METAL IONS IN LIFE SCIENCES 17

Astrid Sigel, Helmut Sigel, Roland K.O. Sigel
Metal Ions in Life Sciences 17

Metal Ions in Life Sciences

Edited by
Astrid Sigel, Helmut Sigel and Roland K.O. Sigel

Volume 17

Lead: Its Effects on Environment and Health

DE GRUYTER

Editors

Astrid Sigel
University of Basel
Department of Chemistry
Inorganic Chemistry
Spitalstrasse 51
CH-4056 Basel
Switzerland
<astrid.sigel@unibas.ch>

Helmut Sigel
University of Basel
Department of Chemistry
Inorganic Chemistry
Spitalstrasse 51
CH-4056 Basel
Switzerland
<helmut.sigel@unibas.ch>

Roland K. O. Sigel
University of Zürich
Department of Chemistry
Rm 34-F-68
Winterthurerstrasse 190
CH-8057 Zürich
Switzerland
<roland.sigel@chem.uzh.ch>

ISBN 978-3-11-044107-9
e-ISBN (PDF) 978-3-11-043433-0
e-ISBN (EPUB) 978-3-11-043301-2
Set-ISBN 978-3-11-043434-7
ISSN 1559-0836
e-ISSN 1868-0402

Library of Congress Cataloging-in-Publication Data
A CIP catalog record for this book has been applied for at the Library of Congress.

Bibliographic information published by the Deutsche Nationalbibliothek
The Deutsche Nationalbibliothek lists this publication in the Deutsche Nationalbibliografie; detailed bibliographic data are available on the Internet at http://dnb.dnb.de.

Cover illustration: The figure on the dust cover shows Pb(II) in the gamma binding site of HIV-1 DIS, which is normally occupied by Mg(II). Innersphere binding is represented by heavy lines and outersphere binding by thinner ones. The second sphere seen in the background is a further Pb(II), which also replaces a Mg(II) (the detailed coordination sphere is not shown). See also Figure 3 in Chapter 12. The figure was prepared by Roland K. O. Sigel based on PDB 1Y95.

Typesetting: Meta Systems Publishing & Printservices GmbH, Wustermark, Germany
Printing and binding: CPI books GmbH, Leck
♾ Printed on acid-free paper
Printed in Germany

For further volumes: www.mils-WdG.com
www.degruyter.com

About the Editors

Astrid Sigel has studied languages; she was an editor of the *Metal Ions in Biological Systems* series (until Volume 44) and also of the "Handbook on Toxicity of Inorganic Compounds" (1988), the "Handbook on Metals in Clinical and Analytical Chemistry" (1994; both with H. G. Seiler), and on the "Handbook on Metalloproteins" (2001; with Ivano Bertini). She is also an editor of the *MILS* series from Volume 1 on.

Helmut Sigel is Emeritus Professor (2003) of Inorganic Chemistry at the University of Basel, Switzerland, and a previous editor of the *MIBS* series until Volume 44. He served on various editorial and advisory boards, published over 350 articles on metal ion complexes of nucleotides, coenzymes, and other ligands of biological relevance, and lectured worldwide. He was named Protagonist in Chemistry (2002) by *ICA* (issue 339); among further honors are the P. Ray Award (Indian Chemical Society, of which he is also an Honorary Fellow), the Alfred Werner Prize (Swiss Chemical Society), a Doctor of Science honoris causa degree (Kalyani University, India), appointments as Visiting Professor (e.g., Austria, China, Japan, Kuwait, UK) and Endowed Lectureships; he is also a Honorary Member of SBIC (Society of Biological Inorganic Chemistry).

Roland K. O. Sigel is Full Professor (2016) of Chemistry at the University of Zürich, Switzerland. In the same year he became Vice Dean of Studies (BSc/MSc) of the Faculty of Science. From 2003 to 2008 he was endowed with a Förderungsprofessur of the Swiss National Science Foundation and he is the recipient of an ERC Starting Grant 2010. He received his doctoral degree summa cum laude (1999) from the University of Dortmund, Germany, working with Bernhard Lippert. Thereafter he spent nearly three years at Columbia University, New York, USA, with Anna Marie Pyle (now Yale University). During the six years abroad he received several prestigious fellowships from various sources, and he was awarded the EuroBIC Medal in 2008 and the Alfred Werner Prize (SCS) in 2009. His research focuses on the structural and functional role of metal ions in ribozymes, especially group II introns, regulatory RNAs, and on related topics. He was also an editor of Volumes 43 and 44 of the *MIBS* series and of the *MILS* series from Volume 1 on.

Historical Development and Perspectives of the Series *Metal Ions in Life Sciences*[*]

It is an old wisdom that metals are indispensable for life. Indeed, several of them, like sodium, potassium, and calcium, are easily discovered in living matter. However, the role of metals and their impact on life remained largely hidden until inorganic chemistry and coordination chemistry experienced a pronounced revival in the 1950s. The experimental and theoretical tools created in this period and their application to biochemical problems led to the development of the field or discipline now known as *Bioinorganic Chemistry*, *Inorganic Biochemistry*, or more recently also often addressed as *Biological Inorganic Chemistry.*

By 1970 *Bioinorganic Chemistry* was established and further promoted by the book series *Metal Ions in Biological Systems* founded in 1973 (edited by H. S., who was soon joined by A. S.) and published by Marcel Dekker, Inc., New York, for more than 30 years. After this company ceased to be a family endeavor and its acquisition by another company, we decided, after having edited 44 volumes of the *MIBS* series (the last two together with R. K. O. S.) to launch a new and broader minded series to cover today's needs in the *Life Sciences.* Therefore, the Sigels new series is entitled

Metal Ions in Life Sciences.

After publication of 16 volumes (since 2006) with various publishers during the past 10 years, we are happy to join forces now in this still growing endeavor with Walter de Gruyter GmbH, Berlin, Germany, a most experienced Publisher in the *Sciences.*

The development of *Biological Inorganic Chemistry* during the past 40 years was and still is driven by several factors; among these are (i) attempts to reveal the interplay between metal ions and hormones or vitamins, etc., (ii) efforts regarding the understanding of accumulation, transport, metabolism and toxicity of metal ions, (iii) the development and application of metal-based drugs,

---

* Reproduced with some alterations by permission of John Wiley & Sons, Ltd., Chichester, UK (copyright 2006) from pages v and vi of Volume 1 of the series *Metal Ions in Life Sciences* (MILS-1).

(iv) biomimetic syntheses with the aim to understand biological processes as well as to create efficient catalysts, (v) the determination of high-resolution structures of proteins, nucleic acids, and other biomolecules, (vi) the utilization of powerful spectroscopic tools allowing studies of structures and dynamics, and (vii), more recently, the widespread use of macromolecular engineering to create new biologically relevant structures at will. All this and more is reflected in the volumes of the series *Metal Ions in Life Sciences*.

The importance of metal ions to the vital functions of living organisms, hence, to their health and well-being, is nowadays well accepted. However, in spite of all the progress made, we are still only at the brink of understanding these processes. Therefore, the series *Metal Ions in Life Sciences* links coordination chemistry and biochemistry in their widest sense. Despite the evident expectation that a great deal of future outstanding discoveries will be made in the interdisciplinary areas of science, there are still ''language'' barriers between the historically separate spheres of chemistry, biology, medicine, and physics. Thus, it is one of the aims of this series to catalyze mutual ''understanding''.

It is our hope that *Metal Ions in Life Sciences* continues to prove a stimulus for new activities in the fascinating ''field'' of *Biological Inorganic Chemistry*. If so, it will well serve its purpose and be a rewarding result for the efforts spent by the authors.

Astrid Sigel and Helmut Sigel
Department of Chemistry, Inorganic Chemistry
University of Basel, CH-4056 Basel, Switzerland

Roland K. O. Sigel
Department of Chemistry
University of Zürich, CH-8057 Zürich, Switzerland

October 2005
and September 2016

Preface to Volume 17

Lead: Its Effects on Environment and Health

Owing to its abundance on earth and its multiple uses by humans, lead is a major toxicant that threatened human health for millenia and continues to do so. There is no safe level of exposure, necessitating a nuanced approach to its control in food. Turnover in soft tissues is within days, but lead accumulates in bone with a half-life of about 30 years, though it can be mobilized under physiological conditions of bone resorption. Children suffer irreversible neurological deficits. In adults chronic exposure leads to elevated blood pressure, development of cancers, and, as suggested more recently, neurodegeneration. Except for its action in δ-aminolevulinate dehydrogenase, its molecular toxicology remains largely speculative in terms of specific targets. One major molecular mechanism seems to be the replacement of zinc by lead in zinc proteins with functional consequences. All this and more is indicated in *Chapter 1*, *The Bioinorganic Chemistry of Lead in the Context of Its Toxicity*, and discussed in detail in the 15 chapters to follow.

Compared to other metals Pb is rather immobile in the environment, but still its biogeochemical cycling is greatly perturbed by human activities. *Chapter 2* deals with the distribution of Pb in crustal materials and the connected natural and anthropogenic processes that contribute to the metal's mobilization in the biosphere. Important in this context are its high volatility, low melting point, and large radius. Its chemical speciation in aqueous systems contributes to its redistribution. Certainly, anthropogenic inputs began already in antiquity, but accelerated during the industrial revolution, which sparked increases in mining and fossil fuel combustion. Its global cycling and tracking of water mass circulation in the ocean is discussed. The methods for the determination of lead in environmental samples are explained in *Chapter 3*, where also sample preparation, speciation for differentiation, as well as applications of its isotope-selective determinations are described. In *Chapter 4* the encapsulation technology as a potential breakthrough solution for a recyclable removal of lead from industrial wastewater is summarized. – At sites more strongly impacted by mining and

Metal Ions in Life Sciences, Volume 17 Edited by Astrid Sigel, Helmut Sigel, and Roland K. O. Sigel

DOI 10.1515/9783110434330-202

urbanization, Pb is found at high nano to low micromolar concentrations in surface waters, yet it can even be higher in soils and sediments. *Chapter 5* surveys the responses of microorganisms to lead exposure, which can range from resistant to highly sensitive. These varying levels of toxicity are to be attributed to the cellular handling of Pb. – Naturally, *Human Biomonitoring of Lead Exposure* (*Chapter 6*) is an important task: The predominant sample matrices considered include blood and bone, as well as urine, hair, nail, and saliva. The so-called "biomarkers of effect" used for diagnostic strategies are also pointed out.

Structural information on the interaction between lead ion and its targeting biological substances is important for various reasons, including the successful treating of lead poisoning which is a present-day problem. Thus, *Chapter 7* provides solid state structures of lead complexes with (i) amino acids and small peptides, (ii) proteins, (iii) nucleic acid constituents, (iv) nucleic acids, (v) simple saccharides, and (vi) other biorelevant molecules, including lead-detoxification agents. As described in *Chapter 8*, the mostly hemidirected lead(II) complexes of amino acids and peptides have a moderate stability owing to the sterical effect of the $6s^2$ lone pair; e.g., a second tridentate ligand, as it occurs in a (NH_2,COO^-,S^-)-coordination of penicillamine, is not able to coordinate. At high ligand excess, however, coordination of three sulfur donors to lead(II) is found with thiolate-containing amino acids and oligopeptides. High-basicity oxygens of hydroxamates, hydroxypyronates, and hydroxypyridinoates are also effective lead-binding donors, though it may be noted that the corresponding thio derivatives are significantly better ligands for lead than their parent oxo molecules, but polymers with poor water solubility are formed in most cases.

Metallothioneins are involved in homeostatic metal response for the essential metals zinc and copper, as well as in the detoxification of heavy metals. In *Chapter 9* efforts are made to understand the role of metallothioneins regarding the metabolism of lead and in *Chapter 10* attempts are provided to understand the biological chemistry of lead using a synthetic biology approach by focusing on thiolate-rich sites that are found in metalloregulatory proteins in which Pb often prefers a hemidirected $Pb(II)(SR)_3^-$ coordination sphere, regardless of the protein fold (α-helices, β-sheet or loop regions). This insight allows to reveal fundamental concepts on how metals behave in biological systems.

As summarized in *Chapter 11*, the coordination chemistry of lead(II) is complicated due to its varying coordination numbers (4 to 10), as well as by the $6s^2$ electron lone pair, which, with CN = 4, can shield one side of the Pb^{2+} coordination sphere. The chapter focuses on complexes formed with nucleotides and their constituents and derivatives, that is, on complexes formed with hydroxy groups, sugar residues, nucleobases, and phosphates. Such Pb^{2+} complexes are compared as far as possible with those of Ca^{2+}, Fe^{2+}, Cu^{2+}, Zn^{2+}, and Cd^{2+} to reveal in this way the special properties of Pb^{2+} for which the *hard-soft rule* fails. For example, the affinities of Pb^{2+} towards S donor sites are difficult to generalize: On the one hand Pb^{2+} forms very stable complexes with nucleoside 5′-*O*-thiomonophosphates, however, on the other hand, once a sulfur atom replaces one of the terminal oxygen atoms in the phosphodiester linkage, macrochelate formation of the phosphate-bound Pb^{2+} occurs with the O and not with the S site. For some

of the purine-nucleotides macrochelate formation takes place by the interactions of the phosphate-coordinated Pb^{2+}, e.g., with the guanine N7/(C6)O site.

As pointed out in *Chapter 12*, lead(II) is not associated naturally with nucleic acids, but it has been applied together with DNA and RNA in various contexts. Pb^{2+} is a hydrolytic metal ion with excellence in catalyzing phosphodiester cleavages and thus, has potential for probing secondary structures and metal ion binding sites. The structures of $tRNA^{Phe}$, RNAse P, the HIV-1 dimerization-initiation site, and the leadzyme are discussed in detail. It is emphasized that derivatives of two lead(II)-dependent DNAzymes have been applied to detect lead(II) in the lower nanomolar range not only in the test tube, but also in body fluids. Due to the toxicity of lead(II) for living beings this is a highly active research field.

Chapter 13 summarizes historical and current views on lead toxicity. It also addresses the development and evolution of exposure prevention policies, and one learns about the progress that has been made through regulations and guidelines to reduce exposure and prevent lead toxicity. As stated in *Chapter 14*, the use of alkyl lead derivatives as anti-knock agents in gasoline can be considered as one of the main pollution disasters of the 20^{th} century because of both the global character of the pollution emitted and the seriousness of the impact on human health. Alkyl lead derivatives by themselves cannot be considered to be persistent pollutants because they readily degrade. However, the inorganic lead they produced has been deposited all over the globe, including remote sites such as polar areas. Whereas the residence time of lead in the atmosphere is short, the very long permanence of inorganic lead in soils is striking and resuspension is a permanent source of toxic lead.

"*Lead Toxicity in Plants*" (*Chapter 15*) looks critically at the relevance of lead toxicity and the proposed mechanisms of Pb^{2+}-induced stress in algae and higher plants. Previous studies suggest three main mechanisms of toxicity of Pb^{2+}: inhibition of photosynthesis, oxidative stress, and "genotoxicity" including DNA damage and defects in mitosis. Considering the applied concentration ranges in these studies it is argued that likely the defects in mitosis are the environmentally most relevant effects; inhibition of photosynthetic light reactions is far less efficient with Pb^{2+} compared to other metal ions, so this Pb^{2+} toxicity seems environmentally not relevant. – For humans it holds: While essential metals have physiological roles, there are no health benefits from lead intake. In *Chapter 16* the sources of lead exposure, the absorption, distribution, and elimination of lead from the human body, as well as molecular mechanisms of lead-induced toxicity are discussed. The effects on the nervous system, kidney, immune system, blood, reproductive system, and bones are highlighted.

To concude, this volume devoted solely to lead is rich on specific information, but it provides also basic insights that should help to promote further our understanding of the unique role which this toxic metal plays in the environment and in human health.

Astrid Sigel
Helmut Sigel
Roland K. O. Sigel

Contents

Contributors to Volume 17

Numbers in parentheses indicate the pages on which the authors' contributions begin.

Henry G. Abadin Agency for Toxic Substances and Disease Registry (ATSDR), US Department of Health and Human Services, Division of Toxicology and Human Health Studies, 1600 Clifton Road, F-57, Atlanta, GA 30333, USA <habadin@cdc.gov> (435)

Ana Carolina B. Almeida Lopes Graduate Program in Public Health, Center of Health Sciences, State University of Londrina, Londrina, Parana, Brazil (501)

Katsuyuki Aoki Department of Environmental and Life Sciences, Toyohashi University of Technology, Tempaku-cho, Toyohashi 441–8580, Japan <ka003@edu.imc.tut.ac.jp> (123)

Michael Aschner Department of Molecular Pharmacology, Albert Einstein College of Medicine, Forchheimer 209, 1300 Morris Park Avenue, Bronx, NY 10461, USA <michael.aschner@einstein.yu.edu> (501)

Miquel Barceló-Oliver University of the Balearic Islands, Department of Chemistry, Bldg. Mateu Orfila i Rotger, Carretera Valldemossa km 7.5, E-07122 Palma (Mallorca), Spain <miquel.barcelo@uib.es> (403)

Josep Bonet SCHEMA, Rue Principale 92, L-6990 Rameldange, Luxembourg (471)

Péter Buglyó Department of Inorganic and Analytical Chemistry, Faculty of Science, University of Debrecen, Egyetem tér 1, H-4032 Debrecen, Hungary <buglyo@science.unideb.hu> (201)

Samuel Caito Department of Molecular Pharmacology, Albert Einstein College of Medicine, Forchheimer 209, 1300 Morris Park Avenue, Bronx, NY 10461, USA (501)

Virginia Cangelosi Department of Chemistry, Michigan State University, 578 S. Shaw Ln., East Lansing, MI 48824-1322, USA <vcangelo@msu.edu> (271)

Jay T. Cullen School of Earth and Ocean Sciences, Bob Wright Centre A415, Box 3065STN CSC, University of Victoria, Victoria, BC, V8W 3V6, Canada <jcullen@uvic.ca> (21)

Etelka Farkas Department of Inorganic and Analytical Chemistry, Faculty of Science, University of Debrecen, Egyetem tér 1, H-4032 Debrecen, Hungary <efarkas@science.unideb.hu> (201)

Montserrat Filella [1]Institute F.-A. Forel, University of Geneva, Boulevard Carl-Vogt 66, CH-1211 Geneva 4, Switzerland <montserrat.filella@unige.ch> and [2]SCHEMA, Rue Principale 92, L-6990 Rameldange, Luxembourg (471)

Thomas Göen Institute and Outpatient Clinic of Occupational, Social and Environmental Medicine, Friedrich-Alexander University (FAU) of Erlangen-Nürnberg, Schillerstr. 25/29, D-91052 Erlangen, Germany (99)

Peter C. Hauser Department of Chemistry, Analytical Sciences, University of Basel, Spitalstrasse 51, CH 4056 Basel, Switzerland <peter.hauser@unibas.ch> (49)

Ning-Hai Hu Changchun Institute of Applied Chemistry, Chinese Academy of Sciences, Changchun 130022, China <hunh@ciac.ac.cn> (123)

Susan Z. Ingber Agency for Toxic Substances and Disease Registry (ATSDR), US Department of Health and Human Services, Division of Toxicology and Human Health Studies, 1600 Clifton Road, F-57, Atlanta, GA 30333, USA <singber@cdc.gov> (435)

Renata Jastrząb Faculty of Chemistry, Adam Mickiewicz University, Umultowska 89b, PL-61-614 Poznán, Poland <renatad@amu.edu.pl> (61)

Katrin Klotz Institute and Outpatient Clinic of Occupational, Social and Environmental Medicine, Friedrich-Alexander University (FAU) of Erlangen-Nürnberg, Schillerstr. 25/29, D-91052 Erlangen, Germany <katrin.klotz@fau.de> (99)

Hendrik Küpper [1]Biology Center of the Czech Academy of Sciences, Institute of Plant Molecular Biology, Department of Plant Biophysics & Biochemistry, and [2]University of South Bohemia, Department of Experimental Plant Biology; Branisovská 31/1160, CZ-370 05, České Budějovice, Czech Republic <hendrik.kuepper@umbr.cas.cz> (491)

Wolfgang Maret King's College London, School of Medicine, Division of Diabetes and Nutritional Sciences and Department of Biochemistry, London Iron Metabolism Group, Franklin-Wilkins Bldg., 150 Stamford St., London SE1 9NH, UK <wolfgang.maret@kcl.ac.uk> (1)

Jason McAlister [2]Department of Earth and Ocean Sciences, University of British Columbia, Vancouver, BC, Canada <jmcalist@eos.ubc.ca> (21)

Maureen E. Merrifield-MacRae Department of Chemistry, The University of Western Ontario, 1151 Richmond Street, London, Ontario N6A 5B7, Canada (241)

Kazutaka Murayama Graduate School of Biomedical Engineering, Tohoku University, Aoba, Sendai 980–8575, Japan <kmura@bme.tohoku.ac.jp> (123)

Bert P. Operschall Department of Chemistry, Inorganic Chemistry, University of Basel, Spitalstrasse 51, CH-4056 Basel, Switzerland (319)

Joana Palou-Mir University of the Balearic Islands, Department of Chemistry, Bldg. Mateu Orfila i Rotger, Carretera Valldemossa km 7.5, E-07122 Palma (Mallorca), Spain <joana.palou@uib.es> (403)

Monica M. B. Paoliello Graduate Program in Public Health, Center of Health Sciences, State University of Londrina, Londrina, Parana, Brazil (501)

Vincent L. Pecoraro Department of Chemistry, University of Michigan, 930 N. University, Ann Arbor, MI 48109-1055, USA <vlpec@umich.edu> (271)

Hana R. Pohl Agency for Toxic Substances and Disease Registry (ATSDR), US Department of Health and Human Services, Division of Toxicology and Human Health Studies, 1600 Clifton Road, F-57, Atlanta, GA 30333, USA <hpohl@cdc.gov> (435)

Leela Ruckthong Department of Chemistry, University of Michigan, 930 N. University, Ann Arbor, MI 48109-1055, USA (271)

Astrid Sigel Department of Chemistry, Inorganic Chemistry, University of Basel, Spitalstrasse 51, CH-4056 Basel, Switzerland <astrid.sigel@unibas.ch> (319)

Helmut Sigel Department of Chemistry, Inorganic Chemistry, University of Basel, Spitalstrasse 51, CH-4056 Basel, Switzerland <helmut.sigel@unibas.ch> (319)

Roland K. O. Sigel University of Zurich, Department of Chemistry, Rm 34-F-68, Winterthurerstrasse 190, CH-8057 Zurich, Switzerland <roland.sigel@chem.uzh.ch> (403)

Theodora J. Stewart King's College London, Division of Diabetes and Nutritional Sciences, Franklin-Wilkins Bldg., 150 Stamford St., London SE1 9NH, UK <theodora.stewart@kcl.ac.uk> (79)

Martin J. Stillman Department of Chemistry, The University of Western Ontario, 1151 Richmond Street, London, Ontario N6A 5B7, Canada <martin.stillman@uwo.ca> (241)

Bartosz Tylkowski Centre Tecnològic de la Química de Catalunya, Carrer de Marcel·lí Domingo, ES-43007 Tarragona, Spain <tylkowski.bt@pg.com> <bartosz.tylkowski@ctqc.org> (61)

Daisy L. Wong Department of Chemistry, The University of Western Ontario, 1151 Richmond Street, London, Ontario N6A 5B7, Canada (241)

Titles of Volumes 1–44 in the *Metal Ions in Biological Systems* Series

edited by the SIGELs
and published by Dekker/Taylor & Francis (1973–2005)

Volume 1: **Simple Complexes**
Volume 2: **Mixed-Ligand Complexes**
Volume 3: **High Molecular Complexes**
Volume 4: **Metal Ions as Probes**
Volume 5: **Reactivity of Coordination Compounds**
Volume 6: **Biological Action of Metal Ions**
Volume 7: **Iron in Model and Natural Compounds**
Volume 8: **Nucleotides and Derivatives: Their Ligating Ambivalency**
Volume 9: **Amino Acids and Derivatives as Ambivalent Ligands**
Volume 10: **Carcinogenicity and Metal Ions**
Volume 11: **Metal Complexes as Anticancer Agents**
Volume 12: **Properties of Copper**
Volume 13: **Copper Proteins**
Volume 14: **Inorganic Drugs in Deficiency and Disease**
Volume 15: **Zinc and Its Role in Biology and Nutrition**
Volume 16: **Methods Involving Metal Ions and Complexes in Clinical Chemistry**
Volume 17: **Calcium and Its Role in Biology**
Volume 18: **Circulation of Metals in the Environment**
Volume 19: **Antibiotics and Their Complexes**
Volume 20: **Concepts on Metal Ion Toxicity**
Volume 21: **Applications of Nuclear Magnetic Resonance to Paramagnetic Species**
Volume 22: **ENDOR, EPR, and Electron Spin Echo for Probing Coordination Spheres**
Volume 23: **Nickel and Its Role in Biology**
Volume 24: **Aluminum and Its Role in Biology**
Volume 25: **Interrelations Among Metal Ions, Enzymes, and Gene Expression**
Volume 26: **Compendium on Magnesium and Its Role in Biology, Nutrition, and Physiology**
Volume 27: **Electron Transfer Reactions in Metalloproteins**

Volume 28: **Degradation of Environmental Pollutants by Microorganisms and Their Metalloenzymes**
Volume 29: **Biological Properties of Metal Alkyl Derivatives**
Volume 30: **Metalloenzymes Involving Amino Acid-Residue and Related Radicals**
Volume 31: **Vanadium and Its Role for Life**
Volume 32: **Interactions of Metal Ions with Nucleotides, Nucleic Acids, and Their Constituents**
Volume 33: **Probing Nucleic Acids by Metal Ion Complexes of Small Molecules**
Volume 34: **Mercury and Its Effects on Environment and Biology**
Volume 35: **Iron Transport and Storage in Microorganisms, Plants, and Animals**
Volume 36: **Interrelations Between Free Radicals and Metal Ions in Life Processes**
Volume 37: **Manganese and Its Role in Biological Processes**
Volume 38: **Probing of Proteins by Metal Ions and Their Low-Molecular-Weight Complexes**
Volume 39: **Molybdenum and Tungsten. Their Roles in Biological Processes**
Volume 40: **The Lanthanides and Their Interrelations with Biosystems**
Volume 41: **Metal Ions and Their Complexes in Medication**
Volume 42: **Metal Complexes in Tumor Diagnosis and as Anticancer Agents**
Volume 43: **Biogeochemical Cycles of Elements**
Volume 44: **Biogeochemistry, Availability, and Transport of Metals in the Environment**

Contents of Volumes in the *Metal Ions in Life Sciences* Series

edited by the SIGELs

Volumes 1–4

published by John Wiley & Sons, Ltd., Chichester, UK (2006–2008)
<http://www.Wiley.com/go/mils>
<http://www.wiley.com/WileyCDA/Section/id-300350.html>

Volumes 5–9

published by the Royal Society of Chemistry, Cambridge, UK (2009–2011)
since 2015 by Walter de Gruyter GmbH, Berlin, Germany
<http://www.bioinorganic-chemistry.org/mils> <http://www.mils-WdG.com>

Volumes 10–16

published by Springer Science & Business Media BV, Dordrecht,
The Netherlands (2012–2014; MILS-10 to MILS-14)
and by Springer International Publishing AG, Cham, Switzerland
(2015–2016; MILS-15 and MILS-16)
<http://www.bioinorganic-chemistry.org/mils>

and from Volume 17 on

published by Walter de Gruyter GmbH, Berlin, Germany
<http://www.mils-WdG.com>

Volume 1: Neurodegenerative Diseases and Metal Ions

Volume 2: Nickel and Its Surprising Impact in Nature

Volume 3: The Ubiquitous Roles of Cytochrome P450 Proteins

Volume 4: Biomineralization. From Nature to Application

Volume 5: Metallothioneins and Related Chelators

Volume 6: Metal-Carbon Bonds in Enzymes and Cofactors

Volume 7: Organometallics in Environment and Toxicology

Volume 8: Metal Ions in Toxicology: Effects, Interactions, Interdependencies

Volume 9: Structural and Catalytic Roles of Metal Ions in RNA

Volume 10: Interplay between Metal Ions and Nucleic Acids

Volume 11: Cadmium: From Toxicity to Essentiality

Volume 12: Metallomics and the Cell
Guest Editor: Lucia Banci

Volume 13: Interrelations between Essential Metal Ions and Human Diseases

Volume 14: The Metal-Driven Biogeochemistry of Gaseous Compounds in the Environment
Guest Editors: Peter M. H. Kroneck and Martha E. Sosa-Torres

Volume 16: The Alkali Metal Ions: Their Roles for Life

Comments and suggestions with regard to contents, topics, and the like for future volumes of the series are welcome.

1

The Bioinorganic Chemistry of Lead in the Context of Its Toxicity

Wolfgang Maret

King's College London, Division of Diabetes and Nutritional Sciences and
Department of Biochemistry, London Iron Metabolism Group, Franklin-Wilkins Bldg.,
150 Stamford St., London SE1 9NH, UK
<wolfgang.maret@kcl.ac.uk>

Metal Ions in Life Sciences, Volume 17 Edited by Astrid Sigel, Helmut Sigel, and Roland K. O. Sigel

DOI 10.1515/9783110434330-001

Abstract: Owing to its abundance on earth and its multiple uses by humans, lead (Pb) is a major toxicant that has threatened human health for millennia and continues to do so. There is no safe level of exposure, necessitating a nuanced approach to its control in the food we consume, the water we drink, and the air we breathe. Turnover in soft tissues is within days. In contrast, lead accumulates in bone and turns over with a half-life of about 30 years, though it can be mobilized from bone under physiological and pathophysiological conditions of bone resorption. Children are particularly vulnerable to lead exposure and suffer irreversible neurological deficits affecting learning ability and behavior. In adults, chronic effects of exposure to lead include elevated blood pressure, development of cancers, and, as suggested more recently, neurodegeneration. Some pathways of systemic and cellular metabolism of Pb(II) are known. However, except for its action in δ-aminolevulinate dehydratase, its molecular toxicology remains largely speculative in terms of specific targets. One major molecular mechanism seems to be the replacement of zinc with lead in zinc proteins with functional consequences. Calcium binding proteins are also being discussed as possible targets. However, the affinities of lead for calcium sites in proteins are orders of magnitude lower than those for zinc sites. Therefore, it remains to be shown whether lead at the concentrations occurring in tissues can replace calcium in proteins *in vivo*. Despite humans having recognized the hazards of lead exposure for a very long time, uncertainties remain as to the threshold for adverse effects on our health and the low levels of exposure during our lives as a risk factor for chronic disease.

Keywords: calcium · lead · protein interactions · toxicity · zinc

1. INTRODUCTION

The chemical symbol for lead is Pb derived from the Latin word plumbum. The root of the word is all too familiar to us in the noun and verb "plumbing". Literature searches on lead face the unique challenge that they also retrieve entries for the verb "to lead". As a consequence, one obtains datasets that are difficult to curate, and given the very extensive literature on this metal, it becomes a daunting task to sift through the information.

The toxicity of inorganic and organic lead compounds is the main focus of the biomedical literature. However, a thorough overview would be incomplete without mentioning that at least two groups of established investigators in the field of trace element research reported beneficial effects of lead in the diet of rats. In one study, the natural lead content in the diet was lowered to 200 μg/kg. Addition of lead at a dose of 1.0–2.5 mg/kg then induced a consistent growth response [1]. Another group observed that lowering the natural lead content in the diet to 10–30 μg/kg resulted in growth depression in several subsequent generations. The investigations were reported in a series of publications [2]. The interpretation of these findings is uncertain. It has not been clarified whether

additional methodological issues need to be considered, inadvertent changes in the diet caused these effects or other factors necessary for growth were affected indirectly. The initial presentation of these observations in this article should not distract from its main theme, namely the toxicity of lead.

Lead can be measured in the human body at levels that are higher than those of some essential metal ions, such as molybdenum, manganese or even copper [3]. What are the consequences of its presence? This article will focus on this question and discuss the effects of lead on humans, though the ecotoxicology of lead is important for virtually all living organisms. Many different disciplines come to bear on defining the effects of lead on humans, e.g., chemistry, biochemistry, toxicology, nutrition, epidemiology, clinical investigations, neurobiology, etc. This chapter attempts to transcend disciplines, lay the foundation for the discussions in this book, and provide a scientific basis for addressing the lingering question whether or not some more general ailments and disorders are due to inadvertent exposure and accumulation of metals with high toxicity in our organs during our lifetime.

2. LEAD CHEMISTRY WITH REGARD TO BIOCHEMISTRY

Metals with significant toxicity, namely cadmium (Cd), mercury (Hg), thallium (Tl), and lead (Pb), cluster in one area of the periodic system of the elements (Figure 1). The closest nutritionally essential element is zinc (Zn) in the same d-group with Cd and Hg. Diagonally across the p-group elements, the metalloids separate metals from non-metals, most of the latter being essential. One chemical property that the elements with high toxicity share is their thiophilicity, i.e., a high affinity for the sulfur donor atoms of ligands. The solubility constants ($-\log K$) of their sulfides are: CdS: 27; HgS: 52; Tl_2S: 22; PbS: 28–29. For bismuth (Bi), it is even higher: Bi_2S_3: 96. For comparison, the value for ZnS is 25. Yet, in spite of similar affinities of cadmium and lead for sulfur, their toxic effects in humans are dissimilar [4]. When comparing the affinities of cadmium and lead for ligand donors relative to those of the transition metals and zinc in the Irving-Williams series, the order is Cd < Pb < Zn for nitrogen coordination environments, Cd < Zn < Pb for oxygen coordination environment, and Zn < Cd < Pb for sulfur coordination environments [5]. Hence, among the three metals, lead is the preferred metal in oxygen and sulfur coordination environments. This feature is important for the following discussion of lead interactions with the oxygen donor-rich sites of calcium in proteins and with the sulfur donor-rich sites of zinc in proteins.

Among the three common valence states of lead (0 (elemental lead), II, and IV), valence state II is the one mostly relevant for biology. The solution chemistry of Pb(II) is illustrated with a Pourbaix diagram (Figure 2). It demonstrates that Pb^{2+}, the plumbous ion, is not very soluble at physiological pH. It forms $Pb(OH)^{+}$ with a pK_a of 7.9 in dilute solutions and the polynuclear species $[Pb_4(OH)_4]^{4+}$ in more concentrated solutions. At higher pH values, additional polynuclear species are formed: $[Pb_3(OH)_4]^{2+}$ and $[Pb_6O(OH)_6]^{4+}$, i.e., $HOPbO^{-}$

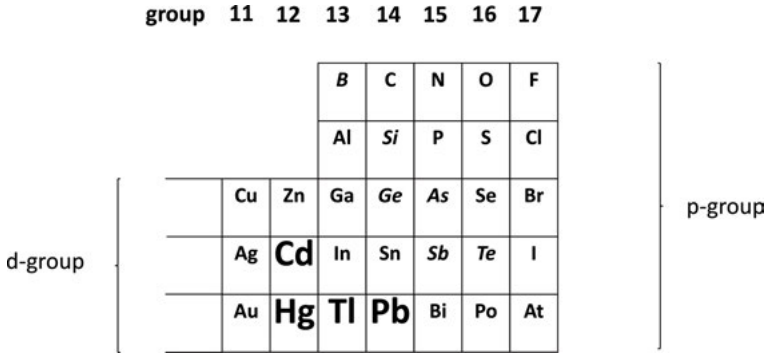

Figure 1. Metals with high toxicity in the periodic system of the elements. Cadmium and mercury, together with zinc in group 12, and thallium and lead following mercury in the same period, form a cluster of metal ions with high toxicity. Metalloids are shown in italics.

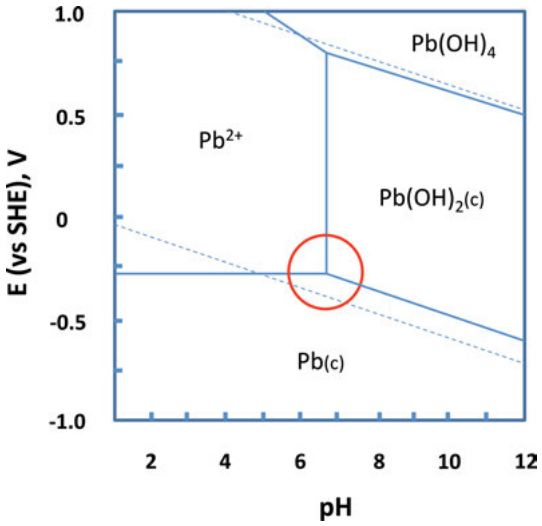

Figure 2. Pourbaix diagram of lead (in the absence of anions with $[Pb^{2+}]_{total} = 10\ \mu M$ at 25 °C). The circle emphasizes the existence of three species, Pb^{2+}, $Pb(OH)_2$, and metallic Pb close to pH 7.0. From http://www.cs.mcgill.ca/~rwest/link-suggestion/wpcd_2008-09_augmented/images/257/25713.png.htm, released into the public domain.

("plumbite"). Pb^{2+} is weakly hydrated because of its low charge density [6]. The presence of other anions influences solubility, in particular carbonate and its pH dependence, and the anions that determine salinity: chloride and sulfate. The solubility products are $pK_L = 4.8$ for lead chloride, 8 for the sulfate, 10.5 for the oxalate, 13.5 for the carbonate, 15.5 for the hydroxide, 28 for the sulfide, and 43.5 for the phosphate. The values for different phosphates range from 10^{-10} M for $PbHPO_4$ to 10^{-77} M for $Pb_5(PO_4)_3OH$ [7]. Only lead acetate, nitrate, and

chlorate/perchlorate have high solubility in water. Because of the solubility of the different salts, the lead salt employed in investigations needs to be specified. Pb^{2+} has relatively fast ligand exchange. This fact has adduced to the notion that lead metabolism is under thermodynamic rather than kinetic control.

In the biological scientific literature, authors usually refer to "lead" in their articles, a term that refers to the element in chemistry. For all purposes, "lead" is the lead(II) ion in biology. Lead(II) in biology does not participate directly in redox reactions. Therefore, lead causing lipid peroxidation and affecting the formation of reactive species in cells must be an indirect action mediated by binding of lead to biological molecules and either activating a process producing reactive species or inhibiting redox enzymes that normally quench reactive species.

Information about the coordination chemistry of lead in solution is rather scarce [6] – even more so with regard to its complexation in biological fluids and in cells. The ionic radius (1.19) is similar to that of Ba^{2+} but larger than those of Ca^{2+} (0.99) and Zn^{2+} (0.74). It is dependent on the coordination number, though, and can vary from 1.00 (CN = 4) to 1.30 (CN = 8) [6]. One factor in the geometry of lead coordination is that Pb^{2+} is stereochemically active, resulting in preferred geometries. This property distinguishes it from Zn^{2+} and Ca^{2+} and is perhaps the single most important issue why coordination environments differ when lead binds in zinc or calcium sites with functional consequences. Whereas a holodirected binding is typical for lead with high coordination numbers, a hemidirected binding occurs at low coordination numbers. In the latter case, the ligands are all on one side leaving one lone electron pair on the opposite site [8].

3. HISTORY AND MANUFACTURING OF LEAD-CONTAINING MATERIALS

Compared to mercury, cadmium, or thallium, lead is a more significant issue in toxicology. Because of its relative abundance on earth and its industrial applications, a particularly problematic relationship with humans and other living organisms developed. Human activities increased lead in the environment from its early uses [9]. The geological record demonstrates an at least 100-fold increase from an original value of 0.4 ng Pb/m^3 soil. In densely populated and industrialized areas, it is now 500 to 10,000 ng Pb/m^3 [10, 11]. In 2012, the worldwide production of lead reached 10 million tonnes [12]. Lead ends up in the environment and in organisms despite efforts in recycling. The effectiveness of human measures to eliminate some sources of lead emissions into the environment is illustrated by the reduction of blood lead levels (BLL) in children (1–5 years) in the US from 15 μg/dL in 1976–1980 to 1.84 μg/dL in 2009–2010 when a ban of leaded gasoline came into effect in 1978 [13]. While industrial hygiene has improved drastically in developed countries, serious issues of pollution remain. Although our knowledge of the toxicity of lead has a very long history, regrettably, human exposure to lead continues to be an issue. As of this writing, the role of lead in the water crisis at Flint near Detroit, MI, is being discussed. In some

households, lead levels were found to be up to 1000 times higher than the US legal limit of 15 ppb.

Sources of available lead are metallurgical processes such as cupellation – treatment of ores at high temperatures to separate noble metals from base metals such as lead – and smelting – treatment of ores at high temperatures in the presence of a reducing agent. The main uses are in acid batteries, lead pipes, roofing and building flashings, ammunition, weights, solders, and radiation shields.

Lead poisoning also is known as saturnism or plumbism. For the poisoning from paint it is known as painter's colic. A historic record over 6000 years describes lead poisoning in humans [14, 15]. The role of lead in the death of the famous such as Benjamin Franklin or Caravaggio leaves a testimony of the dangers of exposure. The Romans boiled grape juice (vinum mustum) in lead containers to produce a syrup called defrutum, which was concentrated further to obtain sapa. These syrups contained lead acetate ("lead sugar"), which was used to sweeten wine and to preserve fruits. It was also used medically in Goulard's exctract as an astringent and has been used in cosmetics. With regard to beverages contaminated with lead, the literature, including the classic literature, is replete with episodes. For example "Devonshire (or Devon) colic" was described to occur with severe abdominal pain. In 1767, Sir George Baker, a physician of king George III of England, discussed eruditely lead poisoning as the probable cause of this ailment as lead vessels were used for making cider or the cider was adulterated with lead sugar as a means to stop fermentation or to sweeten the cider [16]. The "colic of Poitou" is a similar episode attributed to adulterated wine in France. The French physician Louis Tanquerel des Planches (1810–1863) is credited with comprehensively documenting lead poisoning as an occupational illness and describing the neurotoxic effects of lead as "encéphalopathie saturnine" [17].

More recent episodes are well publicized together with fierce and bitter debates juxtaposing commercial interests and scientific findings. Lead additives were patented in the 1920s to boost the octane rating of gasoline and thus increasing fuel efficiency and the performance of engines. Using the lead-based anti-knocking agent tetraethyl lead (TEL), $Pb(C_2H_5)_4$, an organic form of lead, in the combustion releases lead chloride or lead bromide formed due to other additives serving as lead scavengers. While TEL additives were discontinued in the US from 1978, they continued to be used in some countries and phasing out took several decades, even in Europe. Leaded gasoline is still being used in some countries. Concomitantly with the ban of TEL, BLL levels decreased from 16 μg/dL in 1976 to only 3 μg/dL in 1991 in the US [18]. Correlations of the lower BLL and an increase in IQ as well as less violent crime have been reported after TEL addition to gasoline was discontinued. However, the presence of lead in areas of heavy car traffic continues to be a source of exposure.

Lead compounds are used as pigments in paints. While saturnism has been reported to be the cause of disease or even death in some of the greatest artists [19], it is a much wider problem for those working with and being exposed to lead-based paint. The three major pigments in paints are white lead

($PbCO_3$) from the mineral hydrocerrussite, which is basic lead carbonate ($2PbCO_3 \cdot Pb(OH)_2$), red lead (Pb_3O_4), which is Pb_2PbO_4, i.e., lead(II)plumbate(IV), and used as an anticorrosion paint, and chrome yellow ($PbCrO_4$). Lead paints were also banned in the US in 1978. Their use in a significant number of countries continues to be a public health issue.

Lead is also used in the manufacturing of some crystal glass, in glazings of glass, ceramics and pottery, and in some grades of pewter. Lead becomes available from these materials when they are used with acidic drinks or food. Lead nanoparticles are a recent area of manufacturing lead-containing materials for various applications, and pose a potentially new threat to our health.

4. SAFE LEVELS OF EXPOSURES?

Average BLL are 1.6 μg/dL for adults and 1.9 μg/dL for children in the US population. In 2012, the Centers for Disease Control and Prevention (CDC) lowered blood lead levels of concern from 10 μg/dL to ≥ 5 μg/dL for children aged 1–5 to identify children and environments with lead-exposure hazards because cognition and behavior are affected negatively even at previously accepted BLL [20]. The CDC also stipulated that the recommendations ought to be updated every four years. Significantly, the effects of lead on cognitive deficits were non-linear with a greater loss of IQ at lower exposures [21].

The US Environmental Protection Agency (EPA) concludes that there is no safe exposure limit, i.e., there is no RfD (reference dose), the maximum acceptable oral dose of a toxic substance, for lead.

5. REGULATORY LEVELS FOR LEAD IN WATER, FOOD, AND AIR

5.1. Lead in Water

In the US, the limit of lead in water is set at 15 μg/L (ppb). For comparison, the limit for nickel is 20 ppb. The limit for lead is 3 times higher than that for cadmium (5 ppb) or mercury and thallium (2 ppb) set by the US EPA. In the UK, the drinking water inspectorate works with a standard of 10 ppb [22].

5.2. Lead in Food

A panel of the European Food Safety Authority (EFSA) dealing with contaminants in the food chain summarized that the average consumption of lead in food is between 0.36 to 1.24 μg/kg body weight per day (up to 2.43 for high consumers, 0.21 to 0.94 for infants, and 0.80 to 3.10 (up to 5.51) for high consumers) [23]. It defined benchmark dose levels that increase the risk for certain

diseases at certain blood lead levels corresponding to daily intakes: a 1 % increase of development of neurotoxicity 12 (0.50) and systolic blood pressure 36 (1.50), and a 10 % increase of chronic kidney disease 15 (0.63). The panel recommended that efforts should be made to reduce lead exposure from both dietary and non-dietary sources. It identified cereals, leafy vegetables, and tap water as the major sources of ingested lead in Europe.

5.3. Lead in Air

The lead concentrations in urban and industrial areas are 2.5–50 mmol/m^3 against a background of < 0.04 mmol/m^3 [24]. The National Institute for Occupational Safety and Health (NIOSH) considers 50 μg/m^3 over eight hours as the recommended exposure limit but cautions that some investigations suggest that this limit is too high [25]. Aside from exposure at the workplace, one source of lead exposure is inhaled cigarette smoke. Tobacco in different brands of cigarettes contains between 0.38 and 1.16 μg lead per cigarette [26].

It is estimated that 40 % of the lead burden stems from water and food ingested while the remainder is from inhalation. Uptake of lead compounds by inhalation is about 10 times more efficient than uptake by ingestion. Percutaneous absorption can be another source of exposure, in particular for organic lead compounds. Children are more susceptible to lead poisoning than adults with apparently irreversible neurodevelopmental changes. Children have an increased intestinal absorption of lead and a higher mobile pool of lead because they store less lead in bone.

6. TRANSPORT IN BLOOD AND CELLULAR UPTAKE

The transporters on intestinal epithelial cells involved in uptake of lead at the apical site and in the release into blood at the basolateral site are not known with certainty [27]. Divalent metal transporter (DMT-1)-dependent and DMT-1-independent pathways have been described. The absorption is variable, usually < 10 % but higher in children, and it increases after fasting and under conditions of iron deficiency when DMT-1 is up-regulated. In biological monitoring, BLL indicates acute exposure and is important for estimating the risk for a negative outcome on health. In blood, 99 % of lead is in erythrocytes. Uptake into the erythrocytes is mediated by anion exchange and calcium channels. Efflux also occurs through passive diffusion, and via the ATP-dependent calcium transporter. The remainder of lead is rather loosely associated with albumin and other blood proteins such as transferrin.

In erythrocytes and other tissues, lead inhibits the zinc enzyme δ-aminolevulinic acid dehydratase (ALAD), also known as porphobilinogen synthase, the second enzyme in the pathway of porphyrin synthesis [28, 29]. Other enzymes in the heme biosynthetic pathway are also inhibited, mainly coproporphyrinogen

oxidase and ferrochelatase, which inserts iron into protoporphyrin IX to form the heme group. In lead poisoning, the consequences of this inhibition are small erythrocytes and iron deficiency (microcytic anemia), and zinc instead of iron bound to protoporphyrin IX forming a fluorescent compound. However, there are other perturbations of iron metabolism that lead to the formation of zinc protoporphyrin IX (ZPP) and hence its determination is not specific for lead poisoning. ALAD is the single most important molecular target identified for the toxicity of lead. Lead binds 25 times stronger than zinc with a K_I value of 70 fM (pH 7.2, 37 °C, for the common 1-1 allele, ALAD1) [30]. A polymorphism in the enzyme affects lead binding and is responsible for different sensitivity of individuals to lead. Individuals with the minor allele (1-2 heterozygotes and 2-2 homozygotes), which contains an asparagine instead of a lysine at position 59, have higher BLL, and due to the apparently higher affinity of ALAD2 for lead seem to be protected against the hematopoietic effects of lead [31, 32]. Other polymorphisms associated with the toxicokinetics of lead are in the hemochromatosis (HFE) gene and in the vitamin D receptor [33, 34]. Variations in yet other genes, including those of metallothioneins, affect lead distribution and the susceptibility to lead-induced organ damage [35].

In erythrocytes, 12–26 % of lead was found to be associated with the magnesium enzyme pyrimidine 5′-nucleotidase type 1. Lead binds at a position where normally a magnesium-bound water molecule resides [36, 37].

In cells, uptake of lead is thought to involve DMT-1 and Ca^{2+} channels [27]. Membrane transporters are selectivity filters that determine which substances gain access into cells. Lead may compete with or block the transport of other metal ions and substances via membrane transporters.

7. LEAD TOXICITY

7.1. Symptoms of Lead Poisoning

The effects of lead poisoning include primarily the nervous and hematopoietic systems and the kidney. Pathology of the heart, skeleton (bones), intestine, and reproductive system are also described. Symptoms of acute poisoning include abdominal pain, confusion, headache and in cases of severe intoxication, seizures, coma, and death. In a about 70 % of patients, a blue Burton(ian) line on the gums can be detected. It is due to lead sulfide formed from sulfide produced by the oral flora. Other clinical signs of chronic lead poisoning are lead colic, anemia, renal tubulopathies, and motor neuropathies. The symptomatology of acute and chronic lead poisoning has been described in considerable detail [24].

7.2. Chelation Therapy

Decorporation of lead under acute or chronic conditions of lead intoxication can be performed by oral or parenteral chelation therapy. $CaNa_2EDTA$ and

2,3-mercaptopropanol (British anti-Lewisite, BAL) are used for intravenous injections whereas D-penicillamine and meso-dimercaptosuccinic acid (DMSA) are used in oral treatments. There is an extensive clinical literature on the chelating agents to be used depending on BLL and the symptoms of lead poisoning, and the ensuring treatment regime and clinical monitoring of the poisoning during chelation therapy (see also Chapter 8).

7.3. Lead Distribution in the Human Body

For the metabolism of lead, it is characteristic that the half-life in soft tissues is about a month and that lead accumulates in bone with a very long half-life of about 30 years (Figure 3). This turnover is quite different from that of cadmium, which accumulates over time in organs such as the liver. Lead is excreted predominantly through feces. BLL is a measure for acute exposure to lead. Blood concentrations of lead are on average higher than those of essential elements such as manganese, cobalt, and molybdenum, and the overall amount of lead in a human body is even higher than that of copper [38]. Bone lead level is a measure of chronic exposure and the history of exposure. About 90 % of lead is stored in bone, where it is incorporated into hydroxyapatite with very high stability. Control subjects have bone lead levels of about 10 μg/g, whereas subjects occupationally exposed to lead as smelter workers have average lead concentrations of about 106 μg/g in finger bones, which is as high as the concentration of

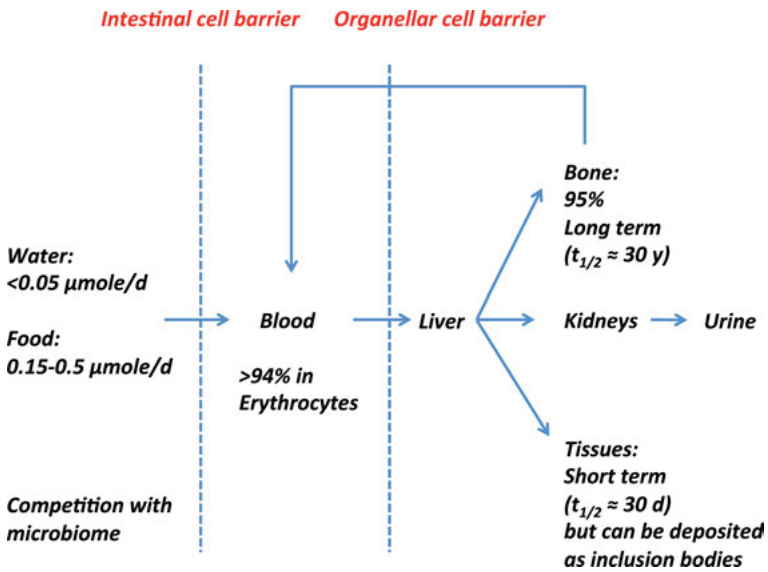

Figure 3. Systemic lead metabolism. The scheme shows the distribution of lead after intestinal uptake in humans (not shown are uptake through the lung, enterohepatic circulation with bile, and the major route of excretion through feces).

zinc (53–190 μg/g) in the bone [39–41]. Lead can be mobilized from bone under the many conditions that cause bone resorption under control of the hormones regulating calcium metabolism. The release of lead from bone is significant during lactation and in ageing, and under pathological conditions such as osteoporosis. Depending on particle size, uptake in the lungs can bring lead directly into the blood and to the heart. Organic compounds such as TEL are taken up through the skin. The intestinal absorption of lead is higher during periods of fasting. Both synergistic and antagonistic interactions with arsenic and cadmium have been reported [42]. There are age-specific effects, e.g., the young and the elderly being more vulnerable to lead intoxication, and there are gender-specific effects (see above).

7.4. Target Organs for Lead Toxicity

Lead has a broad spectrum of toxicity on target organs [42]. Its effect on the hematopoietic system provides one pathway for development of diseases. Causation during chronic exposure is more difficult to prove. Inorganic lead compounds are classified as probably carcinogenic to humans (group 2A) [43].

7.4.1. Nervous System

The effects of lead on the nervous system are one of the hallmarks of poisoning, not only on the central nervous system but also on the neuromuscular junction with manifestation of the clinical sign of wrist and ankle drop. Lead is thought to cross the blood brain barrier as $Pb(OH)^+$ [44]. In addition to psychiatric disease and schizophrenia, lead is now thought to be a factor in neurodegeneration in both Alzheimer's and Parkinson's disease [45–48]. The molecular mechanisms of the toxic effects of lead on the nervous system are largely unknown. The substitution of lead for zinc in zinc finger proteins has been discussed as one aspect of its molecular toxicology [49]. In animal models, exposure of embryos to 10 ppb lead results in changes of the expression of genes involved in neurodevelopment and associated with Alzheimer's disease in the adult brain [50]. As a strong binder and one that alters coordination geometry, one can readily envisage that lead induces protein misfolding. Misfolded proteins serve as seeds for further aggregation in forming amyloid deposits. Together with the effects on brain function and behaviour in children, the possible involvement in neurodegeneration emphasizes the need to revisit guidelines for exposure and to consider further measures for prevention and control of lead in the environment.

7.4.2. Kidneys

Lead exposure affects the proximal tubules and can lead to fibrosis of cells of glomerular and the interstitial capillaries. A direct consequence may be an elevated blood pressure. Worthy of note is the observation that lead exposure af-

fects the renin-angiotensin system [51]. Furthermore, in workers exposed to lead with a mean BLL of 48 μg/dL, a lower urinary excretion of 6-keto prostaglandin 1α (a vasodilatator) and a higher excretion of thromboxane B2 (a vasoconstrictor) were observed above a BLL threshold of 35 μg/dL [52]. In middle-aged and elderly individuals in the Normative Aging Study, decline of renal function was associated with both bone lead levels and BLL in diabetic and hypertensive patients, providing further indications for the health risks associated with lead intoxication [53].

7.4.3. Cardiovascular System

Exposure to lead leads to hypertension. A systematic review supported a causal relationship between lead exposure and blood pressure; however the evidence for a role in cardiovascular outcomes was deemed suggestive but insufficient to suggest causality about ten years ago [54].

7.4.4. Immune System

Both humoral and cellular immune functions are affected in lead poisoning. The extensive role of zinc in the immune system offers a mechanistic aspect of how lead could interfere with zinc-dependent functions [55].

7.4.5. Reproductive System

Lead poisoning has a negative effect on spermatogenesis and therefore the lead burden is associated with male infertility [42]. In females, placental transfer of lead and transfer of lead into the milk during lactation pose risks to the developing embryo and to the nursed child [42].

8. CELLULAR AND MOLECULAR ACTIONS

8.1. Subcellular Distribution of Lead and Lead-Binding Proteins

Once in the cell, lead takes several pathways (Figure 4). Some lead is thought to be bound to glutathione complexes with the composition $Pb(GS)_2$ and $Pb(GS)_3^-$, though information about the low molecular weight pool of lead *in vivo* is scarce [27]. Lead and bismuth are deposited in nuclear inclusion bodies [56]. Nuclear inclusion bodies in renal tubular cells occur in cases of lead intoxication [57]. Nuclear and cytoplasmic inclusion bodies can be detected in many other cells after lead exposure. A recently investigated pathway of how bismuth is deposited as an insoluble sulfide likely applies to lead deposition [58]. The pathway involves transport of metal glutathione complexes via multidrug resistance-associated proteins (MRP) into lysosomes, where the metal sulfide is formed, followed

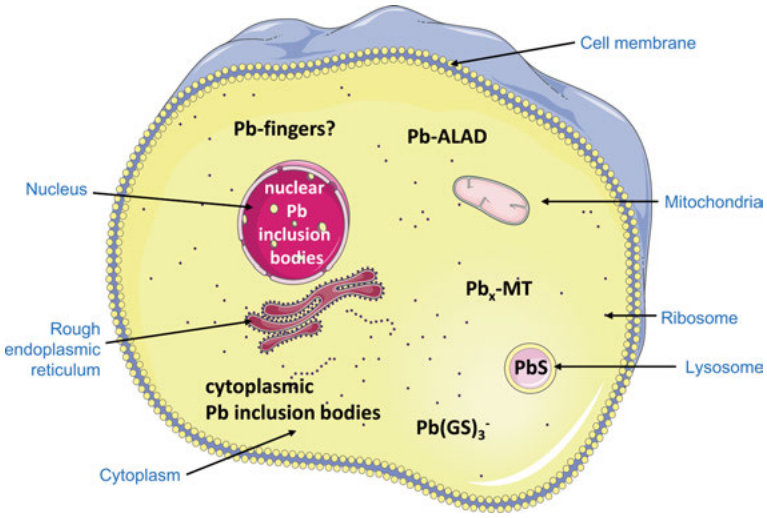

Figure 4. Cellular lead metabolism. The figure shows how lead is bound, transported, and distributed in the cell without emphasizing all the possible interactions discussed to explain its molecular toxicity (drawn with Servier Medical Art software).

by translocation to the nucleus as an inclusion body. ATP-dependent MRP transport also exports the metal glutathione complex from cells. Metallothionein (MT) participates in the formation of inclusion bodies because mice with a double knock-out for both MT-1 and MT-2 are hypersensitive to lead toxicity and kidney carcinogenesis [59, 60].

Metallothionein binds lead *in vitro* but how it contributes to lead binding *in vivo* is not clear [61]. In addition to its role in the formation of inclusion bodies, the observation that mutation(s) in the human MT-2 gene affect the lead body burden supports the notion that MT participates in lead metabolism [62]. MT-3, also known as neuronal growth inhibitory factor, binds seven Pb^{2+} ions in three different populations, and with regard to both the apoprotein (thionein) and the MT with seven zinc ions is thermodynamically favorable. Lead binds one order of magnitude stronger than zinc at pH 6.0 – similar to the difference between lead and zinc binding to other mammalian MTs at pH 7.0 [44].

A rather extensive literature exists about lead binding to proteins. Lead is being used in heavy atom derivatives of proteins in order to solve 3D structures by X-ray diffraction. The majority of sites in 48 proteins investigated have 2–5 ligands, but some have up to 9 ligands [27]. Oxygen ligands make up 79 % of the ligands (Glu: 38.4 %; Asp: 20.3 %; water 20.3 %), sulfur ligands 7 %, and nitrogen ligands only 5 %. It is not clear whether these percentages are representative of the situation *in vivo*. The relatively high affinity of lead to proteins encouraged many model studies in bioinorganic chemistry. Yet, proof that the interactions investigated *in vitro* indeed are physiologically relevant is mostly lacking.

Lead can replace other metal ions in metalloproteins or bind opportunistically at other sites that do not bind native metal ions. A toxic action is not necessarily linked to an inhibition of a process. *In vitro*, lead activates several enzymes or changes their catalytic specificity. For example, lead carboxypeptidase hydrolyses esters but not peptides [63]. Lead also inhibits carboxypeptidase A with a K_I value of 4.8×10^{-5} M (pH 7.5, 25 °C, 0.5 M NaCl) when it binds close to the zinc site [64]. In present day terminology, activation is a gain of function, and it has been discovered in another aspect of how lead may express is toxicity. Lead induces catalytic activity when binding to specific sequences of mammalian 5S rRNA and forming a leadzyme [65].

Genuine lead-binding proteins have been characterized only in bacteria. A few remarks on bacteria are worthwhile though the topic seems not to be relevant for this article with the exception that bacteria are living in a parasitic or commensal relationship with us. Therefore, how microorganisms handle lead may have yet to be discovered consequences. Bacteria demonstrate that mechanisms have evolved to deal with the toxicity of lead. For example, *Cupriavidus metallidurans* has a lead resistance operon encoding a regulator (PbrR), an efflux pump ATPase (PbrA), an uptake protein (PbrT), a phosphatase (PbrB/C) and a lead-binding protein (PbrD) [27]. In essence, some lead is transported into the cell and the lead sensor then activates the expression of the transport protein and the exporter. Phosphate produced by the phosphatase precipitates lead in the periplasmic space. Such a mechanism is not known for humans. However, one could draw a parallel in the way lead is rendered innocuous by phosphate precipitation in bacteria and how sulfide precipitation detoxifies lead when inclusion bodies form in humans. When applying a metallomics approach, in which metalloproteins and their associated metals were screened in the microorganism *Pyrococcus furiosus*, lead was found associated with 34 proteins [66]. Four metalloproteins contained substoichiometric amounts of lead. One protein was identified as a zinc proteinase and the other one as an iron pyrophosphatase.

The interaction of lead with zinc and calcium proteins as major targets has received particular attention and detailed scrutiny. In an attempt to link overall toxicology and molecular properties of lead binding to proteins, it was suggested that the binding affinities of lead measured *in vitro* are physiologically significant [67]. The parameters to consider when drawing this conclusion are the cellular free calcium concentrations (at resting levels about 10^{-7} M) and the cellular free zinc concentrations (at resting levels about 10^{-10} M). Accordingly, lead is expected to bind to zinc or calcium sites if it has at least the same affinity as these metal ions and its free (available) concentrations are higher than the free concentrations of these metal ions. If the affinity of lead is higher, it could bind at about the same or lower free lead ion concentrations. Free lead concentrations, however, are not known.

8.2. Zinc Proteins

For some zinc proteins, the affinity for lead is higher than that for the native metal ion zinc. The connection between properties of an isolated protein and

toxicology is established for ALAD, which binds lead stronger than zinc and out-competes Zn by a factor 500:1 [30]. ALAD has a unique ZnS_3 catalytic site (S = sulfur donor of cysteine) with hemidirected binding of the ligands [27]. Thus, there is a correlation of *in vivo* and *in vitro* data. For zinc finger proteins, there are no *in vivo* data. Among the latter, lead affinities range from 10^{-9} to 10^{-14} M for consensus sequences, but only ZnS_4 coordination environments prefer lead over zinc by a factor of 43. For the other coordination environments, ZnS_3N and ZnS_2N_2 (N = nitrogen donor of histidine), zinc is preferred with competition factors of 0.1 and 0.04 [67]. Because of the lack of biological assays and the limits of analytical techniques, the interaction *in vivo* is unknown. Functional effects are believed to be related to the fact that lead does not provide properly folded sites [68]. In other words, making lead fingers from zinc fingers results in broken fingers.

8.3. Calcium Proteins

Although there are many structures of calcium proteins with lead substituting for calcium, the limited data available indicate that the affinities of lead for calcium proteins are not significantly higher than those for calcium. However, picomolar concentrations of lead activate brain protein kinase C (PKC) [69]. The effect of lead is thought to be a result of binding to the C2 domain of PKC, where lead binds more tightly than calcium. However, there is also a C1 domain in these proteins with two zinc ions in S_4 environments. With the high affinity of lead for these sites, one wonders what the effect of lead on zinc sites is. Synaptotagmin, a protein involved in vesicular exocytosis, also has a C2 domain and the crystal structure demonstrates that lead binds in one of the positions where calcium normally binds. Binding of lead at nanomolar concentrations disrupts the interaction with its partner syntaxin [70].

In calmodulin, lead can replace calcium in the EF hand sites and bind to an allosteric site in the linker region. The interactions are only in the micromolar range of affinities [71]. For example, the affinity of Ca^{2+} for the N-terminal EF hand domain is 11 μM while lead binds < 10-fold stronger; the affinity of Ca^{2+} for the C-terminal EF hand domain is 2 μM while lead binds < 3-fold stronger. The affinity of lead for the additional binding site is only about 2 μM. A comparison of calcium and 21 lead-binding sites in protein structures reported in the Protein Data Bank (RCSB PDB) demonstrates that lead overall has fewer ligands than calcium and that the overall charge is less, –2 for lead and –3 for calcium [72]. Thus, a preference for lead due to a potentially higher coordination number than calcium does not seem to be realized in biological chemistry as calcium is already stabilized with regard to magnesium by having relatively high coordination numbers. Lead also shows a slight preference in binding to Glu instead of Asp. A preference of lead over calcium binding is not typical for all calcium-binding sites [71].

In summary, while there is a copious literature on the effects of lead on cellular calcium, with regard to the much tighter binding of lead to zinc sites, it is not

clear whether lead concentrations in cells are high enough to compete with cellular free Ca^{2+} concentrations of about 100 nM at resting levels. Lead concentrations must be at least as high or higher to compete with calcium in calcium-binding proteins because lead binds only about 3–10 times stronger to some calcium sites. Interference with calcium sites – and many other sites with relatively low affinity – would be possible, however, if the buffering capacity of high affinity sites such as that of some zinc binding sites were so low that lead is not efficiently buffered and reaches rather high cellular concentrations. The argument based on the affinity of lead for calcium sites in proteins does not consider the possible interference of lead with calcium in membrane transporters. Proteins that are thought to be responsible for mediating the effects of lead on brain functions/neurotransmission are the N-methyl-D-aspartate (NMDA) receptor, an ion channel that also transports Ca^{2+}, and the voltage-gated Ca^{2+} channels [21]. On the NMDA receptor, lead may interact with the Zn^{2+} regulatory sites on the NR2A subunit.

9. GENERAL CONCLUSIONS

The number of investigations on lead seems sheer endless and even reviewing reviews is a seemingly impossible endeavor. In this personal view, which serves as an introduction to the topics treated in this book, only a limited number of references are given, and the reader is referred to comprehensive reviews for some of the primary literature.

Lead remains a major ecotoxicant and a threat to human health despite having witnessed a very long history of its toxicity and implementing some necessary and successful measures to lower the lead burden in the environment, e.g., banning leaded gasoline and lead-based paints in many countries. Since no exposure is considered safe, one wonders about the consequences of lead being present and accumulating in our bodies. For example, there is an association of currently acceptable BLL and the prevalence of gout and hyperuricemia [73], and there is renewed interest in a possible causal relationship between lead and chronic diseases such as cancer and neurodegeneration. BLL and its relationship with bone (tibia) lead levels determined by K-shell X-ray fluorescence as a novel biomarker of the cumulative dose for environmental or occupational exposure in combination with evaluation of cognitive performance and clinical parameters of disease will further our understanding of the role of lead in health and disease [74]. Additional preventative measures to limit exposure seem to be warranted.

It remains a challenge to link the symptoms of toxicity and molecular targets. In contrast to unraveling the molecular pathways of essential metal ions where specific proteins and functions have evolved, it turns out to be much more difficult to identify the targets of toxic metals ions because interactions seem to be more pleiotropic and binding adventitious. Yet, since lead is a strong binder, potent effects of lead in experimental systems can be recorded and numerous interactions with proteins have been characterized. Each metal ion is different in terms of its toxicokinetics. For strongly interacting lead, “toxicothermodynam-

ics" is an appropriate term to consider in future investigations. If lead is indeed under thermodynamic control in biology, it is difficult to envisage how low affinity sites can be populated unless the buffering capacity of high affinity sites is rather low.

Analytical challenges remain, in particular identifying lead in low abundance proteins such as zinc finger proteins, many of which are important in developmental processes. Also needed are investigations of lead binding and lead speciation *in vivo* and examination of lead buffering and the lead buffering capacity in cells with fluorescent probes such as Leadmium™. Many experiments suffer from a lack of defining species and uncertainties regarding the physiological relevance of the concentrations of lead used. One should keep in mind that essential metal ions, for which homeostatic mechanisms exist, are also toxic if their concentrations exceed the metal-buffering capacity of cells.

ACKNOWLEDGMENT

I thank Prof. Harold H. Sandstead for discussing clinical aspects of lead intoxication and for sharing his vast experience in the fields of essential and non-essential metal ions.

ABBREVIATIONS

ALAD	δ-aminolevulinic acid dehydratase
ATP	adenosine 5′-triphosphate
BAL	British anti-Lewisite, 2,3-mercaptopropanol
BLL	blood lead levels
CDC	Centers for Disease Control and Prevention
DMT	divalent metal transporter
EDTA	ethylenediamine-N,N′,N″,N‴-tetraacetate
EFSA	European Food Safety Authority
EPA	U. S. Environmental Protection Agency
GS	glutathione
IQ	intelligence quotient
MRP	multidrug resistance-associated protein
MT	metallothionein
NIOSH	National Institute for Occupational Safety and Health
NMDA	N-methyl-D-aspartate
PKC	protein kinase C
RfD	reference dose
TEL	tetraethyl lead
ZPP	zinc protoporphyrin IX

REFERENCES

1. K. Schwarz, in *Clinical Chemistry and Chemical Toxicology of Metals,* Ed. S. S. Brown, Elsevier, New York, 1977, pp. 3–22.
2. M. Kirchgessner, A. M. Reichlmayr-Lais, K. N. Stokl, *J. Trace Elem. Electr. Health Dis.* **1988**, *2*, 149–152.
3. W. Maret, *Int. J. Mol. Sci.* **2016**, *17*, 66.
4. W. Maret, J.-M. Moulis, *Met. Ions Life Sci.* **2013**, *11*, 1–29.
5. R. B. Martin, *J. Chem. Educ.* **1987**, *64*, 402.
6. I. Persson, K. Lyczko, D. Lundberg, L. Eriksson, A. Placzek, *Inorg. Chem.* **2011**, *50*, 1058–1072.
7. H. L. Clever, *J. Phys. Chem. Ref. Data* **1980**, *9*, 751–784.
8. L. Shimoni-Livny, J. P. Glusker, C. W. Bock, *Inorg. Chem.* **1998**, *37*, 1853–1867.
9. C. C. Patterson, *Arch. Environ. Health* **1965**, *11*, 344–369.
10. J. O. Nriagu, *Science* **1998**, *281*, 1622–1623.
11. *Lead in Soil. Recommended Guidelines*, Eds. B. G. Wixson, B. E. Davies, Science Reviews, Northwood, 1993.
12. www.ila-lead.org/lead-facts/lead-production-\-statistics, accessed 26/4/2016.
13. N. Zhang, H. W. Baker, M. Tufts, R. E. Raymond, E. Salihu, M. R. Elliott, *Am. J. Public Health* **2013**, *103*, e72–e77.
14. Nriagu, J., *Lead and Lead Poisoning in Antiquity*, Wiley Interscience, New York, 1983.
15. M. A. Lessler, *Ohio J. Sci.* **1988**, *88*, 78–84.
16. R. M. S. McConaghey, *Med. Hist.* **1967**, *11*, 345–360.
17. L. Tanquerel des Planches, *Traité des maladies de plomb ou saturnines: suivi de l'indication des moyens qu'on doit mettre en usage pour se préserver de l'influence délétère des préparations de plomb*, Ferra, Paris, 1839.
18. J. Wolpaw Reyes, National Bureau of Economic Research Working Paper No. 13097, 2007.
19. J. Montes-Santiago, *Prog. Brain Res.* **2013**, *203*, 223–240.
20. CDC response to advisory committee on childhood lead poisoning prevention recommendations in "Low Level Lead Exposure Harms Children: A Renewed Call of Primary Prevention"; http://www.cdc.gov/nceh/lead/acclpp/blood_lead_levels.htm, pdf accessed 29/11/2015.
21. A. P. Neal, T. R. Guilarte, *Toxicol. Res.* **2013**, *2*, 99–114.
22. www.dwi.defra.gov.uk, accessed 26/4/2016.
23. EFSA Panel on contaminants in the food chain. Scientific opinion on lead in food, *EFSA J.* **2010**, *8*, 1570.
24. J. M. Christensen, J. Kristiansen, in *Handbook on Metals in Clinical and Analytical Chemistry*, Eds. H. G. Seiler, A. Sigel, H. Sigel, Marcel Dekker, New York, NY, 1994, pp. 425–440.
25. www.cdc.gov/niosh/topics/lead/limits.html, accessed 26/4/2016.
26. H. I. Afridi, F. N. Talpur, T. G. Kazi, D. Brabazon, *Clin. Lab.* **2015**, *61*, 1147–1156.
27. V. Cangelosi, V. Pecoraro, in *Binding, Transport and Storage of Metal Ions in Biological Cells,* Eds. W. Maret, A. G. Wedd, The Royal Society of Chemistry, 2014, pp. 843–882.
28. G. Rausa, L. Diana, G. Perin, *Riv. Ital. Ig.* **1968**, *28*, 319–327.
29. D. Bonsignore, C. Cartasegna, C. Vargnano, V. Ardoino, *Med. Lav.* **1968**, *59*, 419–424.
30. T. J. B. Simons, *Eur. J. Biochem.* **1995**, *234*, 178–183.
31. J. G. Wetmur, A. H. Kaya, M. Piewinzka, R. J. Desnick, *Am. J. Hum. Genet.* **1991**, *49*, 757–763.

32. F. Scinicariello, H. E. Murray, D. B. Moffett, H. G. Abadin, M. J. Sexton, B. A. Fowler, *Environ. Health Perspect.* **2007**, *115*, 35–41.
33. N. B. Jain, F. Laden, U. Guller, A. Shankar, S. Kazani, E. Garshick, *Am. J. Epidemiol.* **2001**, *161*, 968–973.
34. C. Gundacker, M. Gencik, M. Hengstschläger, *Mutat. Res.* **2010**, *705*, 130–140.
35. J. Kim, Y. Lee, M. Yang, *J. Environ. Sci. Health Part C* **2014**, *32*, 159–185.
36. I. A. Bergdahl, M. Sheveleva, A. Schütz, V. G. Artamonova, S. Skerfving, *Toxicol. Sci.* **1998**, *46*, 247–253.
37. E. Bitto, C. A. Bingman, G. E. Wesenberg, J. G. McCoy, G. N. Phillips, *J. Biol. Chem.* **2006**, *281*, 20521–20529.
38. Maret, W., *Metallomics. A Primer to Integrated Biometal Sciences*, Imperial College Press, London, 2016.
39. A. Jurkiewicz, D. Wiechuła, R. Nowak, K. Loska, *J. Trace Elem. Med. Biol.* **2005**, *19*, 165–170.
40. L. Gerhardsson, A. Akantis, N.-G. Lundström, G. F. Nordberg, A. Schütz, S. Skerfving, *J. Trace Elem. Med. Biol.* **2005**, *19*, 209–215.
41. G. V. Iyengar, W. E. Kollmer, H. J. M. Bowen, *The Elemental Composition of Human Tissues and Body Fluids*, Verlag Chemie, Weinheim, 1978.
42. B. A. Fowler, in *Cellular and Molecular Biology of Metals*, Eds R. K. Zalups, J. Koropatnick, CRC Press, Boca Raton, FL, 2010, pp. 113–126.
43. International Agency for the Research on Cancer (IARC), *Inorganic and Organic Lead Compounds*, IARC Monographs on the evaluation of carcinogenic risks to humans, Vol. 87, Lyon, France, 2006.
44. M. C. Carpenter, A. Shami Shah, S. DeSilva, A. Gleaton, A. Su, B. Goundie, M. L. Croteau, M. J. Stevenson, D. E. Wilcox, R. N. Austin, *Metallomics* **2016**, *8*, 605–617. DOI 10.1039/C5MT00209E.
45. M. G. Weisskopf, J. Weuve, M. H. Saint-Hilaire, L. Sudarsky, N. K. Simon, B. Hersh, J. Schwartz, R. O. Wright, H. Hu, *Environ. Health Perspect.* **2010**, *118*, 1609–1613.
46. T. R. Guilarte, M. Opler, M. Pletnikov, *Neurotoxicology* **2012**, *33*, 560–574.
47. K. M. Bakulski, L. S. Rozek, D. C. Dolinoy, H. L. Paulson, H. Hu, *Curr. Alzheimer Res.* **2012**, *9*, 563–573.
48. J.-H. Yoon, Y.-S. Ahn, *J. Affective Disord.* **2016**, *190*, 41–46.
49. J. M. Ordemann, R. N. Austin, *Metallomics* **2016**, *8*, 579–588. DOI 10.1039/C5MT00300H.
50. J. Lee, J. L. Freeman, *Metallomics* **2016**, *8*, 589–596. DOI 10.1039/C5MT00267B.
51. H. H. Sandstead, A. M. Michelakis, T. E. Temple, *Arch. Environ. Health* **1970**, *20*, 356–363.
52. A. Cardenas, H. Roels, R. Barbon, A. M. Bernard, R. R. Lauwerys, A. Gelpi, J. Rosello, A. Mutti, I. Franchini, H. Stolte, M. E. De Broe, G. E. Nuyts, S. A. Taylor, R. G. Price, *Brit. J. Ind. Med.* **1993**, *50*, 28–36.
53. S.-W. Tsaih, S. Korrick, J. Schwartz, C. Amarasiriwardena, A. Aro, D. Sparrow, H. Hu, *Environ. Health Perspect.* **2004**, *112*, 1178–1182.
54. A. Navas-Acien, E. Guallar, E. K. Silbergeld, S. J. Rothenberg, *Environ. Health Perspect.* **2007**, *115*, 472–485.
55. H. Haase, L. Rink, *Metallomics* **2014**, *6*, 1175–1180.
56. M. Wachstein, *Am. J. Clin. Pathol.* **1949**, *19*, 608–614.
57. G. W. Richter, Y. Kress, C. C. Cornwall, *Am. J. Pathol.* **1968**, *53*, 189–217.
58. I. Romero-Canelon, P. Sadler, *Proc. Natl. Acad. Sci. USA* **2015**, *112*, 4187–4188.
59. W. Qu, B. A. Diwan, J. Liu, R. A. Goyer, T. Dawson, J. L. Horton, M. G. Cherian, M. P. Waalkes, *Am. J. Pathol.* **2002**, *160*, 1047–1056.
60. M. P. Waalkes, J. Liu, R. A. Goyer, B. A. Diwan, *Cancer Res.* **2004**, *64*, 7766–7772.

61. W. Bernhard, M. Good, M. Vašák, J. H. R. Kägi, *Inorg. Chim. Acta* **1983**, *79*, 154, B7.
62. K. C. M. Fernandes, A. C. Martins Jr., A. A. Soares de Oliveira, L. M. G. Antunes, I. M. de Syllos Colus, F. Barbosa Jr., G. R. M. Barcelos, *Public Health Genomics* **2016**, *19*, 47–52. **2015**, DOI 10.1159/000441713, published online 24 November 2015.
63. B. L. Vallee, D. U. Ulmer, *Annu. Rev. Biochem.* **1972**, *41*, 91–128.
64. K. S. Larsen, D. S. Auld, *Biochemistry* **1991**, *30*, 2613–2618.
65. M. Z. Barciszewska, E. Wyszko, R. Bald, V. A. Erdmann, J. Barciszewski, *J. Biochem.* **2003**, *133*, 309–315.
66. A. Cvetkovic, A. L. Menon, M. P. Thorgersen, J. W. Scott, F. L. Poole 2nd, F. E. Jenney Jr., W. A. Lancaster, J. L. Praissman, S. Shanmukh, B. J. Vaccaro, S. A. Trauger, E. Kalisiak, J. V. Apon, G. Siuzdak, S. M. Yannone, J. A. Tainer, M. W. Adams, *Nature (London)* **2010**, *466*, 779–784.
67. H. A. Goodwin, *Curr. Op. Chem. Biol.* **2001**, *5*, 223–227.
68. J. S. Magyar, T-C. Weng, C. M. Stern, D. F. Dye, B. W. Rous, J. C. Payne, B. M. Bridgewater, A. Mijovilovich, G. Parkin, J. M. Zaleski, J. E. Penner-Hahn, H. A. Godwin, *J. Am. Chem. Soc.* **2005**, *127*, 9495–9505.
69. J. Markovac, G. W. Goldstein, *Nature (London)* **1988**, *334*, 71–73.
70. C. M. L. S. Bouton, L. P. Frelin, C. E. Forde, H. A. Godwin, J. Pevsner, *J. Neurochem.* **2001**, *76*, 1724–1734.
71. R. Gorkhali, K. Huang, M. Kirberger, J. J. Yang, *Metallomics* **2016**, *8*, 563–578. DOI 10.1039/C6MT00038J.
72. M. Kirberger, J. J. Yang, *J. Inorg. Biochem.* **2008**, *102*, 1901–1909.
73. E. Krishnan, B. Lingala, V. Bhatta, *Ann. Intern. Med.* **2012**, *157*, 233–241.
74. H. Hu, R. Shih, S. Rothenberg, B. S. Schwartz, *Environ. Health Perspect.* **2007**, *115*, 455–462.

2

Biogeochemistry of Lead. Its Release to the Environment and Chemical Speciation

Jay T. Cullen [1] ***and Jason McAlister*** [2]

[1]School of Earth and Ocean Sciences, University of Victoria, Victoria, BC, Canada
<jcullen@uvic.ca>

[2]Department of Earth and Ocean Sciences, University of British Columbia, Vancouver, BC, Canada
<jmcalist@eos.ubc.ca>

Metal Ions in Life Sciences, Volume 17 Edited by Astrid Sigel, Helmut Sigel, and Roland K. O. Sigel

DOI 10.1515/9783110434330-002

Abstract: Lead (Pb) is a metal that is not essential for life processes and proves acutely toxic to most organisms. Compared to other metals Pb is rather immobile in the environment but still its biogeochemical cycling is greatly perturbed by human activities. In this review we present a summary of information describing the physical and chemical properties of Pb, its distribution in crustal materials, and the processes, both natural and anthropogenic, that contribute to the metal's mobilization in the biosphere. The relatively high volatility of Pb metal, low melting point, its large ionic radius, and its chemical speciation in aquatic systems contributes to its redistribution by anthropogenic and natural processes. The biogeochemical cycle of Pb is significantly altered by anthropogenic inputs. This alteration began in antiquity but accelerated during the industrial revolution, which sparked increases in both mining activities and fossil fuel combustion. Estimates of the flux of Pb to the atmosphere, its deposition and processing in soils and freshwater systems are presented. Finally, the basin scale distribution of dissolved Pb in the ocean is interpreted in light of the chemical speciation and association with inorganic and organic particulate matter. The utility of stable radiogenic Pb isotopes, as a complement to concentration data, to trace inputs to the ocean, better understand the biogeochemical cycling of Pb and track water mass circulation in the ocean is discussed. An ongoing international survey of trace elements and their isotopes in seawater will undoubtedly increase our understanding of the deposition, biogeochemical cycling and fate of this infamous toxic metal.

Keywords: anthropogenic emissions · biogeochemistry · isotopes · lead · marine biogeochemistry · Pb · pollution · trace metal

1. INTRODUCTION

Lead (Pb) is broadcast to the biosphere from both natural and anthropogenic sources. The metal is acutely toxic to living organisms and given that human activities have greatly increased Pb concentrations in the biosphere [1–4], there is motivation to characterize sources and subsequent mobility of Pb in the environment [5, 6]. Careful measurements of environmental materials in heavily populated regions as well as the most remote reaches of the globe indicate that anthropogenic contamination is systemic and now dominates the biogeochemical cycle for Pb [1, 2, 7–11].

Total industrial and natural weathering cycle mobilizations of Pb to the biosphere by the end of the 1980's are estimated to have been 565,000 t/yr and 180 t/yr respectively, clearly demonstrating the scale of anthropogenic impact [12]. Major, global anthropogenic Pb emissions to the atmosphere are reasonably well constrained and were 332,350 t/yr in 1983 with more recent estimates for the mid-1990's dropping to 119,259 t/yr compared to natural emissions of 12,000 t/yr [12–15]. Thus the major anthropogenic sources to the atmosphere from nonferrous metal production (14,815 t/y) and fossil fuel combustion in stationary (11,690 t/yr) and mobile (76,635–100,842 t/y) platforms exceed major natural sources like wind borne dust (3,900 t/yr), volcanic outgassing (3,300 t/yr), and forest fires (1,900 t/y), by a factor of ~25 [12, 14, 15]. The declining trend in anthropogenic emissions reflects more stringent regulations on Pb use, especially reduced manufacture and combustion of leaded gasoline, capture of Pb at point sources, and more efficient recycling of Pb from consumer goods.

Compared to other metals, Pb is quite particle-reactive and relatively immobile in soils and freshwater systems with lower dissolved concentrations in river and

ocean waters compared to its crustal abundance [16, 17]. Atmospheric deposition and riverine transport ultimately deliver Pb to the ocean, which serves as the repository for much of the Pb released from natural and anthropogenic sources. Together, the variety of stable isotopes of Pb and a thorough understanding of the isotopic composition of crustal components [18], can be used to geochemically fingerprint and identify natural and anthropogenic sources and sinks, and track Pb transport and fate in the natural environment [19, 20]. The biogeochemistry of Pb and the distribution of its isotopes in the ocean is a matter of much interest for oceanographers given the information that temporally variable natural and anthropogenic Pb sources can provide on ocean circulation, atmospheric inputs to the ocean, and particle production, export and recycling in the sea [21–24]. Factors governing the distribution of Pb and its isotopic composition in the major ocean basins will be discussed here in detail.

2. GEOCHEMISTRY OF LEAD

2.1. Chemical Properties

Lead (Z = 82, atomic weight 207.19), is a member of Group 14 of the periodic table and is, therefore, most similar in its chemical properties to tin (Sn) and germanium (Ge) (Table 1) [25]. The metal is bluish-white and lustrous but will oxidize and tarnish to grey when exposed to the atmosphere. Lead is a dense metal but is also soft, flexible, and malleable which suit it to a variety of industrial applications.

This heavy metal has a stable p-block electron configuration ($[Xe]\,4f^{14}\,5d^{10}\,6s^2\,6p^2$) and can exist in the +II and the +IV oxidation states. The divalent state is most common in the environment and forms marginally soluble salts with the most

Table 1. Relevant physical and chemical properties of lead.[a]

Property	
Atomic number	82
Atomic weight (g mol^{-1})[b]	207.19
Atomic radius (pm)[c]	180
Ionic radius of Pb^{2+} (pm)[d]	133
Electron configuration	$[Xe]\,4f^{14}\,5d^{10}\,6s^2\,6p^2$
Melting point (°C)	327.5
Boiling point (°C)	1749
Density at 25 °C (g cm^{-3})	11.342
Oxidation states	+2, +4
Reduction potential (E^0) for $Pb^{2+} + 2e^- = Pb$ (V)	–1.263
First ionization energy (kJ mol^{-1})	715.6
Second ionization energy (kJ mol^{-1})	1,450.5

[a] Adapted from [25].
[b] [180]. [c] [181]. [d] [182].

abundant anions while Pb(IV) is a strong oxidizing agent and comparatively rare at the Earth's surface. Lead has a low melting point (327.5 °C), a boiling point of 1749 °C, and a density equal to 11.34 g/cm^{-3} at 20 °C. The atomic weight of Pb is determined by a mixture of four stable isotopes in addition to the metal having important radioisotopes with environmental science applications (Table 2) [19, 26, 27]. Oxidation of the metal will occur rapidly in moist air, with Pb becoming increasingly soluble in water in the presence of oxygen.

Table 2. Main stable and radioactive isotopes of lead along with their natural abundance[a] or half-life.

Mass number	Half-life[a]	Decay mode	Parent isotope	Half-life of parent isotope (yr)	Parent isotope decay constant λ (yr^{-1})	Natural abundance (%)[b]
204	stable	–	–	–		1
206	stable	–	^{238}U	4.466×10^{9}	1.552×10^{-10}	24
207	stable	–	^{235}U	0.704×10^{9}	9.850×10^{-10}	23
208	stable	–	^{232}Th	1.401×10^{9}	4.948×10^{-11}	52
210	22.2 yr	β^-, α	^{238}U	4.466×10^{9}	1.552×10^{-10}	
212	10.64 h	β^-	^{232}Th	1.401×10^{9}	4.948×10^{-11}	
214	26.8 min	β^-	^{238}U	4.466×10^{9}	1.552×10^{-10}	

[a] Half-life of Pb isotopes reported in [183].
[b] Natural abundance from mole fractions reported in [26].

2.2. Abundance in the Continental Crust

Lead is a rare element in the continental crust with a bulk concentration of 11–14.8 ppm that is roughly 10-fold higher than its Group 14 neighbors Sn and Ge [28, 29]. However, it is the most abundant heavy metal partly owing to the radiogenic nature of its three most abundant isotopes ^{206}Pb, ^{207}Pb, and ^{208}Pb, which result from the decay of primordial uranium and thorium in the crust (Table 2). The abundance of Pb in different crustal constituents is consequently related to the compatibility of U and Th in rock types. In its divalent state Pb is both chalcophilic and lithophilic showing preferential association with sulfur and oxygen respectively. Indeed, the predominant Pb-bearing mineral is galena (PbS) which is roughly 87 % Pb by mass. Under oxidizing conditions at the Earth's surface galena gives way to minerals like anglesite ($PbSO_4$), cerrussite ($PbCO_3$), and pyromorphite ($Pb_4(PbCl)(PO_4)_3$). However, galena is the dominant form of Pb in economically significant ore deposits.

A summary of Pb in crustal materials and soils is presented in Table 3 [25, 29–31]**.** The Pb composition of the mantle is relevant given a later discussion of natural volcanic emissions to the atmosphere and has been estimated to be 185 ppb [32].

Table 3. The concentration of lead in crustal materials and soils.[a]

Type of material	Lead content (μg g^{-1})
Crust[b,c]	11
Upper crust	17
Middle crust	15.2
Lower crust	12.5
Granite[d,e]	18, 17
Basalt[d,e]	8, 6
Shale[d,e]	23, 20
Sandstone[d,e]	10, 7
Limestone[d,e]	9, 9
Soils (general)[d]	19
Soils (world)[f]	30
Soils (UK)[g]	74
Soils (USA)[g]	12

[a] Adapted from [30].
[b] Composition of the average crust and upper and middle units from [28].
[c] Lower continental crust Pb composition from [29].
[d] Values from [184]. [e] Values from [185]. [f] Value from [186]. [g] Values from [187].

3. MOBILIZATION OF LEAD

3.1. Natural Sources

Natural mobilization of Pb contained in the continental crust and mantle can occur through volcanic eruptions, physical and chemical weathering of rock or derived soils, plant exudates and burning of plant biomass, extraterrestrial particles, sea salt spray, and radioactive decay [14, 15, 25, 33–35]. Global estimates of natural Pb fluxes must be interpreted with great caution, as the potential for anthropogenic impact on Pb fluxes is high. Estimates presented in the literature therefore likely represent maximum natural emissions.

Global estimates of natural Pb emissions to the atmosphere suggest that of the ~12,000 (range 970–23,000) t/yr released, roughly 30 % can be attributed to windborne particles, 25 % from volcanic emissions with the remaining flux coming in approximately equal amounts from biogenic sources, forest fires, and sea salt spray [12, 13, 25]. The global volcanic source of Pb is difficult to quantify given the remote location and stochastic nature of most sources, and the variability in Pb in erupted material [36, 37]. Antarctic ice cores record atmospheric deposition of Pb and its isotopic composition over time and indicate that natural sources show significant temporal variability [38, 39]. Measurements indicate that a majority of Pb, and its isotopic composition, in the ice record can be accounted for primarily by long-range transport of quiescent volcanic degassing of Pb with sea salt spray, terrestrial dust, and other natural sources playing less significant roles [38], but that terrestrial dust may be more important during cold climate stands [39].

Estimates of the natural input of Pb to the oceans from continental runoff, based on the weathering cycle, are roughly 295,000 t/yr, roughly 25-fold greater than the natural atmospheric flux [30, 40]. Compilations of Pb abundance in world river water provide an estimate of the mobility of Pb during chemical and physical weathering through the comparison of the concentration in waters with the average crustal concentration (C_w/C_c). The C_w/C_c of Pb is bracketed by that of germanium and iron, placing Pb among the more immobile elements [16]. This analysis, however, does not account for anthropogenic inputs to the watershed and likely underestimates Pb mobility in natural waters. Based on estimates in the literature and further discussed below, natural sources of Pb to the biosphere have been dramatically eclipsed by anthropogenic sources beginning as early as 5000 years before present, continuing through the Roman Empire and reaching a zenith in the 20th century from industrialization and the burning of leaded gasoline [3, 25].

3.2. Anthropogenic Sources

Human perturbation of the natural biogeochemical cycle of Pb is dramatic and pronounced [1, 2, 7–11, 30]. Mobilization of Pb occurs through mining and smelting of ores, combustion of fossil fuels, and use, recycling and disposal of Pb containing products (e.g., batteries). With the exception of years characterized by widespread economic depression in 1930's and 1940's and a significant drop in US production owing to the phase-out of alkyl lead in gasoline in the 1970's and 1980's, there has been a general increase in global Pb production from ~1,000,000 t at the beginning of the 20th century rapidly rising since 2000 to ~5,500,000 t by 2013 (Figure 1). Most recent figures available for 2015 put global mining production at ~4,700,000 t with the great bulk occurring in China (2,300,000 t), and more minor contributions from Australia (633,000 t), and USA (385,000 t) [41, 42].

The most significant uses of Pb and Pb alloys in industry are for Pb-acid batteries, ammunition/ballistics, oxides for glass and ceramic hardening, casting metals, weights and shielding applications [43]. Over the last 20 years, ~80–90 % of Pb consumed in the USA was used to manufacture lead-acid batteries. This type of battery enjoys widespread use in starting-lighting-ignition (SLI) batteries for automobiles and trucks as well heavy industrial vehicles used in the mining, aviation, and construction industries. In addition, Pb containing uninterruptible power sources (UPSs), are essential for medical and computing hardware as well as storage components of load leveling systems associated with commercial power networks. In summary, while the well documented potential for Pb toxicity in the ecosystem has led to regulation and declining use as a fuel additive, increased industrialization in Asia has increased global Pb production.

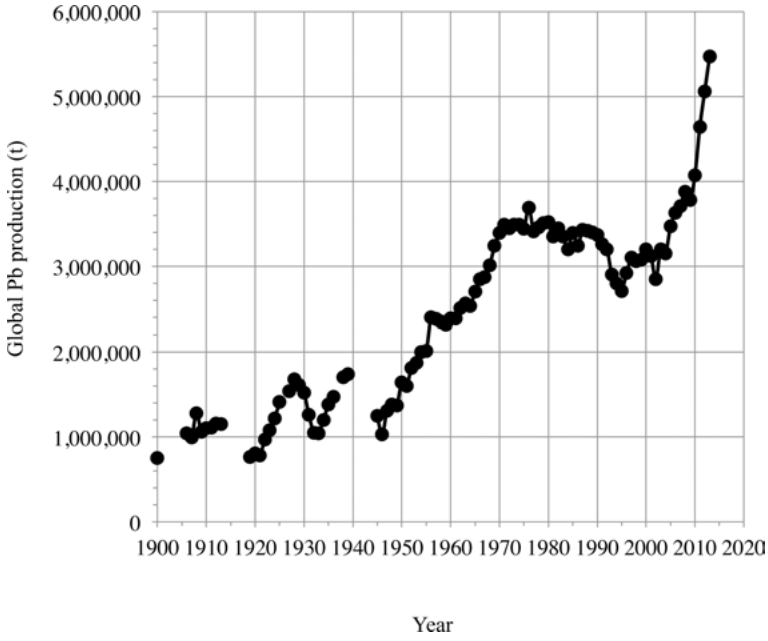

Figure 1. World smelter and mine production of lead with time as reported by the U. S. Geological Survey [188]. World production data were for determined from world smelter production for the period 1900–54 and for world mine production between 1955–98. Data were not available for the years 1901–05, 1914–18, 1926, 1937, and 1940–44.

4. LEAD IN THE ATMOSPHERE

4.1. Sources

As outlined above, anthropogenic emissions of Pb have significantly altered the global biogeochemical cycle and now dominate the natural fluxes of the metal to the atmosphere [11, 12, 14, 33], and there exists enough data to reasonably constrain major sources of Pb to the atmosphere [15, 35, 44, 45]. The most important sources estimated for the mid-1990's include emissions from electricity and heat production (11,690 t/yr), vehicular traffic (77,000–101,000 t/yr), mining of Pb (6,357 t/yr), copper (6,333 t/yr), zinc (2,123 t/yr), iron and steel production (2,926 t/yr), waste disposal (821 t/yr), and cement production (268 t/yr) [14, 15].

Total estimates of the flux of anthropogenic Pb to the atmosphere are approximately 120,000 t/yr compared to median natural fluxes totaling 12,000 t/yr (Table 4) [13, 15]. Anthropogenic contamination can be detected in rain and snow over urban, rural, and remote regions [25, 46, 47]. Indeed, studies of remote snow pack and ice core records recovered from glaciers demonstrate increasing atmospheric transport and deposition of Pb in response to mining activities and industrial emissions [7, 8, 10, 38, 48–54].

Table 4. Global anthropogenic and natural emissions of lead in mid-1990's.[a]

Anthropogenic		**Natural**[b]	
Source	**Pb emission (t yr^{-1})**	**Source**	**Pb emission (t yr^{-1})**
Fossil fuel combustion	11,690	Volcanoes	3,300
Vehicular traffic	88,739		
Non-ferrous metal production	14,815	Biogenic	1,740
Iron and steel production	2,926	Wind-borne dust	3,900
Cement production	268	Terrestrial biomass burning	1,900
Waste disposal	821	Sea-salt spray	1,400
Total	119,259	**Total**	12,340
1983 emission[c]	332,350		

[a] Adapted using data from [15].
[b] Estimates from [13].
[c] Estimate from [14].

4.2. Deposition and Fate

Lead emissions to the atmosphere are largely from anthropogenic sources and show higher levels near urban areas with the fluxes being spatially and temporally variable [13, 25]. Particulate Pb is diverse in size and chemical composition and is easily dispersed by prevailing winds and subsequently delivered to the terrestrial and aquatic environment by wet and dry deposition [14, 25, 33]. Indeed, anthropogenic Pb derived from high temperature processes is largely present in the submicron size fraction and can be dispersed thousands of kilometers through the atmosphere, polluting even the most remote and otherwise pristine environments. A review of measurements during the height of industrial emissions (1960–1970) estimated the bulk occurred in the northern hemisphere with urban areas and rural areas accounting for the majority of emissions and deposition including significant deposition in downwind rural localities [52].

In remote areas of the globe, wet deposition is most important as precipitation leads to washout of the small particulates and aerosols that can be transported long distances in the atmosphere. The Pb associated with these aerosols can be quite labile. For example, the solubility of Pb aerosols is observed to span a wide range with 13–90 % of Pb dissolving within 6 h of exposure to seawater [36]. Wet deposition can account for ~83 % of the depositional flux of Pb to the surface ocean [36, 55]. Measurement of atmospheric Pb in rain and snow around the globe indicate that the primary source of Pb to the atmosphere is anthropogenic and show a pronounced latitudinal gradient in deposition [49, 50, 53, 54, 56–59]. The Pb present in precipitation and bulk aerosol samples is observed to occur at significant crustal enrichment factors (EF_C) where:

$$EF_C = \frac{(Pb/Al)_x}{(Pb/Al)_{crust}} \quad (1)$$

and the Pb concentration ratio to Al in phase x (where x represents an aerosol, rain or snow sample), is compared to the ratio expected in average continental crust. An EF_C greater than 10 is generally accepted as an indication that a significant component of the Pb in the sample is of anthropogenic origin. EF_C for Pb in atmospheric aerosol samples at the height of leaded gasoline use in the 1970's were elevated even in remote locations with values of 2,200 at mid-latitudes in the North Atlantic to approximately 1,100–2,500 at high latitudes in the Antarctic and South Pole [25, 44, 45, 60]. Given the phase-out of leaded gasoline in most industrialized nations EF_C in aerosols has diminished over time with most recent measurements from samples from the Atlantic Ocean in the range of 1.05–112 [61]. Snows deposited in the French Alps (~45–46° N) in 1998 had EF_C's of ~15–200 [59]. Lower EF_C values were found in snows collected in 2005 from the northeastern flank of Mt. Everest (~28° N) with an average of ~3 and as high as ~15 [49].

Snow records from 1991–1995 in central Greenland have Pb EF_C's of 30–50 with a tendency to higher values (~700) in some samples [56]. Ratios of Pb to other heavy metals like Cd in Greenland snows sampled in 1990 suggest that anthropogenic sources in lower latitudes dominate the deposition to this remote area [53]. At higher latitudes in Antarctic snow (~77° S) EF_C values have increased since the beginning of the industrial revolution from 3 to mean values of 56 for the period 1959–1990 [50]. The large range in EF_C for Pb in the atmosphere reflects varying mixtures of high EF_C anthropogenic point source emissions that change in space in time and crustal material from more arid terrestrial regions. High EF_C values for Pb in atmospheric aerosol samples and in precipitation, combined with temporal trends in EF_C with time in snow and ice, suggest that the dominant source of atmospherically transported Pb is from anthropogenic point sources.

Wet deposition removes a significant fraction of Pb from the atmosphere either through the solubilization of aerosols in water droplets or the washout of particles associated with precipitation events. Rainwater Pb concentrations show a considerable range that is related to air mass trajectory and proximity to anthropogenic point sources. Rainwater Pb concentrations over Europe tend to track emissions and have declined from maximum values of 12 μg L^{-1} in the mid-1980's to ~1–2 μg L^{-1} in 2004 [62]. Similar order Pb concentrations exist in rainwater over the North Atlantic in the mid-1980's spanning a wide range from 0.13 to 3.6 μg L^{-1} with EF_C's from 150–2,400 [63, 64]. In remote locations in the South Pacific lower mean Pb concentrations have been measured at American Samoa (0.02 μg L^{-1}) [65], Enewetak Atoll (0.04 μg L^{-1}) [66], and Paradise Beach (New Zealand) (0.02 μg L^{-1}) [67] likely reflecting the predominance of anthropogenic sources in the northern hemisphere.

The depositional flux of Pb comprising both wet and dry components and has been monitored through programs and studies (e.g., AMAP, ADIOS, EMEP) aimed at understanding the temporal and spatial variability in the deposition of

key pollutants. Most recent estimates in Europe and for the Mediterranean Sea indicate that fluxes of Pb from the atmosphere over the period 1986–2002 dropped from 400 ng cm^{-2} yr^{-1} in 1986 to ~100 ng cm^{-2} yr^{-1} in 2002 with some regional variability as Pb emissions for Europe during the same time period dropped from ~80,000 t yr^{-1} to ~1,000 t yr^{-1} [68].

Atmospheric deposition of Pb can be determined using data from snow pits located either at high latitudes or elevations [49, 50, 56–58]. These fluxes appear to vary as a function of latitude with the lowest fluxes in Antarctica and the highest values found at mid-latitudes of the northern hemisphere where point sources to the atmosphere are concentrated. Snows on Mt. Blanc (45.5° N) provide an atmospheric Pb flux estimate of 200 ng cm^{-2} yr^{-1} for the period 1990–1991, while deposition was lower in 2004–2005 at 0.08 ng cm^{-2} yr^{-1} on Mt. Everest (28° N) [49]. At higher latitudes the flux of Pb was 0.39 ng cm^{-2} yr^{-1} in Greenland for the period 1991–1995 [56] and 0.12 ng cm^{-2} yr^{-1} in Antarctica between 1983 and 1986 [57]. Therefore, as atmospheric emissions decreased over time, in response to regulation, depositional fluxes similarly diminished. Still there exists a latitudinal gradient in deposition, with decreasing Pb fluxes as a function of distance from mid-latitude, atmospheric point sources.

5. LEAD IN THE TERRESTRIAL AND FRESHWATER ENVIRONMENT

5.1. Behavior in Soils

The bioavailability, mobility, and transport of Pb present or deposited to the terrestrial environment ultimately depends on the behavior of the metal in soils. As chemical and physical weathering form soils from crustal material the Pb composition should, to a first approximation, represent the Pb content of the parent rocks (Table 3) [30]. However, as discussed above, significant anthropogenic Pb inputs to the atmosphere and natural waters have likely altered soil Pb content. Soils, freshwater courses, and their sediments represent heterogeneous systems where chemical reactions can act to modulate the flux of natural and anthropogenic Pb from the land, via rivers and groundwater, to the ocean. Ultimately the mobility and biological uptake of Pb in freshwater and soil systems depends on its physical and chemical speciation which is a function of the reduction-oxidation potential, pH, and the presence of inorganic and organic ligands and ions in solution [69, 70]. When Pb is introduced to soils, reactions with soil components tend toward the formation of progressively less soluble forms although this tendency is less pronounced than is observed for other metals with smaller atomic radii [71]. Reactive Pb can be incorporated into minerals or bound to soil surfaces through absorption, co-precipitation, ion exchange, and complexation reactions [69, 70].

Given the inherent complexity of natural soils [6], much of the information to follow is derived from experimental work with natural and synthetic soil components such as metal oxyhydroxides, clays, and carbonates in isolation or in mix-

ture [71]. Across environmentally relevant Pb concentrations adsorption tends to follow either the Freundlich or Langmuir isotherm [72]. Carbonates are known to play an important role in controlling Pb partitioning as $PbCO_3$ can form readily in soils under oxidizing and slightly acidic to alkaline pH [69]. When carbonates are not present metal oxides can serve as sites for Pb adsorption. Experiments with iron oxides and oxyhydroxides [73–75] and Mn oxides indicate that Pb shows much more affinity for Mn oxides (~40-fold higher) [76] and that Pb is sparingly soluble in the presences of metal oxides. After an initial fast adsorption period, the degree of Pb adsorption tended to increase with pH and experimental temperature and decreased with the initial concentration of soluble metal and as the material was thermally aged [73].

Organic matter content of soils also plays a role in controlling Pb mobility by particle surface adsorption or solubilization through coordination and complexation in solution [77–79]. Experiments with aluminum oxides indicate that Pb is sorbed quickly to the mineral surface in an initial step forming inner- and outer-sphere complexes [80], followed by a slower adsorption reaction [81]. While useful for understanding the short term processes that can govern Pb behavior in soils, it is likely that experiments with fresh and aged model sediments are not fully representative of Pb mobility in natural soil-porewater systems.

Experiments with natural soils demonstrate that large ionic radii metals like Pb are relatively slow to react within the system compared to other metals of biogeochemical importance, like copper and zinc. The addition of Pb associated with sewage sludge to various soil types indicated that the adsorption of Pb increased with increasing temperature, as determined by the fraction of Pb leached with a H_2O_2-NH_4OAc mixture [82]. Where Pb was introduced to English soils in a predominantly organic matrix (e.g., sewage sludge), there was an appreciable increase in the retention of Pb, presumably because complexing organics allowed for increased adsorption [83]. Generally, the forms and availability of Pb in soils are strongly determined by the origin of the metal and its history since emission to the atmosphere and/or deposition on land. Available literature suggests that while Pb is generally less mobile than other smaller ionic radii metals in soils, reversible adsorption to mineral surfaces can allow Pb to be mobilized, especially under the low pH conditions that predominate in most interstitial waters or in environments where anthropogenic contamination and acidification is significant [84].

5.2. Speciation and Fate in Lakes and Rivers

Mobilization of anthropogenic Pb deposited in the environment has caused freshwater inventories and concentration of Pb to increase. Lead in freshwater systems has increased from pre-industrial background concentrations to an average concentration in world rivers of 0.08 $\mu g\ L^{-1}$ [17, 85]. Similar to atmospheric aerosols, rain and snow, the Pb in the suspended particulate phase carried in world rivers is characterized by high EF_C, on average ~2 and values as high as >20 [17]. A portion of the variability between rivers is likely related to the

Table 5. Dissolved Pb concentration for some major world rivers and estimates of the average concentration and particulate transport.[a]

River[b]	Dissolved Pb concentration ($\mu g\ L^{-1}$)
Africa	
Niger	0.04
Europe	
Seine at Paris, France	0.22
Harz Mountains, Germany	3.8
Idel River[c]	0.12
North America	
St. Lawrence	0.233
Ottawa	0.105
Mistassini, Canada	0.113
Mackenzie	0.771
Peel, Canada	1.13
Beatton	0.269
Upper Yukon, Canada	0.818
Fraser River, Canada	0.078
Upper Mississippi	0.008
Missouri	0.006
Ohio	0.007
Illinois	0.035
Mississippi at Mouth	0.011–0.0016
South America	
Amazon	0.064
Negro	0.170
Solimoes	0.151
Madeira	0.005
Trompetas	0.052
Tapajos	0.061
Asia	
Ob	0.011–0.017
Yenisei	0.005–0.006
Lena	0.019
Changjiang	0.054
Huanghe	0.01–4.1
World Average Dissolved Pb Concentration	0.08
Dissolved Riverine Flux (t yr^{-1})	3,000
Particulate Riverine Flux (t yr^{-1})[c]	916,000

[a] Adapted from Table 1 in [16].
[b,c] Particulate Pb flux associated with suspended material carried by world rivers from [17].

differences in the Pb content of soils and rock in river catchments, but the ~150 % difference in the suspended particulate Pb concentrations relates to point source input of anthropogenic, Pb-rich materials. A compilation of dissolved and particulate Pb in some world rivers is presented in Table 5 [17, 85].

The fate of Pb in freshwater is controlled by its chemical speciation [86]. Thermodynamic calculations show that under typical conditions in freshwaters that are in contact with the atmosphere at circumneutral pH (6–8), Pb is largely present as the $Pb(CO_3)_2^{2-}$ complex and complexes with SO_4^{2-} and OH^- being important at lower and higher pH's respectively [72, 87–89]. Lead tends to be largely complexed by natural organic matter under normal conditions in oxygenated freshwaters [90, 91] although there is a great variability, some of which may be analytical, in the extent of Pb complexation [92]. The degree of complexation with naturally occurring organic ligands depends upon the concentrations and binding characteristics of dissolved organic carbon (DOC; principally humic (HA) and fulvic acids (FA)), pH, and competition with other major and trace cations [72, 93]. Binding of Pb with natural organic ligands from rivers, lakes, and soil solution has been examined (see e.g., [77, 78, 90, 91, 94–97]). Complexation decreases free $[Pb^{2+}]$ so that typically dissolved $[Pb^{2+}]/[Pb]_{Tot}$ range from 0.004–0.005 in rivers [90] to even lower values (< 0.001) in lakes with detectable sulfide [91]. These organic ligands typically have conditional stability constants in the range $\log K = 8.3$–9.4, however, there exists significant variability in the total concentration and stability of these ligands [86, 92].

Suspended particles serve as important sorption sites for Pb in solution or in sediments and represent a significant factor controlling Pb fate in freshwater systems [30, 85, 98–100]. Similar to complexation reactions in solution, the tendency of Pb to adsorb to suspended particles or aquatic sediments will be governed by pH, ionic strength, and the concentration of competing cations, as well as the presence of organic and inorganic ligands [72]. The partitioning of Pb between the dissolved phase and suspended solids, in aquatic sediments and in soil-solution systems can be described by the distribution coefficient (K_d) where

$$K_d = \frac{\textit{amount sorbed per unit mass}}{\textit{equilibrium dissolved concentration}} \tag{2}$$

giving the parameter units of L kg^{-1}. Although somewhat simplistic, using K_d allows for a prediction of the mobility of Pb in freshwater and freshwater-soil systems and can easily be incorporated in models of Pb transport, fate, and bioavailability [101]. There is an astounding range of literature K_d values for Pb in soil-solution systems ranging from 61–2,305,000 L kg^{-1}, with a median value of 102,410 L kg^{-1}. Experiments in the laboratory with a variety of soil components find K_d values for kaolinite (2.68 L kg^{-1}), mica (0.56 L kg^{-1}), vermiculite (117.9 L kg^{-1}), Fe oxide (15.4 L kg^{-1}), while higher values are found for humic acid-rich particles (233 L kg^{-1}) and manganese oxide (1,177 L kg^{-1}) [102]. The greatest predictors of K_d for Pb in freshwater systems are solution pH and total Pb concentration, with the adsorption of Pb to solid phases increasing with each property [85, 100, 101, 103].

Before delivery to the oceans, the flux of particulate and dissolved Pb from world rivers is modulated during transit through estuaries as more saline waters are entrained and mixed [104]. The net effect of this mixing is to alter the speciation of Pb given its particle-reactive nature with the metal showing both quasi-

conservative [105], and non-conservative [106–109], behavior with respect to salinity gradients in the estuaries so that estuaries can behave as both sources and sinks of Pb.

Studies of Pb behavior in the Wanquan River and the Wenchang/Wenjiao River estuaries on Hainan Island (China) demonstrated non-conservative distributions with dissolved Pb diminishing ~100-fold as salinity increased from ~0 in the river to >28 [109]. In the Loire River (France) estuary dissolved Pb (range 0.04–0.26 nmol L^{-1}) was removed from the estuary dropping by a factor of ~2 as salinity increased from 0 to 30 and suspended particulate matter concentrations decreased [110]. Dissolved Pb was removed in the Penzé River estuary (France) in the salinity range 0–10 presumably through flocculation with associated Fe and humic substances [107, 108]. During winter storm activity the estuary behaved as a source of dissolved Pb when erosion and resuspension mobilized particulate Pb in the Penzé [108]. Recent compilations calculate global dissolved and particulate Pb riverine fluxes to the ocean of 3,000 t/yr and 916,000 t/yr, respectively (Table 5) [17, 85]. Seasonal variability in river flow, anthropogenic point sources, dissolved and particulate Pb concentrations, the variable source and sink behavior of different estuaries and the dearth of data in time and space for world rivers require that these estimates remain semi-quantitative [104].

6. LEAD IN OCEAN WATERS

6.1. Distribution

Lead is found at trace concentrations in the ocean at the level of picomoles (10^{-12} moles) per kilogram [21–23, 104, 111–114]. The distribution of Pb and its isotopic composition has evolved in space and time reflecting the influence of anthropogenic activities on the cycling of the metal in the environment [22, 114, 115]. A majority of the Pb present in the oceans is of anthropogenic origin, principally from the combustion of leaded gasoline in the 20th century by North American and European nations (Figure 2), and ongoing emissions associated with mining, smelting, and fossil fuel combustion. Most of this Pb was deposited as aerosols to the ocean surface and variations in the flux of anthropogenic Pb have been documented through measurements of seawater [21, 22, 114–120] and proxy records obtained from calcium carbonate precipitating corals [24]. Changing inputs to the surface of the major ocean basins are propagated into the ocean interior to a first approximation by thermocline ventilation and deepwater formation [117]. Because the residence times of Pb in low productivity surface waters (~2 years) and in the ocean interior (10–10^2 years) [121, 122] are relatively short compared to ocean mixing times, the steady state balance between input and particle scavenging of Pb means that surface water Pb concentrations track changes in input [114]. The distribution of dissolved Pb in the oceans continues to change in response to emissions to the atmosphere from anthropogenic activities [22, 113, 123]. We consider the distribution of dissolved Pb in the major ocean basins below.

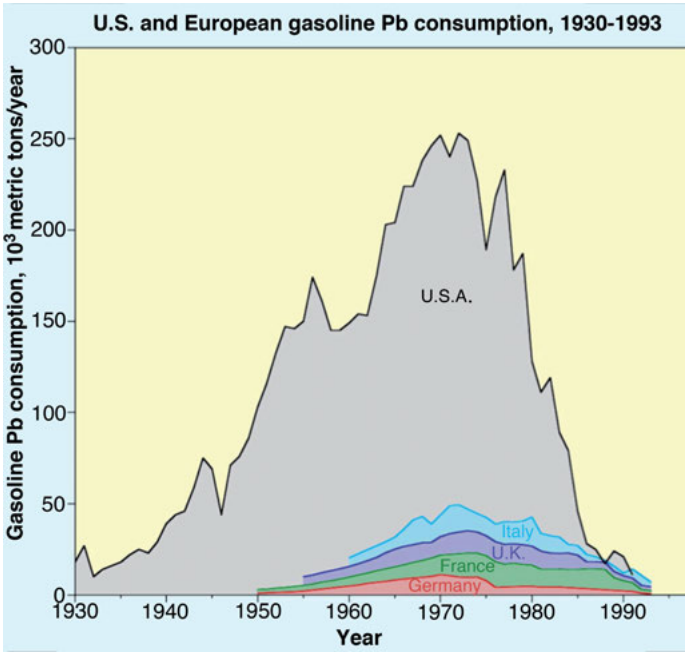

Figure 2. Leaded gasoline consumption for Western European countries and the United States of America from 1930 to 1993. Reproduced with kind permission from [113]; copyright 2014, The Oceanography Society.

Representative depth profiles of dissolved Pb over time in the western North Atlantic since 1979 until 2011 are shown in Figure 3. In the Atlantic Ocean dissolved Pb has been measured periodically near Bermuda since 1979 [24, 113, 124–126]. Near the peak of leaded gasoline inputs to the North Atlantic, surface waters had concentrations of ~160 pmol kg^{-1}, while concentrations were an order of magnitude lower in samples collected in 2011. In each year maximum dissolved concentrations are found in the subsurface (Figure 3). This reflects the sinking of water masses that were last present at the surface during periods of higher Pb in the past. Maximum concentrations diminish from ~170 to ~35 pmol kg^{-1} and deepen from ~400 m to 1,000–2,000 m over time in concert with decreasing anthropogenic leaded gasoline emissions, water mass ventilation and mixing, and scavenging losses of Pb [113, 126]. Given proximity, prevailing atmospheric circulation and the short residence time of Pb-containing aerosols, anthropogenic inputs from North America and Europe in the 20th century led to less acute impacts on distribution of dissolved Pb in the North Pacific [112, 115]. Schaule and Patterson [112] reported upper water column dissolved Pb concentrations near Hawaii of ~65 pmol kg^{-1} which by 1999 had decreased to ~30–35 pmol kg^{-1} [115]. A pronounced zonal gradient exists in the Pacific with surface waters in the western Pacific significantly higher in dissolved Pb compared to the eastern Pacific which is likely related to Pb input from fossil fuel

combustion in Asia [123]. Increased industrialization and later phase out of leaded gasoline in the populated centers around the Indian Ocean are likely responsible for elevated dissolved Pb in surface waters there of 40–80 pmol kg^{-1}, but deepwater in the basin has extremely low values of 2 pmol kg^{-1}. Southern Ocean waters have low concentrations (5–12 pmol kg^{-1}), suggesting little anthropogenic impact [113].

The evolving distribution of dissolved Pb in the ocean in space and time reflects the largely northern hemisphere anthropogenic point sources and records the shift from principal sources in North America and Europe in the mid- to late-20th century to Asian dominance in the 21st century.

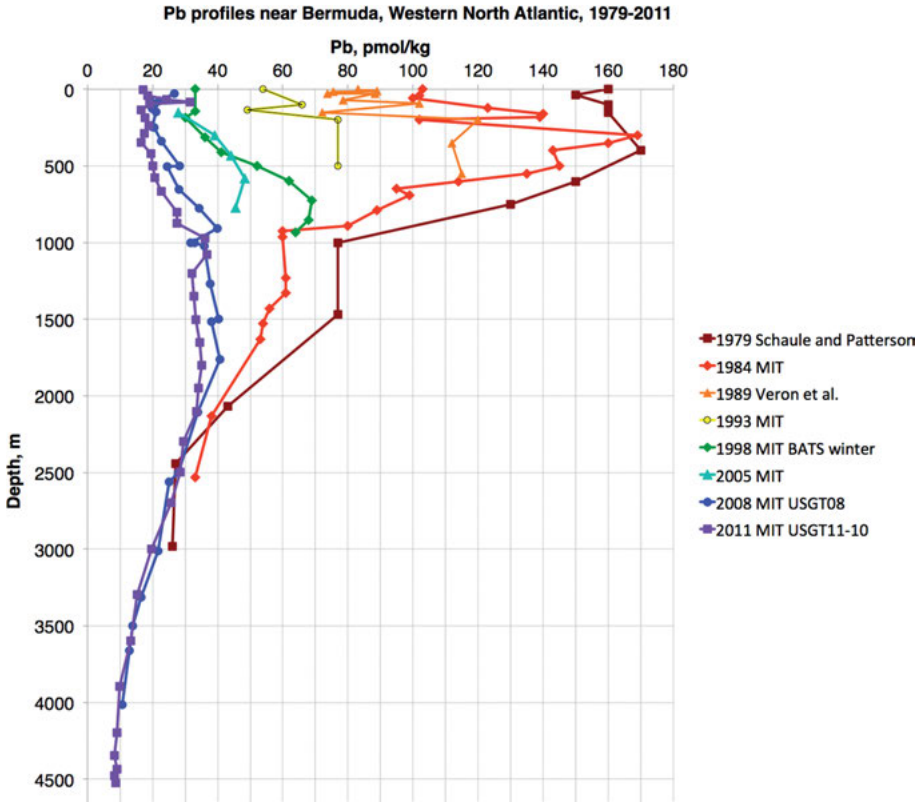

Figure 3. Concentration of Pb in seawater with versus depth from profiles collected near Bermuda in the North Atlantic Ocean for the period 1979–2011. Data from [124] (1979 Schaule and Patterson), [24] (1984 MIT), [125] (1989 Veron et al.), [126] (1993–2008 profiles), and [114] (MIT USGT11–10). Reproduced with kind permission from [113]; copyright 2014, The Oceanography Society.

6.2. Speciation

As in freshwater, the behavior and fate of dissolved Pb in seawater with respect to biological uptake or sorption to particle surfaces depends on its chemical speciation. In estuarine systems, as salinity and pH tend to increase toward the coastal ocean, Pb is predominantly (> 95 %) associated with the particulate or colloidal phase. For the remaining fraction, considered to be in solution, the inorganic equilibrium speciation of Pb in seawater is dominated by its association with Cl^- (46–75 %), CO_3^{2-} (11–42 %), and OH^- (8–9 %) [89, 127, 128]. When dissolved organic carbon concentrations are higher, as they are in estuarine and coastal environments, Pb can be complexed by organic ligands, lowering the concentration of inorganic Pb complexes (Pb') [129–133].

Organic ligands with conditional stability constants (K_{cond}) on the order of $10^{8.6}$–$10^{10.2}$ with respect to the sum of inorganic Pb species (Pb') were detected in waters of Narragansett Bay estuary in Rhode Island (USA) by Kozelka and Bruland [132]. The variation of ligand concentration and affinity in the estuary is such that ~94 % of dissolved Pb is organically complexed in the upper estuary at a salinity of 25 but drops to 67 % in the lower bay where salinity is 30. Organic Pb complexes were similarly important in the San Francisco Bay (USA) (96 %) [131] and estuaries near Southampton (UK) [130]. In open ocean or other low DOC environments, the fraction of strong organic Pb complexes decreases with average values of 70–80 % in waters of the Adriatic Sea, 55–61 % in the Antarctic [134, 135] and 54 % in the North Pacific [136]. Generally, measurements and thermodynamic equilibrium calculations indicate that a greater fraction of Pb is present in more labile inorganic complexes or as Pb^{2+} extending from the coastal zone to open ocean environments.

6.3. Biogeochemical Cycling

Lead's distribution in the ocean and its principal loss from the system through burial in marine sediments is driven by particle scavenging reactions, where Pb is adsorbed to or complexed by particle surfaces [113, 137]. There is no known biological function for Pb, however, metals like Pb, that can be toxic, are concentrated intracellularly by organisms from the seawater in which they grow by various non-selective uptake mechanisms [72, 138, 139]. Phytoplankton represent an important class of particles in the marine environment that can impact Pb distributions by internalizing Pb through surface adsorption of the metal [140]. Zones of high productivity at the ocean margins and in areas of active upwelling are important sites of Pb removal in the ocean [141]. Active uptake of Pb by marine microbes is thought to be governed by the free ion activity model (FIAM), where the bioavailability and intracellular concentration of the metal is controlled by the free ion (Pb^{2+}) or labile inorganic complexes (Pb') [72]. However, lipophilic organic Pb complexes can passively diffuse into marine phytoplankton and organically complexed Pb is demonstrated to adsorb to cell walls, both of which increase the biological scavenging of Pb from seawater [142–144].

Radioisotope uptake experiments indicate that a majority of Pb taken up by the phytoplankton tends to be associated with structural components of cells (cell walls and plasmalemmae) and is therefore unlikely to be easily assimilated by organisms feeding on the algae [145]. It is likely that both passive scavenging and biological uptake in ocean surface waters are important sinks for dissolved Pb while passive scavenging to particle surfaces and sinking is most important for removing Pb from the ocean interior to the sediments.

Organisms interacting with ocean sediments can influence biogeochemical cycling of Pb in the ocean by mobilizing or bioconcentrating Pb. While organisms may not actively take up Pb, filter-feeding organisms such as oysters are at risk of accumulating dissolved or particulate Pb directly from the water column, in addition to ingesting Pb from sediment [146]. Additionally, polychaete worms living in metal-rich sediments can transfer particle-associated Pb to the marine food web [147], but biomagnification of Pb is not thought to occur [148, 149].

6.4. Lead Isotopes as Tracers of Ocean Processes

In addition to information about ocean processes provided by the distribution of Pb in the ocean, its isotopic composition can serve as a fingerprint of sources and sinks, and therefore, Pb isotopes provide an important means to trace Pb in the environment [19, 150, 151]. Within the marine environment, stable radiogenic Pb isotopic composition complements Pb concentration data, providing valuable constraints on the sources of Pb input to the oceans and the marine biogeochemical cycling of Pb [20].

Here we focus on four stable isotopes of Pb including ^{204}Pb which is primordial, and the radiogenic isotopes ^{206}Pb, ^{207}Pb, and ^{208}Pb that are most useful in the environmental sciences [19]. Their relative natural abundance in the crust and in Pb ores shows great variability given that the radiogenic isotopes ^{206}Pb, ^{207}Pb, and ^{208}Pb result from the decay of ^{238}U, ^{235}U, and ^{232}Th, respectively. During ore and mineral formation the compatibility of U, Th, and daughter Pb isotopes can lead to isolation of parent isotopes and Pb which fixes the isotopic ratios found in different end member Pb sources. The radiogenic Pb in a sample depends on the time since the accretion of the Earth and the time since ore emplacement as follows,

$$
\begin{aligned}
^{206}\mathrm{Pb} &= {}^{206}\mathrm{Pb}_0 + {}^{238}\mathrm{U}[\mathrm{e}^{\lambda_{238}t_0} - \mathrm{e}^{\lambda_{238}t}] \\
^{207}\mathrm{Pb} &= {}^{207}\mathrm{Pb}_0 + {}^{235}\mathrm{U}[\mathrm{e}^{\lambda_{235}t_0} - \mathrm{e}^{\lambda_{235}t}] \\
^{208}\mathrm{Pb} &= {}^{208}\mathrm{Pb}_0 + {}^{232}\mathrm{U}[\mathrm{e}^{\lambda_{232}t_0} - \mathrm{e}^{\lambda_{232}t}]
\end{aligned}
$$

where the subscript zero indicates the original isotopic abundance, t_0 is the age of the Earth, t is the time since the ore or mineral was emplaced and the λ term reflects the respective half-lives of the parent isotopes ^{238}U (1.55×10^{-10} yr^{-1}), ^{235}U (9.85×10^{-10} yr^{-1}), and ^{232}Th (4.95×10^{-11} yr^{-1}). The differing source material and emplacement ages of ores mobilized by human activity generate significant

variability in ore isotopic ratios which help to fingerprint the source of anthropogenic contamination in the environment [18, 20, 152].

Isotopic ratios of Pb measured in seawater can therefore be used to identify source inputs of Pb via the atmosphere or from terrestrial runoff. For example, sources of Pb to the North Atlantic from the continents and associated with transport via trade winds are identified based on $^{206}Pb/^{207}Pb$ ratios [21]. Isotope-isotope plots of the $^{206}Pb/^{207}Pb$ ratio with $^{208}Pb/^{206}Pb$ generates a convenient graphical tool for identification of Pb sources and determining whether the composition is representative of one or a mixture of multiple end members. For example, $^{206}Pb/^{207}Pb$ and $^{208}Pb/^{206}Pb$ ratios measured in surface waters of the central and western North Pacific Ocean indicate Pb inputs from Asian leaded gasoline, coal-burning power plants, and trash incineration [123, 153]. In the Atlantic Ocean, decadal time series data reveals precipitous drops in the concentration of Pb measured in the ocean, however, it is the Pb isotope ratios that tell the story of the decline. Inputs of Pb to the central and western Atlantic were initially dominated by aerosols resulting from the use of leaded gasoline in the United States from the 1920s until the product was phased-out over 1970s and 1980s [20, 21, 112]. Subsequently, isotopic ratios of Pb document the geographic source shift in anthropogenic Pb of the Atlantic Ocean from North America to Europe [114, 125].

The historical archive of anthropogenic Pb in seawater is extended from decades to centuries by analysis of Pb isotopes in banded corals growing in the ocean [23, 117, 154–156]. Pb isotope ratios recorded within coral indicate the time scale of anthropogenic impact on Pb inputs to the ocean. For example, in Atlantic corals sampled off Bermuda, shifts in Pb isotope ratios from natural Pb inputs to anthropogenic signals began with the rise of industrialization in the mid 1800s [23]. Analogous shifts in Pb inputs are observed in corals in the Pacific Ocean. Industrial and leaded gasoline emissions from Japan dominated Pb inputs to the western Pacific from the mid 19^{th} century to the 1980s followed by an increased contribution of Pb inputs from China, indicated by transitions in Pb isotope ratios measured in coral [154, 156]. Studies of coral records of Pb isotopes from the Chagos Archipelago in the Indian Ocean document inputs from leaded gasoline and coal combustion in India while corals in the western Indian Ocean near Sumatra indicate that Indonesian leaded gasoline and other anthropogenic sources are the dominant inputs [155]. Further work on calcium carbonate proxy records of seawater Pb isotopic composition will allow a more detailed historical record of the anthropogenic impact of Pb biogeochemistry in the ocean to be constructed.

While frequently applied to determining the source of anthropogenic Pb contamination, Pb isotopes can also assist in delineating sources of essential trace metal nutrients to the ocean. Trace metals such as iron are vital to phytoplankton growth in the ocean [157–160], which may ultimately influence global climate [161, 162]. Inputs of trace metals to the ocean that can stimulate phytoplankton production include atmospheric deposition [163], freshwater inputs from rivers [16], upwelling along the coast [164–167], and transport of coastal sources to the open ocean within eddies [168, 169]. Critically, identification of essential trace

metal inputs is required within large regions of the ocean demonstrating High Nutrient-Low Chlorophyll (HNLC) conditions, where available nutrients such as nitrate and phosphate are underutilized by phytoplankton due to Fe limitation.

Measurements of dissolved Pb isotopes in the eastern subarctic North Pacific HNLC identified distinct ratios between North American river inputs and atmospheric deposition from Asia [170]. HNLC conditions were observed in areas where Pb isotopic ratios were consistent with the major source of Pb, and associated Fe, being atmospheric deposition from Asia. In contrast, in areas with isotopic compositions heavily influenced by North American river input, HNLC conditions were alleviated [170] (Figure 4). One implication of this study is that while atmospheric deposition of trace metals can represent an important, but ephemeral and stochastic, source of trace metals to remote HNLC regions [163, 171–175], continental freshwater inputs and terrestrially derived continental shelf inputs [166, 176–178] allow for the alleviation of Fe limitation near the ocean margins.

The preceding section, while not a comprehensive treatment of applications of Pb isotopes in studies of marine biogeochemistry, demonstrates their versatility and utility for identifying sources of contaminant Pb in the ocean and determining the source of trace metal inputs for phytoplankton.

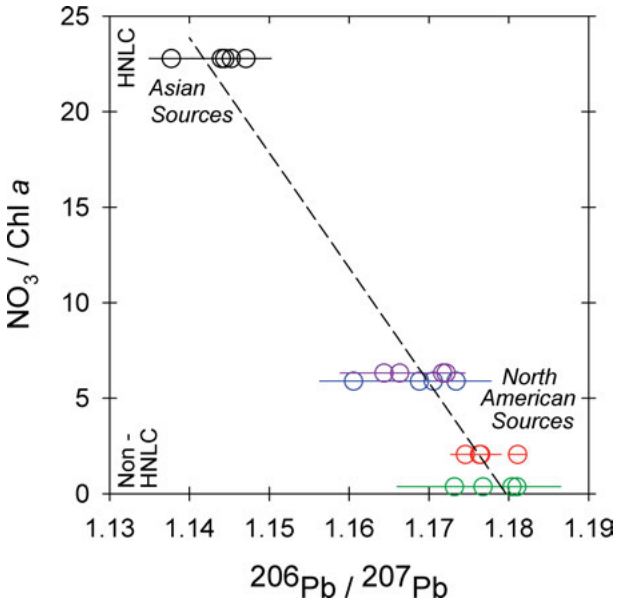

Figure 4. $^{206}Pb/^{207}Pb$ isotope ratios indicative of Pb sources from North America and terrestrial inputs that act to alleviate HNLC conditions in the Northeast Pacific. In contrast, $^{206}Pb/^{207}Pb$ ratios observed in Asian sources are associated with HNLC conditions known to result from a lack of bioavailable Fe.

7. SUMMARY AND CONCLUSIONS

The degree of anthropogenic mobilization of Pb and its inherent, acute toxicity to organisms motivate the scientific community to understand source and sink processes in the environment. Since antiquity humans have altered the biogeochemical cycle of Pb by removing Pb from the crust and mobilizing it in the biosphere. This mobilization occurs primarily through vehicular fuel combustion, non-ferrous metal production, and the burning of fossil fuels. Measurements made on material (both in the dissolved and particulate phase) in the atmosphere, as well as in rainwater, soils, sediments, and aquatic environments demonstrate these anthropogenic activities result in significant enrichment in Pb relative to its average concentration in the continental crust.

Emissions of Pb to the environment appear to have diminished substantially in response to increased regulation, especially the phase out of leaded gasoline in major markets in the 1970s–80s and the implementation of more efficient point source capture and recycling initiatives. Global Pb production continues to increase after a plateau and decline late in the last century to ~5,500,000 t/yr in 2013. Over the past decades there has been a shift on the regions of major Pb production and emissions from Europe and North America to countries in East Asia. This trend mirrors growing demand for energy and rapid industrialization in major population centers in this area. One concern, going forward, is that emissions in Asia are roughly double those of the next nearest continent (Europe) and, although data is sparse, appear to be increasing with time. Whether or not global emissions of Pb will increase in response to continued industrialization of the great population centers in Asia remains to be seen, but should be a focus of monitoring efforts [42].

Radiogenic isotopes of Pb represent a valuable source of information for tracing sources of contaminant Pb in the environment, determining the source of nutrients available to microbes in natural waters, and tracking large scale movements and mixing of water masses in the ocean. The study of Pb isotopes in the environment unite a diverse research community of scientists including chemical and physical oceanographers, biogeochemists, geo- and cosmochemists, environmental scientists, contaminant researchers and ecotoxicolgists, ecologists, and climate scientists. As global efforts, including the multi-decadal international GEOTRACES program [179], to determine Pb and its isotopic composition in environmental samples continue, we can expect to develop a refined understanding of Pb's mobilization, impact on biological systems, and its fate in the biosphere.

ACKNOWLEDGEMENT

This work was supported in part by Canadian Natural Sciences and Engineering Research Council Discovery Grant to JTC.

ABBREVIATIONS AND DEFINITIONS

ADIOS	Atmospheric Deposition and Impact on the Open Mediterranean Sea
AMAP	Arctic Monitoring and Assessment Program
C_w/C_c	water concentration divided by crustal concentration for an element representing a global mobility index
DOC	dissolved organic carbon
EF_C	crustal enrichment factor
EMEP	European Monitoring and Evaluation Programme a Co-operative Programme for Monitoring and Evaluation of the Long-Range Transmission of Pollutants in Europe
FA	fulvic acid
FIAM	free ion activity model
GEOTRACES	an international program dedicated to studying trace elements and isotopes in the ocean
H_2O_2-NH_4OAc	hydrogen peroxide and ammonium acetate mixture
HA	humic acid
HNLC	high nutrient-low chlorophyll region of the ocean
K_d	distribution coefficient
kg	kilogram = 1000 g
Pb'	sum of inorganically complexed Pb and free Pb ion
pH	$-\log\{H^+\}$
SLI	starting-lighting-ignition batteries
t	metric tonne = 1000 kg
UPS	uninterruptible power source
Z	atomic number

REFERENCES

1. C. C. Patterson, *Arch. Environ. Health* **1965**, *11*, 344–360.
2. C. C. Patterson, *Connecticut Medicine* **1971**, *35*, 347–352.
3. J. O. Nriagu, *Lead and Lead Poisoning in Antiquity*, Eds R. L. Metcalf, W. Stumm, John Wiley & Sons, Inc., New York, 1983.
4. D. J. Weiss, M. E. Kylander, M. K. Reuer, *Advances in Earth Science: From Earthquakes to Global Warming* **2007**, *2*, 245–272.
5. J. F. Jaworski, in *Lead, Mercury, Cadmium and Arsenic in the Environment*, Eds T. C. Hutchinson, K. M. Meema, Wiley & Sons, New York, 1987, pp. 3–16.
6. W. Shotyk, G. Le Roux, *Biogeochemical Cycles of Elements*, in *Metal Ions in Biological Systems,* Vol. 43, Eds A. Sigel, H. Sigel, R. K. O. Sigel, Taylor & Francis, CRC Press, Boca Raton, New York, 2005, pp. 239–275.
7. C. F. Boutron, C. C. Patterson, *Nature* **1986**, *323*, 222–225.
8. C. F. Boutron, C. C. Patterson, *J. Geophys. Res.-Atmospheres* **1987**, *92*, 8454–8464.
9. D. M. Settle, C. C. Patterson, *J. Geophys. Res.-Oceans Atmospheres* **1982**, *87*, 8857–8869.
10. M. Murozumi, T. J. Chow, C. Patterson, *Geochim. Cosmochim. Acta* **1969**, *33*, 1247–1294.

11. S. M. Hong, J. P. Candelone, C. C. Patterson, C. F. Boutron, *Science* **1994**, *265*, 1841–1843.
12. J. Nriagu, *Environment* **1990**, *32*, 7–33.
13. J. O. Nriagu, *Nature* **1989**, *338*, 47–49.
14. J. O. Nriagu, J. M. Pacyna, *Nature* **1988**, *333*, 134–139.
15. J. M. Pacyna, E. G. Pacyna, *Environ. Rev.* **2001**, *9*, 269–298.
16. J. Gaillardet, J. Viers, B. Dupré, in *Treatise on Geochemistry*, Eds H. D. Holland, K. K. Turekian, Vol. 7, 2nd edn., Elsevier, Oxford, 2014, pp. 195–235.
17. J. Viers, B. Dupré, J. Gaillardet, *Sci. Total Environ.* **2009**, *407*, 853–868.
18. D. F. Sangster, P. M. Outridge, W. J. Davis, *Environ. Rev.* **2000**, *8*, 115–147.
19. M. Komarek, V. Ettler, V. Chrastny, M. Mihaljevic, *Environ. Int.* **2008**, *34*, 562–577.
20. M. K. Reuer, D. J. Weiss, *Phil. Trans. Roy. Soc. London Series a-Math. Phys. Eng. Sci.* **2002**, *360*, 2889–2904.
21. D. Weiss, E. A. Boyle, J. F. Wu, V. Chavagnac, A. Michel, M. K. Reuer, *J. Geophys. Res.-Oceans* **2003**, *108*.
22. J. F. Wu, E. A. Boyle, *Geochim. Cosmochim. Acta* **1997**, *61*, 3279–3283.
23. A. E. Kelly, M. K. Reuer, N. F. Goodkin, E. A. Boyle, *Earth Planet. Sci. Lett.* **2009**, *283*, 93–100.
24. G. T. Shen, E. A. Boyle, *Earth Planet. Sci. Lett.* **1987**, *82*, 289–304.
25. *The Biogeochemistry of Lead in the Environment: Part A. Ecological Cycles*, in *Topics in Environmental Health*, Ed. J. O. Nriagu, Elsevier/North-Holland Biomedical Press, Amsterdam, The Netherlands, 1978.
26. M. Berglund, M. E. Wieser, *Pure Appl. Chem.* **2011**, *83*, 397–410.
27. J. R. De Laeter, J. K. Bohlke, P. De Bievre, H. Hidaka, H. S. Peiser, K. J. R. Rosman, P. D. P. Taylor, *Pure Appl. Chem.* **2003**, *75*, 683–800.
28. R. L. Rudnick, S. Gao, in *Treatise on Geochemistry*, Eds H. D. Holland, K. K. Turekian, 2nd edn., Vol. 4, Elsevier, Oxford, 2014, pp. 1–51.
29. K. H. Wedepohl, *Geochim. Cosmochim. Acta* **1995**, *59*, 1217–1232.
30. Callender, E., in *Treatise on Geochemistry*, Eds H. D. Holland, K. K. Turekian, 2nd edn., Vol. 11, Elsevier, Oxford, 2014, pp. 59–89.
31. S. R. Taylor, S. M. Mclennan, *Rev. Geophys.* **1995**, *33*, 241–265.
32. H. Palme, H. S. C. O'Neill, in *Treatise on Geochemistry*, Eds H. D. Holland, K. K. Turekian, 2nd edn., Vol. 3, Elsevier, Oxford, 2014, pp. 1–39.
33. Nriagu, J., *Science* **1996**, *272*, 223–224.
34. *Emission Factors of Atmospheric Elements*, in *Toxic Metals in the Atmosphere*, Eds J. O. Nriagu, C. I. Davidson, John Wiley & Sons, New York, 1986.
35. J. N. Rauch, J. M. Pacyna, *Global Biogeochem. Cycles* **2009**, *23*.
36. R. Duce, P. Liss, J. Merrill, E. Atlas, P. Buat-Menard, B. Hicks, J. Miller, J. Prospero, R. Arimoto, T. M. Church, W. Ellis, J. N. Galloway, L. Hansen, T. D. Jickells, A. H. Knap, K. H. Reinhardt, B. Schneider, A. Soudine, J. Tokos, S. Tsunogai, R. Wollast, M. Zhou, *Global Biogeochem.Cycles* **1991**, *5*, 193–259.
37. C. C. Patterson, D. M. Settle, *Geochim. Cosmochim. Acta* **1987**, *51*, 675–681.
38. A. Matsumoto, T. K. Hinkley, *Earth Planet. Sci. Lett.* **2001**, *186*, 33–43.
39. S. M. Hong, Y. Kim, C. F. Boutron, C. P. Ferrari, J. R. Petit, C. Barbante, K. Rosman, V. Y. Lipenkov, *Geophys. Res. Lett.* **2003**, *30*.
40. K. Bertine, E. D. Goldberg, *Science* **1971**, *173*, 233–235.
41. D. E. Guberman, in "Mineral Commodity Summaries: Lead", U.S. Geological Survey, Virgina, 2016, see http://minerals.usgs.gov/minerals/pubs/mcs/2016/mcs2016.pdf.
42. A. R. Flegal, C. Gallon, P. M. Ganguli, C. H. Conaway, *Crit. Rev. Environ. Sci. Technol.* **2013**, *43*, 1869–1944.
43. M. King, V. Ramachandran, R. D. Prengaman, S. C. DeVito, J. Breen, in *Kirk-Othmer Encyclopedia of Chemical Technology*, John Wiley & Sons, Inc., New York, 2000.

44. R. A. Duce, G. L. Hoffman, B. J. Ray, I. S. Fletcher, G. T. Wallace, J. L. Fasching, S. E. Piotrowctz, P. R. Walsh, E. J. Hoffman, J. M. Miller, J. L. Hefter, in *Marine Pollution Transfers*, Eds H. L. Windom, R. A. Duce, D. C. Heath, Lexington, MA, 1976, pp. 77–119.
45. R. A. Duce, G. L. Hoffman, W. H. Zoller, *Science* **1975**, *187*, 59–61.
46. T. Berg, O. Røyset, E. Steinnes, *Atmos. Environ.* **1994**, *28*, 3519–3536.
47. T. Berg, E. Steinnes, *Met. Ions Biol. Syst.* **2005**, *44*, 1–19.
48. S. Hong, *Geophys. Res. Lett.* **2004**, *31*, 5–8.
49. K. Lee, S. D. Hur, S. Hou, S. Hong, X. Qin, J. Ren, Y. Liu, K. J. R. Rosman, C. Barbante, C. F. Boutron, *Sci. Total Environ.* **2008**, *404*, 171–181.
50. F. A. M. Planchon, C. E. Boutron, C. Barbante, G. Cozzi, V. Gaspari, E. W. Wolff, C. P. Ferrari, P. Cescon, *Sci. Total Environ.* **2002**, *300*, 129–142.
51. E. W. Wolff, E. D. Suttie, D. A. Peel, *Atmos. Environ.* **1999**, *33*, 1535–1541.
52. C. C. Patterson, D. M. Settle, *Marine Chemistry* **1987**, *22*, 137–162.
53. R. M. Sherrell, E. A. Boyle, N. R. Harris, K. K. Falkner, *Geochem. Geophys. Geosyst.* **2000**, *1*.
54. K. J. R. Rosman, W. Chisholm, C. F. Boutron, J. P. Candelone, U. Gorlach, *Nature* **1993**, *362*, 333–335.
55. T. Patterson, R. Duce, *Tellus B* **1991**, *43B*, 12–29.
56. C. Barbante, C. Boutron, C. Morel, C. Ferrari, J. L. Jaffrezo, G. Cozzi, V. Gaspari, P. Cescon, *J. Environ. Monit.* **2003**, *5*, 328–335.
57. S. D. Hur, X. Cunde, S. Hong, C. Barbante, P. Gabrielli, K. Lee, C. F. Boutron, Y. Ming, *Atmos. Environ.* **2007**, *41*, 8567–8578.
58. K. Van de Velde, C. Boutron, C. P. Ferrari, A. Moreau, R. Delmas, C. Barbante, T. Bellomi, G. Capodaglio, P. Cescon, *Geophys. Res. Lett.* **2000**, *27*, 249–252.
59. A. Veysseyre, K. Moutard, C. Ferrari, K. Van de Velde, C. Barbante, G. Cozzi, G. Capodaglio, C. Boutron, *Atmos. Environ.* **2001**, *35*, 415–425.
60. W. H. Zoller, E. S. Gladney, R. A. Duce, *Science* **1974**, *183*, 198–200.
61. R. U. Shelley, P. L. Morton, W. M. Landing, *Deep Sea Research Part II: Topical Studies in Oceanography* **2015**, *116*, 262–272.
62. J. M. Pacyna, E. G. Pacyna, W. Aas, *Atmos. Environ.* **2009**, *43*, 117–127.
63. T. Church, J. Tramontano, D. Whelpdale, M. O. Andreae, J. N. Galloway, W. Keene, A. H. Knap, J. Tokos, *J. Geophys. Res.* **1991**, *96*, 18705–18725.
64. T. M. Church, A. Veron, C. C. Patterson, D. Settle, Y. Erel, H. R. Maring, A. R. Flegal, *Global Biogeochem. Cycles* **1990**, *4*, 431–444.
65. R. Arimoto, R. A. Duce, B. J. Ray, A. D. Hewitt, J. Williams, *J. Geophys. Res.-Atmospheres* **1987**, *92*, 8465–8479.
66. R. Arimoto, R. A. Duce, B. J. Ray, C. K. Unni, *J. Geophys. Res.-Atmospheres* **1985**, *90*, 2391–2408.
67. M. J. R. Halstead, R. G. Cunninghame, K. A. Hunter, *Atmos. Environ.* **2000**, *34*, 665–676.
68. C. Guieu, M.-D. Loÿe-Pilot, L. Benyahya, A. Dufour, *Marine Chemistry* **2010**, *120*, 164–178.
69. H. B. Bradl, *J. Colloid Interface Sci.* **2004**, *277*, 1–18.
70. F. Degryse, E. Smolders, D. R. Parker, *Eur. J. Soil Sci.* **2009**, *60*, 590–612.
71. K. Lock, C. R. Janssen, *Rev. Environ. Contam. Toxicol.* **2003**, *178*, 1–21.
72. F. M. M. Morel, J. Hering, *Principles and Applications of Aquatic Chemistry*, John Wiley & Sons, New York, 1993.
73. C. E. Martinez, M. B. McBride, *Clays and Clay Minerals* **1998**, *46*, 537–545.
74. C. E. Martinez, M. B. McBride, *Environ. Sci. Technol.* **1999**, *33*, 745–750.
75. C. E. Martinez, H. L. Motto, *Environ. Pollut.* **2000**, *107*, 153–158.
76. R. M. McKenzie, *Austral. J. Soil Res.* **1980**, *18*, 61–73.

77. J. P. Pinheiro, A. M. Mota, M. F. Benedetti, *Environ. Sci. Technol.* **1999**, *33*, 3398–3404.
78. J. P. Pinheiro, A. M. Mota, M. F. Benedetti, *Environ. Sci. Technol.* **2000**, *34*, 5137–5143.
79. D. G. Strawn, D. L. Sparks, *Soil Sci. Soc. Am. J.* **2000**, *64*, 144–156.
80. D. G. Strawn, D. L. Sparks, *J. Colloid Interface Sci.* **1999**, *216*, 257–269.
81. D. G. Strawn, A. M. Scheidegger, D. L. Sparks, *Environ. Sci. Technol.* **1998**, *32*, 2596–2601.
82. P. S. Hooda, B. J. Alloway, *Int. J. Environ. Anal. Chem.* **1994**, *57*, 289–311.
83. P. S. Hooda, B. J. Alloway, *Water Air Soil Pollut.* **1994**, *74*, 235–250.
84. W. O. Nelson, P. G. Campbell, *Environ. Pollut.* **1991**, *71*, 91–130.
85. J. Gaillardet, J. Viers, B. Dupré, in *Treatise on Geochemistry*, Eds H. D. Holland, K. K. Turekian, Vol. 7, Elsevier Ltd., Amsterdam, 2003, pp. 225–272.
86. M. Filella, R. M. Town, J. Buffle, in *Chemical Speciation in the Environment*, Blackwell Science Ltd, 2007, pp. 188–236.
87. J. Vuceta, J. J. Morgan, *Environ. Sci. Technol.* **1978**, *12*, 1302–1309.
88. J. D. Hem, W. H. Durum, *J. Am. Water Works Assoc.* **1973**, *65*, 562–568.
89. D. R. Turner, in *Lead, Mercury, Cadmium and Arsenic in the Environment*, Eds T. C. Hutchinson, K. M. Meema, John Wiley & Sons, New York, 1987, pp. 175–186.
90. S. E. Mylon, B. S. Twining, N. S. Fisher, G. Benoit, *Environ. Sci. Technol.* **2003**, *37*, 1261–1267.
91. M. Taillefert, C. P. Lienemann, J. F. Gaillard, D. Perret, *Geochim. Cosmochim. Acta* **2000**, *64*, 169–183.
92. R. M. Town, M. Filella, *Aquatic Sci.* **2000**, *62*, 252–295.
93. L. Sigg, R. Behra, in *Metal Ions in Biological Systems,* Vol. 44, Eds. A. Sigel, H. Sigel, R. K. O. Sigel, Taylor & Francis, CRC Press, Boca Raton, New York, 2005, pp. 47–73.
94. G. Abate, J. C. Masini, *Org. Geochem.* **2002**, *33*, 1171–1182.
95. I. Christl, A. Metzger, I. Heidmann, R. Kretzschmar, *Environ. Sci. Technol.* **2005**, *39*, 5319–5326.
96. G. M. Hettiarachchi, G. M. Pierzynski, *Environ. Progress* **2004**, *23*, 78–93.
97. T. F. Rozan, G. W. Luther, D. Ridge, S. Robinson, *Environ. Sci. Technol.* **2003**, *37*, 3845–3852.
98. L. Sigg, M. Sturm, D. Kistler, *Limnol. Oceanogr.* **1987**, *32*, 112–130.
99. Y. Erel, J. Morgan, C. Patterson, *Geochim. Cosmochim. Acta* **1991**, *55*, 707–719.
100. D. P. H. Laxen, *Water Res.* **1985**, *19*, 1229–1236.
101. S. Sauve, W. Hendershot, H. Allen, *Environ. Sci. Technol.* **2000**, *34*, 1125–1131.
102. E. F. Covelo, F. A. Vega, M. L. Andrade, *J. Hazard. Mat.* **2007**, *140*, 308–315.
103. D. P. H. Laxen, *Chem. Geol.* **1984**, *47*, 321–332.
104. K. W. Bruland, R. Middag, M. C. Lohan, in *Treatise on Geochemistry*, Eds H. D. Holland, K. K. Turekian, 2nd edn., Vol. 8, Elsevier, Oxford, 2014, pp. 19–51.
105. A. M. L. Kraepiel, J. F. Chiffoleau, J. M. Martin, F. M. M. Morel, *Geochim. Cosmochim. Acta* **1997**, *61*, 1421–1436.
106. H. L. Windom, R. G. Smith, M. Maeda, *Marine Chem.* **1985**, *17*, 43–56.
107. V. Tanguy, M. Waeles, J. Gigault, J. Y. Cabon, F. Quentel, R. D. Riso, *Marine Freshwater Res.* **2011**, *62*, 329–341.
108. M. Waeles, R. D. Riso, P. Le Corre, *Estuarine Coastal Shelf Sci.* **2007**, *74*, 570–578.
109. J. Fu, X. L. Tang, J. Zhang, W. Balzer, *Continental Shelf Res.* **2013**, *57*, 59–72.
110. M. Waeles, R. D. Riso, J. F. Maguer, J. F. Guillaud, P. Le Corre, *J. Marine Syst.* **2008**, *72*, 358–365.
111. A. R. Flegal, C. C. Patterson, *Earth Planet. Sci. Lett.* **1983**, *64*, 19–32.
112. B. K. Schaule, C. C. Patterson, *Earth Planet. Sci. Lett.* **1981**, *54*, 97–116.

113. E. A. Boyle, J.-M. Lee, Y. Echegoyen, A. Noble, S. Moos, G. Carrasco, N. Zhao, R. Kayser, J. Zhang, T. Gamo, H. Obata, K. Norisuye, *Oceanography* **2014**, *27*, 69–75.
114. A. E. Noble, Y. Echegoyen-Sanz, E. A. Boyle, D. C. Ohnemus, P. J. Lam, R. Kayser, M. Reuer, J. Wu, W. Smethie, *Deep-Sea Research Part II-Topical Studies in Oceanography* **2015**, *116*, 208–225.
115. E. A. Boyle, B. A. Bergquist, R. A. Kayser, N. Mahowald, *Geochim. Cosmochim. Acta* **2005**, *69*, 933–952.
116. E. A. Boyle, S. D. Chapnick, G. T. Shen, M. P. Bacon, *J. Geophys. Res.-Oceans* **1986**, *91*, 8573–8593.
117. G. T. Shen, E. A. Boyle, *J. Geophys. Res.-Oceans* **1988**, *93*, 15715–15732.
118. E. Helmers, L. Mart, M. Schulzbaldes, W. Ernst, *Marine Pollut. Bull.* **1990**, *21*, 515–518.
119. E. Helmers, M. M. Rutgers van der Loeff, *Pangaea* **1993**.
120. E. Helmers, M. M. R. Vanderloeff, *J. Geophys. Res.-Oceans* **1993**, *98*, 20261–20273.
121. M. P. Bacon, D. W. Spencer, P. G. Brewer, *Earth Planet. Sci. Lett.* **1976**, *32*, 277–296.
122. Y. Nozaki, J. Thomson, K. K. Turekian, *Earth Planet. Sci. Lett.* **1976**, *32*, 304–312.
123. C. Gallon, M. A. Ranville, C. H. Conaway, W. M. Landing, C. S. Buck, P. L. Morton, A. R. Flegal, *Environ. Sci. Technol.* **2011**, *45*, 9874–9882.
124. B. K. Schaule, C. C. Patterson, in *Trace Metals in Seawater*, Eds C. S. Wong, E. A. Boyle, K. W. Bruland, J. D. Burton, E. D. Goldberg, Plenum, New York, 1983, pp. 487–504.
125. A. J. Veron, T. M. Church, A. R. Flegal, C. C. Patterson, Y. Erel, *J. Geophys. Res.-Oceans* **1993**, *98*, 18269–18276.
126. J.-M. Lee, E. A. Boyle, Y. Echegoyen-Sanz, J. N. Fitzsimmons, R. Zhang, R. A. Kayser, *Anal. Chim. Acta* **2011**, *686*, 93–101.
127. K. J. Powell, P. L. Brown, R. H. Byrne, T. Gajda, G. Hefter, A.-K. Leuz, S. Sjoberg, H. Wanner, *Pure Appl. Chem.* **2009**, *81*, 2425–2476.
128. R. J. Woosley, F. J. Millero, *Marine Chem.* **2013**, *149*, 1–7.
129. J. Buffle, *Complexation Reactions in Aquatic Systems: An Analytical Approach*, Ellis Horwood Ltd., Chichester, 1988, pp. 692.
130. F. L. L. Muller, *Marine Chem.* **1996**, *52*, 245–268.
131. P. B. Kozelka, K. W. Bruland, *Abstr. Papers Am. Chem. Soc.* **1995**, *209*, 109-GEOC.
132. P. B. Kozelka, K. W. Bruland, *Marine Chem.* **1998**, *60*, 267–282.
133. P. B. Kozelka, S. SanudoWilhelmy, A. R. Flegal, K. W. Bruland, *Estuarine Coastal Shelf Sci.* **1997**, *44*, 649–658.
134. G. Scarponi, G. Capodaglio, G. Toscano, C. Barbante, P. Cescon, *Microchem. J.* **1995**, *51*, 214–230.
135. G. Capodaglio, C. Turetta, G. Toscano, A. Gambaro, G. Scarponi, P. Cescon, *Int. J. Environ. Anal. Chem.* **1998**, *71*, 195–226.
136. G. Capodaglio, K. H. Coale, K. W. Bruland, *Marine Chemistry* **1990**, *29*, 221–233.
137. R. F. Anderson, in *Treatise on Geochemistry*, 2nd edn., Vol. 8, Eds H. D. Holland, K. K. Turekian, Elsevier, Oxford, 2014, pp. 259–280.
138. F. M. M. Morel, A. J. Milligan, M. A. Saito, in *Treatise on Geochemistry*, Eds H. D. Holland, K. K. Turekian, 2nd edn., Vol. 8, Elsevier, Oxford, 2014, pp. 123–150.
139. W. G. Sunda, in *Chemistry of Aquatic Systems: Local and Global Perspectives*, Eds G. Bidoglio, W. Stumm, ECSC, EEC, EAEC, Brussels and Luxembourg, 1994, pp. 213–247.
140. N. S. Fisher, J. K. Cochran, S. Krishnaswami, H. D. Livingston, *Nature* **1988**, *335*, 622–625.
141. K. O. Buesseler, C. Lamborg, P. Cai, R. Escoube, R. Johnson, S. Pike, P. Masque, D. McGillicuddy, E. Verdeny, *Deep-Sea Research Part II-Topical Studies in Oceanography* **2008**, *55*, 1426–1444.

142. J. T. Phinney, K. W. Bruland, *Environ. Sci. Technol.* **1994**, *28*, 1781–1790.
143. J. T. Phinney, K. W. Bruland, *Environ. Toxicol. Chem.* **1997**, *16*, 2046–2053.
144. P. Sanchez-Marin, V. I. Slaveykova, R. Beiras, *Environ. Chem.* **2010**, *7*, 309–317.
145. N. S. Fisher, K. A. Burns, R. D. Cherry, M. Heyraud, *Marine Ecol. Progr. Series* **1983**, *11*, 233–237.
146. J. C. Amiard, H. Ettajani, A. Y. Jeantet, C. Ballandufrancais, C. Amiardtriquet, *Biometals* **1995**, *8*, 280–289.
147. P. S. Rainbow, L. Poirier, B. D. Smith, K. V. Brix, S. N. Luoma, *Marine Ecol. Progr. Series* **2006**, *321*, 167–181.
148. B. C. Suedel, J. A. Boraczek, R. K. Peddicord, P. A. Clifford, T. M. Dillon, *Rev. Environ. Contam. Toxicol.* **1994**, *136*, 21–89.
149. J. R. Reinfelder, N. S. Fisher, S. N. Luoma, J. W. Nichols, W. X. Wang, *Sci. Total Environ.* **1998**, *219*, 117–135.
150. H. Cheng, Y. Hu, *Environ. Pollut.* **2010**, *158*, 1134–1146.
151. B. Gulson, M. Korsch, W. Winchester, M. Devenish, T. Hobbs, C. Main, G. Smith, K. Rosman, L. Howearth, L. Burn-Nunes, J. Seow, C. Oxford, G. Yun, L. Gillam, M. Crisp, *Environ. Res.* **2012**, *112*, 100–110.
152. J. B. Cowart, W. C. Burnett, *J. Environ. Quality* **1994**, *23*, 651–662.
153. W. Wang, X. D. Liu, L. W. Zhao, D. F. Guo, X. D. Tian, F. Adams, *Sci. Total Environ.* **2006**, *364*, 175–187.
154. M. Inoue, M. Tanimizu, *Sci. Total Environ.* **2008**, *406*, 123–130.
155. J.-M. Lee, E. A. Boyle, I. S. Nurhati, M. Pfeiffer, A. J. Meltzner, B. Suwargadi, *Earth Planet. Sci. Lett.* **2014**, *398*, 37–47.
156. K. Ohmori, T. Watanabe, M. Tanimizu, K. Shirai, *Geology* **2014**, *42*, 287–290.
157. C. M. Moore, M. M. Mills, K. R. Arrigo, I. Berman-Frank, L. Bopp, P. W. Boyd, E. D. Galbraith, R. J. Geider, C. Guieu, S. L. Jaccard, T. D. Jickells, J. La Roche, T. M. Lenton, N. M. Mahowald, E. Maranon, I. Marinov, J. K. Moore, T. Nakatsuka, A. Oschlies, M. A. Saito, T. F. Thingstad, A. Tsuda, O. Ulloa, *Nature Geosci.* **2013**, *6*, 701–710.
158. P. W. Boyd, M. J. Ellwood, *Nature Geosci.* **2010**, *3*, 675–682.
159. P. W. Boyd, T. Jickells, C. S. Law, S. Blain, E. A. Boyle, K. O. Buesseler, K. H. Coale, J. J. Cullen, H. J. W. de Baar, M. Follows, M. Harvey, C. Lancelot, M. Levasseur, N. P. J. Owens, R. Pollard, R. B. Rivkin, J. Sarmiento, V. Schoemann, V. Smetacek, S. Takeda, A. Tsuda, S. Turner, A. J. Watson, *Science* **2007**, *315*, 612–617.
160. H. J. W. de Baar, P. W. Boyd, K. H. Coale, M. R. Landry, A. Tsuda, P. Assmy, D. C. E. Bakker, Y. Bozec, R. T. Barber, M. A. Brzezinski, K. O. Buesseler, M. Boye, P. L. Croot, F. Gervais, M. Y. Gorbunov, P. J. Harrison, W. T. Hiscock, P. Laan, C. Lancelot, C. S. Law, M. Levasseur, A. Marchetti, F. J. Millero, J. Nishioka, Y. Nojiri, T. van Oijen, U. Riebesell, M. J. A. Rijkenberg, H. Saito, S. Takeda, K. R. Timmermans, M. J. W. Veldhuis, A. M. Waite, C. S. Wong, *J. Geophys. Res.-Oceans* **2005**, *110*.
161. J. H. Martin, *Paleoceanography* **1990**, *5*, 1–13.
162. J. M. Martin, R. M. Gordon, S. E. Fitzwater, *Limnol. Oceanogr.* **1991**, *36*, 1793–1802.
163. J. K. B. Bishop, R. E. Davis, J. T. Sherman, *Science* **2002**, *298*, 817–821.
164. D. A. Hutchins, G. R. DiTullio, Y. Zhang, K. W. Bruland, *Limnol. Oceanogr.* **1998**, *43*, 1037–1054.
165. K. S. Johnson, F. P. Chavez, V. A. Elrod, S. E. Fitzwater, J. T. Pennington, K. R. Buck, P. M. Walz, *Geophys. Res. Lett.* **2001**, *28*, 1247–1250.
166. K. S. Johnson, F. P. Chavez, G. E. Friederich, *Nature* **1999**, *398*, 697–700.
167. M. C. Lohan, K. W. Bruland, *Environ. Sci. Technol.* **2008**, *42*, 6462–6468.
168. W. K. Johnson, L. A. Miller, N. E. Sutherland, C. S. Wong, *Deep-Sea Research Part II-Topical Studies in Oceanography* **2005**, *52*, 933–953.

169. S. M. Lippiatt, M. T. Brown, M. C. Lohan, K. W. Bruland, *Deep-Sea Research Part I-Oceanographic Research Papers* **2011**, *58*, 1091–1102.
170. J. A. McAlister, *Biogeochemistry of Dissolved Gallium and Lead Isotopes in the Northeast Pacific and Western Arctic Oceans*, Ph.D. Thesis, University of British Columbia, Vancouver, 2015.
171. R. C. Hamme, P. W. Webley, W. R. Crawford, F. A. Whitney, M. D. DeGrandpre, S. R. Emerson, C. C. Eriksen, K. E. Giesbrecht, J. F. R. Gower, M. T. Kavanaugh, M. A. Pena, C. L. Sabine, S. D. Batten, L. A. Coogan, D. S. Grundle, D. Lockwood, *Geophys. Res. Lett.* **2010**, *37*, L19604.
172. A. Krishnamurthy, J. K. Moore, N. Mahowald, C. Luo, C. S. Zender, *J. Geophys. Res.-Biogeosciences* **2010**, *115*.
173. N. M. Mahowald, A. R. Baker, G. Bergametti, N. Brooks, R. A. Duce, T. D. Jickells, N. Kubilay, J. M. Prospero, I. Tegen, *Global Biogeochem. Cycles* **2005**, *19*.
174. N. M. Mahowald, S. Engelstaedter, C. Luo, A. Sealy, P. Artaxo, C. Benitez-Nelson, S. Bonnet, Y. Chen, P. Y. Chuang, D. D. Cohen, F. Dulac, B. Herut, A. M. Johansen, N. Kubilay, R. Losno, W. Maenhaut, A. Paytan, J. A. Prospero, L. M. Shank, R. L. Siefert, *Ann. Rev. Marine Sci.* **2009**, *1*, 245–278.
175. G. S. Okin, A. R. Baker, I. Tegen, N. M. Mahowald, F. J. Dentener, R. A. Duce, J. N. Galloway, K. Hunter, M. Kanakidou, N. Kubilay, J. M. Prospero, M. Sarin, V. Surapipith, M. Uematsu, T. Zhu, *Global Biogeochem. Cycles* **2011**, *25*.
176. S. M. Lippiatt, M. T. Brown, M. C. Lohan, C. J. M. Berger, K. W. Bruland, *Estuarine Coastal Shelf Sci.* **2010**, *87*, 33–42.
177. S. M. Lippiatt, M. C. Lohan, K. W. Bruland, *Geochim. Cosmochim. Acta* **2009**, *73*, A771–A771.
178. M. C. Lohan, K. N. Buck, C. J. Berger, A. M. Aguilar-Islas, B. Sohst, G. J. Smith, K. W. Bruland, *Geochim. Cosmochim. Acta* **2006**, *70*, A369–A369.
179. G. M. Henderson, R. F. Anderson, J. Adkins, P. Andersson, E. A. Boyle, G. Cutter, H. de Baar, A. Eisenhauer, M. Frank, R. Francois, K. Orians, T. Gamo, C. German, W. Jenkins, J. Moffett, C. Jeandel, T. Jickells, S. Krishnaswami, D. Mackey, C. I. Measures, J. K. Moore, A. Oschlies, R. Pollard, M. R. D. van der Loeff, R. Schlitzer, M. Sharma, K. von Damm, J. Zhang, P. Masque, S. W. Grp, *Chemie der Erde-Geochemistry* **2007**, *67*, 85–131.
180. M. E. Wieser, T. B. Coplen, *Pure Appl. Chem.* **2011**, *83*, 359–396.
181. J. C. Slater, *J. Chem. Physics* **1964**, *41*, 3199–&.
182. R. D. Shannon, *Acta Crystallogr. Section A* **1976**, *32*, 751–767.
183. G. Audi, O. Bersillon, J. Blachot, A. H. Wapstra, *Nuclear Physics A* **2003**, *729*, 3–128.
184. D. C. Adriano, *Trace Elements in the Terrestrial Environment*, Springer, New York, 1986.
185. J. I. Drever, *The Geochemistry of Natural Waters*, Prentice-Hall, New York, 1988.
186. A. Kabata-Pendias, *Trace Elements in Soils and Plants*, CRC Press, Boca Raton, 2000.
187. B. J. Alloway, *Heavy Metals in Soils*, Blackie Academic and Professional, London, 1995.
188. U.S. Geological Survey, *Historical statistics for mineral and material commodities in the United States: U. S. Geological Survey Data Series 140*, Eds T. D. Kelly, G. R. Matos, 2014.

3

Analytical Methods for the Determination of Lead in the Environment

Peter C. Hauser

Department of Chemistry, Analytical Sciences, University of Basel,
Spitalstrasse 51, CH 4056 Basel, Switzerland
<peter.hauser@unibas.ch>

Abstract: A survey of the methods for the determination of lead in environmental samples is given. These are mainly based on sensitive atomic spectrometry, but alternatives, such as electrochemical and separation methods are also possible. Discussed are also sample preparation and speciation for differentiation between different organometallic forms as well as applications of isotope-selective determinations.

Keywords: atomic spectroscopy · electrochemical methods · lead isotopes · test kit · tetraalkyl lead · X-ray fluorescence

1. INTRODUCTION

Lead was used widely and continues to be employed for certain applications. The term plumbing derives from its domestic use in piping for water supplies, a

Metal Ions in Life Sciences, Volume 17 Edited by Astrid Sigel, Helmut Sigel, and Roland K. O. Sigel

DOI 10.1515/9783110434330-003

technique which was introduced by the Romans. But even if the actual pipes are not made from lead, the metal may still be present in water service lines of current buildings as part of the solder used for joining of tubings or even in chrome-plated faucets made from brass, which often include a small fraction of lead to render it easier for machining. Lead has also been widely employed as pigment for painting. Red lead, Pb_3O_4, has been in use for rust proofing of iron objects and white lead, $2PbCO_3 \cdot Pb(OH)_2$, has been used widely especially for the painting of wooden buildings. Chrome yellow, $PbCrO_4$, is the original pigment that lent its characteristic golden yellow color to school buses in the US and Canada and to the post offices in large parts of Europe. The metal is used in roofing and guttering especially to make water proof sealings at corners such as around chimneys. It is being used for applications where its high density is desired, such as in diving weights, sinkers for fishing tackle, and as shot for hunting. It is used for shielding against X-rays and radioactivity. It is present in glazed ceramics and leaded crystal. It is used in lead acid batteries, especially for motor vehicles. It was used extensively in petrol in the form of tetraalkyl lead as anti-knock agent and as part of the solder used in electronic equipment.

On the other hand lead has been found to be highly toxic. The Romans used lead acetate as a kind of artificial sweetener, but its toxic nature has long been established since. Among other problems its effects on the central nervous system of children are most pronounced. It has even been suggested that the crime rate in the US, which peaked in about 1990 and has been falling since, correlates with the peak use of lead in petrol approximately 20 years earlier [1]. While it was already reported in the *New York Times* on April 22, 1925, that the use of lead in petrol is a hazard, the general awareness of lead being an environmental and hygienic problem only dates back to the 1970s when generally environmental issues started to be considered. The loss of the freighter Cavtat in the Adriatic Sea in 1974, which carried a large number of barrels containing tetraethyl lead, has been cited as being instrumental in raising the awareness in particular of the environmental hazard of organic lead compounds [2, 3].

The recognition of its toxicity led to a reduction of the use of lead. It is no longer used for water piping or domestic paint. Lead acid batteries are recycled. Leaded petrol was phased-out from the 1970s, even though the initial reason for this was its incompatibility with the catalysts installed in new cars to reduce emission of unburnt hydrocarbons, CO, and NO_x. Except for a few isolated countries and some special aviation fuel, lead is now no longer used in petrol. In 2003 the European Union put in force the RoHS (Restriction of Hazardous Substances) directive, which bans the use of lead in solder for commercial electronic equipment. However, its extensive prior use means that lead is still a substantial menace. Old buildings contain lead-based paint and pipings. Soil around domestic buildings and vegetables grown in this soil may therefore show high levels of lead contamination. The wide use also required lead processing factories and smelters, which have now largely been closed down, but airborne pollution caused significant persistent soil contamination over wide areas surrounding these sites. *US Today* identified about 400 such locations in the US [4]. According to the US EPA (Environmental Protection Agency) lead is the most common

inorganic contaminant at polluted sites in the US. Similarly, mining towns are affected, and the pollution of the landscape in such areas has been found to affect not just humans but also wildlife. While organic lead compounds are mobile, and the rise and fall in the use of leaded petrol can also be tracked by determining organic lead compounds in vintage wines [5], inorganic lead is persistent as the predominant Pb(II) species are mostly water-insoluble. In central areas of large cities with a high volume of road traffic many tons of lead were deposited as dust or via rainfall over the years in which leaded petrol was in use. In the US 5 million tons of lead have been spread in this way, and the soil in inner cities like Sydney in Australia are still found to contain up to 1400 mg of lead per kg even though leaded petrol was phased-out more than 20 years ago [6]. Children playing in the grounds of affected properties are at risk. Highly problematic are also the open fire methods employed in some developing countries for recycling electronic waste.

Given the persistent risks from lead pollution, reliable lead analysis is highly important. At the time of writing two cases involving lead analysis were widely reported in the press. Old water piping is still a problem as highlighted by the Flint water crisis in 2015. Flint is a city of about 100,000 inhabitants in Michigan which were exposed to excessive lead levels in the municipal water supply. Controversial analytical results were part of the ensuing scandal. Also in 2015 Nestlé had to recall a large number of packages of instant noodles produced in India due to alleged contamination with lead. The company however, disputed the analytical results presented by the authorities [7]. The on-going interest in lead analysis is also reflected by the high rate of publications in the scientific literature concerning the determination of lead in different kinds of samples or the development of new methods, which numbers about 50 per month (as shown by a keyword search on the Web of Science). Most commonly atomic spectroscopic methods are used, which have the required sensitivity for the often relatively low concentrations to be determined. Alternatives based on electrochemical methods such as polarography, or separation methods such as ion-chromatography, capillary electrophoresis or even gas-chromatography exist, but generally tend to be less sensitive than the atomic spectrometric methods and are therefore not routinely employed. Chemical sensors for lead have also been proposed, but tend to lack sufficient specificity. Environmental samples usually require extensive pretreatment before quantification can take place. Specification analysis is sometimes needed for environmental studies and special insights can be gained with isotope analysis.

2. SAMPLING

The most simple sampling procedure applies of course to the collection of aqueous specimens. These usually only need to be acidified to prevent precipitation as $Pb(OH)_2$ during storage. If necessary, filtration is carried out with membrane filters, usually with 0.45 μm pore size. When sampling at depths in water bodies is required, this is achieved with special sampling devices that open at desired

levels. For solid samples, e.g., of soils or sediments, care has to be taken to obtain representative samples. As most quantification methods require the sample to be present in liquid form solid samples usually need to be subjected to dissolution or extraction procedures.

Dissolution is first attempted in acids and often this is carried out aided by addition of energy in the form of heat or microwaves. The use of hydrofluoric acid is required for samples containing silicates and some minerals need to be subjected to fusion procedures (dissolution in molten salts). Plant material may be decomposed with ashing procedures such as combustion in closed containers to avoid sample loss.

For the determination of organolead compounds solvent extraction is used. Besides the classical operation with separating funnels a number of newer methods which are more easily automated and require less solvents are available. Most notable is solid phase extraction (SPE) which is based on cartridges containing solid lipophilic materials which trap analytes when the aqueous sample is passed through. The species of interest are then flushed from the cartridge with a small amount of organic solvent prior to quantification. Many of the new developments have focussed on miniaturization to allow working with smaller sample volumes (a comprehensive overview on extraction methods for organometallic species has been prepared by Moreda-Piñeiro et al. [8]). The extraction procedures do not only separate the analytes from the matrix, but can also be employed to achieve a preconcentration so that the demands on the detection limit of the quantification method is relaxed.

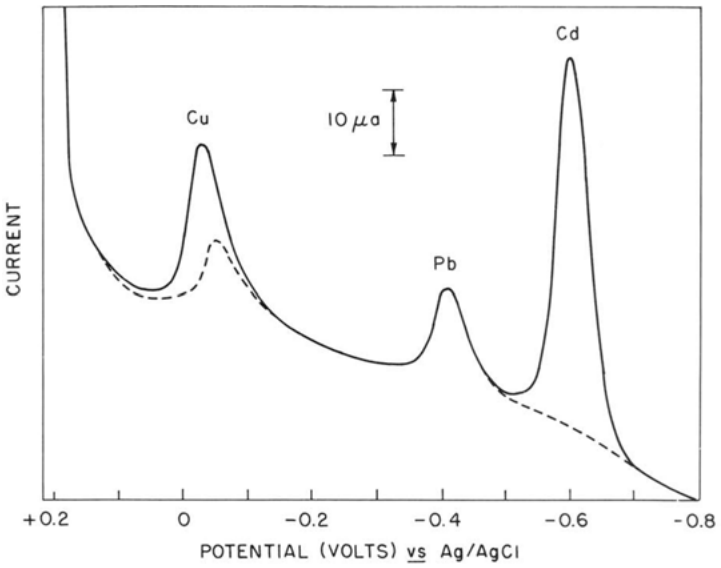

Figure 1. Determination of Pb, besides Cu and Cd, in a sample (solid line) and a blank (broken line) by stripping voltammetry, which gave identical results for Pb due to a contamination of the reagents at approximately 10^{-7} M Pb. Reprinted with permission from G. W. Ewing, *J. Chem. Ed.* **1973**, *50*, p. A131; copyright 1973, American Chemical Society.

As the concentrations of interest are generally at the trace level, proper sampling procedures are essential in order to prevent contamination. This is particularly important when ambient environmental background levels are to be determined. Sampling from boats may need to be carried out from the bow and against the direction of the wind [9]. Containers made from high density polyethylene are generally used for storage, never glass. These have to be subjected to an acid-based precleaning procedure [9]. High purity acids and other reagents have to be employed. For the most demanding applications so-called "electronic" or "semiconductor" grade acids, which are produced for the semiconductor industry, are required. In the laboratory, samples for trace analysis have to be handled on clean benches (under filtered clean air). In the early days of trace metal analysis these requirements were not fully understood and it has been said that much of the environmental data for lead determined prior to about 1975 is not valid due to contamination [10]. This problem is illustrated in Figure 1.

3. SPECTROPHOTOMETRY

Spectrophotometric measurements, i.e., molecular absorption spectrometry, by adding an appropriate color-forming reagent are usually the simplest methods because of the comparatively low cost of the spectrometers. The most common spectrophotometric method employs dithizone as reagent and involves an extraction procedure with an organic solvent in order to achieve selectivity, and quanti-

Figure 2. Test kit for lead as sold in hardware shops.

fication at 520 nm [11]. Simple colorimetric test kits, i.e., methods where a color change is observed by the naked eye, are also available. Such a test kit is shown in Figure 2. These are sold at hardware shops primarily to home owners who wish to test their painting for the presence of lead. They are based on sulfide or rhodizonate as color-forming reagents and contain the reagents in liquid form or are based on a self-contained test device in which a tube containing the reagents is crushed to release the reagents onto a cotton bud which is then used to directly sample the suspected surface.

4. X-RAY FLUORESCENCE

X-ray fluorescence (XRF) [12] has the significant advantage that no sample preparation is necessary, i.e., it is possible to directly analyze solid samples, such as paint and soil. In X-ray fluorescence element-characteristic X-rays are quantified. Excitation is achieved by irradiation with X-rays, hence the name, but it is also possible to employ the gamma rays of a radioactive isotope source such as ^{107}Cd. In one possible method of detection based on semiconductors, namely energy dispersive detection, a spectrum is acquired with a multichannel analyzer which bins the signals according to their peak heights. As can be seen in Figure 3, such instruments can be very compact and battery operated. They are more sensitive and reliable than the colorimetric test kits and this type of instrument is therefore in common use by authorities or companies specializing in remediation of homes or other contaminated sites.

5. ELECTROCHEMICAL METHODS

Several electrochemical methods are available [13], of which polarography has been the most commonly employed technique. This is based on the use of a mercury electrode on which the dissolved analyte ion is reduced. The resulting current is proportional to the concentration. Anodic stripping voltammetry is a technique derived from polarography in which the analyte is first deposited in the metallic form by reduction, followed by re-dissolution by oxidation. The first step leads to an effective preconcentration and the current is measured in the second step. Impressive limits of detection (LOD) in the ppt range are possible employing comparatively simple and inexpensive instruments. Such high sensitivity is otherwise only possible with the much more complex and costly atomic spectroscopic instruments as discussed below. Mercury has generally been employed as electrode material, as the kinetic hindrance of the reduction of water on this metal allows the reduction of heavy metals at negative potentials at which otherwise hydrogen evolution would interfere. Furthermore, the renewal of the electrode surface is readily possible, simply by letting a drop of the liquid metal flow from a capillary. However, due to the toxicity of mercury the method is loosing popularity. The Minamata convention on the ban of the use of mercury

Figure 3. A portable XRF analyzer employed for soil testing. Reprinted with permission; copyright Thermo Fisher Scientific.

signed in 2013 by 128 countries still permits its use in the laboratory, but the use of mercury in polarography has already been banned in Sweden. For this reason alternatives have been extensively researched in recent years. In particular bare or bismuth-coated screen printed carbon electrodes provide a simple replacement. These electrodes can be produced cheaply, so that single use is possible, and are commercially available from several small producers, but have not been adopted widely.

Also possible is the determination of lead ions in solution by potentiometry with ion-selective electrodes. These are either based on crystalline membranes made from pressed PbS or on membranes of plasticized PVC containing an ionophore. Such electrodes have LODs of about 10^{-6} M and are a simple and inexpensive. A special feature of potentiometry with ion-selective electrodes is the fact that only free, but not complexed, lead ions are measured. Careful attention

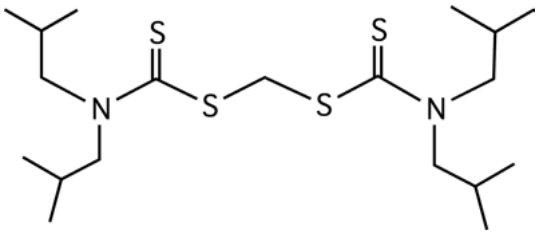

Figure 4. S,S′-Methylenebis(N,N-diisobutyldithiocarbamate), an ionophore for lead employed in ion selective electrodes.

has to be paid to their selectivity, as for example Cd^{2+} is a significant interferent for crystalline membrane-based electrodes. Typical applications are the analysis of plating baths. A commercially available ionophore which selectively binds Pb^{2+} in PVC-based membranes, and thus leads to the creation of an electrode potential in dependence on the lead concentration in the sample solution, is shown in Figure 4.

When the concentrations are high, lead may also be determined by the electrochemical method of electrogravimetry, in which the amount of lead deposited from the sample is determined by weighing, or the related technique of coulometry, where the charge required for complete electrolysis of the lead contained in the sample is determined. Both techniques are relatively time-consuming, and in the case of electrogravimetry it entails significant manual labor, but have the advantage of higher accuracy and precision than other methods.

6. ATOMIC SPECTROSCOPY

Despite their comparatively high cost, most commonly used in practice are the atomic spectroscopic methods. These techniques have very good sensitivity, are robust and are much less prone to interference than most other methods. Atomic absorption spectrometry (AAS) instruments (see Figure 5) are based on absorbance measurements on the free and neutral atoms in the gas phase. The method relies on hollow cathode lamps as light sources, which contain the same metal as the analyte in order to produce matching wavelengths, so that a high reliability is assured. Monochromators are still required to suppress unwanted wavelengths. Most commonly the atomizer consists of a flame into which the samples are introduced as an aerosol. These instruments are widely available. Limits of detection of about 10 ppb are obtained with this method [12]. Lower detection limits of about 0.05 ppb are possible by the more elaborate graphite furnace atomizer, where a small aliquot of the sample is heated electrothermally [12]. A further atomizer variant is the hydride generation technique suitable for elements which form volatile hydrides when sodium borohydride is added to the sample. This is a relatively simple method in that the gaseous hydrides are simply atomized in a resistively heated quartz tube and which generally gives very good

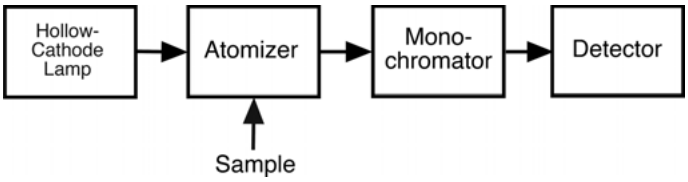

Figure 5. Principle of atomic absorption spectrometry.

detection limits. However the sensitivity of this method for lead, while better than with the most widely used flame AAS, is relatively poor compared to other hydride forming elements such as arsenic [13] with a reported limit of detection for lead of 0.1 ppb [14].

Also common in laboratories for trace analysis of metals are spectrometers employing an inductively coupled plasma (ICP) into which the samples are also introduced as aerosol. These are available in two variants, either based on optical emission spectrometry (ICP-OES) or on mass spectrometry (ICP-MS). The latter is possible as at the high temperature of the plasma (up to about 10,000 °C) the analyte species are not only converted to free elements, but also ionized. These instruments are more expensive in capital outlay and running costs than the AAS instruments, in particular the ICP-MS, but have the advantage of multi-element analysis, in case other analytes besides lead are to be determined. The detection limit for lead obtained with the ICP-OES of about 4 ppm [12] is relatively modest, but with 0.02 ppb excellent for the ICP-MS.

7. SPECIATION

Speciation analysis, i.e., the distinction and quantification of different forms of lead, is important for lead-containing organometallic species. This mainly concerns studies of the environmental fate of the tetraalkyl lead compounds that used to be added to petrol, which was a highly important topic 20–25 years ago but is obviously less relevant now. The main compound which used to be added to petrol was tetraethyl lead, but tetramethyl, and mixed ethyl-methyl compounds were also employed [15]. Their degradation products include singly or doubly charged species such as Et_3Pb^+ and Et_2Pb^{2+}. The speciation of the neutral and charged compounds is generally based on a so-called hyphenated method which combines separation by gas chromatography with sensitive quantification by one of the atomic spectroscopic methods. To allow the separation by gas chromatography the ionic compounds are rendered neutral and volatile by propylation or butylation, rather than methylation or ethylation, to still allow the distinction of all possible species. Hydrogenation is not suitable for this purpose as the dialkyl lead species reportedly do not form hydrides [16].

A different form of speciation analysis is the differentiation between isotopes of lead. This can be achieved by inorganic mass-spectrometry such as ICP-MS. The use of laser ablation ICP-MS or SIMS (secondary ion mass spectrometry)

allows the analysis of small amounts of solid materials. In these methods tiny amounts of sample are vaporized either with high energy laser pulses or by sputtering with an ion beam. Lead has 4 stable isotopes, namely ^{204}Pb, ^{206}Pb, ^{207}Pb, ^{208}Pb. The latter three are the products of the radioactive decay of ^{238}U, ^{235}U, and ^{232}Th, respectively. This means that different sources of lead have different isotopic compositions, which allows the determination of the source of lead samples. A possible application of this is the verification of paintings of the old masters based on the analysis of the white pigment consisting of white lead [17]. Lead isotope analysis is also important in the dating of geological specimens, in the so-called uranium-lead dating method. Due to the long half-lives of the parent elements the determination of the isotopic ratios of the precursor element and the product allows the dating of rocks up to 100s of millions of years old. Often the mineral zircon is employed for this purpose as in its crystallization lead is strongly excluded while uranium is admitted into its crystal structure. Thus, it usually does not contain any naturally occurring lead, but only that produced by the radioactive decay. The determination of both, the ratio of ^{206}Pb/^{238}U and ^{207}Pb/^{235}U, allows a verification of an absence of contamination or loss of either of lead or uranium as both measurements should give identical results.

ABBREVIATIONS

AAS	atomic absorption spectrometry or spectrometer
EPA	Environmental Protection Agency
ICP	inductively-coupled plasma spectrometry or spectrometer
LOD	limit of detection
MS	mass spectrometry or spectrometer
OES	optical emission spectroscopy or spectrometer
PVC	poly(vinyl chloride)
RoHS	restriction of hazardous substances
SIMS	secondary ion mass spectrometry
SPE	solid phase extraction
XRF	X-ray fluorescence

REFERENCES

1. R. Nevin, *Environm. Res.* **2007**, *104*, 315–336.
2. G. Tiravanti, G. Boari, *Environm. Sci. Tech.* **1979**, *13*, 849.
3. M. Branica, Z. Konrad, *Lead in the Marine Environment: Proceedings of the International Experts Discussion on Lead Occurrence, Fate and Pollution in the Marine Environment, Rovinj, Yugoslavia, 18–22 October 1977*, Pergamon, Oxford, 1980.
4. http://content.usatoday.com/news/nation/smelting-lead-contamination, accessed on April 26, 2016.
5. R. Lobinski, C. Witte, F. C. Adams, P. L. Teissedre, J. C. Cabanis, C. F. Boutron, *Nature* **1994**, *370*, 24.

6. http://www.abc.net.au/catalyst/stories/4174798.htm, accessed on April 26, 2016.
7. http://www.nestle.com/ask-nestle/maggi-noodles-india-msg-lead-ban-recall, accessed on April 26, 2016.
8. A. Moreda-Piñeiro, J. Moreda-Piñeiro, P. Bermejo-Barrera, in *Speciation Studies in Soil, Sediment and Environmental Samples*, Ed. S. Bakirdere, CRC Press, Boca Raton, 2014.
9. T. R. Crompton, *Determination of Metals in Natural Waters, Sediments, and Soils*, Elsevier, Amsterdam, 2015.
10. G. Benoit, *Environm. Sci. Tech.* **1994**, *28*, 1987–1991.
11. R. Lobinski, Z. Marczenko, *Spectrochemical Trace Analysis For Metals And Metalloids*, Elsevier, Amsterdam, 1996.
12. R. Jenkins, *X-Ray Fluorescence Spectrometry*, Wiley, New York, 1999.
13. J. A. Plambeck, *Electroanalytical Techniques, Basic Principles and Applications*, Wiley, New York, 1982.
14. J. W. Robinson, *Atomic Spectroscopy*, Marcel Dekker, New York, 1996.
15. B. Welz, M. Sperling, *Atomabsorptionsspektrometrie*, Wiley-VCH, Weinheim, 1997.
16. K. C. Thompson, D. R. Thomerson, *The Analyst* **1974**, *99*, 595–601.
17. R. Lobinski, W. M. R. Dirkx, J. Szpunar-Lobinska, F. C. Adams, *Anal. Chim. Acta* **1994**, *286*, 381–390.
18. J. Szpunar, R. Lobinski, *Hyphenated Techniques in Speciation Analysis*, The Royal Society of Chemistry, Cambridge, 2003.
19. G. Fortunato, A. Ritter, D. Fabian, *The Analyst* **2005**, *130*, 898–906.

4

Smart Capsules for Lead Removal from Industrial Wastewater

Bartosz Tylkowski [1] ***and Renata Jastrząb*** [2]

[1] Centre Tecnològic de la Química de Catalunya, Carrer de Marcel·lí Domingo, ES-43007 Tarragona, Spain
<bartosz.tylkowski@ctqc.org>

[2] Faculty of Chemistry, Adam Mickiewicz University, Umultowska 89b, PL-61-614 Poznan, Poland
<renatad@amu.edu.pl>

Abstract: Ground and especially drinking water could be contaminated by heavy metal ions such as lead and chromium, or the metalloid arsenic, discarded from industrial wastewater. These heavy metal ions are regarded as highly toxic pollutants which could cause a wide range of health problems in case of a long-term accumulation in the body. Thus, there have been many efforts to reduce the concentration of lead ions in effluent wastewater. They have included the establishment of stringent permissible discharge levels and management policies, the

Metal Ions in Life Sciences, Volume 17 Edited by Astrid Sigel, Helmut Sigel, and Roland K. O. Sigel

DOI 10.1515/9783110434330-004

application of various pollution-control technologies, and the development of adsorbent materials for lead reduction. According to *Science* [1] encapsulation, developed approximately 65 years ago, has been defined as a major interdisciplinary research technology. Encapsulation has been used to deliver almost everything from advanced drugs to unique consumer sensory experiences. In this chapter we review the art of encapsulation technology as a potential breakthrough solution for a recyclable removal system for lead ions. Moreover, in order to provide the readers with a comprehensive and in-depth understanding of recent developments and innovative applications in this field, we highlight some remarkable advantages of encapsulation for heavy metal remove, such as simplicity of preparation, applicability for a wide range of selective extractants, large special interfacial area, ability for concentration of metal ions from dilute solutions, and less leakage of harmful components to the environment.

Keywords: alginate · biochar · carbon nanotubes · core-in-hematite shell capsule · encapsulation · industrial wastewater · lead

1. LEAD ION SEPARATION FROM WASTEWATER

Industrial development has always been connected to the growth of civilization, being difficult to imagine a modern society without the benefits of the products and sevices derived from it. Nevertheless, this industralization has led to an overexploitation of natural resources increasing the aquatic enviromental pollution. Amoung such pollutants, heavy metals have received special attention due to their high toxicity or carcinogenicity, long persistence, bioaccumulation in living organisms, and the risk that these substances generate for human health even at low concentration in water. Thus, heavy metal pollution has become one of the most serious enviromental problems today [2].

Lead, a well-known toxic heavy metal, has been widely used in many industrial processes and discharged into water or wastewater systems without proper treatment. Therefore, there have been many efforts to reduce the concentration of lead ions (Pb^{2+}) in effluent wastewater [3]. The efforts have included the establishment of stringent permissible discharge levels and management policies, the application of various pollution-control technologies, and the development of adsorbent materials for lead reduction [4]. Technologies developed or applied in order to remove Pb^{2+} from aqueous solutions include chemical precipitation, electrodialysis, reverse osmosis, adsorption on organic and inorganic materials, aluminium and iron coagulation, electrocoagulation, filtration, ultrafiltration, solvent extraction, ion exchange, and biomass [5, 6].

At low metal concentrations, the practical application of numerous methods can be ineffective, economically unfavorable or technically complicated. Solvent extraction, ion exchange, and zero-valent iron (Fe^0) particles are currently the major industrial-scale techniques used for that purpose. However, they present limitations when applied to aqueous effluent treatments. In the case of solvent extraction, multistage cycles of extraction and back-extraction and the use of organic solvents are required to attain a favorable separation. On the other hand, ion exchange resins have low selectivity in the extraction of metal ions and are highly saturated with ions different to those of interest, thus decreasing the yield. Even highly selective chelating ion exchange resins have slow kinetics in ion

removal [7–9]. In case of using the zero-valent iron particles, nanoscale Fe^0 (NZVI) has been developed, tested and applied as an ideal candidate for *in situ* remediation of metal ions. However, due to the high surface energies and intrinsic magnetic interactions, bare NZVI particles tend to either be oxidized by surrounding media (e.g., dissolved dioxygen) or agglomerated into larger particles in the micro- to millimeter scale or flocs, resulting in loss of surface area, mobility, and reactivity [10]. Furthermore, it is not easy to recycle nanoparticles after application, which requires replenishment of the lost Fe^0 and increases the cost of operation [3, 11].

In order to overcome these limitations, an inexpensive and environmentally friendly adsorbent with high removal efficiency for lead is needed. Considering recent results presented in the literature, encapsulation is one of the smartest, innovative, and breakthrough technologies for lead removal from industrial wastewater. According to Yoshizawa et al. [12] and Zhang et al. [13] encapsulation is a great technique for heavy metal remove/separation, due to some remarkable advantages, such as simplicity of preparation, applicability for a wide range of selective extractants, large special interfacial area, ability for concentration of metal ions from dilute solutions, and less leakage of harmful components to the environment.

2. ENCAPSUALTION TECHNOLOGY

Nanocapsules (10–1000 nm), microcapsules (1–1000 μm), and millicapsules (bigger than 1 mm) are particles which contain an active agent (core, fill, internal phase) surrounded by a coating or shell, as it is shown in Figure 1a [14, 15].

The first encapsulation process was invented in 1953 by Green and Schleicher [16] working in the laboratories of the National Cash Register Company, Dayton, USA, as a way to encapsulate leuco-dyes for carbonless copy paper [17]. Since

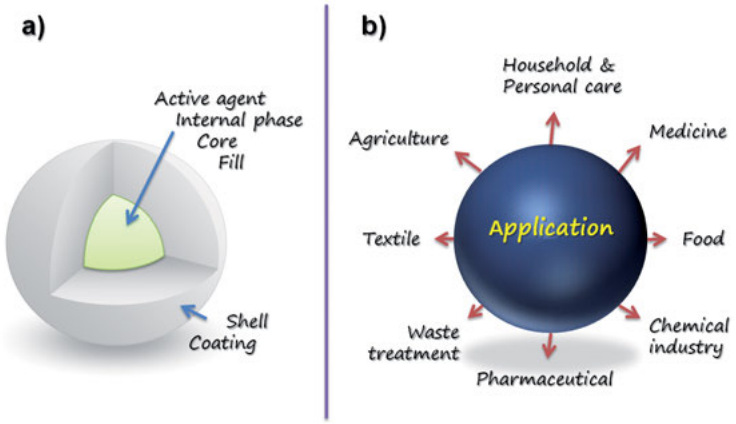

Figure 1. Encapsulation technology capsule scheme (**a**), and capsule applications (**b**).

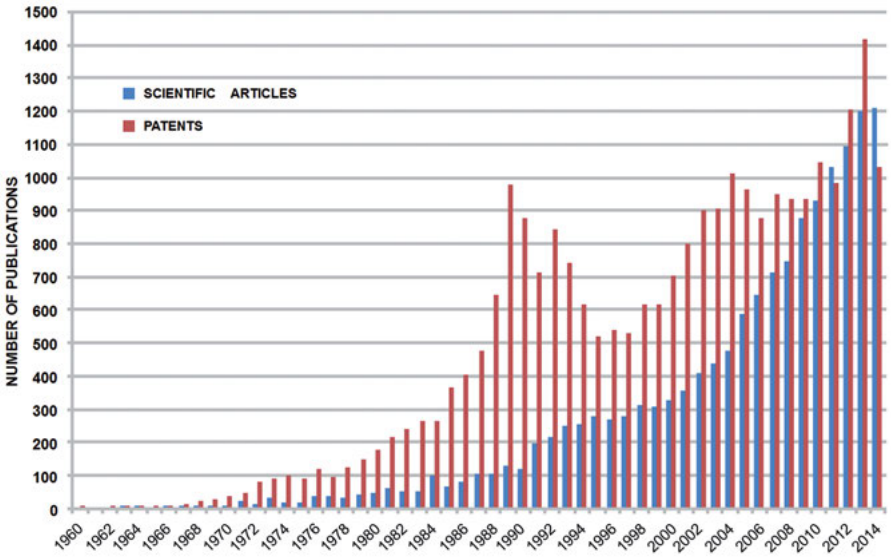

Figure 2. Trends in scientific articles *versus* patent documents on encapsulation. Reproduced with permission from [18], copyright 2015 Walter de Gruyter GmbH, Berlin.

then numerous methods have been investigated for encapsulation of extractants, including *in situ* polymerization, interfacial polymerization, interfacial polycondensation, gelation solvent evaporation, and suspension polymerization. Encapsulation is a knowledge-intensive and dynamic research field with an increasing growth of publications. Trends in patent *versus* non-patent literature on microencapsulation illustrate the growth of basic research (scientific articles), as well as a fast growth of industrial research, represented in waves of patented inventions (Figure 2) [18].

During the last 65 years nano-, micro-, and milli-capsules have been applied in many fields such as medicine, foods, pharmaceuticals, textiles, agriculture, house and personal care products (Figure 1b) [19]. Microcapsules have recently found a new application in the separation and recovery of the following metals: Fe^{2+} [20], Ag^{+} [21], Zn^{2+}, Cu^{2+}, Mn^{2+}, Co^{2+}, and Ni^{2+} [22].

In the following sections we discuss the development and characterization of capsules for lead(II) removal and we demonstrate their outstanding water decontamination efficiency.

3. ALGINATE-BASED CAPSULES

Alginate (alginic acid) is a constituent of brown seaweed and has a characteristic structure that consists of two uronic acids, β-*d*-mannuronic acid and α-*l*-guluronic acid. In the presence of divalent cations, alginic acid forms stable gels as metals

interact ionically with blocks of uronic acid residues, resulting in the formation of a three-dimensional network that is usually described by the 'egg-box' model. According to this model proposed by Morris et al. [23] polyguluronic chains in alginate form electronegative cavities to host divalent cations. In the proposed model, the M^{2+} coordinates in a cavity created by a pair of guluronate sequences along alginate chains where several oxygen atoms are possibly involved in the coordination with the metal cation [24].

The major difficulties in understanding the metal binding of most natural biopolymers, including alginate, results from their (1) polyelectrolytic properties – at circumneutral pH, the carboxylic sites of alginic acid are ionized, thereby creating an electric field which increases complex stability; (2) polyfunctionality – a diversity in the chemical nature and the resulting electronic and steric environment of the coordinating sites; and (3) capacity to change their three-dimensional conformation. The relative importance of each of these effects depends mainly on the physicochemical properties of the external medium including the pH, the ionic strength, and the metal-to-alginate (or metal-to-carboxylic site) ratio. All three effects result in a decreasing metal affinity with increasing metal loading of the biopolymer. Nonetheless, few studies have attempted to separate the effects due to intrinsic chemical binding from the electrostatic or macromolecular (i.e., conformational) contributions. For the most part, metal binding studies have been performed at high metal concentrations (typically mM [25]), in acidic pH (typically between pH 2.0 and pH 4.0 [25]), and at high alginate concentrations (typically between 1 and 5 g L^{-1} [26, 27]). Quantitative information corresponding to low metal-to-alginate ratios, low Pb concentrations, circumneutral pH values, and lower ionic strengths are missing from the literature, despite their obvious environmental and biological relevance.

The conformation of alginate depends on its hydration, the formation of hydrogen bonds or metallic bridges, and the relative proportion of its principal constituents (i.e., β-*d*-mannuronic acid/α-*l*-guluronic acid ratio) [28]. Alginate is by far the most extensively used biopolymer for immobilization and microencapsulation owing to its non-toxicity, biodegradability, ease of usage, and low cost [29, 30]. Particularly, it has a high affinity and binding capacity for metal ions and has already been employed as heavy metal sorbent [31, 32]. Alginate entrapped cells and metal hydroxides have also been used to treat pollutions of heavy metals, organics, and nitrogen compounds [33–35]. As it is described above, the major gelation mechanism in alginate is crosslinking of the polysaccharide carboxyl groups by positively charged metal cations. Thus, alginate may be used to eliminate metal ions from an effluent via two possible mechanisms [36–38]:

- it can serve as the chelating agent itself – in this case the alginate is an active encapsulated agent;
- it can immobilize other types of heavy metal adsorbents – in this case the alginate forms a microcapsule wall.

3.1. Non-crosslinked Alginate Capsules

Recently, Nussinovitch and Dagan [38] from the Hebrew University of Jerusalem, Israel, published a very interesting paper concerning alginate–gellan liquid-core capsules with a non-crosslinked alginate fluidic core surrounded by a gellan membrane for the removal of heavy metal cations from water. The liquid-core capsules are liquids encapsulated in a spherical polymer wall; they have been used in many research fields, including biotechnology, food, and medicine [39].

According to Nussinovitch and Dagan [38], while the literature includes reports of using crosslinked alginate for heavy metal removal, the use of non-crosslinked alginate for Pb^{2+} removal from wastewater has not been mentioned at all. Previously produced liquid-core capsules have consisted mainly of either an alginate membrane or a gellan membrane, but not both together, and the alginate has never been used in its non-crosslinked form. Lim and Sun [40] were the first to describe a method for producing poly-L-lysine–alginate liquid-core microcapsules to encapsulate pancreatic islets. They suspended the cells in a sodium-alginate solution and formed small spherical calcium–alginate beads by crosslinking with calcium ions, and then reacted them with poly-L-lysine to create a poly-L-lysine–alginate membrane around the bead. In the final stage, the bead's core, composed of a calcium-alginate gel, was solubilized, thus forming liquid-core capsules containing cells. Liquid-core capsules with a gellan membrane have also been produced [39]: A mixture of $CaCl_2$, starch and a model drug was dropped into a 0.5 % (w/w) gellan solution. The gellan gel membrane in that case was created by interaction between the gellan solution and the calcium cations that served as the crosslinkers.

As illustrated in Figure 3, Nussinovitch and Dagan [38] fabricated the capsules in a one-step procedure by dropping a mixture of 3 % (w/w) sodium alginate

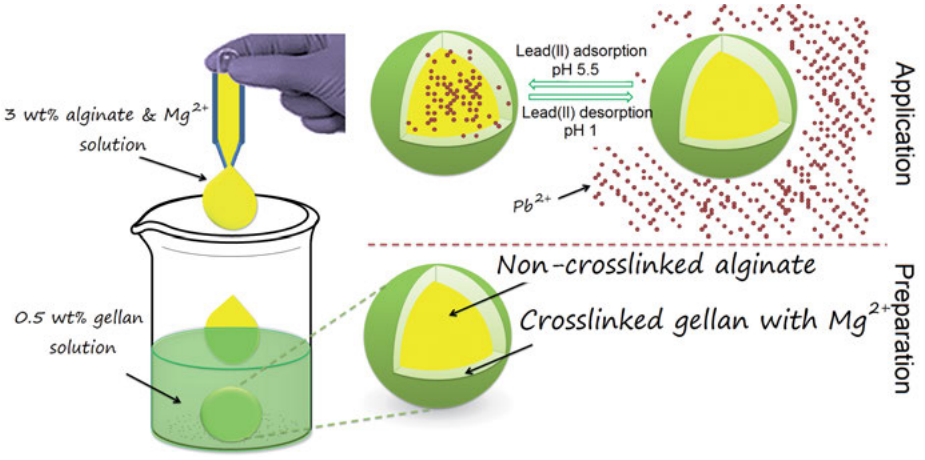

Figure 3. Schematic illustration of the preparation and application of alginate-gellan capsules.

including 5 % (w/w) (0.5 M) $MgCl_2$ salt into a 0.5 % (w/w) gellan solution. The wall of the gellan capsules was formed by reducing the electrostatic repulsion between gellan polysaccharides, allowing the positively charged magnesium to interact with the carboxyl group of the gellan. The authors reported [38] that the obtained capsules were extremely efficient at adsorbing lead cations (267 mg Pb^{2+}/g dry alginate) at 25 °C and pH 5.5. Moreover, the obtained results showed that the metal adsorption by the capsules occurred in two stages:

- the first fast step – during which over 80 % of the Pb^{2+} are adsorbed within the first 60 min (220 mg/g);
- the second slower step – during which the remaining 20 % of the Pb^{2+} are adsorbed over 180 min (47 mg/g) until the maximal lead-cation adsorption was reached.

According to the authors [38], the first adsorption stage included higher concentrations of non-crosslinked gum and lead cations, leading to overly rapid gelling kinetics that favored a spontaneous crosslinking reaction. Later, a slower crosslinking stage occurred due to diffusion via the already formed inner gel, and therefore increased resistance to lead cation diffusion and a slower rate were noted. Similar phenomena have been previously described by Nussinovitch et al. [41] in a publication related to an effect of the hydrocolloid and minerals content on the mechanical properties of alginate gels. Unfortunately, further deep investigations showed that the fabricated alginate–gellan capsules exhibited very poor mechanical properties; they were very weak and brittle. For this reason, in order to improve the mechanical properties of the microcapsules, during the next experiments the authors added surfactant lecithin to the $MgCl_2$/gellan solution. By using this protocol the wall thickness of the microcapsule containing lecithin was reduced as a result of the better wetting ability of the gellan solution due to the reduction in surface tension, resulting in a membrane with less gellan polymer. A similar reduction in capsule wall thickness by the addition of surfactant has been previously reported by Bremond and coworkers [42]. By applying this procedure for the preparation of the alginate–gellan capsules, Nussinovitch and Dagan [38] not only improved their mechanical properties but the capsules also had better adsorption attributes (316 mg Pb^{2+}/g dry alginate *versus* 267 mg Pb^{2+}/g dry alginate without lecithin), most likely due to the thinner membrane and enhanced mass transfer. Additional tests performed by the investigators [38] showed that the alginate–gellan capsules were able to adsorb other heavy metal cations – copper, cadmium, and nickel. Adsorption efficiencies were 219, 197, and 65 mg/g, respectively, and were correlated with the cation's affinity to alginate. In order to investigate the regeneration of the capsules for subsequent reuse, which is of great importance both economically and environmentally, the authors exposed the Pb^{2+}–alginate–gellan capsules to highly concentrated strong acid (HNO_3) for 24 h, in order to replace the adsorbed metal cations with protons. The obtained results demonstrated that the fabricated alginate–gellan capsules could undergo three regeneration cycles before becoming damaged.

3.2. Crosslinked Alginate Capsules

3.2.1. Crosslinked Alginate Capsules Containing a Biochar as the Lead(II) Adsorbent

The research interests of Do and Lee from the University of Ulsan, Republic of Korea, have also been focused on the preparation and characterization of smart capsules based on alginate for lead(II) removal from wastewater [9]. In contrary to Nussinovitch and Dagan, these authors formed biochar–alginate capsules in which the alginate served as a crosslinked polymer to create the microcapsule walls and the biochar as the chelating agent.

Biochar has a large specific surface area, microporous structure, active functional groups, and high pH, which may be good for its use as a surface sorbent [43]. If converted from agricultural residues such as poultry waste, it can have a large adsorption capacity for lead removal from wastewater.

Lu and coworkers [44] evaluated the application potential of biochar as a cost-effective and environment-friendly sorbent material for removing heavy metal

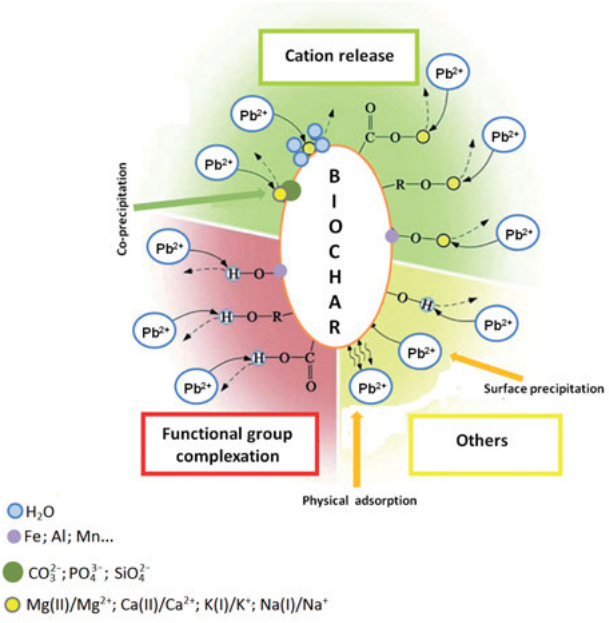

Figure 4. Schematic illustration of the lead adsorption mechanism on biochar including (1) metal exchange with Ca^{2+} and Mg^{2+}, attributing to co-precipitation and innersphere complexation with complexed humic matter and mineral oxides of biochar; (2) surface complexation with free carboxyl and hydroxyl functional groups, and innersphere complexation with the free hydroxyl of mineral oxides and other surface precipitation; (3) others, like innersphere complexation with the free hydroxyl of mineral oxides and other surface precipitation.

ions with Pb^{2+} as the representative, in aqueous solutions at different initial pH values varying from 2.0 to 5.0. The authors comprehensively investigated mechanisms of Pb^{2+} sorption by biochar by using different approaches, including isotherm and kinetics models, desorption studies, and instrumental analysis, such as X-ray diffraction, Fourier transform infrared spectroscopy, and scanning electron microscopy with energy dispersive X-ray spectroscopy. Besides, the authors reported that during the Pb^{2+} sorption, a certain amount of Ca^{2+}, Mg^{2+}, K^{+}, and Na^{+} was released from the biochar, likely due to electrostatic cation exchange, or metal exchange reactions for surface innersphere complex or co-precipitation.

As illustrated in Figure 4, Pb^{2+} sorption may involve the electrostatic attraction, innersphere surface complex formation with free and complexed carboxyl, alcoholic hydroxyl or phenolic hydroxyl groups in humic substances (such as –COOH, –COOM, –R-OH, –R-O-M, where M represents the central metal atoms), or hydroxyl groups on the edges of clay minerals and oxides (such Al/Fe/Mn-OH, Al/Fe/Mn-O-M), as well as co-precipitation or surface precipitation. Some alkali or alkaline earth metals (such as Ca^{2+}, Mg^{2+}, K^{+}, Na^{+}) in the original biochar, retained through electrostatic effects, innersphere complexes with carboxyl and hydroxyl groups as well as precipitation, can be replaced by Pb^{2+} in solution during the sorption process. However, some biochar forms are not sufficient to efficiently remove Pb^{2+}, and it is not easy to collect and recover it in powder form. For this reason, in order to produce the biochar–alginate capsules for Pb^{2+} removal from aqueous solution, Do and Lee [9] have combined the biochar with sodium alginate (Figure 5).

As illustrated in Figure 5, for the preparation of the capsules the authors [9] dropped a solution containing 5 % (w/v) of biochar, 1 % (w/v) of $CaCl_2$, and 0.15 % (w/v) of xanthan gum into a 0.6 % (w/v) of sodium alginate solution containing 0.1 % (v/v) Tween 20 surfactant. During the experiment a magnetic

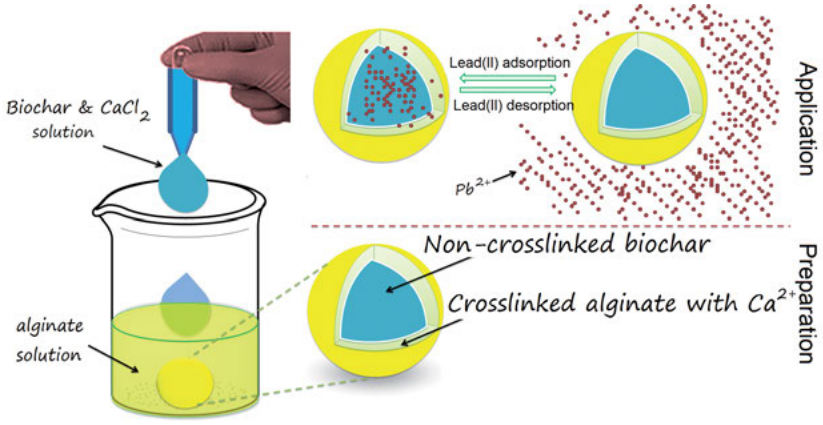

Figure 5. Schematic illustration of the preparation and application of biochar–alginate capsules.

stirrer was used in order to avoid aggregation of the prepared capsules, as well as the xanthan gum Tween 20 was used to create clean spherical capsules.

The surface morphology of the biochar–alginate capsule was studied by the authors [9] using scanning electron microscopy, and their specific surface areas were measured using a Brunauer–Emmett–Teller analyzer. Reported results showed that the obtained capsules were almost spherical in shape with a diameter of 3 ± 0.2 mm and with a surface area of the capsules, of 314.54 m^2/g. This high surface area of the biochar–alginate capsules permits adsorption of a large amount of contaminant and leads to a high adsorption capacity of Pb^{2+} from aqueous solution. Indeed, the authors reported that 236 mg of Pb^{2+} was adsorbed from the water solution by 1g of the capsules during 120 min at pH 5.

The presented results have similar values as those reported by Nussinovitch and Dagan [38] about the alginate–gellan without lecithin capsules (236 mg Pb^{2+}/g dry capsules); however, it is important to mention that the capsules produced by Do and Lee [9] contain biochar as adsorbent, which is cheaper than the alginate-adsorbent gel used by Nussinovitch and Dagan [38]. The regeneration performance determined by analyzing the Pb^{2+} desorption capacity of the Pb-loaded biochar–alginate capsules after the removal of lead(II) cations by adsorption showed that the capsules can be reused up to 10 times [9]. The biochar–alginate capsules maintained almost 70 % of the initial adsorption capacity even after being regenerated 10 times, while the capsules obtained by Nussinovitch and Dagan could be regenerated only 3 times [38]. When the low costs needed to develop the biochar–alginate capsules and the high regeneration feasibility of the adsorbent capsules are taken into consideration, the biochar–alginate capsules are expected to have extensive applicability for the treatment of lead-contaminated water as a low-cost adsorbent that effectively removes Pb^{2+} ions.

3.2.2. Crosslinked Alginate Capsules Containing Zero-valent Iron Particles as the Lead(II) Adsorbent

Another excellent example of microcapsule shells formed by the crosslinked alginate for lead(II) removal was reported by the research group of J. D. Gu from the University of Hong Kong, China [45]. The authors have developed a new type of microcapsule spheres based on an alginate-crosslinked polymer in which NZVI − as an active chelating agent − were immobilized (Figure 6).

During this study, the researchers controlled both the size and shape of microcapsules by a water/oil microemulsion system. The investigators reported that the spherical M-NZVIs had particle diameters, which varied from several hundred nanometers to several micrometers. By using Fourier transform infrared spectroscopy, the authors [45] were able to indicate that alginate adsorbed onto NZVI via both carboxyl groups and oxygen atoms to form bindings. Moreover, due to the protection of alginate, the M-NZVI had good stability against oxidation. Under the conditions of 0.5 g L^{-1} of M–NZVI, 88 % of Pb(II) was removed from a solution containing 300.0 mg L^{-1} of Pb(II). The removal of Pb(II) was found to be closely related to the solution pH, and the optimal solution pH

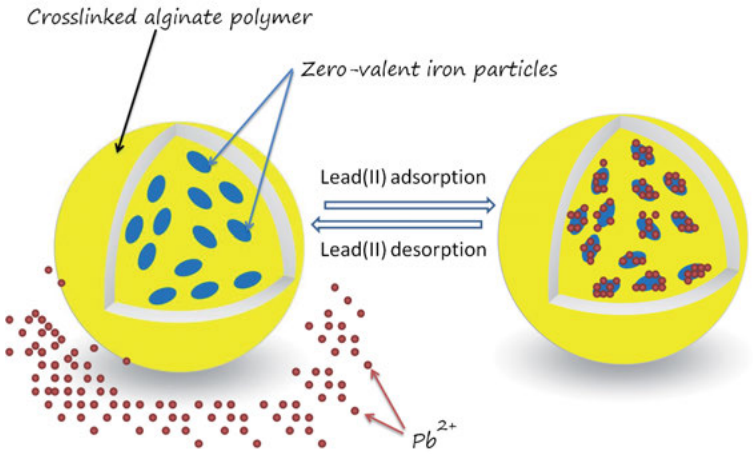

Figure 6. Schematic illustration of alginate–zero-valent iron capsules.

range was determined to be between 4.0–6.0. According to published data, the M-NZVI could be reused at least 4 times when the initial concentration of Pb(II) is below 200.0 mg L^{-1}. The results reported by Luo and coworkers [45] are very useful for further design and improvement of efficient treatment processes for the removal of Pb(II) from wastewater and source water. In addition, successful encapsulation of N-ZVI is expected to lead to the development of more effective and robust environmental remediation technologies, involving co-encapsulation of nanoparticles, microorganisms, and/or enzymes.

4. CARBON NANOTUBES CORE-IN-HEMATITE CAPSULES

As mentioned above, among various candidates, hierarchically structured metal oxide materials have been widely used as removal agents for various heavy metal ions and their removal capacity was found to be relatively reliable. In the case of metal oxide species, the removal mechanism for heavy metal ions is thought to be the formation of a strong bond between metal ions and metal oxide surfaces. This strong complex formation is advantageous for complete removal of heavy metal ions but it presents a drawback if one wants to design a reusable agent by reviving the reaction site for heavy metal ions. Precisely, because the removal mechanism is based on strong complex formation between metal ions and oxide surfaces, recycling of these removal agents has proved to be difficult. It still remains a great challenge to regenerate the active surface after a metal ion complexion reaction. If one could build a recyclable agent for removal of heavy metal ions this would be a very beneficial way to reduce the cost for purification of water and an environment-friendly way for using the material at the same time. Offering a potential solution, Choi and coworkers [46] demonstrated a recyclable removal agent for lead(II) ions by fabricating a core-in-shell

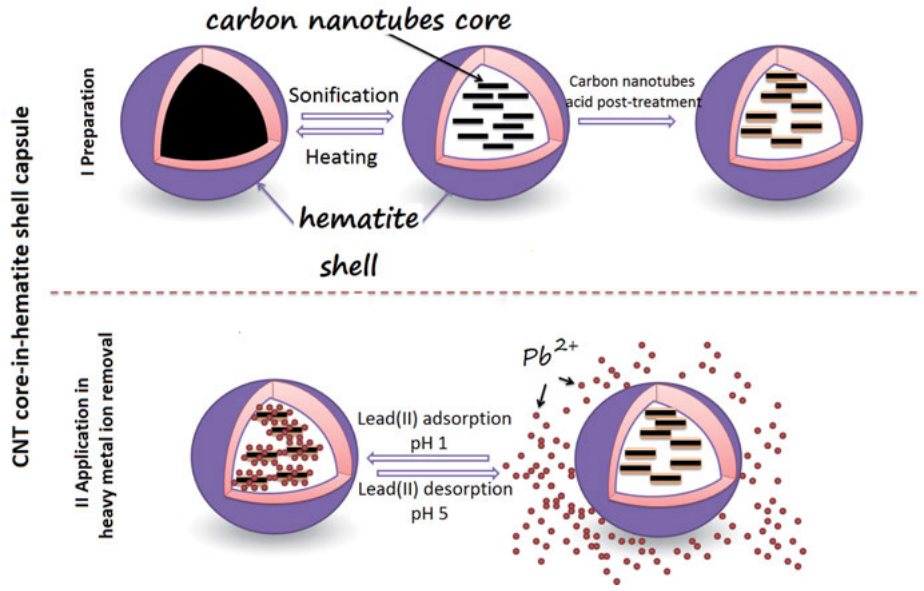

Figure 7. Schematic illustration of the preparation and application of carbon nanotube core-in-hematite capsules.

structure based on a core of carbon nanotubes (CNT) and an iron oxide (hematite) microcapsule structure (shell) – a structure they refer to as CNT core-in-hematite shell capsule (Figure 7).

Since their discovery in 1991, CNTs have been the subject of extensive research due to their unique structure-dependent properties [47]. CNTs have been widely investigated for use in various fields including composites, electrochemical devices, field-emission devices, and nanoscale electronic devices [48–50]. For advanced applications, functionalization and assembly of CNTs into desired nanostructures are priorities. As one of the novel assembly techniques for CNTs, a CNT-based hollow capsule structure has been the subject of extensive research in recent years. There are a number of methods for integration of CNTs into a capsule structure. These include non-covalent self-assembly of CNTs, or the use of a sacrificial template such as polymer colloids or emulsions [51]. Such systems open up new ways to assemble CNTs for the creation of more complicated structures. However, real applications of these CNT-based capsules have not been reported. Recently, core-in-shell capsule structures equipped with a solid core in their cavity have attracted considerable attention as a new class of hierarchically structured materials due to their unique structure, which is characterized by an interstitial space between the core and shell. These structures have great potential for application in various fields including chemical reactors, chemical sensors, catalysts, batteries, drug carriers, and encapsulation. Because the possibility of such applications is due to the cores within the capsules, control of both the properties (functionalization) and structure of core materials is also of interest for many applications.

By unsing a layer-by-layer technique, Choi and coworkers [46] fabricated hematite (α-Fe_2O_3) microcapsules, whose average sizes of the CNT core and hematite shell were 290 and 980 nm, respectively; however, according to the authors, the size could be controlled by changing the species of CNT. The authors reported that the individual CNTs conglomerated and formed a core inside the capsule upon exposure to high temperature (approximately 600 °C), while they scattered when subjected to mild sonication at low pH 1. It is important to underline that when the same calcination process was carried out by the researchers on the particles with CNT layers without an iron oxide shell, conglomerates of CNTs did not form. According to Choi et al. [46] this result suggests that the presence of a robust, spherical outer shell was crucial for the successful formation of CNT cores. Moreover the authors discovered that the assembly/disassembly of CNTs within the capsule was reversible and could be repeated by alternate heating and sonication.

In order to demonstrate the feasibility of using the capsules for lead(II) removal from wastewater, the researchers first performed acid post-treatment of the carbon nanotubes because most of the functional groups on the capsules became chemically inert after calcination, and then they dispersed them in Pb^{2+} aqueous solution. The results obtained showed that most of the lead ions were rapidly removed within 10 min when the CNT core-in-hematite shell capsules were added to the lead(II) ion solution. The removal capacity was 46.6 mg/g. According to the authors this Pb^{2+} removal by CNT core-in-hematite shell capsules was attributed to the high surface area of the CNTs. To confirm this hypothesis, the authors performed additional experiments, in which CNT core-only structures were prepared by dissolution of the hematite capsule and exposure to metal ion solutions at identical concentrations. The surface areas of the CNT core-only structures were lower than those of the CNT core-in-hematite capsule (98 ± 2 and $125 \pm 1\ m^2/g$ for the former and latter, respectively). Thus, the CNT cores in hematite capsules had a greater chance to adsorb Pb^{2+} ions than the core-only structures. Indeed, the removal ability of the CNT core particles without hematite shells was not impressive due to the decrease in the CNT surface areas that resulted from massive aggregation of each CNT core. Reported results indicated that the hematite shell of core-in-shell structures prevents aggregation and outflow of CNTs, thus enhancing the ability to remove lead(II) ions using an environmentally friendly method.

Construction of a recyclable agent for the removal of heavy metal ions should involve reversible desorption of adsorbed metal ions by external stimuli. To investigate the desorption abilities of studied core-in-shell capsules, Choi and coworkers [46] measured the concentration of lead(II) ions released from the capsules at various pH values (1–5). The authors demonstrated that in the case of hematite capsules with CNT cores, the adsorbed lead ions were easily desorbed from the capsules within a short period of time at low pH. Thus, the capsules showed excellent removal ability and recyclability having also use for many potential applications including chemical sensors, microreactors, catalysts, and drug carriers.

5. POLYMER SWELLING CAPSULES

The research group of Chu from the School of Chemical Engineering at the Sichuan University, China, has developed novel smart responsive microcapsules capable to recognize Pb^{2+} ions and self-regulatively they adjust their conformation of the wall material [52]. By using an oil-in-water-in-oil double emulsion method, the authors prepared crosslinked poly(*N*-isopropylacrylamide-*co*-benzo-18-crown-6-acrylamide) (P(NIPAM-*co*-BCAm)) microcapsules (Figure 8).

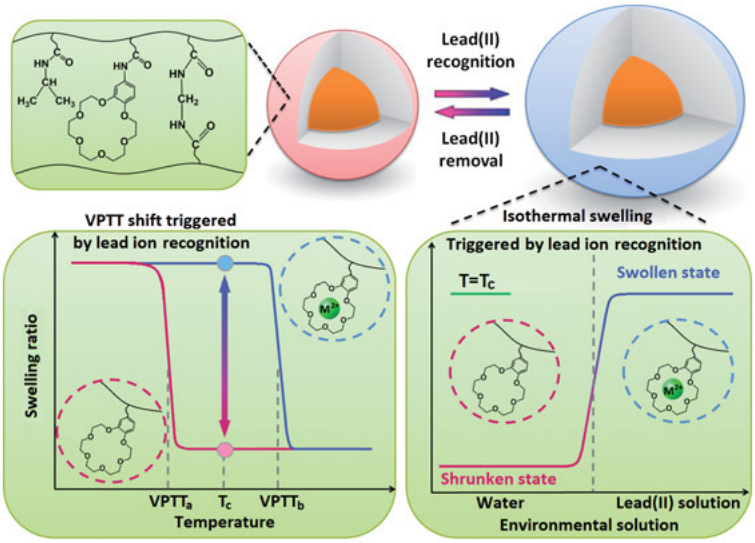

Figure 8. Schematic illustration of the proposed lead ion-recognizable smart microcapsules with a crosslinked P(NIPAM-*co*-BCAm) wall. The volume phase transition temperature (VPTT) of the P(NIPAM-*co*-BCAm) microcapsule shifts from $VPTT_a$ to $VPTT_b$ when the crown ether unit in the P(NIPAM-*co*-BCAm) wall recognizes Pb^{2+} ions. When the environmental temperature (T_c) is located between $VPTT_a$ and $VPTT_b$, the proposed microcapsule exhibits an isothermal and significant swelling by recognizing Pb^{2+} ions and a reversible shrinking by removing the lead ion from the crown ether.

As schematically illustrated in Figure 8, the wall of the proposed microcapsule was made of a crosslinked P(NIPAM-*co*-BCAm) hydrogel, in which the ion-recognizable crown ether 18-crown-6 (18C6) serves as an ion signal-sensing receptor and the thermo-responsive poly(*N*-isopropylacrylamide) (PNIPAM) acts as an actuator. The crown ether 18C6 is a well-known host molecule in supramolecular "host–guest" systems to selectively recognize potassium ion by forming a stable "host–guest" complex. It has been reported that when the pendant 18-crown-6 receptors capture specific ions such as K^+, the lower critical solution temperature of the linear P(NIPAM-*co*-B18C6Am) copolymers shift to higher

temperature due to the enhancement of hydrophilicity of the copolymer when specific ions are captured [53–55].

Moreover, it has been reported that the grafted P(NIPAM-*co*-B18C6Am) copolymers and crosslinked P(NIPAM-*co*-B18C6Am) hydrogels could respond more significantly by recognizing some heavy metal ions such as lead(II) [56, 57] than by recognizing potassium ions. When the BCAm receptors in the crosslinked P(NIPAM-*co*-BCAm) hydrogels or microgels capture lead(II) ions [57], the volume phase transition temperature (VPTT) of crosslinked P(NIPAM-*co*-BCAm) hydrogels or microgels shifts from a lower value ($VPTT_a$ in Figure 8) to a higher one ($VPTT_b$ in Figure 8). As a result, when the environmental temperature (T_c in Figure 8) is located between $VPTT_a$ and $VPTT_b$, the proposed microcapsules could exhibit isothermal and significant swelling by recognizing special heavy metal ions such as lead(II) ions, and reversible shrinking by removing the heavy metal ions from the crown ethers.

Pi and coworkers [52] reported that by recognizing special heavy metal ions, the microcapsule illustrated in Figure 8 exhibits an isothermal and significant swelling, i.e., the crosslinked polymeric network of the microcapsule membrane changes isothermally from a shrunken state to a swollen state. As a result, the permeability of substances diffusing through the microcapsule membrane increases. Such a self-regulated smart conformational change behavior triggered by ion recognition is reversible. The authors have investigated lead(II) as the model heavy metal ion, and sodium, potassium, and calcium ions as reference ions because they are important for chemical signals in biomembranes. The obtained results clearly demonstrate that developed microcapsules can selectively recognize lead(II) ions very well by the BCAm units in the P(NIPAM-*co*-BCAm) membranes, but they cannot recognize either sodium, potassium or calcium ions selectively. The stable "host–guest" BCAm/Pb^{2+} complexes in the P(NIPAM-*co*-BCAm) membrane cause a positive shift of the VPTT of crosslinked P(NIPAM-*co*-BCAm) hydrogel to a higher temperature, and the repulsion among the charged BCAm/Pb^{2+} complexes and the osmotic pressure within the P(NIPAM-*co*-BCAm) walls results in the swelling of the microcapsules.

6. GENERAL CONCLUSIONS

Numerous materials are in various stages of research and development, each possessing unique functionalities that are potentially applicable to the remediation of industrial wastewater, groundwater, surface water, and drinking water. The main goal for most of these investigations is to develop low-cost and environmentally friendly materials for removal of heavy metals from water. To date, smart capsules are widely explored in China as support for highly efficient adsorbents for lead(II) removal from water/wastewater. Encapsulation is a great technique for heavy metal removal/separation and exhibits various advantages: simplicity of preparation, applicability for a wide range of selective extractants, a large special interfacial area, the ability for concentration of metal ions from dilute solutions, and less leakage of harmful components to the environment.

Nevertheless, to further promote the practical application of capsules in the abatement of heavy metal pollution, there still exist some technical bottlenecks which need to be solved. For instance, new cheap polymers for microcapsule walls have to be developed. In addition, how to separate the exhausted capsules from water/wastewater efficiently and at a low cost still remains an interesting but challenging task.

ACKNOWLEDGMENTS

Financial support from European Community's Seventh Framework Programme (FP/2007–2013) under the Individual Outgoing Marie Curie Grant agreement no. 328794, and the Incoming Tecniospring Marie Curie Actions (COFUND) Grant agreement no. TECSPR15-1-044 are gratefully acknowledged by BT.

ABBREVIATIONS AND DEFINITIONS

18C6	18-crown-6 ether
BCAm	benzo-18-crown-6-acrylamide
CNT	carbon nanotube
M-NZVI	nanoscale zero-valent iron particles
NZVI	nanoscale zero-valent iron
P(NIPAM-*co*-BCAm)	poly(*N*-isopropylacrylamide-*co*-benzo-18-crown-6-acrylamide)
PNIPAM	poly(*N*-isopropylacrylamide)
VPTT	volume phase transition temperature

REFERENCES

1. J. Zhang, R. J. Coulston, S. T. Jones, J. Geng, O. A. Scherman, C. Abell, *Science* **2012**, *335*, 690–694.
2. S. K. Srivastava, M. Guix, O. G. Schmidt, *Nano Lett.* **2016**, *16*, 817–821.
3. A. Heidari, H. Younesi, Z. Mehraban, H. Heikkinen, *Int. J. Biol. Macromol.* **2013**, *61*, 251–263.
4. J. Goel, K. Kadirvelu, C. Rajagopal, V. K. Garg, *J. Hazard. Mater.* **2005**, *125*, 211–220.
5. Y. Qi, M. Jiang, Y.-L. Cui, L. Zhao, X. Zhou, *Nanoscale Res. Lett.* **2015**, *10*, 408.
6. O. S. Amuda, A. A. Giwa, I. A. Bello, *Biochem. Eng. J.* **2007**, *36*, 174–181.
7. H. Lu, W. Zhang, Y. Yang, X. Huang, S. Wang, R. Qiu, *Water Res.* **2012**, *46*, 854–862.
8. S. Lacour, J. C. Bollinger, B. Serpaud, P. Chantron, R. Arcos, *Anal. Chim. Acta* **2001**, *428*, 121–132.
9. X.-H. Do, B.-K. Lee, *J. Environ. Manag.* **2013**, *131*, 375–382.
10. F. He, D. Zhao, *Environ. Sci. Technol.* **2005**, *39*, 3314–3320.
11. S. Venkateswarlu, M. Yoon, *ACS Appl. Mat. Interfaces* **2015**, *7*, 25362–25372.

12. H. Yoshizawa, Y. Uemura, Y. Kawano, Y. Hatate, *J. Chem. Eng. Jpn.* **1993**, *26*, 198–204.
13. L. Zhang, D. Wu, B. Zhu, Y. Yang, L. Wang, *J. Chem. Eng. Data* **2011**, *56*, 2280–2289.
14. B. Tylkowski, M. Pregowska, E. Jamowska, R. Garcia-Valls, M. Giamberini, *Eur. Polym. J.* **2009**, *45*, 1420–1432.
15. K. B. d. S. Lobato, K. Paese, J. C. Forgearini, S. S. Guterres, A. Jablonski, A. d. O. Rios, *Food Chem.* **2013**, *141*, 3906–3912.
16. B. Green, L. Schleicher, *Manifold Record Material*, in *http://www.freepatentsonline.com/2730456.html*, Ed. NCRCO, United States, 1956.
17. L. Marteaux, in *Microencapsulation Innovative Applications*, Eds M. Giamberini, S. Fernandez Prieto, B. Tylkowski, DeGruyter, Berlin, 2015, pp. 187–216.
18. B. Boh Podgornik, M. Starešinič, in *Microencapsulation Innovative Applications*, Eds M. Giamberini, S. Fernandez Prieto, B. Tylkowski, DeGruyter, Berlin, 2015, pp. 37–69.
19. M. Giamberini, S. Fernandez Prieto, B. Tylkowski, *Microencapsulation, Innovative Applications*, DeGruyter, Berlin, 2015, pp 220.
20. B. Ding, X. Zhang, K. Hayat, S. Xia, C. Jia, M. Xie, C. Liu, *J. Food Eng.* **2011**, *102*, 202–208.
21. M. Outokesh, Y. Niibori, H. Mimura, S. J. Ahmadi, *Ind. Eng. Chem. Res.* **2008**, *47*, 6742–6752.
22. K. Radhakrishnan, L. Sethuraman, R. Panjanathan, A. Natarajan, V. Solaiappan, W. R. Thilagaraj, *Desalination and Water Treatment* **2016**, *57*, 3572–3587.
23. E. R. Morris, D. A. Rees, D. Thom, J. Boyd, *Carbohydr. Res.* **1978**, *66*, 145–154.
24. S. K. Papageorgiou, E. P. Kouvelos, E. P. Favvas, A. A. Sapalidis, G. E. Romanos, F. K. Katsaros, *Carbohydr. Res.* **2010**, *345*, 469–473.
25. M. Fukushima, K. Tatsumi, S. Wada, *Anal. Sci.* **2001**, *17*, 663–666.
26. P. Lodeiro, B. Cordero, Z. Grille, R. Herrero, M. E. Sastre de Vicente, *Biotechnol. Bioeng.* **2004**, *88*, 237–247.
27. O. Raize, Y. Argaman, S. Yannai, *Biotechnol. Bioeng.* **2004**, *87*, 451–458.
28. C. Lamelas, F. Avaltroni, M. Benedetti, K. J. Wilkinson, V. I. Slaveykova, *Biomacromolecules* **2005**, *6*, 2756–2764.
29. D.-G. Ahn, J. Lee, S.-Y. Park, Y.-J. Kwark, K. Y. Lee, *ACS Appl. Mater. Interfaces* **2014**, *6*, 22069–22077.
30. M. C. Jonathan, G. Bosch, H. A. Schols, H. Gruppen, *J. Agric. Food. Chem.* **2013**, *61*, 553–560.
31. C. Gok, S. Aytas, *J. Hazard. Mater.* **2009**, *168*, 369–375.
32. S.-F. Lim, Y.-M. Zheng, S.-W. Zou, J. P. Chen, *Environ. Sci. Technol.* **2008**, *42*, 2551–2556.
33. C. Escudero, N. Fiol, I. Villaescusa, J.-C. Bollinger, *J. Hazard. Mater.* **2009**, *164*, 533–541.
34. S. Önal, Ş. H. Baysal, G. Ozdemir, *J. Hazard. Mater.* **2007**, *146*, 417–420.
35. S. L. Zala, J. Ayyer, A. J. Desai, *World J. Microbiol. Biotechnol. 20*, 661–665.
36. W. Plazinski, *Environ. Sci. Pollut. Res.* **2012**, *19*, 3516–3524.
37. Y.-L. Lai, M. Thirumavalavan, J.-F. Lee, *Toxicol. Environ. Chem.* **2010**, *92*, 697–705.
38. A. Nussinovitch, O. Dagan, *J. Hazard. Mater.* **2015**, *299*, 122–131.
39. A. Schützendübel, A. Polle, *J. Exp. Bot.* **2002**, *53*, 1351–1365.
40. F. Lim, A. M. Sun, *Science* **1980**, *210*, 908–910.
41. A. Nussinovitch, I. J. Kopelman, S. Mizrahi, *Food Hydrocolloids* **1990**, *4*, 257–265.
42. N. Bremond, E. Santanach-Carreras, L. Y. Chu, J. Bibette, *Soft Matter* **2010**, *6*, 2484–2488.
43. J. Paul Chen, M. Lin, *Water Res.* **2001**, *35*, 2385–2394.

44. H. Lu, W. Zhang, Y. Yang, X. Huang, S. Wang, R. Qiu, *Water Res.* **2012**, *46*, 854–862.
45. S. Luo, T. Lu, L. Peng, J. Shao, Q. Zeng, J.-D. Gu, *J. Mater. Chem. A* **2014**, *2*, 15463–15472.
46. W. S. Choi, H. M. Yang, H. Y. Koo, H.-J. Lee, Y. B. Lee, T. S. Bae, I. C. Jeon, *Adv. Funct. Mater.* **2010**, *20*, 820–825.
47. S. Iijima, *Nature* **1991**, *354*, 56–58.
48. R. H. Baughman, *Science* **2000**, *290*, 1310–1311.
49. M. Daniel, S. Leland, S. Kyeong-Sik, C. Chi On, D. Bruce, *Translat. Mater. Res.* **2015**, *2*, 015001.
50. A. Bachtold, P. Hadley, T. Nakanishi, C. Dekker, *Science* **2001**, *294*, 1317–1320.
51. M. Sano, A. Kamino, J. Okamura, S. Shinkai, *Nano Lett.* **2002**, *2*, 531–533.
52. S.-W. Pi, X.-J. Ju, H.-G. Wu, R. Xie, L.-Y. Chu, *J. Colloid Interface Sci.* **2010**, *349*, 512–518.
53. M. Irie, Y. Misumi, T. Tanaka, *Polymer* **1993**, *34*, 4531–4535.
54. Z. Liu, X. J. Ju, Y. H. Huang, R. Xie, W. Wang, K. R. Lee, L. Y. Chu, *J. Membrane Sci.* **2016**, *497*, 328–338.
55. H. R. Yu, J. Q. Hu, X. H. Lu, X. J. Ju, Z. Liu, R. Xie, W. Wang, L. Y. Chu, *J. Phys. Chem. B* **2015**, *119*, 1696–1705.
56. T. Ito, T. Hioki, T. Yamaguchi, T. Shinbo, S. I. Nakao, S. Kimura, *J. Am. Chem. Soc.* **2002**, *124*, 7840–7846.
57. X. J. Ju, S. B. Zhang, M. Y. Zhou, R. Xie, L. Yang, L. Y. Chu, *J. Hazard. Mater.* **2009**, *167*, 114–118.

5

Lead Speciation in Microorganisms

Theodora J. Stewart

King's College London, Division of Diabetes and Nutritional Sciences,
Franklin-Wilkins Bldg., 150 Stamford St., London SE1 9NH, UK
<theodora.stewart@kcl.ac.uk>

Metal Ions in Life Sciences, Volume 17 Edited by Astrid Sigel, Helmut Sigel, and Roland K. O. Sigel

DOI 10.1515/9783110434330-005

Abstract: The biogeochemical cycles of lead (Pb) have been largely affected by anthropogenic activities as a result of its high natural abundance and use over the centuries [1]. At sites more strongly impacted by urbanization [2] and mining [3], Pb is found at high nano to low micromolar concentrations in surface waters, and can be significantly higher in soil and sediment [4]. Microorganisms are found everywhere and their responses to Pb exposure can range from resistant to highly sensitive [5, 6]. These varying levels of toxicity can be attributed to the cellular handling of Pb, making it important to understand the role of intracellular Pb speciation for more accurate toxicity predictions.

Keywords: detoxification · intracellular speciation · lead · metal speciation · microorganisms

1. INTRODUCTION

1.1. A Shift from Extra- to Intracellular Metal Speciation

Over 40 years ago, Zitko et al. were one of the first to demonstrate that the external free metal ion was a better predictor of metal toxicity in an organism than the total dissolved concentration [7]. This seemingly simple observation highlighted the importance of metal speciation. As a result of decades of scientific work, we now have a large data set relating to metal complexation equilibria [8]. These results helped form conceptual equilibrium-based metal speciation models, such as the Free Ion Activity Model (FIAM) [9] and subsequently the Biotic Ligand Model (BLM) [10].

However, this great scientific effort has also revealed the complexity in predicting metal toxicity from *external* metal speciation. Species-specific responses occur in part from different intracellular detoxification mechanisms and toxic modes of action [11]. In many metal toxicity studies a target binding site on the surface of an organism is considered. However, to more accurately predict metal toxicity, we must proceed further and consider subcellular targets. To which biomolecules are metals bound? Where are they localized? What are the molecular mechanisms behind disruption of vital cellular processes leading to measured effects? As eloquently expressed by Lucia Banci and the late Ivano Bertini, the question remains if we can ultimately place the correct metal, with the correct biomolecule, in the correct subcellular location, at the correct time [12]. This seemingly simple idea is clearly a non-trivial task, but one with immense scientific significance and one that requires a shift of focus from *extracellular* to *intracellular* metal speciation.

1.2. Intracellular Metal Speciation

Metal speciation within the cell is ultimately a question of identifying to which ligand or biomolecule a metal is bound, which includes determining a metals

valence or spin state. Under certain circumstances, information on the oxidation state for redox active metals or the local chemical environment surrounding a metal at the atomic scale for non-redox active metals may suffice, depending on the scientific question. However, often identification of the metal complexing ligand or of entire biomolecules is desired, requiring a host of complimentary methods. It is important to note that the subcellular localization of a metal alone should not be considered metal speciation and rather falls under the category of subcellular metal distribution. Although subcellular metal distribution itself does not provide direct information on speciation, the ability to localize specific metal species is invaluable when addressing the role of metal chemistry in cellular processes.

Pb can form strong complexes through coordination with both oxygen and sulfur [13] originating from both inorganic and organic ligands. For microorganisms, these species include oxides, polyphosphates, sulfides, and mercaptans, both originating from small peptides and larger proteins. The Pb^{2+} ion is the biologically active form normally accumulated. However, as discussed below, certain microorganisms appear to biotransform Pb^{2+} into volatile methylated compounds.

Intracellular metal species determine their biological effects. This concept holds true for both essential and non-essential metals in all organisms. In the case of non-essential metals like Pb, effects typically correspond to the total intracellular metal content: the greater the metal uptake, the greater the adverse biological effect. However, the threshold amount that an organism accumulates before such effects are observed for a given biological endpoint can vary greatly between species. The types of intracellular Pb species, their relative amounts, subcellular localization and even temporal dynamics are important factors. Therefore, to gain a greater mechanistic understanding of detoxification processes and toxic modes of action at the sub-cellular level, quantification and localization of specific Pb species is critical.

In this chapter, techniques for the speciation of metals at the atomic and molecular scales are introduced, as well as for the localization of specific metal species. Although many associate microorganisms with prokaryotes, intracellular Pb speciation is discussed for a range of microorganisms that include bacteria, fungi and algae within the context of detoxification strategies. The chapter is concluded with extending the discussion to future trends in intracellular metal speciation determination for a better integration of intracellular metal speciation and biological effects.

2. INTRACELLULAR METAL SPECIATION TECHNIQUES

The identification, quantification, and localization of specific non-essential metal species within a cell are challenging. Non-essential metals can be present in low amounts, which can be an analytical obstacle with respect to limits of detection. To overcome this limitation, intracellular contents can be extracted, isolated and concentrated to identify and quantify metal complexes. Because this process in-

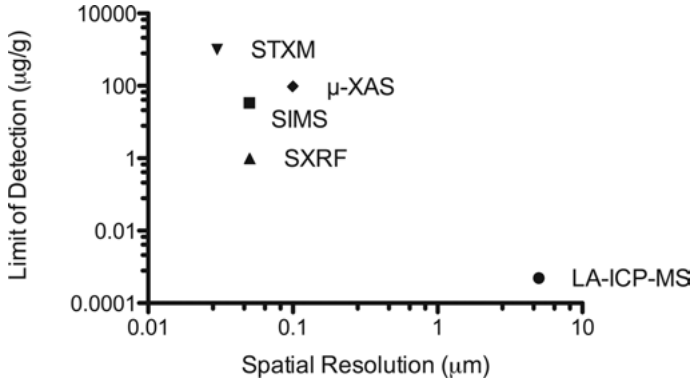

Figure 1. Comparison of metal speciation techniques as a function of detection limit and spatial resolution. Values taken from [25] and [38] are approximations, as detection limits are dictated by metal and beam line optics for synchrotron-based techniques.

volves the physical disruption of an organism, one must be aware of the potential redistribution of metals. Techniques should be metal-specific, ideally non-destructive, and have low limits of detection that reveal not only the local coordination environment, but also identify the biological ligand or biomolecule to which the metal of interest is bound. However, there is no silver bullet for intracellular metal speciation, and a host of complimentary techniques are required to achieve such a comprehensive picture (Figure 1). Techniques are broadly categorized as non-destructive, in the sense that analyses are conducted on intact cells, and destructive, which first require the extraction of intracellular contents prior to analysis. Techniques are presented within the broader context of intracellular metal speciation, but all are applicable to Pb speciation.

2.1. Non-destructive Techniques

The intracellular domain of all living organisms is a highly complex environment and characterized by a continuity of dynamic pathways and processes. Whether it be for the maintenance of essential metal homeostasis or the detoxification of non-essential metals, the dynamics, localization, and concentration of metal species are crucial for the optimal functioning of an organism. To accurately identify, quantify and locate specific intracellular metal species, it is important to mitigate any physical disruption to this environment. In this section, a selection of synchrotron based spectroscopy methods are presented, which are suitable for non-invasive metal speciation.

2.1.1. X-Ray Absorption Spectroscopy

X-ray absorption spectroscopy (XAS) allows for the determination of metal speciation in hydrated biological samples both in bulk as well as at the subcellular

level with ~100 nm scale resolution [14]. In XAS, elemental speciation is obtained when the energy from a monochromatic X-ray beam corresponds to the binding energy of an inner shell electron of a specific element of interest, producing an element-specific feature called an absorption edge. The region around this absorption edge is referred to as the X-ray absorption near edge structure (XANES) and can provide information on the oxidation state and molecular geometry of a specific metal complex. When the incident energy is sufficiently high, a core electron is ejected and the ejected photoelectron wave is scattered by surrounding atoms producing an extended X-ray absorption fine structure (EXAFS). The EXAFS provides information on the identity of neighboring atoms, coordination geometry and bond distances. XAS can be measured in transmission mode but can also be performed in fluorescence mode, utilizing radiative decay of the excited states, which is proportional to the absorption coefficient. This strategy enhances sensitivity, as measurements are collected outside the direct beam path and almost all background counts are eliminated. Therefore, XAS in fluorescence mode is ideal for dilute samples, which is often the case for non-essential metals in microorganisms.

Microorganisms must be measured in either a frozen hydrated state or carefully dried and stored to prevent oxidation of redox-active metal complexes. X-ray spectroscopy cannot be performed on hydrated living organisms at ambient temperature due to radiation damage caused by the X-ray beam. XAS can be performed as a bulk technique, providing information on the local coordination environment surrounding a specific metal without the spatial localization of these metal species. In this case, the signal obtained from the bulk sample is assumed to be representative of the average metal speciation (dominated by the major species) within a single microorganism. Both micro- and nano-XAS can also be performed on specimens and provide additional insight on spatial localization with resolutions down to approximately 100 nm [15]. However, reducing the beam size to obtain better spatial resolution also reduces the signal intensity measured. In all types of XAS, relative amounts of metal species can be quantified by implementing fitting procedures with known biologically relevant metal standards.

One main caveat of XAS is the near impossibility of distinguishing between different types of ligand donors that lie next to each other in the periodic table (O *versus* N). It is an additional challenge to determine differences in elements present in the second coordination shell (Pb-O-S *versus* Pb-O-P) [16]. These challenges are exacerbated for Pb, which often forms complexes with distorted geometries because of an inert pair of electrons [17]. Together, these factors make it challenging to proceed beyond direct coordination towards ligand identification [18]. However, to have a mechanistic understanding of the biological effects of Pb in microorganisms, it is important to obtain such information.

2.1.2. Resonant X-Ray Emission Spectroscopy

Some of the limitations associated with XAS spectral resolution can be addressed with resonant X-ray emission spectroscopy (RXES). RXES is often re-

ferred to as a photon–in/photon–out process, where an incoming photon is absorbed that is in resonance with a specific absorption edge. An excited intermediate state is produced that contains a core hole. The subsequent photon emission results in a final state, which possesses a higher energy relative to the initial state and contains a core hole with a longer lifetime relative to XAS. This phenomenon decreases the core hole broadening of spectral lines and increases spectral resolution. Thus, RXES combines both XAS and X-ray emission spectroscopy (XES). RXES is a widely used tool to probe the electronic structure of matter [19], but has only recently found application in the biological field [16, 20]. In an RXES experiment, highly resolved spectra of metal complexes are obtained by combining both XAS and XES, producing planes analogous to a metal-ligand fingerprint. Discernment between different types of oxygen and sulfur ligand bound Pb complexes becomes possible [16]. This degree of detailed metal speciation is not possible with XAS or any other technique [20].

2.1.3. X-Ray Diffraction

X-ray diffraction (XRD) is useful for the study of crystalline structures, as each structure produces a characteristic diffraction pattern analogous to a fingerprint. Within the intracellular domain, this technique can be particularly helpful in identifying intracellular metal precipitates. In addition, XRD and EXAFS go hand-in-hand, where the geometry obtained from XRD measurements is required to begin iterative calculations in EXAFS, and EXAFS can be helpful in confirming structures obtained from XRD [14].

2.1.4. Scanning Transmission X-Ray Microscopy

One promising technique utilizing XAS is scanning transmission X-ray microscopy (STXM). In STXM, a sample is scanned across a focused X-ray beam and can be measured in both transmission and fluorescence modes. Both imaging and spectroscopy are possible at the nano scale [21]. An additional advantage is the ability to probe elements, such as carbon, nitrogen, oxygen and sulfur, which can provide insight into the composition of proteins, polysaccharides, or lipids [22] surrounding a metal. Due to typically low concentrations of intracellular trace metals, analysis is often limited to the XANES region and can only be applied to the EXAFS region when the required signal-to-noise ratio is met [15]. Therefore, oxidation states of the metal of interest can be easily obtained, whereas neighboring atoms, coordination geometry, and bond distances become more challenging to deduce. STXM imaging has been reviewed [21].

2.2. Destructive Techniques

X-ray spectroscopic techniques are powerful in describing the atomic environment surrounding a metal, however it is also of interest to identify the biomole-

cule to which a metal is bound. To achieve this, molecular and elemental mass spectrometry (MS) are useful approaches. However, unlike in the intact cell analysis previously described, MS is normally performed on isolated cellular fractions. It should be noted that complexes, which are chemically labile run the risk of metal redistribution during cellular fractionation and separation. Metal speciation work often uses hyphenated analytical techniques that include some type of liquid chromatography (LC) or gel/capillary electrophoresis (GE or CE) for the separation of biomolecules, molecular MS for the identification of biomolecules, and inductively coupled plasma mass spectrometry (ICP-MS) for the identification and quantification of metals or elements such as sulfur. A selection of techniques is presented, which are suitable for the identification and quantification of metal bound biomolecules in microorganisms. However, these techniques are by no means limited to those described in the following sections. Comprehensive reviews of bioinorganic analytical techniques can be found elsewhere [23–25].

2.2.1. High Performance Liquid Chromatography-Inductively Coupled Plasma-Mass Spectrometry

The use of HPLC-ICP-MS is a commonly used technique for the determination of metal species in isolated fractions. It is versatile, able to accommodate a range of analytes, and HPLC can be easily coupled to ICP-MS [26]. Biomolecules are fractionated based on polarity, charge, or size, and multi-elemental quantification of metals in these fractions are carried out using ICP-MS. Particularly useful for single cell analysis is the use of nano-HPLC-ICP-MS, which significantly reduces the volume of sample required. Electrospray ionization-mass spectrometry (ESI-MS) can be used in parallel to identify biomolecules present in the respective fractions. Together, these two techniques offer the most robust approach for the *in vitro* identification of metal complexes in the pM to nM range [24].

2.2.2. Gel Electrophoresis-Laser Ablation Inductively Coupled Plasma-Mass Spectrometry

Although recent published work in laser ablation (LA) ICP-MS reported resolution down to 1 μm [27], spatial resolutions of LA ICP-MS are generally in the range of 5 μm, limiting its use in smaller microorganisms [25]. However, LA ICP-MS can be used to analyze bands and spots obtained from 1D and 2D gel-electrophoresis gels. GE, more commonly operated in 2D, is routinely utilized for protein separation and can be used to separate metal complexes when under non-denaturing conditions [28]. By coupling GE with LA ICP-MS, metals are quantified in specific bands or spots. When used in combination with molecular MS for protein identification, the speciation of protein bound metals can be achieved [29]. GE-LA ICP-MS was shown to be particularly useful in identifying increased metal–protein complexes formed as a result of metal stress [30]. The reader is directed to a comprehensive review for more information [31].

2.2.3. Electrospray Ionization-Mass Spectrometry

Electrospray ionization-mass spectrometry (ESI-MS) is a sensitive soft ionization technique that allows for the identification of large biomolecules with little or no fragmentation. Additionally advantageous is that metal complexes can also be transferred to the gas-phase [32]. By using nano-ESI-MS, significantly lower concentration and sample volume is required, and increased tolerance to solvents and salt contamination is achieved [23]. This technique was used to identify the stoichiometry of Pb-phytochelatin complexes (Pb-PC) *in vitro* and indicated likely competition of Zn and Cu for M-PC complex formation [33].

3. INTRACELLULAR METAL LOCALIZATION TECHNIQUES

Determination of intracellular metal species in microorganisms is most valuable when these species can be spatially located within the subcellular domain. To obtain meaningful spatial localization of metal species in microorganisms, resolution should be $\leq 1\ \mu m$. In achieving this minimum resolution, one can probe organelles such as the nucleus, lysosomes, vesicles, and the mitochondrial network [14]. Incoming monochromatic X-ray beams can now be focused down to spot sizes between 150–300 nm to obtain metal speciation information at intracellularly relevant spatial scales [34].

3.1. Synchrotron X-ray Fluorescence

In synchrotron X-ray fluorescence (SXRF) characteristic photons are emitted from the absorption and relaxation process described in XAS. With SXRF one can easily identify and quantify elements at 100 nm spatial resolutions, making this technique valuable in probing subcellular metal localization. With SXRF, attogram levels of transition metals are detected and multiple elements can be simultaneously mapped for co-localization studies [35]. Spatial resolutions down to approximately 30 nm are now being reported in the literature [36]. Work with SXRF has been typically conducted in 2D. Although challenging, translation to 3D is possible with XRF tomography. For example, de Jonge et al. successfully mapped the 3D distribution of ten trace elements in the diatom *Cyclotella meneghiniana* with 400 nm spatial resolution [37].

3.2. Secondary Ion Mass Spectrometry

The use of secondary ion mass spectrometry (SIMS) is an emerging tool for the quantification and distribution of ions in biological samples [38]. In SIMS, a primary ion beam is scanned across a sample, which sputters away the surface, ejecting both atoms and atomic clusters. These ionized atoms and clusters are the

secondary ions, which are measured and from which spatial maps are generated. Measurements are performed under high vacuum, making *in vivo* measurements not possible. SIMS can be operated in either static or dynamic mode, which refers to the intensity of the primary ion beam and the degree of fragmentation from the sample surface. In static SIMS, a time-of-flight (TOF) mass spectrometer is often used in conjunction with a second ion beam used to sputter the surface of the sample. After each pulse, secondary ions are measured based upon their mass-to-charge (m/z) ratio. In TOF-SIMS one is able to simultaneously map all metal ions as well as other molecular ions. In contrast, dynamic SIMS, referred to in the literature as NanoSIMS, requires a pre-selection of up to seven masses. However, better sensitivity is achieved, allowing for spatial resolutions down to 50 nm [38]. A study using NanoSIMS conducted on Cu uptake in *C. kesslerii* indicated possible Cu interaction with phosphate granules, proteins, and the nucleus [39]. These conclusions were made based upon the co-localization of $^{63}Cu^-$ and varying intensities of ^{12}C, $^{12}C^{14}N^-$, and $^{31}P^-$. Co-localization and quantification of specific elemental isotopes is possible, but direct identification of intracellular metal complexes is not achieved with NanoSIMS. One significant drawback is an inability to resolve subcellular organelle distribution because organelle membranes have similar structural compositions.

3.3. Lead-Specific Probes and Sensors

Metal-specific probes and sensors can also be employed to localize intracellular metals. This technique is based upon converting the binding of a specific metal to a measurable optical signal. Fluorescence-based probes and sensors are the most prevalent type and include small-molecule sensors, protein-based biosensors, and hybrid probes genetically encoding small-molecule sensors [40]. Each type has strengths and weaknesses dependent upon the requirement of the system being studied: requirement of specificity, dissociation constants, signal intensity, dynamic range, and subcellular localization capabilities [40]. Fluorescence imaging for Pb^{2+}-specific sensors can, in theory, supply information on the spatial localization and temporal dynamics of the intracellular labile Pb pools, if such pools even exist. However, despite the existence of Pb^{2+}-specific fluorescent probes [41–43], relatively few Pb^{2+}sensors are available for application in living cells. Leadmium™Green AM is the only known commercially available probe for detecting nM concentrations of intracellular Pb^{2+} but it also binds to Cd^{2+}. However, He et al. synthesized Leadfluor-1 (LF1) utilizing a fluorescein-type scaffold [44]. This Pb^{2+}-specific sensor is insensitive to Cd^{2+} as well as other major cations found at μM to mM concentration within the cell and is able to monitor changes in intracellular Pb^{2+} levels within living mammalian cells. Recently, a FRET-based Pb^{2+} sensor referred to as Met-lead 1.59, was developed for use in detecting intracellular Pb [45]. This sensor is based upon the Pb^{2+} binding domain of PbrR, a bacterial metalloregulatory protein, which is described in greater detail in the following section.

4. LEAD SPECIATION IN MICROORGANISMS

Microorganisms have developed mechanisms to prevent metal toxicity and maintain physiologically required cellular concentrations of essential metals [46, 47]. In the case of Pb, toxicity can occur from the replacement of essential metals with Pb, demonstrated by the exchange of Zn from the family of Zn finger proteins [48]. Lead has also been reported to interfere in electron transfer reactions in mitochondria [49] and chloroplasts [50], affecting respiration and photosynthesis [51]. Other physiological disruptions have been observed in algae [52]. In addition to these direct effects, indirect effects can occur through an increase in metal-induced reactive oxygen species (ROS). These ROS lead to the radical attack on proteins, lipids, and nucleic acids, which can ultimately lead to cell death. To avoid such deleterious effects, microorganisms employ several key detoxification strategies that influence intracellular Pb speciation and ameliorate toxic effects. Binding to cellular wall components may serve to slow the internalization of Pb. However, once taken up, formation of insoluble Pb precipitates, vacuolar sequestration, and excretion of Pb are major detoxification mechanisms.

4.1. Bacteria

Bacterial Pb detoxification strategies mainly comprise of intracellular precipitation, efflux, and in some cases the methylation of Pb^{2+} to more volatile organic lead compounds [5]. Precipitation of Pb with phosphate seems to serve as a particularly common sequestration mechanism, and the type of lead phosphate precipitated is often species-specific. For example, *Staphylococcus aureus* precipitates internalized Pb as $Pb_3(PO_4)_2$ [53], whereas *Vibrio harveyi* sequesters intracellular Pb as $Pb_9(PO_4)_6$, determined using XRD [54]. *Burkholderia cepacia* sequesters Pb as $Pb_5(PO_4)_3Cl$, which was shown using EXAFS [55]. The different intracellular Pb phosphate species likely arise from different species-specific subcellular processes involved in detoxification. However, there are no known systematic studies that compare types of phosphate precipitation with different known detoxification pathways. Intracellular precipitation has also been observed with sulfur. When taking up Pb under phosphate-limiting conditions, PbS was found in *Klebsiella aerogenes* NCTC418 [56]. It has also been shown with XRD that sulfate-reducing bacteria are able to use $PbSO_4$ as an electron acceptor to form PbS [57].

Metallothioneins (MTs) are low-molecular-weight metal-binding proteins encoded by the smt locus and are well known for their essential role in Zn homeostasis [58]. It has been shown that Pb induces smtA expression and MT synthesis in a handful of bacterial species [59–62], which may also serve as a detoxification mechanism. However, this does not seem to be a primary Pb detoxification strategy among bacteria.

Bacteria are also able to excrete Pb via established efflux systems. These include P-type ATPase-mediated transport [63]. CadA from *S. aureus*, ZntA from

E. coli, CadA2 from *Ps. putida* KT2440, and PbrA from *Cupriavidus metallidurans* CH34 all seem to transport Pb^{2+} out of the cytoplasm into the periplasmic space [64–67].

C. metallidurans CH34 is a model bacterium often used for metal tolerance studies and particularly interesting within the context of intracellular Pb speciation and detoxification. The Pbr efflux system removing intracellular Pb^{2+} was first reported in this bacterium [68], and it is the only system known to combine both efflux with precipitation in its detoxification strategy against Pb. This efflux system is encoded by pbr, and includes PbrT, a membrane protein, PbrA, a PIB-type ATPase, PbrB, a phosphatase membrane protein, PbrC, a putative signal peptidase, PbrD, a putative intracellular Pb binding protein, and PbrR, a positive regulator [68]. PbrT is partially responsible for the uptake of Pb^{2+} into the cytoplasm, whereby it is thought that the PbrD protein binds Pb, making it less available to sensitive subcellular targets while simultaneously activating PbrA. PbrA is responsible for the efflux of Pb into the periplasm and works in conjunction with PbrB, which releases inorganic phosphate into the periplasmic space and allows for the precipitation of Pb phosphates. This periplasmic precipitation is thought to prevent re-entry of Pb into the cytosol [65].

Some bacteria have an ability to transform various Pb^{2+} species into methylated Pb species, which seems to play a role in detoxification [69]. This process is referred to as biomethylation, but the exact mechanisms have not been unequivocally established because of the instability of monomethyl lead(IV) as a result of the labile nature of the methyl-lead linkage [69]. Both tetramethyl (Me_4Pb) and trimethyl (Me_3Pb) lead have been identified as products of microbial biomethylation. It was shown that *Aeromonas sp.* transformed lead acetate into Me_4Pb [70]. Several other types of bacteria showed similar transforming capabilities, but there is also evidence questioning if biomethylation of Pb occurs at all in the environment [71–74]. Despite these claims, a form of arctic marine bacteria was reported to produce Me_3Pb [75].

4.2. Fungi

Much less is known about Pb detoxification mechanisms in fungi. The work that has been conducted indicates similar mechanisms of detoxification as seen in bacteria. In *S. cerevisiae*, Pb is easily taken up via an unknown transport mechanism, which is independent of cellular metabolism and accumulated in the cytosol. In the cytoplasm, Pb binds to glutathione (GSH) and the ATP-binding cassette transporter cadmium factor 1 transports this complex to the vacuole [76]. The importance of GSH in Pb detoxification was also observed for *Schizosaccharomyces pombe* [77]. Additionally, the copper-transporting ATPase CAD2 appears to be important for the efflux of Pb^{2+} [78]. Fungi also protect themselves against Pb toxicity through the precipitation and formation of $Pb_5(PO_4)_3Cl$, determined using XRD, which appear to significantly influence the biogeochemical cycles of Pb in the environment [79]. Interestingly, the fungus *Aspergillus niger*

was shown to solubilize $Pb_5(PO_4)_3Cl$ and subsequently sequestered Pb as oxalates, observed from differences in XRD spectra [80].

4.3. Algae

Algae avoid toxic effects through metal sequestration either by complexation with phytochelatins (PCs), important peptides in metal detoxification [81, 82], or through metal immobilization in intracellular precipitates, such as polyphosphate vacuolar granules [83, 84]. Although not well studied, efflux may be a potential mechanism of detoxification.

Chlamydomonas reinhardtii is a particularly important model algal species, as it has been well studied within the context of intracellular metal homeostasis and tolerance [85]. Rapid induction of PCs in *C. reinhardtii* was measured upon both short- and long-term Pb exposures down to 1 nM Pb^{2+} [51]. Several studies have also shown that Pb induces PCs in other algal species [86, 87]. Yet, Scheidegger et al. [81] observed that although Pb induced the production of PCs in *C. reinhardtii*, the amount was not high enough to bind all intracellular Pb. As no observable toxic effects were measured, other sequestration processes mitigating toxicity were assumed to be present. Studies indicate that, in addition to PC induction, polyphosphate-containing vacuoles appear to serve an important role in intracellular metal sequestration [83, 84].

Antioxidant mechanisms are also critical in mitigating the indirect effects of metal toxicity brought upon by ROS. GSH is one of the most abundant cellular thiols found in millimolar concentrations [51]. In addition to being a precursor for PC production, GSH plays an integral role in cellular antioxidant responses. Direct involvement of GSH in metal detoxification in algae has been proposed [88], but little is known if GSH directly binds intracellular Pb. With respect to Pb efflux, several metal tolerance proteins (MTPs), related to the family of cation diffusion facilitator (CDF) transporters involved in the efflux of Zn^{2+}, have been identified in the green algae *C. reinhardtii* and *C. merolae* [89]. No known studies have determined the specific role of these transporters in the efflux of Pb as a detoxification mechanism in algae. However, as observed in bacteria, it is plausible that algae may also utilize such Zn^{2+} efflux systems to remove accumulated Pb.

Recent work [16] was conducted using *C. reinhardtii* to understand the temporal evolution of intracellular Pb species, how these species relate to measurable effects on both growth and photosynthesis, and how extracellular Pb speciation influences intracellular speciation. Samples analyzed using RXES showed that when *C. reinhardtii* was exposed to 0.1 nM Pb^{2+}, sequestration of intracellular Pb as PbO and $Pb_3(PO_4)_2$ occurred within the first five hours (Figure 2a) [16]. Within this time a decrease in PbO and corresponding proportionate increase of $Pb_3(PO_4)_2$ was attributed to Pb redistribution. The exact mechanism is unknown but likely originated from precipitation with phosphate released from polyphosphatase-mediated hydrolysis of inorganic polyphosphate [90] present in elevated concentrations within vacuoles of *C. reinhardtii* [91]. Upon longer exposure

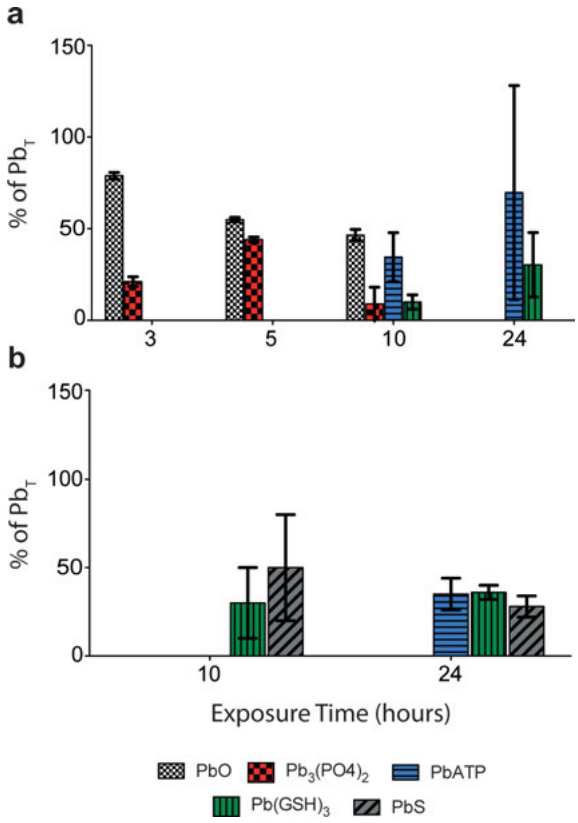

Figure 2. Intracellular Pb speciation in *C. reinhardtii* as a function of exposure time to (**a**) 0.1 nM Pb^{2+} and (**b**) 25 nM Pb^{2+}. Figure 2a reproduced by permission from [16] (copyright 2015, American Chemical Society) for comparison with unpublished data in Figure 2b (T. J. Stewart, unpublished data from the Dissertation [16]) .

times, further redistribution to organic phosphate and tridentate thiol complexation was measured, likely from thiol-mediated dissolution of inorganic lead phosphate precipitates [92]. Relative to inorganic precipitation, less Pb was complexed by thiols. This finding was in contrast to proposed detoxification strategies involving thiol complexation by PCs.

Interestingly, Pb speciation in the exposure solution influences intracellular Pb speciation. In the same study [16], changing the exposure solution composition to 25 nM Pb^{2+}, while maintaining a similar total Pb concentration, resulted in different intracellular species but similar intracellular concentrations (T. J. Stewart, unpublished data from the Dissertation [16]) (Figure 2b). Similar thiol complexation was observed, but PbS precipitation was also measured after both 10 and 24 hours of exposure. Only after 24 hours of exposure was Pb complexation to organic phosphate measured. These results showed that increasing the bioavailability of Pb did not significantly increase total intracellular Pb content, but did lead to the formation of different intracellular Pb species.

The free metal ion is often the species that dictates the concentration of metal-cell surface complexes, which in turn can influence uptake kinetics, the amount of accumulated metal, and toxicity [93]. A positive correlation between Pb^{2+} concentration and the internalization flux in the green alga *Chlorella vulgaris* in both the presence and absence of labile Pb complexes was observed [94]. With more Pb^{2+} present in the exposure medium, a faster internalization of Pb would be expected. This may have caused an initially higher internal Pb concentration resulting in the measured precipitation of PbS. Formation of PC-coated CdS nanocrystals has been reported in *C. reinhardtii* [95] but this is the first known study to measure PbS in *C. reinhardtii*. These collective observations indicate that metal uptake kinetics may dictate intracellular metal speciation and corresponding biological responses. As novel and informative as this study was, information regarding the spatial localization of specific Pb complexes was missing. This lack of spatial resolution makes it challenging to place metal species within the context of biological responses and highlights the importance of nano scale spatial visualization of metal species.

5. REMAINING QUESTIONS AND FUTURE DIRECTIONS

The ability to identify Pb species, or any metal species, at the subcellular level is critical in understanding of how cells handle both essential and non-essential metals. It is also clear that a multitude of techniques are required to deduce intracellular metal speciation. A fundamental question thus remains: how does one correlate these techniques so that a complete picture is achieved? The trend in correlative microscopy has already been successfully demonstrated in the combination of cryo-fluorescence with cryo-electron microscopy and cryo-fluorescence with soft X-ray cryo-microscopy [96, 97]. These pioneering techniques have allowed us to obtain detailed views of the subcellular structures within a cell. What is not addressed in these techniques is metal speciation within such structures.

The direct comparison between complementary speciation techniques is precisely what is required for the field of intracellular metal speciation. Fluorescent probes labeling specific subcellular organelles can be used in conjunction with both SXRF and XAS to directly correlate metal speciation and subcellular localization [36]. However, this approach has only been utilized in a handful of studies. The major advantage lies in its compatibility with live cell imaging with minimal disruption to ion homeostasis [36]. Other beneficial approaches would include fluorescence microscopy with 3D elemental mapping using SXRF, and the combination of SXRF with phase contrast imaging techniques such as ptychography [98], where resolutions beyond the limitations of X-ray lenses are obtained by using diffraction patterns generated from coherently illuminated non-crystalline samples [99].

The ultimate goal of single cell metal speciation determination would be to obtain 3D chemical maps of any element of interest. Combining STXM with tomographic techniques has yielded promising results (Figure 3) [100], but is far

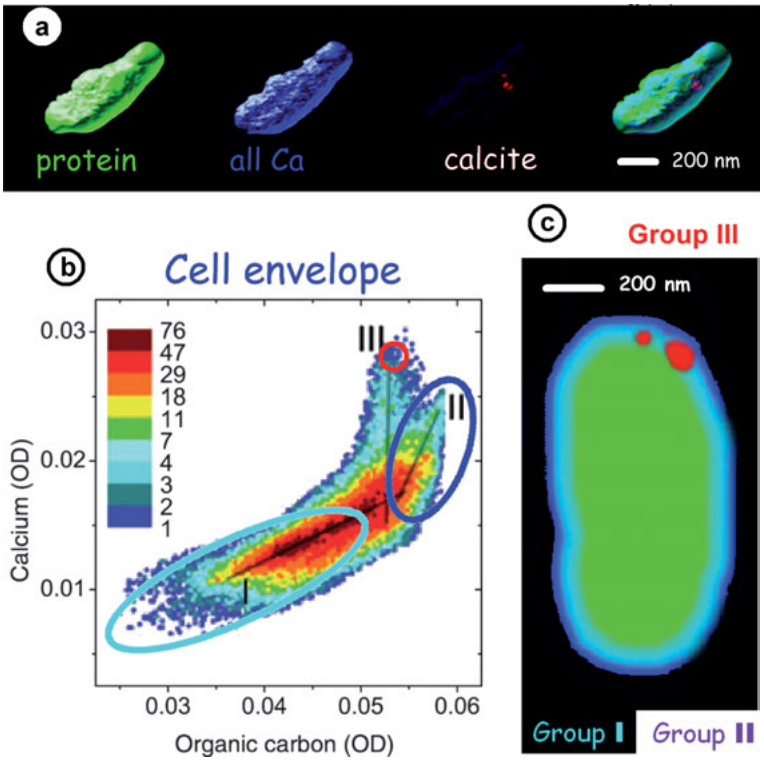

Figure 3. 3D renderings of protein (green), total Ca (blue), calcite (red), and overlaid images from a single *Synechococcus leopoliensis* PCC 7942 bacterium (**a**). Analysis of 3D spatial and compositional correlations of Ca^{2+} and organic carbon signals (**b, c**). Reproduced by permission from [100]; copyright 2010, Cambridge University Press.

from routine largely due to slow acquisition time leading to radiation damage [101]. The field of intracellular metal speciation has a multitude of incredibly promising tools at its fingertips. Through fruitful collaborations with synchrotron beam line scientists, significant strides can be made in advancing these techniques and our understanding of subcellular metal speciation.

ACKNOWLEDGMENT

I would like to thank Wolfgang Maret for internal review of the manuscript.

ABBREVIATIONS

BLM	biotic ligand model
CDF	cation diffusion facilitator
ESI	electrospray ionization

EXAFS	extended X-ray absorption fine structure
FIAM	free ion activity model
GE/CE	gel electrophoresis/capillary electrophoresis
GSH	glutathione
HPLC	high performance liquid chromatography
ICP-MS	inductively coupled plasma-mass spectrometry
LA	laser ablation
LC	liquid chromatography
M	metal
Me	methyl
MS	mass spectrometry
MT	metallothionein
MTP	metal tolerance protein
PC	phytochelatin
ROS	reactive oxygen species
RXES	resonant X-ray emission spectroscopy
SIMS	secondary ion mass spectrometry
STXM	scanning transmission X-ray microscopy
SXRF	synchrotron X-ray fluorescence
TOF	time of flight
XANES	X-ray absorption near edge structure
XAS	X-ray absorption spectroscopy
XES	X-ray emission spectroscopy
XRD	X-ray diffraction

REFERENCES

1. J. O. Nriagu, *Science* **1996**, *272*, 223–223.
2. P. Bradac, B. Wagner, D. Kistler, J. Traber, R. Behra, L. Sigg, *Environ. Pollut.* **2010**, *158*, 641–648.
3. A. M. Farag, D. A. Nimick, B. A. Kimball, S. E. Church, D. D. Harper, W. G. Brumbaugh, *Arch. Environ. Contam. Toxicol.* **2007**, *52*, 397–409.
4. J. N. Rauch, J. M. Pacyna, *Global Biogeochem. Cy.* **2009**, *23*, 1–16.
5. A. Jarosławiecka, Z. Piotrowska-Seget, *Microbiology* **2014**, *160*, 12–25.
6. K. A. C. De Schamphelaere, C. Nys, C. R. Janssen, *Aquat. Toxicol.* **2014**, *155*, 348–359.
7. V. Zitko, W. V. Carson, W. G. Carson, *Bull. Environ. Contam. Toxicol.* **1973**, *10*, 265–271.
8. R. M. Town, M. Filella, *Aquat. Sci.* **2000**, *62*, 252–295.
9. P. G. C. Campbell, in *Metal Speciation and Bioavailability in Aquatic Systems*, Eds A. Tessier, D. R. Turner, John Wiley & Sons, Inc, New York, 1995, pp. 45–102.
10. P. R. Paquin, R. C. Santore, K. B. Wu, C. D. Kavvadas, D. M. Di Toro, *Environ. Sci. Policy* **2000**, *3*, S175–S182.
11. P. R. Paquin, J. W. Gorsuch, S. Apte, G. E. Batley, K. C. Bowles, P. G. C. Campbell, C. G. Delos, D. M. Di Toro, R. L. Dwyer, F. Galvez, R. W. Gensemer, G. G. Goss, C. Hostrand, C. R. Janssen, J. C. McGeer, R. B. Naddy, R. C. Playle, R. C. Santore,

U. Schneider, W. A. Stubblefield, C. M. Wood, K. B. Wu, *Comp. Biochem. Physiol. C Toxicol. Pharmacol.* **2002**, *133*, 3–35.
12. L. Banci, I. Bertini, in *Metallomics and the Cell*, Vol. 12 of *Metal Ions in Life Sciences*, Ed. L. Banci, Series Eds A. Sigel, H. Sigel, R. K. O. Sigel, Springer, Dordrecht, 2013, 1–10.
13. R. G. Pearson, *Inorg. Chim. Acta* **1995**, *240*, 93–98.
14. R. Ortega, A. Carmona, I. Llorens, P. L. Solari, *J. Anal. At. Spectrom.* **2012**, *27*, 2054–2065.
15. R. Ortega, *J. Anal. At. Spectrom.* **2010**, *26*, 23–29.
16. T. J. Stewart, J. Szlachetko, L. Sigg, R. Behra, M. Nachtegaal, *Environ. Sci. Technol.* **2015**, *49*, 11176–11181. See also: T. J. Stewart, *Lead Bioavailability and Effects to Periphyton*, Dissertation, ETH-Zürich, Switzerland, 2014, http://e-collection.library.ethz.ch/view/eth:46986.
17. L. Shimoni-Livny, J. P. Glusker, C. W. Bock, *Inorg. Chem.* **1998**, *37*, 1853–1867.
18. A. Manceau, M. Boisset, G. Sarret, R. Hazemann, M. Mench, P. Cambier, R. Prost, *Environ. Sci. Technol.* **1996**, *30*, 1540–1552.
19. U. Bergmann, P. Glatzel, *Photosyn. Res.* **2009**, *102*, 255–266.
20. J. C. Swarbrick, U. Skyllberg, T. Karlsson, P. Glatzel, *Inorg. Chem.* **2009**, *48*, 10748–10756.
21. B. Kaulich, P. Thibault, A. Gianoncelli, M. Kiskinova, *J. Phys. Condens. Matter* **2011**, *23*, 083002.
22. J. R. Lawrence, G. D. W. Swerhone, G. G. Leppard, T. Araki, X. Zhang, M. M. West, A. P. Hitchcock, *Appl. Environ. Microbiol.* **2003**, *69*, 5543–5554.
23. J. Szpunar, *Analyst* **2005**, *130*, 442–465.
24. S. Mounicou, J. Szpunar, R. Lobinski, *Chem. Soc. Rev.* **2009**, *38*, 1119–1138.
25. W. Maret, J. A. Caruso, C. H. Contag, D. P. Giedroc, P.-L. Hagedoorn, A. Matusch, E. P. Skaar, R. B. Thompson, in *Trace Metals and Infectious Diseases*, Eds. J. O. Nriagu, E. P. Skaar, MIT Press, Cambridge, MA, 2015, pp. 1–61.
26. M. Montes-Bayón, K. DeNicola, J. A. Caruso, *J. Chromatogr. A* **2003**, *1000*, 457–476.
27. G. Schwarz, H. A. O. Wang, C. Giessen, D. Schapiro, B. Hattendorf, B. Bodenmiller, D. Günther, *Chimia (Aarau)* **2015**, *69*, 637–637.
28. D. E. Garfin, *Trends Analyt. Chem*. **2003**, *22*, 263–272.
29. A. Cvetkovic, A. L. Menon, M. P. Thorgersen, J. W. Scott, F. L. Poole, F. E. Jenney, W. A. Lancaster, J. L. Praissman, S. Shanmukh, B. J. Vaccaro, S. A. Trauger, E. Kalisiak, J. V. Apon, G. Siuzdak, S. M. Yannone, J. A. Tainer, M. W. W. Adams, *Nature* **2010**, *466*, 779–782.
30. M. R. B. Binet, R. Ma, C. W. McLeod, R. K. Poole, *Anal. Biochem.* **2003**, *318*, 30–38.
31. S. R. Haider, B. L. Sharp, H. J. Reid, *Trends Analyt. Chem*. **2011**, *30*, 1793–1808.
32. J. C. Traeger, *Int. J. of Mass Spectrom.* **2000**, *200*, 387–401.
33. C. Scheidegger, M. J. F. Suter, R. Behra, L. Sigg, *Front. Microbiol.* **2012**, *3*, 1–7.
34. M. J. Pushie, I. J. Pickering, M. Korbas, M. J. Hackett, G. N. George, *Chem. Rev.* **2014**, *114*, 8499–8541.
35. C. J. Fahrni, *Chemical Biology* **2007**, *11*, 121–127.
36. S. Roudeau, A. Carmona, L. Perrin, R. Ortega, *Anal. Bioanal. Chem.* **2014**, *406*, 6979–6991.
37. M. D. De Jonge, J. Diaz, D. Howard, C. Holzner, S. B. Baines, D. Legnini, B. S. Twining, B. Twining, K. Ignatyev, J. Diaz, D. L. Howard, D. Legnini, A. Miceli, I. McNulty, C. J. Jacobsen, S. Vogt, *Proc. Natl. Acad. Sci. USA* **2010**, *107*, 15676–15680.
38. R. Lobinski, C. Moulin, R. Ortega, *Biochimie* **2006**, *88*, 1591–1604.
39. V. I. Slaveykova, C. Guignard, T. Eybe, H.-N. Migeon, L. Hoffmann, *Anal. Bioanal. Chem.* **2008**, *393*, 583–589.

40. K. M. Dean, Y. Qin, A. E. Palmer, *Biochim. Biophys. Acta* **2012**, *1823*, 1406–1415.
41. S. Deo, H. A. Godwin, *J. Am. Chem. Soc.* **2000**, *122,* 174–175.
42. Y. Lu, J. Liu, *J. Am. Chem. Soc.* **2004**, *126*, 12298–12305.
43. P. Chen, B. Greenberg, S. Taghavi, C. Romano, D. van der Lelie, C. He, *Angew. Chem.* **2005**, *117*, 2775 –2779.
44. Q. He, E. W. Miller, A. A. P. Wong, C. J. Chang, *J. Am. Chem. Soc.* **2006**, *128*, 9316–9317.
45. T.-Y. Chiu, D.-M. Yang, *Toxicol. Sci.* **2012**, *126*, 436–445.
46. S. Clemens, *Planta* **2001**, *212*, 475–486.
47. A. Z. Mason, K. D. Jenkins, in *Metal Speciation and Bioavailability in Aquatic Systems,* Eds A. Tessier, D. R. Turner, John Wiley & Sons, Inc, New York, 1995, pp. 479–608.
48. H. A. Godwin, *Curr. Opin. Chem. Biol.* **2001**, *5*, 223–227.
49. J. E. Bittell, D. E. Koeppe, R. J. Miller, *Physiol. Plant* **1974**, *30*, 226–230.
50. C. D. Miles, J. R. Brandle, D. J. Daniel, O. Chu-Der, P. D. Schnare, D. J. Uhlik, *Plant Physiol.* **1972**, *49*, 820–825.
51. C. Scheidegger, R. Behra, L. Sigg, *Aquat. Toxicol.* **2010**, *101*, 423–429.
52. J. Vymazal, *Acta Hydrochim. Hydrobiol.* **1990**, *18*, 513–535.
53. H. S. Levinson, I. Mahler, *FEMS Microbiol. Lett.* **1998**, *161*, 135–138.
54. C. E. Mire, J. A. Tourjee, W. F. O'Brien, K. V. Ramanujachary, G. B. Hecht, *Appl. Environ. Microbiol.* **2004**, *70*, 855–864.
55. A. S. Templeton, A. M. Spormann, G. E. Brown, *Environ. Sci. Technol.* **2003**, *37*, 2166–2172.
56. H. Aiking, H. Govers, J. van't Riet, *Appl. Environ. Microbiol.* **1985**, *50*, 1262–1267.
57. O. Karnachuk, S. Kurochkina, O. Tuovinen, *Appl. Microbiol. Biotechnol.* **2002**, *58*, 482–486.
58. C. A. Blindauer, *J. Biol. Inorg. Chem.* **2011**, *16*, 1011–1024.
59. J. W. Huckle, A. P. Morby, J. S. Turner, N. J. Robinson, *Mol. Microbiol.* **1993**, *7*, 177–187.
60. S. Murthy, G. Bali, S. K. Sarangi, *Afr. J. Biotechnol.* **2011**, *10*, 15966–15972.
61. M. M. Naik, A. Pandey, S. K. Dubey, *Ecotoxicol. Environ. Saf.* **2012**, *79*, 129–133.
62. H. M. Rifaat, K. F. Mahrous, W. Khalil, *J. App. Sc. Environ. San*. **2009**, *4*, 197–206.
63. H.-J. Apell, *Bioelectrochemistry* **2004**, *63*, 149–156.
64. J. M. Argüello, *J. Membrane Biol.* **2003**, *195*, 93–108.
65. A. Hynninen, T. Touzé, L. Pitkänen, D. Mengin Lecreulx, M. Virta, *Mol. Microbiol.* **2009**, *74*, 384–394.
66. A. Leedjärv, A. Ivask, M. Virta, *J. Bacteriol.* **2008**, *190*, 2680–2689.
67. C. Rensing, Y. Sun, B. Mitra, B. P. Rosen, *J. Biol. Chem.* **1998**, *273*, 32614–32617.
68. B. Borremans, J. L. Hobman, A. Provoost, N. L. Brown, D. van der Lelie, *J. Bacteriol.* **2001**, *183*, 5651–5658.
69. J. S. Thayer, *Appl. Organomet. Chem.* **2002**, *16*, 677–691.
70. B. A. Silverberg, P. T. Wong, Y. K. Chau, *Appl. Environ. Microbiol.* **1976**, *32*, 723–725.
71. M. N. Hughes, R. K. Poole, *Metals and Micro-Organisms*, Chapman and Hall, London, 1989, 252–301.
72. K. Reisinger, M. Stoeppler, H. W. Nürnberg, *Nature* **1981**, *291*, 228–230.
73. J. S. Thayer, F. E. Brinckman, in *Advances in Organometallic Chemistry*, Eds F. G. A. Stone, R. West, Academic Press, New York, 1982, 313–356.
74. P. T. S. Wong, Y. K. Chau, P. L. Luxon, *Nature* **1975**, *253*, 263–264.
75. R. Pongratz, K. G. Heumann, *Chemosphere* **1999**, *39*, 89–102.
76. J. H. Suh, J. W. Yun, D. S. Kim, *Bioprocess Eng.* **1999**, *21*, 383–387.
77. A. Coblenz, K. Wolf, *FEMS Microbiol. Rev.* **1994**, *14*, 303–308.

78. E. Shiraishi, M. Inouhe, M. Joho, H. Tohoyama, *Curr. Genet.* **2000**, *37*, 79–86.
79. N. Clipson, D. B. Gleeson, *Curr. Biol.* **2012**, *22*, R82–R84.
80. J. A. Sayer, J. D. Cotter-Howells, C. Watson, S. Hillier, G. M. Gadd, *Curr. Biol.* **1999**, *9*, 691–694.
81. C. Scheidegger, R. Behra, L. Sigg, *Aquat. Toxicol.* **2011**, *101*, 423–429.
82. S. Le Faucheur, R. Behra, L. Sigg, *Environ. Toxicol. Chem.* **2005**, *24*, 1731–1737.
83. Y. Komine, L. L. Eggink, H. Park, J. K. Hoober, *Planta* **2000**, *210*, 897–905.
84. M. Siderius, A. Musgrave, H. Ende, H. Koerten, P. Cambier, P. Meer, *J. Phycol.* **1996**, *32*, 402–409.
85. M. Hanikenne, *New Phytol.* **2003**, *159*, 331–340.
86. B. A. Ahner, F. Morel, *Limnol. Oceanogr.* **1995**, *40*, 658–665.
87. S. Le Faucheur, F. Schildknecht, R. Behra, L. Sigg, *Aquat. Toxicol.* **2006**, *80*, 355–361.
88. G. Howe, S. Merchant, *Plant Physiol.* **1992**, *98*, 127–136.
89. M. Hanikenne, U. Krämer, V. Demoulin, D. Baurain, *Plant Physiol.* **2005**, *137*, 428–446.
90. J. D. Keasling, *Ann. NY Acad. Sci.* **1997**, *829*, 242–249.
91. F. A. Ruiz, N. Marchesini, M. Seufferheld, Govindjee, R. Docampo, *J. Biol. Chem.* **2001**, *276*, 46196–46203.
92. C. E. Martínez, A. R. Jacobson, M. B. McBride, *Environ. Sci. Technol.* **2004**, *38*, 5584–5590.
93. P. G. C. Campbell, O. Errécalde, C. Fortin, V. P. Hiriart-Baer, B. Vigneault, *Comp. Biochem. Physiol C* **2002**, *133*, 189–206.
94. V. I. Slaveykova, K. J. Wilkinson, *Environ. Sci. Technol.* **2002**, *36*, 969–975.
95. S. Hu, K. W. K. Lau, M. Wu, *Plant Sci.* **2001**, *161*, 987–996.
96. M. Schorb, J. A. G. Briggs, *Ultramicroscopy* **2014**, *143*, 24–32.
97. E. A. Smith, G. McDermott, M. Do, K. Leung, B. Panning, M. A. Le Gros, C. A. Larabell, *Biophys. J.* **2014**, *107*, 1988–1996.
98. J. Deng, D. J. Vine, S. Chen, Y. S. G. Nashed, Q. Jin, N. W. Phillips, T. Peterka, R. Ross, S. Vogt, C. J. Jacobsen, *Proc. Natl. Acad. Sci. USA* **2015**, *112*, 2314–2319.
99. J. Miao, P. Charalambous, J. Kirz, D. Sayre, *Nature* **1999**, *400*, 342–344.
100. A. P. Hitchcock, J. Wang, M. Obst, *Microsc. Microanal.* **2010**, *16*, 850–851.
101. M. Obst, G. Schmid, in *Electron Microscopy: Methods and Protocols, Methods in Molecular Biology,* Ed. J. Kuo, Humana Press, New Jersey, 2013, pp. 757–781.

6

Human Biomonitoring of Lead Exposure

Katrin Klotz and Thomas Göen

Institute and Outpatient Clinic of Occupational, Social and Environmental Medicine,
Friedrich-Alexander University (FAU) of Erlangen-Nürnberg, Schillerstr. 25/29,
D-91052 Erlangen, Germany
<katrin.klotz@fau.de>

Metal Ions in Life Sciences, Volume 17 Edited by Astrid Sigel, Helmut Sigel, and Roland K. O. Sigel

DOI 10.1515/9783110434330-006

Abstract: After a chronic exposure, lead accumulates in the human body, especially in bones and teeth. Critical effects of lead affect the nervous system, reproduction, fertility as well as genotoxicity and carcinogenicity [1].

Analyses of lead concentrations in human biological material are performed using inductively coupled plasma mass spectrometry and atomic absorption spectrometry, but also electrochemical methods and X-ray fluorescence spectroscopy. The predominant sample matrices include blood and bone, as well as urine, hair, nail, and saliva.

To characterize first biological effects, diverse parameters are discussed as "biomarkers of effect". These include δ-aminolevulinic acid dehydratase (ALAD) and erythrocyte porphyrins (EPs) in blood as well as δ-aminolevulinic acid (ALA) in urine and plasma and coproporphyrin in urine. However, biomarkers of effect alone are not sufficiently sensitive for an early detection of a health impairment caused by lead.

In summary, lead in blood is the most prominent and best validated biomarker for a lead exposure. A recommended diagnostic strategy for revealing lead-induced effects is the determination of lead in whole blood combined with the analysis of different effect parameters like ALA and coproporphyrin in urine and ALAD and zinc protoporphyrin (ZPP) in blood.

Keywords: AAS · analysis · biomonitoring · blood · ICP-MS · lead · toxicokinetics · urine

1. INTRODUCTION

Lead exposure results in a lot of adverse effects, of which the hematopoietic system, the nervous system, the kidneys, the reproductive organs, and the cardiovascular system are the most important targets [1–3]. The effects of lead on the hematopoietic system include both, effects on the erythrocyte production and on the hemoglobin synthesis. Neurotoxic effects of lead include central nervous disorders and disorders of the peripheral motor and smooth muscular function. Moreover, inorganic lead compounds have clastogenic and weak mutagenic potential, both *in vitro* and *in vivo*. Lead is assigned as carcinogenic to animals (carcinogenic group 2) [4]. Lead is a cumulative poison. Even low concentrations have toxic effects on various organic systems. The mode of action of lead is not fully confirmed. It is presumed that lead interacts with biological systems either via its affinity to proteins or via its ability to displace calcium in the organism. By binding to SH groups, lead can inactivate certain enzymes, for example, δ-aminolevulinic acid dehydratase. The binding of lead to proteins such as Na-K-ATPase or carboxylic acid anhydrase can also result in changes in the conformation of the protein structure. The displacement of calcium by lead results in disturbance of calcium signals and this in turn can cause chronic neurotoxicity or effects on the cardiovascular function [5].

Sources of lead intake may be linked to an occupational exposure, but also to lead water pipes, lead-glazed ceramic pottery, lead-based paint, sport shooting, etc. In former times, the lead content in gasoline was an important source of lead exposure [2].

With an ambient monitoring, the lead concentration in air, soil, water, diet, etc. can be determined. However, biological monitoring can describe the body burden of the individual considering all exposure routes. For a diagnostic examination of the internal lead exposure, lead levels in human biological material, e.g., lead in blood and urine, are analyzed. Since the disturbance of heme synthesis is one of the most sensitive effects of lead in humans, parameters of these effects can be used as biological effect parameters. The effect of lead exposure in the human body is characterized by measuring the biological parameters (e.g., δ-aminolevulinic acid dehydratase (ALAD) and erythrocyte porphyrins (EPs) in blood; δ-aminolevulinic acid (ALA) in urine and plasma). However, it has to be considered that these parameters are not specific for a lead exposure alone, but may also be influenced by secondary factors like drugs, hormones, alcohol, hepatic damage, etc. [6].

Figure 1 gives an overview about different strategies for lead monitoring. It demonstrates that biological monitoring is an excellent tool for the toxicological risk assessment of lead exposure.

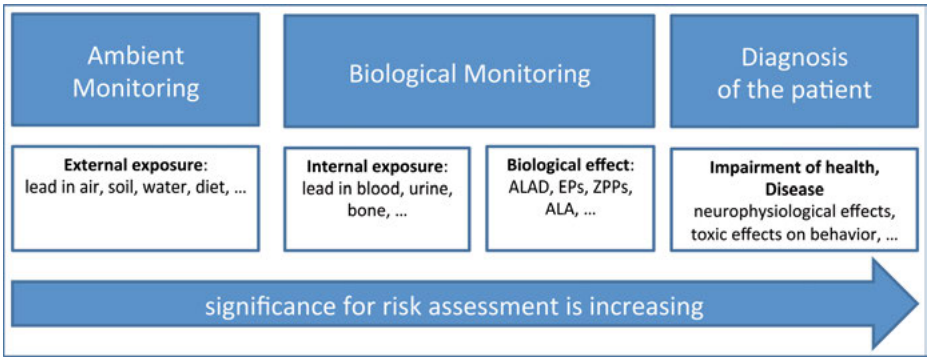

Figure 1. Lead monitoring strategies for risk assessment.

This chapter presents different biomonitoring strategies as well as analytical procedures for lead biomonitoring, which are recommended to quantify the biomarkers of exposure (concentration of lead in human biological material) as well as biomarkers of effect. Preferably, well-established standard methods of analysis are presented. In Germany, standard procedures for the biological monitoring are published by the Working Group "Analyses of Hazardous Substances in Biological Materials" of the "Commission for the Investigation of Health Hazards of Chemical Compounds in the Work Area" (AibM) [7–10]. An overview of lead biomonitoring methods is also presented in a compendium of the World Health Organization [11].

2. PHARMACOKINETICS

There are numerous studies available on the absorption, distribution, retention and excretion of lead in the human organism [1, 2, 12, 13].

2.1. Absorption and Distribution

Lead and its compounds are absorbed by the human organism via the lungs and the gastrointestinal tract. Organic lead compounds, e.g., tetraethyl lead and tetramethyl lead, can also be resorbed in toxicologically relevant amounts via the skin. At the workplace, inhalation is the most important route of absorption for lead and its inorganic compounds. In contrast, ingestions by food and drinking water are generally the most important absorption routes for the general population. However, special life style factors, e.g., smoking and sport shooting, can lead to a considerable inhalative exposure of lead [2, 14].

On average 30 % of the inhaled lead is resorbed via the lung. However, the retention depends on the solubility of the lead compound and the diameter distribution of the particles. The highest retention of lead particles in the lung has been found in about 60 % for particle diameters of > 1 μm and in 40 % for particle diameters of 0.1 μm. About 5–10 % of the ingested lead can be resorbed gastrointestinally. Under certain workplace situations, about 6 % of a dermal dose of alkyl lead compounds can be absorbed via the skin [15].

After resorption, lead appears rapidly in blood, where 94–99 % are absorbed by the red blood cells and only < 1–6 % remain in the plasma fraction [16–20]. The association between lead in plasma (Pb-P) and lead in whole blood (Pb-B) was found to be non-linear, indicating an increase of the Pb-P/Pb-B ratio with an increase of exposure [17–19, 21]. *In vitro* experiments demonstrated that the great majority of lead penetrates the erythrocyte membrane and binds at hemoglobin (80 %), whereas the minor part (14 %) is absorbed by the red blood cell membrane [22]. In plasma, the majority of lead is bound to proteins (4.5 % of blood content) and lipids (1.3 %) and only the minority of lead exists unbound. Although the red blood cells represent the main compartment of lead in blood, it is questionable whether this part is sufficiently exchangeable. Thus, the fraction of lead in plasma is supposed to exchange with the different tissues in the body [18, 23].

After distribution by blood transport, lead can be stored in different tissues of the body. One fraction of the tissues can be assigned as soft tissue compartments with a high lead exchange turnover (e.g., brain, kidney), whereas other tissues constitute a hard tissue fraction (dense bone, teeth, hair), in which lead is strongly bound and can poorly be extracted. In the steady state, the skeleton contains approximately 80–90 % of the total body lead burden [23]. The kinetic of lead in bones depends on the kind of bone compartment. Lead in the trabecular bone compartment can be extracted and represents the displaceable lead portion in bones, whereas lead in the cortical bone fraction is strongly bound and therefore displays a repository of lead. Lead readily passes the placental barrier. Fetal blood therefore has more or less the same lead concentration as the maternal

blood [24]. Lead also passes the blood–brain barrier, but is not supposed to accumulate in the brain.

2.2. Metabolism

After distribution in the organism, tetraethyl lead is metabolized via oxidative dealkylation to triethyl lead, diethyl lead, and inorganic lead [25, 26]. Oxidative dealkylation is catalyzed in the endoplasmatic reticulum of the liver cells by cytochrome P450 [26, 27]. The urine metabolites triethyl and diethyl lead have, in contrast to tetraethyl lead, ionic character and therefore their distributional behavior in the organism is different from that of tetraethyl lead. The application of an analytical procedure to tetramethyl lead-exposed individuals indicates a similar metabolism of tetramethyl and tetraethyl lead [28–30].

2.3. Elimination

The main elimination route of lead is the urinary passage, which accounts for 75–80 % of the total excretion. The secondary route is the gastrointestinal elimination pathway. Other elimination routes, e.g., hair, nails and sweat, cover altogether less than 8 % of the total excretion [2]. Additional elimination takes place within the lactation period by breast milk. In general, the rate of elimination is very slow. As the various tissues and compartments provide different characteristics of lead storage and exchange, the lead blood level displays multiphase elimination kinetics. After cessation of lead exposure the blood concentration decreases in the first phase with a half-time of 29–36 days [31–33]. Due to counterbalancing from soft tissues and the different bone compartments, further compartment elimination processes have to be considered with half-time values of 1.2 years for a second compartment and 13 years for a third compartment [31]. *In vivo* studies on the decrease of the lead concentration in bone demonstrated half-times of 6–37 years [31, 34, 35].

3. BIOMARKERS OF EXPOSURE

3.1. Review on Probable Biomarkers of Lead Exposure

The incorporated lead was found in several matrices of the human body [36–45]. Data exist for the following parameters: Lead in whole blood, in plasma or serum, in saliva, in urine, in bone, in teeth, in hair, in nails, and in breast milk.

3.1.1. Lead in Blood and Blood Compartments

The determination of lead in whole blood is the most prominent and extensively applied parameter for the biological exposure monitoring of lead. Macroscopi-

cally, the parameter provides a high sensitivity for current lead exposure and depicts an intermediate observation time featured by an elimination half-time of about one month. Moreover, the parameter is positively and adequately associated with the external exposure [19, 32, 46]. The crucial advantage of this parameter is its frequent implementation in studies on lead toxicity and thereby high availability of valid exposure limits and assessment values. Nevertheless, it has to be pointed out that whole blood is composed of two compartments with different behavior and lead kinetics. The erythrocyte fraction contains more than 90 % of the whole blood lead amount, and thus possesses the higher detectability of lead. However, the lead is absorbed in the red blood cell or adsorbed at the cell membranes, which results in a low ability to exchange the element with other tissues. In contrast, blood plasma regularly contains only 1 % of lead (in special instants up to 6 %), but displays a compartment that enables the exchange of lead with other compartments and tissues without restriction [17–19, 21, 45, 47].

Whereas no special investigations of erythrocyte lead have been reported, several studies presented the levels of plasma lead and their association with other parameters of internal exposure, particularly with bone lead [17, 36, 47]. Thus, lead in plasma was supposed to represent the interchangeable and therefore capable of acting internal lead fraction [36]. The determination of lead in plasma and serum is challenged by the very low concentration. Contradicting results in former studies were explained by insufficient analytical techniques and the high risk of contamination [36, 37]. However, the progress in analytical performance within the last two decades may have improved the ability to gain valid data for lead in plasma. Nevertheless, the lack of data inhibits the evaluation of this parameter to date [37].

3.1.2. Lead in Saliva

Saliva is a biological matrix which is considered as a surrogate of blood levels, particularly of the plasma compartment [39]. Saliva lead biomonitoring was applied to occupationally exposed subjects as well as in general populations [48–54]. Consistently, all studies revealed a correlation between saliva lead and blood lead only above the current occupational exposure limits. Furthermore, the saliva lead levels in occupationally not exposed subjects differ distinctly between the different studies, which may be explained by different saliva sampling techniques and procedures [39, 51]. In summary, this parameter might be suitable for lead exposure assessment in principle, but has the disadvantage of its low sensitivity and the lack of sampling standardization.

3.1.3. Lead in Urine

Another probable biomonitoring parameter is the determination of lead in urine. This approach is supported by the fact that urinary excretion is the major elimination route of lead. Moreover, a significant correlation was found between urine lead and blood lead in both, occupationally exposed employees and indi-

viduals of the general population without occupational exposure [19, 21, 43, 55–57]. However, the comparison of both parameters by a linear correlation model showed high variance and uncertainty in general, which may be explained by different kinetic behavior of both parameters.

The correlation between urine lead and plasma lead was found to be comparable or slightly stronger than between urine lead and blood lead [19, 21]. Presently, scientific knowledge on the association between urinary lead levels and toxic effects is poor, which contradicts the evaluation of health-based exposure limits for this parameter. Consequently, the use of the parameter for risk assessment of lead exposure is limited.

3.1.4. Lead in Bone

On the one hand, the skeleton contains approximately 80–90 % of the total body lead burden in the steady state [23]. On the other hand, lead exchange between bone and the distribution media blood occurs very slowly, which is characterized by elimination half-times of 6–37 years, depending on the bone compartment [31, 34, 35, 58]. Consequently, the bone lead level shows the strongest correlation with the cumulative lead exposure [38, 59]. Nevertheless, the rapid exchange pool in the trabecular bone compartment is also correlated with the lead blood concentration during regular exposure situations. In summary, bone lead represents the cumulative exposure, but is disadvantaged for reflecting fluctuating acute exposure to lead.

3.1.5. Lead in Other Materials

Data on lead contents also exists for hair of different body regions [49,50,60,61], teeth [42, 62, 63], finger and toe nails [41, 60, 61, 64], sweat [52], and breast milk [44]. However, the studies did not reveal any of these parameters as powerful biomarkers of lead exposure.

Overviews of analytical methods for determining lead in human biological material are given in Tables 1 to 3 below. For biomonitoring after occupational as well as environmental exposure to lead, the quantification of **lead in whole blood** has been established as the most suitable parameter to date.

3.2. Pre-analytical Phase

The ubiquitous presence of lead in the environment has to be considered during the analytical process. There is a contamination risk during the whole process of sampling and analysis, which has to be minimized by a strict laboratory practice.

As in any trace element analysis, it is of major importance to use reagents of the highest purity and contaminant-free tips of automatic pipettes, tubes, and glassware. Plastic tubes used for specimen collection and treatment must be individually cleaned with 1 M nitric acid to avoid exogenous contamination. There-

fore, the tubes are filled with acid and allowed to stand for at least two hours. Afterwards, they are rinsed two to three times with deionized water and then with ultrapure water before drying them. The cleaning can be made more effectively by warming the nitric acid [8].

3.3. Analytical Methods for the Determination of Lead

Standard procedures for analyzing lead concentrations in blood and urine are inductively coupled plasma mass-spectrometry (ICP-MS) and atomic absorption spectrometry (AAS) [65–67]. Furthermore, electrochemical methods can be applied. Several factors influence the choice of the analytical method, e.g., the matrix, the required detection limit as well as the competence of the laboratory staff.

3.3.1. Inductively Coupled Plasma-Mass Spectrometry

The inductively coupled plasma-mass spectrometry is a multi-element technique enabling the very sensitive quantification of a number of trace elements in one analytical run. Briefly, the sample is heated in argon-plasma activated by a high-voltage field. Thereby, atoms in the sample are ionized. Using an electric field, the generated ions are extracted from the plasma and accelerated to the analyzer of the mass spectrometer, where they are separated according to the mass-to-charge-ratio of the specific isotopes. Sector field as well as quadrupole instruments are suitable for this approach.

With ICP-MS methods, lead in **urine and blood** after occupational or environmental exposure can be determined sensitively, specifically, and with little effort of sample preparation. Sample preparation is mostly acidic digestion or dilution. Triton® X-100 is added for the solubilization of blood cell membranes and proteins [68]. Detection limits for ICP-MS analysis in blood or urine are reported in the range from 0.008 μg/L to 1.0 μg/L [8, 68–80] (see Table 1).

The MAK Commission has published a standard procedure for the determination of lead in urine. Briefly, after UV digestion of the urine samples, a solution of rhodium and iridium is added as internal standard and the samples are introduced into the quadrupole ICP-MS with a pneumatic nebulizer. Quantification is carried out using the standard addition procedure. With a detection limit of 0.03 μg/L urine, this method can be applied to the occupational as well as environmental exposure range [8]. Besides blood and urine, ICP-MS methods are presented for other biological materials such as plasma, saliva, hair, and nails [48, 64, 71, 81].

Table 1. Lead analysis with ICP in human biological materials.

Analytical method	Sample matrix	Preparation method	LOD	Ref.
ICP-SF-MS	blood	microwave digestion with nitric acid	0.1 μg/L	[74]
ICP-MS	blood	acidic dilution with butanol, nitric acid, and Triton® X-100	0.02 μg/L	[70]
LA-ICP-MS	blood	drying on filter membrane	0.1 μg/L	[73]
ICP-MS	blood	dilution with Triton® X-100 and NH_4OH	0.008 μg/L (LOQ)	[72]
ICP-MS	blood	wet digestion with nitric acid and perchloric acid	0.1 ppb	[79, 128]
ICP-MS	blood	dilution with tetramethylammonium hydroxide, Triton® X-100, ammonium pyrrolidinedithiocarbamate, and isopropanol	4.8 μg/L	[68]
ICP-MS	blood	dilution with HNO_3, Triton® X-100 as well as Rh and Ir (as internal standards)	0.5 μg/L	[77]
ICP-MS	blood serum	dilution with ammonia, Triton® X-100 and EDTA	1.0 μg/L blood 0.1 μg/L serum	[69, 129]
DRC-ICP-MS	blood urine	dilution with *t*-butanol, HCl, and Au	0.38 μg/L	[76]
ICP-MS	whole blood, plasma, urine, hair	dilution with nitric acid, Triton® X-100 and butanol; hair: mineralization with nitric acid, dilution with nitric acid, Triton® X-100 and butanol	0.019 μg/L (blood), 0.028 μg/L (plasma), 0.017 μg/L (urine), 0.0003 μg/g (hair)	[71]
ICP-QMS	urine	UV digestion with HNO_3/H_2O_2	0.03 μg/L	[8]
LA-ICP-MS	urine	drying	0.03 μg/g creatinine	[75]
HR-ICP-MS	urine	dilution with HNO_3, In as internal standard	< 8 pg/g	[80]
ICP-MS	urine	dilution with HNO_3/HCl	0.03 μg/L	[78]
ICP-MS	finger and toe nails	mineralization with nitric acid, dilution with nitric acid, Triton® X-100, and butanol	0.0003 μg/g	[64]
IH-ETV-ICP-MS	hair	IH-ETV	0.04 μg/g	[81]
ICP-MS	saliva, plasma	dilution with ammonia Na_2EDTA and Triton® X-100	0.02 μg/L saliva 0.03 μg/L plasma	[48]

DRC = dynamic reaction cell; HR = high resolution; ICP = inductively coupled plasma; IH-ETV = induction heating-electrothermal vaporizer; LA = laser ablation; LOD = limit of detection; LOQ = limit of quantification; MS = mass spectrometry; QMS = quadrupole mass spectrometry; SF-MS = sector field mass spectrometry.

3.3.2. Atomic Absorption Spectrometry

Another standard procedure for a lead quantification is the atomic absorption spectrometry. Here, the sample is heated by a flame or in a furnace, until the element atomizes. The atoms absorb light at their resonance line. The attenua-

Table 2. Lead analysis with AAS in human biological materials.

Analytical method	Sample matrix	Preparation method	LOD	Ref.
F-AAS	blood	complexation with APDC, extraction with methyl isobutyl ketone	15 µg/L	[7]
GF-AAS (EC-THGA)	blood	dilution with Triton® X-100, nitric acid and trichloroacetic acid; W, Rh, and $NH_4H_2PO_4$ as modifiers	0.65 µg/L	[85]
GF-AAS	blood	dilution with diammonium hydrogen phosphate and Triton® X-100	2.0 µg/L	[87]
GF-AAS (THGA)	blood	dilution with $NH_4H_2PO_4$ modifier, Triton® X-100 and HNO_3	10 µg/L	[77]
GF-AAS	blood, food	wet ashing with nitric acid and perchloric acid	not specified	[128]
GF-AAS	urine	acidification, microwave digestion with HNO_3/HCl, modifier $Mg(NO_3)_2$	0.2 µg/L	[84]
GF-AAS	human milk	digestion with HNO_3/H_2O_2	3.4 µg/L	[83]
GF-AAS	blood, urine, hair, saliva	hair: dilution with HNO_3, HCl, H_2O_2 and microwave digestion blood, urine, hair, saliva: dilution with matrix modifier $NH_4H_2PO_4$, Triton® X-100 and nitric acid	0.8 µg/L	[49, 86]
GF-AAS	blood, urine, scalp hair	microwave digestion with HNO_3/H_2O_2	~1 µg/L	[82]
HR-CS AAS	tissue, human hair, bovine blood	direct solid sampling	0.01 µg/g	[130]
GF-AAS	blood, serum, hair	microwave digestion with HNO_3/ H_2O_2, colloidal Pd as modifier	1.2 µg/L	[88]
AAS	saliva, hair	digestion with HNO_3	1.5 µg/L saliva; 0.2 µg/g hair	[50, 131]

AAS = atomic absorption spectrometry, APDC = ammonium pyrrolidin dithiocarbamidate, EC-THGA = end-capped transversal heating graphite tubes, F-AAS = flame atomic absorption spectrometry, GF-AAS = graphite furnace atomic absorption spectrometry, HR-CS AAS = high-resolution continuum source AAS.

tion of intensity of the light beam can be measured. Using the AAS procedure, every element has to be analyzed separately at a special wavelength.

In clinical chemistry, the parameter lead in **blood** is predominantly chosen and quantified with graphite furnace atomic absorption spectrometry (GF-AAS), also known as electrothermal AAS (ET-AAS). In general, blood samples are directly analyzed after dilution and addition of a matrix-modifier. Solubilizers (Triton® X-100) or modifiers (e.g., diammonium hydrogen phosphate, Pd components) are added to minimize matrix effects. For samples with very low lead concentrations, a pre-concentration can be achieved by chelation and extraction with a mixture of organic solvents. Additionally, there are many different methods for lead determination in **urine, hair, saliva, serum, tissue, and human milk** in the literature (for some examples, see Table 2). Flame AAS is still used in many laboratories because of a good precision at low costs and a high sample throughput. However, for the determination of low physiological concentrations like lead in blood, the limit of detection is not sufficient. The detection limits for AAS methods are in the range of 0.2 to 15 μg/L [7, 50, 77, 79, 82–88]. Thus, for the quantification of lower lead concentrations, high resolution AAS or the ICP-MS technique are needed.

3.3.3. Electrochemical Methods

Voltammetry is described as a very sensitive, but also a very time-consuming analytical technique [89]. Thus, it is not established for application in routine analytics [90]. Nevertheless, this thechnique can be applied as an independent reference procedure for quality control of the mainly applied AAS and ICP-MS-procedures in environmental as well as occupational-medical samples [9] (Table 3).

In **differential pulse anodic stripping voltammetry (DPASV)**, lead ions are first reduced and amalgamated at the working electrode, which is a hanging mercury drop electrode or a mercury film electrode, during pre-electrolysis at a suitable applied potential. In the second step, the reduced amalgamated lead is re-oxidized by means of a potential ramp imposed between the working electrode and a platinum rod electrode [91]. When the specific voltage for lead is reached, the ions are released ("stripped") from the electrode and can be measured as current. The resulting peak is proportional to the lead concentration of the solution. The procedure is influenced by water-soluble proteins present in urine samples because surface active substances may influence the hanging mercury drop. Therefore, the complete elimination of the biological matrix has to be achieved with digestion [9, 92]. Additionally, intermetallic interferences may influence the results. For example, if lead and thallium are present in the same sample, their peaks are observed at very similar voltages [9]. DPASV procedures have been applied to analyze lead in blood and urine [9, 91–93] and in human hair [94]. The samples were prepared by digestion with acids.

During **potentiometric stripping analysis (PSA)**, trace elements or ions are pre-concentrated by potentiostatic deposition on an electrode (e.g., mercury film on a glassy-carbon electrode). In contrast to DPASV, PSA is not subject to background interferences from organic electroactive constituents in the sample or to

Table 3. Analytical procedures using electrochemical methods (stripping voltammetry) for lead analysis in biological materials.

Analytical method	Sample matrix	Preparation method	LOD	Ref.
DPASV	blood and urine	digestion with HNO_3/H_2SO_4; acetate buffer and citrate solution	10 μg/L blood 3 μg/L urine	[9]
DPASV	blood	digestion with $HNO_3/HClO_4$	0.5 μg/L	[93]
ASV	blood			[132]
DPASV	urine	microwave digestion with nitric acid; acetate buffer for pH adjustment	0.0033 μg/L	[91]
DPASV	urine	digestion with HNO_3, acetate buffer	not specified	[92]
DPASV	hair	microwave digestion with HNO_3/ H_2O_2	0.04 μg/g	[94]
PSA	blood	dilution with solution of KCl, $HgCl_2$, $NiCl_2$, 2-octanol and Triton® X-100, adjustment to pH 1,3–1,4 with 6 M HCl	10 μg/L	[95]
PSA	blood	HCl, $HgCl_2$ in HCl	not specified	[93]
PSA	blood	dissolve in tetramethylammonium hydroxide, dilution with Hg(II) in HCl as matrix modifier	2.5 μg/L	[96]
PSA	blood	dilution with 0.5 M HCl	0.1 μg/L	[89]
PSA	urine	HCl	1 nM	[97]

DPASV = differential pulse anodic stripping voltammetry, PSA = potentiometric stripping analysis.

the presence of dissolved oxygen [89]. Blood samples are diluted with HCl because the hemoglobin as predominant protein of the erythrocytes is soluble only in hydrochloric acid, but not in nitric or perchloric acid [95]. PSA is used to analyze lead in whole blood [89, 93, 95, 96] and urine [97].

3.3.4. Further Methods

As described before, bone lead features as biomarker for long-term exposure to lead [58, 98]. Lead concentrations in bones can be measured with **X-ray fluorescence spectroscopy (XRF)**. This method depends on the detection of photons generated in lead by an externally incident beam of radiation. Photon emission is produced by an incident beam of X-rays or gamma rays interacting with the atomic electrons of lead, resulting in the emission of characteristic fluorescent photons [98, 99]. The discrete energy of emitted X-rays is specific for each element. This enables the determination of the atomic number as well as the concentration of the element by measuring the energy and fluence rate of the X-rays [58]. In the past, different XRF approaches have been developed, although the one using ^{109}Cd excited K XRF is most widely used [100]. With XRF, analysis

of lead concentrations in the bones can be carried out *in vivo;* it is mainly applied for clinical measurements in the bones of persons occupationally exposed to lead [100, 101]. The radiation dose has to be kept as low as possible and in every case within the range of other diagnostic procedures.

3.4. Quality Assurance

To ensure the quality of the analysis, an internal quality control should be performed with each analytical run. Control materials for an internal lead quality control are commercially available, e.g., certified reference material for trace elements in urine and whole blood.

An appropriate external quality assessment is necessary to assure the accuracy and comparability of the results with other laboratories. For external quality control, participation in a round robin test is a helpful tool. There are various quality control programs containing lead in blood and urine (see Table 4). One example is the international program of the German External Quality Assessment Scheme (G-EQUAS), where lead analysis can be tested for the concentrations found in the occupational as well as environmental exposure range [102]. Other prominent international proficiency test programs, which include lead in blood, are PCI and QMEDQAS from Canada as well as LAMP and a proficiency testing program from the USA (Table 4).

Table 4. Examples for quality control programs for the determination of lead in different matrices.

Country	Program	Matrix	Reference
Germany	G-EQUAS	Pb in blood Pb in urine δ-aminolevulinic acid (ALA)	http://www.g-equas.de/
Canada	PCI	Pb in blood Pb in urine	https://www.inspq.qc.ca/en/ctq/eqas
	QMEQAS	Pb in hair, blood, serum, urine	https://www.inspq.qc.ca/en/ctq/eqas
USA	LAMP	Pb in blood	http://www.cdc.gov/labstandards/lamp.html
	proficiency test program	Pb in blood	http://www.wadsworth.org/regulatory/clep/pt

3.5. Evaluation of Human Biomonitoring

The reference value describes the background levels of lead in the environment in a reference population which is not occupationally exposed to lead (95th per-

centile). The Human Biomonitoring Commission of the German Federal Environment Agency published reference values (95th percentile of the lead background exposure) of 70 μg/L for women and 90 μg/L for men (aged 18–69 years) as well as 35 μg/L for children aged 3–14 years [103]. The MAK Commission evaluated a reference value for the population of working age (BAR) of 70 μg lead/L blood for women [4]. The lead concentration is influenced by age, hematocrit, lead concentration in the domestic drinking water, and the consumption of drinks with a low alcohol concentration. The data are based on the German Environmental Survey 1998. Compared to the former Environmental Survey from 1990/92, the lead concentration in blood decreased around 30 % over the time, e.g., because of reduced concentrations in gasoline [104]. A revision of the reference values is expected.

For occupational exposure assessment a biological guidance value (BLW) of 300 μg/L blood for men and women older than 45 years is established by the MAK Commission [105]. This value covers the most toxic effects of lead except carcinogenicity. For women of child-bearing age, a reference value (BAR) of 70 μg/L should be considered. The European "Scientific Committee on Occupational Exposure Limits" (SCOEL) recommends a biological limit value of 300 μg/L for lead in blood [3]. The "American Conference of Governmental Industrial Hygienists" (ACGIH) recommends a Biological Exposure Index of 300 μg lead/L blood. Moreover, they emphasize that women of child-bearing potential, with lead concentrations in blood exceeding 100 μg/L, are at risk for delivering a child with elevated blood Pb. These children may encounter an increased risk of cognitive deficits, if the blood Pb remains elevated. They recommend regular monitoring and appropriate steps for minimizing the child's exposure to environmental lead [106].

4. BIOMARKERS OF EFFECT

4.1. Overview

Long term exposure to lead may cause a disturbance of the porphyrin synthesis. In the hematopoietic system, δ-aminolevulinic acid is generated from the succinyl coenzyme A. Influenced by the enzyme δ-aminolevulinic acid dehydratase, ALA can form porphobilinogen, a basis for heme biosynthesis. Increasing levels of Pb^{2+} ions may inhibit ALAD [6,107]. This effect may be recognized in humans by the following parameters:

- δ-aminolevulinic acid dehydratase, erythrocyte porphyrins or zinc protoporphyrins in erythrocytes
- δ-aminolevulinic acid in urine and plasma
- coproporphyrin in urine

Effect parameters alone are not recommended for the characterization of the internal lead exposure, either for methodological or practical reasons, or for

reasons of inadequate sensitivity because the levels of exposure to lead at the workplace are lower than in former times [90].

4.2. Analytical Methods for Biomarkers of Effect

4.2.1. δ-Aminolevulinic Acid Dehydratase

The activity of the enzyme ALAD in blood can be quantified with a standard procedure of the AibM working group [108]. Therefore, ALAD is incubated with a maximum of the substrate concentration of ALA. The new generated porphobilinogen reacts with the modified Ehrlich's solution, and can be quantified photometrically at 555 nm against a blank.

4.2.2. Free Erythrocyte Porphyrins and Zinc Protoporphyrins

Free erythrocyte porphyrins do (contrary to heme) not contain iron, thus they are referred to as iron "free." Erythrocytes protoporphyrins are other names for EPs, because the erythrocytes contain mainly protoporphyrin IX. Predominantly, EPs are bound to zinc and therefore are called zinc protoporphyrins (ZPP) [109, 110].

In isolated erythrocytes, the free EPs can be quantified with **fluorescence spectroscopy**. The free EPs are extracted with ethyl acetate and acetic acid. After centrifugation, the EPs are extracted with hydrochloric acid solution. The extinctions of these acidic extracts are analyzed at 405/610 nm against a blank [110].

A **hematofluorometer** measures the ratio between the amount of ZPP fluorescence and the amount of light absorbed by oxyhemoglobin [111,112].

In addition, ZPP and PP can be quantified using **high performance liquid chromatography** (**HPLC) methods** with fluorescence detection [112–114].

4.2.3. δ-Aminolevulinic Acid in Urine and Plasma

In older publications, ALA in urine is analyzed mainly photometrically. Briefly, ALA is separated from the matrix using ion exchange columns. ALA is eluated from the cation exchanger with sodium acetate solution and reacts with 2,4-pentanedione to a pyrrol ring. After adding the Ehrlich's solution (4-(dimethylamino)-benzaldehyde hydrochloric acid solution), a red dye can be quantified photometrically at 553 nm [107].

Newer methods use HPLC and liquid chromatography tandem mass spectrometry (LC-MS/MS) procedures for the determination of ALA in urine and plasma. For the HPLC procedures, ALA in urine is derivated with acetylacetone and formaldehyde [115–117] or dansyl chloride [118], separated with HPLC and quantified using fluorescence detection. The LC-MS/MS procedures require a solid phase extraction and butanol derivatization [119], acidification with trichlo-

roacetic acid and filtration [120] or dilution with acetonitrile and centrifugation [121] as sample preparation prior to the analysis.

4.2.4. Coproporphyrin in Urine

The coproporphyrin in urine is extracted with diethyl ether. The organic phase is washed and re-extracted with a hydrochloric acid solution. The extinctions of this acidic extract are determined spectrophotometrically at 380, 401, and 421 nm. For quantification, urine is spiked with a reference standard and processed in the same way as the urine samples [122].

Newer publications describe procedures using HPLC or ultra high performance liquid chromatography, which even enable a separation of coproporphyrin isomer I and III [123, 124].

4.3. Evaluation of Biological Effect Data

The normal ranges for laboratory parameters of the porphyrin metabolism are shown in Table 5. An **acute lead intoxication** may cause a sharp increase in ALA (> 300 μmol/24 h) and coproporphyrin III (total porphyrin up to 15 μmol/24 h, > 80 % coproporphyrin) and a minor increase in porphobilinogen in urine. In erythrocytes, zinc protoporphyrin is increased, while the ALAD activity is strongly reduced [6,125].

Table 5. Reference ranges for parameters of porphyrin and porphyrin metabolism (according to [6]).

Parameter	Matrix	Reference range
δ-aminolevulinic acid dehydratase	erythrocytes	varies in wide range
zinc protoporphyrin	erythrocytes	0.09–0.15 μmol/L blood
δ-aminolevulinic acid	urine	2–49 μmol/24 h
total porphyrin	urine	< 0.12 μmol/24 h
thereof coproporphyrin isomer I		17–31 %
thereof coproporphyrin isomer III		69–83 %

A **chronic lead intoxication** leads to moderate coproporphyrinuria (0.5–2.0 μmol/24 h). The ALA excretion is in the range of 10–50 μmol/24 h [6]. The ALA level in urine will increase, when Pb-B is in excess of 170–340 μg/L blood [126]. For protoporphyrin (as ZPP), even a minor increase over the reference range is relevant, while concentrations up to 6 μmol/L are characteristic after a lead intoxication [6]. The activity of ALAD is inhibited by lead to less than 10 % of the normal activity. Due to the genetic variability, the normal activity of ALAD in the general population varies over a wide range [6]. Willi et al. [127]

published a reference range for ALAD of 761–1211 mmol/L/h. In lead-exposed workers, they found an ALAD concentration of 13–350 mmol/L/h, while blood lead concentrations are 192–671 μg/L.

5. CONCLUSIONS

The analysis of lead concentrations in biological material is mainly performed with ICP-MS or AAS. In general, ICP-MS attains higher sensitivity and specifity than AAS. Additionally, electrochemical methods can be applied, which are specific and may serve as a reference procedure. XRF techniques are applied to an *in vivo* quantification of lead in bones. The predominant sample matrices include blood and bone, but urine, hair, saliva, and tissue are also analyzed.

For a characterization of biological effects of lead in humans, the determination of several laboratory parameters in blood and urine (ALAD, ZPP, ALA, coproporphyrins) is recommended. For their interpretation, the combination with lead exposure assessment is essential.

ABBREVIATIONS AND DEFINITIONS

AAS	atomic absorption spectrometry
ACGIH	American Conference of Governmental Industrial Hygienists
AibM	Working Group "Analyses of Hazardous Substances in Biological Materials" of the "Commission for the Investigation of Health Hazards of Chemical Compounds in the Work Area"
ALA	δ-aminolevulinic acid
ALAD	δ-aminolevulinic acid dehydratase
APDC	ammonium pyrrolidine dithiocarbamidate
BAR	reference value ("Biologischer Arbeitsstoff Referenzwert")
BLW	biological guidance value ("Biologischer Leitwert")
DRC	dynamic reaction cell
DPASV	differential pulse anodic stripping voltammetry
EC-THGA	end-capped transversal heating graphite tubes
EDTA	ethylenediamine-N,N′,N″,N‴-tetraacetate
EP	erythrocyte porphyrins
ET-AAS	electrothermal atomic absorption spectrometry
ETV-ICP-MS	electrothermal vaporization inductively coupled plasma-mass spectrometry
F-AAS	flame atomic absorption spectrometry
G-EQUAS	German External Quality Assessment Scheme
GF-AAS	graphite furnace atomic absorption spectrometry

HPLC	high performance liquid chromatography
HR-CS AAS	high-resolution continuum source AAS
ICP-MS	inductively coupled plasma-mass spectrometry
IH-ETV	induction heating-electrothermal vaporizer
LA-ICP-MS	laser ablation inductively coupled plasma-mass spectrometry
LAMP	Lead and Multielement Proficiency Program
LC-MS/MS	liquid chromatography tandem mass spectrometry
LOD	limit of detection
LOQ	limit of quantification
MAK Commission	German Commission for the Investigation of Health Hazards of Chemical Compounds in the Work Area
MS	mass spectrometry
PCI	Interlaboratory Comparison program for Metals in Biological Matrices
PSA	potentiometric stripping analysis
Pb-P	lead concentration in plasma
Pb-B	lead concentration in whole blood
QMEQAS	Quebec Multielement External Quality Assessment Scheme
QMS	quadrupole mass spectrometry
SCOEL	Scientific Committee on Occupational Exposure Limits
SF-MS	sector field mass spectrometry
XRF	X-ray fluorescence spectroscopy
ZPP	zinc protoporphyrins

REFERENCES

1. *Lead and Its Inorganic Compounds*, *Occupational Toxicants. Critical Data Evaluation for MAK Values and Classification of Carcinogens*, Ed. H. Greim, Vol. 17, Wiley, Weinheim, 2002.
2. WHO, "Inorganic Lead", IPCS (International Programme on Chemical Safety). *Environmental Health Criteria* 165, World Health Organization, Geneva, 1995.
3. SCOEL, "Recommendation from the Scientific Committee on Occupational Exposure Limits for lead and its inorganic compounds: SCOEL/SUM/83", 2002.
4. Deutsche Forschungsgemeinschaft, *List of MAK and BAT Values 2016: Maximum Concentrations and Biological Tolerance Values at the Workplace (http://onlinelibrary.wiley.com/book/10.1002/3527600418/homepage/access_to_the_list_of_mak_and_bat_values.htm)*, Wiley VCH, Weinheim, 2016.
5. T. Sanders, Y. Liu, V. Buchner, P. B. Tchounwou, *Rev. Environ. Health* **2009**, *24,* 15–45.
6. L. Thomas, *Labor und Diagnose, Indikation und Bewertung von Laborbefunden für die medizinische Diagnostik*, TH-Books Verlagsgesellschaft mbH, Frankfurt/Main, 2012.
7. K. H. Schaller, W. Pilz, *Lead. Determination in Blood (Atomic absorption spectrometry)*, in *Analyses of Hazardous Substances in Biological Materials.* Eds J. Angerer, K. H. Schaller, D. Henschler, Vol. 2, VCH, Weinheim, 1985.

8. P. Schramel, I. Wendler, L. Dunemann, H. Fleischer, H. Emons, *Lead in Urine (ICP-MS)*, in *Analyses of Hazardous Substances in Biological Materials. The MAK Collection for Occupational Health and Safety.* Eds J. Angerer, K. H. Schaller, H. Greim, Vol. 2, Wiley-VCH, Weinheim, 1999.
9. H. Seiler, J. Angerer, *Lead (Inverse voltammetry)*, in *Analyses of Hazardous Substances in Biological Materials.* Eds J. Angerer, K. H. Schaller, D. Henschler, Vol. 2, VCH, Weinheim, 1988.
10. T. Göen, E. Eckert, A. Schäferhenrich, A. Hartwig, *Int. J. Hyg. Envir. Heal.* **2012**, *215*, 233–237.
11. WHO, "Biological monitoring of chemical exposure in the workplace, Guidelines", 1, World Health Organization, Geneva, 1996.
12. A. C. Chamberlain, *P. Roy. Soc. B-Biol. Sci.* **1985**, *224*, 149–182.
13. S. Skerfving, U. Nilsson, A. Schütz, L. Gerhardsson, *Scand. J. Work Env. Health* **1993**, *19*, 59–64.
14. E. Ochsmann, T. Göen, K. H. Schaller, H. Drexler, *Int. J. Hyg. Envir. Health* **2009**, *212*, 557–561.
15. E. P. Laug, F. M. Kunze, *J. Ind. Hyg. Toxicol.* **1948**, *30*, 256–259.
16. A. Cavalleri, C. Minoia, *Scand. J. Work Env. Health* **1987**, *13*, 218–220.
17. W. I. Manton, J. D. Cook, *Bri. J. Ind. Med.* **1984**, *41*, 313–319.
18. A. Schütz, I. A. Bergdahl, A. Ekholm, S. Skerfving, *Occup. Environ. Med.* **1996**, *53*, 736–740.
19. A. Schütz, M. Olsson, A. Jensen, L. Gerhardsson, J. Börjesson, S. Mattsson, S. Skerfving, *Int. Arch. Occ. Env. Health* **2005**, *78*, 35–43.
20. M. R. Moore, *Sci. Total Environ.* **1988**, *71*, 419–431.
21. I. A. Bergdahl, S. Skerfving, *Am. J. Ind. Med.* **1997**, *32*, 317–318.
22. C. N. Ong, W. R. Lee, *Br. J. Ind. Med.* **1980**, *37*, 78–84.
23. R. W. Baloh, *Arch. Environ. Health* **1974**, *28*, 198–208.
24. H. Roels, G. Hubermont, J. P. Buchet, R. Lauwerys, *Environ. Res.* **1978**, *16*, 236–247.
25. J. E. Casida, E. C. Kimmel, B. Holm, G. Widmark, *Acta Chem. Scand.* **1971**, *25*, 1497.
26. J. E. Cremer, *Br. J. Ind. Med.* **1959**, *16*, 191–199.
27. D. F. Da Silva, H. Diehl, *Xenobiotica* **1985**, *15*, 789–797.
28. M. Blaszkewicz, G. Baumhoer, B. Neidhart, Z. Myslak, T. Rest, E. Wandel, *Verh. Dt. Ges. Arbeitsmed.* **1988**, *28*, 603–605.
29. M. Blaszkewicz, G. Baumhoer, B. Neidhart, R. Ohlendorf, M. Linscheid, *J. Chromatogr.* **1988**, *439*, 109–119.
30. W. Zhang, G. G. Zhang, H. Z. He, H. M. Bolt, *Int. Arch. Occ. Env. Health* **1994**, *65*, 395–399.
31. U. Nilsson, R. Attewell, J. O. Christoffersson, A. Schutz, L. Ahlgren, S. Skerfving, S. Mattsson, *Pharmacol. Toxicol.* **1991**, *68*, 477–484.
32. M. B. Rabinowitz, G. W. Wetherill, J. D. Kopple, *J. Clin. Invest.* **1976**, *58*, 260–270.
33. A. Schütz, S. Skerfving, J. Ranstam, J. O. Christoffersson, *Scand. J. Work Env. Health* **1987**, *13*, 221–231.
34. J. O. Christoffersson, L. Ahlgren, A. Schütz, S. Skerfving, S. Mattsson, *Arch. Environ. Health* **1986**, *41*, 312–317.
35. J. Price, A. W. Grudzinski, P. W. Craswell, B. J. Thomas, *Arch. Environ. Health* **1992**, *47*, 256–262.
36. F. Barbosa, J. E. Tanus-Santos, R. F. Gerlach, P. J. Parsons, *Environ. Health Persp.* **2005**, *113*, 1669–1674.
37. I. A. Bergdahl, S. Skerfving, *J. Toxicol. Env. Health A* **2008**, *71*, 1235–1243.
38. M. L. Bleecker, F. E. Mcneill, K. N. Lindgren, V. L. Masten, D. P. Ford, *Toxicol. Lett.* **1995**, *77*, 241–248.

39. B. Michalke, B. Rossbach, T. Göen, A. Schäferhenrich, G. Scherer, *Int. Arch. Occup. Environ. Health* **2015**, *88*, 1–44.
40. P. S. Barry, *Br. J. Ind. Med.* **1975**, *32*, 119–139.
41. B. L. Gulson, *Sci. Total Environ.* **1996**, *177*, 323–327.
42. B. L. Gulson, *Environ. Health Persp.* **1996**, *104*, 306–312.
43. B. L. Gulson, M. A. Cameron, A. J. Smith, K. J. Mizon, M. J. Korsch, G. Vimpani, A. J. McMichael, D. Pisaniello, C. W. Jameson, K. R. Mahaffey, *Environ. Res.* **1998**, *78*, 152–160.
44. B. L. Gulson, C. W. Jameson, K. R. Mahaffey, K. J. Mizon, N. Patison, A. J. Law, M. J. Korsch, M. A. Salter, *Environ. Health Perspect.* **1998**, *106*, 667–674.
45. W. I. Manton, S. J. Rothenberg, M. Manalo, *Environ. Res.* **2001**, *86*, 263–273.
46. M. Kentner, T. Fischer, G. Richter, *Int. Arch. Occup. Environ. Health* **1994**, *66*, 23-31.
47. M. Hernandez-Avila, D. Smith, F. Meneses, L. H. Sanin, H. Hu, *Environ. Health Perspect.* **1998**, *106*, 473–477.
48. F. Barbosa, M. Heloisa, C. Rodrigues, M. R. Buzalaf, F. J. Krug, R. F. Gerlach, J. E. Tanus-Santos, *Arch. Toxicol.* **2006**, *80*, 633–637.
49. F. Gil, A. F. Hernández, C. Márquez, P. Femia, P. Olmedo, O. López-Guarnido, A. Pla, *Sci. Total Environ.* **2011**, *409*, 1172–1180.
50. M. Wilhelm, A. Pesch, U. Rostek, J. Begerow, N. Schmitz, H. Idel, U. Ranft, *Sci. Total Environ.* **2002**, *297*, 109-118.
51. D. Koh, V. Ng, L. H. Chua, Y. Yang, H. Y. Ong, S. E. Chia, *Occup. Environ. Med.* **2003**, *60*, 696–698.
52. F. O. Omokhodion, G. W. Crockford, *Sci. Total Environ.* **1991**, *103*, 113–122.
53. A. Y. S. Pan, *J. Toxicol. Env. Health* **1981**, *7*, 273–280.
54. J. F. Staff, A. H. Harding, J. Morton, K. Jones, E. A. Guice, T. McCormick, *Toxicol. Lett.* **2014**, *231*, 270-276.
55. S. Skerfving, *Arbeite och Hälsa* **1993**, *1*.
56. Y. Fukui, M. Miki, H. Ukai, S. Okamoto, S. Takada, K. Higashikawa, M. Ikeda, *Int. Arch. Occup. Environ. Health* **1999**, *72*, 516–520.
57. S. W. Tsaih, J. Schwartz, M. L. T. Lee, C. Amarasiriwardena, A. Aro, D. Sparrow, H. Hu, *Environ. Health Persp.* **1999**, *107*, 391–396.
58. J. Börjesson, S. Mattsson, *X-Ray Spectrom.* **2008**, *37*, 58–68.
59. I. A. Bergdahl, U. Stromberg, L. Gerhardsson, A. Schütz, D. R. Chettle, S. Skerfving, *Scand. J. Work Env. Health* **1998**, *24*, 38–45.
60. M. Wilhelm, D. Hafner, I. Lombeck, F. K. Ohnesorge, *Sci. Total Environ.* **1991**, *103*, 199–207.
61. M. Kim, K. Kim, *Biol. Trace Elem. Res.* **2011**, *143*, 794–802.
62. G. R. C. de Almeida, C. D. Guerra, G. D. S. Leite, R. C. Antonio, F. Barbosa, J. E. Tanus-Santos, R. F. Gerlach, *Sci. Total Environ.* **2011**, *409*, 1799–1805.
63. U. Ewers, A. Brockhaus, G. Winneke, I. Freier, E. Jermann, U. Kramer, *Int. Arch. Occup. Environ. Health* **1982**, *50*, 139–151.
64. J. P. Goullé, E. Saussereau, L. Mahieu, D. Bouige, S. Groenwont, M. Guerbet, C. Lacroix, *J. Anal. Toxicol.* **2009**, *33*, 92–98.
65. K. H. Schaller, F. Alt, M. Fleischer, R. Heinrich-Ramm, H. Seiler, *The Use of ICP-MS for Human Biomonitoring*, in *The MAK Collection for Occupational Health and Safety. Analyses of Hazardous Substances in Biological Materials.* Eds. J. Angerer, K. H. Schaller, H. Greim, Vol. 4, Wiley-VCH, Weinheim, 1994, pp. 1–50.
66. V. A. Lemos, A. L. de Carvalho, *Environ. Monit. and Assess.* **2010**, *171*, 255-265.
67. P. Schramel, J. Begerow, H. Emons, *The Use of ICP-MS for Human Biomonitoring*, in *Analyses of Hazardous Substances in Biological Materials. The MAK Collection*

for Occupational Health and Safety. Eds J. Angerer, K. H. Schaller, H. Greim, Vol. 6, Wiley-VCH, Weinheim, 1999, pp. 1–45.
68. W. J. Mc Shane, R. S. Pappas, V. Wilson-McElprang, D. Paschal, *Spectrochim. Acta B* **2008**, *63*, 638–644.
69. E. Barany, I. A. Bergdahl, A. Schütz, S. Skerfving, A. Oskarsson, *J. Anal. Atom. Spectrom.* **1997**, *12*, 1005–1009.
70. A. Cesbron, E. Saussereau, L. Mahieu, I. Couland, M. Guerbet, J. P. Goulle, *J. Anal. Toxicol.* **2013**, *37*, 401–405.
71. J. P. Goullé, L. Mahieu, J. Castermant, N. Neveu, L. Bonneau, G. Lainé, D. Bouige, C. Lacroix, *Forensic Sci. Int.* **2005**, *153*, 39-44.
72. P. Heitland, H. D. Köster, *J. Trace Elem. Med. Biol.* **2006**, *20*, 253–262.
73. H. F. Hsieh, W. S. Chang, Y. K. Hsieh, C. F. Wang, *Talanta* **2009**, *79*, 183–188.
74. M. Ikeda, F. Ohashi, Y. Fukui, S. Sakuragi, J. Moriguchi, *Int. Arch. Occup. Environ. Health* **2011**, *84*, 139–150.
75. U. Kumtabtim, A. Siripinyanond, C. Auray-Blais, A. Ntwari, J. S. Becker, *Int. J. Mass Spectrom.* **2011**, *307*, 174–181.
76. D. E. Nixon, K. R. Neubauer, S. J. Eckdahl, J. A. Butz, M. F. Burritt, *Spectrochim. Acta B* **2004**, *59*, 1377–1387.
77. C. D. Palmer, M. E. Lewis, C. M. Geraghty, F. Barbosa, P. J. Parsons, *Spectrochim. Acta B* **2006**, *61*, 980–990.
78. P. Schramel, I. Wendler, J. Angerer, *Int. Arch. Occup. Environ. Health* **1997**, *69*, 219-223.
79. Z. W. Zhang, S. Shimbo, N. Ochi, M. Eguchi, T. Watanabe, C. S. Moon, M. Ikeda, *Sci. Total Environ.* **1997**, *205*, 179–187.
80. A. T. Townsend, K. A. Miller, S. McLean, S. Aldous, *J. Anal. Atom. Spectrom.* **1998**, *13*, 1213–1219.
81. R. Lam, E. D. Salin, *J. Anal. Atom. Spectrom.* **2007**, *22*, 1430–1433.
82. H. I. Afridi, T. G. Kazi, M. K. Jamali, G. H. Kazi, M. B. Arain, N. Jalbani, G. Q. Shar, R. A. Sarfaraz, *Toxicol. Ind. Health* **2006**, *22*, 381–393.
83. E. García-Esquinas, B. Pérez-Gómez, M. A. Fernández, A. M. Pérez-Meixeira, E. Gil, C. D. Paz, A. Iriso, J. C. Sanz, J. Astray, M. Cisneros, A. D. Santos, A. Asensio, J. M. García-Sagredo, J. F. García, J. Vioque, M. Pollán, G. López-Abente, M. J. González, M. Martínez, P. A. Bohigas, R. Pastor, N. Aragonés, *Chemosphere* **2011**, *85*, 268–276.
84. C. J. Horng, J. L. Tsai, P. H. Horng, S. C. Lin, S. R. Lin, C. C. Tzeng, *Talanta* **2002**, *56*, 1109–1115.
85. F. Kummrow, F. F. Silva, R. Kuno, A. L. Souza, P. V. Oliveira, *Talanta* **2008**, *75*, 246–252.
86. P. Olmedo, A. Pla, A. F. Hernández, O. López-Guarnido, L. Rodrigo, F. Gil, *Anal. Chim. Acta* **2010**, *659*, 60–67.
87. K. S. Subramanian, J. C. Meranger, *Clin. Chem.* **1981**, *27*, 1866–1871.
88. A. Viitak, A. B. Volynsky, *Talanta* **2006**, *70*, 890–895.
89. P. Ostapczuk, *Clin. Chem.* **1992**, *38*, 1995–2001.
90. H. M. Bolt, *Lead and Its Compounds*, in *The MAK-Collection for Occupational Health and Safety. BAT Value Documentations.* Eds H. Greim, G. Lehnert, Wiley-VCH, Weinheim, 2001.
91. C. J. Horng, *Analyst* **1996**, *121*, 1511–1514.
92. A. N. Onar, A. Temizer, *Analyst* **1987**, *112*, 227–229.
93. M. A. Moreno, C. Marin, F. Vinagre, P. Ostapczuk, *Sci. Total Environ.* **1999**, *229*, 209–215.
94. W. Wasiak, W. Ciszewska, A. Ciszewski, *Anal. Chim. Acta* **1996**, *335*, 201–207.
95. D. I. Bannon, J. J. Chisolm, Jr., *Clin. Chem.* **2001**, *47*, 1703–1704.

96. A. Viksna, E. S. Lindgren, *Anal. Chim. Acta* **1997**, *353*, 307–311.
97. D. Jagner, M. Josefson, S. Westerlund, *Anal. Chim. Acta* **1981**, *128*, 155–161.
98. H. Hu, *Environ. Health Persp.* **1998**, *106*, 961–967.
99. M. C. Scott, D. R. Chettle, *Scand. J. Work Env. Health* **1986**, *12*, 81–96.
100. D. R. Chettle, *J. Radioanal. Nucl. Chem.* **2006**, *268*, 653–661.
101. U. Nilsson, S. Skerfving, *Scand. J. Work Env. Health* **1993**, *19*, 54–58.
102. T. Göen, K. H. Schaller, H. Drexler, *Int. J. Hyg. Environ. Health* **2012**, *215*, 229–232.
103. C. Schulz, M. Wilhelm, U. Heudorf, M. Kolossa-Gehring, *Int. J. Hyg. Environ. Health* **2012**, *215*, 150–158.
104. H. M. Bolt, *Lead and Its Compounds (in German language)*, in *The MAK-Collection for Occupational Health and Safety. BAT Value Documentations.* Eds A. Hartwig, H. Drexler, Vol. 20, Wiley-VCH, Weinheim, 2013.
105. H. M. Bolt, *Lead and Its Compounds (in German language)*, in *The MAK-Collection for Occupational Health and Safety. BAT Value Documentations.* Eds A. Hartwig, H. Drexler, Vol. 21, Wiley-VCH, Weinheim, 2014.
106. ACGIH, *TLVs and BEIs Based on the Documentations of the Threshold Limit Values & Biological Exposure Indices*, Signature Publications, 2014.
107. J. Angerer, K. H. Schaller, *δ-Aminolävulinsäure in Harn*, in *Analyses of Hazardous Substances in Biological Materials.* Eds J. Angerer, K. H. Schaller, D. Hentschler, Vol. 2, VCH, Weinheim, 1978.
108. K. H. Schaller, J. Angerer, *δ-Aminolävulinsäure-Dehydrase*, in *Analyses of Hazardous Substances in Biological Materials.* Eds J. Angerer, K. H. Schaller, D. Hentschler, Vol. 2, VCH, Weinheim, 1976.
109. A. A. Lamola, T. Yamane, *Science* **1974**, *186*, 936–938.
110. J. Lewalter, K. H. Schaller, C. Domik, *Erythrozytenporphyrine (in German language)*, in *Analyses of Hazardous Substances in Biological Materials.* Eds J. Angerer, K. H. Schaller, D. Hentschler, Vol. 9, VCH, Weinheim, 1988.
111. W. E. Blumberg, J. Eisinger, A. A. Lamola, D. M. Zuckerman, *J. Lab. Clin. Med.* **1977**, *89*, 712–723.
112. Y. M. Roh, K. Kim, H. Kim, *Ind. Health* **2000**, *38*, 372–379.
113. H. Sato, K. I. Ido, K. Kimura, *Clin. Chem.* **1994**, *40*, 1239–1244.
114. E. Rossi, P. Garcia-Webb, *Biomed. Chromatogr.* **1986**, *1*, 163–168.
115. H. Oishi, H. Nomiyama, K. Nomiyama, K. Tomokuni, *J. Anal. Toxicol.* **1996**, *20*, 106–110.
116. K. Tomokuni, M. Ichiba, Y. Hirai, *Ind. Health* **1992**, *30*, 119–128.
117. K. Tomokuni, M. Ichiba, Y. Hirai, *Clin. Chem.* **1993**, *39*, 169–170.
118. E. I. Minder, *Clin. Chim. Acta* **1986**, *161*, 11–18.
119. J. L. Zhang, M. Yasuda, R. J. Desnick, M. Balwani, D. Bishop, C. L. Yu, *J. Chrom. B* **2011**, *879*, 2389–2396.
120. N. M. Felitsyn, G. N. Henderson, M. O. James, P. W. Stacpoole, *Clin. Chim. Acta* **2004**, *350*, 219–30.
121. C. M. Benton, L. Couchman, J. T. Marsden, D. C. Rees, C. Moniz, C. K. Lim, *Biomed. Chromatogr.* **2012**, *26*, 1033–1040.
122. K. H. Schaller, J. Angerer, *Koproporphyrin*, in *Analyses of Hazardous Substances in Biological Materials.* Eds J. Angerer, K. H. Schaller, D. Hentschler, Vol. 2, VCH, Weinheim, 1978.
123. C. M. Benton, C. K. Lim, C. Moniz, D. J. L. Jones, *Biomed. Chromatogr.* **2012**, *26*, 714–719.
124. M. Danton, C. K. Lim, *Biomed. Chromatogr.* **2006**, *20*, 612–621.
125. M. Doss, F. Laubenthal, M. Stoeppler, *Int. Arch. Occup. Environ. Health* **1984**, *54*, 55–63.

126. Y. Fukui, M. Miki, H. Ukai, S. Okamoto, S. Takada, M. Ikeda, *Ind. Health* **2005**, *43*, 691–698.
127. R. F. Willi, N. Felgenhauer, F. Eyer, J. T. Buters, T. Zilker, *Deutsche Med. Wochenschr.* **2009**, *134*, 2556–2560.
128. Z. W. Zhang, C. S. Moon, T. Watanabe, S. Shimbo, F. S. He, Y. Q. Wu, S. F. Zhou, D. M. Su, J. B. Qu, M. Ikeda, *Int. Arch. Occup. Environ. Health* **1997**, *69*, 273–281.
129. E. Barany, I. A. Bergdahl, L. E. Bratteby, T. Lundh, G. Samuelson, A. Schutz, S. Skerfving, A. Oskarsson, *Sci. Total Environ.* **2002**, *286*, 129–141.
130. D. L. G. Borges, A. F. da Silva, B. Welz, A. J. Curtius, U. Heitmann, *J. Anal. Atom. Spectrom.* **2006**, *21*, 763–769.
131. M. Wilhelm, I. Lombeck, D. Hafner, F. K. Ohnesorge, *J. Trace Elem. Elect. H.* **1989**, *3*, 165–170.
132. S. Jaenicke, R. M. Sabarathinam, B. Fleet, H. Gunasingham, *Talanta* **1998**, *45*, 703–711.

7

Solid State Structures of Lead Complexes with Relevance for Biological Systems

Katsuyuki Aoki, [1] ***Kazutaka Murayama,*** [2] ***and Ning-Hai Hu*** [3]

[1] Department of Environmental and Life Sciences, Toyohashi University of Technology, Tempaku-cho, Toyohashi 441-8580, Japan
<ka003@edu.imc.tut.ac.jp>

[2] Graduate School of Biomedical Engineering, Tohoku University, Aoba, Sendai 980-8575, Japan
<kmura@bme.tohoku.ac.jp>

[3] Changchun Institute of Applied Chemistry, Chinese Academy of Sciences, Changchun 130022, China
<hunh@ciac.ac.cn>

Metal Ions in Life Sciences, Volume 17 Edited by Astrid Sigel, Helmut Sigel, and Roland K. O. Sigel

DOI 10.1515/9783110434330-007

Abstract: Structural information on the interaction between lead ion and its targeting biological substances is important not only for enriching coordination chemistry of lead but for successfully treating lead poisoning that is a present-day problem. This chapter provides structural data, mainly metal binding sites/modes, observed in crystal structures of lead complexes with

biorelevant molecules, obtained from the Cambridge Structural Database (the CSD version 5.36 updated to May 2015) and the Protein Data Bank (PDB updated to February 2016). Ligands include (i) amino acids and small peptides, (ii) proteins, (iii) nucleic acid constituents, (iv) nucleic acids, (v) simple saccharides, and (vi) other biorelevant molecules involving lead-detoxification agents. For representative complexes of these ligands, some details on the environment of the metal coordination and structural characteristics are described.

Keywords: amino acids · crystal structures · detoxification agents · lead ion · nucleic acids · nucleic acid constituents · peptides · proteins · saccharides · stereochemically active lone pair effect

1. INTRODUCTION

Lead poisoning is one of the most common environmental as well as health problems [1–3]. In order to fully understand its mechanism with the goal of successfully treating lead poisoning, in addition to improve methods for detecting lead poisoning, structural information on the interaction between lead ion and its targeting biological substances is indispensable. In a detailed review by Claudio, Godwin, and Magyar [1], devoted to the fundamental coordination chemistry, environmental chemistry, and biochemistry of Pb(II), one of the sections deals with structural investigations on Pb(II) complexes, where crystal structures of Pb(II) complexes with small biomolecules (gluconic acid, isoalloxazine, and citric acid), lead detoxification and related agents, Ca(II)- and Zn(II)-binding proteins, and $tRNA^{Phe}$ were described. Extensive reviews on crystal data of Pb(IV) and Pb(II) coordination compounds by Holloway and Melnik [4], Shimoni-Livny, Glusker, and Bock [5], and Godwin et al. [1] revealed some general aspects on the structural properties of Pb(IV)/Pb(II): (i) The preferred coordination numbers for lead were found to be 4 for Pb(IV) and 4 and 6 for Pb(II). (ii) Especially, Pb(II) is capable of exhibiting variable coordination numbers and geometries; the geometries are describable in terms of (1) *holodirected, in which the bonds to ligand atoms are distributed throughout the surface of an encompassing globe*, and (2) *hemidirected, in which the bonds to ligand atoms are directed throughout only part of an encompassing globe, i.e., there is an identifiable void in the distribution of bonds to the ligands* [5], where the void is occupied by a 'stereochemically active' $6s^2$ lone pair of electrons of Pb(II). (iii) All *Pb(IV)* structures in the CSD had a *holodirected* coordination geometry; *Pb(II)* compounds are *hemidirected* for low coordination numbers (2–5) and *holodirected* for high coordination numbers (9, 10), but for intermediate coordination numbers (6–8), examples of either type of stereochemistry were found [5].

In this chapter, we provide structural information observed in crystal structures of lead ion complexes with, among a variety of biomolecules, amino acids and small peptides, proteins, nucleic acid constituents, nucleic acids, simple carbohydrates, and other small biomolecules of special relevance involving lead detoxification agents, obtained from the Cambridge Structural Database (the CSD version 5.36 updated to May 2015) or the Protein Data Bank (PDB updated to February 2016), above all focusing on the metal binding sites/modes. Thus, this

chapter relies heavily on previous reviews [1, 4, 5] and attempts to give an up-to-data overview of lead interaction with biorelevant molecules in the solid state.

The ionic radius (Å) of Pb(IV)/Pb(II) varies depending on the coordination number: 0.65 and 0.775 for four- and six-coordinated Pb(IV), respectively, and 1.19, 1.29, and 1.40 for six-, eight-, and ten-coordinated Pb(II), respectively [6]; van der Waals radius of Pb is 2.02 Å [7]; and van der Waals radii (Å) of the ligating atoms are 1.52 for O, 1.55 for N, and 1.80 for S [7]. Based on these values, in this review, we set our standard values for Pb(II) separately for a 'normal' coordination bond length and for a 'weak' interaction: the former is assumed to be less than 2.9 Å for O and N and 3.1 Å for S; the latter to be in the range of 2.9–3.5 Å for O and N and 3.1–3.8 Å for S. In each table in this chapter, *normal* coordination bonds and *weak* interactions are separately listed (the latter in parenthesis). For each compound, structural data were used from the original paper or the CIF of the CSD in some cases.

2. AMINO ACID, SMALL-PEPTIDE, AND PROTEIN COMPLEXES

2.1. Amino Acid Complexes

Amino acids are not only the building blocks of proteins but are also used in the biosynthesis of other molecules involving porphyrins and neurotransmitters (such as γ-amino-butyric acid, serotonin, dopamine, epinephrine, or norepinephrine) and they are among the most common nutritional supplements. Amino acids contain amine (NH_2) and carboxyl (COOH) functional groups along with a side chain (R) specific to each amino acid with the general formula $H_2NCHRCOOH$ for α-amino acids. At physiological pH (6.7 ~ 7.4), they exist as zwitterions with the amino group protonated and the carboxyl group deprotonated. We deal here with the twenty standard α-amino acids, which make up proteins. The twenty amino acids can be classified here for convenience into four broad groups according to the properties of the side chains: Group *1* amino acids with nonpolar and electrically neutral (at pH 7.4) side chains; Group *2*, with polar and neutral side chains; Group *3*, with basic polar side chains; and Group *4*, with polar and acidic side chains.

Table 1 lists the total number of so far reported crystal structures of lead complexes with the twenty standard amino acids including their substituted ones [8–31] and Table 2 summarizes metal binding sites/modes observed in the individual complexes. Among a total of 39 complexes [8–31], only a small number of crystal structures are available for amino acids whose amino and carboxyl groups both are free: two complexes [8] for Gly, four [17–19] for Val, one [19] for Leu, three [18] for Ile, four [18, 23, 24] for Phe, one [27] for Cys, one [18] for Arg, and one [28] for Asp; all the others are blocked at the amino group but free at the carboxyl group. No crystal structure of Pb(II) ion is reported for Trp, Met, Ser, Thr, Asn, Gln, Lys, and His, and their derivatives.

Table 1. Total number of lead complexes with the standard twenty amino acids and their substituents in the solid state.[a]

Amino acid	Number of complexes	CSD ID	Ref.	CSD ID	Ref.	CSD ID	Ref.
Glycine (Gly)	12	WEQPEO	[8]	WEQPAK	[8]	None	[9]
		TEZMOA	[10]	INAJAJ	[11]	UCAPIZ	[12]
		XAQNAE	[13]	IZIPIQ	[14]	IZIPOW	[14]
		EZENOM	[15]	TEZMUG	[10]	TEZMIU	[10]
Alanine (Ala)	1	IKEWAW	[16]				
Valine (Val)	4	ESAPET	[17]	ESAPET01	[18]	EWEBAK	[18]
		BOHNIW	[19]				
Leucine (Leu)	1	BOHNES	[19]				
Isoleucine (Ile)	3	EWEBAK	[18]	BOHNAO	[19]	BOHNAO01	[18]
Proline (Pro)	3	RIRRUG	[20]	EQIXOR	[21]	WERGAC	[22]
Phenylalanine (Phe)	5	QIXHUB	[23]	QIXHUB01	[18]	EWAZUY	[18]
		ODEWEA	[24]	FELJAJ	[25]		
Tryptophan (Trp)	0						
Methionine (Met)	0						
Serine (Ser)	0						
Threonine (Thr)	0						
Tyrosine (Tyr)	1	FIFWAT	[26]				
Cysteine (Cys)	1	NARLID	[27]				
Asparagine (Asn)	0						
Glutamine (Gln)	0						
Histidine (His)	0						
Lysine (Lys)	0						
Arginine (Arg)	1	EWAZEI	[18]				
Aspartic acid (Asp)	2	XARQAI	[28]	NIZDAC	[29]		
Glutamic acid (Glu)	5	RAXPIR	[30]	PAXPOX	[30]	RAXPUD	[30]
		SEFYEI	[31]	SEFYIM	[31]		
Total	39						

[a] Obtained from the Cambridge Structural Database (CSD version 5.36 updated to May 2015).

Table 2. Lead binding sites/modes on amino acids in the solid state.[a,b]

Complex[c]		Coordination number[d] and geometry[e]	Metal binding sites[f] on amino acid ligand and other ligands/comments, if any	CSD code	Ref.
Glycine complexes					
$[PbCl_2\{Cu_{0.5}(Gly - H)\}]_n$	Pb (Cu	8 Hemi. 6 Holo.	O_A,O_B [α-CO_2^- (Mol.1): 2.585, 2.777][g], O_A [α-CO_2^- (Mol.1′): 2.682][h], 5 Cl [2.796–3.120] N,O_B [Mol.1, amino N: 1.959; α-CO_2^-: 1.976][i], N,O_B [Mol.1′, amino N: 1.959; α-CO_2^-: 1.976], 2 Cl [2.995, 2.995]) The Cu atom locates on an inversion center.	WEQPEO	[8]
$[PbBr_2\{Cu_{0.5}(Gly - H)\}]_n$	Pb (Cu	8 Hemi. 6 Holo.	O_A,O_B [α-CO_2^- (Mol.1): 2.599, 2.820], O_A [α-CO_2^- (Mol.1′): 2.720], 5 Br [2.928–3.237] N,O_B [Mol.1, amino N: 1.972; α-CO_2^-: 1.967], N,O_B [Mol.1′, amino N: 1.972; α-CO_2^-: 1.967], 2 Br [3.167, 3.167]) The Cu atom locates on an inversion center.	WEQPAK	[8]
$[Pb(bphmGly - 2H)(H_2O)]$		6 (7) Hemi.	O [α-CO_2^- (Mol.1): 2.816], 4 O [phosphonate: 2.364 (Mol.1′), 2.678 (Mol.1″), 2.649 (Mol.1‴), 2.381 (Mol.1⁗)], O [aqua: 2.441] (O [phosphonate: 2.957 (Mol.1⁗)])	None	[9]
$[Pb(bzGly - H)_2(H_2O)_2]_n \cdot 2nH_2O$		8 –[j]	O_A,O_B [α-CO_2^- (Mol.1): 2.75, 2.46], O_A,O_B [α-CO_2^- (Mol.1′): 2.75, 2.46], 2 O_B [α-CO_2^- (Mol.1″, (Mol.1‴): 2.75, 2.75], 2 O [aqua (Mol.1, Mol.1′): 2.62, 2.62] The Pb atom locates on a twofold axis.	TEZMOA	[10]
$[Pb(cpsGly - 2H)(4,4'\text{-bpy})_{0.5}]_n$		6 –	O_A,O_B [α-CO_2^- (Mol.1): 2.455, 2.532], O,O [phenyl-CO_2^- (Mol.1′): 2.539, 2.642], O [phenyl-CO_2^- (Mol.1″): 2.722], N [bpy: 2.590]	INAJAJ	[11]

$[Pb_2(FcCO_2)_2(FcCO\text{-}Gly - H)_2(phen)_2] \cdot 6H_2O$		7 Hemi	O_A,O_B [α-CO_2^- (Mol.1): 2.569, 2.803], O_B [α-CO_2^- (Mol.1′): 2.718], O,O [$FcCO_2^-$: 2.432, 2.548], 2 N [phen: 2.556, 2.675] The dimeric structure with two Pb atoms related by an inversion center.	UCAPIZ	[12]
$[Pb(npsGly - 2H)]_n$		6 Hemi.	N,O_A [Mol.1, sulfonamide N: 2.450; α-CO_2^-: 2.402], O_A [α-CO_2^- (Mol.1′): 2.530], 2 O [sulfonyl (Mol.1″, Mol.1‴): 2.461, 2.961], O [nitro (Mol.1⁗): 2.897]	XAQNAE	[13]
$[Pb_3\{phm(m)Gly - 3H\}_2]_n \cdot nH_2O$ (monoclinic)	Pb1	5 Hemi.	N,O_A,O [Mol.1, amide N: 2.577; α-CO_2^-: 2.476; phosphonate: 2.642], 2 O [phosphonate (Mol.1′, Mol.2): 2.811, 2.269]	IZIPIQ	[14]
	Pb2	5 Hemi.	N,O_A,O [Mol.2, amide N: 2.598; α-CO_2^-: 2.420; phosphonate: 2.592], 2 O [phosphonate (Mol.1′, Mol.1″): 2.437, 2.661]		
	Pb3	5 Hemi.	2 O_A [α-CO_2^- (Mol.1, Mol.2′): 2.533, 2.594], 3 O [phosphonate (Mol.1′, Mol.2, Mol.2′): 2.704, 2.378, 2.379]		
$[Pb_3\{phm(m)Gly - 3H\}_2]_n \cdot nH_2O$ (triclinic)	Pb1	6 Hemi.	N,O_A,O [Mol.1, amide N: 2.599; α-CO_2^-: 2.519; phosphonate: 2.461], 3 O [phosphonate (Mol.1′, Mol.2, Mol.2′): 2.776, 2.533, 2.631]	IZIPOW	[14]
	Pb2	6 Hemi.	N,O_A,O [Mol.2, amide N: 2.621; α-CO_2^-: 2.625; phosphonate: 2.466], 3 O [phosphonate (Mol.1, Mol.1″, Mol.2′): 2.527, 2.571, 2.819]		
	Pb3	6 –	O_A [α-CO_2^- (Mol.2): 2.780], O_A [α-CO_2^- (Mol.1⁗): 2.356], O_B [α-CO_2^- (Mol.1⁗): 2.843], O_B [α-CO_2^- (Mol.2′): 2.759], 2 O [phosphonate (Mol.1, Mol.2′): 2.332, 2.435]		

Complex[c]		Coordination number[d] and geometry[e]	Metal binding sites[f] on amino acid ligand and other ligands/comments, if any	CSD code	Ref.
$[Pb_3\{phm(m)Gly-3H\}(BTS)(H_2O)]_n \cdot nH_2O$	Pb1	5 Hemi.	O_A [α-CO_2^- (Mol.1): 2.639], O [phosphonate (Mol.1′): 2.387], O,O [CO_2^- (BTS Mol.1″): 2.518, 2.721], O [aqua: 2.694]	EZENOM	[15]
	Pb2	5 Hemi.	O_B [α-CO_2^- (Mol.1): 2.415], O [CO_2^- (BTS Mol.1″): 2.628], O,O [CO_2^- (BTS Mol.1‴): 2.463, 2.625], O [sulfonate (BTS Mol.1): 2.672]		
	Pb3	4 Hemi.	O_A [α-CO_2^- (Mol.1): 2.554], N,O [N-C-PO_3^{2-} (Mol.1): 2.637 (N); 2.363 (O)], O [phosphonate (Mol.1′): 2.359]		
$[Pb(tsGly-H)_2(bpy)]_n$		7 Hemi.	O_A,O_B [α-CO_2^- (Mol.1): 2.627, 2.827], O_B [α-CO_2^- (Mol.1′): 2.745], 2 O_A [α-CO_2^- (Mol.2, Mol.2′): 2.523, 2.649], 2 N [bpy: 2.612, 2.609]	TEZMUG	[10]
$[Pb(tsGly-2H)(H_2O)]_n$		6 Hemi.	N,O_A [Mol.1, amide N: 2.38; α-CO_2^-: 2.314], O_A,O_B [α-CO_2^- (Mol.1′): 2.827, 2.78], O [sulfonic (Mol.1″): 2.683], O [aqua: 2.423]	TEZMIU	[10]
Alanine complex					
$[Pb(pym\text{-}L\text{-}Ala-H)(ClO_4)]_n$		4 (6) Hemi.	O_A,N,N [Mol.1, α-CO_2^-: 2.321; amino N: 2.455; pyridyl ring N: 2.577], O_B [α-CO_2^- (Mol.1′): 2.538] (2 O [ClO_4^- (Mol.1, Mol.1′): 2.936, 2.903])	IKEWAW	[16]

Valine complexes					
$[Pb(L\text{-}Val)_2(NO_3)(H_2O)_2]_n \cdot (NO_3)_n$		7 (8) Holo.	O_A [α-CO_2^- (Mol.1): 2.44], O_A,O_B [α-CO_2^- (Mol.2): 2.36, 2.87], 2 O [nitrate (Mol.1): 2.78, 2.85], 2 O [aqua (Mol.1, Mol.2): 2.50, 2.89] (O [nitrate: (Mol.1′): 2.95])	ESAPET	[17]
$[Pb(L\text{-}Val)_2(NO_3)(H_2O)_2]_n \cdot (NO_3)_n$		6 (10) Hemi.	O_A [α-CO_2^- (Mol.1): 2.459], O_A,O_B [α-CO_2^- (Mol.2): 2.356, 2.892], 2 O [nitrate (Mol.1): 2.790, 2.847], O [aqua (Mol.1): 2.512] (O_B [α-CO_2^- (Mol.1): 3.266], 2 O [nitrate (Mol.1′): 3.174, 2.969], O [aqua (Mol.2): 2.915])	ESAPET01	[18]
$[Pb(L\text{-}Val)(L\text{-}Ile)(NO_3)(H_2O)_2] \cdot NO_3$		7 (10) Hemi.	O_A,O_B [Val α-CO_2^-: 2.379, 2.828], O_A [Ile α-CO_2^-: 2.475], 2 O [nitrate (Mol.1): 2.819, 2.827], 2 O [aqua: 2.484, 2.886] (O_B [Ile α-CO_2^-: 3.463], 2 O [nitrate (Mol.1′): 2.925, 3.126])	EWEBAK	[18]
$\{[Pb_4(L\text{-}Val)_{10}] \cdot (ClO_4)_8 \cdot 4\,H_2O\}_n$	Pb1	6 (7) Hemi.	O_A,O_B [α-CO_2^- (Mol.1): 2.63, 2.73], O_A,O_B [α-CO_2^- (Mol.2): 2.68, 2.55], O_A,O_B [α-CO_2^- (Mol.3): 2.43, 2.84] (O_A [α-CO_2^- (Mol.10′): 2.92])	BOHNIW	[19]
	Pb2	6 (7) Hemi.	O_A [α-CO_2^- (Mol.1): 2.55], O_B [α-CO_2^- (Mol.2): 2.73], O_A,O_B [α-CO_2^- (Mol.4): 2.50, 2.55], O_A [α-CO_2^- (Mol.5): 2.35], O_B [α-CO_2^- (Mol.8): 2.88] (O_B [α-CO_2^- (Mol.5): 2.92])		
	Pb3	7 Hemi.	O_A,O_B [α-CO_2^- (Mol.6): 2.62, 2.64], O [α-CO_2^- (Mol.4): –], O_A,O_B [α-CO_2^- (Mol.7): 2.65, 2.65], O_A,O_B [α-CO_2^- (Mol.8): 2.43, 2.78]		

Complex[c]		Coordination number[d] and geometry[e]	Metal binding sites[f] on amino acid ligand and other ligands/comments, if any	CSD code	Ref.
	Pb4	6 Hemi.	O_B [α-CO_2^- (Mol.6): 2.49], O_B [α-CO_2^- (Mol.7): 2.62], O_A,O_B [α-CO_2^- (Mol.9): 2.45, 2.58], O_B [α-CO_2^- (Mol.10): 2.31], O_B [α-CO_2^- (Mol.3′): 2.84]		
Leucine complex					
$[Pb_2(L\text{-Leu} - H)_2(NO_3)_2]_n$	Pb1	7 Hemi.	N,O_A [Mol.1, amide N: 2.420; α-CO_2^-: 2.419], O_A,O_B [α-CO_2^- (Mol.1′): 2.590, 2.775], O [nitrate (Mol.1): 2.693], 2 O [nitrate (Mol.1′): 2.772, 2.845]	BOHNES	[19]
	Pb2	7 Hemi.	N,O_A [Mol.2, amide N: 2.423; α-CO_2^-: 2.410], O_A,O_B [α-CO_2^- (Mol.2′): 2.582, 2.772], 2 O [nitrate (Mol.2): 2.699, 2.913], O [nitrate (Mol.2′): 2.768]		
Isoleucine complexes					
$[Pb(L\text{-Ile})(L\text{-Val})\ (NO_3)(H_2O)_2]\cdot NO_3$		7 (10) Hemi.	O_A [Ile α-CO_2^-: 2.475], O_A,O_B [Val α-CO_2^-: 2.379, 2.828], 2 O [nitrate (Mol.1): 2.819, 2.827], 2 O [aqua: 2.484, 2.886] (O_B [Ile α-CO_2^-: 3.463], 2 O [nitrate (Mol.1′): 2.925, 3.126])	EWEBAK	[18]
$[Pb(L\text{-Ile})_2(NO_3)(H_2O)_2]\cdot NO_3$		7 Hemi.	O_A,O_B [α-CO_2^- (Mol.1): 2.374, 2.849], O_A [α-CO_2^- (Mol.2): 2.487], 2 O [nitrate: 2.804, 2.824], 2 O [aqua: 2.508, 2.890] This is the same compound as BOHNAO01 [18].	BOHNAO	[19]

$[Pb(L\text{-}Ile)_2(NO_3)(H_2O)_2]\cdot NO_3$		6 (10) Hemi.	O_A,O_B [α-CO_2^- (Mol.1): 2.379, 2.816], O_A [α-CO_2^- (Mol.2): 2.492], 2 O [nitrate (Mol.1): 2.809, 2.824], O [aqua: 2.497] (O_B [α-CO_2^- (Mol.2): 3.467], 2 O [nitrate (Mol.1′) : 2.934, 3.106], O [aqua: 2.907]) This is the same compound as BOHNAO [19].	BOHNAO01	[18]
Proline complexes					
$[Pb(L\text{-}Pro - 2\,H)(H_2O)]_n$		4 (6) Hemi.	N,O_A [Mol.1, ring N: 2.49; α-CO_2^-: 2.347], N,O_A [Mol.1′, ring N: 2.49; α-CO_2^-: 2.347], (2 O [aqua (Mol.1, Mol.1′: 2.928, 2.928]) The Pb atom locates on a twofold axis.	RIRRUG	[20]
$[Pb_2(phm\text{-}DL\text{-}Pro - 2H)Cl_2]_n$	Pb1	6 Hemi.	O_A [α-CO_2^- (Mol.1′): 2.572], O_B [α-CO_2^- (Mol.1″): 2.851], O [phosphonate (Mol.1): 2.400], 2 O [phosphonate (Mol.1′): 2.482, 2.824], O [phosphonate (Mol.1″): 2.842]	EQIXOR	[21]
	Pb2	6 Hemi.	O_B [α-CO_2^- (Mol.1‴): 2.747], 3 O [phosphonate (Mol.1, Mol.1′, Mol.1″): 2.749, 2.421, 2.811], 2 Cl [2.684, 2.767]		
$[Pb_4O(phm\text{-}DL\text{-}Pro - 3\,H)_2]_n$	Pb1	4 –	O_A [α-CO_2^- (Mol.1′): 2.699], 3 O [phosphonate (Mol.1′, Mol.1″, Mol.2): 2.373, 2.459, 2.513]	WERGAC	[22]
	Pb2	4 –	O_A [α-CO_2^- (Mol.2): 2.511], 2 O [phosphonate (Mol.1, Mol.2): 2.554, 2.452], O [Pb2-O-Pb4: 2.598]		
	Pb3	5 –	2 O_B [α-CO_2^- (Mol.1′, Mol.2‴): 2.643, 2.637], 2 O [phosphonate (Mol.1, Mol.2‴): 2.510, 2.616], O [Pb2-O-Pb4: 2.189]		

Complex[c]		Coordination number[d] and geometry[e]	Metal binding sites[f] on amino acid ligand and other ligands/comments, if any	CSD code	Ref.
	Pb4	4 –	O_A [α-CO_2^- (Mol.2): 2.647], O [phosphonate (Mol.2‴): 2.504], O [Pb2-O-Pb4: 2.324], O [(Pb2-O-Pb4)‴: 2.290]		
Phenylalanine complexes					
$[Pb(L\text{-}Phe)_2(NO_3)(H_2O)_2]\cdot NO_3$		6 (9) Hemi.	O_A,O_B [α-CO_2^- (Mol.1): 2.354, 2.979], O_A,O_B [α-CO_2^- (Mol.2: 2.628, 2.886), 2 O [nitrate (Mol.1): 2.453, 2.791], (2 O [aqua (Mol.1, Mol.2): 2.927, 2.994], O [nitrate (Mol.1′): 3.035]) This is the same compound as QIXHUB01 [18].	QIXHUB	[23]
$[Pb(L\text{-}Phe)_2(NO_3)(H_2O)_2]\cdot NO_3$		6 (10) Hemi.	O_A,O_B [α-CO_2^- (Mol.1): 2.442, 2.747], O_A [α-CO_2^- (Mol.2): 2.343], O [nitrate (Mol.1): 2.857], 2 O [aqua (Mol.1, Mol.2): 2.640, 2.871] (O_B [α-CO_2^- (Mol.2): 2.962], O [nitrate (Mol.1): 3.033], 2 O [nitrate (Mol.1′): 3.016, 3.373]) This is the same compound as QIXHUB [117].	QIXHUB01	[18]
$[Pb(L\text{-}Phe)_2(NO_3)(H_2O)_2]\cdot NO_3\cdot H_2O$		5 (9) Hemi.	O_A [α-CO_2^- (Mol.1): 2.381], O_A,O_B [α-CO_2^- (Mol.2): 2.380, 2.827], O [nitrate (Mol.1): 2.602], O [aqua (Mol.1): 2.617] (O_B [α-CO_2^- (Mol.1): 2.966], O [nitrate (Mol.1): 2.962], O [aqua (Mol.2): 2.966])	EWAZUY	[18]
$[Pb(L\text{-}Phe - H)_2]_n$		6 Hemi.	O_A [α-CO_2^- (Mol.1): 2.748], O_A [α-CO_2^- (Mol.1′): 2.748], N,O_A [Mol.2, amide N: 2.435; α-CO_2^-: 2.442], N,O_A [Mol.2′, amide N: 2.435; α-CO_2^-: 2.442] The Pb atom locates on a twofold axis.	ODEWEA	[24]

[Pb{pbic-di(L-Phe – H)}(DMF)]·H_2O		7 Hemi.	O_A,O_B [α-CO_2^- (L-Phe1 Mol.1): 2.824, 2.373], O_A [α-CO_2^- (L-Phe1 Mol.1′): 2.717], O_A [α-CO_2^- (L-Phe2 Mol.1″): 2.387], O_B [α-CO_2^- (L-Phe2 Mol.1‴): 2.387, 2.752], O_B [α-CO_2^- (L-Phe2 Mol.1⁗): 2.885], O [DMF: 2.454] pbic-di(Phe – H) = ^-O_2C-Phe1-NH-C(O)-NH-C_6H_4-NH-C(O)-NH-Phe2-CO_2^-.	FELJAJ	[25]
Tyrosine complex					
$[Pb(3,5\text{-dinitro-L-Tyr} - 2\,H)]_n$·$0.5\,nH_2O$		4 Hemi.	N,O_A [Mol.1, amino N: 2.389; α-CO_2^-: 2.305], O_B [α-CO_2^- (Mol.1′): 2.454], O [phenolic O^- (Mol.1″): 2.466]	FIFWAT	[26]
Cysteine Complex					
$[Pb\{Mo_2O_2S_2(L\text{-Cys} - 2\,H)_2\}]_n$·$2\,nH_2O$	Pb	6 (7) –	S [Cys (Mol.1) sulfide: 2.739], S [Cys (Mol.2) sulfide: 2.928], O_A,O_B [α-CO_2^- (Mol.1′): 2.736, 2.775], O_A,O_B [α-CO_2^- (Mol.2′): 2.878, 2.834] (S [Mo-S2-Mo: 3.250])[f]	NARLID	[27]
	(Mo1	7	N,O_B,S [Cys (Mol.1) amino N: 2.256; α-CO_2^-: 2.234; sulfide: 2.544], Mo [Mo2: 2.8428], S [Mo-S1-Mo: 2.321], S [Mo-S2-Mo: 2.346], O [Mo=O: 1.677])		
	(Mo2	7	N,O_B,S [Mol.2, amino N: 2.236; α-CO_2^-: 2.265; sulfide: 2.508], Mo [Mo1: 2.8428], S [Mo-S1-Mo: 2.352], S [Mo-S2-Mo: 2.326], O [M=O: 1.690]) Pb–S(Cys)–Pb–S(Cys)–(1D chain).		

Complex[c]		Coordination number[d] and geometry[e]	Metal binding sites[f] on amino acid ligand and other ligands/comments, if any	CSD code	Ref.
Arginine complex					
$[Pb_2(L\text{-}ArgH)_3(NO_3)_7(H_2O)]\cdot 3H_2O$	Pb1	6 (10) Hemi.	O_A,O_B [α-CO_2^- (Mol.1): 2.519, 2.518], O_A,O_B [α-CO_2^- (Mol.2): 2.617, 2.401], O [nitrate (Mol.1): 2.657], O [nitrate (Mol.3): 2.803] (O [nitrate (Mol.1): 3.312], 2 O [nitrate (Mol.2): 2.902, 3.124] O [nitrate (Mol.3): 3.163])	EWAZEI	[18]
	Pb2	7 (11) Hemi.	O_A,O_B [α-CO_2^- (Mol.3): 2.494, 2.656], 2 O [nitrate (Mol.4): 2.721, 2.803], O [nitrate (Mol.5): 2.626], O [nitrate (Mol.7): 2.800], O [aqua: 2.576] (O [nitrate (Mol.5): 3.425], O [nitrate (Mol.5′): 3.031], O [nitrate (Mol.6): 3.133], O [nitrate (Mol.7): 3.150])		
Aspartic acid complexes					
$[Pb(L\text{-}Asp - H)(NO_3)]_n$		6 Hemi.	O_A [α-CO_2^- (Mol.1): 2.493], O_A [β-CO_2^- (Mol.1′): 2.743], O_A,O_B [β-CO_2^- (Mol.1″): 2.706, 2.500], O_B [α-CO_2^- (Mol.‴): 2.536], O [nitrate (Mol.1): 2.730] Formation of 18-membered [–Pb–{α-CO_2^--$CH(CH_2)$-β-CO_2^-}–]$_3$ trimeric framework.	XARQAI	[28]
$[Pb_{2.5}(Asp\text{-}dimer - H)(H_2O)_2]_n$	Pb1	7 Hemi.	O_A,O_B [Mol.1, β-CO_2^- (Asp2): –, –], O_A [Mol.1′, α-CO_2^- (Asp1): –], O_A [Mol.1″, β-CO_2^- (Asp1): –], O_A [Mol.1‴, α-CO_2^- (Asp2): –], O_B [Mol.1⁗, β-CO_2^- (Asp2): –], O [aqua: –]	NIZDAC	[29]

	Pb2 Hemi.	6	O_B,N,O_A,O_A [Mol.1, α-CO_2^- (Asp1): –; amine N^-: 2.518; α-CO_2^- (Asp2): –; β-CO_2^- (Asp2): –], O_B [Mol.1″, β-CO_2^- (Asp1):–], O [aqua: –]		
	Pb3 Holo.	8	O_B [Mol.1, α-CO_2^- (Asp2): –], O_B [Mol.1‴, α-CO_2^- (Asp2): –], O_A [Mol.1⁗, β-CO (Asp1): –], O_A [Mol.1⁗, β-CO_2^- (Asp1): –], 4 O [aqua: –, –, –, –] Average Pb–O(aqua) bond length of 2.684 Å; Pb–O (carboxylate) bond lengths in the range of 2.408–2.672 Å. The Pb3 atom locates on an inversion center. Asp-dimer – H = $[^-O_2C$-Asp1-N^--Asp2-$CO_2^-]^{5-}$.		
Glutamic acid complexes					
$[Pb(ts\text{-}DL\text{-}Glu - 2\,H)(H_2O)]_n$		7 Holo.	O_A,O_B [α-CO_2^- (Mol.1): 2.479, 2.618], O_B [α-CO_2^- (Mol.1′): –], O_A,O_B [γ-CO_2^- (Mol.1″): 2.333, 2.718], O_B [γ-CO_2^- (Mol.1‴): 2.514], O [aqua: 2.842] Formation of the dimeric [–Pb–{α-CO_2^--$CH(CH_2)_2$-γ-CO_2^-}–]$_2$ framework.	RAXPIR	[30]
$[Pb(ts\text{-}DL\text{-}Glu - 2\,H)(phen)]_2$		6 Hemi.	O_A,O_B [α-CO_2^- (Mol.1): 2.753, 2.283], O_A,O_B [γ-CO_2^- (Mol.1′): 2.489, 2.490], 2 N [phen: 2.724, 2.638] Formation of the center-of-symmetry related [–Pb–{α-CO_2^--$CH(CH_2)_2$-γ-CO_2^-}–]$_2$ dimeric structure.	RAXPOX	[30]

Complex[c]		Coordination number[d] and geometry[e]	Metal binding sites[f] on amino acid ligand and other ligands/comments, if any	CSD code	Ref.
$[Pb(ts\text{-}DL\text{-}Glu-2H)(bpy)]_2$		6 Hemi.	O_A,O_B [α-CO_2^- (Mol.1): 2.720, 2.292], O_A,O_B [γ-CO_2^- (Mol.1′): 2.505, 2.468], 2 N [bpy: 2.722, 2.619] Formation of the center-of-symmetry related [–Pb–{α-CO_2^--$CH(CH_2)_2$-γ-CO_2^-}–]$_2$ dimeric structure.	RAXPUD	[30]
$[Pb_2(bs\text{-}L\text{-}Glu-2H)_2(bpy)_2]_n$	Pb1	7	O_A,O_B [α-CO_2^- (Mol.2): 2.406, 2.715], O_A,O_B [γ-CO_2^- (Mol.1): 2.402, 2.620], 2 N [bpy (Mol.2): 2.730, 2.869], $O^{\#1}$ [γ-CO_2^- (Mol.2″): –]	SEFYEI	[31]
	Pb2	8 Hemi.	O_A,O_B [α-CO_2^- (Mol.1): 2.699, 2.552], O_A,O_B [γ-CO_2^- (Mol.2): 2.352, 2.573], 2 N [bpy (Mol.1): 2.572, 2.619], $O^{\#2}$ [α-CO_2^- (Mol.2″): –], $O^{\#3}$ [γ-CO_2^- (Mol.1′): –] The Pb–$O^{\#1}$/$O^{\#2}$/$O^{\#3}$ distances are in the range of 2.873–3.087 Å. Formation of the [–Pb1–{α-CO_2^--Glu1-γ-CO_2^-}– Pb2–{α-CO_2^--Glu1-γ-CO_2^-}–] dimeric framework.		
$[Pb_2(bs\text{-}L\text{-}Glu-2H)_2(phen)_2]_n$	Pb1	7 –	O_A,O_B [α-CO_2^- (Mol.1): 2.513, –], O_A,O_B [γ-CO_2^- (Mol.2): 2.368, 2.608], 2 N [phen (Mol.1): 2.631, 2.618], O [γ-CO_2^- (Mol.1′): –]	SEFYIM	[31]
	Pb2	7 –	O_A,O_B [α-CO_2^- (Mol.2): 2.681, 2.613], O_A,O_B [γ-CO_2^- (Mol.1): 2.404, 2.509], 2 N [bpy (Mol.2): 2.635, 2.579], O [γ-CO_2^- (Mol.2″): –] Formation of the [–Pb1–{α-CO_2^--Glu1-γ-CO_2^-}–Pb2–{α-CO_2^--Glu1-γ-CO_2^-}–] dimeric framework.		

[a] Obtained from the Cambridge Structural Database (CSD version 5.36 updated to May 2015).
[b] Abbreviations: aqua: water ligand; Ala, zwitterionic alanine with α-COO^- and $-NH_3^+$; Ala – H, alaninate monoanion with COO^- and $-NH_2$; ArgH, argininium monocation with α-COO^- and $-NH_3^+$, and $-NHC(NH_2)(=NH_2^+)$; Asn, zwitterionic asparagine with α-COO^-, $-NH_3^+$, and γ-$C(O)NH_2$; Asp-dimer – H, $[N^-\{CH(CO_2^-)CH_2CO_2^-\}_2]^{5-}$; Asp – H, aspartate monoanion with α-COO^-, β-COO^-, and $-NH_3^+$; bphmGly – 2 H, *N*-bis(phosphonomethyl)glycinate dianion with α-CO_2^- and PO_3H^-; bpy, 2,2′-bipyridine; 4,4′-bpy, 4,4′-bipyridine; bsGlu – 2 H, *N*-benzenesulfonylglutamate dianion with α-COO^-, γ-COO^-, and –NH–; BTS, 5-sulfoisophthalate trianion; bzGly – H, *N*-benzoylglycinate mononion with α-COO^- and $-NH_2$; Cp*, pentamethylcyclopentadienyl; cpsGly – 2 H, *N*-(3-carboxyphenylsulfonyl)glycinate dianion with α-COO^-, –NH–, and phenyl –COO^-; Cys – 2 H, cysteinate dianion with –COO^-, $-NH_2$, and $-S^-$; DMF, dimethylformamide; Fc, ferrocene; FcCO-Gly – H, *N*-ferrocenylformylglycinate monoanion with α-COO^- and –NH–; Glu – H, glutamate monoanion with α-COO^-, γ-COO^-, and $-NH_3^+$; Glu – 2 H, glutamate dianion with α-COO^-, β-COO^-, and $-NH_2$; Gly – H, glycinate monoanion with α-COO^- and $-NH_2$; Ile, zwitterionic isoleucine with α-COO^- and $-NH_3^+$; Leu – H, leucinate monoanion with α-COO^- and $-NH_2$; M, metal ion; npsGly – 2 H, *N*-(2-nitrophenylsulfonyl)glycinate dianion with α-COO^- and $-N^-$–; pbic-di(Phe – H), *N*,*N*′-[1,4-phenylenebis(iminocarbonyl)]di(phenylalanate) dianion with α-COO^- for both Phe entities; Phe, zwitterionic phenylalanine with α-COO^- and $-NH_3^+$; Phe – H, phenylalaninate monoanion with α-COO^- and $-NH_2$; phm(m)Gly – 3 H, *N*-(phosphonomethyl)-*N*-methyl-glycinate trianion with α-COO^-, –NH–, and $-PO_3^{2-}$; phmPro – 2 H, *N*-phosphomethylprolinate dianion with α-COO^- and $-PO_3H^-$; phmPro – 3 H, *N*-phosphomethylprolinate trianion with α-COO^- and $-PO_3^{2-}$; pymAla – H, *N*-(2-pyridylmethyl)alaninate monoanion with α-COO^- and –NH–; Pro – 2 H, prolinate dianion with α-COO^- and $-N^-$– (pyrrolidine ring); tsGlu – 2 H, *N*-(*p*-tolylsulfonyl)glutamate dianion with α-COO^-, –NH–, and γ-COO^-; TsGly – H, *N*-(*p*-tolylsulfonyl)glycinate monoanion with α-COO^- and –NH–; tsGly – 2 H, *N*-(*p*-tolylsulfonyl)glycinate dianion with α-COO^- and $-N^-$–; Tyr – 2H, tyrosinate dianion with α-COO^-, $-NH_2$, and phenolic $-O^-$; Val, zwitterionic valine with α-COO^- and $-NH_3^+$.
[c] Including lead complexes with *substituted* amino acids.
[d] The coordination number is counted for the *normal* coordination bond whose distance is less than 2.9 Å for O and N and 3.1 Å for S; the value in parentheses refers to the coordination number when the *weak* interaction (2.9–3.5 Å for O and N and 3.1–3.8 Å for S) is further considered.
[e] In the *hemidirected* coordination geometry the bonds to ligand atoms are directed throughout only part of an encompassing globe, while in the *holodirected* coordination mode the bonds to ligand atoms are distributed throughout the surface of an encompassing globe.
[f] When the Pb–O/N/S bond distance falls in the range of *weak* interaction[d], it is given in parentheses.
[g] For example, 'O_A,O_B [α-CO_2^- (Mol.1): 2.585, 2.777]' denotes that the metal ion binds to two α-carboxylate oxygens of the amino acid molecule 1 (Mol.1; Gly in this case), forming an O_A–M–O_B chelation, and their bond distances (Å), where O_A denotes one of the two carboxylate oxygens and O_B denotes the other one.
[h] 'O [α-CO_2^- (Mol.1′): 2.682]' denotes that the metal ion binds to an α-CO_2^- oxygen of Mol.1′, which is symmetry-related to the parent Mol.1 in the crystal lattice, and its bond distance (Å).
[i] 'N,O_B [Mol.1, amino N: 1.959; α-CO_2^-: 1.976]' denotes that the metal ion binds to the amino nitrogen and the carboxylate oxygen O_B of Mol.1, forming an N–M–O chelation, and their bond distances (Å).
[j] No mention is made about hemidirected or holodirected coordination geometries in the literature.

2.1.1. Group 1 Amino Acids

Group 1 amino acids with nonpolar and electrically neutral (at pH 7.4) side chains are glycine (Gly), alanine (Ala), valine (Val), leucine (Leu), isoleucine (Ile), proline (Pro), phenylalanine (Phe), tryptophan (Trp), and methionine (Met). Among the Group 1 amino acids, a total of 27 crystal structures of Pb(II) complexes are reported: twelve [8–15] are Gly complexes, one [16] for Ala, four [17–19] for Val, one [19] for Leu, two [18, 19] for Ile, three [20–22] for Pro, and four [18, 23–25] for Phe, and none for Trp and Met. In these complexes, when the amino acid exists as a zwitterionic form, $H_3N^+CHRCOO^-$, the carboxylate group is the only choice for metal binding: this is the case for three complexes of Val, $[Pb(\text{L-Val})_2(NO_3)(H_2O)_2]_n \cdot (NO_3)_n$ [17, 18], $[Pb(\text{L-Val})(\text{L-Ile})(NO_3)(H_2O)_2] \cdot NO_3$ [18], and $\{[Pb_4(\text{L-Val})_{10}] \cdot (ClO_4)_8 \cdot 4H_2O\}_n$ [19]; two for Ile, $[Pb(\text{L-Ile})(\text{L-Val})(NO_3)(H_2O)_2] \cdot NO_3$ [18] and $Pb(\text{L-Ile})_2(NO_3)(H_2O)_2] \cdot NO_3$ [18, 19]; and two for Phe, $[Pb(\text{L-Phe})_2(NO_3)(H_2O)_2] \cdot NO_3$ [18, 23] and $[Pb(\text{L-Phe})_2(NO_3)(H_2O)_2] \cdot NO_3 \cdot H_2O$ [18]. When the protonated ammonium group loses a proton to give $H_2NCHRCOO^-$ [8, 19, 24], the amino group becomes a possible metal binding site: this is the case for a Leu complex $[Pb_2(\text{L-Leu} - H)_2(NO_3)_2]_n$ [19] and a Phe complex $[Pb(\text{L-Phe} - H)_2]_n$ [24], where Pb(II) binds to the primary amine nitrogen and simultaneously to the carboxylate oxygen to form a five-membered N–M (metal ion)–O (carboxylate) chelate ring. But this is not always the case: the Pb(II) ion binds solely to the carboxylate oxygens in two isomeric Gly complexes, $[PbX_2\{Cu_{0.5}(\text{Gly} - H)\}]_n$ (X = Cl [8] or Br [8]).

For Pb(II) complexes of Group 1 amino acids whose amino group is *singly* substituted (this holds for eight complexes [10–13, 16, 25] excluding two complexes of proline [21, 22]), the secondary amino group –NH– *hardly* takes part in metal coordination: this is the case for four complexes [10–13, 25]), and only one complex $[Pb(\text{pym-L-Ala} - H)(ClO_4)]_n$ (pymAla – H = *N*-(2-pyridylmethyl)-alaninate monoanion) [16] provides a rare example showing Pb(II)–N bonding for an amino acid having the –NH– functional group. On the other hand, when the –NH– group is deprotonated, the resulting $-N^-$– entity is *always* involved in metal coordination, accompanying the N–M–O (carboxylate) chelation, in two complexes $[Pb(\text{tsGly} - 2H)(H_2O)]_n$ (tsGly – 2 H = *N*-(*p*-tolylsulfonyl)glycinate dianion) [10] and $[Pb(\text{npsGly} - 2H)]_n$ (npsGly – 2 H = *N*-(2-nitrophenylsulfonyl)glycinate dianion) [13].

For Group 1 amino acids whose amino group is *doubly* substituted (four glycine complexes [9, 15]), the tertiary amine nitrogen *does not* participate in metal coordination in two complexes, $[Pb(\text{bphmGly} - 2H)(H_2O)]$ (bphmGly – 2 H = *N*-bis(phosphonomethyl)glycinate dianion with $\alpha\text{-}CO_2^-$ and PO_3H^-) [9] and $[Pb\{\text{phm(m)Gly} - 3H\}(\text{BTS})(H_2O)]_n \cdot nH_2O$ (phm(m)Gly – 3 H = *N*-(phosphonomethyl)-*N*-methyl-glycinate trianion with $\alpha\text{-}CO_2^-$ and $-PO_3^{2-}$, and BTS = 5-sulfoisophthalate trianion) [15], while interestingly, the same ligand [15] containing two polymorphic compounds $[Pb_3\{\text{phm(m)Gly} - 3H\}_2]_n \cdot nH_2O$ (monoclinic [14] and triclinic [14]) carries Pb(II)–N bonding through to form an N–M–O (carboxylate) chelate ring.

Proline is unique in that its side chain binds to the main chain to form the pyrrolidine ring. Among three Pb(II)-proline complexes reported [20–22], the unsubstituted Pro complex, $[Pb(\text{L-Pro} - 2\,H)(H_2O)]_n$ [20], is noticeable in that Pb(II) binds, in addition to the carboxylate oxygen, to the deprotonated secondary amine ring-nitrogen $-N^-$–, forming an N–M–O chelation; on the other hand, in the other two substituted Pro complexes, $[Pb_2(\text{phm-DL-Pro} - 2\,H)Cl_2]_n$ (phmPro – 2 H = *N*-phosphomethylprolinate dianion with α-CO_2^- and $-CH_2PO_3H^-$) [21] and $[Pb_4O(\text{phm-DL-Pro} - 3\,H)_2]_n$ (phmPro – 3 H = *N*-phosphomethylprolinate trianion with α-CO_2^- and $-CH_2PO_3^{2-}$) [22], the tertiary amine ring-nitrogen *does not* participate in metal coordination and, as expected, the phosphonate functional group of the substituent *does* extensively, involving the O (phosphonate)–M–O (carboxylate) chelation.

2.1.2. Group 2 Amino Acids

Group 2 amino acids with polar and neutral side chains are serine (Ser), threonine (Thr), tyrosine (Tyr), cysteine (Cys), asparagine (Asn), and glutamine (Gln). Only two complexes are available, one each for Tyr [26] and Cys [27] and none for others (penicillamine, a dimethyl derivative of cysteine, is separately dealt with in Section 5). In the polymeric tyrosine complex $[Pb(\text{3,5-dinitro-L-Tyr} - 2\,H)]_n \cdot 0.5\,nH_2O$ [26], Pb(II) binds to three Tyr molecules in the crystal lattice: The first ligand binds through both the amino NH_2 and carboxylate groups to form the N–M–O chelation, the second one through the other carboxylate oxygen, and the third one through the phenolate oxygen $-O^-$ attached to the side chain.

In the polymeric cysteine complex $[Pb\{Mo_2(\mu\text{-}S)_2O_2(\text{L-Cys} - 2\,H)_2\}]_n \cdot 2\,nH_2O$ [27], the Pb(II) ion bridges between thiolate ($-S^-$) side chain groups of two cysteine ligands within a sulfur-bridged dinuclear anion $[Mo_2(\mu\text{-}S)_2O_2(\text{L-Cys} - 2\,H)_2]^{2-}$ in which two tridentate cysteine ligands are coordinated with the two Mo(V) atoms each via carboxylate, amino NH_2, and thiolate groups, giving a 1D chain structure.

2.1.3. Group 3 Amino Acids

Group 3 amino acids with basic polar side-chains are lysine (Lys), arginine (Arg), and histidine (His). Only one complex [27] is available for Arg. $[Pb_2(\text{L-ArgH})_3(NO_3)_7(H_2O)] \cdot 3\,H_2O$ involves two Pb(II) ions and three protonated arginine molecules (with α-CO_2^-, amino $-NH_3^+$, and guanidinium $-NHC(NH_2)(=NH_2^+)$ groups): the first Pb(II) binds to two arginine ligands while the second Pb(II) to only one arginine ligand, each through carboxylate oxygens (bidentate) by forming a four-membered O–M–O chelate ring.

2.1.4. Group 4 Amino Acids

Group 4 amino acids with acidic polar side chains are aspartic acid (Asp) (pK_a = 3.9 for β-COOH) and glutamic acid (Glu) (pK_a = 4.1 for γ-COOH). Two complexes [28, 29] are reported for Asp, and five complexes [30, 31] for Glu. In all of these complexes, in addition to the α-carboxylate oxygens, the deprotonated β-carboxylate group of Asp or γ-carboxylate group of Glu are always involved in metal binding. In the Asp complex, $[Pb(\text{L-Asp} - H)(NO_3)]_n$ [28], Pb(II) binds to four crystallographically related monoanionic aspartate molecules (with α-CO_2^-, amino $-NH_3^+$, and β-CO_2^-), forming a polymeric structure: two aspartate ligands through the α-carboxylate group (monodentate for each ligand) and the other two ligands through the β-carboxylate group (monodentate for one ligand and bidentate for the other ligand). In the dimerized Asp complex, $[Pb_{2.5}(\text{Asp-dimer} - H)(H_2O)_2]_n$ [29] (which was prepared under high temperature and basic conditions), where a secondary amine was formed by the dimerization of aspartic acid and acts as the ligand (Asp-dimer – H = $[N^-\{CH(CO_2^-)CH_2CO_2^-\}_2]^{5-}$ = $[^-O_2C\text{-Asp1-}N^-\text{-Asp2-}CO_2^-]^{5-}$), one of the three independent Pb(II) ions binds to five Asp-dimer ligands through an α-carboxylate oxygen belonging to Asp1; the second Pb(II) binds to two ligands, one ligand through a β-carboxylate oxygen of Asp1 and the other through four sites, one site being another α-carboxylate oxygen of Asp1 and the remaining three sites belonging to Asp2, that is, an α-carboxylate oxygen, a β-carboxylate oxygen, and the deprotonated secondary amine, thus forming three kinds of chelate rings in the Asp2 fragment; the third Pb(II), which rides on a two-fold rotation axis, binds to two symmetry-related ligands each through another α-carboxylate oxygen of Asp2, resulting in the formation of a polymeric structure of the complex.

In all of the five reported Pb(II) complexes of Glu whose amino group is substituted, $[Pb(\text{ts-DL-Glu} - 2H)(H_2O)]_n$ (ts = *N*-(*p*-tolylsulfonyl)) [30], $[Pb(\text{ts-DL-Glu} - 2H)(\text{bpy or phen})]_2$ [30], and $[Pb_2(\text{bs-L-Glu} - 2H)_2(\text{bpy or phen})_2]_n$ (bs = *N*-benzenesulfonyl) [31], each glutamate dianion (with α-CO_2^-, amino –NH–, and γ-CO_2^-) coordinates to two or more Pb(II) ions via both the α- and γ-carboxylate groups, forming the discrete dimeric $[-Pb-\{\alpha\text{-}CO_2^-\text{-}CH(CH_2)_2\text{-}\gamma\text{-}CO_2^-\}-]_2$ structure in $[Pb(\text{ts-DL-Glu} - 2H)(\text{bpy or phen})]_2$ or such a structural framework as a part of the polymeric structure in the other three complexes.

2.1.5. Summary

Among the functional groups of amino acids, the α-carboxyl group, which is always deprotonated, is involved in metal coordination in all of so far reported Pb(II) complexes with the twenty standard amino acids (including the amino group-substituted ones). The amino group also binds to Pb(II) in any form of primary, secondary, or tertiary amines with different degrees of occurrence. For amino acids having a neutral amino group $-NH_2$, among the five complexes reported (Gly [8], Leu [19], Phe [24], Tyr [26], and Cys [27] complexes), Pb(II)–

N bonding occurs in three complexes [19, 24, 26]. For the neutral secondary amine –NH–, Pb(II)–N bonding is quite rare, only one complex is available (Ala [16]) among ten complexes of singly *N*-substituted amino acids [9–11, 16, 25, 30, 31], whereas the deprotonated $–N^{-}–$ secondary amine always takes part in metal binding in three complexes (Gly [10, 13] and Asp-dimer [29]). Of the four complexes of doubly *N*-substituted amino acids, which are all Gly complexes [9, 14, 15], two polymorphic compounds $[Pb_3\{phm(m)Gly - 3\,H\}_2]_n \cdot n H_2O$ (monoclinic [14] and triclinic [14]) are of special interest in that the tertiary amine achieves Pb(II)–N bonding. It is noticeable that, whenever Pb(II) binds to an amino group in any form, Pb(II) simultaneously also binds to the carboxylate oxygen to form the five-membered N–M–O chelate ring.

Among the four groups of amino acids, of special interest from the viewpoint of not only coordination chemistry but their possible interactions with metal ions as amino acid residues of proteins, are those that belong to Groups 2 and 4, whose side chains contain polar functional groups: –OH of Ser, Thr, and Tyr, –SH of Cys, and $–CONH_2$ of Asn and Gln in Group 2 amino acids and β-COOH of Asp and γ-COOH of Glu in Group 4 amino acids. Available examples (only two complexes) show that Pb(II) binds to the hydroxyl group of Tyr [26] and the sulfhydryl group of Cys [27], both in the deprotonated forms $–O^{-}$ and $–S^{-}$, however. On the other hand, in all of two Asp complexes [28, 29] (involving Asp dimer [29]) and five Glu complexes [30, 31], deprotonated β- and γ-CO_2^{-} groups of Asp and Glu, respectively, are always involved in metal coordination.

As expected, in most of Pb(II) complexes with amino acids, Pb(II) exhibits a 'stereochemically active' $6s^2$ lone pair effect (ligands are *hemidirected*) (see Table 2, which lists the coordination geometry for each complex). In only a few complexes (Val [17], Asp-dimer [29], and Glu [30] complexes), the $6s^2$ lone pair on Pb(II) is 'stereochemically inactive' (the ligands are *holodirected*). In the crystal lattice, most complexes form polymeric structures (26 complexes) due to the existence of multiple functional groups on amino acids (including *N*-substituted derivatives); some others are monomeric (seven complexes [9, 18, 19, 23, 25]) or dimeric (four complexes [12, 18, 30]).

2.2. Small-Peptide Complexes

For peptides, possible ligation sites are the amide oxygen and the nitrogen (but only when deprotonated) within the peptide backbone, polar functional groups on the side chains of the amino acids belonging to Groups 2 and 4 in Section 2.1, and the amino terminal nitrogen and the carboxyl terminal oxygens. Table 3 lists metal binding sites/modes on the peptide ligands [32, 33].

Unfortunately, only two crystal structures of small peptides are available: $[Pb(Gly\text{-}L\text{-}Glu)(H_2O)_{0.5}]_n \cdot n ClO_4$ [32] and a cyclic peptide complex $[Pb\{cyclo(Gly\text{-}L\text{-}Ser\text{-}L\text{-}Pro\text{-}L\text{-}Glu)\}(NO_3)]_n \cdot 2n H_2O$ [33], both containing Group 2 and/or Group 4 amino acids (Ser and/or Glu).

In the $[Pb(Gly\text{-}L\text{-}Glu)(H_2O)_{0.5}]_n \cdot n ClO_4$ complex [32], where the GlyGlu molecule exists as a monovalent anion with both α- and γ-carboxyl groups (of Glu)

Table 3. Pb(II) ion binding sites/modes on small peptides in the solid state.[a,b]

Complex	Coordination number and geometry[c]	Metal binding sites on peptide ligand and other ligands/ comments, if any	CSD code	Ref.
$[Pb(Gly\text{-}L\text{-}Glu)(H_2O)_{0.5}]_n \cdot n ClO_4$	6 Hemi.	O_A,O_B [α-CO_2^- (Mol.1 Glu): 2.734, 2.657][d], O_A,O_B [γ-CO_2^- (Mol.1′ Glu): 2.571, 2.451], O_A [α-CO_2^- (Mol.1″ Glu): 2.576], O [aqua: 2.593] The aqua ligand lies on a two-fold axis. Formation of the [–Pb–{α-CO_2^--$CH(CH_2)_2$-γ-CO_2^-}–] helical structure and the [–Pb–{α-CO_2^--$CH(CH_2)_2$-γ-CO_2^-}–]$_2$ dimeric framework.	OHETEA	[32]
$[Pb\{cyclo(Gly\text{-}L\text{-}Ser\text{-}L\text{-}Pro\text{-}L\text{-}Glu)\}(NO_3)]_n \cdot 2nH_2O$	7 Holo.	O,O [Ser (Mol.1) amide[e]: 2.489; hydroxyl: 2.475], O_A,O_B [γ-CO_2^- (Mol.1′ Glu): 2.463, 2.644], O [amide (Mol.1″ Glu): 2.833], 2 O [nitrate (Mol.1, Mol.1′): 2.571, 2.755] Naturally occurring cyclic tetrapeptide. See Figure 1.	LEYBUO	[33]

[a] Obtained from the Cambridge Structural Database (CSD version 5.36 updated to May 2015).
[b] Abbreviations: aqua, water ligand; *cyclo*(Gly-L-Ser-L-Pro-L-Glu), *cyclo*(glycyl-L-seryl-L-propyl-L-glutamyl) monoanion with –OH (Ser) and γ-COO^- (Glu); Gly-L-Glu, glycyl-L-glutamate monoanion with –NH_3^+ (Gly), α-COO^- (Glu), and γ-COO^- (Glu).
[c] See footnote 'e' in Table 2.
[d] 'O_A,O_B [α-CO_2^- (Mol.1 Glu): 2.734, 2.657]' denotes that the metal ion binds to two α-carboxylate oxygens O_A and O_B of the amino acid residue of the molecule 1 (Glu of Mol.1 in this case), forming an O_A–M–O_B chelation, and their bond distances (Å).
[e] 'amide' denotes the amide oxygen of the peptide backbone.

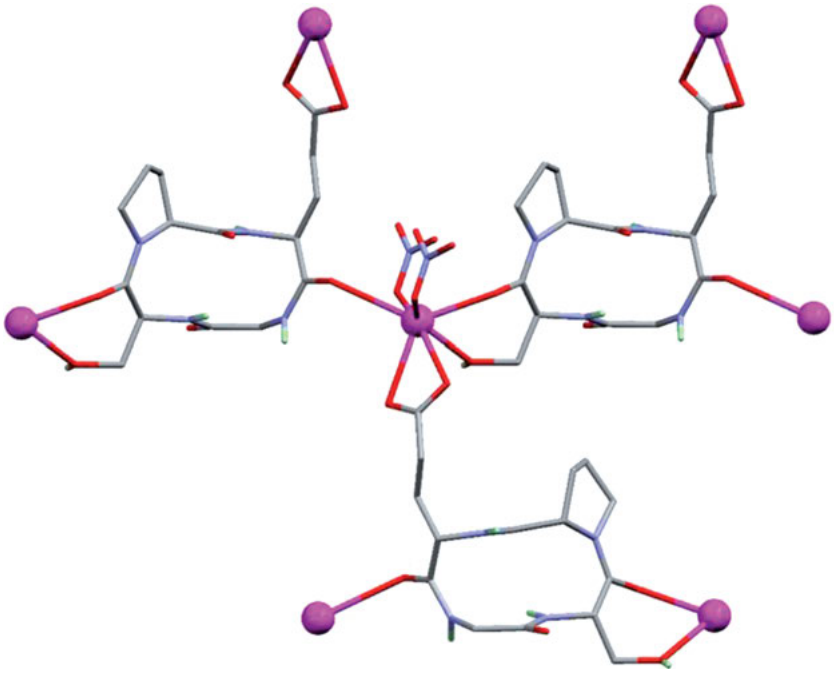

Figure 1. A segment of the polymeric structure of the [Pb{*cyclo*(Gly-L-Ser-L-Pro-L-Glu)}$(NO_3)]_n$ complex [33], shown with color-coded atoms (*red*, oxygen; *blue*, nitrogen; *grey*, carbon; *green*, hydrogen; *purple*, lead). The residues bound to the metal ion are depicted as 'sticks' and the metal ion as 'ball'. The peptide ligand, a marine cyclic tetrapeptide, binds to three Pb(II) ions, through amide carbonyl and hydroxyl oxygens of Ser, through γ-carboxylate oxygens of Glu, and through an amide carbonyl oxygen of Glu, respectively. Note that the seven-coordinated Pb(II) center shows an uncommon *holodirected* coordination sphere. Similar color codes are also used in subsequent diagrams of molecular structures.

deprotonated and the amino group (of Gly) protonated, Pb(II) binds to three symmetry-related peptide molecules (Mol.1, Mol.1′, and Mol.1″) through only carboxylate groups of Glu: through α-CO_2^- (bidentate binding) of Mol.1 and γ-CO_2^- (bidentate) of Mol.1′ (related to Mol.1 by a twofold screw-axis symmetry), thus forming the [–Pb–{α-CO_2^--$CH(CH_2)_2$-γ-CO_2^-}–]$_n$ helical structure, and further through γ-CO_2^- (monodentate) of Mol.1″ (related to Mol.1 by a unit-cell translation), forming the [–Pb–{α-CO_2^--$CH(CH_2)_2$-γ-CO_2^-}–]$_2$ dimeric framework, which is analogous to that observed in *N*-substituted Glu complexes [Pb_2(bs-L-Glu – 2 H)$_2$(bpy/phen)$_2$]$_n$ [31]. The geometry around the six-coordinated Pb(II) center appears *hemidirected* due to its stereochemically active lone pair.

Cyclo(Gly-L-Ser-L-Pro-L-Glu) is a naturally occurring cyclic tetrapeptide, which was first isolated from the *Ruegeria* strain of marine bacteria and was found to possess moderate antibacterial activity against *Bacillus subtilis* [34]. Figure 1 shows the binding mode of *cyclo*(Gly-L-Ser-L-Pro-L-Glu) to Pb(II) in the [Pb{*cyclo*(Gly-L-Ser-L-Pro-L-Glu)}$(NO_3)]_n \cdot 2n H_2O$ complex [33]. The Pb(II)

ion binds to three cyclic peptide molecules (Mol.1, Mol.1′, and Mol.1″), which are symmetry-related to each other, through amide carbonyl and hydroxyl oxygens of Ser (of Mol.1), forming a six-membered chelate ring, through γ-carboxylate oxygens (bidentate) of Glu (Mol.1′), and through an amide oxygen of Glu (Mol.1″). The Pb(II) center in a seven coordination environment shows an uncommon *holodirected* coordination sphere.

These two peptide complexes, though limited, show that oxygen-containing functional groups are all involved in Pb(II) bonding: carboxylate groups of the carboxyl-terminal and the side chain of Glu, the hydroxyl group of Ser, and the amide oxygen of the main chain. As is mentioned below in Section 2.3, the side chain of Glu and the main chain carbonyl are involved in Pb(II) binding in crystal structures of Pb(II)-bound proteins: in fact, Glu is observed as the most predominant ligand for Pb(II) bonding [35].

2.3. Protein Complexes

Lead is used to prepare heavy atom derivatives of protein and nucleic acid crystals for use in their structure determination by isomorphous replacement [36] or anomalous dispersion [37] approaches that can solve the 'phase problem' in X-ray crystallography.

We searched the Protein Data Bank (PDB updated to February 2016) (http://www.rcsb.org/pdb/) for Pb(II)/Pb(IV) compounds. A total of 45 Pb(II) structures were found: 41 protein structures (including three protein/RNA structures) and four RNA structures. Next we checked the primary literature for these 41 lead-derivatized protein structures and noticed that, unfortunately, in the majority of these compounds in which lead was used exclusively for phase determination, little attention was given to lead binding sites/modes. We deal here with ten protein crystal structures in which Pb-binding sites/modes are well defined: those include Ca(II)-binding proteins [PDB ID: 1N0Y [38], 2V01 [39], 3TWY [40]], one Zn(II)-binding protein [PDB ID 1QNV] [41], and other proteins [PDB ID: 1QR7 [42], 1EQN [43], 1HD7 [43], 2G0A [44], 2FJQ [45], 2QD5 [46]].

Godwin et al. once reviewed [1] crystal structures of Pb(II) complexes with Ca(II)-binding proteins (calmodulin [PDB ID 3CLN] [47] and synaptotagmin [PDB ID 1RSY] [48] and [PDB ID 1DQV] [49]) and those with Zn(II)-binding proteins (δ-aminolevulinate dehydratase [PDB ID 1AW5] [50] and carboxypeptidase A [no PDB ID: not deposited in the PDB] [51]). These crystal structures along with several $Me_3Pb(IV)^+$-derivatized protein crystal structures [52] are also mentioned here briefly.

For a general review for lead-binding proteins refer to [53] and for lead toxicity refer to [54].

2.3.1. Calcium-Binding Proteins

Pb(II) is known [55] that its disruptive effect on transmitter release at synapses and in neurons is primarily due to inhibition of voltage-gated calcium channels as

well as its interaction with Ca(II)-binding proteins, including calmodulin (CaM), synaptotagmin (SYT), or protein kinase C (PKC), which regulate the synaptic vesicle mobilization, docking, and exocytosis processes.

2.3.1.1. Calmodulin

CaM, a Ca(II)-binding protein, exists in all eukaryotic cells as a major intracellular Ca(II) ion receptor and mediates a variety of physiological processes in a calcium-dependent manner [56]. Lead is known to have a very high affinity towards CaM and to displace bound Ca(II) from CaM [57] and it is able to falsely activate CaM even at low concentrations [58–60] but inhibits it at high concentrations [61, 62]. Pb(II)–CaM may play a role in Pb(II) toxicity [63, 64].

Three crystal structures of the *Pb(II)-bound CaM* have so far been reported [PDB ID: 3CLN [47], 1N0Y [38], and 2V01 [39]]. The crystal structure of the *native mammalian CaM* at 2.2 Å resolution [PDB ID 3CLN] [47] revealed the four calcium binding loops in CaM, which have the typical EF-hand conformation (helix-loop-helix structural motif), and each loop binds a Ca(II) ion (see Figure 6 in [47]) (for a review on the structure and function of the EF-hand motif, refer to [65]). The four Ca(II)-binding loops consist of 12-residue segments. All four Ca(II)-binding sites exhibit seven-fold coordination: the first Ca(II)-binding ligand in each loop is furnished by an Asp or Asn side chain; the next five ligands are by three side chains and one carbonyl oxygen atom; a water molecule completes the coordination shell; the residues at the first, third, and fifth positions in each loop contribute a carboxylate oxygen atom; the residue at the seventh position contributes its carbonyl oxygen; the 12^{th} residue in each loop is a glutamate that binds to Ca(II) through both carboxylate oxygens. In loops 2, 3, and 4, the residue in the ninth position are Asp, Ser, and Asn, respectively.

On the other hand, the crystal structure of the *Pb(II)-bound CaM* at 2.2 Å resolution [no PDB ID] [47], which was prepared by soaking $Pb(OAc)_2$, showed five Pb(II)-binding sites, two of which correspond to the Ca-binding sites in the first two Ca(II) binding loops. This means, Ca(II)-binding sites are formed by Asp20, Asp22, Asp24, Thr26, and Glu31 for Pb-1 in EF-hand-1 while they are formed by Asp56, Asp58, Asn60, Thr62, and Glu67 for Pb-2 in EF-hand-2. Of the other three Pb(II) sites, one Pb(II) is bound to side chains from Asp118 and Asp122; the other two Pb(II) are coordinated to side chains from Glu14 and Glu87, respectively [47].

The crystal structure of the *Pb(II)-bound CaM* (from *Paramecium tetraurelia*) at 1.75 Å resolution [PDB ID 1N0Y] [38], prepared by soaking $Pb(OAc)_2$, was determined. Unfortunately, for each of the two independent molecules in the asymmetric unit, only a portion of the structure could be modeled due to their structural disordering. A total of 14 Pb(II) sites were found, four of which are located in the EF-hand loops and seven Pb(II) are scattered around the CaM surface (see Figure 1c in [66]). In all four metal-binding loops of CaM, the Pb(II) coordination is essentially identical to that of Ca(II), including the seventh water ligand to the metal ion (see Figure 5 in [66]). Comparison of the structures of

Ca(II)–CaM (from *Paramecium tetraurelia*) at 1.0 Å resolution [PDB ID 1EXR] [67] (see Figure 1a in [66]) and Pb(II)–CaM [PDB ID 1N0Y] [38] (see Figure 1b in [66]) shows close agreement in the C-terminal domain but significant structural differences in the N-terminal domain (but the flexibility of the N-terminal domain is an intrinsic property of the protein and not an effect specific to Pb(II)–CaM [38]).

The crystal structure of the *Pb(II)-bound human CaM* at 2.15 Å resolution, prepared by soaking $PbCl_2$ ([PDB ID 2V01] [39]), revealed a total of eight Pb(II) ions (see Figure 1a in [39]), four of which replace Ca(II) ions in all four EF-hands in native CaM and one Pb(II) is located close to EF-hand-2, being coordinated by Asp58 and Asp64. The other three Pb(II) ions are scattered around the CaM surface, interacting with negatively charged CaM surface residues, as is observed in the Pb–CaM (from *Paramecium tetraurelia*) structure [38]. The authors suggest [39] that this could be a mechanism for the reported decrease in CaM activation by Pb at higher concentrations [61, 62] and, since no such Ca atoms are observed upon crystallization in Ca-containing solutions, the affinity of Pb for non-EF-hand sites in CaM seems to be higher than that of Ca; thus, the toxicity-related activation mechanism of CaM by lead may have two aspects: hyperactivation at low concentrations of Pb and inactivation at high concentrations.

2.3.1.2. Synaptotagmins

SYTs are synaptic vesicle-associated, phospholipid-binding proteins most commonly associated with Ca(II)-dependent exocytotic and Ca(II)-independent endocytotic events [68]. SYTs constitute a family of membrane-trafficking proteins that are characterized by an N-terminal transmembrane region, a variable linker, and two C-terminal C2 domains (C2A and C2B). The C2A and C2B domains have similar protein folding to each other (composed of a stable eight-stranded β-sandwich with flexible loops emerging from the top and bottom) with three and two Ca(II)-binding sites, respectively, but with different functions (C2A acts as a Ca(II) sensor). Ca(II) ions bind exclusively to the top loops and the binding pockets are coordinated by five conserved aspartate residues: three calcium ions bind to the C2A domain via Asp172, Asp178, Asp230, Asp232, Ser235, and Asp238 (see Figure 6A in [69]), and two calcium ions bind to C2B via Asp303, Asp309, Asp363, Asp365, and Asp371 (see Figure 6B in [69]) (for review on details of the structure and function of C2 domains, refer to [70]).

Crystal structures of two *synaptotagmins* were solved using $Me_3Pb^{IV}(OAc)$ as a heavy atom derivative: one is the C2A domain (residues 140–267) of native rat synaptotagmin-1 (SYT-1) at 1.9 Å resolution [PDB ID 1RSY] [48] and the other is the C2 domain (residues 295–569 including C2A and C2B domains) of the mouse synaptotagmin-3 (SYT-3) at 3.2 Å resolution [PDB ID 1DQV] [49]. SYT-1 functions as the Ca(II) sensor for rapid, synchronous synaptic vesicle exocytosis and is one of the most significant molecular targets for lead [71, 72]. One of the characteristic properties of SYT-3 is the ability to bind divalent cations and accessory proteins promiscuously [49].

Unfortunately, the original literature of the *SYT-1* crystal structure [PDB ID 1RSY] made no mention about lead binding, but Godwin et al. noted in their

review [1] that a Pb(IV) ion binds only to the high-affinity calcium-binding site between two loops, the site corresponding to the Ca1 site in Figure 6A in [69], which is made up of β-carboxylate groups of four Asp residues (Asp172 and Asp179 in the loop 1, and Asp230 and Asp232 in the loop 3) in the multinuclear calcium-binding site of the C2A domain.

On the other hand, in the crystal structure of the *C2 domain of SYT-3* [PDB ID 1DQV], three Pb(IV)-binding sites were found, one of which is located at the same site (the Ca1 site in Figure 6A in [69]) on the C2A domain as the one corresponding to the high-affinity Ca(II)-binding site in the CYT-1 structure [PDB ID 1RSY]. The second site is on a minor Ca(II)-binding site (the Ca2 (or Ca3) site in Figure 6A in [69]) on the C2A domain and the third site is in Ca(II)-binding loops of the C2B domain (see Figure 6B in [69]).

2.3.1.3. Protein kinase C

Protein kinase C isozymes (PKCs) constitute a family of Ser- and Thr-specific protein kinases that control signaling pathways essential for cell proliferation, differentiation, and survival. All PKCs have a conserved kinase domain at the carboxyl terminal side and more variable regulatory domains at the amino terminal side. Among these PKC isozymes, Ca(II)-dependent PKC isozymes (called conventional PKCs (α, β, and γ)) have the regulatory domain composed of H_2N–pseudosubstrate motif–C1 domain (diacylglycerol-binding domain)–C2 domain (Ca(II)-binding domain), among which the C2 domain anchors the parent enzyme to lipid membranes in response to binding Ca(II) ions. It has been shown that the Ca(II)-dependent binding of the protein kinase C-α isozyme (PKC-α) to membranes presents a high specificity for a short chain lipid 1,2-dicaproyl-*sn*-phosphatidyl-L-serine (PtdSer) and this binding is mediated by the C2 domain (for details of the structure and function of PKCs, refer to [73]). The C2 domain of conventional PKCs is a well-documented molecular target of lead [72, 74].

Four crystal structures including the C2 domain of rat PKC-α (designated C2α [40]) (residues 155–293) are available: C2α apo (Ca- and Pb-free) at 1.9 Å resolution [PDB ID 3TWJ] [40], the binary C2α–Ca(II) complex at 2.4 Å resolution [no PDB ID] [75], the ternary C2α–Ca(II)–PtdSer complex at 2.6 Å resolution [PDB ID 1DSY] [75], and the binary *C2α–Pb(II) complex* at 1.5 Å resolution, prepared by soaking $Pb(OAc)_2$ [PDB ID 3TWY] [40]. NMR and isothermal titration calorimetry techniques established [40] that C2α binds Pb(II) with higher affinity than its natural cofactor Ca(II) and that there are two Pb(II)-binding sites on the C2α domain with a 2000-fold difference between the Pb(II) affinities of the two sites.

Commonly in these four crystal structures, the C2 domain has an antiparallel β-sandwich composed of eight β-strands, a topology being similar to the C2A domain of synaptotagmin-1 [48]. The two Ca(II) ions (Ca1 and Ca2) in both the binary C2α–Ca(II) and ternary C2α–Ca(II)–PtdSer complexes or the two Pb(II) ions in the C2α–Pb(II) complex bind in a cavity formed by the first and final loops of the C2 domain, as a binuclear cluster in which the two Ca(II) are related to each other by a pseudo-dyad symmetry axis, similar to what had been observed in most C2 structures [76], whereas the two Pb(II) are partly deviated

from the pseudo-dyad symmetry due to the difference in coordination geometries between the two Pb(II), one being *holodirected* and the other *hemidirected* (as noted below). Non-specific association of Ca(II) or Pb(II) ions with the charged side chains on the protein surface is not observed. It should be noted that these Ca1 and Ca2 sites correspond to the Ca1 and Ca2 sites in the C2A domain of synaptotagmin-1 (compare with Figure 6A in [69]). A comparison of the metal coordination sites between the Ca(II) and the Pb(II) complexes shows (see Figure 4C in [40]) that the Ca1 site and the Pb1 site (high-affinity site) are superimposable, thereby containing a total of nine oxygens that coordinate to Pb1, seven are from the same ligand as those [four Asp side chains 187 (bidentate), 193, 246 (bidentate), and 248 and a Trp247 carbonyl] bound to Ca1 in the C2α–Ca(II) and C2α–Ca(II)–PtdSer complexes, and the remaining two oxygens are from two water molecules, adopting the *holodirected* coordination geometry.

On the other hand, the Pb2 site (low affinity site) is slightly shifted from the Ca2 site to lead in the absence of Pb2 bonding to the carbonyl oxygen of Met186, which is coordinated to Ca2 in the Ca(II) complexes, though six of the eight oxygen atoms that are coordinated to Pb2 are still from the same ligand as those [four Asp side chains 187, 246, 248 (bidentate), and 254 (monodentate for Ca2; bidentate for Pb2)] bound to Ca2 and the remaining two oxygens are from two water molecules, showing the *hemidirected* coordination geometry for Pb2 in contrast to the *holodirected* one for Ca2. The backbone superposition of apo C2α, C2α–Pb(II), and C2α–Ca(II)–PtdSer complexes shows that the binding of divalent metal ions has little effect on the backbone conformation of the whole C2 domain (Figure 4A in [40]), and thus the slight movement of the Pb2 site from the Ca2 site is possibly due to the stereochemically active lone pair effect of Pb(II) against the carbonyl oxygen of Met186.

2.3.2. Zinc-Binding Proteins

2.3.2.1. δ-Aminolevulinate dehydratase (ALAD or porphobilinogen synthase PBGS)

ALAD is a zinc-protein that catalyzes the formation of porphobilinogen from δ-aminolevulinic acid (ALA) in the metabolic pathway of the heme biosynthesis. ALAD is known to be one of the most lead-sensitive enzymes [77]: human ALAD binds lead tightly with a sub-picomolar inhibition constant, and Zn(II) and Pb(II) compete for the same binding site [78].

The crystal structure of the *native yeast ALAD* enzyme at 2.3 Å resolution [PDB ID 1AW5] [79] revealed the two zinc binding sites (Zn1 as the major site and Zn2 as the minor site), where the Zn1 site is formed by three cysteine residues (called Cys3: Cys133, Cys135, and Cys143) while the Zn2 site involves Cys234 and His142 (see Figure 6 in [79]).

On the other hand, the crystal structure of the *Pb(II)-bound yeast ALAD* at 2.5 Å resolution [PDB ID 1QNV] [41, 79], prepared by soaking $Pb(OAc)_2$, showed that one of the two lead ions replaces the catalytic Zn1 ion bound to the Cys3 site (see Figure 6 in [79] and Figure 7 in [41]). This represents a possible

mechanism for the neurological symptoms of lead toxicity, that is, the incorporation of lead into the enzyme reduces the affinity for substrate ALA non-competitively to result in the accumulation of ALA [79]. No apparent Pb(II) binding at the Zn2 binding site was observed but instead, the minor lead-binding site was found near the main triple-cysteine site in the active site of the enzyme (see Figure 7 in [41]). A kinetic study of *human* ALAD proposed [80] that the chemically active lone pair effect of Pb(II) could alter the active site environment and disfavor substrate binding and subsequent catalysis of ALAD. Preference of Pb(II) toward the Cys3 site in ALAD was later borne out by a model study [81] showing that lead binds more tightly than zinc (about 500 to 1) to a tris-thiol ligand tris(mercaptophenylimidazolyl)hydroborate (Tm^{Ph}), a model ligand for the Cys3 cite in ALAD, and the structure of $[Pb(Tm^{Ph})]^+$ (see Figure 8 in Section 5) is very similar to the structure of $[Pb(Cys)_3]$ formed at the active site of Pb(II)–ALAD: both possess a trigonal pyramidal geometry with very similar average Pb–S bond lengths of 2.7 and 2.8 Å, respectively.

2.3.2.2. Metallocarboxypeptidases

Carboxypeptidases catalyze the hydrolysis of polypeptides and esters at the C-terminal peptide or ester bond. Metallocarboxylases, which comprise the largest class of carboxypeptidases having a single Zn(II) at the active site, can be classified by their substrate specificities. Carboxypeptidase A (CPA) is specific for neutral, preferably hydrophobic amino acids. It has been shown [82] that lead hydroxide $[Pb(OH)]^+$ inhibits the bovine CPA catalysis by binding to the catalytic residue Glu270.

The high-resolution (1.6 Å) crystal structure [PDB ID 3CPA] [83] of the *native bovine CPA* complexed with the slowly hydrolyzed CPA substrate, Gly-L-Tyr, revealed a Zn(II) ion at the active site. The Zn(II) ion is five-fold coordinated by three enzyme residues (His69, Glu72, and His196) and the Gly-L-Tyr peptide ligand through chelate formation via the carbonyl oxygen and the neutral amino terminus (see Figure 5 in [83]).

On the other hand, the crystal structure of the *Pb(II)-bound bovine CPA* complexed with Gly-L-Tyr at 2.0 Å resolution [no PDB ID] [84], prepared by soaking $PbCl_2$, revealed two Pb(II) ions, one of which binds to a citrate (used in crystallization) and the other to the catalytic residue Glu270, as suggested [82], but does not well overlap with the Zn(II)-binding site in the native CPA structure [PDB ID 3CPA] (see the disposition of Glu270 in Figure 5 in [83]).

The crystal structure of the *Pb(II)-bound PfuCP* (a carboxypeptidase from the hyperthermophilic Archaeon *Pyrococcus furiosus*) at 3.0 Å resolution [PDB ID 1KA4] [85], prepared by soaking $PbBr_2$, was determined, in addition to the apo-PfuCP structure at 2.2 Å resolution [PDB ID 1KA2] [85]. PfuCP is an unusual metalloprotease in that (i) it misses the $HisXXGlu(X)_{123–132}His$ motif characteristic of classical metallocarboxypeptidases and instead contains the HisGluXXHis motif, (ii) the Zn(II)-bound form is inactive, while binding of other metals, such as Mn(II) [85] and Co(II) [86], promotes its catalytic activity, and (iii) it has a broad substrate specificity that includes basic, aromatic, neutral, and polar amino acids. The Pb–PfuCP structure revealed a four-fold coordinated

Pb(II) bound to the two histidine residues (269 and 273 corresponding the HisGluXXHis motif) and Glu299 at the catalytic site and the fourth ligand is a water molecule (see Figure 4 in [86]). In the apo-PfuCP structure, the metal ion occupying the equivalent position is presumed to be a Mg(II) from the crystallization condition. The origin of the metal-dependent differences in the activities of PfuCP remains unresolved.

2.3.3. Other Proteins

2.3.3.1. 3-Deoxy-D-arabino-heptulosonate-7-phosphate synthase (DAHPS)
DAHPS, a metal-activated enzyme, catalyzes the stereospecific condensation of phospho*enol*pyruvate (PEP) and D-erythrose-4-phosphate (E4P) giving rise to 3-deoxy-D-*arabino*-heptulosonate-7-phosphate (DAHP), the first step in the common pathway leading to the biosynthesis of aromatic compounds in microorganisms and plants. The identity of the activating metal *in vivo* remains unclear, although evidence for both Fe(II) [87] and Cu(II) [88] has been reported. Pb(II) activates DAHPS (phenylalanine-regulated form) only poorly (to 3 % of the level achievable with Mn(II), the most effective metal ion *in vitro* [87]).

Two crystal structures of the *Pb(II)-bound* and the *Mn(II)-bound Escherichia coli DAHPS* (phenylalanine-regulated form) were determined at 2.6 Å and 2.0 Å resolution, respectively, where substrate PEP and substrate-analog 2-phosphoglycolate (PGL) were co-crystalized in both the Pb(II)-DAHPS complex [PDB ID 1QR7] [42] prepared by soaking $Pb(OAc)_2$ and the Mn(II)-DAHPS complex [PDB ID 1GG1] [89]. A single metal ion, Pb(II) or Mn(II), was found at the active site of DAHPS. The coordination sphere of Pb(II) or Mn(II) commonly includes side-chains of four protein residues (Cys61, His268, Glu302 as bidentate, and Asp326 as monodentate) and a water molecule, and the sixth site is from PEP for Pb(II) or PGL for Mn(II) (see Figure 3 in [42] for the Pb(II) complex and Figure 3 in [89] for the Mn(II) complex). The four protein residues are dispersed throughout the polypeptide chain and are not part of a localized metal-binding motif. The most striking differences were the metal-binding modes toward substrate PEP or substrate-analog PGL ligands: the Pb(II) ion approaches the four atoms (three carbons and one carboxylate oxygen) that comprise the planar part of PEP, with the approximately equal and rather long interatomic distances (3.6–3.9 Å) due to two factors, metal–π-bond conjugation and the inert electron pair effect, providing the *hemidirected* coordination geometry (see Figure 5 in [42]); in contrast, Mn(II) was coordinated to PGL through the carboxylate oxygen with the usual interatomic distance (2.45 Å) and it showed the *holodirected* coordination geometry (see Figure 4 in [89]). These differences in metal coordination are assumed [42] to be the basis for the striking differences in activation by the most efficient metal activator Mn(II) and the poorly activating Pb(II).

2.3.3.2. Apurinic/apyrimidinic endonuclease (Ape1)
Ape1 is an essential DNA repair enzyme that initiates the removal of apurinic/apyrimidinic sites from DNA by hydrolyzing the DNA backbone [43] and it can

utilize Mg(II) or Mn(II) as a cofactor in catalysis [90]. Ape1 is not known to be inhibited by lead.

Two crystal structures of the *Pb(II)-bound human Ape1*, each prepared by soaking $Pb(OAc)_2$, were determined, one acidic pH structure at 1.95 Å resolution [PDB ID 1HD7] [43] and one neutral pH structure at 2.20 Å resolution [PDB ID 1E9N] [43]. The low pH structure and the neutral structure contain one Pb(II) ion and two Pb(II) ions, respectively, both in the active site. One of the Pb ions in the *neutral* pH structure superimposes closely on the Pb(II) ion in the *low* pH structure and is four-fold coordinated by the carboxylates of Asp70 (monodentate) and Glu96 (bidentate) and a water molecule, and the second Pb(II) ion is four-fold coordinated by the side chains of Asp210 (monodentate), Asn212, and His309 and a water molecule (see Figure 3 in [43]). The two metal ions are 5.0 Å apart. Based on the neutral pH structure and kinetic data, the two-metal (most probably Mg(II)) catalytic mechanism is presumed for the phosphodiester bond hydrolysis [43].

2.3.3.3. Pyrimidine 5′-nucleotidase type 1 (P5N-1)

P5N-1 catalyzes the Mg(II) ion-dependent dephosphorylation of pyrimidine 5′-mononucleotides [91]. Human P5N-1 is one of several enzymes readily inhibited by Pb(II) during lead poisoning [92, 93] and the P5N-1 enzyme deficiency is either familial or can be acquired through lead poisoning [94, 95].

Five crystal structures of the *mouse P5N-1* (mP5N-1) have been reported [44]: these are (i) native P5N-1 with bound Mg(II) at 2.25 Å resolution [PDB ID 2G06], (ii) P5N-1 complexed with a phosphoenzyme intermediate analog at 2.30 Å [PDB ID 2G07], (iii) P5N-1 with a product-transition complex analog at 2.35 Å [PDB ID 2G08], (iv) P5N-1 with a product complex at 2.1 Å [PDB ID 2G09], and (v) *Pb(II)-bound P5N-1* at 2.35 Å prepared by soaking $Pb(OAc)_2$ [PDB ID 2G0A].

The *Mg(II)-bound P5N-1* structures [PDB ID: 2G06, 2G07, 2G08, and 2G09] (Figures 4*B*-4*F* in [44]) revealed one Mg(II) in the active site, which is octahedrally coordinated by the side-chains of two Asp residues (49 and 238), the main-chain carbonyl oxygen of Asp51, and two water molecules, and either an additional water [PDB ID 2G06] or an oxygen of the phosphate group in the product complex [PDB ID 2G09] (Figures 4*E* and 5*A* in [44]) or fluorine of phosphate analogs [PDB ID: 2G07and 2G08] in the reaction cycle. The phosphate group of the substrate binds within a 'cationic cavity' (Figure 5*A* in [44]), which is required for the recognition and binding of the phosphate group of nucleotides.

On the other hand, the *Pb(II)-bound P5N-1* structure [PDB ID 2G0A] revealed one Pb(II) which binds also within the active site of P5N-1 (Figure 4*F* in [44]) with partial occupancy (assuming 25 %) but the binding mode of Pb(II) differs from that of Mg(II) in the Mg(II)-bound P5N-1 structures: the position of Pb(II) coincides approximately with the position of one of the water molecules that coordinates Mg(II); Pb(II) is not coordinated by the backbone carbonyl of Asp51 but stabilized by a rather weak interaction with Asp242 [2.8 Å]. Importantly, Pb(II) is clearly located away from the cationic cavity. Based on these

observations, a mechanism for the P5N-1 inhibition by Pb(II) is proposed [44]: the Pb(II) inhibition is based on the *lowered* affinity of the cationic cavity for the phosphate group (and possibly also on improper positioning of the catalytic residue Asp49 for in-line attack), since a properly positioned metal ion within the active site is directly coordinated by the phosphate bound in the cationic cavity and further stabilizes the negatively charged phosphate through electrostatic interaction. On the other hand, Pb(II) shows a much higher affinity for the active site than Mg(II) [96]. It thus outcompetes Mg(II) and *poisons* the active site of P5N-1 because simultaneous binding of Mg(II) and Pb(II) is not possible.

2.3.3.4. Acyl-CoA-binding protein (ACBP)

ACBP, an intracellular carrier of acyl-CoA esters, is essential for the fatty acid metabolism, membrane structure, membrane fusion, and ceramide synthesis [97]. Human ACBP is known to be one of the proteins that binds lead ions with high affinity *in vivo* [98].

The high-resolution crystal structure of the *Pb(II)-bound human apo ACBP* at 1.6 Å resolution [PDB ID 2FJ9] [45], prepared by soaking $Pb(NO_3)_2$, revealed one Pb(II) site (and one Zn(II) site due to $ZnSO_4$ used in crystallization). The Pb(II) ion is bound at a protein-protein contact in a way that it is complexed to the side chains of Glu69 of a ACBP molecule and Glu61of a neighboring molecule. These side chains are not near the acyl-CoA binding pocket. The Zn(II) ion is also bound at a protein-protein contact, complexed to the side chains of Glu11/His15 and Glu11/His15 of a neighboring molecule, respectively.

2.3.3.5. Ferrochelatase (protoheme ferrolyase)

Ferrochelatase is the terminal enzyme in heme biosynthesis and catalyzes the insertion of ferrous iron into protoporphyrin IX to form protoheme IX (heme) [99]. The enzyme is known to be inhibited by a number of divalent cations including lead [100].

The crystal structure of the *Pb(II)-bound human ferrochelatase* enzyme at 2.3 Å resolution [PDB ID 2QD5] [46] has been reported. The crystal was prepared by incubating the enzyme with protoporphyrin IX and $Pb(OAc)_2$ during crystallization. The enzyme forms a homodimeric structure (subunits A and B) in which Pb(II) is inserted into protoporphyrin IX but not into the protein in each subunit. Unfortunately, the potential lead position could not be refined suggesting a partially occupied or poorly defined site, so that the lead atom was modeled with partial occupancy on either side of the protoporphyrin IX, consistent with the known lead-porphyrin compounds [101, 102] in which the lead is highly disordered and situated out of the mean plane of the porphyrin. The atomic details of the lead inhibition of ferrochelatase remain to be accurately described based on higher resolution data.

2.3.3.6. $Me_3Pb(IV)^+$-derivatized proteins

Metal binding properties of trimethyl lead(IV) acetate toward several proteins, where $Me_3Pb(IV)^+$ was used as a first-choice heavy-atom derivative, were re-

ported [52] by Holden and Rayment: these proteins include insecticyanin from *Manduca sexta* L [103], cytochrome c2 from *Rhodobacter capsulatus* [104], cytochrome c2 from *Paracoccus denitrificans* [105], apolipophorin-III from *Locusta migratoria* [106], the [2 Fe-2 S] ferredoxin from *Anabaena* 7120 [107], the high-potential iron-sulfur protein ([4 Fe-4 S] ferredoxin) from *Ectothiorhodospira halophila* [108], and UDP-Gal-4-epimerase from *Escherichia coli* [109]. These proteins are not known to be inhibited by lead.

The crystal structure at 2.6 Å resolution of *insecticyanin* [PDB ID 1Z24] [103], which plays a key role in the cryptic coloration of the insect [110], revealed that one Me_3Pb^+ ion is bound to the surface amino acid residue Glu68, in both subunits, among ten Glu residues per subunit.

In the crystal structure of *cytochrome c2* from *Rhodobacter capsulatus* (including one heme moiety) at 1.8 Å resolution [PDB ID 1C2R] [104], there was only one Pb(IV)-binding site, which was not located near Glu residues but at the interface between the two independent cytochrome molecules in the asymmetric unit.

In the crystal structure at 1.7 Å resolution of *cytochrome c2* from *Paracoccus denitrificans* [PDB ID 1COT] [105], there were four major Pb(IV) binding sites: one site wedged between the side chain carboxylates of Asp93 and Glu61, a second site located between the side chain carboxylates of Asp92 and Glu11, a third site situated between two glutamate residues, Glu51 and Glu73, and a fourth binding site lying next to the carboxylate side chain of Glu9.

In the *Apolipophorin-III* structure at 3.0 Å resolution [PDB ID 1EAP] [106], one $Me_3Pb(IV)^+$ was bound only to the side chain of Glu10 in a total of thirteen Glu residues.

The *[2 Fe-2 S] ferredoxin* structure at 2.5 Å resolution [PDB ID 1FXA] [107] revealed three Pb(IV)-binding sites: two sites were located between the side chains of Glu24 and Glu32 in each of the two ferredoxin molecules in the asymmetric unit. The third Pb(IV) binding site was located between the interface of the two ferredoxin molecules in the crystal lattice.

The *high-potential iron-sulfur protein (HiPIP)* structure at 2.5 Å resolution [PDB ID 2HIP] [108] revealed four Pb(IV)-binding sites in one HiPIP molecule (Mol.1) and only one site (side chain of Asp11) in the other molecule (Mol.2) in the asymmetric unit: the former four sites in Mol.1 were located at the side chains of Glu15, Glu27, and Glu32 (in a total of eight Glu residues in a HiPIP molecule) and the remaining one was near the carbonyl oxygen of Asp18.

The crystal structure at 2.3 Å resolution of *UDP-Gal-4-epimerase* (from *E. coli*) (no PDB ID) [109], which is involved in the conversion of galactose to glucose, revealed two Pb(IV) binding sites near Glu 320 and Asp271 in the same monomer within a dimer composed of chemically identical but crystallographically different subunits.

These studies reveal that there are two metal-binding modes [52]: (i) the Me_3Pb^+ ion is coordinated by two carboxylate groups that lie in close proximity or (ii) the Me_3Pb^+ site is in a small hydrophobic pocket either within the protein or formed by protein-protein contacts in the crystal lattice. In general, the occupancy of the former (i) is higher than the latter (ii) and occurs more frequently. It is emphasized [52] that Me_3PbOAc fulfills requirements for an ideal heavy

atom derivative that is soluble in all commonly employed precipitants and demonstrates a limited number of binding sites on the protein, the latter being a benefit for the structure determination.

2.3.4. Summary

Crystal structures of the lead-bound proteins dealt with here reveal that there are two modes of metal binding for lead: a site-specific binding (*ionic displacement* binding [66, 111]) and a site-non-specific binding (involving *opportunistic* binding [39, 66, 111] with the charged side chains on the protein surface). The former case is typically observed for Ca(II)- and Zn(II)-binding proteins, that is, lead can bind to the calcium- and zinc-binding sites by substituting for Ca(II) and Zn(II) despite their different size [ionic radii (Å) [6]: 1.19, 1.00, and 0.74 for Pb(II), Ca(II), and Zn(II), respectively] and this is believed to be the primary mechanism of lead toxicity. The *opportunistic* binding of Pb(II) is also noticeable as a possible mechanism of lead toxicity [66], as demonstrated in a Pb(II)–calmodulin (CaM) system, where both the *ionic displacement* and the *opportunistic* bindings coexist in the crystal structure [39] and, in addition, fluorescence and NMR studies showed [111] that the *opportunistic* binding has a profound impact on the conformation and dynamics of the essential molecular recognition sites of the central helix, providing a structural basis for two biological activities of lead, initial activation followed by inhibition in response to increasing concentrations of lead [61, 62], as noted above in Section 2.3.1.

Oxygen atoms present the major ligand sites for lead, most frequently from the carboxylate side chains of Glu and Asp or water, followed by, albeit much less frequently, the carbonyl of the main chain, and the neutral side chain of Asn at the active site of Ca(II)-dependent CaM [38, 39] and at the non-active site of Mg(II)- or Mn(II)-dependent apurinic/apyrimidinic endonuclease (Ape-1) [43] and that of Thr at the active site of CaM [38, 39]; *sulfur* acts as the ligand in the case of displacement of zinc by lead at the zinc-binding sites in δ-aminolevulinic acid dehydratase (ALAD) [79] and at the active site of Fe- or Cu-dependent 3-deoxy-D-arabino-heptulosonate-7-phosphate synthase (DAHPS) [42]; *nitrogen* of His presents the minor ligand at the active site of DAHPS [79], at the active site of carboxypeptidase A [85], and at the nonactive site of Ape-1 [43]. Kirberger and Yang reported [66] that the binding ligand preference for Pb(II) is in the order of side chain Glu (38.4 %) > side chain Asp (20.3 %) = water (20.3 %) > sulfur (7.3 %), based on the data analysis of the PDB.

The stereochemically active lone pair effect of Pb(II) on metal binding/recognition mode in proteins has received attention [80, 112] but X-ray studies of this topic are still limited. In the Pb(II)–C2α (protein kinase C-α) structure [40], *holodirected* and *hemidirected* coordination geometries for the two Pb(II) ions coexist within a single protein molecule: one Pb(II) that occupies the *high*-affinity site has a *holodirected* geometry while the other Pb(II) ion that takes the *low*-affinity site adopts a *hemidirected* geometry. In the Pb(II)–DAHPS structure [42], a Pb(II) ion forms a *hemidirected* geometry with its lone pair directed to-

ward a coexisted phosphoenolpyruvate (PEP) substrate, which thereby locates far from the Pb(II) center, a situation being unfavorable for the catalytic reaction; this structural basis may provide an explanation for the poorly activating Pb(II) [42, 89].

3. NUCLEIC ACID CONSTITUENT COMPLEXES

There are three potential metal-binding groups on nucleic acids: phosphate, sugar, and base moieties. X-ray studies/data on metal ion interactions with nucleic acid constituents have been repeatedly reviewed: these include transition/heavy metal ion complexes [113–123] and alkali/alkaline earth metal ion complexes [118, 122] of *nucleobases*, transition/heavy metal ion complexes [113–118, 124–128] and alkali/alkaline earth metal ion complexes [114, 122, 125, 126, 128] of *nucleosides*/*nucleotides*, and metal ion complexes of *double-helical oligonucleotides* [126, 128, 129]; in addition, special reviews on metal ion complexes of adenosine 5′-triphosphate (ATP) are available [130, 131].

These studies revealed that the phosphate groups of nucleotides involving oligonucleotides are good ligands for alkali and alkaline earth metal ions as well as transition and heavy metal ions. Sugar hydroxyl groups are good ligands for alkali and alkaline earth metal ions but not for transition and heavy metal ions. Ring nitrogens of bases are good targets for all types of metal ions, particularly for transition and heavy metal ions. Coordination to the ring nitrogens is favored over binding to the exocyclic amino and keto groups: the N7 site is the most preferred metal binding site for purine bases and the N3 site for cytosine. Keto substituents at O2 of cytosine and O2 and O4 of thymine and uracil are usual metal binding sites for alkali and alkaline earth metal ions. As a rule, amino substituents at N6 of adenine, N2 of guanine, and N4 of cytosine become good ligands only when they are deprotonated, with two exceptions, namely, the N7–Ru–N6(NH_2) chelation in [Ru(9-methyladenine)(trithiacyclononane)(DMSO)]$^{2+}$ [132] and the K–N2(NH_2) bonding or π-interaction with the C2–N2 bond in $[K_6(H_2O)_6\{Pt(9\text{-methylguanine})(MeNH_2)_2\}\{Pt(CN)_4\}_3]_n$ [133]. Nomenclature and chemical structure of the common nucleotides are presented in Figure 2. For the conformational terms of the nucleotide structures refer to [134].

Table 4 summarizes metal binding sites/modes observed in crystal structures of Pb(II) complexes with the common nucleobases and nucleosides including their substituted ones. Unfortunately, only a limited number of crystal structures of lead complexes are available with nucleic acid constituents: five complexes for nucleobases (a hypoxanthine complex [135] and four uracil complexes [136–138], where these bases are all carboxyl- or acetic acid-functionalized ones), one complex for nucleosides (a sugar-modified guanosine complex [139]) but none for mononucleotides or oligonucleotides whose residues are less than ten. For short or small RNA polynucleotides, seven crystal structures of Pb(II) complexes are reported: three tRNA complexes [140, 141], one leadzyme complex [142], and three other ribozyme complexes [143–145] but none for a DNA polynucleotide.

Table 4. Pb(II) ion binding sites/modes on nucleobases and nucleosides in the solid state.[a,b]

Complex	Coordination number[c] and geometry[d]	Metal binding sites[e] on nucleic acid constituents and other ligands/comments, if any	CSD code	Ref.
Nucleobase complexes				
$[Pb(Hyp\text{-}1\text{-}OAc)_2(H_2O)_2]_n$	6 Holo.	2 *N7* [Hyp: 2.676 (Mol.1), 2.676 (Mol.1′)][f], O [-CO_2^-: 2.653 (Mol.1″)], O [-CO_2^-: 2.653 (Mol.1‴)], 2 O [aqua: 2.629 (Mol.1), 2.629 (Mol.1′)] The Pb atom rides on an inversion center.	VIXMUM	[135]
$[Pb(Ura\text{-}5\text{-}carboxylato)_2(H_2O)]_n$	7 (10) Holo.	*O4*,O_A[g] [Mol.1: 2.667 (Ura), 2.491 (-CO_2^-)], O_A [-CO_2^-: 2.498 (Mol.1′)], *O2* [Ura: 2.725 (Mol.2)], O_A [-CO_2^-: 2.651 (Mol.2′)], O_B[f] [-CO_2^-: 2.843 (Mol.2″)], O [aqua: 2.496] (O_B [-CO_2^-: 3.134 (Mol.2′)], O_A [-CO_2^-: 3.179 (Mol.2″)], O_B [-CO_2^-: 3.241 (Mol.1′)])[d]	AQEGUZ	[136]
$[Pb(Ura\text{-}5\text{-}carboxylato - H)(H_2O)]_n$	6 (9) Holo.	*O4*,O_A [Mol.1: 2.560 (Ura), 2.508 (-CO_2^-)], *N1* [Ura: 2.646 (Mol.1′)], O_A,O_B, [-CO_2^-: 2.787, 2.650 (Mol.1″)], O5 [aqua: 2.455] (O_B [-CO_2^-: 2.915 (Mol.1‴)], *O2* [Ura: 3.066 (Mol.1⁗)], *O2* [Ura: 3.215 (Mol.1′)])	AQEHAG	[136]
$[Pb(Ura\text{-}6\text{-}carboxylato - H)(H_2O)]_n$	6 (8) Holo.	*N1*,O_A [Mol.1: 2.429 (N1), 2.464 (-CO_2^-)], *O2* [Ura: 2.637 (Mol.1′)], *O4* [Ura: 2.680 (Mol.1″)], *O4* [Ura: 2.801 (Mol.1‴)], O [aqua: 2.551] (O_B [-CO_2^-: 2.997 (Mol.1⁗)], O_A [-CO_2^-: 3.064 (Mol.1⁗)])	POQXOJ	[137]

$[Pb(5\text{-F-Ura-1-OAc})_2]_n$		6 (8) Holo.	O_A,O_B [-CO_2^-: 2.444, 2.804 (Mol.1)], O_B [-CO_2^-: 2.529 (Mol.1′)], O_A [-CO_2^-: 2.591 (Mol.2)], O_B [-CO_2^-: 2.360 (Mol.2′)], O_B [-CO_2^-: 2.689 (Mol.2″)] (*O4* [Ura: 2.937 (Mol.2‴)], *O2* [Ura: 3.174 (Mol.2⁗)])	OCEQOD	[138]
Nucleoside complex					
2 [Pb(O2′,O3′,O5′-substituted Guo)$_8$]$_2$ · (picrate)$_8$ · $(MeCN)_{10.4}$ · $(CHCl_3)_{14.4}$ · 18.4 (H_2O)	Pb1	8 Holo.	8 *O6* [Guo: 2.659 (Mol.1), 2.717 (Mol.2), 2.723(9) (Mol.3), 2.707 (Mol.4), 2.618 (Mol.5), 2.648 (Mol.6), 2.565 (Mol.7), 2.588 (Mol.8)]	GUPWIX	[139]
	Pb2	8 Holo.	8 *O6* [Guo: 2.678 (Mol.9), 2.617 (Mol.10), 2.627 (Mol.11), 2.604 (Mol.12), 2.640 (Mol.13), 2.711 (Mol.14), 2.740 (Mol.15), 2.727 (Mol.16)]		
	Pb3	8 Holo.	8 *O6* [Guo: 2.709 (Mol.17), 2.678 (Mol.18), 2.723 (Mol.19), 2.667 (Mol.20), 2.648 (Mol.21), 2.612 (Mol.22), 2.608 (Mol.23), 2.611 (Mol.24)]		
	Pb4	8 Holo.	8 *O6* [Guo: 2.598 (Mol.25), 2.526 (Mol.26), 2.656 (Mol.27), 2.625 (Mol.28), 2.698 (Mol.29), 2.709 (Mol.30), 2.689 (Mol.31), 2.672 (Mol.32)] See Figure 3.		

[a] Obtained from the Cambridge Structural Database (CSD version 5.36 updated to May 2015).
[b] Abbreviations: aqua, water ligand; 5-F-Ura-1-OAc = 5-fluorouracil-1-acetate monoanion; Hyp-1-OAc = hypoxanthine-1-acetate monoanion; O2′,O3′,O5′-substituted Guo, 5′-*tert*-butyl-dimethylsilyl-2′,3′,-di-O-isopropylidene guanosine; Ura-5-carboxylate, uracil-5-carboxylate monoanion; Ura-5-carboxylate – H, uracilate-5-carboxylate dianion with both the carboxyl group and the N1 site deprotonated; Ura-6-carboxylate – H, uracil-6-carboxylate dianion with both the carboxyl group and the N1 site deprotonated.
[c] See footnote 'd' in Table 2.
[d] See footnote 'e' in Table 2.
[e] When the Pb–O (N) bond distance falls in the range of *weak* interaction[c], it is given in parentheses.
[f] '2 *N7* [Hyp: 2.676 (Mol.1), 2.676 (Mol.1′)]' denotes that the metal ion binds to two hypoxanthine molecules, Mol.1 and its symmetry-related Mol.1′, each through the N7 site, and their bond distances (Å).
[g] O_A and O_B denote the two carboxylate oxygens, respectively.

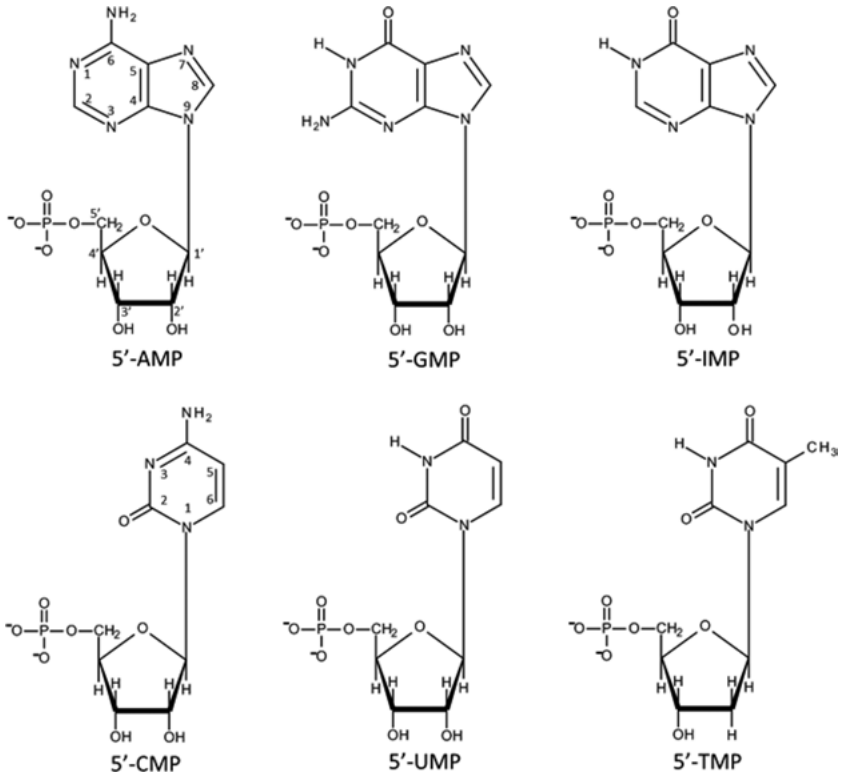

Figure 2. Nomenclature and chemical structures of the common nucleotides. The nucleotides are shown in the *syn* conformation (to save space) even though they mostly occur in the *anti* form.

3.1. Nucleobase and Nucleoside Complexes

3.1.1. Purine Nucleobases

For adenine and guanine bases, no crystal structure of a Pb(II) complex has so far been reported, and only one example is available solely for hypoxanthine. In the acetate-functionalized hypoxanthine complex $[Pb(Hyp\text{-}1\text{-}OAc)_2(H_2O)_2]_n$ [135], the distorted octahedral Pb(II), which rides on an inversion center, is bound to four hypoxanthine bases, two of which are through the ring N7 site and the other two are through the carboxylate oxygen, and two water molecules. In return, each hypoxanthine base coordinates in a bidentate fashion to two Pb(II) ions, one through N7 and the other through the acetate oxygen, forming helical, polymeric molecular chains along the crystallographic two-fold screw axis. The Pb−O and Pb−N bond lengths are from 2.629(4) to 2.676(4) Å, providing a typical example for a *holodirected* coordination geometry about the octahedral Pb(II) atom.

3.1.2. Pyrimidine Nucleobases

Four Pb(II) complexes are reported for carboxyl- or acetate-functionalized uracils [136–138] and none for cytosine and thymine.

The reactions of uracil-5-carboxylic acid, $PbCl_2$ and NaOH gave two complexes $[Pb(Ura\text{-}5\text{-}carboxylato)_2(H_2O)]_n$ [136] and $[Pb(Ura\text{-}5\text{-}carboxylato - H)(H_2O)]_n$ [136]. In $[Pb(Ura\text{-}5\text{-}carboxylato)_2(H_2O)]_n$ [136], ignoring *weak* Pb–O interactions, the Pb(II) ion is seven-coordinated by five Ura-5-carboxylato$^-$ ligands (two independent molecules Mol.1 and Mol.2 and three symmetry-related Mol.1′ and Mol.2′ and Mol.2″), through the O4 (keto)–Pb–O (carboxylate) chelation for Mol.1, the keto O2 for Mol.2, and through three carboxylate oxygens (each monodentate) for Mol.1′, Mol.2′, and Mol.2″, and by a water ligand completing the seventh site. The seven *normal* coordination bonds are in the range of 2.491(3)–2.843(3) Å and are distributed roughly in a whole sphere around the Pb(II) ion, thus forming a *holodirected* coordination geometry. When three *weak* interactions [3.134(3)–3.241(3) Å] are considered, alternate carboxylate oxygens of Mol.1′, Mol.2′, and Mol.2″ are further involved in the metal ion coordination. The ligands Mol.1 and Mol.2 in return coordinate to two and three Pb(II) ions, respectively, forming a three-dimensional framework in the crystal lattice.

On the other hand, in $[Pb(Ura\text{-}5\text{-}carboxylato - H)(H_2O)]_n$ [136], ignoring *weak* Pb–O interactions, Pb(II) is six-coordinated by three Ura-5-carboxylato^{2-} ligands (Mol.1 and symmetry-related Mol.1′ and Mol.1″), through the O4 (keto)–Pb–O (carboxylate) chelation for Mol.1, the deprotonated ring N1 of the base for Mol.1′, and through two carboxylate oxygens (bidentate) for Mol.1″, and by a water molecule. The Pb–O bond lengths are in the range of 2.455(6)–2.787(5) Å and there is a void space in one side of the metal coordination sphere. When three *weak* interactions [2.915(6)–3.215(7) Å] are considered, the keto O2 of Mol.1′ (forming an N1–Pb–O2 chelation), the keto O2 of Mol.1‴, and carboxylate oxygen of Mol.1‴ are involved in metal coordination to occupy the void space. In return, the Ura-5-carboxylato^{2-} ligand binds to three Pb(II) ions when only *normal* coordination bonds are considered, or to five Pb(II) ions when *weak* interactions are additionally considered, forming a two-dimensional sheet structure.

In the crystal structure of the Pb(II) complex with uracil-6-carboxylic acid (orotic acid), $[Pb(Ura\text{-}6\text{-}carboxylato - H)(H_2O)]_n$ [137], prepared under alkaline conditions, the Pb(II) ion is six-coordinated, when *weak* interactions are ignored, to the four orotate ligands (Mol.1 and its symmetry-related Mol.1′, Mol.1″, and Mol.1‴) and to a water molecule: it binds to Mol.1 through the formation of a five-membered N1 (deprotonated)–Pb–O_A (one of the two carboxylate oxygens) chelate ring, Mol.1′ through the keto O2, and Mol.1″ and Mol.1‴ each through the keto O4. These six *normal* coordination bonds locate at one side of the coordination sphere with their bond distances in the range of 2.429(4)–2.801(4) Å. When *weak* interactions are considered, the other side is occupied by two additional atoms (carboxylate O_B (the other carboxylate oxygen) of Mol.1⁗ and carboxylate O_A of Mol.1⁗) with the bond distances of 2.997(4) and 3.064(5) Å, respectively. Considering these *weak* interactions, the orotate ligand

exhibits a hexametallic coordination mode through chelating and bridging O and N atoms, constructing a three-dimensional polymer.

In the Pb(II) complex with 5-fluorouracil-1-acetic acid, $[Pb(5\text{-F-Ura-1-OAc})_2]_n$ [138], ignoring *weak* interactions, Pb(II) is coordinated to six oxygen atoms of five 5-F-Ura-1-OAc^- ligands (Mol.1 and Mol.2 and their symmetry-related Mol.1′, Mol.2′, and Mol.2″): it binds to Mol.1 through the carboxylate oxygens (bidentate), Mol.2 through the carboxylate oxygen O_A, Mol.1′ through the carboxylate oxygen O_B, Mol.2′ through the carboxylate O_B, and Mol.2″ through the carboxylate O_B. The Pb–O bond lengths are in the range of 2.444(4)–2.804(4) Å and the coordination sphere around the Pb(II) leaves a vacant space, where the keto O4 of Mol.2‴ and the keto O2 of Mol.2⁗ locate with *weak* Pb–O interactions of 2.937(4) and 3.174(4) Å, respectively. In return, considering these two weak interactions, the ligands Mol.1 and Mol.2 bind to two and five Pb(II) ions, respectively, forming a two-dimensional polymeric structure.

3.1.3. Purine Nucleosides

Only one Pb(II) complex is reported for guanosine [139] and none for adenosine and inosine. A lipophilic guanosine derivative, 5′-*tert*-butyl-dimethylsilyl-2′,3′-di-O-isopropylidene guanosine (O2′,O3′,O5′-substituted Guo) extracts Pb(II) picrate over K(I) picrate from water into organic solvents with at least a 100 : 1 extraction selectivity [139]. The crystal structure of the extracted compound, $2\,[Pb(O2',O3',O5'\text{-substituted Guo})_8]_2 \cdot (picrate)_8 \cdot (MeCN)_{10.4} \cdot (CHCl_3)_{14.4} \cdot 18.4\,(H_2O)$ [139], shows that the complex contains crystallographically independent four Pb(II) ions and 32 guanosine ligands, which self-associate to form four sets of $(Guo)_8$-Pb(II) octamers. Each octamer is constructed by two sets of guanosine-tetramers, where four guanine bases self-associate to form a hydrogen-bonded, cyclic 'G-quartet', and by a Pb(II), which is sandwiched between the G-quartet layers. In addition, two coaxial $(Guo)_8$-Pb(II) octamers form a G-quadruplex (see Figure 3), totally two sets of G-quadruplexes in the asymmetric unit.

In each $(Guo)_8$-Pb(II) octamer, the Pb(II) ion binds to eight guanine bases (four from one G-quartet and the other four from the other G-quartet) through the keto O6 of each guanine. The Pb–O6 bond lengths are in the range of 2.526(10)–2.740(12) Å for a total of 32 bonds and the coordination geometry around each of the four Pb(II) ions is a typical *holodirected* one. A structural comparison of the $(Guo)_8$-Pb(II) octamer with an analogous $(Guo)_8$-K(I) octamer formed in $[CsK_3(O2',O3',O5'\text{-substituted Guo})_{16}] \cdot (picrate)_4 \cdot (MeCN)_x$ [146] indicates [139], judged by the M–O6 bond length, O6–O6 diagonal distance, and inter-tetramer separation, that the smaller and more highly charged Pb(II) cation templates a smaller G8 octamer cage than does K(I) (Pb(II) has an ionic radius of similar to but smaller than that of K(I): 1.29 Å of Pb(II) while 1.51 Å of K(I) for the *octa*-coordinate cations [6]), correlating with NMR data [139, 146] indicating that N2–N7 hydrogen bonds in $(Guo)_8$-Pb(II) are kinetically more stable than in $(Guo)_8$-K(I). It is known [147] that Pb(II) significantly pro-

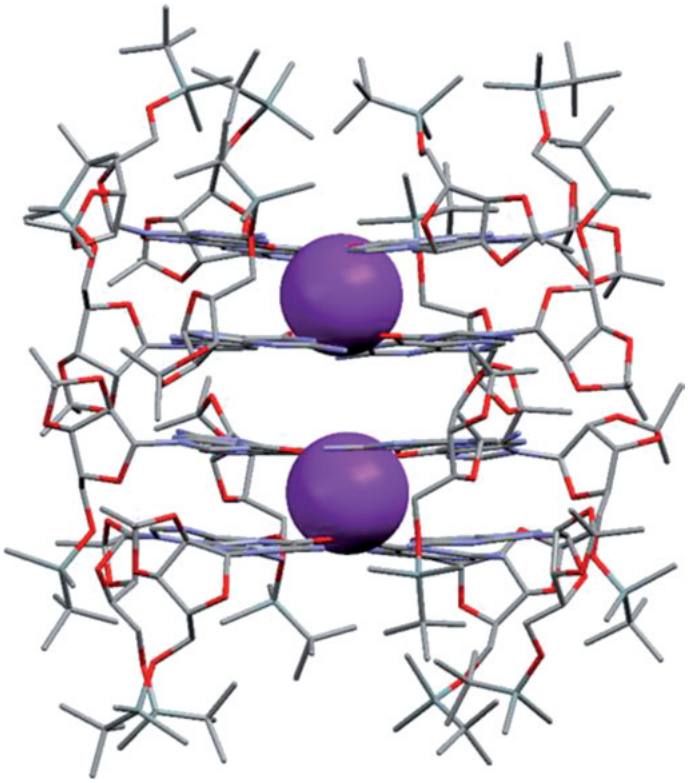

Figure 3. Structure of the lead-filled G-quadruplex, [Pb(O2′,O3′,O5′-substituted Guo)$_8$]$_2^{4+}$ [139], where the G-quadruplex is composed of two coaxial (Guo)$_8$-Pb octamers. Each Pb(II) ion is bound to eight keto O6 oxygens from eight Guo ligands. The metal coordination geometry is *holodirected*.

motes folding of a DNA G-quadruplex, i.e., more than does K(I) (for review on G-quadruplex nucleic acid structure, refer to [148]). Pb(II) also replaces K(I) in a K(I)-induced G-quadruplex in a DNA oligonucleotide (termed PS2.M) to generate a more compact Pb(II)-PS2.M structure [149]. These solid and solution data provide a rationale for why Pb(II) binds more tightly and more efficiently to a G-quadruplex than does K(I) [139].

3.1.4. Pyrimidine Nucleosides

None.

3.1.5. Summary

Though only a limited number of crystal structures are available, that is, for hypoxanthine and uracil bases only, both substituted by a carboxylate functional

group, and only for the guanosine nucleoside, they show that the preferred metal-binding sites observed for other transition and heavy metal ions apply also to Pb(II): N7 of the purine base (hypoxanthine) [135], keto O6 of oxopurine (guanine) [139], and keto O2 and O4 of uracil [136, 137]. With the uracil moiety, Pb(II) binds to the deprotonated ring nitrogen N1 under alkaline conditions, accompanying a weak interaction with the keto O2 to form a pseudo four-membered chelate ring in the uracil-5-carboxylate complex [136] or simultaneous binding to the carboxylate oxygen to form a five-membered chelate ring in the uracil-6-carboxylate complex [138]. Structural similarities between the K(I)– and Pb(II)–G-quadruplexes, but structurally and kinetically more tight binding of the latter than the former, are suggestive of the ability of Pb(II) to substitute for K(I) in nucleic acid structures, while it remains to be seen if Pb(II)-binding to DNA G-quartets has a role in the cause and effect of lead's genotoxicity [139]. The metal coordination geometry about the Pb(II) center is *holodirected* in all six crystal structures.

3.2. Nucleotide and Nucleic Acid Complexes

Unfortunately, no crystal structure of a Pb(II) complex with mononucleotides (including their di- and triphosphates) and oligonucleotides (composed of less than ten residues) is available. We describe here a total of seven crystal structures of Pb(II)-bound RNA (with more than eleven residues) [140–145], but none of Pb(II)-bound DNA, which were sought out from the PDB.

3.2.1. RNA Complexes

There is an increasing interest in interactions between metal ions and RNA because RNA biopolymers can act, in addition to their function as genetic carriers, as rigid structural scaffolds, conformational switches, and catalysts for chemical reactions, and in these cases, metal ions play a crucial role in RNA function (for review, refer to [150–164]).

Pb(II) is highly effective in forming oligoadenylic acids from adenosine 5′-phosphorimidazolide, an activated derivative of adenylic acid [165]. Pb(II) is well known to induce cleavage at specific positions in tRNA and mRNA, and thereby Pb is commonly used as a chemical probe for RNA structures [164]. Pb(II) can also play a role as a cofactor in the single-stranded DNA-catalyzed, site-specific cleavage of RNA [166, 167].

RNA sequences are abbreviated as AGCU from 5′- to 3′-ends. When attention is focused on the particular residues of polynucleotides, they are abbreviated $A_{18}GC_{20}U$ (suffix denotes sequence numbering taken from the original literature).

3.2.1.1. Transfer RNA (tRNA)

tRNAs are small RNA molecules containing 75 to 95 nucleotides (nt); they help to decode messenger RNA (mRNA) sequences into proteins. Pb(II) brings about site-specific cleavage of tRNAs [168].

Two crystal structures at 3.0 Å resolution of Pb(II)-bound yeast $tRNA^{Phe}$ (composed of 76 nt) in the *monoclinic* form, one prepared at pH 5.0 [PDB ID 1TN1] and the other at pH 7.4 [PDB ID 1TN2] by soaking 1 mM $Pb(OAc)_2$ with the Pb(II)/$tRNA^{Phe}$ ratio of 5 : 1, were determined [140]. Three Pb(II) binding sites (Pb1, Pb2, and Pb3 ions) were revealed (see Figure 3 in [140b]), which have essentially the same positions at either pH. However, at pH 7.4, sugar-phosphate backbone cleavage of the $tRNA^{Phe}$ molecule occurred between residues D_{17} and G_{18}, whereas at pH 5.0 the cleavage reaction did not proceed to any observable extent (D = dihydrouracil and the numerals represent the numbering in the sequence of the tRNA [169]). The Pb1 ion is bound in the TψC loop region of the $tRNA^{Phe}$ molecule, by replacing the Mg(II) ion in the native structure [170], to O4 of U_{59} [Pb–O4 = 2.2 Å], N3 of C_{60} [2.8 Å], and phosphate oxygen of G_{19} [3.4 Å]; the Pb2 ion is bound in the extra loop region to O6 of G_{45} [2.5 Å]; the Pb3 ion is bound to N7 of Y_{37} (a hypermodified base) [2.4 Å] in the anticodon loop. The Pb1 site is close to the major cleavage between D_{17} and G_{18}; the Pb2 site is near the minor cleavage between G_{22} and A_{23}; no sugar-phosphate backbone cleavage is observed near the Pb3 site. The cleavage mechanism was proposed (Figure 10 in [140b]). The cleavage could occur via a $Pb(OH)^+$ at the Pb1 site ($Pb \cdots O2'$ (C_{17}) = 6.0 Å was observed in the crystal) that abstracts the proton from 2′-OH, thus facilitating nucleophilic attack of the resulting 2′-O^- on the phosphorus atom of G_{18}; the reaction proceeds through a pentacovalent phosphorus intermediate to produce a 2′,3′-cyclic phosphate at C_{17} and a free 5′-OH at G_{18}, cleaving the chain. Though this mechanism is similar to that observed for the first step of the reaction in ribonuclease [171, 172], the reaction in tRNA is proposed to proceed via an 'adjacent' mechanism rather than the 'in-line' mechanism observed for ribonuclease (for 'adjacent' and 'in-line' mechanisms, refer to Figures 9 and 10 in [140b]). The pK_a of a Pb(II)-bound water molecule falls around pH 7.4 [173] (that is, physiological pH), thus facilitating the reaction at pH 7.4 and slowing it substantially at pH 5.0.

The crystal structure at 5.5 Å resolution of Pb(II)-bound yeast $tRNA^{Phe}$ in the *orthorhombic* form, prepared by soaking saturated $PbCl_2$ at pH 6.5, was determined [PDB ID 1TRA] [141]. Three Pb(II) ion-binding sites were found and they are identical to the sites observed in the *monoclinic* crystals [140] mentioned above.

3.2.1.2. Leadzymes

The leadzyme is a small RNA motif, derived from *in vitro* selection, which catalyzes a site-specific, Pb(II)-dependent RNA cleavage reaction [174]. Like naturally occurring ribozymes, the resulting leadzyme cleaves a phosphodiester bond to give a 5′-hydroxyl and a 2′,3′-cyclic phosphate as products, the latter further undergoes hydrolysis to yield a 3′-phosphomonoester. The minimal secondary structure of leadzyme comprises an asymmetric purine-rich internal loop composed of six nucleotides and a helical region on each side of the internal loop; the cleavage site of the leadzyme is located within a four-nucleotide long asymmetric internal loop. The targeting of these RNA motifs by lead is considered as a

possible mechanism for lead-mediated toxicity resulting in cell death, since these motifs occur with a high frequency in human mRNA sequences [175].

The crystal structure at 2.7 Å resolution (space group $P6_122$) of the Pb(II)-bound leadzyme, termed ZL4 [174] composed of the combination of two separate RNA fragments, 5′-$C_{18}GGACC_{23}G_{24}A_{25}G_{26}CCAG_{30}$-3′ (13 nt; the numbering of the residue corresponds to that of $tRNA^{Phe}$) and 5′-$G_{39}CUG_{42}GGAGUCC_{49}$-3′ (11 nt), prepared by soaking $Pb(OAc)_2$ (0.05 mM–19 h or 1.0 mM–2 min), was reported [PDB ID 429D] [142]. The two independent ZL4 RNA molecules, Mol.1 and Mol.2, were found in the asymmetric unit. Both molecules form an A-form RNA duplex with a central asymmetric internal loop ($C_{23}G_{24}A_{25}G_{26}$) in which a bulged purine base stack twists away from the helical stem. Although both molecules share a similar bulged structure, their conformations differ significantly, primarily in the catalytic core: in Mol.1, the purine rings of the three 'flipped-out' nucleotides GAG are stacked, while in Mol.2, A_{25} and G_{26} are stacked, but G_{24} is not. This unstacking sharply kinks the phosphoribose backbone at the scissile bond of Mol.2, rendering the C_{23}–O3′–P–O5′–G_{24} phosphodiester bond susceptible to cleavage; this does not occur in Mol.1. Mol.1 coordinates to Mg(II) or Ba(II), whereas Mol.2 binds to Pb(II) or Ba(II) but not to Mg(II) (Figure 2 in [142]); the Pb(II)-binding site in Mol.2 corresponds to an equivalent Mg(II) position of the two Mg(II) sites in Mol.1 in the native structure or occupies essentially the same site as does one of the three Ba(II) sites in Mol.2 of the Ba(II)-soaked (10 mM–10 min) crystal, indicating that this site is a dominant metal-binding site in the RNA structure. The Pb(II) ion binds to G_{42} through N7 and O6 [with the distances of 3.1 and 3.5 Å, respectively] and to U_{41} through O4 [3.5 Å] in Mol.2 but it is remote from the cleavage site and thus metal ions bound at this position may serve a structural role rather than a catalytic one. Instead, a Ba(II) ion was found near the scissile bond through four first sphere contacts to N1 of A_{45}, O2 and ribose 2′-OH of C_{23}, and C3′-phosphate oxygen of G_{24}. By modeling a $Pb(OH)^+$ ion in the active site of Mol.2 in lieu of Ba(II), a plausible scenario for the lead-dependent cleavage mechanism was presented (see Figure 5 in [142]): $Pb(OH)^+$ that coordinates to the 2′-hydroxyl of C_{23} and other ligands could abstract the hydroxyl proton to form the 2′-oxyanion; once activated, the leadzyme nucleophile moves *in-line* with the 5′-O leaving group as the C_{23} ribose pucker changes to a C3′-*endo* conformation; this concomitantly places atom O(P) of the scissile bond into the $Pb(H_2O)^{2+}$ coordination sphere, thereby polarizing the electrophilic phosphorus of G_{24}, and dissipating negative charge build-up in the trigonal bipyramidal transition state; the cleavage products are the 2′,3′-cyclic phosphodiester of C_{23} and the 5′-OH of G_{24}; the former product is further hydrolyzed to generate a final product 3′-phosphomonoester (two-step reaction mechanism similar to that in protein ribonuclease [171, 172]). The reaction of the first step is proposed to proceed in an 'in-line' mechanism.

Later, high-resolution crystal structures at 1.8 Å (space group $P6_1$) of native (involving Mg(II) only) [PDB ID 1NUJ] and Sr(II)-soaked (involving Mg(II)) [PDB ID 1NUV] LZ4 leadzymes were determined [176]. Higher resolution data allowed to adopt the lower symmetry space group $P6_1$ that has an exact twofold-

axis symmetry, which was treated with a pseudo-two-fold symmetry in the 2.7 Å resolution structure [142], noted above by adopting the space group $P6_122$. This revealed more structural details and presented a further defined model for the lead-dependent cleavage mechanism, which is essentially the same as that noted above (see Figure 5 in [176]).

3.2.1.3. RNA dimerization initiation site of the HIV-1 RNA genome (DIS RNA)

An important step in retroviral replication is dimerization of the genomic RNA prior to encapsidation; dimerization is initiated by the formation of a transient 'kissing-loop complex' that is thought to be subsequently matured into an extended duplex by the nucleocapsid protein (NCp) [143].

The crystal structure of the Pb(II) complex with the DIS RNA fragment (subtype-A), a 23-nt RNA fragment, 5′-CUUGCUGA$_8$G$_9$GUGCACA$_{16}$CAGCAAG-3′, at 2.8 Å resolution, prepared by soaking $Pb(OAc)_2$, was reported [PDB ID 1Y95] [143]. Thanks to a complementary sequence, the DIS fragment forms an 'extended duplex' with two bulges at the A_8 residue for each (*a* or *b*) chain. Two Pb(II) ions were found at 'Hoogsteen' sites (forming G$_9$*a*–A$_{16}$*b* and A$_{16}$*a*–G$_9$*b* base-pairings) located around the two bulges (see Figure 6 in [143]). These two sites correspond to the γ and γ′ Mg(II)-binding sites among the eight specific binding sites (see Figure 6 in [143]) in the parent crystal structure of the DIS RNA fragment [code: ur0005 in the Nucleic Acid Data Base], in which two partially dehydrated Mg(II) ions are coordinated to G$_9$*a* and G$_9$*b* guanine residues each through N7 and to phosphate oxygens of A$_8$*a* and A$_8$*b* in the structurally equivalent γ and γ′ sites, respectively, indicating that metal binding at these sites might be important to promote and stabilize the observed extrahelical conformation of these bulges.

3.2.1.4. Ribonuclease P (RNase P) RNA

RNase P is one of the first ribozymes identified [177]. RNase P is a divalent metal ion (preferably magnesium)-dependent, site-specific endonuclease that catalyzes the hydrolysis of the phosphodiester bond of pre-tRNA as well as other RNA substrates, generating products with 5′-monophosphates and 3′-hydroxyls ([178–180] for review). RNase P is a ribonucleoprotein complex containing one RNA subunit and as few as one protein subunit; in bacteria and in some archaea, the RNA subunit alone can support catalysis and it consists of two domains: a specificity domain (S-domain) and a catalytic domain (C-domain).

Two Pb(II)-soaked crystal structures, one of the S-domain RNA [PDB ID 1NBS] [144] and the other one of the whole RNA [PDB ID 2A64] [145] of bacterial (*Bacillus subtilis*) RNase P were reported. Unfortunately, Pb(II) binding in the crystal structure of the S-domain RNA (composed of 154 nt) at 3.15 Å resolution is not described [144]. The crystal structure at 3.3 Å resolution of the entire RNase P RNA (composed of 417 nt including both the S- and C-domains), prepared by soaking $Pb(OAc)_2$, revealed two Pb(II)-binding sites [145], both of which are found in the major grooves of helices distorted from the A-RNA geometry. One Pb(II) site (the site A in Figure 4 in [145]) is formed by consecu-

tive base pairs U_{56}–A_{392} and G_{57}–C_{391} in the vicinity of the highly conserved helix P4-stem in the C-domain (for the numbering of the stems, see Figure 1 in [145]); the P4-stem plays a role, together with the P4/P5 coaxial stem, to recognize the acceptor stem of tRNA, as revealed in the crystal structure of a bacterial RNase P holoenzyme in complex with $tRNA^{Phe}$ [PBD ID 3Q1Q] [181]. This site overlaps with one of the Os(III) hexamine sites in the Os(III)-soaked RNase P RNA structure [145] and with the one of the assumed Mg(II) sites [145], suggesting low cation specificity for this site. It is proposed [145] that the primary role of the metal-binding sites in helix P4 is to screen electronegative repulsion between the negatively charged tRNA substrate and ribozyme RNAs. The other Pb(II) site is not mentioned.

3.2.2. DNA Complexes

Although not yet found in nature, a large number of so-called DNAzymes, single-stranded small DNAs, which catalyze various chemical reactions in the presence of different metal ions, have been isolated from *in vitro* selection [163]. Among these, the first known DNAzyme, termed GR-5, catalyzes the Pb(II)-dependent cleavage of a single RNA linkage within a DNA substrate at a rate that is more than 100-fold compared to the uncatalyzed reaction [182]. Other known Pb(II)-dependent DNAzymes include 8–17 DNAzyme [183–185], and Mg5 DNAzyme [183, 184]. Unfortunately, no crystal structure of a Pb(II)-bound DNAzyme is available yet. Most recently, the first crystal structure of a metal-bound DNAzyme, the Mg(II)- and RNA (substrate)-ligating DNAzyme (termed 9DB1) [PDB ID 5CKK], was reported [186].

3.2.3. Summary

In Section 3.2, X-ray studies have revealed that tRNA [140, 141], leadzymes [142], DIS RNA [143], and RNase P [144, 145] have specific Pb(II)-binding sites that utilize both nucleobase and phosphate ligands in intricately folded single-stranded regions. X-ray crystallography, corroborated by biochemical experiments, has also provided significant insight into the reaction mechanism for Pb(II)-mediated RNA cleavage. For the scission to occur, three factors are important [140]: (i) the pK_a value of a Pb(II)-bound water molecule has to have a value near 7 (physiological pH), (ii) a hydroxyl group of $[Pb(OH)]^+$ must be in the correct orientation at a correct distance from the 2′-OH group which is to be activated via proton abstraction, and (iii) the cleavage site has to be structurally flexible. In conclusion, cleavages occur only when several necessary conditions are met simultaneously by fortunate circumstances, wherein rigorous stereochemical requirements need to be met after a minimal conformational change of the bulge region (especially for the sugar pucker of the cleaved residues) so as to greatly accelerate a specific reaction [140, 143].

Unfortunately, in all seven Pb(II)-bound RNA structures [140–145], the limited atomic resolution of X-ray data has precluded the detection/identification of any

other ligand (water molecule or any solvent molecule) bound to Pb(II) as well as of any stereochemically active lone pair effect of Pb(II), which both could also affect RNA folding in the crystal lattice.

4. SIMPLE-CARBOHYDRATE COMPLEXES

As simple carbohydrates, we surveyed saccharides that are of special biological relevance, including monosaccharides (five-membered ribose, ribulose, and xylulose; six-membered glucose, mannose, galactose, fructose and their phosphate esters), disaccharides (sucrose, maltose, and lactose), and oligosaccharides (α-, β-, and γ-cyclodextrins). Among these targeted saccharides, the CSD search provided four Pb(II) complexes only for cyclodextrins (CDs): none for α-CD, two structures [187, 188] for β-CD, and two structures [187, 189] for γ-CD, which are described here. Most recently, a review on crystal structures of metal complexes based on cyclodextrins, involving Pb(II) complexes, was reported [190]. A D-gluconate complex of Pb(II) [191] was reviewed by Godwin et al. [1], which is not duplicated here but its structural data is given in Table 5.

4.1. Cyclodextrins

As shown in Figure 4, cyclodextrins are cyclic saccharides composed of α-1,4-linked, 6–8 glucose units (α-, β-, and γ-CD, respectively), produced mainly from starch by the catalytic reaction of cyclodextrin glucanotransferase [192]. CDs have a toroidal shape with a hydrophobic interior and a hydrophilic exterior, which give CDs the ability to interact with both polar and nonpolar compounds. Table 5 summarizes metal binding sites/modes observed in crystal structures of Pb(II/IV) ion complexes with cyclodextrins.

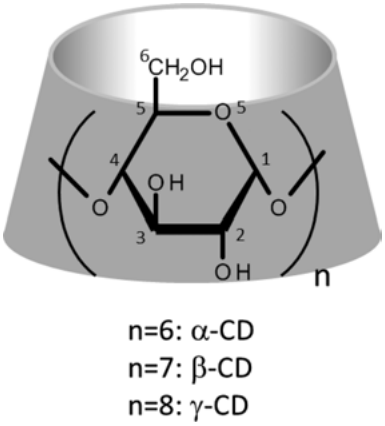

Figure 4. Structure of α-, β-, and γ-cyclodextrins with the numbering.

Table 5. Pb(II) ion binding sites/modes on saccharides in the solid state.[a,b]

Complex		Coordination number[c] and geometry[d]	Metal binding sites[e,f] on saccharide ligands and other ligands/comments, if any	CSD code	Ref.
$[Pb(D\text{-gluconate})_2]_n$		6 Holo.	O,O_A [Mol.1: 2.48 (α-hydroxyl), 2.43 (carboxylate)][g], O,O_A [Mol.1′[h]: 2.48 (α-hydroxyl), 2.43 (carboxylate)], $2\,O_B$ [Mol.1″[h], Mol.1‴[h]: 2.71 (carboxylate)] The Pb(II) atom rides on a twofold axis.	ZZZWCW01	[191]
$[\{Pb^{IV}(\beta\text{-CD} - 2\,H)_3\} - H]\cdot [Li(H_2O)_4]_3\cdot 5\,MeOH\cdot 34\,H_2O$		6 Holo.	3 O [O2 (Mol.1, Mol.1′, Mol.1″: 2.174][i], 3 O [O3 (Mol.1, Mol.1′, Mol.1″): 2.144] One proton is lost from any site of the $[Pb^{IV}(\beta\text{-CD} - 2\,H)_3]^{2-}$ entity. The bucket-wheel-shaped $[\{Pb^{IV}(\beta\text{-CD} - 2\,H)_3\} - H]^{3-}$ structure has a C_3-symmetry with the Pb(IV) atom on a threefold rotational axis. Tris(diolato) metal-binding. See Figure 5.	VERDOM	[187]
$[Pb_{14}(\beta\text{-CD} - 14\,H)_2(H_2O)]\cdot (cyclohexanol)_3\cdot 34\,H_2O$	Pb1	5 Hemi.	2 O [Mol.1, Glc1(O2, O3): 2.510, 2.280][j], 2 O [Mol.2, Glc1(O2, O3): 2.511, 2.244], O [Mol.1′, Glc1(O6): 2.830]	TEVZOL	[188]
	Pb2	4 (6) Hemi.	2 O [Mol.1, Glc1(O3): 2.314; Glc2(O2): 2.369], 2 O [Mol.2, Glc1(O2): 2.348; Glc7(O3): 2.353] (O [Mol.1, Glc2(O1): 3.264], O [Mol.2, Glc1(O1): 3.315])		
	Pb3	4 Hemi.	2 O [Mol.1, Glc2(O2, O3): 2.473, 2.282], 2 O [Mol.2, Glc7(O2, O3): 2.474, 2.259]		
	Pb4	4 (6) Hemi.	2 O [Mol.1, Glc2(O3): 2.379; Glc3(O2): 2.387], 2 O [Mol.2, Glc7(O2): 2.294; Glc6(O3): 2.389] (O [Mol.1, Glc3(O1): 3.265], O [Mol.2, Glc7(O1): 3.158])		

	Pb5	4 Hemi.	2 O [Mol.1, Glc3(O2, O3): 2.525, 2.228], 2 O [Mol.2, Glc6(O2, O3): 2.460, 2.278]		
	Pb6	4 (6) Hemi.	2 O [Mol.1, Glc3(O3): 2.347; Glc4(O2): 2.356], 2 O [Mol.2, Glc6(O2): 2.348; Glc5(O3): 2.352] (O [Mol.1, Glc4(O1): 3.241], O [Mol.2, Glc1(O1): 3.277])		
	Pb7	5 Hemi.	2 O [Mol.1, Glc4(O2, O3): 2.525, 2.250], 2 O [Mol.2, Glc5(O2, O3): 2.420, 2.295], O [aqua: 2.803]		
	Pb8	4 (6) Hemi.	2 O [Mol.1, Glc4(O3): 2.352; Glc5(O2): 2.368], 2 O [Mol.2, Glc5(O2): 2.335; Glc4(O3): 2.414] (O [Mol.1, Glc5(O1): 3.156], O [Mol.2, Glc5(O1): 3.131])		
	Pb9	4 Hemi.	2 O [Mol.1, Glc5(O2, O3): 2.410, 2.261], 2 O [Mol.2, Glc4(O2, O3): 2.576, 2.255]		
	Pb10	4 (6) Hemi.	2 O [Mol.1, Glc5(O3): 2.373; Glc6(O2): 2.385], 2 O [Mol.2, Glc4(O2): 2.369; Glc3(O3): 2.348] (O [Mol.1, Glc6(O1): 3.227], O [Mol.2, Glc4(O1): 3.106])		
	Pb11	4 Hemi.	2 O [Mol.1, Glc6(O2, O3): 2.453, 2.275], 2 O [Mol.2, Glc3(O2, O3): 2.541, 2.288]		
	Pb12	4 (6) Hemi.	2 O [Mol.1, Glc6(O3): 2.361; Glc7(O2): 2.359], 2 O [Mol.2, Glc3(O2): 2.369; Glc2(O3): 2.365] (O [Mol.1, Glc7(O1): 3.316], O [Mol.2, Glc3(O1): 3.239])		
	Pb13	4 Hemi.	2 O [Mol.1, Glc7(O2, O3): 2.517, 2.270], 2 O [Mol.2, Glc2(O2, O3): 2.471, 2.269]		
	Pb14	4 (6)	2 O [Mol.1, Glc7(O3): 2.355; Glc1(O2): 2.326], 2 O [Mol.2, Glc2(O2): 2.349; Glc1(O3): 2.317] (O [Mol.1, Glc1(O1): 3.373], O [Mol.2, Glc2(O1): 3.237]) See Figure 6.		

Complex		Coordination number[c] and geometry[d]	Metal binding sites[e,f] on saccharide ligands and other ligands/comments, if any	CSD code	Ref.
$[Pb_{16}(\gamma\text{-CD} - 16\,H)_2] \cdot 14\,H_2O$	Pb1	4 Hemi.	2 O [Mol.1, Glc1(O2, O3): 2.419, 2.227], 2 O [Mol.2, Glc1(O2, O3): 2.493, 2.241]	TEVZIF	[188]
	Pb2	4 (6) Hemi.	2 O [Mol.1, Glc1(O3): 2.363; Glc2(O2): 2.330], 2 O [Mol.2, Glc1(O2): 2.352; Glc8(O3): 2.349] (O [Mol.1, Glc2(O1): 3.148], O [Mol.2, Glc1(O1): 3.288])		
	Pb3	4 Hemi.	2 O [Mol.1, Glc2(O2, O3): 2.448, 2.290], 2 O [Mol.2, Glc8(O2, O3): 2.546, 2.211]		
	Pb4	4 (6) Hemi.	2 O [Mol.1, Glc2(O3): 2.446; Glc3(O2): 2.334], 2 O [Mol.2, Glc8(O2): 2.311; Glc7(O3): 2.337] (O [Mol.1, Glc3(O1): 3.203], O [Mol.2, Glc8(O1): 3.308])		
	Pb5	4 (5) Hemi.	2 O [Mol.1, Glc3(O2, O3): 2.476, 2.257], 2 O [Mol.2, Glc7(O2, O3): 2.466, 2.312] (O [Mol2′, Glc6(O2): 2.913])		
	Pb6	4 (6) Hemi.	2 O [Mol.1, Glc3(O3): 2.377; Glc4(O2): 2.363], 2 O [Mol.2, Glc7(O2): 2.313; Glc6(O3): 2.342] (O [Mol.1, Glc4(O1): 3.273], O [Mol.2, Glc7(O1): 3.283])		
	Pb7	4 Hemi.	2 O [Mol.1, Glc4(O2, O3): 2.412, 2.260], 2 O [Mol.2, Glc6(O2, O3): 2.471, 2.298]		
	Pb8	4 (6) Hemi.	2 O [Mol.1, Glc4(O3): 2.373; Glc5(O2): 2.437], 2 O [Mol.2, Glc6(O2): 2.372; Glc5(O3): 2.373] (O [Mol.1, Glc5(O1): 3.181], O [Mol.2, Glc6(O1): 3.097])		
	Pb9	4 Hemi.	2 O [Mol.1, Glc5(O2, O3): 2.523, 2.249], 2 O [Mol.2, Glc5(O2, O3): 2.417, 2.247]		
	Pb10	4 (6) Hemi.	2 O [Mol.1, Glc5(O3): 2.413; Glc6(O2): 2.379], 2 O [Mol.2, Glc5(O2): 2.409; Glc4(O3): 2.358] (O [Mol.1, Glc6(O1): 3.086], O [Mol.2, Glc5(O1): 3.121])		

	Pb11	4 Hemi.	2 O [Mol.1, Glc6(O2, O3): 2.431, 2.263], 2 O [Mol.2, Glc4(O2, O3): 2.497, 2.267]		
	Pb12	4 (6) Hemi.	2 O [Mol.1, Glc6(O3): 2.348; Glc7(O2): 2.283], 2 O [Mol.2, Glc4(O2): 2.337; Glc3(O3): 2.374] (O [Mol.1, Glc7(O1): 3.145], O [Mol.2, Glc4(O1): 3.201])		
	Pb13	5 Hemi.	2 O [Mol.1, Glc7(O2, O3): 2.652, 2.269], 2 O [Mol.2, Glc3(O2, O3): 2.337, 2.302], O [Mo1′, Glc1(O2): 2.803]		
	Pb14	4 (6)	2 O [Mol.1, Glc7(O3): 2.406; Glc8(O2): 2.384], 2 O [Mol.2, Glc3(O2): 2.381; Glc2(O3): 2.333] (O [Mol.1, Glc8(O1): 3.162], O [Mol.2, Glc3(O1): 3.296])		
	Pb15	4 Hemi.	2 O [Mol.1, Glc8(O2, O3): 2.389, 2.261], 2 O [Mol.2, Glc2(O2, O3): 2.450, 2.280]		
	Pb16	4 (6) Hemi.	2 O [Mol.1, Glc8(O3): 2.441; Glc1(O2): 2.399], 2 O [Mol.2, Glc2(O2): 2.375; Glc1(O3): 2.376] (O [Mol.1, Glc1(O1): 3.184], O [Mol.2, Glc2(O1): 3.237]) Refer to Figure 6.		
$[Pb_{16}(\gamma\text{-CD} - 16\,H)_2] \cdot 20\,H_2O$	Pb1	4 Hemi.	2 O [Mol.1, Glc1(O2, O3): 2.456, 2.261], 2 O [Mol.2, Glc1(O2, O3): 2.449, 2.26]	POJGOK	[189]
	Pb2	4 (6) Hemi.	2 O [Mol.1, Glc1(O3): 2.379; Glc2(O2): 2.399], 2 O [Mol.2, Glc1(O2): 2.397; Glc8(O3): 2.390] (O [Mol.1, Glc2(O1): 3.173], O [Mol.2, Glc1(O1): 3.100])		
	Pb3	4 Hemi.	2 O [Mol.1, Glc2(O2, O3): 2.484, 2.23], 2 O [Mol.2, Glc8(O2, O3): 2.473, 2.213]		
	Pb4	4 (6) Hemi.	2 O [Mol.1, Glc2(O3): 2.38; Glc3(O2): 2.293], 2 O [Mol.2, Glc8(O2): 2.365; Glc7(O3): 2.396] (O [Mol.1, Glc3(O1): 3.159], O [Mol.2, Glc8(O1): 3.173])		

Complex		Coordination number[c] and geometry[d]	Metal binding sites[e,f] on saccharide ligands and other ligands/comments, if any	CSD code	Ref.
	Pb5	5 Hemi.	2 O [Mol.1, Glc3(O2, O3): 2.636, 2.272], 2 O [Mol.2, Glc7(O2, O3): 2.364, 2.343], O [Mol.1′, Glc5(O2): 2.815]		
	Pb6	4 (6) Hemi.	2 O [Mol.1, Glc3(O3): 2.434; Glc4(O2): 2.396], 2 O [Mol.2, Glc7(O2): 2.395; Glc6(O3): 2.33] (O [Mol.1, Glc4(O1): 3.140], O [Mol.2, Glc7(O1): 3.162])		
	Pb7	4 Hemi.	2 O [Mol.1, Glc4(O2, O3): 2.422, 2.283], 2 O [Mol.2, Glc6(O2, O3): 2.496, 2.26]		
	Pb8	4 (6)	2 O [Mol.1, Glc4(O3): 2.380; Glc5(O2): 2.419], 2 O [Mol.2, Glc6(O2): 2.41; Glc5(O3): 2.36] (O [Mol.1, Glc5(O1): 3.169], O [Mol.2, Glc6(O1): 3.214])		
	Pb9	4 Hemi.	2 O [Mol.1, Glc5(O2, O3): 2.417, 2.248], 2 O [Mol.2, Glc5(O2, O3): 2.50, 2.27]		
	Pb10	4 (6) Hemi.	2 O [Mol.1, Glc5(O3): 2.397; Glc6(O2): 2.329], 2 O [Mol.2, Glc5(O2): 2.33; Glc4(O3): 2.360] (O [Mol.1, Glc6(O1): 3.142], O [Mol.2, Glc5(O1): 3.252])		
	Pb11	4 Hemi.	2 O [Mol.1, Glc6(O2, O3): 2.485, 2.27], 2 O [Mol.2, Glc4(O2, O3): 2.465, 2.22]		
	Pb12	4 (6) Hemi.	2 O [Mol.1, Glc6(O3): 2.45; Glc7(O2): 2.358], 2 O [Mol.2, Glc4(O2): 2.37; Glc3(O3): 2.338] (O [Mol.1, Glc7(O1): 3.208], O [Mol.2, Glc4(O1): 3.220])		
	Pb13	4 Hemi.	2 O [Mol.1, Glc7(O2, O3): 2.501, 2.254], 2 O [Mol.2, Glc3(O2, O3): 2.450, 2.309]		

Pb14	4 (6) Hemi.	2 O [Mol.1, Glc7(O3): 2.386; Glc8(O2): 2.37], 2 O [Mol.2, Glc3(O2): 2.359; Glc2(O3): 2.367] (O [Mol.1, Glc8(O1): 3.263], O [Mol.2, Glc3(O1): 3.273])
Pb15	4 Hemi.	2 O [Mol.1, Glc8(O2, O3): 2.420, 2.27], 2 O [Mol.2, Glc2(O2, O3): 2.437, 2.242]
Pb16	4 (6) Hemi.	2 O [Mol.1, Glc8(O3): 2.33; Glc1(O2): 2.40], 2 O [Mol.2, Glc2(O2): 2.383; Glc1(O3): 2.41] (O [Mol.1, Glc1(O1): 3.253], O [Mol.2, Glc2(O1): 3.168])
		Refer to Figure 6.

[a] Obtained from the Cambridge Structural Database (CSD version 5.36 updated to May 2015).
[b] Abbreviations: aqua, water ligand; CD, cyclodextrin; β-CD – 2 H, β-CD anion with two hydroxyl groups deprotonated; β-CD – 14 H, β-CD anion with all of 14 hydroxyl groups deprotonated; γ-CD – 16 H, γ-CD anion with all of 16 hydroxyl groups deprotonated.
[c] See footnote 'd' in Table 2.
[d] See footnote 'e' in Table 2.
[e] For atom numbering of cyclodextrin, see Figure 4.
[f] When the Pb–O bond distance falls in the range of *weak* interaction[c], it is given in parentheses.
[g] 'O,O_A [Mol.1: 2.48 (α-hydroxyl), 2.43 (carboxylate)]' denotes that the metal ion binds to two oxygens of a gluconate molecule Mol.1, one through the α-hydroxyl oxygen and the other through the carboxylate oxygen O_A to form an O–M–O_A chelation, and their bond distances (Å), where O_A denotes one of the two carboxylate oxygens.
[h] Mol.1′, Mol.1″, and Mol.1‴ are symmetry-related to the parent molecule Mol.1 (twofold symmetry in this case).
[i] '3 O [O2 (Mol.1, Mol.1′, Mol.1″: 2.174]' denotes that the metal ion binds to three O2 oxygens belonging to each of the three CD molecules Mol.1, Mol.1′, and Mol.1″, which are related to each other by a symmetry (C_3 symmetry in this case), and the bond distance (Å).
[j] '2 O [Mol.1, Glc1(O2, O3): 2.244, 2.511]' denotes that the metal ion binds to two oxygens O2 and O3 attached to the first glucose unit Glc1 belonging to the CD molecule Mol.1, and their bond distances (Å).

4.1.1. β-Cyclodextrin

Two crystal structures of a Pb(IV) [187] and a Pb(II) complex [188], which were prepared under alkaline conditions, are available. Figure 5 shows the $[\{Pb^{IV}(\beta\text{-CD} - 2\,H)_3\} - H]^{3-}$ structure (in which one proton is lost from any site of the $[Pb^{IV}(\beta\text{-CD} - 2\,H)_3]^{2-}$ entity) in $[Li(H_2O)_4]_3 \cdot [\{Pb^{IV}(\beta\text{-CD} - 2\,H)_3\} - H] \cdot 5\,MeOH \cdot 34\,H_2O$ [187]. The Pb(IV) ion binds to three β-CD molecules each through two deprotonated hydroxyl oxygens O2 and O3 (for the atom numbering, see Figure 4) to form a bucket-wheel-shaped $M^{IV}(\beta\text{-CD})_3$ motif that has a C_3 symmetry with the Pb(IV) atom riding on a threefold rotational axis. The tris(diolato) bonding to the Pb(IV) center forms a *holodirected* coordination geometry with the Pb–O2 and Pb–O3 bond distances of 2.174(3) and 2.144(3) Å, respectively.

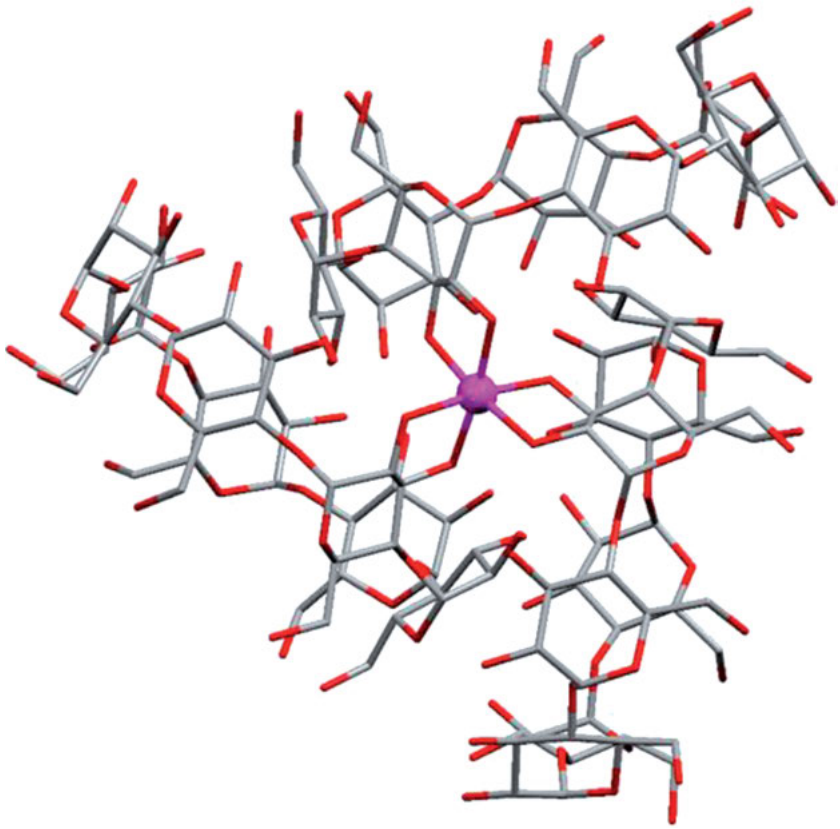

Figure 5. Structure of the $[\{Pb^{IV}(\beta\text{-CD} - 2\,H)_3\} - H]^{3-}$ complex [187] with a $Pb^{IV}(\beta\text{-CD})_3$ bucket-wheel motif, viewed along the three-fold symmetry axis running through the Pb atom. The Pb(IV) atom is bound to three β-CD ligands, to each ligand through two deprotonated diol oxygens O2/O3 to form a five-membered chelate ring. The metal coordination geometry is *holodirected*, as usually observed for Pb(IV).

Figure 6 shows the $[Pb_{14}(\beta\text{-CD} - 14H)_2]$ structure in the Pb(II) complex $[Pb_{14}(\beta\text{-CD} - 14\,H)_2(H_2O)] \cdot (\text{cyclohexanol})_3 \cdot 34\,H_2O$ [188], where a total of 14 Pb(II) ions are bound to two β-CD molecules (Mol.1 and Mol.2) through a total of 28 deprotonated O2/O3 hydroxyl oxygen atoms to generate a head-to-head arranged, sandwich-type molecule, connected by a tetradecanuclear metallomacrocycle ring [–Pb1-Pb2-···-Pb14–] along the equator. Guest solvents of cyclohexanol molecules were trapped in the cavity of the β-CD-based tube (not shown in the figure). There are two types of Pb atoms: the outer Pb(II) atoms (Pb1, Pb3, ···, Pb13 in Table 5) are part of two five-membered chelate rings; on the other hand, the inner Pb(II) atoms (Pb2, Pb4, ···, Pb14) are bound to four alcoxide O atoms from four different anhydroglucose units.

It is noticeable that the Pb–O2 bond length is always longer than the Pb–O3 bond length for the *outer* Pb atoms whereas there is no significant difference between the Pb–O2 and Pb–O3 bond lengths for the *inner* Pb atoms: for the *outer* Pb atoms, the bond lengths of a total of fourteen Pb–O2 bonds are in the range of 2.410(7) to 2.576(7) Å while those of 14 Pb–O3 bonds are in the range of 2.228(6) to 2.295(7) Å; on the other hand, for the *inner* Pb atoms, each of the Pb-O2 and Pb-O3 bond lengths for 14 Pb–O bonds are in the range of 2.294(7) to 2.387(6) and 2.314(6) to 2.414(7) Å, respectively (Table 5). In addition, each

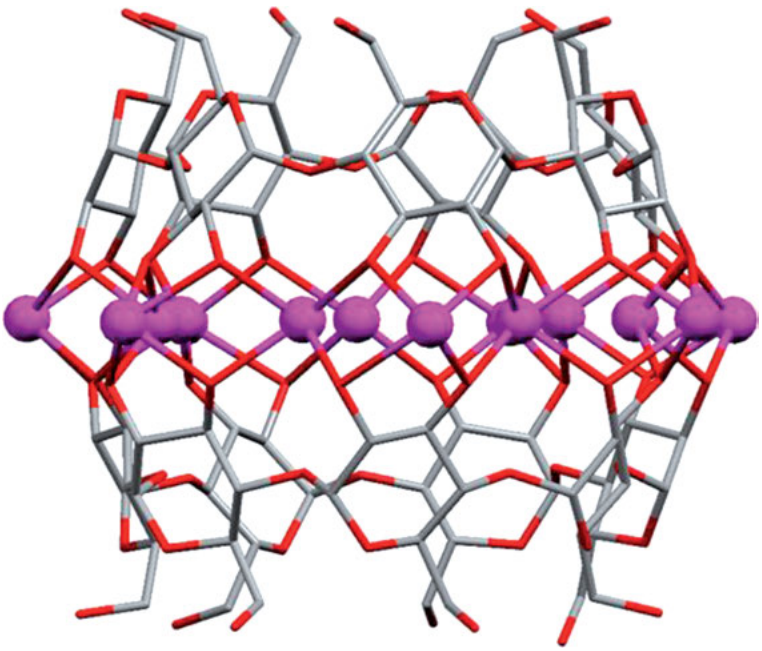

Figure 6. Sandwich-type structure in the $[Pb_{14}(\beta\text{-CD} - 14\,H)_2(H_2O)]$ complex [188] (one water ligand is omitted). A total of 14 Pb(II) ions are bound to two β-CD molecules through a total of 28 deprotonated O2/O3 diol oxygens. Each Pb(II) atom adopts a *hemi-directed* coordination geometry. An analogous hexadecanuclear Pb(II)–γ-CD complex, $[Pb_{16}(\gamma\text{-CD} - 16\,H)_2]$ [188, 189], is reported.

inner Pb atom weakly interacts with the bridging ether oxygen O1: the Pb–O1 distances are in the range of 3.156 to 3.373 Å for Mol.1 and 3.106 to 3.315 Å for Mol.2. One hydroxyl O6 oxygen of glucose, among a total of the fourteen O6 hydroxyls in the dimer molecule, binds to an outer Pb atom of the neighboring molecule with the bond length of 2.830 Å. All of the 14 Pb(II) atoms exhibit a *hemidirected* coordination geometry.

4.1.2. γ-Cyclodextrin

Two crystal structures of the Pb(II) complexes, $[Pb_{16}(\gamma\text{-CD} - 16\,H)_2] \cdot 14\,H_2O$ [188] and $[Pb_{16}(\gamma\text{-CD} - 16\,H)_2] \cdot 20\,H_2O$ [189], which were prepared under alkaline conditions, were reported. The $[Pb_{16}(\gamma\text{-CD} - 16\,H)_2]$ structures of both complexes are essentially the same and are isotypes of the tetradecanuclear Pb(II)–β-CD complex [188] described above. Thus, the two fully deprotonated γ-CD molecules are connected through a hexadecanuclear metallomacrocycle, forming a sandwich-type molecular tube. There were no solvents in the cavity of the γ-CD-based tube. Here also, the Pb–O2 bond length is always longer than the Pb–O3 bond length for the *outer* Pb atoms whereas there is no significant difference between the Pb–O2 and Pb–O3 bond lengths for the *inner* Pb atoms, and each *inner* Pb atom interacts weakly with the bridging ether oxygen O1: for the *outer* Pb atoms in the $[Pb_{16}(\gamma\text{-CD} - 16\,H)_2] \cdot 14\,H_2O$ complex [188], the Pb–O2 and Pb–O3 bond lengths are in the ranges of 2.337(16) to 2.652(15) and 2.211(14) to 2.312(14) Å, respectively; for the *inner* Pb atoms, the Pb–O2 and Pb–O3 bond lengths are in the ranges of 2.283(13) to 2.437(16) and 2.333(14) to 2.446(14) Å, respectively, and the Pb–O1 distances are in the range of 3.086 to 3.308 Å. For the *outer* Pb atoms in the $[Pb_{16}(\gamma\text{-CD} - 16\,H)_2] \cdot 20\,H_2O$ complex [189], the Pb–O2 and Pb–O3 bond lengths are in the ranges of 2.364(13) to 2.636(15) and 2.213(14) to 2.343(13) Å, respectively; for the *inner* Pb atoms, the Pb–O2 and Pb–O3 bond lengths are in the ranges of 2.293(14) to 2.419(14) and 2.329(14) to 2.434(15) Å, and the Pb–O1 distances are in the range of 3.100 to 3.273 Å. All the 16 Pb(II) atoms exhibit a *hemidirected* coordination geometry in both complexes.

4.1.3. Summary

Among possible metal-binding sites for cyclodextrins, which are the ether oxygen O1 that bridges between two glucose units, O2/O3 hydroxyls, ring ether oxygen O5, and hydroxyl O6, the most frequently observed sites are deprotonated O2/O3, followed by bridging ether O1 (weak), and hydroxyl O6 (once). With regard to the five-membered [–M-O2-C-C-O3–] chelate ring, the Pb–O bond distances are shorter for Pb(IV) than Pb(II) due to their ionic sizes (0.775 Å for sixfold-coordinated Pb(IV) and 0.96 and 1.19 Å for fourfold- and sixfold-coordinated Pb(II), respectively [6]), and the Pb–O2 and Pb–O3 bond distances are essentially the same for Pb(IV) whereas the former is significantly longer than the latter for Pb(II). The coordination geometry about the metal center is *holodirected* for a Pb(IV) atom in the β-CD complex [187] while it is *hemidirected* for all of the

Pb(II) atoms in the β-CD complex [188] and two γ-CD complexes [188, 189]. The diol-O2/O3 functional groups self-assemble via metal bonding to generate supramolecules, a mononuclear $M(CD)_3$ bucket-wheel molecule in the Pb(IV)–β-CD complex or a $M_n(CD)_2$ ($n = 14$ or 16) sandwich-type molecule connected by a multinuclear metallocycle in the Pb(II)–β-CD and Pb(II)–γ-CD complexes. Cyclodextrins are fascinating ligands for forming well defined, various structural motifs for CD-based metal complexes, which are ranging from monomeric species, dinuclear systems, homo- and heterometallic sandwich-type complexes to cylindrical, extended structures [190].

5. COMPLEXES OF OTHER BIORELEVANT LIGANDS

As *other* biorelevant ligands, we searched the CSD for water-soluble vitamins, natural ionophores, major hormones, major neurotransmitters, and some common detoxification agents, among which only one vitamin complex [193] and several complexes of detoxification agents [194–199] were found and are described here, along with a related-ligand complex [81]. As common chelating agents for the treatment of lead poisoning are known [200]: calcium disodium ethylenediaminetetraacetic acid ($CaNa_2EDTA$), D-penicillamine (DPA), *meso*-2,3-dimercaptosuccinic acid (DMSA), sodium-2,3-dimercaptopropane-1-sulfonate (DMPS), or dimercaprol (BAL). Among these targeted ligands, we found a penicillamine complex [194, 195] and six EDTA complexes [196–199]. Table 6 lists metal binding sites/modes observed in crystal structures of Pb(II) ion complexes with biorelevant ligands. Godwin et al. reviewed [1] crystal structures of Pb(II) complexes with 10-methylisoalloxazine [193] and citric acid [201] as small biomolecules and those of D-penicillamine [194], EDTA [196, 197], and ethylenediaminetetraacetamide (EDTA-N_4) [202], thiohydroxamic acids [203, 204], and hydroxypyridinethione [205] as detoxification agents or related ligands, which are updated here by the recent literature and search of the CSD, included in Table 6, and briefly described here.

5.1. Isoalloxazine

Isoalloxazine is a tricyclic, heterocyclic amino cofactor associated with riboflavin (vitamin B2) and is active in oxidation-reduction reactions with metal ions such as Mo and Fe [206]. In the $[Pb(10\text{-methylisoalloxazine})_2(H_2O)_4]\cdot(ClO_4)_2$ complex [193], when considering a normal coordination distance, the four-coordinated Pb(II) ion binds to two flavin ligands each through the ring keto oxygen and to two water molecules with the Pb–O bond distances in the range of 2.38(2) to 2.69(2) Å. When considering a weak interaction, a water molecule and the ring nitrogen of the same pyrimidine moiety are included in metal bonding (3.21 and 2.99 Å, respectively), the latter forming a five-membered [–M-O-C-N–] chelate ring. The coordination geometry around the Pb center is *hemidirected*.

Table 6. Pb(II) ion binding sites/modes on *other* biorelevant ligands in the solid state[a,b]

Complex		Coordination number[c] and geometry[d]	Metal binding sites[e] on ligands/comments, if any	CSD code	Ref.
Flavin					
$[Pb(10\text{-methyl-isoalloxazine})_2 \cdot (H_2O)_4] \cdot (ClO_4)_2$		4 (6) Hemi.	O [Mol.1, keto: 2.46], O [Mol.1′, keto: 2.63][f], O [Mol.1, aqua: 2.69], O [Mol.1′, aqua: 2.38] (N [Mol.1, pyrimidine ring N: 2.99], O [Mol.2, aqua: 3.21]) Five-membered [–M-O-C-N–] chelation.	MIAXPB10	[193]
Citric acid					
$[Pb(citratoH)]_n \cdot nH_2O$		7 (9) Hemi.	O,O_A [Mol.1: 2.527 (hydroxyl), 2.395 (carboxylate1)][g], O_A [Mol.1', carboxylate1: 2.510], O_A,O_B [Mol.1″, carboxylate2: 2.416, 2.847], O_B [Mol.1‴, carboxylate1: 2.805], O [aqua: 2.883] (O_B [Mol.1′, carboxylate1: 3.271], O [aqua: 3.216])	MAKZON	[201]
$[Pb_3(citrato)_2(H_2O)]_n \cdot 1.5\,nH_2O$	Pb1	7 Hemi.	O_A,O,O_A [Mol.1: 2.639 (carboxylate1), 2.389 (hydroxyl), 2.645 (carboxylate3)], O_A [Mol.2, carboxylate3: –], O_B [Mol.1′, carboxylate1: –], O_A [Mo.2′, carboxylate2: –], O [aqua: –]	FOZTEU	[209]
	Pb2	4 Hemi.	O [Mol.1, carboxylate3: 2.625], O_A,O [Mol.2: – (carboxylate3), – (hydroxyl)], O_A [Mol.2′, carboxylate1: –]		
	Pb3	5 Hemi.	O_A,O_B [Mol.1, carboxylate2: –, –], O_A,O_B [Mol.2, carboxylate2: –, –], O_B [Mol.1″, carboxylate3: –]		

$[Na(H_2O)_3]_n \cdot [Pb_5(citrato)_3(citratoH)(H_2O)_3]_n \cdot 9.5\,nH_2O$	Pb1	6 (9) Hemi.	O_A,O_B [Mol.1, carboxylate1: 2.553, 2.625], O_A,O_B [Mol.1′, carboxylate3: 2.521, 2.842], O_A [Mol.2, carboxylate2: 2.399], O [aqua: 2.677] (O_B [Mol.2, carboxylate2: 3.074], O_A [Mol.3′, carboxylate1: 2.993], O_B [Mol.4′, carboxylate1: 3.056])	YABREA	[210]
	Pb2	8 (9) Hemi.	O_A [Mol.1, carboxylate1: 2.797], O_B [Mol.1, carboxylate3: 2.611], O_A [Mol.1′, carboxylate3: 2.844], O_A,O,O_A [Mol.2: 2.641 (carboxylate2), 2.610 (hydroxyl), 2.552 (carboxylate3)], O_B [Mol.3, carboxylate1: 2.577], O [aqua: 2.749] (O_A [Mol.3, carboxylate1: 2.948])		
	Pb3	6 (10) Hemi.	O_A,O,O_B [Mol.1: 2.547 (carboxylate2), 2.840 (hydroxyl), 2.565 (carboxylate3)], O_A [Mol.4, carboxylate3: 2.763], O_A,O_B [Mol.4′, carboxylate1: 2.595, 2.484] (O_A [Mol.2, carboxylate3: 3.321], O_B,O_A [Mol.3: 2.979 (carboxylate 1), 2.934(carboxylate3)], O_B [Mol.4, carboxylate3: 2.903])		
	Pb4	10 Hemi.	O_A,O_B [Mol.1, carboxylate2: 2.752, 2.579], O_A,O_B [Mol.3′, carboxylate2: 2.778, 2.557], O_A,O_B [Mol.3″, carboxylate2: 2.784, 2.727], O_A,O_A [Mol.4: 2.718 (carboxylate1), 2.723 (carboxylate3)], O_A,O_B [Mol.4′: 2.852(carboxylate1), 2.717 (carboxylate3)]		
	Pb5	8 Hemi.	O_B [Mol.1″, carboxylate2: 2.631], O_A,O_B [Mol.2, carboxylate1: 2.455, 2.851], O_A,O,O_A [Mol.3: 2.828 (carboxylate2), 2.761 (hydroxyl), 2.545 (carboxylate3)], O_A [Mol.3′, carboxylate2: 2.805], O [aqua: 2.515]		

Complex		Coordination number[c] and geometry[d]	Metal binding sites[e] on ligands/comments, if any	CSD code	Ref.
D-*Penicillamine*					
$[Pb(D\text{-penicillaminato})]_n$		4 (6) Hemi.	N,O_A,S [Mol.1, amino N: 2.444; α-CO_2^- : 2.444; thiolate S: 2.716], O_A [Mol.1′, α-CO_2^-: 2.768] (2 S [Mol.1″, Mol.1‴, thiolate S: 3.160, 3.480]) This compound is the same as DPENPB01 [195]. See Figure 7.	DPENPB	[194]
$[Pb(D\text{-penicillaminato})]_n$		5 (7) Hemi.	N,O_A,S [Mol.1, amino N: 2.444; α-CO_2^- : 2.451; thiolate S: 2.714], O_A [Mol.1′, α-CO_2^-: 2.720], S [Mol.1″: 3.091], (O_B [Mol.1′, α-CO_2^-: 3.470], S [Mol.1‴: 3.464]) This compound is the same as DPENPB [194].	DPENPB01	[195]
Ethylenediaminetetraacetic acid (EDTAH_4)					
$[Pb(EDTAH_2)(H_2O)]_2 \cdot H_2O$	Pb1	6 (7) Hemi.	4 O,2 N [Mol.1, 4carboxylate: 2.570, 2.494, 2.567, 2.735; 2amine: 2.518, 2.604] (O [aqua: 2.967])	BIYLOK	[196]
	Pb2	7 (8) Holo.	4 O,2 N [Mol.2, 4carboxylate: 2.590, 2.645, 2.555, 2.565; 2amine: 2.573, 2.624], O [Mol.2′, carboxylate: 2.824] (O [aqua: 2.953]) This compound is the same as BIYLOK01 [197].		
$[Pb(EDTAH_2)(H_2O)]_2 \cdot H_2O$	Pb1	6 (8) Hemi.	4 O,2 N [Mol.1, 2carboxylate: 2.578, 2.492; 2carboxyl: 2.743, 2.568; 2amine: 2.635, 2.587] (O [Mol.1′, carboxylate: 3.196], O [aqua: 2.971])	BIYLOK01	[197]
	Pb2	7 (8) Holo.	4 O,2 N [Mol.2, 2carboxylate: 2.533, 2.572; 2carboxyl: 2.662, 2.571; 2amine: 2.578, 2.624], O [Mol.2′, carboxylate: 2.841] (O [aqua: 2.930]) This compound is the same as BIYLOK [196].		

$(NH_4)_{2n}[Pb(EDTA)]_n \cdot 2.5\,nH_2O$	Pb1	8 Hemi.	4 O,2 N [Mol.1, 4carboxylate: 2.534, 2.573, 2.696, 2.584; 2amine: 2.567, 2.619], O [Mol.1′, carboxylate: 2.898], O [Mol.2″, carboxylate: 2.890]	LORLIN	[198]
	Pb2	8 Hemi.	4 O,2 N [Mol.2, 4carboxylate: 2.558, 2.634, 2.664, 2.618; 2amine: 2.593, 2.606], O [Mol.1, carboxylate: 2.815], O [Mol.2′, carboxylate: 2.894]		
$Na_{2n}[Pb(EDTA)]_n \cdot 2\,nH_2O$	Pb	6 (7) Hemi.	4 O,2 N [Mol.1, 4carboxylate: 2.640, 2.486, 2.639, 2.485; 2amine: 2.513, 2.519] (O [Mol.1′, carboxylate: 3.280])	LORLOT	[198]
$Cs_{2n}[Pb(EDTA)]_n \cdot 3.5\,nH_2O$	Pb1	7 (8) Hemi.	4 O,2 N [Mol.1, 4carboxylate: 2.58, 2.79, 2.574, 2.511; 2amine: 2.639, 2.552], O [Mol.1′, carboxylate: 2.89] (O [Mol.2, carboxylate: 2.924])	LORLUZ	[198]
	Pb2	6 (8) Hemi.	4 O,2 N [Mol.2, 4carboxylate: 2.60, 2.53, 2.472, 2.72; 2amine: 2.580, 2.64], (O [Mol.2′, carboxylate: 2.98]; O [Mol.1″, carboxylate: 3.04])		
$Tl_{2n}[Pb(EDTA)]_n \cdot 3\,nH_2O$	Pb	6 (8) Hemi.	4 O,2 N [Mol.1, 4carboxylate: 2.53, 2.75, 2.560, 2.56; 2amine: 2.589, 2.499] (O [Mol.1′, carboxylate: 2.91], O [Mol.1″, carboxylate: 3.07])	LORMAG	[198]
$K_2[Pb(EDTA)] \cdot 4\,H_2O$	Pb1	6 Hemi.	4 O,2 N [Mol.1, 4carboxylate: 2.623, 2.473, 2.653, 2.536; 2amines: 2.561, 2.561]	BEJCOJ	[199]
$[Pb(EDTA\text{-}N_4)] \cdot (NO_3)_2$		6 Hemi.	4 O,2 N [Mol.1, 4acetamide: 2.693, 2.597, 2.439, 2.632; 2amine: 2.620, 2.605]	QIDKOD	[202]

Complex	Coordination number[c] and geometry[d]	Metal binding sites[e] on ligands/comments, if any	CSD code	Ref.
Thiohydroxamic acid				
$[Pb(MBTHX)_2]_n$	4 (6) Hemi.	S,O [Mol.1: 2.7462 (thiolate), 2.383 (*N*-hydroxylate)], S,O [Mol.1′: 2.7462 (thiolate), 2.383 (*N*-hydroxylate)], (O [Mol.1′: 2.935 (*N*-hydroxylate)], O [Mol.1″: 2.935 (*N*-hydroxylate)],) The Pb atom rides on a twofold axis. Five-membered [–M-O-N-C-S–] chelation.	KEGZAX	[203]
$[Pb(MATHX)_2]_n$	4 (7) Hemi.	S,O [Mol.1: 2.859 (thiolate), 2.371 (*N*-hydroxylate)], S,O [Mol.2: 2.744 (thiolate), 2.448 (*N*-hydroxylate)], (O [Mol.1′: 2.996 (*N*-hydroxylate)], O [Mol.2′: 2.880 (*N*-hydroxylate)], S [Mol.2′: 3.358]) Five-membered [–M-O-N-C-S–] chelation.	KEGZEB	[203]
$[Pb(CPATHX)_2]$	4 Hemi.	S,O [Mol.1: 2.685 (thiolate), 2.374 (*N*-hydroxylate)], S,O [Mol.1′: 2.685 (thiolate), 2.374 (*N*-hydroxylate)] The Pb atom rides on a twofold axis. Five-membered [–M-O-N-C-S–] chelation.	ZOXGAU	[204]
$[Pb(MPTHX)_2]_n$	5 (6) Hemi.	S,O [Mol.1: 2.725 (thiolate), 2.497 (*N*-hydroxylate)], S,O [Mol.2: 2.809 (thiolate), 2.349 (*N*-hydroxylate)], O [Mol.1′: 2.81 (*N*-hydroxylate)] (O [Mol.2′: 3.13 (*N*-hydroxylate)]) Five-membered [–M-O-N-C-S–] chelation.	ZOXGEY	[204]

Hydroxypyridinethione				
$[Pb(DECHPT)_2]$	4 (6) Hemi.	S,O [Mol.1: 2.696 (thiolate), 2.419 (*N*-hydroxylate)], S,O [Mol.2: 2.720 (thiolate), 2.407 (*N*-hydroxylate)] (O,O [Mol.2′: 3.036 (*N*-hydroxylate), 3.143 (carbamoyl)]) Five-membered [–M-O-N-C-S–] chelation. Six-membered [–M-O-N-C-C-O–] chelation.	WATSEP	[205]
3 S Ligand				
$[Pb(Tm^{Ph})] \cdot ClO_4$	3 (4) Hemi.	3 S [Mol.1: 2.693, 2.693, 2.693] (O [perchlorate: 2.94]) The $[Pb(Tm^{Ph})]^+$ structure has a C_3 symmetry with the threefold symmetry axis passing through the Pb atom. Tm^{Ph} is a tris-thio ligand as a model for the Cys3 site in ALAD [41, 79]. See Figure 8.	EBEXEO	[81]

[a] Obtained from the Cambridge Structural Database (CSD version 5.36 updated to May 2015).
[b] Abbreviations: ALAD, δ-aminolevulinate dehydratase; aqua, water ligand; citrato, fully deprotonated citrate trianion; citratoH, doubly deprotonated citrate dianion; EDTA, fully deprotonated ethylenediaminetetraacetate tetraanion; $EDTAH_2$, doubly deprotonated EDTA dianion; EDTA-N_4, ethylenediaminetetraacetamide; CPATHX, *N*-cyclohexyl-phenylacetothiohydroxamate; DECHPT, 6-(diethylcarbamoyl)-1-hydroxy-2(1H)-pyridine-2-thionate; M, metal ion; MATHX, *N*-met hylacetothiohydroxamate; MBTHX, *N*-methylbenzothiohydroxamate; MPTHX, *N*-methyl-3-pyridothiohydroxamate; Tm^{Ph}, tris(2-mercapto-1-phenylimidazolyl)hydroborate.
[c] See footnote 'd' in Table 2.
[d] See footnote 'e' in Table 2.
[e] When the Pb–O/N/S bond distance falls in the range of *weak* interaction[c], it is given in parentheses.
[f] 'O [Mol.1′, keto: 2.63]' denotes that the metal ion binds to the keto oxygen of the ligand molecule Mol.1′, which is symmetry-related to the parent molecule Mol.1 (flavin in this case), and the bond distance (Å).
[g] 'O,O_A [Mol.1: 2.527 (hydroxyl), 2.395 (carboxylate1)]' denotes that the metal ion binds to Mol.1 (citrate in this case) at the hydroxyl oxygen and the carboxylate oxygen O_A of one (carboxylate1) of the three carboxylate groups and their bond distances (Å), where O_A denotes one of the two carboxylate oxygens (and O_B denotes the other one in the table).

5.2. Citric Acid

Citric acid (2-hydroxypropane-1,2,3-tricarboxylic acid), a tribasic acid, is an intermediate in the citric acid cycle (Krebs cycle) in the metabolism of all organisms [207]. Many organisms have evolved primary or secondary membrane transporters that transport citrate coupled to Na^+ or H^+ or certain metal ions, particularly iron, and most bacterial citrate transporters carry free citrate but some transporters specifically recognize citrate in complexes with divalent metal ions, involving Pb(II) [208]. Citric acid is well known as an excellent chelating agent [208]. Three carboxylic groups of citric acid are denoted below in the deprotonated form as carboxylate1, carboxylate2, and carboxylate3, respectively.

Three Pb(II)–citrate crystal structures are available: $[Pb(citratoH)]_n \cdot nH_2O$ [201], $[Pb_3(citrato)_2(H_2O)]_n \cdot 1.5\,nH_2O$ [209], and $[Na(H_2O)_3]_n[Pb_5(citrato)_3(citratoH)(H_2O)_3]_n \cdot 9.5\,nH_2O$ [210]. In the *[Pb(citratoH)]* complex [201], when ignoring weak Pb(II)–O interactions, the seven-coordinated Pb(II) binds to four doubly-deprotonated citrate ligands (Mol.1, Mol.1′, Mol.1″, and Mol.1‴, which are symmetry-related to each other): Mol.1 through the hydroxyl oxygen and the carboxylate1 oxygen (O_A) to form a five-membered [–M-O_A-C-C-O(H)–] chelate ring, Mol.1′ through the carboxylate1 oxygen O_A, Mol.1″ through two oxygens (O_A and O_B) of the carboxylate2, and Mol.1‴ through the carboxylate1 oxygen O_B, and the seventh position is occupied by a water molecule. The Pb(II)–O bond distances are in the range of 2.395(7)–2.883(1) Å with a *hemidirected* coordination geometry around the Pb center. In return, the citrate ligand is bound to four Pb(II) atoms: Pb1 in an *O*,*O*-bidentate mode through the carboxylate1 O_A and the hydroxyl oxygen, Pb1′ through the carboxylate1 O_A, Pb1″ through the carboxylate2 oxygens (bidentate), and Pb‴ through the carboxylate1 O_B. This Pb(II)–citrate binding mode is termed here as *motif 1* [210] in order to compare with the other six different binding modes, which are described below.

In the *[$Pb_3(citrato)_2(H_2O)$]* complex [209], three crystallographically independent Pb(II) ions exist (Pb1, Pb2, and Pb3) and two citrate ligands (Mol.1 and Mol.2) with the three carboxyl groups fully deprotonated. Each citrate ligand is bound to five Pb(II) atoms with different binding motifs. For Mol.1, as *Pb(II)–citrate binding motif 2*, Pb1 binds in an *O*,*O*,*O*-tridentate mode through the carboxylate1 O_A, the hydroxyl oxygen, and the carboxylate3 O_A; Pb2 through the carboxylate3 O_A; Pb3 through the carboxylate2 O_A and O_B; and Pb1′ and Pb3′ each through the monodentate bonding to the carboxylate1 O_B and the carboxylate3 O_B, respectively. For Mol.2 [*Pb(II)–citrate binding motif 3*], Pb1 binds through the carboxylate3 O_A; Pb2 in an *O*,*O*-bidentate mode through the carboxylate3 O_A and the hydroxyl oxygen; Pb3 through the carboxylate2 O_A and O_B; and Pb1″ and Pb2′ each through the monodentate bonding to the carboxylate2 O_A and carboxylate1 O_A. The coordination geometry is *hemidirected* for Pb1 and Pb2.

On the other hand, in the *[$Pb_5(citrato)_3(citratoH)(H_2O)_3$]$^-$* complex [210], five crystallographically independent Pb(II) ions exist (Pb1–Pb5) and four citrate

ligands, three (Mol.1–Mol.3) of which are triply-deprotonated and one (Mol.4) doubly-deprotonated. Ignoring weak interaction, for Mol.1 [*Pb(II)–citrate binding motif 4*], six Pb atoms bind as follows: Pb1, Pb4, and Pb1′ each through bidentate bonding to carboxylate1, carboxylate2, and carboxylate3, respectively; Pb2 bridging between carboxylate1 and carboxylate3, Pb3 in a tridentate fashion through carboxylate2 O_A and carboxylate3 O_B and the hydroxyl group; and Pb5″ through the carboxylate2 O_B. For Mol.2 [*Pb(II)–citrate binding motif 5*], three Pb atoms bind: Pb1 and Pb5 each in a bidentate fashion to carboxylate2 and carboxylate1, respectively, and Pb2 in a tridentate fashion as the same as Pb3 for Mol.1. For Mol.3 [*Pb(II)–citrate binding motif 6*], six Pb atoms bind: Pb2, Pb4′, and Pb4″ each through bidentate bonding to carboxylate1, carboxylate 2, and carboxylate3, respectively; Pb3 bridging between carboxylate1 and carboxylate3; Pb5 in a tridentate fashion as the same as Pb3 for Mol.1; and Pb5′ through the carboxylate2 O_A. For Mol.4 [*Pb(II)–citrate binding motif 7*], four Pb atoms bind: Pb3 and Pb3′ each through bidentate bonding to carboxylate3 and carboxylate1, respectively; and each of Pb4 and Pb4′ bridges between carboxylate1 and carboxylate3.

In the three reported Pb(II)–citrate complexes [201, 209, 210], seven metal binding motifs for citrate are observed, which are different in the ligand dentate number (the number of metal ions attached) and their binding sites (refer to Figure 5 in [207], where these seven motifs are schematically drawn). The carboxylate and the hydroxyl groups are always involved in metal coordination, except for one case [210] for the hydroxyl group. The bidentate or tridentate binding motifs involving the *hydroxyl* group have received attention in connection with the citric acid metabolism, that is, metal complexes that have tridentate binding motifs were not metabolized, whereas metal complexes that bind through a dicarboxyl but not through the *hydroxyl* group were metabolized [211], implying that the *hydroxyl* group needs to be uncoordinated so that aconitase can recognize the citrate [210].

5.3. D-Penicillamine

D-Penicillamine (DPA) is a dimethyl derivative of D-cysteine and is used as a chelating agent in the treatment of intoxications with metal compounds, especially for copper [200]. The crystal structure of $[Pb(D\text{-penicillaminato})]_n$ was first reported in 1974 [194] and was later redetermined [195]. As Figure 7 shows, the D-penicillaminate ligand, with the carboxyl and the sulfhydryl groups doubly deprotonated, coordinates to the Pb(II) ion in an *N*,*S*,*O*-tridentate mode. In the crystal lattice, Pb(II) further binds to symmetry-related, three DPA ligands: two ligands through the S atom and one ligand through the carboxylate oxygens (bidentate), forming a three-dimensional polymeric structure. Taken together, the Pb(II) atom is six-coordinated with a *hemidirected* coordination geometry.

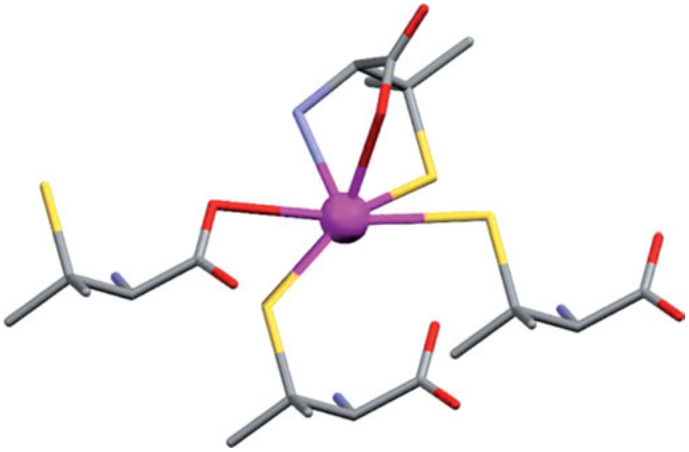

Figure 7. Structure of the [Pb(D-penicillaminato)]$_n$ complex [194, 195]. The Pb(II) atom is bound to four D-penicillaminato ligands, the first ligand through an *S*(thiolate),*O*(carboxylate),*N*(amino)-tridentate chelation, the second ligand through a carboxylate oxygen, and the last two ligands each through a thiolate sulfur. The Pb(II) shows a *hemidirected* coordination geometry. Sulfur atoms are drawn in yellow color.

5.4. Ethylenediaminetetraacetic Acid ($EDTAH_4$)

Six Pb(II)–EDTA crystal structures are available: $[Pb(EDTAH_2)(H_2O)]_2 \cdot H_2O$ [196, 197], $X_{2n}[Pb(EDTA)]_n \cdot y\,nH_2O$ [X = NH_4, y = 2.5; X = Na, y = 2; X = Cs, y = 3.5; X = Tl, y = 3] [198], and $K_2[Pb(EDTA)] \cdot 4\,H_2O$ [199]. The Pb(II)–$EDTAH_2$ complex [196, 197] involves two crystallographically independent but structurally equivalent $[Pb(EDTAH_2)(H_2O)]$ units. In each unit, Pb(II) is capped by an $EDTAH_2^{2-}$ ligand through four Pb–O (carboxylate) and two Pb–N (amine) bonds with normal distances (termed as a 2 *N*/4 *O*-hexadentate chelation mode). In addition, a water molecule and one carboxylate oxygen of the neighboring molecular unit, which is related to the parent unit by an inversion center, coordinate to the Pb(II) atom with longer bond distances, thus forming a dimeric structure. The resulting metal coordination geometry is *hemidirected* for one Pb(II) atom and *holodirected* for the other one. Similarly, the other five Pb(II)–$EDTA^{4-}$ complexes commonly form EDTA-capped $[Pb(EDTA)]^{2-}$ structural units with the Pb(II) atom coordinated in a 2 *N*/4 *O*-hexadentate mode. The NH_4^+ and Cs^+ salt complexes [198] involve two independent [Pb(EDTA)] structural units, each of which self-contacts across an inversion center through a long Pb–O bond with a carboxylate oxygen of a neighboring EDTA molecule to form a dimeric structure; in addition, these two independent structural units are further connected in parallel through another long Pb–O bond to result in the formation of a double-layered polymeric structure. On the other hand, in the Tl^+ and Na^+ salt complexes [198], which contain one independent [Pb(EDTA)] structural unit, a

dimeric structure having an inversion center also forms in the Tl^+ salt complex while the Na^+ complex has a monomeric structure; an additional intermolecular Pb–O bond creates a polymeric structure in both complexes. The coordination geometry around each Pb(II) is *hemidirected*. No intermolecular Pb–O contact in the K^+ salt complex is mentioned [199].

5.5. Ethylenediaminetetraacetamide (EDTA-N_4)

In the crystal structure of the Pb(II)–EDTA-N_4 complex [Pb(EDTA-N_4)]$\cdot(NO_3)_2$ [202], the Pb(II) ion is six-coordinated to both ethylenediamino nitrogens and all four carbonyl oxygens in the amido functionalities. The metal coordination geometry is *hemidirected*.

5.6. Thiohydroxamic Acids

Thiohydroxamic acids are the sulfurous equivalent of the hydroxamic functionality frequently found in naturally occurring iron chelators (refer to [212] for a review on siderophores) and exhibit high affinity for Pb(II) and excellent selectivity over Zn(II) and Ca(II) [205]. Four Pb(II)–thiohydroxamate complexes are reported: [Pb(*N*-methylbenzothiohydroxamato)$_2$]$_n$ [203], [Pb(*N*-methylacetothiohydroxamato)$_2$]$_n$ [203], [Pb(*N*-cyclohexyl-phenylacetothiohydroxamato)$_2$] [204], and [Pb(*N*-methyl-3-pyridothiohydroxamato)$_2$]$_n$ [204]. In the four thiohydroxamate complexes, ignoring weak interactions, Pb(II) binds to two thiohydroxamate ligands each through an *S,O*-bidentate mode to form a five-membered [–M-O-N-C-S–] chelate ring in the first three complexes, and additionally to a third ligand through the *N*-hydroxylate oxygen from the symmetry-related neighboring molecule in the fourth complex. An additional weak interaction is formed with two, three, or one neighboring thiohydroxamate ligand(s) in the first, second, and fourth complex, respectively, but none in the third complex, where the bulkiness of the ligands prevents the metal atom from increasing its coordination number by intermolecular contacts. In all four complexes, the metal coordination geometry is *hemidirected*.

5.7. Hydroxypyridinethione

The structure of the [Pb(diethylcarbamoyl-hydroxypyridinethionato)$_2$] complex [205] is based on a four-coordinated geometry formed by two sets of an *S,N*-bidentate chelation mode similar to that observed in the thiohydroxamate structures. In addition, weak Pb–O interactions occur from ligation by the *N*-hydroxyl and carbonyl oxygens of a neighboring molecule, forming a twofold-symmetry related dimeric structure. The metal coordination geometry is *hemidirected*.

5.8. Tris(mercaptophenylimidazolyl)hydroborate (Tm^{Ph})

Figure 8 shows the $[Pb(Tm^{Ph})]^+$ structure in the $[Pb(Tm^{Ph})]\cdot ClO_4$ complex [81], where the trigonal pyramidal Pb(II) is capped by the Tm^{Ph} ligand bound in an *S*,*S*,*S*-tridentate mode and the axial position is occupied by the stereochemically active electron lone pair on Pb(II).

As noted in Section 2.3, the $[Pb(Tm^{Ph})]^+$ structure serves as a model for a $[Pb(Cys)_3]$ adduct that forms by replacing a native Zn(II) at the active site of δ-aminolevulinate dehydratase [41], a suggested mechanism of lead poisoning. That is, the stereochemically active Pb(II) lone pair that occupies the vacant place may prevent the aminolevulinic acid substrate from forming a tetrahedral species of the type $[(Cys)_3Pb(ALA)]$, a required intermediate in the proposed mechanisms of action of ALAD. The authors pointed out [81] that the degree of the activation of ALA by interaction of the ketone group with the Zn(II) center is a function of the Lewis acidity of the metal center, which is considerably greater for a tetrahedral Zn(II) center than for a trigonal pyramidal Pb(II) center, presumably associated with the stereochemically active Pb(II) lone pair which tempers its electrophilicity.

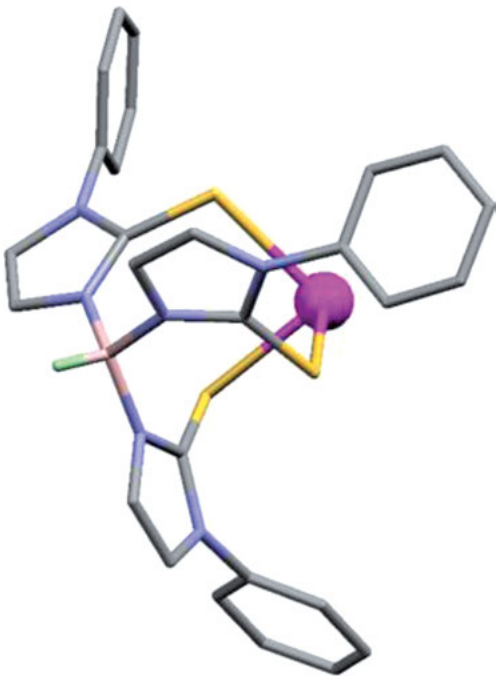

Figure 8. Structure of the $[Pb(Tm^{Ph})]^+$ complex [81], where Tm^{Ph} is a tris-thio ligand as a model for the Cys3 cite in ALAD [41] (see text). The Pb(II) ion is bound to a $[Tm^{Ph}]^-$ ligand in an *S*,*S*,*S*-tridentate chelation mode. The metal coordination geometry is *hemidirected*. Sulfur and boron atoms are drawn yellow and pink in color, respectively.

5.9. Summary

A still limited number of lead complexes with *other* biorelevant small molecules have been reported, the majority of which are those of detoxification agents and their derivatives. Detoxifying and related ligands exhibit characteristic metal binding modes/motifs: an *S*,*N*,*O*-tridentate chelation mode for penicillamine, a 2*N*/4*O*-hexadentate chelation mode for EDTA and EDTA-N_4, and an *S*,*O*-bidentate chelation mode for thiohydroxamate and hydroxypyridinethione. EDTA, EDTA-N_4, and thiohydroxamate and hydroxypyridinethione derivatives are structurally rigid and are spatially well 'preorganized' as chelating agents to give discrete Pb(II) complexes that have a stereochemically active lone pair on one side, thus improving solubility, one of the major factors required for a detoxification agent; this provides a strategy for designing detoxification agents. On the other hand, citrate, which has one hydroxyl group in addition to three carboxylate groups, is so structurally flexible that it is subject to a variety (seven) of metal binding motifs accompanying the formation of a polymeric structure, where the hydroxyl group was not deprotonated in any instance and involved in two types of metal bonding: one *O*,*O*,*O*-tridentate chelation (in motifs 2, 4, 5, and 6 noted above) and the other *O*,*O*-bidentate chelation (in motifs 1 and 3). The tris(mercaptophenylimidazolyl)hydroborate complex [81] is doubly significant in that it displays an *S*,*S*,*S*-tridentate chelation mode and serves as a model for a [$Pb(Cys)_3$] adduct formed at the active center of δ-aminolevulinate dehydratase [41].

6. CONCLUDING REMARKS

In this chapter, we attempted to provide structural information on lead interactions with amino acids and small peptides, proteins, nucleic acid constituents, nucleic acids, small saccharides, and other biorelevant small molecules, based on crystal structural data. It is evident that the trends exhibited by Pb(II) in small molecule structures [1, 4, 5] are also seen/reconfirmed in biological molecules: (i) commonly observed donor atoms include the relatively hard oxygen and nitrogen atoms as well as the softer sulfur atom, consistent with the chemical nature of Pb(II) as an intermediate acid according to the hard and soft acid-base rule, and their relative frequency of occurrence is in that order; (ii) Pb(II) adopts variable coordination numbers (four to eleven) and geometries as a consequence of the large radius and the possible occurrence of a stereochemically active lone pair of electrons, which arises from mixing of 6s and 6p orbitals and results in a *hemidirected* structure. (iii) Most Pb(II) compounds exhibit a *hemidirected* metal coordination geometry.

Somewhat surprisingly, the crystal structures that have so far been reported for Pb(II)/Pb(IV) coordination compounds of biomolecules are still quite limited. Further X-ray studies should be promoted in a more systematic way in order to accumulate more data with an aim to get trends/rules and with a goal to gain the whole picture of lead interactions with biomolecules. In this regard, it should

be emphasized that more attention should be paid to lead-bound crystal structures of proteins or nucleic acids that are prepared even as heavy-atom derivatives since they are a treasury of potential information on lead interactions with large molecules of biological origin, and especially, since a high-resolution structure provides a rare chance to investigate the stereochemically active lone-pair effect of Pb(II) in such a particular system.

X-ray studies of lead complexes relevant to biological systems are *continuously* important in providing structural information inevitable not only for the understanding of the mechanism of lead toxicity but also for the successful treatment of lead poisoning, including the rational design of detoxification agents, a today's subject to be tackled. Of course, such studies have to be complemented by solution studies.

ABBREVIATIONS

Regarding the abbreviations of amino acids and their derivatives, see Tables 1 and 2, respectively.

ACBP	acyl-CoA binding protein
ALA	δ-aminolevulinic acid
ALAD	δ-aminolevulinate dehydratase
Ape1	apurinic/apyrimidinic endonuclease
A-RNA	double-stranded ribonucleic acid with an A-type conformation
ATP	adenosine 5′-triphosphate
BAL	dimercaprol
bpy	2,2′-bipyridine
CaM	calmodulin
CIF	Crystallographic Information File
citrateH	doubly deprotonated citrate dianion
CD	cyclodextrin
CD – 2 H	cyclodextrin dianion
CD – 14 H	cyclodextrin tetradecaanion
CD – 16 H	cyclodextrin hexadecaanion
CPA	carboxypeptidase A
CSD	Cambridge Structural Database
D	dexter (optical isomer named after Latin)
DAHP	3-deoxy-D-arabino-heptulosonate-7-phosphate
DAHPS	3-deoxy-D-arabino-heptulosonate-7-phosphate synthase
DIS RNA	RNA dimerization initiation site of the HIV-1 RNA genome
DMPS	2,3-dimercaptopropane-1-sulfonate
DMSA	*meso*-2,3-dimercaptosuccinic acid
DMSO	dimethylformamide
DPA	D-penicillamine
E4P	D-erythrose-4-phosphate

$EDTAH_4$	ethylenediamine-N,N′,N″,N‴-tetraacetic acid
$EDTAH_2$	ethylenediaminetetraacetate dianion
EDTA-N_4	ethylenediaminetetraacetamide
5-F-Ura-1-OAc	5-fluorouracil-1-acetate
Gal	galactose
GlyGlu	glycylglutamate
GlySerProGlu	glycylserylprolylglutamyl
GlyTyr	glycyltyrosine
Guo	guanosine
HiPIP	high-potenial iron-sulfur protein
Hyp-1-OAc	hypoxanthine-1-acetate
L	laevus (optical isomer named after Latin)
M	metal ion
mP5N-1	mouse pyrimidine 5′-nucleotidase type 1
mRNA	messenger RNA
NCp	nucleocapsid protein
nt	number of nucleotide units constituting a nucleic acid
OAc	acetate
O(P)	oxygen atom of the phosphate group
P5N-1	pyrimidine 5′-nucleotidase type 1
PBGS	porphobilinogen synthase
PDB	Protein Data Bank
PDB ID	PDB identification code
PEP	phosphoenolpyruvate
PGL	2-phosphoglycolate
PKC	protein kinase C
PfuCP	carboxypeptidase from the hyperthermophilic Archaeon *Pyrococcus furiosus*
phen	1,10-phenanthroline
PS2.M	K(I)-induced G-quadruplex in a DNA oligonucleotide
PtdSer	1,2-dicaproyl-*sn*-phosphatidyl-L-serine
R	side chain of amino acid
RNase P	ribonuclease P
SYT	synaptotagmin
Tm^{Ph}	tris(2-mercapto-1-phenylimidazolyl)hydroborate
tRNA	transfer RNA
$tRNA^{Phe}$	phenylalanyl transfer ribonucleic acid
UDP	uridine 5′-diphosphate
Ura	uracil

REFERENCES

1. E. S. Claudio, H. A. Godwin, J. S. Magyar, *Progr. Inorg. Chem*. **2003**, *51*, 1–144.
2. *Lead: Chemistry, Analytical Aspects, Environmental Impact and Health Effects*, Eds J. S. Casas, J. Sordo, Elsevier, Amsterdam, 2006, pp. 1–366.

3. G. Flora, D. Gupta, A. Tiwari, *Interdiscip. Toxicol.* **2012**, *5*, 47–58.
4. C. E. Holloway, M. Melnik, *Main Group Metal Chem*. **1997**, *20*, 399–495.
5. L. Shimoni-Livny, J. P. Glusker, C. W. Bock, *Inorg. Chem*. **1998**, *37*, 1853–1867.
6. R. D. Shannon, *Acta Cryst.* **1976**, *A32*, 751–767.
7. A. Bondi, *J. Phys. Chem.* **1964**, *68*, 441–451.
8. W. Bi, N. Mercier, N. Louvain, M. Latroche, *Eur. J. Inorg. Chem.* **2006**, 4225–4228.
9. K. D. Demadis, E. Armakola, K. E. Papathanasiou, G. Mezei, A. M. Kirillov, *Cryst. Growth Des.* **2014**, *14*, 5234–5243.
10. G. Battistuzzi, M. Borsari, L. Menabue, M. Saladini, M. Sola, *Inorg. Chem.* **1996**, *35*, 4239–4247.
11. G.-L. Wen, S. Yuan, *Synth. React. Inorg. Met.-Org. Nano-Met. Chem.* **2010**, *40*, 207–210.
12. S.-N. Qin, J.-R. Hu, Z.-L. Chen, F.-P. Liang, *J. Coord. Chem.* **2011**, *64*, 3718–3728.
13. D. Iacopino, L. Menabue, M. Saladini, *Aust. J. Chem.* **1999**, *52*, 741–748.
14. C. Lei, J.-G. Mao, Y.-Q. Sun, *J. Solid State Chem.* **2004**, *177*, 2449–2455.
15. J.-L. Song, C. Lei, Y.-Q. Sun, J.-G. Mao, *J. Solid State Chem.* **2004**, *177*, 2557–2564.
16. X. Wang, J. J. Vittal, *Inorg. Chem. Commun.* **2003**, *6*, 1074–1077.
17. N. Burford, M. D. Eelman, W. G. LeBlanc, T. S. Cameron, K. N. Robertson, *Chem. Commun.* **2004,** 332–333.
18. C. D. L. Saunders, L. E. Longobardi, N. Burford, M. D. Lumsden, U. Werner-Zwanziger, B. Chen, R. McDonald, *Inorg. Chem.* **2011**, *50*, 2799–2810.
19. L. Gasque, M. A. Verhoeven, S. Bernès, F. Barrios, J. G. Haasnoot, J. Reedijk, *Eur. J. Inorg. Chem.* **2008**, 4395–4403.
20. F. Marandi, N. Shahbakhsh, *J. Coord. Chem.* **2007**, *60*, 2589–2595.
21. B.-P. Yang, J.-G. Mao, Y.-Q. Sun, H.-H. Zhao, A. Clearfield, *Eur. J. Inorg. Chem.* **2003**, 4211–4217.
22. Z.-G. Sun, L.-Yi Cui, Z.-M. Liu, D.-P. Dong, L. Meng, H. Chen, L.-C. Zhang, Z.-M. Zhu, W.-S. You, *Inorg. Chem. Commun.* **2006**, *9*, 1121–1124.
23. S. Bernès, L. Gasque, *Acta Cryst.* **2008**, *E64*, m566–m567.
24. F. Marandi, N. Shahbakhsh, *Z. Anorg. Allg. Chem*. **2007**, *633*, 1137–1139.
25. M. Stapf, T. Böhle, W. Seichter, F. O. R. L. Mertens, E. Weber, *Z. Naturforsch., Teil B* **2012**, *67*, 1166–1172.
26. Q. Ye, Y.-H. Li, Q. Wu, Y.-M. Song, J.-X. Wang, H. Zhao, R.-G. Xiong, Z. Xue, *Chem. Eur. J.* **2005**, *11*, 988–994.
27. R. Yoshida, S. Ogasahara, H. Akashi, T. Shibahara, *Inorg. Chim. Acta* **2012**, *383*, 157–163.
28. L. Gasque, S. Bernès, R. Ferrari, C. R. de Barbarín, M. de J. Gutiérrez, G. Mendoza-Díaz, *Polyhedron* **2000**, *19*, 649–653.
29. A. Ghosh, R. A. Sanguramath, *J. Chem. Sci.* **2008**, *120*, 217–222.
30. L.-L. Wu, H.-H. Song, *J. Coord. Chem.* **2012**, *65*, 2135–2146.
31. L.-F. Ma, L.-Y. Wang, J.-G. Wang, Y.-F. Wang, X. Feng, *Z. Anorg. Allg. Chem.* **2006**, *632*, 487–490.
32. R. Ferrari, S. Bernés, C. R. de Barbarín, G. Mendoza-Díaz, L. Gasque, *Inorg. Chim. Acta* **2002**, *339*, 193–201.
33. S. Chakraborty, P. Tyagi, D.-F. Tai, G.-H. Lee, S.-M. Peng, *Molecules* **2013**, *18*, 4972–4985.
34. M. Mitova, S. Popov, S. De Rosa, *J. Nat. Prod.* **2004**, *67*, 1178–1181.
35. M. Kirberger, J. J. Yang, *J. Inorg. Biochem.* **2008**, *102*, 1901–1909.
36. T. L. Blundell, L. N. Johnson, *Protein Crystallography*, Academic, New York, 1976.
37. W. A. Hendrickson, *Q. Rev. Biophys.* **2014**, *47*, 49–93.
38. M. A. Wilson, A. T. Brunger, *Acta Cryst.* **2003**, *D59*, 1782–1792.
39. P. Kursula, V. Majava, *Acta Cryst*. **2007**, *F63*, 653–656.

40. K. A. Morales, M. Lasagna, A. V. Gribenko, Y. Yoon, G. D. Reinhart, J. C. Lee, W. Cho, P. Li, T. I. Igumenova, *J. Am. Chem. Soc.* **2011**, *133*, 10599–10611.
41. P. T. Erskine, E. M. H. Duke, I. J. Tickle, N. M. Senior, M. J. Warren, J. B. Cooper, *Acta Cryst.* **2000**, *D56*, 421–430.
42. I. A. Shumilin, R. H. Kretsinger, R. H. Bauerle, *Structure* **1999**, *7*, 865–875.
43. P. T. Beernink, B. W. Segelke, M. Z. Hadi, J. P. Erzberger, D. M. Wilson III, B. Rupp, *J. Mol. Biol.* **2001**, *307*, 1023–1034.
44. E. Bitto, C. A. Bingman, G. E. Wesenberg, J. G. McCoy, G. N. Phillips, Jr., *J. Biol. Chem*. **2006**, *281*, 20521–20529.
45. J. P. Taskinen, D. M. van Aalten, J. Knudsen, R. K. Wierenga, *Proteins: Struct. Funct. Bioinf.* **2007**, *66*, 229–238.
46. A. E. Medlock, T. A. Dailey, T. A. Ross, H. A. Dailey, W. N. Lanzilotta, *J. Mol. Biol*. **2007**, *373*, 1006–1016.
47. Y. S. Babu, C. E. Bugg, W. J. Cook, *J. Mol. Biol.* **1988**, *204*, 191–204.
48. R. B. Sutton, B. A. Davletov, A. M. Berghuis, T. C. Südhof, S. R. Sprang, *Cell* **1995**, *80*, 929–938.
49. R. B. Sutton, J. A. Ernst, A. T. Brunger, *J. Cell. Biol.* **1999**, *147*, 589–598.
50. P. T. Erskine, N. Senior, S. Awan, R. Lambert, G. Lewis, I. J. Tickle, M. Sarwar, P. Spencer, P. Thomas, M. J. Warren, P. M. Shoolingin-Jordan, S. P. Wood, J. B. Cooper, *Nat. Struct. Biol*. **1997**, *4*, 1025–1031.
51. W. N. Lipscomb, L. G. N. Reeke, J. A. Hartsuck, F. A. Quiocho, P. H. Bethge, *Philos. Trans. R. Soc. London, Ser. B* **1970**, *257*, 177–214.
52. H. M. Holden, I. Rayment, *Arch. Biochem. Biophys.* **1991**, *291*, 187–194.
53. H. C. Gonick, *J. Toxicol.* **2011**, *2011*, Article ID 686050.
54. B. L. Vallee, D. D. Ulmer, *Annu. Rev. Biochem*. **1972**, *41*, 91–128.
55. J. B. Suszkiw, *Neurotoxicology* **2004**, *25*, 599–604.
56. D. Chin, A. R. Means, *Trends Cell Biol.* **2000**, *10*, 322–328.
57. J. M. Aramini, T. Hiraoki, M. Yazawa, T. Yuan, M. Zhang, H. J. Vogel, *J. Biol. Inorg. Chem.* **1996**, *1*, 39–48.
58. E. Habermann, K. Crowell, P. Janicki, *Arch. Toxicol.* **1983**, *54*, 61–70.
59. G. Richardt, G. Federolf, E. Habermann, *Biochem. Pharmacol*. **1986**, *35*, 1331–1335.
60. M. Kern, M. Wisniewski, L. Cabell, G. Audesirk, *Neurotoxicology* **2000**, *21*, 353–363.
61. R. Sandhir, K. D. Gill, *Exp. Mol. Pathol*. **1994**, *61*, 69–75.
62. J. Weaver, S. Porasuphatana, P. Tsai, G.-L. Cao, T. A. Budzichowski, L. J. Roman, G. M. Rosen, *J. Pharmacol. Exp. Ther*. **2002**, *302*, 781–786.
63. P. L. Goering, *Neurotoxicology* **1993**, *14*, 45–60.
64. G. W. Goldstein, *Neurotoxicology* **1993**, *14*, 97–102.
65. A. Lewit-Bentley, S. Réty, *Curr. Opin. Struc. Biol.* **2000**, *10*, 637–643.
66. M. Kirberger, J. J. Yang, *J. Inorg. Biochem*. **2008**, *102*, 1901–1909.
67. M. A. Wilson, A. T. Brunger, *J. Mol. Biol*. **2000**, *301*, 1237–1256.
68. T. C. Südhof, *J. Biol. Chem*. **2002**, *277*, 7629–7632.
69. I. Fernandez, D. Araç, J. Ubach, S. H. Gerber, O.-H. Shin, Y. Gao, R. G. W. Anderson, T. C. Südhof, J. Rizo, *Neuron* **2001**, *32*, 1057–1069.
70. J. Rizo, T. C. Südhof, *J. Biol. Chem.* **1998**, *273*, 15879–15882.
71. C. M. L. S. Bouton, L. P. Frelin, C. E. Forde, H. A. Godwin, J. Pevsner, *J. Neurochem.* **2001**, *76*, 1724–1735.
72. J. B. Suszkiw, *Neurotoxicology* **2004**, *25*, 599–604.
73. S. F. Steinberg, *Physiol. Rev.* **2008**, *88*, 1341–1378
74. X. Sun, X. Tian, J. L. Tomsig, J. B. Suszkiw, *Toxicol. Appl. Pharmacol*. **1999**, *156*, 40–45.
75. N. Verdaguer, S. Corbalan-Garcia, W. F. Ochoa, I. Fita, J. C. Gómez-Fernández, *EMBO J.* **1999**, *18*, 6329–6338.

76. X. Shao, B. A. Davletov, R. B. Sutton, T. C. Südhof, J. Rizo, *Science* **1996**, *273*, 248–251.
77. M. J. Warren, J. B. Cooper, S. P. Wood, P. M. Shoolingin-Jordan, *Trends Biochem. Sci.* **1998**, *23*, 217–221.
78. T. J. B. Simons, *Eur. J. Biochem.* **1995**, *234*, 178–183.
79. P. T. Erskine, N. Senior, S. Awan, R. Lambert, G. Lewis, I. J. Tickle, M. Sarwar, P. Spencer, P. Thomas, M. J. Warren, P. M. Shoolingin-Jordan, S. P. Wood, J. B. Cooper, *Nat. Struct. Biol*. **1997**, *4*, 1025–1031.
80. E. K. Jaffe, J. Martins, J. Li, J. Kervinen, R. L. Dunbrack, Jr., *J. Biol. Chem*. **2001**, *276*, 1531–1537.
81. B. M. Bridgewater, G. Parkin, *J. Am. Chem. Soc.* **2000**, *122*, 7140–7141.
82. K. S. Larsen, D. S. Auld, *Biochemistry* **1991**, *30*, 2613–2618.
83. D. W. Christianson, W. N. Lipscomb, *Proc. Natl. Acad. Sci. USA* **1986**, *83*, 7568–7572.
84. W. N. Lipscomb, G. N. Reeke, Jr., J. A. Hartsuck, F. A. Quiocho, P. H. Bethge, *Phil. Trans. Roy. Soc. Lond*. **1970**, *B257*, 177–214.
85. J. W. Arndt, B. Hao, V. Ramakrishnan, T. Cheng, S. I. Chan, M. K. Chan, *Structure* **2002**, *10*, 215–224.
86. T. C. Cheng, V. Ramakrishnan, S. I. Chan, *Protein Sci.* **1999**, *8*, 2474–2486.
87. C. M. Stephens, R. H. Bauerle, *J. Biol. Chem*. **1991**, *266*, 20810–20817.
88. T. Baasov, J. R. Knowles, *J. Bacteriol.* **1989**, *171*, 6155–6160.
89. T. Wagner, I. A. Shumilin, R. Bauerle, R. H. Kretsinger, *J. Mol. Biol*. **2000**, *301*, 389–399.
90. C. M. Kane, S. Linn, *J. Biol. Chem*. **1981**, *256*, 3405–3414.
91. A. Amici, M. Emanuelli, G. Magni, N. Raffaelli, S. Ruggieri, *FEBS Lett.* **1997**, *419*, 263–267.
92. D. E. Paglia, W. N. Valentine, J. G. Dahlgren, *J. Clin. Invest.* **1975**, *56*, 1164–1169.
93. Sakai, T., *Ind. Health* **2000**, *38*, 127–142.
94. D. E. Paglia, S. W. Renner, K. Bhambhani, *Clin. Biochem.* **1999**, *32*, 193–199.
95. Y. Kim, H. Lee, C. R. Lee, D. U. Park, J. S. Yang, I. J. Park, K. Y. Lee, M. Lee, T.-K. Kim, N.-S. Sohn, Y. S. Cho, N. Lee, H. K. Chung, *Sci. Total Environ.* **2002**, *286*, 181–189.
96. D. E. Paglia, W. N. Valentine, *J. Biol. Chem.* **1975**, *250*, 7973–7979.
97. J. Knudsen, T. B. F. Neergaard, B. Gaigg, M. V. Jensen, J. K. Hansen, *J. Nutr.* **2000**, *130*, 294S–298S.
98. D. R. Smith, M. W. Kahng, B. Quintanilla-Vega, B. A. Fowler, *Chem. Biol. Interact.* **1998**, *14*, 39–52.
99. H. A. Dailey, *Biochem. Soc. Trans.* **2000**, *30*, 590–595.
100. H. A. Dailey, *Ann. N. Y. Acad. Sci*. **1987**, *514*, 81–86.
101. K. M. Barkigia, J. Fajer, A. D. Adler, G. J. B. Williams, *Inorg. Chem*. **1980**, *19*, 2057–2061.
102. M. J. Plater, S. Aiken, T. Gelbrich, M. B. Hursthouse, G. Bourhill, *Polyhedron* **2001**, *20*, 3219–3224.
103. H. M. Holden, W. R. Rypniewski, J. H. Law, I. Rayment, *EMBO J.* **1987**, *6*, 1565–1570.
104. M. M. Benning, G. Wesenberg, M. S. Caffrey, R. G. Bartsch, T. E. Meyer, M. A. Cusanovich, I. Rayment, H. M. Holden, *J. Mol. Biol.* **1991**, *220*, 673–685.
105. M. M. Benning, T. E. Mayer, H. M. Holden, *Arch. Biochem. Biophys.* **1994**, *310*, 460–466.
106. D. R. Breiter, M. R. Kanost, M. M. Benning, G. Wesenberg, J. H. Law, M. A. Wells, I. Rayment, H. M. Holden, *Biochemistry* **1991**, *30*, 603–608.
107. W. R. Rypniewski, D. R. Breiter, M. M. Benning, G. Wesenberg, B.-H. Oh, J. L. Markley, I. Rayment, H. M. Holden, *Biochemistry* **1991**, *30*, 4126–4131.

108. D. R. Breiter, T. E. Meyer, I. Rayment, H. M. Holden, *J. Biol. Chem.* **1991**, *266*, 18660–18667.
109. A. J. Bauer, I. Rayment, P. A. Frey, H. M. Holden, *Proteins Struct. Funct. Genet.* **1991**, *9*, 135–142.
110. J. K. Kawooya, P. S. Keim, J. H. Law, C. T. Riley, R. O. Ryan, J. P. Shapiro, *ACS Symp.* **1985**, *Ser. 276*, 511–521.
111. M. Kirberger, H. C. Wong, J. Jiang, J. J. Yang, *J. Inorg. Biochem.* **2013**, *125*, 40–49.
112. G. Zampella, K. P. Neupane, L. De Gioia, V. L. Pecoraro, *Chem. Eur. J.* **2012**, *18*, 2040– 2050.
113. D. J. Hodgson, *Prog. Inorg. Chem.* **1977**, *23*, 211–254.
114. V. Swaminathan, M. Sundaralingam, R. Bau, *CRC Crit. Rev. Biochem.* **1979**, *6*, 245–336.
115. L. G. Marzilli, T. J. Kistenmacher, G. L. Eichhorn, in *Metal Ions in Biology*, Ed T. G. Spiro, Vol. 1, John Wiley and Sons, New York, 1980, pp. 180–250.
116. K. Aoki, *J. Cryst. Soc. Jpn*. **1981**, *23*, 309–327.
117. W. Saenger, *Principles of Nucleic Acid Structure*, Springer-Verlag, New York, 1984, pp. 201–219.
118. M. Sundaralingam, P. T. Haromy, in *Landolt-Börnstein: Nukleinsäuren; Teilband a*; Kristallographische und Structurelle Daten I, Ed W. Saenger, Springer-Verlag, Berlin, 1989, pp. 22–256.
119. B. Lippert, *Coord. Chem. Rev.* **2000**, *200–202*, 487–516.
120. D. K. Patel, A. Domínguez-Martín, M. P. Brandi-Blanco, D. Choquesillo-Lazarte, V. M. Nurchi, J. Niclós-Gutiérrez, *Coord. Chem. Rev.* **2012**, *256*, 193–211.
121. K. Aoki, I. Fujisawa, K. Murayama, N.-H. Hu, *Coord. Chem. Rev.* **2013**, *257*, 2798–2813.
122. K. Aoki, K. Murayama, N.-H. Hu, *Met. Ions Life Sci.* **2016**, *16*, 27–101.
123. M. S. Rahman, M. A. Salam, N.-H. Hu, K. Murayama, K. Aoki, in press, *Inorg. Chim. Acta 2016*.
124. R. W. Gellert, R. Bau, *Met. Ions Biol. Syst.* **1979**, *8*, 1–55.
125. K. Aoki, in *Landolt-Börnstein: Nukleinsäuren; Teilband b*; Kristallographische und structurelle Daten II, Ed W. Saenger, Springer-Verlag, Berlin, 1989, pp. 171–246.
126. K. Aoki, *Met. Ions Biol. Syst*. **1996**, *32*, 91–134.
127. A. Terrón, *Comm. Inorg. Chem*. **1993**, *14*, 63–88.
128. K. Aoki, K. Murayama, *Met. Ions Life Sci.* **2012**, *10*, 43–102.
129. K. Aoki, in *Comprehensive Supramolecular Chemistry*, Ed. J.-M. Lehn, Vol. 5, Pergamon Press, Oxford, 1996, pp. 249–294.
130. R. Cini, *Comm. Inorg. Chem*. **1992**, *13*, 1–34.
131. K. Aoki, I. Fujisawa, in *Nucleoside Triphosphates and Their Analogs*, Ed. M. Vaghefi, Taylor and Francis, Boca Raton, London, New York, 2005, pp. 115–132.
132. N. Shan, S. J. Vickers, H. Adams, M. D. Ward, J. A. Thomas, *Angew. Chem. Int. Ed.* **2004**, *43*, 3938–3941.
133. B. Müller, W.-Z. Shen, P. J. S. Miguel, F. M. Albertí, T. van der Wijst, M. Noguera, L. Rodríguez-Santiago, M. Sodupe, B. Lippert, *Chem. Eur. J.* **2011**, *17*, 9970–9983.
134. W. Saenger, *Principles of Nucleic Acid Structure*, Springer-Verlag, New York, 1984, pp. 17–24.
135. X. Yuan, X. Zhang, H. Zhao, L. Liu, B. Wu, *Cryst. Growth Des.* **2013**, *13*, 4859–4867.
136. Z. Chen, J. Yan, H. Xing, Z. Zhang, F. Liang, *J. Solid State Chem.* **2011**, *184*, 1063–1069.
137. H. Yin, S.-X. Liu, *Inorg. Chem. Commun.* **2009**, *12*, 187–190.
138. J.-X. Yuan, M.-L. Hu, A. Morsali, *Inorg. Chem. Commun.* **2006**, *9*, 277–280.
139. F. W. Kotch, J. C. Fettinger, J. T. Davis, *Org Lett.* **2000**, *2*, 3277–3280.

140. (a) R. S. Brown, B. E. Hingerty, J. C. Dewan, A. Klug, *Nature* **1983**, *303*, 543–546. (b) R. S. Brown, J. C. Dewan, A. Klug, *Biochemistry* **1985**, *24*, 4785–4801.
141. J. R. Rubin, M. Sundaralingam, *J. Biomol. Struct. Dyn*. **1983**, *1*, 639–646.
142. J. E. Wedekind, D. B. McKay, *Nat. Struct. Biol*. **1999**, *6*, 261–268.
143. E. Ennifar, P. Walter, P. Dumas, *Nucleic Acids Res.* **2003**, *31*, 2671–2682.
144. A. S. Krasilnikov, X. Yang, T. Pan, A. Mondragón, *Nature* **2003**, *421*, 760–764.
145. A. V. Kazantsev, A. A. Krivenko, D. J. Harrington, S. R. Holbrook, P. D. Adams, N. R. Pace, *Proc. Natl. Acad. Sci. USA* **2005**, *102*, 13392–13397.
146. S. L. Forman, J. C. Fettinger, S. Pieraccini, G. Gottarelli, J. T. Davis, *J. Am. Chem. Soc.* **2000**, *122*, 4060–4067.
147. I. Smirnov, R. H. Shafer, *J. Mol. Biol.* **2000**, *296*, 1–5.
148. E. Largy, J.-L. Mergny, V. Gabelica, *Met. Ions Life Sci.* **2016**, *16*, 203–258.
149. W. Liu, H. Zhu, B. Zheng, S. Cheng, Y. Fu, W. Li, T.-C. Lau, H. Liang, *Nucleic Acids Res.* **2012**, *40*, 4229–4236.
150. R. Hanna, J. A. Doudna, *Curr. Opin. Chem. Biol*. **2000**, *4*, 166–170.
151. H. Sigel, C. P. Da Costa, R. B. Martin, *Coord. Chem. Rev*. **2001**, *219–221*, 435–461.
152. A. M. Pyle, *J. Biol. Inorg. Chem*. **2002**, *7*, 679–690.
153. V. J. DeRose, *Curr. Opin. Struct. Biol*. **2003**, *13*, 317–324.
154. D. M. J. Lilley, *Curr. Opin. Struct. Biol*. **2005**, *15*, 313–323.
155. D. E. Draper, D. Grilley, A. M. Soto, *Annu. Rev. Biophys. Biomol. Struct.* **2005**, *34*, 221–243.
156. M. R. Stahley, S. A. Strobel, *Curr. Opin. Struct. Biol*. **2006**, *16*, 319–326.
157. A. Torres-Larios, K. K. Swinger, T. Pan, A. Mondragón, *Curr. Opin. Struct. Biol*. **2006**, *16*, 327–335.
158. S. A. Strobel, J. C. Cochrane, *Curr. Opin. Chem. Biol*. **2007**, *11*, 636–643.
159. R. K. O. Sigel, A. M. Pyle, *Chem. Rev.* **2007**, *107*, 97–113.
160. E. Freisinger, R. K. O. Sigel, *Coord. Chem. Rev.* **2007**, *251*, 1834–1851.
161. N. Toor, K. S. Keating, A. M. Pyle, *Curr. Opin. Struct. Biol*. **2009**, *19*, 260–266.
162. A. M. Pyle, *Crit. Rev. Biochem. Mol. Biol.* **2010**, *45*, 215–232.
163. *Metal Ions in Life Sciences*, Vol. 9, Eds A. Sigel, H. Sigel, R. K. O. Sigel, Royal Society of Chemistry, Cambridge, UK, 2011, pp. 1–391.
164. W. L. Ward, K. Plakos, V. J. DeRose, *Chem. Rev.* **2014**, *114*, 4318–4342.
165. H. Sawai, *J. Am. Chem. Soc*. **1976**, *98*, 7037–7039.
166. T. Lan, Y. Lu, *Met. Ions Life Sci.* **2012**, *10*, 217−248.
167. M. Hollenstein, *Molecules* **2015**, *20*, 20777–20804.
168. G. Dirheimer, J. P. Ebel, J. Bonnet, J. Gangloff, G. Keith, B. Krebs, B. Kuntzel, A. Roy, J. Weissenbach, C. Werner, *Biochimie* **1972**, *54*, 127–l44.
169. A. Jack, J. E. Ladner, A. Klug, *J. Mol. Biol*. **1976**, *108*, 619–649.
170. A. Jack, J. E. Ladner, J. E. Rhodes, R. S. Brown, A. Klug, *J. Mol. Biol*. **1977**, *111*, 315–328.
171. D. A. Usher, *Proc. Natl. Acad. Sci. USA* **1969**, *62*, 661–667.
172. G. C. K. Roberts, E. A. Dennis, D. H. Meadows, J. S. Cohen, O. Jardetzky, *Proc. Natl. Acad. Sci. USA* **1969**, *62*, 1151–1158.
173. C. F. Baes, Jr., R. E. Mesmer, *The Hydrolysis of Cations*, Wiley–Interscience, New York, 1976.
174. T. Pan, O. C. Uhlenbeck, *Nature* **1992**, *358*, 560–563.
175. M. Z. Barciszewska, M. Szymanski, E. Wyszko, J. Pas, L. Rychlewski, J. Barciszewski, *Mutat. Res., Rev. Mutat. Res.* **2005**, *589*, 103–110.
176. J. E. Wedekind, D. B. McKay, *Biochemistry* **2003**, *42*, 9554–9563.
177. C. Guerrier-Takada, K. Gardiner, T. Marsh, N. Pace, S. Altman, *Cell* **1983**, *35*, 849–857.
178. A. V. Kazantsev, N. R. Pace, *Nat. Rev. Microbiol*. **2006**, *4*, 729–740.

179. M. C. Marvin, D. R. Engelke, *J. Cell Biochem*. **2009**, *108*, 1244–1251.
180. O. Esakova, A. S. Krasilnikov, *RNA* **2010**, *16*, 1725–1747.
181. N. J. Reiter, A. Osterman, A. Torres-Larios, K. K. Swinger, T. Pan, A. Mondragón, *Nature* **2010**, *468*, 784–789.
182. R. R. Breaker, G. F. Joyce, *Chem. Biol*. **1994**, *1*, 223–229.
183. Q.-C. He, J.-M. Zhou, D.-M. Zhou, Y. Nakamatsu, T. Baba, T. Taira, *Biomacromolecules* **2002**, *3*, 69–83.
184. A. K. Brown, J. Li, C. M. B. Pavot, Y. Lu, *Biochemistry* **2003**, *42*, 7152–7161.
185. J. Li, Y. Lu, *J. Am. Chem. Soc*. **2000**, *122*, 10466–10467.
186. A. Ponce-Salvatierra, K. Wawrzyniak-Turek, U. Steuerwald, C. Höbartner, V. Pena, *Nature* **2016**, *529*, 231–234.
187. K. Benner, J. Ihringer, P. Klüfers, *Angew. Chem. Int. Ed*. **2006**, *45*, 5818–5822.
188. Y. Wei, D. Sun, D. Yuan, Y. Liu, Y. Zhao, X. Li, S. Wang, J. Dou, X. Wang, A. Hao, D. Sun, *Chem. Sci*. **2012**, *3*, 2282–2287.
189. P. Klüfers, J. Schuhmacher, *Angew. Chem. Int. Ed*. **1994**, *33*, 1863–1865.
190. D. Prochowicz, A. Kornowicz, I. Justyniak, J. Lewiński, *Coord. Chem. Rev*. **2016**, *306*, 331–345.
191. T. Lis, *Acta Cryst*. **1984**, *C40*, 374–376.
192. E. M. M. D. Valle, *Process Biochem*. **2004**, *39*, 1033–1046.
193. M. W. Yu, C. J. Fritchie, Jr., *J. Chem. Soc. Dalton Trans.* **1975**, 377–380.
194. H. C. Freeman, G. N. Stevens, I. F. Taylor, Jr., *J. Chem. Soc., Chem. Commun.* **1974**, 366–367.
195. A. C. Schell, M. Parvez, F. Jalilehvand, *Acta Cryst*. **2012**, *E68*, m489–m490.
196. P. G. Harrison, A. T. Steel, *J. Organomet. Chem.* **1982**, *239*, 105–113.
197. A. L. Poznyak, G. N. Kupriyanova, I. F. Burshtein, A. B. Ilyukhin, *Koord. Khim.* **1998**, *24*, 825–827.
198. A. B. Ilyukhin, V. B. Logvinova, R. L. Davidovich, *Zh. Neorg. Khim.* **1999**, *44*, 1654–1660.
199. J. Wang, Z.-R. Liu, X.-D. Zhang, W.-G. Jia, D.-M. Fan, *J. Struct. Chem. (Jiegou Huaxue)* **2003**, *22*, 454–458.
200. Y. Cao, M. A. Skaug, O. Andersen, J. Aaseth, *J. Trace Elem. Med. Biol*. **2015**, *31*, 188–192.
201. M. Kourgiantakis, M. Matzapetakis, C. P. Raptopoulou, A. Terzis, A. Salifoglou, *Inorg. Chim. Acta* **2000**, *297*, 134–138.
202. E. S. Claudio, M. A. ter Horst, C. E. Forde, C. L. Stern, M. K. Zart, H. A. Godwin, *Inorg. Chem.* **2000**, *39*, 1391–1397.
203. K. Abu-Dari, F. E. Hahn, K. N. Raymond, *J. Am. Chem. Soc*. **1990**, *112*, 1519–1524.
204. S. Rupprecht, S. J. Franklin, K. N. Raymond, *Inorg. Chim. Acta* **1995**, *235*, 185–194.
205. K. Abu-Dari, T. B. Karpishin, K. N. Raymond, *Inorg. Chem.* **1993**, *32*, 3052–3055.
206. R. Miura, Y. Miyake, H. Tojo, T. Yamano, in *Metalloproteins*, Eds S. Otsuka, T. Yamanaka, Kodansha, Elsevier, Tokyo, Amsterdam, 1988, pp. 443–455.
207. M. Matzapetakis, N. Karligiano, A. Bino, M. Dakanali, C. P. Raptopoulou, V. Tangoulis, A. Terzis, J. Giapintzakis, A. Salifoglou, *Inorg. Chem.* **2000**, *39*, 4044–4051.
208. B. Huta, J. J. Lensboeur, A. J. Lowe, J. Zubieta, R. P. Doyle, *Inorg. Chim. Acta* **2012**, *393*, 125–134.
209. J. Shi, J.-N. Xu, P. Zhang, Y. Fan, L. Wang, M.-H. Bi, K.-R. Ma, T.-Y. Song, *Gaodeng Xuexiao Huaxue Xuebao (Chem. J. Chin. Uni.)* **2007**, *28*, 1617–1621.
210. C. Chu, K. Darling, R. Netusil, R. P. Doyle, J. Zubieta, *Inorg. Chim. Acta* **2011**, *378*, 186–193.
211. A. J. Francis, C. J. Dodge, *Environ. Sci. Technol*. **2008**, *42*, 8277–8282.
212. K. N. Raymond, B. E. Allred, A. K. Sia, *Acc. Chem. Res.* **2015**, *48*, 2496–2505.

8

Lead(II) Complexes of Amino Acids, Peptides, and Other Related Ligands of Biological Interest

Etelka Farkas and Péter Buglyó

Department of Inorganic and Analytical Chemistry, University of Debrecen,
Egyetem tér 1, H-4032 Debrecen, Hungary
<efarkas@science.unideb.hu> <buglyo@science.unideb.hu>

Metal Ions in Life Sciences, Volume 17 Edited by Astrid Sigel, Helmut Sigel, and Roland K. O. Sigel

DOI 10.1515/9783110434330-008

Abstract: Lead(II) forms (NH_2,COO^-)-chelated mono- and bis-complexes with simple amino acids, while mono-complexes with pH-dependent coordination modes exist with simple dipeptides. These mostly hemidirected complexes have moderate stability. While a weak interaction of side chain imidazole and carboxylate in lead(II)-aminoacidato complexes is found, the thiolate group has an exceptionally high affinity to this metal ion. For example, tridentate (NH_2,COO^-,S^-)-coordination of penicillamine (Pen) and cysteine (Cys) results in an extremely strong interaction with lead(II), but, owing to the sterical effect of the $6s^2$ pair, a second ligand is not able to coordinate in the above mentioned tridentate way. Although there is no example for a lead(II)-induced deprotonation and coordination of a peptide-amide and the side-chain thiolate in oligopeptides has a somewhat lower basicity compared to that of Pen or Cys, still the Cys-containing peptides interact rather strongly with lead(II). Interestingly, the position of Cys in the peptide influences significantly both the lead-binding ability via different bonding modes and the selectivity for lead(II) against other metal ions, like zinc(II) or cadmium(II). At high ligand excess, however, coordination of three sulfur donors to lead(II) is found with thiolate-containing amino acids and oligopeptides.

High basicity oxygens of hydroxamates, hydroxypyronates, and hydroxypyridinonates are also effective lead-binding donors. Some factors affecting the complexation of these ligands with lead(II) are: (i) A larger extent of delocalization along the ring in hydroxypyridinonate results in a more favored metal-binding ability over hydroxypyronate. (ii) Even monohydroxamates are good ligands and form mono- and bis-complexes with lead(II). (iii) In general, dihydroxamates and trihydroxamate-based siderophores, like desferrioxamine B (DFB) and desferricoprogen (DFC), are better binding agents for Pb(II) than the monohydroxamates, but the length and structure of linkers connecting the hydroxamate moieties have a significant impact on the complexation and selectivity for lead(II). (iv) The corresponding thio derivatives are significantly better ligands for lead than their parent oxo molecules, but polymeric complexes with poor water solubility are formed in most cases. (v) Out of the hydroxamate derivatives of amino acids the α-ones are the most effective ligands, provided polynuclear species involving the hydroxamate-oxygens, amino-N and hydroxamate-N can be formed.

Keywords: amino acids · cysteine · glutathione · hydroxamic acids · lead(II) · peptides · phytochelatins · selectivity · solution equilibrium · speciation · stability constant · thiolate ligands

1. INTRODUCTION

Lead, a widely distributed metal on Earth, has played an important role for thousands of years in human activities. A large variety of products and also large

quantities of them have been produced and used for many centuries. Although very serious health and environmental problems were known to be associated with this metal and despite very strict regulations regarding its application (e.g., the use of organic lead-containing compounds as antiknock additives in gasoline has been banned in many countries), living beings are still exposed to, and contaminated by lead, both in developed and developing countries. The predominant part of lead absorbed in the body, is found in bones, but it is also known to have a well-defined affinity towards proteins, e.g., serum albumins and zinc finger proteins [1–3]. The toxicity of lead(II), at least to some part, is attributed to the displacement of the physiologically relevant metal ions like zinc(II) or calcium(II) in proteins [1, 4–6]. A detailed discussion of these issues is beyond the aim of this chapter, they will only be explained shortly and will be covered in other chapters of this volume. However, it is worth emphasizing that any knowledge on the complexation of Pb(II) with amino acids and derivatives might provide useful support in understanding the interaction of Pb(II) with large biomolecules because the so-called "side-chain donor atoms" of their amino acid units often play a crucial role in binding of metal ions. This is one reason, why a large part of this chapter will focus on the interpretation of major characteristics of complexation and the main factors affecting the interactions of lead(II) with various amino acids and small peptides. Results on various natural or synthetic thiol-rich molecules being able to bind lead(II) very effectively and sometimes with good selectivity are also emphasized.

In addition to amino acids and oligopeptides, numerous other types of biologically relevant small molecules are known to interact with lead(II) ion and many of them will be discussed in other chapters of this volume. Furthermore, because the analysis of relevant solution equilibrium results is one of the main aims in this chapter, a presentation of results published with molecules, which show a weak interaction with lead(II) and/or form poorly water-soluble or non-soluble oligo- or polynuclear species with lead(II) is beyond our aim. For example, some recently published results on lead complexation with hydroxycarboxylic acids, such as citric acid or tartaric acid will not be discussed [7, 8]. Therefore, in addition to amino acids and small peptides, this chapter will focus only on a few effective lead chelators, such as various hydroxamate-based compounds or hydroxy(thio)pyrones and hydroxy(thio)pyridinones.

Natural compounds, for example, hydroxamic acid derivatives of amino acids are considered as strong binding agents of several metal ions, including Pb(II). Followed by the introduction of a hydroxamate function as effective Pb(II) chelator and also by the main results on lead(II) complexes formed with trihydroxamate-type natural siderophores, the relevant results published with aminohydroxamic acids and also the main conclusions will be shortly presented.

Not only the hydroxamate-based siderophore desferrioxamine B (DFB), but also the best known hydroxypyridinone derivative Dhp (also named Deferiprone) is used as iron-sequestering agent in the therapy of Thalassemian patients and, in several cases, its scaffold is considered as a "privileged" structure in the design of new chelating drugs [9]. Recently published results on Pb(II) complexation of Dhp, together with the relevant results obtained with maltol and thiomaltol will also be covered.

In addition to the effectivity, also the selectivity of lead binding by a certain molecule against related metal ions has a similar importance and is also discussed in a short section.

2. COMPLEXATION OF LEAD(II)

2.1. General Characterization of Lead(II) Complexes

Of the p-block elements, the coordination chemistry of lead(II) has received significant interest during the past several decades. Out of the readily accessible oxidation states of this metal ion the lead(IV) form is easily reduced, but the lead(II) ion is stable and is the most common form of lead in the environment. Consequently, most interest has been focused on the coordination compounds involving the 2+ oxidation state and a wide variety of the ligands has been involved in the studies on complexation with this metal ion. In the investigated ligands not only the types of the donor atom(s) have been varied, but a large variety of open chain and macrocyclic ligands, as well as chelating and non-chelating ones have been studied.

There is no doubt that the following characteristics play a crucial role in the complexation with lead(II) ion:

(i) In aqueous solution, the hydroxide ion can behave as an effective ligand towards this metal ion. This means that OH^- can compete with other ligands in complexation reactions of Pb(II) and this has to be taken into account in the evaluation of equilibrium studies. Critical analysis of previous results published for the Pb(II)–hydroxide ion system concluded that the interaction between these two components starts at about pH ca. 5 in a diluted solution ($c_{Pb(II)}$ = ca. 10^{-3} M) and depending on the analytical concentration of Pb(II) and the pH different mono- and polynuclear complexes are formed. In very diluted solution ($c_{Pb(II)}$ = as low as 10^{-6} M) only mononuclear hydroxo complexes, $[Pb(OH)]^+$, $[Pb(OH)_2]$, $[Pb(OH)_3]^-$, exist [10], but in the concentration range of ca. 10^{-4} to 10^{-3} M polynuclear complexes already dominate above pH 7 [10–12]. The hydrolysis model obtained at $1 \cdot 10^{-3}$ to $4 \cdot 10^{-3}$ M range (I = 0.2 M, KNO_3), together with the stability constants (log β) calculated for the indicated equilibria is as follows [12]:

$$Pb^{2+} + H_2O \rightleftharpoons [Pb(OH)]^+ + H^+: \quad -7.32$$

$$4\,Pb^{2+} + 4\,H_2O \rightleftharpoons [Pb_4(OH)_4]^{4+} + 4\,H^+: \quad -19.98$$

$$6\,Pb^{2+} + 8\,H_2O \rightleftharpoons [Pb_6(OH)_8]^{4+} + 8\,H^+: \quad -42.62$$

(ii) Lead(II) as a central ion can adopt many different geometries in its complexes and also the coordination number can vary within a large range (2–12). These interesting features are associated with the effects of its $6s^2$ electrons, the so-called "inert electron pair". Because knowledge of these effects is of considerable importance in attempts to design ligands for selective binding of lead(II) [13, 14], they are discussed shortly in the following section.

2.2. Effect of the Lone Pair Electrons on Lead(II) Complexation

Divalent lead, with its electronic configuration [Xe] $4f^{14}$ $5d^{10}$ $6s^2$, is one of the post-transition metal elements that exhibits the so-called "inert pair effect". The concept of a chemically inert but stereochemically active $6s^2$ lone pair is commonly associated with this metal ion. Depending on whether the $6s^2$ lone pair causes a spherical or non-spherical charge distribution around the Pb(II) cation, complexes with symmetrical or distorted geometries are formed. Among others, Shimony-Livny et al. [15] have made detailed investigations on the role of the lone pair on the coordination geometry for a large number of Pb(II) complexes. They have classified two general structural types of the studied compounds and named them holodirected and hemidirected structures [15]. In the holodirected complexes the bonds to ligand atoms are directed throughout the whole space, while in the hemidirected ones the bonds are directed only throughout part of the space (see Scheme 1). As a consequence, in the hemidirected (asymmetrical) complexes there is a void in liganding that is not found in the holodirected (symmetrical) ones.

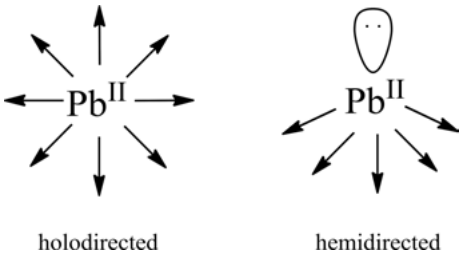

Scheme 1.

Different factors determine whether the attitude of the $6s^2$ electron pair is stereochemically active or inactive in a complex:

(i) The stereochemical activity of the lone pair and hence the geometry of the formed complex, seems to depend strongly on the nature of the donor

atoms (soft or hard), the charge of them, and also the interactions (attractive or repulsive) among the coordinated ligands [1, 15–21]. Namely, hemidirected structures are favored in complexes, in which the ligands are coordinated via their electronegative donor atoms such as oxygen or nitrogen [1]. At the same time, molecular orbital calculations suggest some preference of holodirected stuctures of complexes formed with very polarizable ligands [1, 16].

(ii) The denticity of the ligand and the charge of the donor atoms were also found to be important factors. In complexes containing high denticity ligands hemidirected geometries were found in the presence of donor atoms with a high affinity towards Pb(II). In fact, it was observed that a soft donor atom, such as sulfur, which is usually found in holodirected Pb(II) complexes, was able to enforce a hemidirected structure, when it was part of an anionic group in a polydentate molecule [18].

(iii) An interesting observation is that the stereoactivity of the lone pair correlates with the coordination number. It was quite generally detected that lead(II) compounds are hemidirected when the number of coordinating donor atoms is low (<6), and holodirected if it is high (9 to 10). Both types are found for coordination numbers 6–8 [1, 15, 21].

Stereochemical activity or non-activity of the lone pair in complexes formed between lead(II) and a large variety of N- and O-donor containing macrocyclic ligands was investigated in several studies [20–22]. It was found that in a series of macrocyclic ligands where oxygen donors were replaced by nitrogen ones, a change happens from a stereochemically inactive lone pair to an active lone pair if approximately two or fewer nitrogen donors are present [20]. The importance of steric factors, whether or not the lone pair is stereochemically active, was concluded by detailed spectroscopic investigations and DFT calculations on the Pb(II)-DOTA complex [21]. A very effective chelator of Pb(II), N,N′-bis[(6-carboxy-2-pyridyl)methyl]-4,13-diaza-18-crown-6, was found to coordinate to this metal ion via its 10 donor atoms. In spite of this high coordination number, all X-ray and theoretical calculations supported that the compound is hemidirected and the lone pair of electrons is stereochemically active [22].

Since amino acids, peptides and derivatives have the above mentioned types of donor atoms (N, O or S), and furthermore, their denticities and charges also vary, the information discussed above is useful for the evaluation and interpretation of results on Pb(II) complexes formed with amino acid- and peptide-based ligands or related compounds.

2.3. Correlation between Toxicity, Sequestration, and Complexation of Lead(II)

It is well-known and was also indicated in the Introduction, that lead has widely been used in different human activities during the past thousands of years. Different compounds of this metal have been and in part still are used in industry,

in products such as construction materials, paints, batteries, and piping. In the past century a huge amount of it was also used as gasoline additive. Although the many lead-related health problems led to the implementation of various regulations, such as the introduction of unleaded gasoline in many countries, or the ban of lead-based paints, lead can be found in a wide variety of geochemical environment and it has accumulated there much above its natural level. As a consequence, lead is still a serious environmental poison and people are still being exposed to it.

Despite the numerous studies made on the binding characteristics of Pb(II) in biological systems, many questions are still open. It is clearly known that the absorption and biological effects of lead are modified by numerous factors, including nutritional status, health, and age (e.g., children are much more sensitive to lead exposure than adults) [23]. Likewise, it is known that the predominant part of Pb(II) absorbed into the body is found in bones, but it has also a well-defined affinity towards different biomolecules, such as proteins [1–6, 24, 25]. Evidently, the ability of this non-essential metal to interact with binding sites for essential metal ions is serious because this can result in its ability to gain access to cellular compartments and to disrupt normal biochemical or physiological functions [26]. Therefore, a broad range of dysfunctions can be caused by Pb(II) such as oxidative stress by inducing the generation of reactive oxygen species (ROS) and subsequent DNA damage [1, 27–29]. Thus, lead exposure results in many health problems caused by its toxicity to liver, kidneys, and the nervous system [30–32].

From a coordination chemical point of view, studies focused on the determination of the coordination mode of Pb(II) in proteins are especially interesting [2–6]. For example, the binding sites for Pb(II) in human serum (HSA) and bovine serum albumins (BSA) were determined under physiological conditions using a constant protein concentration and various Pb(II) contents. Fourier transform infrared spectroscopy (FTIR), UV-visible, circular dichroism (CD), fluorescence, and X-ray photoelectron spectroscopic (XPS) methods were used to analyze the binding modes, the binding constants, and the effect of metal ion complexation on the stability and conformations of HSA and BSA. The obtained results showed strong hydrophilic contacts between lead and HSA or BSA, and protein N and O atoms as binding sites were proven. Moreover, Pb(II) was found to alter protein conformation by a major reduction of the α-helical structure from 57 % (free HSA) to 48 % (metal complex) and 63 % (free BSA) to 52 % (metal complex). These changes in the conformation resulted in partial protein destabilization [2]. ^{207}Pb NMR was used to monitor the coordination of Pb(II) to a thiol-rich small molecule, glutathione, as well as to zinc finger proteins and a PbS_3 environment was supported [5]. In another electrochemical work, binding between Pb(II) and the high-abundance bovine serum proteins, serum albumin, bovine transferrin and bovine immunoglobulin as well as the proteome of fetal bovine serum were investigated. Interestingly, the binding constants calculated for the interaction of Pb(II) with the protein mixture was not the sum of the complex stabilities with the single proteins. From these results, effects of protein-protein interactions and microenvironmental influences on lead(II)-protein interactions were concluded [24].

The replacement of physiologically relevant metal ions, like zinc(II) or calcium(II), by Pb(II) in proteins is known from numerous studies [1, 3–6, 25]. To investigate the potential relationship between the existence of Pb(II)-protein complexes and the toxicity of this metal ion, structural properties of Pb(II) and Ca(II) binding sites were compared by analyzing data from the Protein Data Bank. It was concluded that although oxygen is the dominant donor atom for both metal ions, e.g., in calmodulin, there are some differences in the number of liganding sites, geometries, and also in the site of the coordinating donors [4]. A mass spectroscopy study on zinc finger-like peptides led to the observation that whereas lead prefers cysteine-S donors, Zn(II) binds primarily to histidine residues and only secondarily to cysteine ones [3]. In the presence of Pb(II), a significant change in the conformation of the Zn transcription factor IIIA and an inhibition of the formation or decomposition of the adduct formed previously between this protein and DNA was detected [25]. Based on numerous previous results, it is now commonly accepted that the change in the coordination preferences enforced by Pb(II) results in a new environment compared to the native proteins; these imposed structures frequently do not stabilize the proper protein forms and as a consequence, disrupt the normal functions [6, 33].

Although different techniques are known to remove this metal ion from a contaminated environment or living organism [1, 23, 30, 34], often efficiency and mainly selectivity problems arise during the decontamination process. Chelate-forming compounds are the most frequently used Pb(II)-sequestering agents. Because a clear preference of Pb(II) for S-donors over O or N donors and 5-membered chelate rings is known [1, 35], it is not a surprise that penicillamine was the first chelating agent in the treatment of lead poisoning. In addition to this molecule, ligands mainly used nowadays as lead-sequestering chelators include dimercaptosuccinic acid, dimercaptopropane sulfonate, dimercaprol, anti-Lewisite, and $CaNa_2EDTA$ [1, 30, 34] and efforts to find new molecules with higher selectivity are in progress in several laboratories [22, 36–38]. According to the results, it seems relatively easy to achieve good selectivity for Pb(II) over Ca(II) with chelating agents, but this is not the case over Zn(II) because this latter metal ion frequently forms complexes with a similar stability as Pb(II) [20, 36]. Because Pb(II) causes oxidative stress, supplementation of antioxidants (some of them are at the same time also chelating agents) following lead exposure was also studied [28].

3. LEAD(II) COMPLEXES OF AMINO ACIDS AND DERIVATIVES

Amino acids (Table 1) are an important class of biomolecules and can be found in varying concentrations in the various compartments of the body. At pH 7.4 most of these ligands are in the zwitterionic form. In the absence of side chain donor atom(s) all the natural amino acids are capable of metal ion binding via the carboxylate-O and amino-N donors that are in a chelatable position and can form a five-membered chelate. With strongly coordinating side chain donors a

tridentate binding mode is also possible resulting in the formation of complexes with typically higher stability.

As lead(II) is an emerging pollutant, studies on Pb(II)-amino acid interactions date back several decades. Practically all naturally occuring amino acids have been involved in these investigations carried out both in solution and in the solid state. Lead(II) is typically considered as borderline metal ion but its affinity to negatively charged O-donor(s) (e.g., hydroxide ion) is also well known. This difficulty in the classification is also reflected in the wide variety of composition, stability, and detected coordination modes in the amino acid complexes. Nevertheless, sulfur-containing amino acids and derivatives have the highest affinity to the metal ion and will be addressed separately in Section 3.2.3.

Table 1. Amino acids, $H_3^+NCH(R)COOH$, and their acidity constants (pK_a) [39–45].

Name	Symbol*	R	pK_a values
Alanine	Ala	CH_3	2.31, 9.70
Arginine	Arg	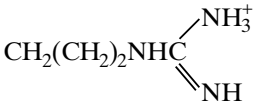	2.03, 9.02 (12.1)
Asparagine	Asn	CH_2CONH_2	2.15, 8.72
Aspartic acid	Asp	CH_2COOH	1.94, 3.70, 9.62
Cysteine	Cys	CH_2SH	1.91, 8.16, 10.29
Glutamine	Gln	$CH_2CH_2CONH_2$	2.16, 9.96
Glumatic acid	Glu	CH_2CH_2COOH	2.18, 4.20, 9.59
Glycine	Gly	H	2.36, 9.56
Histine	His	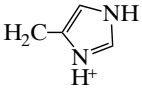	1.7, 6.02, 9.09
Isoleucine	Ile	$CH(CH_3)C_2H_5$	2.21, 9.56
Leucine	Leu	$CH_2CH(CH_3)_2$	2.27, 9.28
Lysine	Lys	$CH_2(CH_2)_3NH_3^+$	2.19, 9.12, 10.68
Methionine	Met	$CH_2CH_2SCH_3$	2.10, 9.06
Phenylalanine	Phe	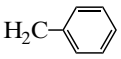	1.9, 10.41
Serine	Ser	CH_2OH	2.13, 9.05
Threonine	Thr	$CH(OH)CH_3$	2.20, 8.96
Tryptophan	Trp	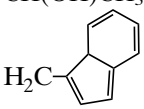	2.34, 9.32
Tyrosine	Tyr	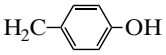	2.17, 9.04, 10.11
Valine	Val	$CH(CH_3)_2$	2.26, 9.49
Proline	Pro	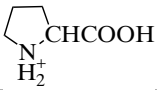	1.9, 10.41

*The symbols stand for the completely deprotonated forms of the amino acids.

Table 2. Stability constants (log β) of Pb(II) complexes formed with amino acids (I = 0.1–3.0 M, T = 298 K).

	$[PbH_2L]$	$[PbHL]$	$[PbL]$	$[PbL(OH)]$	$[PbH_2L_2]$	$[PbHL_2]$	$[PbL_2]$	$[PbL_2(OH)]$	$[PbL_3]$	medium	Refs.
Asn			4.91				7.82		8.82	3 M $NaClO_4$	[48]
Asp		12.28	6.67				9.43			3 M $NaClO_4$	[48]
		11.28	6.02	–3.54						1 M $NaClO_4$	[46]
		11.39	5.95	–2.14						0.2 M KNO_3	[51]
Cys			13.16				19.20		22.47	3 M $NaClO_4$	[48]
		17.35	12.21			27.48	18.57	7.33		3 M $NaClO_4$	[47]
		16.16	12.20	2.04		25.10				1 M $NaClO_4$	[45]
			12.20							0.15 M KNO_3	[54]
	22.72	17.77	13.12	2.49			17.56			0.1 M $NaNO_3$	[55]
	22.28	17.21	12.58	2.09			17.00			0.5 M $NaNO_3$	[55]
	21.93	16.78	12.16	1.79			16.57			1 M $NaNO_3$	[55]
Gln			4.68				8.36		10.12	3 M $NaClO_4$	[48]
Gly		11.88	5.75	–1.89						3 M $NaClO_4$	[57]
		12.60	5.46	–2.77			9.32			1 M $NaClO_4$	[46]
			4.68	–2.84						0.2 M KNO_3	[51]
D-His			5.93		23.35	17.17	10.10			0.1 M KNO_3	[50]
L-His			6.90				9.81			3 M $NaClO_4$	[48]
			5.95		23.39	17.13	10.11			0.1 M KNO_3	[50]
			5.96	–2.28						0.2 M KNO_3	[51]
Leu			5.07	–3.64						0.1 M KNO_3	[56]
Met			4.39	–3.18						0.2 M KNO_3	[51]
Me-Cys			4.43				7.97			0.1 M $NaClO_4$	[53]
			4.05				7.40			0.1 M $NaClO_4$	[52]
			4.49	–3.50						0.2 M KNO_3	[51]
Phe			4.63				8.35			3 M $NaClO_4$	[48]

Ser			5.05				8.27		9.96	3 M $NaClO_4$	[48]
		11.00	4.86	–3.15						1 M $NaClO_4$	[46]
			4.66	–3.53						0.1 M KNO_3	[56]
Trp			4.89				10.27			3 M $NaClO_4$	[48]
D-Pen		17.72	14.32		34.04	27.98	19.05	7.55		3 M $NaClO_4$	[47]
DL-Pen			12.88							0.1 M KNO_3 [a]	[49]
		16.28	13.06	7.33						0.15 M NaCl [b]	[45]
		17.30	13.0							0.15 M KNO_3	[53]
	20.97	17.11	13.37	3.19			16.93			0.1 M $NaNO_3$	[55]
	20.99	16.84	12.93	2.74			16.66			0.5 M $NaNO_3$	[55]
	21.23	16.76	12.66	2.39			16.59			1 M $NaNO_3$	[55]
L-Pen			13.18							0.1 M KNO_3 [a]	[49]
			13.21			26.65	17.52			0.2 M KNO_3	[51]

[a] T = 295 K, [b] T = 310 K.

In the field of solution equilibrium studies typically pH potentiometry was carried out to estimate the stoichiometry and thermodynamic stability constants of Pb(II) complexes. As $PbCl_2$ has a limited aqueous solubility, the measurements are made in a perchlorate or nitrate medium. Table 2 provides an overview on the literature data of the stability constants of various amino acidato complexes.

With respect to other types of interactions, structures of some bare and hydrated $[Pb(aminoacidato)]^+$ complexes were studied using infrared multiple photon dissociation spectroscopy (IRMPD) [58], the water binding energies of $[Pb(aminoacidato)H_2O]^+$ species were determined by blackbody infrared radiative dissociation [59], and correlation between bond activation and gas-phase acidity of lead(II)-aminoacidato complexes was also investigated [60].

3.1. Complexes of Amino Acids with Non-coordinating Side Chains

Based on equilibrium studies, typically carried out by pH potentiometry, stability constants of the Pb(II) complexes of glycine [46, 57] and various amino acids containing hydrophobic [45, 48] and polar [45, 46, 48] non-coordinating side chains were published. The results supported an interaction of Pb(II) with simple amino acids only above pH 5 and hydrolysis started at pH ca. 8 [51]. The complexation scheme in these systems is relatively simple. A monoprotonated [PbHL] complex was found with Gly in a few cases [46, 57], mono- and bis-complexes (in one work also some tris-complexes with Asn and Gln [48]) were found and just before the precipitation of hydroxo complexes, formation of a mixed hydroxo species, $[PbH_{-1}L]$, was suggested (see Table 2). Comparison of the data reveals that for this class of 1:1 complexes, where (NH_2,COO^-)-coordination can be assumed, the log β values are in the range 4.4 to 5.1, while the $[PbL_2]$ ones in the range 7.8 to 8.4, obeyed the expected statistical considerations. These values are roughly one log unit higher than those of the corresponding Cd(II) complexes and comparable with those of the Zn(II) ones for this type of amino acids [61].

In recent years numerous studies of solid state structures of such complexes have also been reported; these are discussed in Chapter 7 of this book and are only shortly mentioned here. With valine $[Pb(Val)_2(H_2O)_2(NO_3)_3]$ coordination of one monodentate and one bidentate carboxylate function was identified [62]. Based on X-ray diffraction, the PbO_8-type complex has a holodirected structure. In the case of a phenylalanine complex, $[Pb(Phe)_2]_n$, that was also characterized by elemental analyses, IR, and ^1H NMR spectroscopy, the single crystal structure shows that the complex is a 2D chain polymer due to phenylalaninate bridging [63]. With proline a single crystal X-ray structural analysis of $[Pb(Pro)_2(H_2O)]_n$ shows that the (NH,COO^-)-coordinated complex is a 1D chain polymer as a result of water bridging. The chains interact with each other via weak Pb···O interactions and hydrogen bonding to create a 2D framework [64]. In both of the above complexes the coordination number of the Pb(II) is six, PbN_2O_4, with

"stereo-chemically active" electron lone pairs and a hemidirected coordination sphere [63, 64]. In a solid state ^{207}Pb NMR and X-ray diffraction study [65] by Gasque et al. $[Pb(IleH)_2(NO_3)(H_2O)_2]NO_3$, $[Pb_2(ValH)_5](ClO_4)_4 \cdot 2\,H_2O$, and $[Pb(Leu)(NO_3)]$ were found to contain a seven-coordinated metal ion surrounded by mono- and bidentate carboxylates for the protonated Ile and Val complexes, while (NH_2,COO^-)-chelation occurs in the case of the Leu compound [65]. Both the Leu and ValH complexes are 1D polymers. In a more recent study on the Pb(II)-Phe, -Ile, -Val, and -Arg systems, complexes with 1 : 2 stoichiometry and carboxylate coordination of the first three ligands occur, while a $[Pb_2(OH)_2(HArg)_3(NO_3)_7]$ cluster for the latter one was identified by single crystal X-ray diffraction [66].

3.2. Complexes of Amino Acids with Coordinating Side Chains

N/O/S donor atom(s) in the side chains of amino acids are also capable of participating in metal ion binding if they are in a chelatable position to the amino and/or carboxylate moiety or have an exceptionally high affinity to the metal ion. Although the increased stability of amino acid complexes with subsequent carboxylate (Asp, Glu), hydroxyl (Tyr, Thr, Ser), amino (Orn, Lys) or imidazole N (His) side chains cannot be ruled out either, owing to the high preference of Pb(II) toward sulfur donors, for the thiolate containing Cys and Pen a significant increase in stability or alteration in the nucleation of the complexes can be expected.

3.2.1. Complexes of Amino Acids with Side Chain O Donors

Even though data on the stoichiometry and stability constants of the lead(II) complexes with these ligands available in the literature are rather scarce, it is evident that the presence of a –OH group does not play a measureable role in metal ion binding. A slight stability increase, however, can be assumed with Asp suggesting tridentate coordination of the ligand in solution with the involvement of the second carboxylate group too. Solid state results on $[PbAspH(NO_3)]$ revealed its 3D polymeric structure with each Pb(II) coordinated to five carboxylate and one nitrate oxygen atoms and the bridging role of both the α- and the β-carboxylates [65, 67]. For [PbAsp], however, the involvement of the amino group in the coordination was also suggested based on spectroscopic data [67]. In the case of 3,5-dinitrotyrosine (dnTyr), having a phenolic OH in the side chain, the solid state structure of $[Pb(dnTyr)(0.5\,H_2O)]$ revealed a tetradentate bridging coordination of the ligand to three Pb(II) via a (NH_2,COO^-)-chelate; the other carboxylate-O binds in a monodentate manner as does the phenolate-O [68].

3.2.2. Complexes of Amino Acids with Side Chain N Donors

In principle, Lys and Orn are capable of tridentate coordination too due to the presence of an NH_2 group in the side chain, however, this donor atom would

form large (eight or seven membered) chelates with the (NH_2,COO^-) set in the metal complex and this is disfavored. The very little information on the complex-forming behavior of these amino acids in solution with Pb(II) seems to support the general trend that the side chain amino groups do not increase the thermodynamic stability of the metal complexes but may alter their stoichiometry owing to the positive charge of these functions below pH 9.

As it is generally known, histidine with the imidazole group in the side chain is one of the most important binding sites for various metal ions in biological systems. Unlike with Lys or Orn, with His stable six-membered fused (NH_2,COO^-,N_{im})-type chelates can be formed in the metal complexes. As the data in Table 1 clearly reveal, an increased stability for the Pb(II)–His species supports the above mentioned tridentate coordination. This behavior was further proven with NMR measurements by the comparison of the chemical shift values of the C2(H) and C(5)H signals of His in the absence and presence of Pb(II) [51]. Although the low affinity of Pb(II) toward aliphatic N donors is found in many cases, the direct and strong interaction in the Pb(II)-N-methylimidazole system counts for the increased affinity of the metal ion even for the imidazole N as single donor [69].

3.2.3. Complexes of Amino Acids and Analogous Ligands Containing Sulfur Donor Atoms

Owing to the high preference of Pb(II) toward the sulfur donor atom with soft character, a strong interaction with this subclass of ligands can be expected. Thioether S donors in Met, S-methyl-cysteine (MeCys) or related ligands, however, are characterized by a rather low basicity compared to the thiolate-type S donor atoms in Cys, Pen or other derivatives (Table 1). This remarkable difference is also reflected in the large difference of the thermodynamic stability of the Pb(II) complexes between these two types of sulfur-containing molecules. Solution studies with Met or MeCys indicated that a negligible increase in the stability of the Pb(II) complexes with these ligands compared to the Gly complexes with a possible (NH_2,COO^-)-coordination can be observed (see the data in Table 2). Furthermore, unlike Asp or His, the thioether-type amino acids, Met or MeCys, are unable to prevent Pb(II) hydrolysis at elevated pH indicating the lack of involvement of these S donors in Pb(II) binding [51]. On the contrary, complexes with high thermodynamic stability are reported for the Cys- and Pen-containing systems (Table 2), though in some cases equilibrium studies were hindered by the formation of a precipitate in aqueous solution due to polymerization of the complexes [51]. The increased stability, e.g., of the [PbL] species with Cys or Pen compared to that of Gly, unambiguously supports the involvement of the thiolate moiety and therefore the likely tridentate coordination of these ligands via the (NH_2,COO^-,S^-)-donor set. Coordination of the second Pen to [PbL], however, was shown to be disfavored due to steric hindrance by the $6s^2$ lone electron pair of Pb(II). As a consequence, depending on the pH range, [$PbHL_2$] or [PbL_2] complexes were detected with non-coordinating ammonium or amino groups of the second ligand, respectively [51].

Jalilehvand et al. [70] studied the Pb(II)-D-Pen system in the range $9.6 < pH < 11.0$, $10\ mM < c_{Pb(II)} < 100\ mM$ using up to a ten-fold excess of ligand. The combined spectroscopic (UV-Vis, EXAFS, NMR, XANES) and ESI-MS results are consistent with the existence of a 1 : 2 Pb(II) : Pen complex as major species with $(NH_2,COO^-,S^-)(S^-)$-coordination [70]. With Cys, under very similar conditions, a mixture of species with $(NH_2,S^-)(NH_2, S^-)$- and $(NH_2,COO^-,S^-)(S^-)$-chelating sets, were identified at low (2–3) Cys/Pb(II) mole ratios. At high (> 0.7 M) Cys concentration a tris-complex with $(NH_2,S^-)(S^-)(S^-)$-coordination was also proven to occur [71]. Results on the Pb(II)-N-acetylcysteine system by the same group applying the same methodology revealed that at a ligand-to-lead(II) mole ratio of 2.1 thiolate-bridged dimeric or oligomeric species, in which three S-donors are coordinating to the metal ions, are likely, while at higher ligand excess a trithiolate $[Pb(NAC)_3]^{4-}$ complex is present as major species [72].

Besides solution studies, a large number of solid state reports are also available in the literature on the sulfur-containing amino acid systems. In an early IR study on the Pb(II)-Cys system tridentate coordination of the ligand with a strong Pb-S interaction was suggested [73]. The molecular structure of [Pb(D-Pen)] accessed by X-ray diffraction provided direct proof for (NH_2,COO^-,S^-)-coordination [74]. Redetermination of the molecular structure of $[Pb(D\text{-}Pen)]_n$ indicated that Pen coordinates to Pb(II) in a (NH_2,S^-,COO^-)-tridentate mode. While the S atom acts as a bridge to two neighboring Pb(II), thereby forming a double thiolate chain, the coordinating carboxylate O forms bridges to the metal ions in the adjacent chain [75].

4. LEAD(II) COMPLEXES OF HYDROXAMIC ACIDS, RELATED SMALL LIGANDS, AND HYDROXAMIC ACID DERIVATIVES OF AMINO ACIDS

Hydroxamic acids contain the hydroxamic moiety, $R_CC(O)NR_NOH$ ((R_C = alkyl/aryl; R_N = alkyl/aryl or H). This weakly acidic chelating group can be obtained via the reaction of a carboxylic acid derivative with hydroxylamine or alkylated/arylated hydroxylamines, and, depending on the substituents, the pK values typically fall into the range 8.2 to 9.5 [76]. The hydroxamic acids are important bioligands with numerous applications in nature and medicine [77, 78]. For example: (i) one type of the microbial siderophores involve hydroxamic functions (most commonly three) to chelate iron(III) with perfect selectivity in complexes with extremely high stability and transport this metal ion into the cells in adequate amount; (ii) a trihydroxamate-based siderophore, desferrioxamine B (DFB), as sequestering agent, has been clinically used for decades to treat iron-overload desease or aluminum poisoning; (iii) antifungal, antimalarial, and anticancer properties of hydroxamate-based compounds are also well known [77, 79, 80].

As ligands, hydroxamic acids typically coordinate to metal ions via a 5-membered (O,O)-chelate (through the carbonyl oxygen atom and the deprotonated

hydroxyl group), but other types of coordination modes, such as monodentate coordination via one of the oxygens or the deprotonated hydroxamato-N atom are also known [76, 78, 80, 81]. In addition, metal ion-induced deprotonation of a hydroxamato moiety (with or without coordination of the N-donor), where both the N and O atoms of the hydroxamic acid are deprotonated (named as hydroximate moiety), can also occur [81, 82]. With the involvement of the hydroximato group, formation of polynuclear metallacrown-type complexes is especially interesting [83, 84].

The complexation behavior of hydroxamic acids can be enhanced by the incorporation of ancillary coordinating groups, such as an amino group in amino acid derivatives, at adjacent sites in the molecule [85].

Most of the investigations made on metal complexes with various hydroxamic acids have been performed on Fe(III) complexes, but numerous other metal ions, including Pb(II) have been involved in some studies. Investigations on Pb(II)-hydroxamic acid and -aminohydroxamic acid complexes have been initiated by the following goals: to obtain new information for the development of effective and selective chelating agents for binding this toxic metal ion and/or to investigate different hydroxamate-based compounds as potential Pb(II)-sequestering or -mobilizing agents [12, 86–93]. The results obtained and discussed below show that hydroxamate-based compounds can be highly effective chelators of Pb(II).

4.1. Complexes with Mono- and Dihydroxamic Acids

The first solution equilibrium results on Pb(II) complexes formed with a simple monohydroxamic acid, acetohydroxamic acid (HAha), were published many decades ago by Anderegg et al. [86]. They and later also others found that in the maximum two Aha ligands, through two 5-membered (O,O)-chelates, coordinate to a Pb(II) ion, and, as it can be seen in Table 3, only the basicity differences appear in the differences of stability constants of the complexes formed with Aha and another simple monohydroxamate, *N*-methyl-acetohydroxamate (MeAha) [87]. Interestingly, however, the stability of the hydroxamate-type chelate formed with *N*-methyl-acrylhydroxamate (MeAcrha) is higher than expected on the basicity. In this latter case, the conjugation between the double bond and the hydroxamate moiety (they are situated in β-position to each other), was suggested to increase the stability of the chelate. Any such indication was not observed for the Pb(II)-induced H release from the hydroxamic NH of (O,O)-coordinated Aha, but the hydroxide ion was found to compete with this ligand as well as with other studied monohydroxamic acids above pH ca. 8 and the formation of a mixed hydroxo complex with the stoichiometry $[PbH_{-1}L]$ was found [87].

Complexation between Pb(II) and several desferrioxamine B (H_4DFB) model dihydroxamic acids, namely $HO(CH_3)NCO\text{-}(CH_2)_x\text{-}CO\text{-}NH\text{-}(CH_2)_yCON(CH_3)OH$ (x = 2–3; y = 2–5; the compounds are abbreviated as H_2(2,5-DIHA), H_2(2,4-DIHA), H_2(2,3-DIHA), H_2(2,2-DIHA), H_2(3,4-DIHA), and H_2(3,3-DIHA), respectively), have been studied. The linker in H_2(2,5-DIHA) is exactly the same as the two ones in H_4DFB. Potentiometric pH measurements, spectrophotome-

Table 3. Protonation constants of the ligands (log K) and stability constants (log β) of various Pb(II)-monohydroxamate complexes at T = 298 K and I = 0.2 M (KNO_3) [87].

Species	**Aha**	**MeAha**	**MeAcrha**
	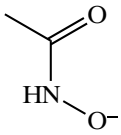	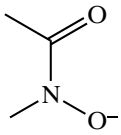	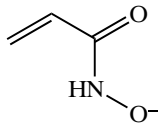
	log K		
$[L]^-$	9.24	8.68	8.35
	log β		
$[PbL]^+$	6.56	5.83	6.18
$[PbL_2]$	10.72	9.53	10.75
$[PbH_{-1}L]^-$	–2.46	–3.4	–2.7

try, NMR, and ESI-MS supported the chelation of Pb(II), and also the fact that only 1 : 1 complexes ([PbHL] mono-chelated and [PbL] bis-chelated) are formed. Coordination of more than one dihydroxamic acid to a lead(II) ion was not found even at ligand excess. This means that the maximum coordination number is 4 (the same as was found with the monohydroxamic acids). A distorted geometry of the complexes caused by the large space requirement of the stereoselectively active lone electron pair of Pb(II) was assumed, and this resulted in the packed arrangement of the two coordinated hydroxamates in the bis-chelated complexes. This arrangement of the coordinated chelates was suggested by the highest stability of the bis-chelated complex, [PbL], with 2,2-DIHA, in which the shortest linker between the two chelating functions exists [12].

4.2. Complexes with Trihydroxamate-Based Natural Siderophores

Trihydroxamate-based microbial siderophores are very effective Fe(III) chelators [88], but they are also able to bind other metal ions, including Pb(II), with high stability. Out of these natural compounds, the most well-known and most extensively studied is desferrioxamine B (H_4DFB) (Scheme 2), which, as mentioned above, has been used in the clinical practice as one of the metal ion-sequestering agents [79]. This fact and also the possibility of immobilization of Pb(II) by microbal siderophores in soil have initiated several investigations on the Pb(II)-DFB system [87, 89–93]. The only other hydroxamate-based siderophore, which was also involved in a detailed equilibrium investigation with Pb(II), is desferricoprogen (H_3DFC) [87]. The formula of the completely protonated forms of the two siderophores (H_4DFB and H_3DFC), together with the corresponding logarithmic dissociation constants (pK_a values), are shown in Scheme 2.

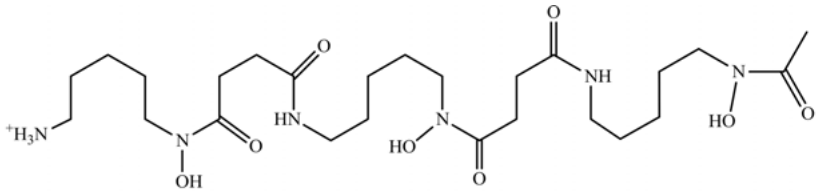

H_4DFB^+, $pK_1 = 8.33$ $pK_2 = 8.96$ $pK_3 = 9.52$ $pK_4 = 10.85$

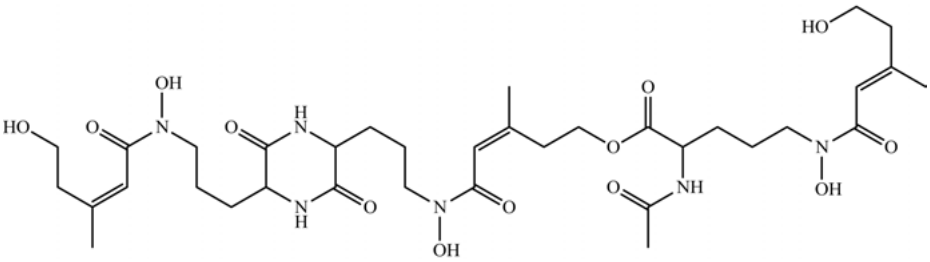

H_3DFC, $pK_1 = 7.93$ $pK_2 = 8.84$ $pK_3 = 9.82$

Scheme 2.

Stability constants calculated from the overall values in Ref. [87] for the different stepwise processes in the Pb(II)-DFB and -DFC systems are summarized in Table 4.

The values in Table 4, which refer to the formation of the 1 : 1 complexes of DFB are in quite acceptable agreement with the ones published in other papers [86, 89], but the value for a dinuclear species, $[Pb_2H_2L_2]$, is found only in [89] and that for a trinuclear species, $[Pb_3H_2L_2]^{2+}$, in [87]. In Table 4 coordination of one hydroxamate chelate of this siderophore is indicated by the value for $[PbH_3L]^{2+}$; the other two hydroxamic functions plus the terminal ammonium moiety still carry dissociable protons. Two hydroxamic functions are already de-

Table 4. Logarithmic stability constants (log K) calculated for the indicated equilibria of the Pb(II)-DFB and Pb(II)-DFC complexes [87].

Equilibrium	**log *K***	
	DFB	**DFC**
$Pb^{2+} + L \rightleftharpoons [PbL]$	10.05	13.0
$Pb^{2+} + HL \rightleftharpoons [PbHL]$	10.13	11.24
$Pb^{2+} + H_2L \rightleftharpoons [PbH_2L]$	9.36	–
$Pb^{2+} + H_3L \rightleftharpoons [PbH_3L]$	5.78	–
$3\,Pb^{2+} + 2\,L \rightleftharpoons [Pb_3L_2]$	–	36.9
$3\,Pb^{2+} + 2\,HL \rightleftharpoons [Pb_3H_2L_2]$	32.72	–

protonated and coordinated in the $[PbH_2L]^+$ complex, the stability constant of which (Table 4) is similar to the constants of $[PbL_2]$ complexes of monohydroxamic acids (Table 3). Compared to the constant of $[PbH_2L]^+$ ($\log K = 9.36$), the value, which belongs to the formation of [PbHL] ($\log K = 10.13$) is only slighly higher. Although there is some contradiction in the literature, whether a third hydroxamate chelate can or cannot be accepted by Pb(II) [87, 89, 90, 92], the results suggest that coordination of two hydroxamate moieties occurs in the maximum to Pb(II). A similar binding mode in $[PbL]^-$ compared to [PbHL] is suggested, they differ only in the protonation stage of the non-coordinated terminal amino moiety. These suggestions are supported also by the favored capability of DFB to bind Pb(II) excess in di- or trinuclear-type complexes. For example, in the millimolar concentration range, even at a 1 : 1 metal to ligand ratio ca. 70 % of the metal ion exists in the trinuclear complex [87]; its suggested binding mode is depicted in Scheme 3.

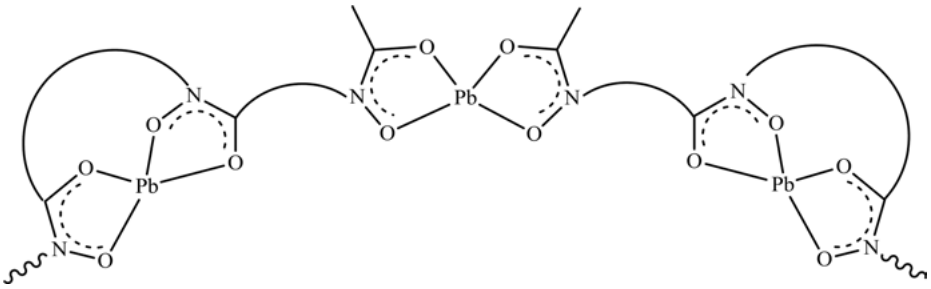

Scheme 3.

Unexpectedly, a significantly different behavior of DFC was found in its interaction with Pb(II) compared to that of DFB. In fact, dissociable protons of H_3DFC are displaced at lower pH compared to H_4DFB^+ and in highly overlapping processes. As a result, it was not possible to calculate a stability constant for the monochelated species $[PbH_2L]^+$ and the values obtained for [PbHL] and especially $[PbL]^-$ with DFC were significantly higher than the corresponding ones with DFB. An almost negligible ratio of the metal ion was found in the trinuclear complex of the Pb(II)-DFC system at a 1 : 1 metal to ligand ratio (this was ca. 70 % with DFB). All the mentioned results demonstrate that DFC is a significantly more effective Pb(II) chelator than DFB. The reason for this difference obviously originates from some structural difference(s) of the ligands. In this respect, out of the several differences existing between the linkers of DFC and DFB, the double bond in β-position to each hydroxamic function in DFC, was suggested to be the most significant one [87]. Like in the situation with the monohydroxamate MeAcrha (see Table 3), a conjugation between the double bonds and the hydroxamate moieties results in an increased electron density at the carbonyl-O and an increased stability of the hydroxamate chelates with DFC. Furthermore, also some involvement of the $6s^2$ electrons of Pb(II) in the coordi-

nation and a higher symmetry allowing more favored binding of three hydroxamates to Pb(II) with DFC compared to DFB was assumed [87].

4.3. Complexes of Thiohydroxamic Acids

In thiohydroxamic acids, the carbonyl oxygen of the hydroxamic function is replaced by a sulfur atom ($R_CC(S)NR_NOH$). The very large overall stability constant (log $\beta_2 = 20.7$ in a 70 % 1,4-dioxane-water mixture) for the bis-complex of Pb(II) formed with *N*-phenylthiobenzohydroxamic acid was published some decades ago [94]. This result initiated a project in the laboratory of Raymond, in which several new mono- and bis-thiohydroxamic acids have been synthesized as potential and powerful Pb(II)-specific sequestering agents and their Pb(II) complexation was studied [95–98]. In addition to derivatives of simple monohydroxamic acids, *N*-methylthiobenzohydroxamic acid, *N*-methylthioacetohydroxamic acid, *N*-methyl-3-pyridothiohydroxamic acid, *N*-cyclohexyl-phenylacetothiohydroxamic acid [95, 97], also a derivative involving a cyclic thiohydroxamato moiety [96] was synthesized and investigated. Bis-complexes formed with Pb(II), one of these was characterized in the solid state [96].

According to the X-ray results, the thiohydroxamic acids typically formed bis-complexes with a coordination number of five. Two isomers were found in all cases. One of them contained both sulfurs in the equatorial plane, while the other involved one sulfur and one oxygen in these positions. In either case, the lone pair occupied a position in the equatorial plane of the trigonal bipyramidal geometry [95–97]. Unfortunatelly, the above mentioned ligands (and also their complexes) had poor water solubility. To overcome this handicap and also to increase further the thermodynamic stability of the Pb(II) complexes, a series of bis-thiohydroxamic acids with linkers of varying lengths and rigidities as well as their Pb(II) complexes were synthesized and characterized. Unfortunately, instead of discrete mononuclear complexes, polymers were found to exist in most cases [98].

4.4. Complexes of Aminohydroxamic Acids

In aminohydroxamic acids the carboxylic moiety of the parent amino acid is modified to a hydroxamic one (deprotonated form: hydroxamate). In a recent study [99], complexation of many aminohydroxamates, DL-α-alaninehydroxamate (α-Alaha), sarcosinehydroxamate (Sarha), DL-*N*-methyl-α-alaninehydroxamate (*N*-Me-α-Alaha), β-alaninehydroxamate (β-Alaha), L-aspartic acid-β-hydroxamate (Asp-β-ha), L-glutamic acid-γ-hydroxamate (Glu-γ-ha) and L-histidinehydroxamate (Hisha), with Pb(II) in aqueous solution was investigated by pH potentiometry, ^{1}H NMR, and ESI-MS and the effects of α-, β- or γ-amino-N, together with additional so called "side chain" donors on Pb(II) complexation were evaluated [99]. If the analytical concentrations were within the range of ca. 10^{-3} to 10^{-1} M, measurable complexation, via competition between the Pb(II)

and the corresponding dissociable proton(s), starts at pH ca. 3.5. At this pH both the amino and hydroxamate moieties of the non-complexed ligands and in the case of Hisha also the imidazole group are still in the protonated form. With these ligands, as bonding isomers, in addition to the formation of the so called hydroxamate-type (O,O)-chelate (Scheme 4, structure **I**), if R_N = H, also "amine-type" (N,N)-chelates (structure **II,** x = 1–3) through the amino-N and deprotonated hydroxamate-N donors can be formed, and, if the ligand is Asp-β-ha or Glu-γ-ha, formation of an "amino acid-type" (N,O)-chelate (structure **III**) can be expected as well.

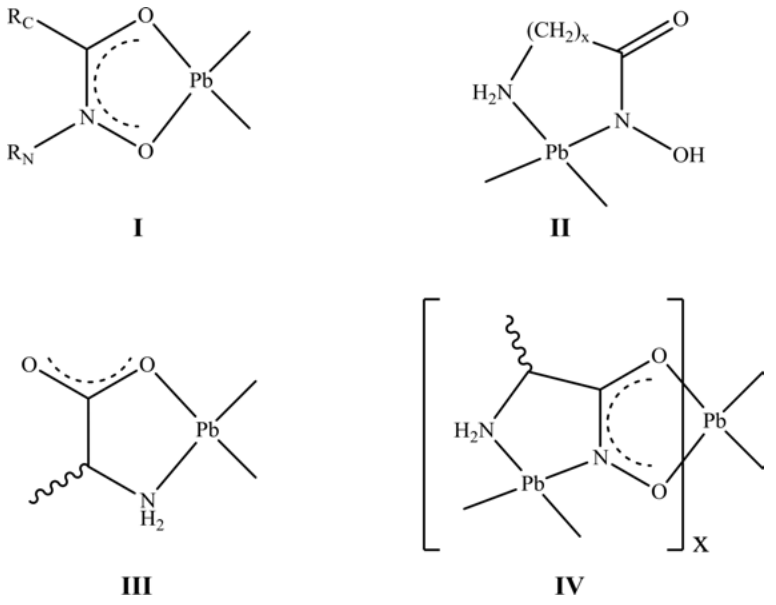

Scheme 4.

In all the systems studied, predominance of the hydroxamate-type coordination was supported by ^{1}H NMR results and also by the fact that the stability constants obtained for the mono- and bis-chelated complexes containing amino-hydroxamate, [PbL] and [PbL_2], are similar to those of the corresponding complexes with Aha (Table 1). Further evaluations can be made, e.g., by calculating the pH-dependent conditional stability constants for the different types of possible chelates and comparing them with each other. The dominant coordination modes follow from the relative stability order of the possible chelates. To calculate the conditional stability constants for the different linkage-isomers of [PbL], the following ligands were selected: L = Aha for (O,O)-hydroxamate-type chelate, L = en for the "amine-type" (N,N) coordination, and L = Gly for the "amino acid-type" (N,O)-chelate. Because higher-membered chelates are usually less stable than the corresponding 5-membered ones, these were not considered in the evaluation.

The calculated pH-dependent conditional stability constants are depicted in Figure 1. The corresponding overall stability constants (log β_{PbL}) were taken from [45, 51, 99]. The conditional stability constant can be defined as:

$$\beta' = \beta_{PbL}/\alpha_H$$

where β_{PbL} = the corresponding overall stability constant, β_{HiL} = the protonation constants of the ligands [45, 51, 99].

$$\alpha_H = 1 + \sum_{i=1}^{n} \beta_{H_iL}[H]^i$$

L = totally deprotonated form of Gly, en, and Aha; n = number of protons competing with the formation of the chelate. This value is 1 in the case of the hydroxamate function, 2 for the other two types of chelates.

Figure 1 shows that the conditional stability constant of the hydroxamate-type O,O-chelate is the highest through the whole evaluated pH range. This supports the hydroxamate-type chelate coordination in the [PbL] complex with hydroxamic acid derivatives of simple amino acids.

Compared to the corresponding stability constants obtained for the complexes of simple aminohydroxamic acids, somewhat higher values (0.5 to 1 log units) of the complexes formed with Asp-β-ha and Glu-γ-ha were found. This was explained by the additional coordination of the β- and γ-carboxylates present in these ligands, respectively [99].

Significant differences between the coordination modes of α- and β-/γ-derivatives were observed above pH 6, where the ammonium group starts to release its proton. All results indicate that primary α-amino acid derivatives, i.e., α-Alaha, Sarha, Hisha (R_N = H), parallel the hydroxamate-type (O,O)-chelate, forming in addition a five-membered (N,N)-type chelate (Scheme 4, structure **IV**). In these

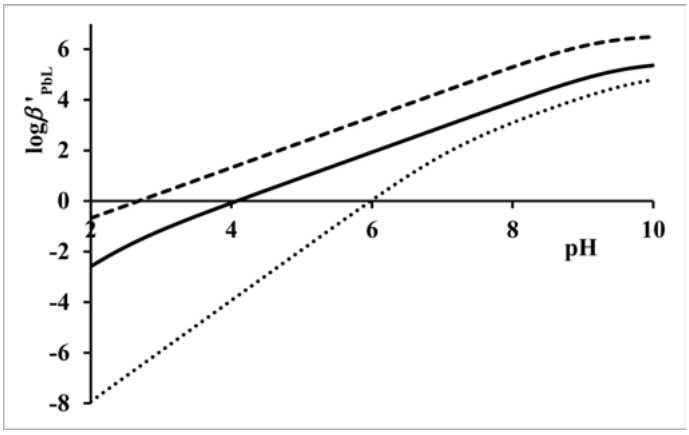

Figure 1. pH dependence of the conditional stability constants (log β'_{PbL}) of Pb(II)-Aha (----), Pb(II)-Gly (——), and Pb(II)-en (· · · · · ·).

stable, most probably polynuclear complexes, a 1:1 metal to ligand ratio was found and the stoichiometric formula of these species is $[PbH_{-1}L]_x$ [99].

The possibility of an even stronger interaction was checked by using the newly synthesized dipeptidedihydroxamic acids, AlaAlaNHOH and AlaAlaNMeOH, as ligands for Pb(II). With the former molecule, if both of the N-terminal amino and C-terminal hydroxamate moieties would coordinate to the same metal ion in joined chelates via the deprotonated and coordinated peptide-amide this would result in the formation of a complex with very high stability. Unfortunately, all the results obtained by pH potentiometry, ^{1}H NMR, and ESI-MS do not support this hypothesis. The two ends of these molecules were not found to coordinate simultaneously to the same Pb(II), but, to some extent, they linked two different metals ($[Pb_2L_2]$), and also different bonding isomers of [PbL] were formed [51].

4.5. Hydroxy(thio)pyrones and Hydroxy(thio)pyridinones as Lead(II) Chelators

Besides various hydroxamate-based compounds, also simple heterocyclic molecules, involving a 6-membered ring and being effective metal ion chelators in their deprotonated forms, received increasing interest as potential metal ion-sequestering and/or therapeutic agents [5]. In recent years this interest initiated some studies on their Pb(II) complexes. Inspired by previous work on the solid state Pb(II)-3-hydroxy-1,2-dimethyl-4-pyridinonato (Pb(II)-Dhp) dinuclear bis-complex [100], Pb(II) complexation in solution has been investigated with 3-hydroxy-2-methyl-4-pyrone (maltol, HMalt), and its two derivatives, 3-hydroxy-2-methyl-4*H*-pyran-4-thione (thiomaltol, HThiomalt) and 3-hydroxy-1,2-dimethyl-4-pyridinone (HDhp) (see Scheme 5 for their general formulae) [101]. The acidity order of the hydroxyl goups in these molecules is HThiomalt > HMalt > HDhp. In Dhp (its completely protonated form is H_2Dhp^+), although the existence of different bonding isomers is assumed, the first protonation constant is attributed to the negatively charged oxygen on the pyridinone ring while the second one is attributed to the N-pyridinyl group [101].

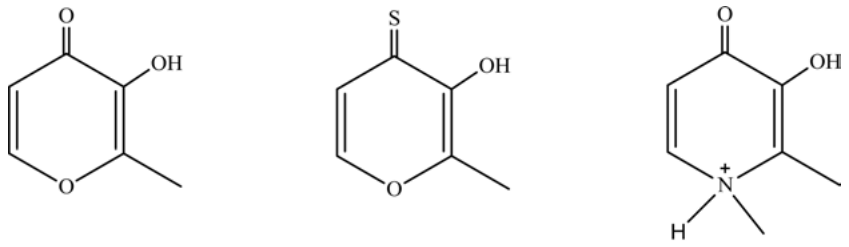

HMalt **HThiomalt** **H_2Dhp^+**

Scheme 5.

In the solid dimeric complex, each Pb(II) was found to have five oxygens in its coordination sphere and the arrangement of these oxygens strongly indicated the stereoactive behavior of the $6s^2$ lone pair [100].

In solution, out of the studied ligands, the (S,O)-chelating thiomalt was found to form the most stable mono-, bis-chelated, and dinuclear-type species, $[PbL]^+$, $[PbL_2]$, and $[Pb_2L_3]^+$, but limited water solubility hindered the examination of this system above pH 7. The Pb(II)-binding abilities of Malt and especially Dhp were proven to be still very good. At a 1:2 Pb(II) to ligand ratio only two complexes, $[PbL]^+$ and $[PbL_2]$, were found to exist in measurable concentrations below pH 9. Above this pH mixed hydroxo species, $[PbH_{-1}L]$, appeared with both ligands, but $[PbL_3]^-$ formed only with Dhp. The significantly increased Pb(II)-binding ability of Dhp compared to Malt was partly attributed to the higher basicity of the former ligand, but besides this, also the possibility of some involvement of the $6s^2$ lone electron pair of Pb(II) in the bonding with Dhp was suggested. Furthermore, Dhp, compared to Malt, was found not just to be a more effective Pb(II) chelator, but also to bind Pb(II) with a rather good selectivity against Zn(II) [101].

5. COMPLEXES OF LEAD(II) WITH SMALL PEPTIDES AND RELATED LIGANDS

Since the typical coordination sites of amino acids, the carboxylate and amino functions, are not in chelatable position to each other in common oligopeptides anymore, in the absence of further side chain donor atoms, strong metal ion binding can only be expected with the involvement of the amide-N as donor after metal ion-assisted deprotonation has occurred. This is unambiguously supported by a huge number of data on various metal (e.g., Cu(II), Ni(II), Zn(II)) complexes obtained both in solution and in the solid state. Up to date, Pb(II)-assisted deprotonation of the peptide bond, however, has not been reported, most likely owing to the low affinity of this metal ion to amide-N. Therefore, common oligopeptides without strongly coordinating side chain donor atom(s) have to be classified as weak Pb(II) binders. This is also in accord with the small number of publications on this topic.

Owing to the borderline character of Pb(II) and its high affinity to the S^- of Cys and other thiol-containing amino acids together with oligopeptides containing these amino acids, formation of Pb(II) complexes with high stability and often remarkable selectivity can be expected. The vast majority of papers on Pb(II)-peptide interactions, therefore, deals with cysteine-containing peptides focusing especially on complexes with glutathione, phytochelatins, and thioneins. Since several chapters of this book are devoted to this important class of ligands, the aim of the following sections is restricted to the discussion of (i) the Pb(II) complexes of common small oligopeptides regarding their structural features, binding modes, and thermodynamic stabilities (Section 5), and (ii) the Pb(II) complexes of peptides containing Cys or related ligands with an emphasis on glutathione and some structural models of phytochelatins (Section 6).

5.1. Complexes of Peptides with Non-coordinating Side Chains

Studies on the interaction of lead(II) with common di- or tripeptides having non-coordinating side chains are very limited. In earlier ^{1}H NMR, potentiometric, and calorimetric studies polyglycine peptides ($(Gly)_n$, n = 2–4) were shown to interact with Pb(II) via a C-terminal COO^- coordination below pH 4, while a (NH_2,CO) binding fashion was suggested above pH 4 in 1 : 1-type species [57, 102]. Recent results of equilibrium work on the Pb(II) systems with GlyGly, GlyVal, and GlyGlyGly revealed the formation of 1 : 1 complexes with different protonation degrees as major species in aqueous solution [51]. Based on potentiometric evidence, in [PbHL] coordination of the terminal carboxylate occurs while in [PbL] that of the (NH_2,CO)-chelating set is likely but the ligands are not capable of preventing the metal ion from partial hydrolyis at pH = 7.4 even at a 1 : 2 metal ion to ligand ratio [51]. The reported values ($\log \beta_1 = 2.73$–3.35) for [PbL] of these di- or tripeptides are similar to that of [CdL] ($\log \beta_1 = 2.86$) for GlyGly [103] but smaller than that of [ZnL] for the same ligand ($\log \beta_1 = 3.75$) [104] indicating that common dipeptides are better ligands for essential transition metal ions, that is, Cu(II), Ni(II), Co(II) or Zn(II), than for the toxic Pb(II) or Cd(II).

5.2. Complexes of Peptides with Coordinating O/N Donors in the Side Chains

Type and number of additional side chain donor atoms, besides the terminal amino, the terminal carboxylate, and the peptide group(s), in small or oligopeptides may alter significantly the metal ion binding capabilities of these ligands as well as the stoichiometry and thermodynamic stability of the complexes formed.

Among the side chain O donors the alcoholic OH group of Ser and Thr typically do not play an important role in metal ion binding as a part of a peptide even with Cu(II) which is known to form stable peptide complexes. Most likely the same applies for the phenolate O of the Tyr residue. Carboxylate O donors of the Asp and Glu residues, however, are considered to be the most effective side chain O donors with Cu(II) and the same trend can be seen from the few studies available for Pb(II). In particular, comparison of the Pb(II) binding capabilities of SerGly, GlyAsp, AspGly, GlyGlu, and GluVal indicated a slightly enhanced stability of [PbHL] with GlyAsp only, when the side chain carboxylate is in a chelatable position to the terminal carboxylate function [51]. On increasing the pH, in the [PbL] species a (NH_2,CO) coordination of all these dipeptides with a moderate stability is plausibly assumed. In another study GlyGlu was found to form complexes with identical stoichiometry and very similar stability as the above dipeptides. However, solid state information on $[PbHGlyGlu]ClO_4$ revealed an exclusive carboxylate binding with a hemidirected Pb(II) sphere due to the stereochemically active $6s^2$ lone pair [105]. Based on isothermal titration calorimetry, cyclopeptides, such as cyclo[D-Glu-Glu-D-Glu-Glu-D-Leu-Leu-D-

Leu-Trp] and cyclo[Glu-D-Leu-Glu-D-Leu-Glu-D-Leu-Glu-D-Trp], were shown to bind lead(II) in a L/Pb^{2+}/L sandwich-like fashion [106].

Although the imidazole N of the His residue is one of the most effective side chain donors and proven to be the major binding site for numerous metal ions in various peptides and proteins, only a very limited number of publications is available regarding Pb(II) binding of His-containing oligopeptides. With GlyHis and HisGly the results of an equilibrium study [51] revealed that the former ligand binds Pb(II) in a very similar manner as the previously discussed dipeptides forming 1 : 1 complexes with different protonation degrees. On the contrary, HisGly, in which the side chain imidazole-N is in a chelatable position to the terminal amino group, can bind Pb(II) via the (NH_2, N_{im}) chelating set and this coordination mode was also supported by NMR [51].

5.3. Complexes of Peptides with Side Chain Sulfur Donors

Lead(II) exhibits a high tendency to interact with the soft S donors of various bioligands. Therefore, sulfur-containing amino acid residues of oligopeptides are expected to enhance significantly metal ion binding. Among the proteinogenic amino acids methionine contains a thioether-type S donor with very low basicity while cysteine bears a thiol group with a pK_a value of 10.3 (see Table 1).

As recent results of Pb(II) systems with MetGly, GlyMet, GlyMetGly, GlyGlyMet, and MetMetMet show, the thioether-type S is not a sufficient anchor for Pb(II) because only a negligible effect of this side chain on complex stability was found [51]. Moreover, if Met is in the N-terminal position, the (NH_2,CO) chelate in the complexes is significantly less stable (both with the di- and tripeptides) due to sterical hindrance of the S-methyl group [51].

Table 5. Overall protonation constants of the ligands [51, 107] and stability constants (log β) of the complexes formed in aqueous solution at 25 °C in the Pb(II)-AlaCys [51], Pb(II)-CysGly [51] (I = 0.2 M, KNO_3), and Pb(II)-GSH [55] systems (I = 0.1 M, $NaNO_3$).

log β	**AlaCys**	**CysGly**	**GSH**
HL	9.64	9.36	9.50
H_2L	17.60	16.32	18.20
H_3L	20.55	19.50	21.76
H_4L	–	–	23.94
[PbH_2L]	20.49	17.96	22.14
[PbHL]	15.99	13.78	17.05
[PbL]	8.32	10.40	9.67
[$PbH_{-1}L$]	0.80	2.32	–
[PbH_2L_2]	30.06	28.46	32.59
[$PbHL_2$]	22.0	23.26	24.51
[PbL_2]	13.67	15.96	15.48
[PbL_3]	–	19.0	–

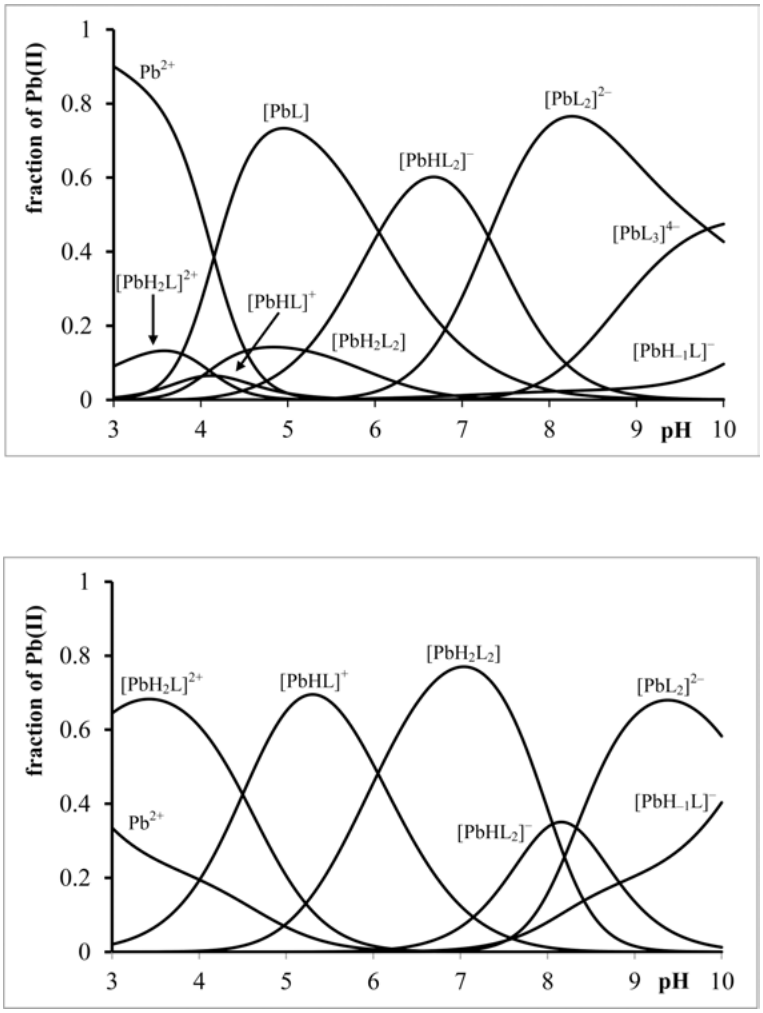

Figure 2. Concentration distribution curves for the Pb(II)-CysGly (top) and Pb(II)AlaCys (bottom) systems using data from Ref. [51], metal ion to ligand ratio = 1 : 3, $c_{Pb(II)}$ = 2 mM.

Due to the presence of the thiolate side chain with high basicity in AlaCys and CysGly, these dipeptides turned out to be much more effective ligands for Pb(II), although the deprotonation and coordination of the peptide group was not detected in these systems [51]. The stoichiometry and the determined stability constants for the Pb(II) complexes with these dipeptides are summarized in Table 5. Although the models in Table 5 are very similar, differences in the corresponding stability constants strongly suggest different coordination modes of the ligands depending on the position of the side chain thiolate. This is also reflected in the formation degrees of the species plotted as a function of pH for the two ligands

as shown in Figure 2. In particular, with CysGly (S^-,NH_2,CO)-binding occurs while with AlaCys only C-terminal (S^-,COO^-)-coordination takes place, resulting in the formation of $[PbHL]^+$ with a higher stability, as is suggested from the beginning of the interaction under acidic conditions. On increasing the pH, formation of 1:2 complexes with a (S,NH_2,CO)(S^-)-binding mode in $[PbHL_2]^-$ (CysGly) or (S^-,COO^-)(S^-,COO^-), in $[PbH_2L_2]$ (AlaCys) at neutral pH are revealed (see Figure 2) [51]. Impressive is the high stability of $[PbL_2]^{2-}$ in the CysGly system.

6. COMPLEXES OF LEAD(II) WITH THIOL-RICH NATURAL PEPTIDES

Naturally occurring proteins or peptides that are considered as thiol-rich, e.g., containing several cysteinyl amino acids, are the phytochelatins, metallothioneins, and zinc finger proteins. The structural features and biological role of metallothioneins together with their Pb(II) complexes are the subject of Chapter 9 of this book while Chapter 10 also involves Pb(II)-zinc finger interactions. Though glutathione (γ-GluCysGly) cannot be considered directly as a thiol-rich peptide, its highest natural abundance as a Cys-containing tripeptide together with its pivotal role in the synthesis of phytochelatins account for the present discussion of its interaction with Pb(II).

6.1. Complexation of Glutathione with Lead(II)

Reduced glutathione, γ-GluCysGly (GSH), is a highly abundant tripeptide that plays a protective role against oxidative damage of various cellular components. This important antioxidant effect is connected to the reaction of its thiol function with reactive oxygen species (ROS) or toxic metal ions in the defence mechanism of the cells in animals and plants. In GSH, beside the thiolate function the carboxylate and amino groups of the N-terminal Glu, the C-terminal carboxylate of Gly and, after metal ion-assisted deprotonation, the two peptide nitrogens may provide donors for complex formation. These reactions were the subject of previous reviews [108, 109]. Further reviews centered on GSH itself [110] and on the binding of GSH to toxic metal ions are also available [111].

In an early work the interaction of Pb(II) with GSH at a 1:2 metal ion to ligand ratio was studied by ^{13}C NMR. The results revealed the coordination of the thiolate function of the tripeptide in the range $5.4 < pD < 12.0$ (outside of this range precipitation was detected) together with a minor involvement of the Gly carboxylate function [112]. In a thermodynamic study formation of [PbL] was suggested with Pb(II) binding to the Glu carboxylate and amino groups as well as the thiolate and Gly carboxylate groups [57]. With an excess of GSH leading to $[PbHL_2]$, the coordination of the second ligand via the thiolate was proposed [57]. ^1H and ^{13}C NMR data led to the conclusion that in both [PbL] and $[PbL_2]$

as formed in alkaline solution, monodentate coordination of the S^- group only occurs [113]. Based on differential pulse polarography data, in the Pb(II)-GSH system a 1 : 2 complex with $2 \times (S^-)$ coordination of the two tripeptides and a 2 : 2 species with a $(S^-,COO^-)(S^-,COO^-)$-binding mode were suggested, resulting in a strongly sulfur-coordinated and a weakly carboxylate-bound Pb(II) in the latter species [114]. In an ESI-MS study [PbL]- and $[Pb_2L]$-type species were indentified [115]. IR information supported thiolate coordination of GSH in a series of complexes with $[PbL(X)] \cdot H_2O$ stoichiometry ($L = GSH$, $X = Cl^-$, NO_3^-, CH_3COO^-, NCS^-) [116]. Investigation of the Pb(II)-GSH interaction by SEC-ICP/ESI-MS showed the presence of a variety of species with 1 : 1 to 1 : 4, 2 : 2, and 2 : 3 stoichiometry [117].

More recently ^{207}Pb NMR and UV-Vis spectroscopy were successfully used to study the complex formation in the Pb(II)-GSH system. It was reported that at a 1 : 3 metal ion to ligand mole ratio at and above pH 7.5 a $[PbS_3]$-type species with the involvement of the thiolate functions of the GSH ligands and with a trigonal pyramidal geometry is present in solution as major species [5]. In a comprehensive solution and solid state study at a 1 : 2 Pb(II) to GSH mole ratio it was demonstrated that Pb(II) binds via the thiolate and N-terminal amino or Glu carboxylate groups in complexes with $PbS_2(N/O)$ or $PbS_2(N/O)_2$ stoichiometry. On increasing the excess of GSH (1 : 3 ratio) a mixture of $Pb(GSH)_2$ and $Pb(GSH)_3$ with PbS_2N_2 and PbS_3 coordination modes were detected while at higher than 1 : 4 mole ratios the PbS_3-type complex with $3 \times (S^-)$ binding of GSH was found to predominate in aqueous solution [118]. EXAFS results on the solid compound with the empirical formula of $[PbH_2L]ClO_4$ support $(S^-,CO/COO^-)$ coordination of GSH and a network of dimers in which the thiolate group forms an asymmetrical bridge between two lead(II) ions [118]. Very recently a paper was published with equilibrium models and thermodynamic data for systems involving Pb(II) and Pen, Cys or GSH [55]. To allow a comparison between the corresponding data, the stability constants for the complexes identified in the Pb(II)-GSH system are listed together with those determined for the complexes with AlaCys and CysGly in Table 5.

6.2. Lead(II)-Phytochelatin Complexes

Phytochelatins (PC) are Cys-rich peptides with the general stoichiometry of $(\gamma\text{-GluCys})_n$Gly where $n = 2$ to 6 in most cases. PC are intracellular metal ion-binding peptides produced by plants, algae or some yeasts against toxic metal ion stress. Phytochelatins, synthesized from GSH by the specific enzyme, phytochelatin synthase, can act as chelating agents to bind soft or borderline metals in form of stable complexes as part of a widespread defence mechanism developed by the above biological systems. Production of PC is rapid and activated by the presence of metal ions. Since the presence of intracellular PC is an early and specific signal of metal ion stress this class of compounds might be considered as suitable biochemical indicators for metal ion exposure [119].

PC containing multiple Cys residues are considered as excellent Pb(II) binders, however, due to the larger number of thiolates present the complexity of the equilibria involved in complex formation is even higher than that with GSH.

Based on UV-Vis and CD information, PC with the structure $(\gamma\text{-GluCys})_n\text{Gly}$ (n = 2 to 4) have been shown to bind one Pb(II) per peptide molecule for n = 2 and 3, while in the case of $(\gamma\text{-GluCys})_4\text{Gly}$ two distinct complexes with one and two Pb(II) per peptide molecule were identified. The results were consistent with the formation of two-, three-, and four-coordinate Pb(II)-thiolate complexes [120]. Comparison of the Pb(II)-binding capability of $(\text{GluCys})_2\text{Gly}$ with that of its phytochelatin analogue $(\gamma\text{-GluCys})_2\text{Gly}$, revealed similar metal ion chelating properties of the oligopeptides being capable of complexing one Pb(II) per peptide molecule. $(\text{GluCys})_2\text{Gly}$, that can be encoded by a gene, was also found to chelate quantitatively the metal ion from the Pb(II)-GSH complex [121]. The applicability of the Pb(II)–thiolate charge transfer bands (250–400 nm) to monitor lead binding to cysteine-rich sites in proteins together with the determination of Pb(II) binding to a series of structural Zn(II)-binding domains is also reported [122].

Using laboratory cultures of the marine diatom *Phaeodactylum tricornutum* exposed to Pb(II), the synthesis of PC showed a direct relationship to metal ion exposure [123, 124]. In another experiment with the same phytoplankton it was detected that increasing cellular PC concentration increases free Pb(II) in EDTA-buffered artifical seawater, giving thus rise to a bioassay to assess Pb(II) pollution in aquatic environments [119]. In an electrochemical study it has been demonstrated that the biohomopolymer $(\text{L-Cys})_n$ ($n \sim 50$) can be used as an effective metal chelator (including Pb(II)) using only electrochemical potentials to reversibly control the reactivity and binding strength of the ligand without altering the redox state of Pb(II) [125].

Reexamination of the Pb(II) coordination preferences in sulfur-rich structural Zn(II)-binding peptides suggested that, unlike Zn(II), Pb(II) prefers to avoid tetradentate coordination, binding instead in a trigonal pyramidal Pb(II)–S_3 manner or as $\text{Pb(II)–S}_{5–8}$ [127]. In a differential pulse polarographic study Pb(II) binding capabilities of $(\gamma\text{-GluCys})_2\text{Gly}$ (PC_2) and $(\gamma\text{-GluCys})_3\text{Gly}$ (PC_3) were studied. Complexes with 1:1 and 2:1 metal ion to ligand stoichiometry and thiolate binding of the ligands were identified. In particular, (S^1,S^2) in PbL for PC_2 while (S^2,S^3) in PbL and $(S^1)/(S^2,S^3)$ coordination modes in Pb_2L for PC_3 were detected [127]. Natural abundance ^{207}Pb NMR was succesfully used to probe a homoleptic PbS_3 coordination environment in three-strand coiled-coil Cys-containing peptides [128]. The same binding mode for Pb(II) was detected using a single polypeptide chain capable of forming a three-helix bundle with a tris(Cys) environment [129]. In an ESI-MS study on the Pb(II) binding of Cys-rich peptides multiple losses of water and a single methane loss provided a sensitive tool for locating Pb(II) and therefore elucidating its coordination [3].

7. FACTORS DETERMINING LEAD SELECTIVITY AGAINST ZINC, CALCIUM OR CADMIUM

The aim of this short section is to analyze and evaluate the main factors affecting the Pb(II)-binding ability of amino acids, small peptides and other bio-relevant small molecules discussed in the preceding sections as well as to find some factors determining their selectivity for Pb(II) against Ca(II), Zn(II), and Cd(II). In this respect, Ca(II) and Zn(II) can be interesting because Pb(II) is known to be able to substitute them in proteins [1, 4, 5]. Consequently, evaluation of the competition between Pb(II) and these metal ions for the ligands discussed might prove useful in developing specific chelators for Pb(II). Since in many cases the Ca(II)-binding ability of a given ligand (including amino acids and related compounds) is much weaker compared to that of Pb(II), to overcome the problem of selectivity for Pb(II) *versus* Ca(II) can be relatively easy [41, 42]. In the relation of Pb(II) and Zn(II), however, the situation is more complex because the preferences of these two metal ions towards N or O donors are often very similar [42, 45, 51]. Therefore, sulfur-containing amino acids, derivatives, and small peptides can be promising in this respect because Pb(II) exibits a clear preference for thiols over oxygen- and nitrogen-containing functions while this is not the case with Zn(II). In the interaction with a sulfur-containing molecule, however, other soft metal ions, such as Cd(II), might be strong competitors of Pb(II) [61].

There is no doubt that the question of selectivity is especially of relevance in the cases, in which the ligands are capable of binding Pb(II) with high effectiveness. This is not the situation with simple amino acids and simple oligopeptides, as it is described in Sections 3.1, 3.2.1, and 3.2.2. (NH_2,COO^-)-coordinated mono- and bis-complexes are formed with simple amino acids, while mono-complexes with pH-dependent coordination modes dominate with simple dipeptides. It follows clearly from the presented results that in solution most probably hemidirected complexes, with low coordination number (ca. 4 to 5) are formed in these systems and that the Pb(II)-binding ability of most of the amino acids, di- or tripeptides, even in the presence of a weakly coordinating carboxylate or imidazole moiety, is only moderate. For example, in the millimolar concentration range, at a 1 : 2 Pb(II) to ligand ratio and pH 7.4, a measurable (in some systems significant) concentration of the metal ion exists in a non-complexed, so-called "free metal ion" form (see Table 6).

Looking at the corresponding values in Table 6, one can conclude that, even if the interaction of Pb(II) with simple amino acids and simple oligopeptides is considerably more significant than that of Ca(II) [45] and the corresponding stability constants are measurably higher (1 to 2 log units per chelate) compared to those of Cd(II) [61], simple amino acids and small peptides cannot be suggested to be used as Pb(II)-sequestering agents. The stability of the Pb(II) complexes is increased a little bit in the presence of side chain-imidazole or -carboxylate in chelatable position, but even in the presence of Asp or His ~6.5 % and ~2.5 % free metal ion, respectively, exists under the conditions defined in Table 6. More-

Table 6. Calculated percentage of free Pb(II) for various Pb(II)-ligand systems at pH = 7.4, at 1 : 2 Pb(II) to ligand mole ratio, and $c_{Pb} = 1 \cdot 10^{-3}$ M.

Type of ligand	% of free Pb(II)	Refs.
Simple amino acid with non-coordinating side chain	20–25	[26]
Amino acid with weekly coordinating side chain donor	3–7	[26]
Simple dipeptide/tripeptide	25–40	[26]
Asp- or His-containing dipeptide	10–15	[26]
Pen	$1.85 \cdot 10^{-5}$	[26]
Cys-containing dipeptide with C/N-terminal Cys	$5.37 \cdot 10^{-2}/2.10 \cdot 10^{-4}$	[83]
Monohydroxamic acids	0.3–2.0	[12]
Dihydroxamic acids	ca. $5 \cdot 10^{-2}$	[83]
DFB/DFC	$9 \cdot 10^{-3}/9 \cdot 10^{-5}$	[95]
Aminohydroxamic acids: α/β-Alaha/N-Me-α-Alaha	0.1/1.8/4.0	[26]
Peptidehydroxamic acids: AlaAlaNHOH/AlaAlaNMeOH	2.7/3.1	[26]

over, the stability of the corresponding complexes with Zn(II) shows a similar increase indicating no selectivity for Pb(II) *versus* Zn(II) with these ligands [45].

It is well known that Pb(II) preferentially binds to sulfur donors, but its interaction is negligible (if there is any) with a thioether group. The thiol-containing molecules, discussed in Sections 3, 5, and 6, are extremely effective ligands for Pb(II) as quantitative binding occurs as seen from the corresponding data in Table 6.

As discussed in Section 3.2.3, in amino acids and related ligands containing a side-chain thiolate function (Pen, Cys, NAC), the sulfur donor plays a predominant role in the interaction with Pb(II). While formation of polynuclear complexes (in most cases with poor water solubility) is favored with Cys and NAC, this tendency is reduced by sterical hindrance with Pen. A tridentate (NH_2,COO^-,S^-) coordination mode of Pen and Cys can result in an extremely strong interaction with Pb(II). Owing to the sterical effect of the $6s^2$ pair, however, only one ligand is found to coordinate to Pb(II) in the tridentate fashion while the second one can bind through a S^- alone. Furthermore, with Cys, a mixture of bis-complexes with (NH_2, S^-)(NH_2, S^-) and (NH_2,COO^-, S^-)(S^-) coordination modes were also identified.

The selectivity of the thiol derivatives Cys and Pen for Pb(II) against Ca(II) and Zn(II) seems to be very good, and, in the case of Pen, also against Cd(II) a reasonable selectivity is indicated by the difference between the corresponding stability constants [45, 55, 61]. Looking at the differences, the stability constant of the complex [Pb(Pen)] (log β_{ML}) is more than three orders of magnitude higher than that of [Zn(Pen)] and a stability difference of almost two log units can be seen in favor of Pb(II) by the comparison with Cd(II). The affinity of Pen for Pb(II) over Cd(II) seems to be confirmed by the fact that Pen can be a useful molecule for the treatment of toxic effects of a Pb(II) exposure, but it is not efficient against Cd(II) poisoning [130].

Although deprotonation and coordination of peptide-amide was not found in any Pb(II)-small peptide system, peptides containing a side-chain thiol moiety

are still very effective Pb(II)-binding agents. At the same time, the Pb(II)-binding ability of Cys-containing small peptides, like the natural tripeptide GSH or the synthetic dipeptides CysGly and AlaCys, is measurably less than that of Cys or Pen. For example, log β_{PbL} is 13.37, 13.12 , 9.67, 9.64, and 9.36 for the complexes formed with Pen, Cys, GSH, AlaCys and CysGly, respectively [51, 55]. The sequestering ability of Pen, Cys and GSH towards Pb(II) follows the above trend of the stability constants [55]. It is also shown from the results with CysGly and AlaCys (see Section 5.3) that the position of the S-donor atom within the molecule affects significantly both the bonding modes and the selectivity. Compared to Pen these two Cys-containing dipeptides are somewhat poorer Pb(II) chelators, but the selectivity of AlaCys for this metal ion over Zn(II) was found to be even slightly better than that of Pen [51]. The Cd(II)- and Pb(II)-binding capability of small peptides, such as GSH, is often comparable [54], but synthesized Cys-rich polypeptides with coiled-coil motifs were shown to provide noticeable selectivity for Pb(II) even over Cd(II) [131].

Compared to simple amino acids and small peptides, hydroxamic acids are significantly more efficient Pb(II)-binding agents (Table 6). Even with a simple monohydroxamic acid complex formation is almost quantitative. Comparison of the stability of Pb(II)-monohydroxamate complexes with those of the corresponding Ca(II), Zn(II), and Cd(II) ones clearly shows the following trend: log β (Pb(II) complexes) > log β (Zn(II) complexes) > log β (Cd(II) complexes) $\gg$ log β (Ca(II) complexes). For example, the log β_{ML} values for $[PbAha]^+$, $[ZnAha]^+$, $[CdAha]^+$, and $[CaAha]^+$ are 6.56, 5.32, 4.25, and 2.40, respectively [132, 133]. Replacement of the carbonyl-oxygen by a sulfur atom in a hydroxamic acid moiety results in a thiohydroxamic acid with a much stronger Pb(II)-binding ability compared to the parent molecule. However, in most cases polynuclear complexes with poor solubility are formed. Compared to the corresponding monohydroxamate-based derivatives, similar factors were found to determine the Pb(II)-binding capability and selectivity against Zn(II) with the investigated hydroxypyronate, hydroxypiridinonate, and thiohydroxypyronate ligands [101].

If a hydroxamic function is also present in an amino acid derivative (aminohydroxamic acids), the effectivity of the interaction with Pb(II) depends very much, both, on the position of the amino-group (α, β, or γ) compared to the hydroxamic moiety and on the substituent at the hydroxamate-N (R_N = H or Me). In particular, α-aminohydroxamic acids with R_N = H (like α-Alaha) show the best Pb(II)-binding ability above pH 6, where they form very stable oligonuclear, water-soluble complexes, with the involvement of both the hydroxamate-type (O,O)- and the amine-type (N,N)-chelates (see Scheme 4, Structure IV). Because none of the other three metal ions are capable of forming this latter type species with high stability [85], complexation with α-aminohydroxamic acids is not only effective, but also rather selective for Pb(II) against Ca(II), Zn(II), and Cd(II).

A significantly better effectiveness of the AlaAlaNHOH and AlaAlaNMeOH peptidehydroxamic acids, as Pb(II) chelators was found, compared to that of the corresponding dipeptides, but the discrimination is less than that with monohydroxamic acids (Table 6). Their selectivity for Pb(II) *versus* Zn(II) was evaluated and a similar ability for binding of these two metal ions was concluded [26].

Dihydroxamic acids and especially trihydroxamic acid-based siderophores are very effective Pb(II) binding agents, their binding ability approximates to that of sulfur-containing small molecules (Table 6). However, interesting factors can be found to modify the selectivity of these molecules for Pb(II) over the other three metal ions discussed:

(i) While for Zn(II) and Cd(II) the complexes with 2,5-DIHA, containing the longest connecting chain between the two chelating functions, have the highest stability, Pb(II), due to the large space requirement of its $6s^2$ lone pair, prefers 2,2-DIHA a bit over the other dihydroxamic acids, including 2,5-DIHA. This results in a slightly increased selectivity towards 2,2-DIHA compared to 2,5-DIHA for Pb(II) over Zn(II) and Cd(II) (see Table 7).
(ii) Out of DFB and DFC, however, not the former one, containing the shorter connecting chains, forms Pb(II) complexes with a higher stability; just the opposite is shown by the results in Table 7.

This interesting finding most probably originates from the somewhat different behavior of the lone pair of Pb(II) in the complexes with these two siderophores. It is very likely that the behavior of the lone pair is highly affected by the double bonds, situated in β-position to each hydroxamic moiety in the linkers of DFC. As detailed in Section 4, the conjugation between the double bonds and the hydroxamate functions not just increases the stability of the chelates a little bit, but some involvement of the lone pair in bonding also occurs. The chelates formed with DFC might have a higher symmetry compared to the very packed arrangement assumed with DFB. As a consequence, the longer linkers of DFC compared to those of DFB might be beneficial. As the corresponding values in Table 7 show, DFC is not just simply a better Pb(II)-binding chelator compared to DFB, but it also demonstrates better selectivity for Pb(II) against the other three metal ions studied. In particular, both siderophores form much less stable complexes with Ca(II) than with Pb(II) indicating good selectivity in this rela-

Table 7. Stability constants (log β) of various metal(II) complexes formed with di- and trihydroxamic acids.

Complex	**log β_{ML}**		**Refs.**
	L = 2,2-DIHA	**L = 2,5-DIHA**	
[ZnL]	7.95	8.74	[12]
[CdL]	6.08	6.56	[12]
[PbL]	10.11	9.80	[12]
Complex	**log β_{ML}**		
	L = DFB	**L = DFC**	
[ZnL]	10.36	11.80	[134]
[CdL]	7.36	8.66	[87]
[CaL]	3.03	3.77	[87]
[PbL]	10.05	13.00	[87]

tion. On the contrary, the difference of the stability constants for the corresponding [PbL] and [CdL] complexes provides perfect selectivity only in the case of DFC. Regarding Zn(II) there is no selectivity with DFB and just a moderate one exists with DFC (Table 7).

ACKNOWLEDGMENTS

The authors thank the members of the EU COST Action CM1105 for motivating discussions. This work was supported by the Hungarian Scientific Research Fund (OTKA K112317). The research was also supported by the EU and co-financed by the European Regional Development Fund under the project GINOP-2.3.2-15-2016-00008.

ABBREVIATIONS AND DEFINITIONS

The list below does not contain abbreviations for essential amino acids because these are shown in Table 1. Furthermore, abbreviations for compounds which are mentioned only once in the text are not listed here either, those are defined within the corresponding part of the Chapter. In general, charges are omitted for clarity throughout the text, except in those cases where the formula refers to an individual species.

Aha	acetohydroxamate
AlaAlaNHOH	alanyl-alaninehydroxamic acid
AlaAlaNMeOH	alanyl-alanine-N-methylhydroxamic acid
AlaCys	alanyl-cysteine
α-Alaha	DL-α-alaninehydroxamate
β-Alaha	DL-β-alaninehydroxamate
Asp-β-ha	L-aspartic acid-β-hydroxamate
BSA	bovine serum albumin
CD	circular dichroism
CysGly	cysteinyl-glycine
DFB	desferrioxamine B, deprotonated form
DFC	desferricoprogen, deprotonated form
DFT	density functional theory
Dhp	1,2-dimethyl-3-hydroxy-4(1H)-pyridinone, Deferiprone
DIHA	dihydroxamate
dnTyr	3,5-dinitrotyrosine
DOTA	1,4,7,10-tetraazacyclododecane- 1,4,7,10-tetraacetic acid
EDTA	ethylenediamine,N,N′,N″,N‴-tetraacetate
en	ethylenediamine
ESI-MS	electrospray ionization mass spectrometry
EXAFS	extended X-ray absorption fine structure

FTIR	Fourier transform infrared spectroscopy
Glu-γ-ha	L-glutamic acid-γ-hydroxamate
GlyGly	glycylglycine
GSH	glutathione, γ-GluCysGly
HDhp	3-hydroxy-1,2-dimethyl-4-pyridinone
Hisha	L-histidinehydroxamate
HMalt	maltol, 3-hydroxy-2-methyl-4-pyrone
HSA	human serum albumin
ICP-MS	inductively coupled plasma mass spectrometry
IR	infrared
IRMPD	infrared multiple photon dissociation spectroscopy
L	general ligand
MeCys	S-methylcysteine
NAC	*N*-acetylcysteine
NMeAcrha	*N*-methyl-acrylhydroxamate
NMeAha	*N*-methyl-acetohydroxamate
NMR	nuclear magnetic resonance
Pen	penicillamine
PC	phytochelatin
ROS	reactive oxygen species
Sarha	sarcosinehydroxamate
SEC	size exclusion chromatography
UV-Vis	ultraviolet visible
XANES	X-ray absorption near-edge structure
XPS	X-ray photoelectron spectroscopy

REFERENCES

1. E. S. Claudio, H. A. Godwin, J. S. Magyar, in *Progr. Inorg. Chem*. Vol. 51, Ed. K. D. Karlin, John Wiley and Sons Inc., New York, 2003, pp. 1–144.
2. A. Belatik, S. Hotchandani, R. Carpentier, H.-A. Tajmir-Riahi, *PLoS ONE,* **2012**, *7*, e36723, doi:10.1371/journal.pone.0036723.
3. L. Banu, V. Blagojevic, D. K. Bohme, *J. Am. Soc. Mass. Spectrom*. **2013**, *24*, 1534–1542.
4. M. Kirberger, J. J. Yang, *J. Inorg. Biochem*. **2008**, *102*, 1901–1909.
5. K. P. Neupane, V. L. Pecoraro, *J. Inorg. Biochem.* **2011**, *105*, 1030–1034.
6. M. Razmiafshari, J. Kao, A. d'Avignon, N. H. Zawia, *Toxicol. Appl. Pharmacol*. **2000**, *166*, 1–12.
7. M. Kourgiantakis, M. Matzapetakis, C. P. Raptopoulou, A. Terzis, A. Salifoglou, *Inorg. Chim. Acta,* **2000**, *297*, 134-138.
8. M. Weil, *Acta Christ.* **2015**, 171, 82-84.
9. M. A. Santos, S. M. Marques, S. Chaves, *Coord. Chem. Rev.* **2012**, *256*, 240– 259.
10. K. J. Powell, B. L. Brown, R. H. Byrne, T. Gajda, G. Hefter, A. Leuz, S. Sjöberg, H. Wanner, *Pure Appl. Chem.* **2009**, *81*, 2425–2476.
11. R. N. Sylva, P. L. Brown, *J. Chem. Soc. Dalton Trans.* **1980**, 1577–1581.
12. E. Farkas, D. Bátka, Z. Pataki, P. Buglyó, M. A. Santos, *Dalton Trans.* **2004**, 1248–1253.

13. R. D. Hancock, A. E. Martell, *Chem. Rev.* **1989**, *89*, 1875–1914.
14. B. P. Hay, R. D. Hancock, *Coord. Chem. Rev.* **2001**, *212*, 61–78.
15. L. Shimony-Livny, J. P. Glusker, C. W. Bock, *Inorg. Chem.* **1998**, *37*, 1853–1867.
16. J. Masternak, B. Barszcz, M. Hodorowicz, O. V. Khavryuchenko, A. Majka, *Spectrochim. Acta Part A: Mol. Biomol. Spectr.* **2015**, *136*, 1998–2007.
17. D. Esteban-Gomez, C. Platas-Inglesias, T. Enriquez-Perez, F. Avecilla, A. de Blas, T. Rodriguez-Blas, *Inorg. Chem.* **2006**, *45*, 5407–5416.
18. M. Imran, A. Mix, B. Neumann, H. G. Stammler, U. Monkowius, P.Gründlinger, N. W. Mitzel, *Dalton Trans.* **2015**, *44*, 924–937.
19. A. Walsh, G. W. Watson, *J. Solid State Chem.* **2005**, *178*, 1422–1428.
20. R. D. Hancock, M. S. Shaikjee, S. M. Dobson, J. C. A. Boeyens, *Inorg. Chim. Acta* **1988**, *154*, 229–238.
21. J. W. Nugent, H-S. Lee, J. H. Reibenspies, R. D. Hancock, *Polyhedron* **2015,** *91*, 120–127.
22. R. Ferreiros-Martınez, D. Esteban-Gomez, É. Tóth, A. de Blas, C. Platas-Inglesias, T. Rodriguez-Blas, *Inorg. Chem*. **2011**, *50*, 3772–3784.
23. R. C. Gracia, W. R. Snodgrass, *Am. J. Health. Syst Pharm*. **2007**, *64*, 45–53.
24. M. Guo, L. He, P. J. Strong, H. Wang, *Chemosphere* **2014**, *112*, 472–480.
25. M. Huang, D. Krepkiy, W. Hu, D. H. Petering, *J. Inorg. Biochem.* **2004**, *98*, 775–785.
26. N. Ballatori, *Environ. Health Persp.* **2002**, *110*, 689–694.
27. S. M. McKelvey, K. A. Horgan, R. A. Murphy, *J. Trace Elem. Med. Biol.* **2015**, *29*, 151–169.
28. H. Gurer, N. Ercal, *Free Radical Biol. Med.* **2000**, *29*, 927–945.
29. J. Gastaldo, M. Viau, Z. Bencokova, A. Joubert, A-M. Charvet, J. Balosso, N. Foray, *Toxicol. Lett*. **2007**, *173*, 201–214.
30. H.-C. Kim, T.-W. Jang, H.-J. Chae, W.-J. Choi, M.-N. Ha, B.-J. Ye, B.-G. Kim, M.-J. Jeon, S.-Y. Kim, Y.-S. Hong, *Annals. Occup. Environ. Med*. **2015**, *27*, 30, DOI 10.1186/s40557-015-0085-9
31. Y. Finkelstein, M. E. Markowitz, J. F. Rosen, *Brain Res. Rev.* **1998**, *27*, 168–176.
32. C. D. Toscano, T. R. Guilarte, *Brain Res. Rev.* **2005**, *49*, 529–554.
33. A. A. Jarzecki, *J. Phys. Chem. A* **2012**, *116*, 571–581.
34. M. Blanusa, V. M. Varnai, M. Piasek, K. Kostial, *Curr. Med. Chem.* **2005,** *12*, 2771–2794.
35. J. Parr, *Polyhedron* **1997**, *16*, 551–566.
36. R. Ferreiros-Martinez, D. Esteban-Gomez, A. de Blas, T. Rodrıguez-Blas, *Inorg. Chem*. **2009**, *48*, 11821–11831.
37. R. Ferreiros-Martinez, D. Esteban-Gomez, C. Platas-Inglesias, A. de Blas, T. Rodriguez-Blas, *Inorg. Chem*. **2009**, *48*, 10976–10987.
38. B. T. Farrer, V. L. Pecoraro, *Curr. Opin. Drug Discov. Devel.* **2002**, *5*, 937–943.
39. S. L. Laurie, *Metal-Ligand Interactions in Biological Fluids*, in *Bioinorganic Chemistry*, Ed. G. Berthon, Vol. 1, Part 3, Chapter 2, Marcel Dekker, New York, 1995, pp. 603–724.
40. T. Kiss, I. Sóvágó, A. Gergely, *Pure Appl. Chem.* **1991**, *63*, 597–638.
41. I. Sóvágó, T. Kiss, A. Gergely, *Pure Appl. Chem.* **1993**, *65*, 1029–1080.
42. G. Berthon, *Pure Appl. Chem.* **1995**, *67*, 1117–1240.
43. O. Yamauchi, A. Odani, *Pure Appl. Chem.* **1996**, *68*, 469–496.
44. S. Sjoberg, *Pure Appl. Chem.* **1997**, *69*, 1549–1570.
45. L. D. Pettit, K. J. Powell, IUPAC Stability Constants Database, Version 5.7, Academic Software, Otley, Yorkshire, UK, **2005**.
46. Y. Khayat, M. Cromer-Morin, J.-P. Scharff, *J. Inorg. Nucl. Chem.* **1979**, *41*, 1496–1498.
47. A. M. Corrie, M. D. Walker, D. R. Williams, *J. Chem. Soc., Dalton* **1976**, 1012–1015.

48. A. M. Corrie, M. L. D. Touche, D. R. Williams, *J. Chem. Soc., Dalton* **1973**, 2561–2565.
49. Y. Sugiura, A. Yokoyama, H. Tanaka, *Chem. Pharm. Bull.* **1970**, *18*, 693–701.
50. L. D. Pettit, J. L. M. Swash, *J. Chem. Soc., Dalton* **1976**, 588–594.
51. E. Farkas, B. Bóka, B. Szőcs, A. J. Godó, I. Sóvágó, *Inorg. Chim. Acta* **2014**, *423*, 242–249.
52. B. B. Tewari, *Russ. J. Coord. Chem.* **2005**, *31*, 344–348.
53. A. E Martell, R. M. Smith, *Critical Stability Constants*, Vol. 1, Plenum Press, New York, **1977**.
54. C. Norman, R. A. Manning, *J. Am. Chem. Soc.* **1955**, *77*, 5225–5228.
55. F. Crea, G. Falcone, C. Foti, O. Giuffrè, S. Materazzi, *New. J. Chem.* **2014**, *38*, 3973–3983.
56. F. Rey, J. M. Antelo, F. Arce, F. J. Penedo, *Polyhedron* **1990**, *9*, 665–668.
57. A. M. Corrie, D. R. Williams, *J. Chem. Soc. Dalton* **1976**, 1068–1072.
58. M. B. Burt, S. G. A. Decker, C. G. Atkins, M. Rowsell, A. Peremans, T. D. Fridgen, *J. Phys. Chem. B* **2011**, *115*, 11506–11518.
59. M. B. Burt, S. G. A. Decker, T. D. Fridgen, *Phys. Chem. Chem. Phys.* **2012**, *14*, 15118–15126.
60. L. Banu, V. Blagojevic, D. K. Bohme, *Int. J. Mass Spectrom*. **2012**, *316–318*, 23–30.
61. I. Sóvágó, K. Várnagy, *Cadmium(II) Complexes of Amino Acids and Peptides,* in *Metal Ions in Life Sciences*, Vol. 11, Eds A. Sigel, H. Sigel, R. K. O. Sigel, Springer Science & Business Media, Dordrecht, 2013, pp. 275–302.
62. N. Burford, M. D. Eelman, W. G. LeBlanc, T. S. Cameron, K. N. Robertson, *Chem. Commun*. **2004**, 332–333.
63. F. Marandi, N. Shahbakhsh, *Z. Anorg. Allg. Chem.* **2007**, *633*, 1137–1139.
64. F. Marandi, N. Shahbakhsh, *J. Coord. Chem*. **2007**, *60*, 2589–2595.
65. L. Gasque, M. A. Verhoeven, S. Bernès, F. Barrios, J. G. Haasnoot, J. Reedijk, *Eur. J. Inorg. Chem*. **2008**, 4395–4403.
66. C. D. L. Saunders, L. E. Longobargi, N. Burford, M. D. Lumsden, U. Werner-Zwanziger, B. Chen, R. McDonalds, *Inorg. Chem*. **2011**, *50*, 2799–2810.
67. L. Gasque, S. Bernès, R. Ferrari, C. R. de Barbarín, J. Gutiérrez, G. Mendoza-Díaz, *Polyhedron* **2000**, *19*, 649–653.
68. Q. Ye, Y.-H. Li, Q. Wu, Y.-M. Song, J.-X. Wang, H. Zhao, R.-G. Xiong, Z. Xue, *Chem. Eur. J.* **2005**, *11*, 988 –994.
69. V. Jószai, Z. Nagy, K. Ősz, D. Sanna, G. Di Natale, G. La Mendola, G. Pappalardo, E. Rizzarelli, I. Sóvágó, *J. Inorg. Biochem*. **2006**, *100*, 1399–1409.
70. N. S. Sisombath, F. Jalilehvand, A. C. Schell, Q. Wu, *Inorg. Chem*. **2014**, *53*, 12459–12468.
71. F. Jalilehvand, N. S. Sisombath, A. C. Schell, G. A. Facey, *Inorg. Chem*. **2015**, *54*, 2160–2170.
72. N. S. Sisombath, F. Jalilehvand, *Chem. Res. Toxicol*. **2015**, *28*, 2313–2324.
73. H. Shindo, T. L. Brown, *J. Am. Chem. Soc*. **1965**, *87*, 1904–1909.
74. H. C. Freeman, G. N. Stevens, I. F. Taylor, *J. Chem. Soc., Chem. Commun*. **1974**, 366–367.
75. A. C. Schell, M. Parvez, F. Jalilehvand, *Acta Cryst*. **2012**, *E68*, m489–m490.
76. E. Farkas, É. A. Enyedy, H. Csóka, *J. Inorg. Biochem*. **2000**, *79*, 205–211.
77. Codd, R., *Coord. Chem. Rev.* **2008**, *252*, 1387–1408.
78. *Hydroxamic Acids: A Unique Family of Chemicals with Multiple Biological Activities*, Ed. S. P Gupta, Springer-Verlag, Berlin, 2013.
79. E. M. F. Muri, M. J. Nieto, R. D. Sindelar, J. S. Williamson, *Curr. Med. Chem.* **2002**, *9,* 1631–1653.
80. C. J. Marmion, D. Griffith, K. B. Nolan, *Eur. J. Inorg. Chem*. **2004**, *15*, 3003–3016.

81. P. Buglyó, K. Lénárt, M. Kozsup, A. C. Bényei, É. Kováts, I. Sóvágó, E. Farkas, *Polyhedron* **2015**, *100*, 392–399.
82. E. Farkas, E. Kozma, M. Pethő, K. M. Herlihy, G. Micera, *Polyhedron* **1998**, *17*, 3331–3342.
83. B. Kurzak, E. Farkas, T. Glowiak, H. Kozlowski, *J. Chem. Soc. Dalton Trans.* **1991**, 163–167.
84. J. J. Bodwin, A. D. Cutland, R. G. Malkani, V. L. Pecoraro, *Coord. Chem. Rev.* **2001**, *216–217*, 489–512.
85. B. Kurzak, H. Kozłowski, E. Farkas, *Coord. Chem. Rev.* **1992**, *114*, 169–200.
86. G. Anderegg, F. L'Eplattenier, G. Schwarzenbach, *Helv. Chim. Acta* **1963**, *154***,** 1400–1408.
87. E. Farkas, D. Bátka, G. Kremper, I. Pócsi, *J. Inorg. Biochem.* **2008**, *102*, 1654–1659.
88. A.-M. Albrecht-Gary, A. L. Crumbliss, in *Metal Ions in Biological Systems*, Vol. 35, Eds A. Sigel, H. Sigel, Marcel Dekker, New York, 1998, pp. 239–327.
89. B. J. Hernlem, L. M. Vane, G. D. Sayles, *Inorg. Chim. Acta* **1996**, *244*, 179–184.
90. B. I. Kruft, J. M. Harrington, O. W. Duckworth, A. A. Jarzecki, *J. Inorg. Biochem.* **2013**, *129*, 150–161.
91. S. M. Kraemer, J. Xu, K. N. Raymond, G. Sposito, *Environ. Sci. Technol.* **2002**, *36*, 1287–1291.
92. B. Mishra, E. A. Haack, P. A. Maurice, B. A. Bunker, *Environ. Sci. Technol.,* **2009**, *43*, 94–100.
93. N. K. Adam, *J. Geochem*. **2014**, Article ID 168938.
94. R. Dietzel, Ph. Thomas, *Z. Anorg. Allg. Chem.* **1971**, *381*, 214–218.
95. K. Abu-Dari, F. E. Hahn, K. N. Raymond, *J. Am. Chem. Soc.* **1990**, *112*, 1519–1524.
96. K. Abu-Dari, T. B. Karpishin, K. N. Raymond, *Inorg. Chem.* **1993**, *32*, 3052–3055.
97. S. Rupprecht, S. J. Franklin, K. N. Raymond, *Inorg. Chim. Acta* **1995**, *235*, 185–194.
98. S. Rupprecht, K. Langemann, T. Lügger, J. M. McCormick, K. N. Raymond, *Inorg. Chim. Acta* **1996**, *243*, 79–90.
99. E. Farkas, D. Bátka, *J. Inorg. Biochem.* **2006**, *100*, 27–35.
100. S. I. Ahmed, J. Burgess, J. Fawcett, S. A. Parsons, D. R. Russel, S. H. Laurie, *Polyhedron* **2000**, *19*, 129–135.
101. P. Buglyó, L. Bíró, I. Nagy, B. Szőcs, E. Farkas, *Polyhedron* **2015**, *92*, 7–11.
102. D. L. Rabenstein, S. Libich, *Inorg. Chem*. **1972**, *11*, 2960–2967.
103. A. P. Brunetti, E. J. Burke, M. C. Lim, G. H. Nancollas, *J. Sol. Chem*. **1972**, *1*, 153–164.
104. A. Vaidyan, P. Bhattacharya, *Ind. J. Chem*. **1994**, *33A*, 1003–1007.
105. R. Ferrari, S. Bernés, C. R. de Barbarín, G. Mendoza-Díaz, L. Gasque, *Inorg. Chim. Acta* **2002**, *339*, 193–201.
106. M. Ngu-Schwemlein, W. Gilbert, K. Askew, S. Schwemlein, *Bioorg. Med. Chem*. **2008**, *16*, 5778–5787.
107. P. Cardiano, G. Falcone, C. Foti, O. Giuffrè, A. Napoli, *J. Inorg. Biochem*. **2013**, *129*, 84–93
108. H. Sigel, R. B. Martin, *Chem. Rev.* **1982**, *82*, 385–426.
109. I. Sóvágó, in *Biocoordination Chemistry*, Ed. K. Burger, Ellis Horwood, New York, 1990, pp. 135–184.
110. A. Krezel, W. Bal, *Acta Biochim. Pol.* **1999**, *46*, 567–580.
111. F. M. Rubino, *Toxics* **2015**, *3*, 20–62.
112. B. J. Fuhr, D. L. Rabenstein, *J. Am. Chem. Soc*. **1973**, *95*, 6944–6950.
113. L. A. P. Kane-Maguire, P. J. Riley, *J. Coord. Chem*. **1993**, *28*, 105–120.
114. B. H. Cruz, J. M. Díaz-Cruz, M. S. Díaz-Cruz, C. Ariño, M. Esteban, R. Tauler, *J. Electroanal. Chem*. **2001**, *516*, 110–118.
115. N. Burford, M. D. Eelman, K. Groom, *J. Inorg. Biochem*. **2005**, *99*, 1992–1997.

116. B. K. Singh, R. K. Sharma, B. S. Garg, *J. Them. Anal. Cal*. **2006**, *84*, 593–600.
117. K. Polec-Pawlak, R. Ruzik, E. Lipiec, *Talanta* **2007**, *72*, 1564–1572.
118. V. Mah, F. Jalilehvand, *Inorg. Chem*. **2012**, *51*, 6285–6298.
119. E. Morelli, L. Fantozzi, *Bull. Environ. Contam. Toxicol*. **2008**, *81*, 236–241.
120. R. K. Mehra, V. R. Kodati, R. Abdullah, *Biochem. Biophys. Res. Commun*. **1995**, *215*, 730–736.
121. W. Bae, R. K. Mehra, *J. Inorg. Biochem*. **1997**, *68*, 201–210.
122. J. C. Payne, M. A. ter Horst, H. A. Godwin, *J. Am. Chem. Soc*. **1999**, *121*, 6850–6855.
123. E. Morelli, G. Scarano, *Marine Environ. Res.* **2001**, *52*, 383–395.
124. G. Scarano, E. Morelli, *BioMetals*, **2002**, *15*, 145–151.
125. A. M. Johnson, J. A. Holcombe, *Anal. Chem*. **2005**, *77*, 30–35.
126. J. S. Magyar, T-C. Weng, C. M. Stern, D. F. Dye, B. W. Rous, J. C. Payne, B. M. Bridgewater, A. Mijovilovich, G. Parkin, J. M. Zaleski, J. E. Penner-Hahn, H. A. Godwin, *J. Am. Chem. Soc*. **2005**, *127*, 9495–9505.
127. A. Alberich, C. Ariño, J. M. Díaz-Cruz, M. Esteban, *Talanta*, **2007**, *71*, 344–352.
128. K. P. Neupane, V. L. Pecoraro, *Angew. Chem. Int. Ed*. **2010**, *49*, 8177–8180.
129. S. Chakraborty, J. Y. Kravitz, P. W. Thulstrup, L. Hemmingsen, W. F. Degrago, V. L. Pecoraro, *Angew. Chem. Int. Ed*. **2011**, *50*, 2049–2053.
130. F. Jalilehvand, B. O. Leung, V. Mah, *Inorg. Chem*. **2009**, *48*, 5758–5771.
131. M. Matzapetakis, D. Ghosh, T.-C. Weng, J. E. Penner-Hahn, V. L. Pecoraro, *J. Biol. Inorg. Chem*. **2006**, *11*, 876–890.
132. E. Farkas, É. A. Enyedy, H. Csóka, *J. Inorg. Biochem*. **2000**, *79*, 205–211.
133. E. Farkas, D. Bátka, *unpublished result* (log β[CdAha]$^{+}$ = 5.32).
134. É. A. Enyedy, I. Pócsi, E. Farkas, *J. Inorg. Biochem*. **2004**, *98*, 1957–1966.

9

Lead(II) Binding in Metallothioneins

Daisy L. Wong, Maureen E. Merrifield-MacRae, and Martin J. Stillman *

Department of Chemistry, The University of Western Ontario, London, Ontario N6A 5B7, Canada
<martin.stillman@uwo.ca>

Metal Ions in Life Sciences, Volume 17 Edited by Astrid Sigel, Helmut Sigel, and Roland K. O. Sigel

DOI 10.1515/9783110434330-009

Abstract: Heavy metal exposure has long been associated with metallothionein (MT) regulation and its functions. MT is a ubiquitous, cysteine-rich protein that is involved in homeostatic metal response for the essential metals zinc and copper, as well as detoxification of heavy metals; the most commonly proposed being cadmium. MT binds *in vivo* to a number of metals in addition to zinc, cadmium and copper, such as bismuth. *In vitro*, metallation with a wide range of metals (especially mercury, arsenic, and lead) has been reported using a variety of analytical methods. To fully understand MT and its role with lead metabolism, we will describe how MT interacts with a wide variety of metals that bind *in vitro*. In general, affinity to the metal-binding cysteine residues of MT follows that of metal binding to thiols: Zn(II) < Pb(II) < Cd (II) < Cu(I) < Ag(I) < Hg(II) < Bi(III). To introduce the metal binding properties that we feel directly relate to the metallation of metallothionein by Pb(II), we will explore MT's interactions with metals long known as toxic, particularly, Cd(II), Hg(II), and As(III), along with xenobiotic metals, and how these metal-binding studies complement those of lead binding. Lead's effects on an organism's physiological functions are not fully understood, but it is known that chronic exposure inflicts amongst other factors pernicious anemia and developmental issues in the brain, especially in children who are more vulnerable to its toxic effects. Understanding the interaction of lead with metallothioneins throughout the biosphere, from bacteria, to algae, to fish, to humans, is important in determining pathways for lead to enter and damage physiologically significant protein function, and thereby its toxicity.

Keywords: arsenic MT · cadmium MT · electrospray ionization mass spectrometry · *Fucus vesiculosus* · isothermal titration calorimetry · ITC · lead MT · mercury MT · metallothionein · metal-thiolate cluster formation · MT · NMR · ^{207}Pb nuclear magnetic resonance · zinc MT

1. INTRODUCTION

1.1. Essential Metals and Toxic Metals

The inorganic elements such as copper, iron, and zinc, once solubilized from the earth's crust, can greatly affect all natural chemistries, so in many cases the physiological chemistries that result from their cellular transport and accessible cellular concentrations are controlled by highly regulated homeostatic control based on numerous proteins [1, 2]. Metallic elements are found in all living organisms and serve a multitude of functions. In almost all biological roles, metals are coordinated by ligand donor atoms of chaperones or metal-dependent proteins, and in many cases, for the softer metals in particular, cysteinyl thiols serve as major donor atoms.

A brief comment about the term "soft" applied here to both metals and donor atoms of ligands may be useful. This nomenclature arose from the development of inorganic coordination chemistry, with the major statement being made by Pearson. His "hard/soft – acid/base" concepts allowed a much better understanding of the selection of donor atoms by metals in isolated metal complexes, or, in the case of metalloproteins, the selection by donor atoms on specific amino acids of metals in solution, typically bound to chaperone molecules. For the discussion in this review, we are specifically interested in donor atoms N and S, which can

be classified as intermediate/soft bases, and a range of metals, including Pb(II), that can also be classified as intermediate/soft. The essence of the Pearson theory is that soft bind soft with a much greater binding affinity than soft binding to hard (whichever way round one sets up the reaction) [3].

In the case of cysteines, we recognize that the thiol groups are defined as soft donor atoms. The cysteines can be just a few of many residues in very large proteins, for example, in the zinc finger proteins, or represent a significant fraction of the sequence, for example, in the metallothioneins, or even a very simple tripeptide like glutathione. The key concept for this chapter is that for each of these physiologically significant actors, not only are their functions disrupted when metals other than the 'correct' one bind, but toxic metals that humans are commonly exposed to from both the environment and diet will bind to thiols with binding affinities often greater than the 'correct' physiological metal.

Essential elements may be structural elements, stabilizers of biological structures, components of control mechanisms (e.g., in nerves and muscles), and, in particular, can be activators or components of redox systems. Essential metals can be characterized because their deficiency results in impairment of biological functions [4]. The trace metals generally regarded as essential for human health include iron, zinc, copper, manganese, chromium, molybdenum, and selenium. Toxic metals have no known biological requirement in humans, and exposure is linked to demonstrable toxicity.

The severity of the toxicity increases with increase in dosage. There may be a lower limit of exposure where toxicity may not be detected, or there may be no amount at the molecular level that does not have an adverse effect [5]. A common denominator is that these 'soft' metals bind with high binding affinities to biological thiols resulting in changed function and, therefore, a toxic response. Metallothioneins (MTs), being rich in thiols, are a prime target for these metals. To put lead-binding to MT in perspective, we first consider briefly the binding to metallothionein of zinc, the essential metal with binding affinities great enough to reduce free cellular ion concentration to picomolar levels. Then, we will move to describe characterization of the metallation of MT with cadmium, mercury, and, in more detail, arsenic. Arsenic binding would be expected to mirror that of lead.

1.2. Metallothioneins – Overview

Metallothioneins are metalloproteins that are cysteine-rich, and bind Group 11 and 12 metals with a two domain structure comprised of two metal-thiolate clusters. Metallothioneins are characterized by a low molecular mass (6000–7000 Da for the mammalian protein), with about 30 % cysteinyl residues (mammalian MT has 20 cysteines out of 62), and a complete absence of aromatic amino acids in the primary sequence. Metallothioneins are capable of binding metals with stoichiometries of 7, 12, or even 18 Group 11 and 12 metals (commonly Cu(I), Cd(II), Hg(II), and Zn(II)), in either a single (yeast or fungus) or two (mammalian and crustacean) clustered domains. The formation of these clustered domains

typically involve bridging cysteinyl thiolates. The first characterization of a cadmium-zinc metallothionein was reported by Kägi and Vallee in the 1950s [6].

The early techniques used to characterize metallothionein included electronic absorption, circular dichroism, and atomic absorption spectroscopy. The establishment of new analytical techniques has greatly increased the ability of researchers to characterize MT. Techniques such as electrospray ionization mass spectrometry (ESI-MS), which provides a method to directly characterize the molar mass of all species coexisting in solution, have dramatically increased our understanding of metalation pathways. The early chemical and spectroscopic studies reported on the speciation of Cd(II), Zn(II), and Cu(I) binding, where these different species exhibited specific spectral properties. Nuclear magnetic resonance (NMR) spectroscopy and X-ray diffraction studies showed that these metal-thiolate complexes adopted a three-dimensional structure in mammalian metallothionein containing Cd(II) and Zn(II), involving two separate metal-thiolate cluster domains (β-domain at the N-terminus, α-domain at the C-terminus) [7–10]. In general, structural properties that are characteristic of metallothionein are the formation of metal-thiolate clusters that involve terminal and/or bridging cysteinyl thiolate groups in the peptide chain. This determines the secondary structure of the metallated protein in which the peptide chain wraps around the clusters [7].

1.3. Mammalian Metallothioneins

Current studies show that in mammalian species, multiple MT genes code for a family of isoforms. For mammals, MTs fall into at least four subgroups: MT-1, MT-2, MT-3, and MT-4. The MT-1 and MT-2 isoforms are the most widely expressed isoforms, predominantly found in the liver and kidneys, respectively, and differ by only a single negative charge. The human MT genes are found concentrated on a single locus of chromosome 16 (16q13), where at least 10 of the 17 genes identified are functional. They encode multiple isoforms of MT-1 and a single isoform of MT-2. For MT-3 and MT-4, only single genes have been detected [11]. MT-3 is preferentially expressed in the brain, but has also been detected in reproductive tissues, the tongue, stomach, heart, and kidney. The MT-4 genes from mice and humans have been cloned and the expression of the gene appears to be restricted to squamous epithelial cells.

Numerous stimuli are able to induce MTs, including metal ions, hormones, cytokines, inflammation, and stress. The predominantly studied inducers of metallothioneins are metal ions and glucocorticoids. In humans, metal ions induce all of the MT isoforms, while glucocorticoids induce only MT-2a and MT-1e. Human metallothionein isoforms are regulated independently of each other. Only metal ions are capable of inducing MT-1 isoforms, which shows the straightforward nature of the human MT-1 promoter region compared with the numerous enhancer regions in the regulator of MT-2a [12].

1.4. Metallothioneins from Non-Mammalian Sources – Snail, *Fucus vesiculosus*, and Yeast

Reports of recently-described metallothioneins now include structural and functional forms of non-mammalian MTs. The ability of these MTs to be induced by heavy metals and their accumulation of them intracellularly have been used as biomarkers in environmental toxicology. Metallothionein is expressed in many vertebrates, fungi, plants, algae, and metal-resistant bacteria [13–16]. We describe three examples here as an introduction to the metallation properties of MT under polluted environmental conditions.

The snail *Helix pomatia* expresses a newly discovered metallothionein. Terrestrial snails have the ability to tolerate high concentrations of cadmium while accumulating copper at high levels, required for the production of the Cu-dependent oxygen carrier, hemocyanin. In these snails, cadmium accumulates in the midgut gland, and copper is found in the foot and mantel. There are tissue-specific MT forms which contain 18 conserved cysteine residues, with the midgut-gland MT binding Cd(II) and the mantle MT binding Cu(I) [17].

Brown algae contain greater concentrations of arsenic than either green or red algae. *Fucus vesiculosus,* a brown algae, thrives in heavily polluted aquatic environments. Brown alga *Fucus gardneri* cells have been shown to accumulate significant concentrations of arsenic. Work within the Stillman group showed that As(III) binding takes place in two metal-binding domains, a smaller, 7 cysteine region separated by a 14 residue linker region from the larger 9-cysteine region. For Cd(II) and Zn(II), we expect a cluster structure in which bridging and terminal sulfurs from the 16 cysteines will form a cage- or adamantine-like three-dimensional structure. Metallation of *Fucus vesiculosus* with Zn(II) and Cd(II) requires four thiols arranged in tetrahedral geometry around the six divalent metals. In the case of arsenic, metallation conforms to its usual inorganic chemistry with each trivalent arsenic atom binding up to 3 cysteinyl sulfurs in a trigonal pyramid configuration. Five As(III) atoms bind to the 16-cysteine mammalian protein, leaving one cysteine free. The mass spectral data suggest that the structure is far more open than that observed when six divalent metal ions (Zn or Cd) bind to the *Fucus*-MT [18].

The first detailed report of a copper-binding protein from yeast cells was in 1975 [19]. The same protein from *Saccharomyces cerevisiae* has been called copper-thionein, copper-chelatin, or Cu-MT. This low molecular-weight, cysteine-rich protein belongs to the metallothionein family. The yeast protein is inducible only by copper, not by cadmium or zinc. The metal composition of the MT is determined by the extent of the organism's exposure to different metals. The isolated copper MT contains 7 (or 8, depending on the report) moles of copper ligated to 10 cysteines per mole of protein. The yeast MT can also bind Ag(I), Cd(II), Zn(II), and Co(II). The stoichiometry of Ag(I) binding is similar to Cu(I); Cd(II) and Zn(II) coordinate with the 10 cys in the yeast MT with a maximum stoichiometry of four metal ions per mole of protein [20]. The X-ray structure of the yeast Cu-MT is only the second structure for any MT determined at this resolution [21].

1.5. Reactions of Metallothioneins with Essential Metals – Zinc and Copper

The most studied member of the MT family, the mammalian MTs, comprise 20 cysteine residues that act to encapsulate two metal-thiolate cores (β and α) using a combination of bridging and terminal thiolates from the cysteinyl residues (Figure 1). The two separate metal binding domains adopt a dumbbell-like structure, as determined by the analysis of X-ray diffraction data in crystals isolated from rat liver tissue [22]. The β-domain, with 9 cysteine residues, is capable of binding 3 Cd(II) or Zn(II), or 6 Cu(I), while the α-domain, with 11 cysteine residues, is capable of binding 4 Cd(II) or Zn(II), or 6 Cu(I). Molecular modelling and later experimental data from solution studies suggests that the two domains are not isolated, but somewhat coalesced [23].

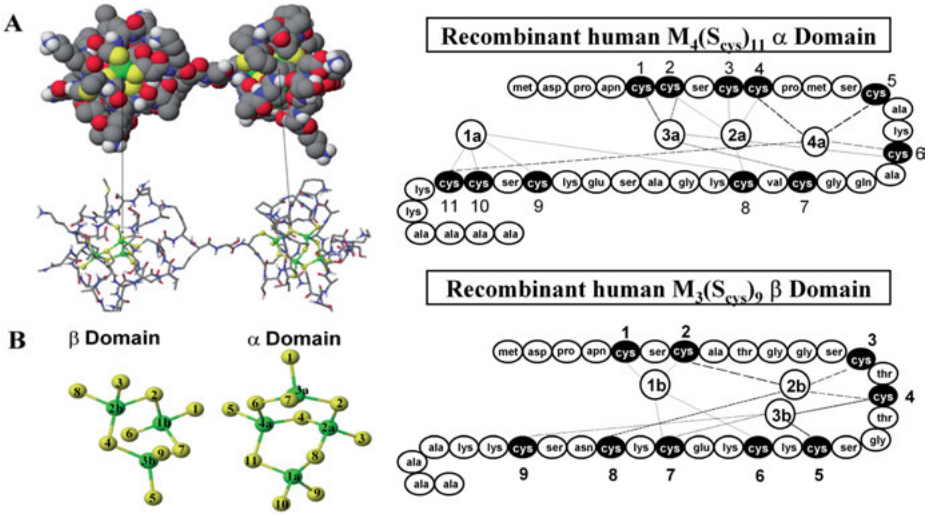

Figure 1. Structural properties of human metallothionein 1a. **Left:** (**A**) Space filling model with 7 divalent metals bound. (**B**) The formation of two clustered domains involving, both terminal and bridging cysteinyl thiols. The numbering is taken from the ^{113}Cd NMR data of Armitage and coworkers [86]. **Right:** The sequence of recombinant human MT1a showing the metal-thiolate connections. The numbering here is related to the fragment domains, not the full protein. Reproduced with permission of the Royal Society for Chemistry 2011 [8].

Naturally occurring MTs are usually isolated as either Zn-MT, Cu-MT or as the mixed metal species Zn-Cu-MT and Zn-Cd-MT. In the case of mammals, Zn-MT is the dominant form, however, Cu-MT has been isolated from several sources including fetal liver MT, bovine calf liver MT, rat kidney MT, as well as brain specific MT-3. For yeast and fungi, Cu-MT is the dominant species. At the cellular level, both toxic and nontoxic metals are tightly controlled, as estimates

of free Cu(I) and Zn(II) ion concentrations suggest that neither is available in the cytosol. The absence of freely available Cu(I) and Zn(II) suggests that an organism is able to exist in this state by using metallochaperones to transport these ions in a controlled manner. MT is considered one such metallochaperone, a protein capable of transporting Zn(II) and Cu(I) to apo-enzymes. Metal exchange experiments have been conducted in which Zn(II) from Zn_7-βα-MT has been transferred to Zn-dependent enzymes, such as m-aconitase, carbonic anhydrase, and the prototypical transcription factor, Gal4.

Removal of Zn(II) from the zinc finger-containing transcription factor Sp1 demonstrates that MT may also act as a Zn(II) acceptor. The association of MT with the biologically essential Zn(II) and Cu(II) has suggested that its function is the maintenance of metal ion homeostasis. While metal exchange to apo-enzymes requiring these metals has been reported, there has been no mechanism elucidated. The role of MT as a metallochaperone is demonstrated in the transcription of DNA to RNA, which has been shown to be strongly controlled by exposure to metal ions. In the case of mammals, of the four isoforms (MT-1 to -4), only two (MT-1 and MT-2) are heavily upregulated by metal ions [8, 24–26].

1.5.1. Specific Reactions of Metallothioneins with Zinc

The reactivity and structural properties of Pb-MT described below require reflection with respect to the metallation data reported for reactions of metallothioneins with zinc and cadmium. We briefly bring forward the metallation properties of zinc binding to MT. The spectroscopic data for Cu-MT has been described previously and are more complicated than those reported for either Zn(II) or Cd(II). The properties of Cd-MT are described in Section 2.1.

In humans, zinc is important for the quantity and quality of new tissue synthesis. Zinc has also been found to stabilize plasma and intracellular membranes, as confirmed in animal studies. There are also a wide array of regulatory functions associated with zinc. It has been shown to regulate the activity of 5′-nucleotidase activity in human lymphoblast plasma membranes to inhibit guanylate and adenylate cyclase, to modify phosphorylation of mouse epithelial cell membrane receptors, to aid in the binding of insulin to cell membrane receptors and of androgens to nuclear receptors and to act as a calcium antagonist in regulating calmodulin activity [27].

Although Zn-MTs have been well characterized, it is only recently that a consistent model describing the metallation pathways in a systematic manner has emerged. ESI-mass spectral data taken as a function of both the stepwise binding of Zn(II) and the dependence of the Zn atom coordination site on the total number of Zn atoms bound provide a view of fundamentally important metallation properties. The power of the ESI-MS experiment and its significant results are evident when comparing the data reported for Zn and Cd binding.

Figure 2 shows that for Zn(II) binding to human MT-1a, the reaction at physiological pH follows a non-cooperative, distributed pathway, named a “bead-pathway” to emphasize the formation of a number of (up to 5) $Zn(S_{CYS})_4$ beads before the familiar clusters with bridging thiolates begin to form. Figure 2 dem-

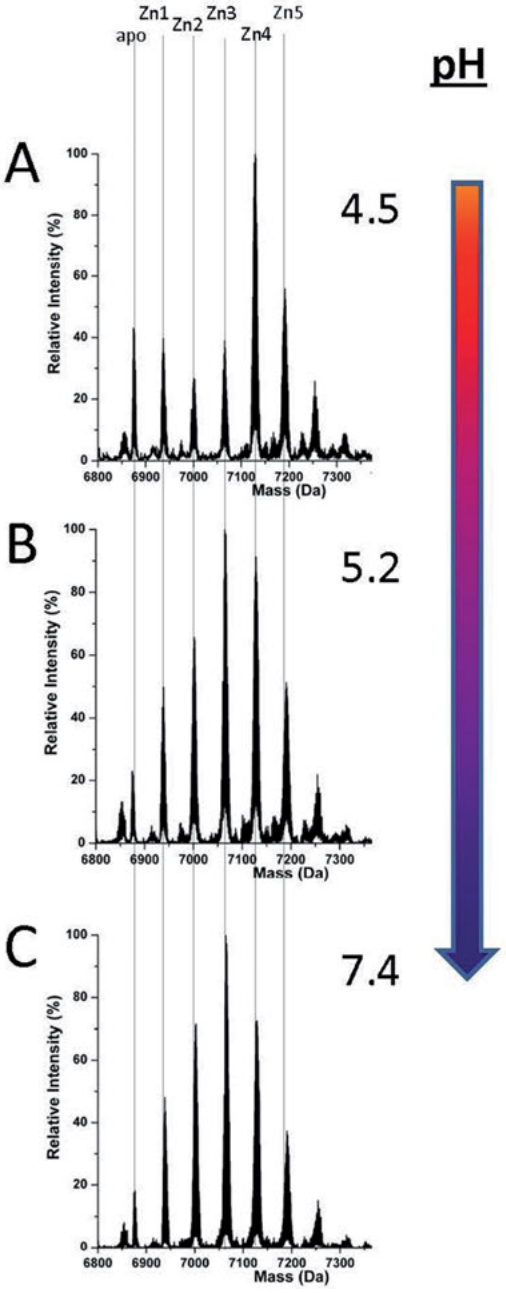

Figure 2. Representative ESI-MS spectra recorded during the pH titration of Zn_xMT (x = 0–5) after approximately 2.5 equivalents of Zn(II) had been added. The spectrum at pH 4.5 (**A**) shows a mixed binding mechanism, whereas by pH 5.2 (**B**), it is largely distributive and terminally bound, remaining unchanged to pH 7.4 (**C**). Reproduced with permission of the Royal Society of Chemistry, Metallomics 2016 [28].

onstrates the complete pH-dependence of the structure and stoichiometry of the individual metal-binding sites as only the pH is changed (decreased) for a single aliquot addition of 2.5 molar equivalents (out of a maximum of 7). This is further demonstrated schematically in Figure 3. The ESI-MS data change systematically, showing how near neutral pH the Zn(II) atoms distribute to bind using 4 cysteinyl thiolates, while at low pH the clustered $Zn_4(S_{CYS})_4$ binding structure begins to dominate. The data show that the distributed pathway applies at all pH values

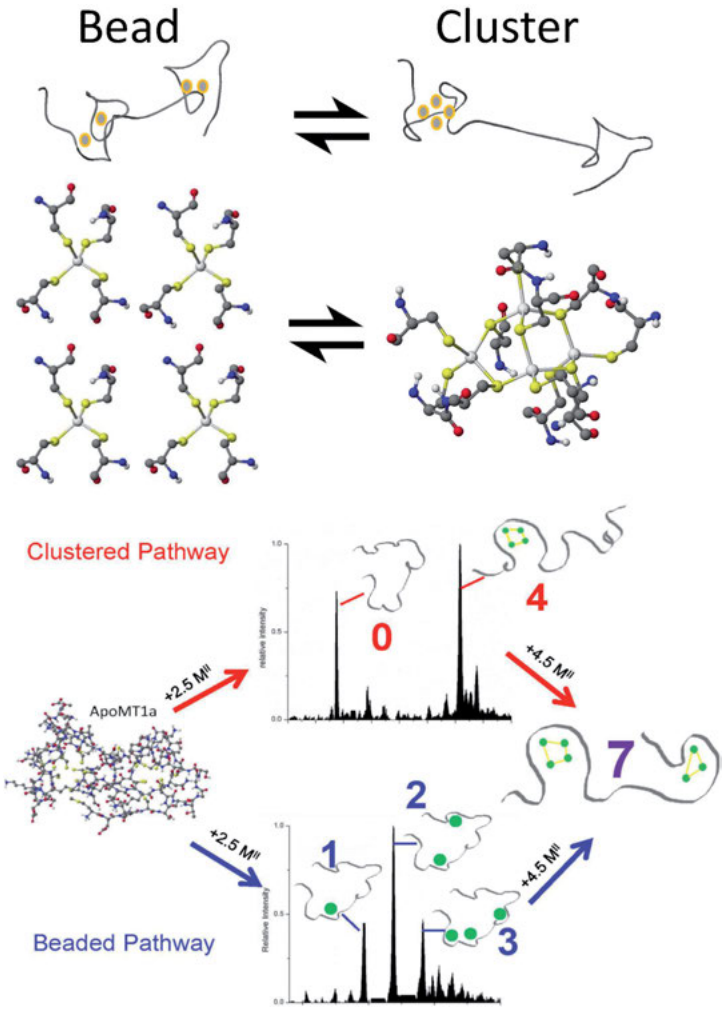

Figure 3. Zinc and cadmium binding to apo-rhMT-1a follow one of two pathways. **Top**: The possible metallation structures when 4 divalent metals, M(II), bind to the 20 cysteines of MT-1a. The metals either bind separately involving terminal cysteines forming beads of $M(S_{CYS})_4^{2-}$, or the four metals bind in a cluster of $M_4(S_{CYS})_{11}^{3-}$ in the α-domain. **Bottom**: Diagrammatic view of the two pathways followed during metallation of apo-MT-1a. Reproduced with permission of the Royal Society of Chemistry, 2016 [28].

above 6. In the text below where Cd-MT is discussed, we will show how Cd binding is quite different, adopting a clustered structure at a pH close to neutral (just below pH 6) at the expense of the beaded model (see Figure 4 in Section 2.1). This bead/cluster model for zinc binding to MT was used to explain the Zn(II) distribution in the presence of the Zn-dependent carbonic anhydrase [28, 29].

The pathways followed are likely common for MTs when cluster formation is possible. For As(III) and possibly Pb(II), cluster formation is unlikely. For As-MT, it has been shown that the stoichiometry is exactly 1 As(III) : 3 S_{CYS}.

2. METALLOTHIONEINS AND TOXIC METALS

2.1. Reactions of Metallothioneins with Cadmium

Cadmium is a naturally occurring metal, in the same triad as Zn and Hg in the Periodic Table of the Elements, with its chemical behavior similar to zinc in many aspects. However, significant for this chapter, we note that Cd(II) binds to thiols with binding affinities about 10^4 times greater than Zn(II), such that cadmium will displace zinc in many of the binding sites in Zn-dependent proteins, and particularly in MT. Cadmium exists in the earth's crust at 0.1 ppm, and is an impurity in zinc or lead deposits. It is also a by-product of zinc or lead smelting. For commercial uses, cadmium is used in television screens, lasers, batteries, paint pigments, cosmetics, and in galvanizing steel [30].

Cadmium is a ubiquitous environmental pollutant, is toxic, and is not nutritionally essential [31]. It is known to interact with the metabolism of three essential metals: calcium, zinc, and iron. The source of cadmium uptake by humans is food, where it is found in leafy vegetables, grains, and cereals. Cadmium accumulates in the liver and the kidneys, and has a long biological half-life in humans, ranging anywhere from 10–30 years. The toxicity route primarily involves the renal and skeletal systems, and is a result of the interactions between cadmium and essentials metals, in particular calcium. Cadmium interferes with calcium and vitamin D metabolism in the kidneys. There have been epidemiological studies that have shown human populations in areas of cadmium pollution show signs of hypocalcaemia, such as in Japan where the severe disease called Itai-Itai affected many people as a result of excess cadmium exposure through the consumption of rice grown in contaminated waters [32, 33]. The interaction of cadmium and calcium in bone can result in disorders of bone metabolism. Cadmium that is deposited in osteoid tissue interferes with calcification, decalcification, and bone remodeling [34]. Pregnancy increases cadmium accumulation in the kidneys and mobilizes copper and zinc bound to metallothionein. This effect supports the role of metallothionein in the storage of zinc and copper, and their transport from the placenta to the fetus, where the metals are needed for growth and development [30].

From ^{113}Cd NMR and X-ray structures, the two-domain binding arrangement in which all 7 Cd(II) are tetrahedrally coordinated has been established for mam-

malian proteins. Only recently have the metallation pathways for Cd(II) binding to both the apo-MT and Zn_7MT been described [28, 35]. The pathways were elucidated primarily from metallation studies using ESI-MS, which provides the individual speciation up to metal saturation. Two pathways were described that were pH-dependent (Figure 4). At low pH, Cd(II) binds in a cooperative cluster-driven pathway, whereas at physiological pH, Cd(II) binds in a non-cooperative beaded pathway involving individual Cd-Cys_4 coordination [28]. While the saturation of MT with 7 divalent metals was long considered to be the end of the reaction, ESI-MS data showed that supermetallated structures formed that could be characterized by ^{113}Cd NMR for $Cd_5\alpha$MT-1 and Cd_8MT-1 [23, 36]. These structures suggest a flexibility in the MT chain previously unexpected and unreported. Although mammalian MT binds cadmium, it is not clear whether detoxification is a major role. Detailed analysis of the ESI-MS data over the course of metallation using a two-way competition with carbonic anhydrase (CA) supported a binding model at physiological pH for which five M-Cys_4 (where M = Zn or Cd) formed prior to the rearrangement to the two well-established clusters, with two additional metals [28].

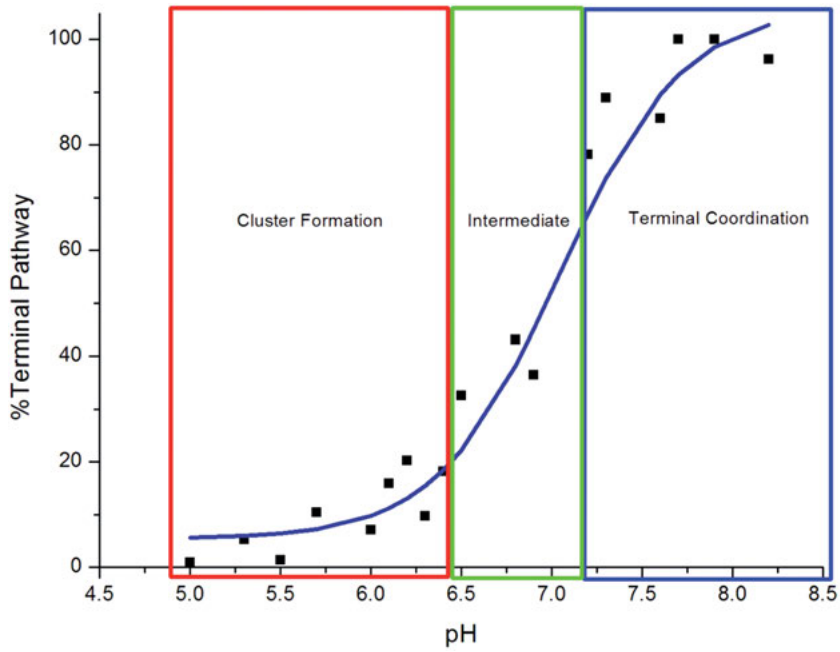

Figure 4. Change in cadmium binding pathway to apo-MT-1 as a function of pH. The "%Terminal Pathway" was calculated from the individually measured ESI-MS data for a single addition of Cd(II) at each pH. The cluster formation pathway dominates below pH 6.5, while between pH 6.5–7.2 the two pathways compete. The terminal pathway based on "beads" dominates above pH 7.2. Reproduced with permission of the Royal Society of Chemistry, 2016 [28].

2.2. Reactions of Metallothioneins with Arsenic

Arsenic has been listed as number one in the Comprehensive Environmental Response Compensation and Liability Act Priority List of Hazardous Substances that is published by the Agency for Toxic Substances and Disease Registry [37]. To understand the toxicity of arsenic, it is imperative to understand the toxicology of this metalloid, an element that has properties of metals and non-metals. Arsenic in the environment is found in both inorganic and organic forms, as well as in different oxidation states. Toxicologically, the notable valence states of arsenic are the trivalent (III) and pentavalent (V) states, which humans are most exposed to. The most toxic arsenic compounds are those in the trivalent oxidation state. This is due to their reactivity with sulfur-containing compounds and generation of reactive oxygen species (ROS).

Historically, arsenic has been used to treat certain ailments: in the 1700s it was used as a 1 % solution of potassium arsenite to treat malaria, syphilis, asthma, chorea, eczema, and psoriasis. It was used in a drug called Salvarsan that was introduced in 1910 to treat syphilis until penicillin came up in the 1940s, and was subsequently glorified by the Warner Bros. movie *Dr. Ehrlich's Magic Bullet*. Arsenic has also been used as a cancer chemotherapeutic and is used as drug for treating acute promyelocytic leukemia. Arsenic was heavily used as a pigment (e.g., Paris Green) in the 1800s and was a large cause of unintentional arsenic poisoning, as it was employed heavily in wallpaper at the time. Paris Green was also served as an insecticide from 1867 until 1900 to control Colorado potato beetles and mosquitoes. Lead arsenate was heavily used as a pesticide for apple and cherry orchards in the early 1900s, being phased out in the 1960s. Until 1900s, concerns regarding arsenic toxicity focused on acute effects. However, the use of arsenic in insecticides increased the understanding of how low levels of exposure over long periods of time affected public health [4]. Early studies in orchard workers showed the correlation between arsenic exposure and cancer. Although the use of lead arsenate pesticides was eliminated 50 years ago, its environmental persistence continues, as it is estimated that millions of acres of land are still contaminated with lead arsenate residues. This poses a potentially significant public health concern in some areas of the United States (e.g., New Jersey, Washington, and Wisconsin). Arsenic in drinking water is mainly in an inorganic form and can be stable as both arsenite and arsenate, which are trivalent and pentavalent, respectively. Where levels in the groundwater concentration are typically 1 μg/L or less, some levels in Nevada were found to be about 8 μg/L. Outside of the United States, there are cases of several hundred μg/L concentrations, causing significant human exposure through drinking water. Many foods contain organic arsenic compounds, though they are typically considered to have low toxicity. Some of these compounds are mono- and dimethylarsenic acids, arsenobetaine, arsenocholine, arsenosugars, and arsenolipids [37].

Arsenic binds strongly to MT. These metallation reactions have yielded the first reported stepwise kinetic data [38]. A problem with measuring kinetics for most metals with MT is that binding rates are fast. In most methods, the signal is an average, as each chromophore is essentially identical over the course of the

reaction. However, with As(III), the binding reaction is slow enough that the ESI mass spectrometric technique is able to measure the presence of all species formed in the reaction, allowing a full kinetic analysis. An important feature of the kinetic data is that at any single point in the metal titration, a range of intermediately metallated species exist. With the knowledge of the super-saturation and metal fluxionality properties, this shows that simply adding a stoichiometric amount of metal to the protein does not guarantee that the species numerated by the stoichiometry will in fact dominate. We illustrate this with the figure for As-binding kinetics (Figure 5) [38].

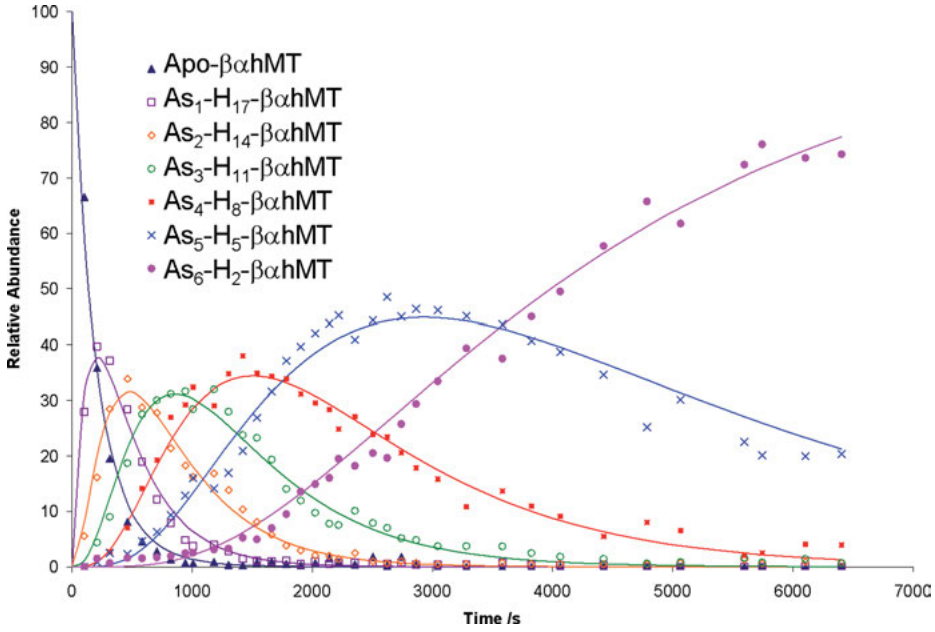

Figure 5. Time-resolved ESI-MS relative abundances for apo-βαMT, following reaction with up to 6 As(III) at 25 °C and pH 3.5 to form As_N-MT (N = 1–6). Reaction was carried out with an As(III) : MT stoichiometric ratio of 11 : 1. Relative abundances for each species are shown as data points on the graphs, with different symbols indicating each component species. The smooth lines are calculated based on the complete analysis of kinetic data for the relative abundance at the specified times. The lines are connected by the series of sequential reactions, as described in reference [38]. Reproduced with permission of the American Chemical Society, 2008 [38].

The data were fit with a single multiparameter algorithm, refined to find 6 binding constants. The most significant result was that the binding constants fell on a nearly linear negative slope as a function of metals bound, indicating that the metalation of the last site was the slowest, and therefore had the lowest binding affinity. This important property was also later determined for Cd(II) and Zn(II) binding to metallothionein, again indicating that for multi-metal

binding site proteins, the first metal will bind faster than the last. Molecular mechanics/molecular dynamics (MM/MD) for the As-MT structure revealed that As(III) bound to three cysteines, and that 6 As(III) coalesced into a 3D ball-like structure. This structure is important in the context of Pb-MT because Pb(II) is expected to bind as PbS_3, and so a Pb-MT structure may have similarities with the As_6-MT structure. We have also studied As(III) binding to the *Fucus vesiculosus* algal MT protein and were able to calculate binding constants that showed the presence of two As-binding domains, such that As_2S_7 and As_3S_9 formed over time. The importance of this analysis was that the arsenic bound solely to 3 cysteine thiols, and the stoichiometric ratio is dependent on this numeracy. Benzoquinone modification of unattached cysteines was used to prove that arsenic did not involve coordination by other amino acids, showing that for the mammalian As_6MT two benzoquinones bound to the free thiols [39].

2.3. Reactions of Metallothioneins with Mercury

Every form of mercury is toxic to humans. The toxic effects are organ-specific and depend upon the chemical form of mercury, along with the duration, route, and level of exposure. The differing forms of mercury are known to deposit preferentially in different tissue compartments, this being the result of differing toxic profiles. Methylmercury (MeHg) is almost entirely absorbed across the intestines and through the blood-brain barrier, whereas inorganic mercury follows the same absorption route but at a more inefficient level. Methylmercury is the most toxic form of mercury, which has a half-life of 70 days in humans. Its route of transport demonstrates its high rate of deposition in hematopoietic and neural tissues.

There are 3 chemical forms of mercury: elemental (mercury with no other atoms attached to it), organic, and inorganic. These forms are interconvertible and are all capable of producing systemic toxicity. At ambient temperature, metallic mercury is a liquid and is released into the atmosphere as mercury vapor. Methylmercury is formed from the methylation of inorganic mercury by microorganisms found in soil, water, and in the human mouth when mercury vapor is released from amalgam dental fillings. It is also formed through non-enzymatic methylation. Methylmercury in tissues binds to sulfhydryl molecules (compounds that contain a functional group of a sulfur atom and a hydrogen atom, or -SH) which could be L-cysteine, glutathione (GSH), hemoglobin, albumin, metallothionein, or other cysteine-containing polypeptides.

Once mercury is in the body, it binds to sulfur-containing molecules such as glutathione, along with any protein-based cysteine, including MT. Mercury vapor, once absorbed through the lungs, is converted by catalase to divalent mercury in tissues, and then is excreted in bile as a glutathione conjugate. This is eliminated by the body in feces. MeHg is also eliminated through conjugation with glutathione in the liver, again being excreted as bile. When bound to glutathione or cysteine, inorganic mercury is filtered through glomeruli and then reabsorbed in the renal proximal tubule.

Mercury exposure can come from numerous sources, such as silver amalgam dental fillings, and fish consumption (such as mackerel, shark, swordfish, tilefish, and tuna). There have also been cases reported in dietary supplements and Chinese medicine [40].

Mercury binds strongly to metallothionein, forming a range of species that were identified through titrations monitored by CD spectroscopy and ESI-MS [41]. The important stoichiometric ratios identified through the CD data were Hg : MT of 7, 11, and 18 : 1. The presence of three unique species suggests that Hg adopts three different coordination geometries, and that in addition to the flexibility of MT, one must also consider the coordination flexibility of the metal being bound. In this case, the Hg_7MT was assigned as tetrahedral coordination, the Hg_{11}MT to trigonal coordination, and the Hg_{18}MT to the supermetallated single domain with digonal coordination. We comment that similar fluxional behavior of both the metal and the protein have been reported for Cu(I) binding [42].

3. METALLOTHIONEINS AND LEAD

3.1. Overview of Papers and Their General Results − A Summary

Human manipulation of lead in industrial activities has resulted in heavy metal pollution in the environment since ancient times, an exposure risk that remains of great concern today for human health.

Currently, the body burden of lead in the general population has been estimated to be 1000 times higher than that of the prehistoric human. The primary routes of lead exposure are lead added to gasoline, industrial emissions, lead solder, lead batteries, and lead in glazes and paints. For industrialized, wealthy countries, the exposure to lead has decreased significantly with the removal of lead additives to gasoline. In developing countries, the exposure to lead is still very high. For inhalation, exposure from the air is dependent on the use of leaded gasoline; in areas where levels of lead are low, food is the dominant source. Areas where the air concentration is high list inhalation as the largest route of exposure. A study in Tokyo and Kyoto (where leaded gasoline is still used) found that gasoline contributed to 50 % of the lead absorbed by humans. The cities that still use leaded gasoline (or have only recently phased it out) have air lead levels around 200–400 ng/m^3, while in areas with heavy traffic the levels are much higher, in the range of 2000–3900 ng/m^3. Lead inhalation in areas near lead-emitting industrial centers is also a significant source of exposure [43].

For ingestion as a route of exposure, the ingestion of lead objects (e.g., fishing sinkers, curtain weights) by small children can cause dangerously high levels of lead in the body. Lead content in drinking water varies greatly. Daily consumption in Sweden is estimated at 1 μg/day, whereas in Hamburg, Germany, where lead pipes are common, the range in lead concentration is between 5 μg/L and 330 μg/L. Lead intake also occurs through food consumptions; it is present in

vegetables from the deposition of lead from air. The lead exposure through foods varies by country, with the standard American adult having an intake of 3 μg/day, compared with a typical adult in the United Kingdom, who takes in 27 μg/day. In diet, the items containing the highest amounts of lead are fruits, vegetables, cereals, baked goods, and beverages [4]. Sequestration of a variety of heavy metals by metallothioneins, as discussed earlier in the chapter, is believed to be related to an organism's defence against enzyme inhibition, where divalent metals like Zn(II) and Cu(II) are cofactors that can be replaced by Pb(II), disrupting function. Studies of lead exposure to various species of fish and rats show that there is a positive correlation between lead uptake and metallothionein biosynthesis [44–46].

A review by Fowler discusses several papers that examine the intracellular bioavailability of lead at low dosages in rat kidney and brain [47]. In rat kidneys there were several low-molecular-weight protein peaks found in the cytosol, which could possibly be a tetramer and demonstrate stable binding of ^{203}Pb on SDS gels. It was demonstrated that *in vitro*, cadmium and zinc were the most effective competitors for inhibiting Pb binding to the lead-binding protein, which correlates to an *in vivo* study. In the rat brain, the lead-binding protein was an acidic protein with a high content of glutamic and aspartic amino acids and ion-exchange chromatographic characteristics similar to renal lead-binding proteins. In human kidneys there are two lead-binding proteins identified as diazepam-binding inhibitor and thymosin β_4. Brain studies have shown that lead is endogenously bound to thymosin β_4. The intracellular partitioning of Pb in target organs can be involved in mediating the low dose effects of lead, as these proteins are chemically similar and vary between species and target organs, with K_d values for lead around 10^{-8} M. The *in vitro* studies show the binding of Pb is very stable and represents the Pb pool in the cytosolic compartments. Fowler hypothesized that the soluble Pb-binding proteins in major target tissues such as the brain and kidney are involved in mediating these individual differences in susceptibility, particularly at low-dose exposures.

In the paper by Galano and coworkers, the effects of cadmium and lead on the viability of human primary renal cells (HRCE cell line) and their impact on cell proteome were evaluated [48]. The kidney was chosen as it is a primary target organ of heavy metals due to its ability to reabsorb and accumulate divalent metals. Comparisons between lead and cadmium suggest that different apoptosis mechanisms may be activated with lead, that toxic effects are dose- and time-dependent, and that these effects were more evident with cadmium. In the case of lead, the observed cell death was not exclusively due to apoptosis activation. There is more than one mechanism that can be activated by lead; this study showed an increase in DNA fragmentation and caspase-3 activation upon heavy metal treatment and is in line with *in vivo* studies demonstrating apoptotic cell death in proximal renal tubules of experimental animals post cadmium exposure. The proteins involved in cell metabolism are also affected by metal exposure, as shown in Table 3 of [48]. For example, Enolase 1 (ENO1), a major glycolytic enolase in non-muscle and neuronal cells, showed an increased exposure upon lead exposure, but was unaffected by cadmium.

A review paper by Gonick describes studies of a variety of lead binding proteins, most notably δ-aminolevulinic acid dehydratase (ALAD) and metallothionein [49]. ALAD is a zinc-dependent enzyme involved in heme synthesis and is both induced and inhibited by lead in humans, with lead exposure leading to increased amounts of ALAD. Various isoforms of ALAD exist, with ALAD-2 binding lead ions more strongly, a characteristic associated to its higher electronegativity when compared to ALAD-1. In the presence of zinc-bound metallothionein, Zn(II) is donated to activate ALAD from MT, with Pb(II) preferring to form lead-metallothionein (termed lead-thionein in their paper).

Gonick also summarizes the results of biological studies involving lead injections into rats and the resulting induced expression of metallothionein. Metallothionein-null phenotypic mice demonstrate nephromegaly, decreased renal function, as well as metastatic renal cell carcinoma upon lead exposure, which does not appear in wild-type mice. It also appears that in wild-type mice, exposure to lead resulted in metallothionein-based inclusion bodies that are not induced in null-type mice [49].

In a series of papers, Jalilehvand and coworkers have reported on the structures of several compounds that model the interactions between Pb(II) and cysteine, in cysteine itself, in glutathione, and in penicillamine [50–53]. The Jalilehvand group combine the structural power of X-ray absorption methods, both EXAFS and XANES, to provide good bond lengths with reasonable coordination numbers. Donor atom identification information was obtained from the descriptive power of UV-visible absorption spectroscopy identifying ligand-to-metal charge transfer bands, and ^{207}Pb NMR. The significant value of the ^{207}Pb NMR is that the chemical shift between peaks is so wide that it allows discrimination between donor atoms quite clearly.

Their results for Pb(II) reactions with glutathione (GSH) are of direct interest in the later description of Pb(II) binding to metallothioneins. The 2012 paper used ESI-MS data for a solution of GSH and Pb(II) to identify formation of a mixture of $Pb(GSH)_3$, $Pb(GSH)_2$, and $Pb(GSH)_1$ [51]. These results do indicate the issue of mixtures that compounds form in solution gives difficulty in structural assignment for nearly all characterization methods but for X-ray diffraction (as illustrated in the As-MT data, Figure 5). Mah and Jalilehvand tried to systematize the species formed between Pb(II) and GSH by varying the pH and using the Pb coordination sensitivity of ^{207}Pb NMR, however, the results were somewhat ambiguous [51]. The authors stated in their summary of the results that "…The combined results from the UV-Vis, ^{207}Pb NMR, and Pb LIII-edge EXAFS spectroscopic studies suggest, therefore, that solution B contains a mixture of Pb^{2+}-GSH complexes with PbS_3 and PbS_2N_2 geometries (Scheme 3 of [51]), where GSH coordinates via its NH_2 and thiol groups to the Pb^{2+} ions, …". Later, in 2015, Sisombath and Jalilehvand noted the very close overlap of the ligand-to-metal charge transfer bands and EXAFS spectra for acetylcysteine in the GSH/Pb(II) complexes, and concluded that in complexes of Pb(II) with GSH at basic pH and with Pb : GSH ratios near 2, the Pb(II) likely forms a dimeric or oligomeric species for tetrahedral coordination by 4 S donor atoms [52].

Their XANES data for a series of Pb(II)-GSH solutions (with different Pb(II) : GSH stoichiometric ratios) indicated a mixture of coordinations was likely present [51]. Analysis of the associated EXAFS data suggested that for $Pb(GSH)_2$, the Pb(II) was 4 coordinated (2 N;2 S) with a non-bonding pair acting as a 5th site; for $Pb(GSH)_3$, the coordination number was 3 with 3 thiolate donor atoms where the Pb-S bond length average was 265 ± 4 pm. It is clear from all the data described in this paper that unravelling the complexes formed in solution with ligands that provide more than one donor atom (here O, N, and S) requires the combination of a number of probes – and those sensitive to the donor atom identity provide very useful information, here the ^{207}Pb NMR in conjunction with the XAS methods. Interestingly, the ESI-MS data were not as informative as one might hope. In 2015, their work with another good model for the MT peptide, N-acetylcysteine, again using a combination of ^{207}Pb NMR, ESI-MS and EXAFS, suggested that the initial assessment of the coordination in $Pb(GSH)_2$ being a mixture of 2 N and 2 S, might be incorrect and that dimers or oligomers form with the Pb(II) coordination being the same 3 S as in $Pb(II)(GSH)_3$ [52]. This latter study reinforces the need for the use of multiple methods when studying complex formation for metals that can readily bind to different donors.

Studying Pb(II) binding to biological thiol complexes provides the groundwork for investigating larger thiol containing proteins, like metallothionein. To elucidate protein-metal binding reactions, *in vitro* analysis must be carried out to give the detailed information necessary. Below, we discuss the many reports using spectroscopy, mass spectrometry, isothermal titration calorimetry, X-ray absorption, ^{207}Pb NMR, and computational studies to uncover the structure and metal binding properties of lead to metallothioneins.

3.2. UV-Visible and Circular Dichroism Spectroscopic Data

The spectroscopic properties of Pb-MT have been demonstrated to be pH-dependent. Early spectroscopic studies by Bernhard et al. showed Pb_7MT displaying a ligand-to-metal charge transfer (LMCT) band at approximately 350 nm at pH 8, with supporting magnetic CD and CD spectra [54]. However, alkaline conditions cause $Pb(OH)_2$ precipitation, resulting in broad absorption from scattering between 300–350 nm. This may have skewed early results. More recently, He et al. described the difference in the two states through spectroscopic studies [55]. At neutral (pH 7.0), solutions of Pb(II) bound to rabbit liver apo-MT-2 exhibiting a LMCT band at 330 nm ($\varepsilon \sim 3500\,M^{-1}\,cm^{-1}$), which was consistent with PbS absorption in small molecule studies, with no CD bands being observed. The lack of a CD spectrum differs from the distinct CD spectra observed for Cd_7- and Zn_7MT, indicating that a different binding structure occurs in the case of Pb_7MT. However, at weakly acidic (pH 4–5) conditions, there were drastically different spectra with two new bands appearing at 325 and 375 nm, and a shoulder at 400nm. The CD spectra show maxima at 240 (+), 265 (+), 320 (−), 350 (+), 370 (+), and 395 nm (−), with isodichroic points at 280, 340, and 375 nm. The change in acidic structure has been associated with increased pro-

tein flexibility, allowing Asp 2 and 56 to coordinate each Pb(II), as suggested by molecular modelling [55].

In a comparison with Pb(II) replacement of Zn(II) in Zn_7MT, and for the Pb-MT formed following reconstitution of apo-MT (both rabbit liver MT-2), Chu et al. demonstrated that the Pb_7MT product of these two reactions resulted in very different UV-visible absorption and CD spectra [56]. In the UV absorption spectrum, the Pb-MT formed by the replacement of Zn(II) in Zn_7MT by Pb(II) showed a strong shoulder at approximately 350 nm, while the apo-MT reconstituted with Pb(II) resulted in absorption bands forming at 330 nm and 375 nm, with a slight shoulder at 400 nm. The CD spectra of the Zn_7MT replacement showed a strong maximum at 275 (+) after Pb(II) addition, which did not appear in the apo spectra. These results are further supplemented by microcalorimetry data, as discussed in the thermodynamic studies section below [56].

3.3. Electrospray Ionization Mass Spectral Data

ESI-MS is a soft ionizing technique, useful for studying small proteins such as metallothioneins. The high resolution capabilities allow for the monitoring of reactions in real time, providing a vast amount of information not limited to binding stoichiometry and kinetics. ESI-MS has already been employed in studies of metallothionein binding to a wide variety of metals, including Zn(II), Bi(III), As(III), Cd(II), Ru(II), Rh(II), Pt(II), Cu(I), Hg(II), Ag(I), and Au(I), as well as studies regarding its role in metal exchange to enzymes [41, 57–64]. In 2004, RP-HPLC-ICP-TOF-MS was used to identify heterogeneous metal Pb-containing proteins in carp liver metallothioneins [65]. Palacios et al., in 2007, reported findings involving ESI-MS studies for Pb(II) metal displacement in recombinant mouse Zn_7MT and its domain fragments at both pH 7 and pH 4.5, where the apo species predominates [66].

Under neutral conditions, Pb(II) titrations of the full protein resulted in metal displacement of Zn(II) in Zn-MT by Pb(II). For example, a titration using 7 mol. eq. of Pb(II) resulted in formation of mixed Zn-Pb-MT species together with the homogenous Pb-MT species, with up to Pb_9MT visible upon addition. After 2, 6, and 24 hours post metal incubation, these homogenous Pb-MT species disappeared, with only the original Zn_7MT remaining. With excess additions of Pb(II) (~35 mol. eq.), a stoichiometry of up to 12 Pb(II) ions bound to the MT was measured, with the heterogeneous Zn-Pb-MT species also formed [66].

Under acidic conditions (pH 4.5), Zn-MT solutions also contain the metal-free (apo) species, as Zn ions are weakly bound. Addition of Pb(II) into acidic apo-to $Zn_3\beta$-MT created both mixed and homogenous Pb-MT with up to Pb_4-MT formed. As above, after 24 hrs, the predominant species were apo-β-MT with small amounts of Zn_{1-3}-MT species (see Figure 5 of [66]). In both cases, the Pb-MT is lost over time. While Pb(II) has a higher affinity for cysteine binding than Zn(II), Pb_7MT formation appears to be favored kinetically. However, it is not thermodynamically stable as a result of the competing formation of $Pb(OH)_2$ [66].

3.4. Thermodynamic Studies

Isothermal titration calorimetry (ITC) provides thermodynamic information for reactions in solution. In the case of metal binding to metallothionein, the change in Gibbs free energy (ΔG), entropy (ΔS), and enthalpy (ΔH) can be determined through the course of the reaction. As well, stoichiometry and reaction equilibrium constants for each binding event can also be calculated, meaning ITC gives rich information for protein-substrate interactions.

Two groups have used ITC for investigating lead binding to metallothionein. In 2000, Chu et al. showed that metal replacement in Zn_7MT and reconstitution of apo-MT with Pb(II) are spontaneous, exothermic, and entropy-increasing with each molar addition [56]. For each molar equivalent addition of Pb(II) to Zn_7MT, the thermodynamic parameters were reported as $\Delta G = -28.7$ kJ/mol, $\Delta H = -25.2$ kJ/mol, and $\Delta S = 11.6$ J/mol K, whereas for reconstituted apo-MT, each molar equivalent addition of Pb(II) had thermodynamic values of $\Delta G = -32.4$ kJ/mol, $\Delta H = -17.8$ kJ/mol, and $\Delta S = 48.8$ J/mol K.

In 2016, Carpenter et al. used a different procedure to determine the thermodynamic parameters of Pb(II) binding to human recombinant Zn_7MT-3 [68]. They explored the titration of Pb(II) into Zn_7MT, as well as the demetalation of Pb_7-MT using competitive EDTA chelation. For both, the resulting isotherm curve displayed three inflection points, indicating that metallation and demetallation was triphasic. The reaction began exothermically, then became endothermic, with the final stage being again exothermic. This triphasic binding process complements results reported of multiphasic rates of zinc metallation of MT. This three-stage binding process indicates a significant sequence of structural changes as the protein folds to accommodate the metals, and that Pb(II) binding to MT is an overall thermodynamically favored process [68].

3.5. X-ray-Absorption Data

X-ray absorption spectroscopy (XAS) provides several extremely powerful spectroscopic techniques for use in the analysis of metal-binding sites in proteins, since crystals are not required for accurate bond lengths and fairly precise coordination numbers. An example of the use of EXAFS in the determination of the coordination of lead in cysteine-rich proteins is provided by Magyar et al., in which they challenge the Zn binding sites in a number of zinc-finger proteins by replacing Zn(II) with Pb(II) [69]. They calibrated their Pb-protein data using small molecule models. The data reported illustrates the detail that may be obtained from EXAFS data. Their consensus fits to their protein data for lead resulted in coordination numbers of 3 with a Pb-S bond length of approximately 264 pm, though in some data sets, a coordination number of 2 also fit the data with low error. Their associated absorption spectra for the Pb(II) complexes are similar to those reported for Pb-MT and described above.

Hasnain et al. in 1987 reported the only data available for X-ray absorption spectra of Pb-MT [70]. In their paper from the *Metallothionein II* conference,

they compared EXAFS data for Zn, Cu, Cd, Ag, Hg, and Pb-MT. At that time, they did not report fitted data. However, the alignment of the EXAFS spectra of Hg_7MT and Pb_7MT suggested similar environments, and their preliminary analysis provided a Pb-S bond length of 265 pm, compared with 240 pm for Hg-S in Hg_7MT. Unfortunately, there are no details of the preparative methods used to obtain either the Hg_7-MT or Pb_7-MT, so the stoichiometry of both is, to some extent, uncertain [70]. Studies by Cai and Stillman have shown that for rabbit liver MT-2 a range of stoichiometries exists, such that a single species may not be obtained by simply adding the theoretical molar equivalents [41]. This is more clearly observed in the data for As(III) binding to metallothionein from Ngu et al., where several species coexist at each theoretical mole equivalent added to the protein (see Figure 5) [38].

3.6. ^{207}Pb NMR Data

^{207}Pb NMR has a large range in chemical shift (ppm), which is useful for probing the binding behavior of lead in proteins. In relation to sulfur-rich zinc proteins, ^{207}Pb NMR can provide strong evidence for binding stoichiometry and ligand identity. In a study by Neupane and Pecoraro, ^{207}Pb NMR was employed for the investigation of proteins with cysteine in their metal coordination sites, including glutathione and zinc finger proteins, in addition to *de novo* synthesized peptides [71]. They showed that the Pb-S chemical shift of the NMR peak in the Pb-glutathione complex occurred at ~5750 ppm (pH-dependent), confirming the PbS_3 binding motif. However, Pb binding in the zinc finger with Cys_2His_2 as its Zn coordination site showed two chemical shifts, at 5790 and 5744 ppm, arising from two species, only one of which was stable at higher temperatures.

He et al. reported the ^{207}Pb NMR spectra of the two species of rabbit liver Pb_7MT-2 formed, one at pH 7.0 and the other at pH 4.5 [55]. The NMR data were completely different, with the appearance of a peak at 4348 ppm assigned to an oxygen-containing ligand for the pH 4.5 Pb_7-MT species. They assigned the lead coordination in MT-2 at pH 4.5 species as PbS_3O_1. They concluded, following other tests, that Asp was the ligand providing the oxygen coordination, and that the low pH UV absorption and CD spectral data were a result of said oxygen coordination. The neutral pH Pb_7-MT species showed only a single peak at 5679 ppm, consistent with a trigonal pyramidal coordination for each PbS_3. Despite the lack of detail in the ^{207}Pb NMR data, the extremely large chemical shifts, which are sensitive to the coordinated ligand, allowed for quite precise determination of a solution structure in the absence of a crystal structure.

3.7. Molecular Modelling

Molecular modelling has long proven an invaluable source of information about geometric possibilities for metal-ligand coordination complexes in the absence of X-ray structures, for reaction pathway excited state geometries, and as a basis

for the interpretation of spectroscopic data (including X-ray, UV-visible, and IR optical data, as well as Raman and NMR spectral data). The methods available for small coordination complexes have been extended to the metal binding sites in metalloproteins using a combination of the non-quantum-based molecular mechanics and dynamics methods (termed for simplicity, MM), up to the near-*ab initio* quality of DFT methods (termed, QM). A recent review illustrates this latter quality in the analysis of heme protein reaction pathways [72]. For molecules as large as a metalloprotein, the DFT methods become far too costly in terms of computational resources, however, a neat approach is to split the computational job between molecular mechanics (MM) and DFT, which can be expressed as a QM/MM hybrid calculation. One approach that offers the user a range of computational methods is ONIOM (short for "our own n-layered integrated molecular orbital and molecular mechanics"), developed by K. Morokuma and his team since 1996 [73]. ONIOM is fully parameterized in the computational program Gaussian [9].

One of the issues with using any form of computational method is determining the accuracy of the result. The accuracy of the calculated geometry and the calculated spectral data may be difficult to resolve due to inherent errors in the key facets of the methods chosen, such as the force fields in MM and the functionals in the DFT approach. For metalloproteins without available X-ray structures as guides for at the least some aspect of the computational work, X-ray absorption-based techniques (EXAFS and XANES), metal-based NMR, Raman, and even optical spectroscopic data can be used, though each of these techniques suffers from being both deficient in a specific part of the binding site properties required (either geometry, coordination number, or exact donor atoms) or by being averages of the properties of many different coexisting species. Thus, computational models need to be judged based on as many predicted properties as possible.

Early molecular dynamics calculations of rabbit liver Cd_7-Zn_7- and Hg_7-MT-2 and of Cu_{12}-MT-2 were based on the atomic coordinates derived from the X-ray structure of rat liver Cd_5Zn_2-MT-2 and compared with the NMR data [22, 74–76]. While the NMR data summarized in this last paper provided a very accurate description of the protein backbone, no data were provided explicitly for the metal-thiolate bonding, and, particularly, the metal-thiolate bond angles were far from optimum for the tetrahedral structure of each Cd(II). This was essentially unrealistic when compared with experimental data for Cd(II)-thiolate models. To provide good force field parameters for Cd_7-MT-2, Chan et al. compared simulated XANES data based on models with experimental XANES data. The conclusions reached were that the $Cd_4S_{11\text{-}CYS}$ and $Cd_3S_{9\text{-}CYS}$ metal-thiolate cluster structures needed to be more symmetric than as proposed in either the NMR or X-ray structures [77]. Later studies by Soldatov and coworkers introduced higher level calculation for the geometry in each cluster [78]. The conclusion from this work was that experimental data should be predicted and then obtained when calculating geometries as fluxional as those found for the 7 divalent metals bound to MT. These authors used predictions of the XANES data from the Cd-edge to calibrate the force fields in the MM calculation of Cd-MT [78].

The most detailed MM and MD studies of metal-free MT (fragments and full protein), partially metallated-MTs, and MT fragments and full protein metallated with Cd(II) and separately, Cu(I) and As(III), have been reported by Stillman and coworkers [10, 38, 75, 77, 79–82].

The question of the possible structural properties of the metal-free MT (apo-MT) was addressed by Rigby and Stillman in 2004, with the MD trajectory data showing that the protein coalesced into a 3-dimensional structure with the cysteinyl thiolates located near the outer surface [82]. This structure was supported experimentally in a combined metal-binding kinetic and ESI-MS study where metallation rates for the folded and unfolded α-fragment were determined. Under folded conditions near pH 7, the metallation was significantly faster than at low pH, or in the presence of guanidine hydrochloride reversible denaturing agent, with the interpretation that metallation when the cysteinyl thiols were on the surface allowed formation of the tetrahedral site faster than when the peptide was completely unwound [81, 82]. In all of these MD calculations, it was found that the apo-peptide arranged itself into a globular conformation, one with similar dimensions to that of the metallated protein. ESI-MS data at a range of pH values for the apo-MT supported a conformation that above pH of about 5 was similar to that of the metallated protein in terms of surface area, due to the charge states being constant over a range of metallation states [81, 83].

The most ambitious MM/MD study concerned the multiple α domains of the double and triple α proteins. As shown in Figure 6, the demetallation of the recombinant human Cd_{12}-ααα-MT-1 was studied with respect to the available pH-dependent ESI-mass spectral data. This showed the first effect of an acidic pH, which was to lose 4 Cd(II), then the remaining 8 Cd(II), demetallated over a very narrow pH range. This again couples computational results with experimental data [79].

Since 2007, a number of advanced calculations have been reported (for example, those of Greisen et al. [84] and Kepp [85]) that are of significance when we address the detailed ONIOM calculation of He et al. [55]. He et al. compared their method to the published NMR data, though this seems somewhat odd in view of the paper of Chan et al. [77] described above, where the Cd-S bond angles and the bond lengths were found to be unreasonably distorted in both the X-ray data and the NMR data sets published on the Protein Data Bank [55, 77]. The spectroscopic and computational modeling of Chan et al. was conclusive in showing that actually the Cd(II) adopted a very symmetric coordination geometry. Indeed, for He et al. to state that the coincidence of their computational results with the NMR data secured their ONIOM calculations requires critical re-evaluation [55].

The results from the ONIOM calculation by He et al. [55], do, however, provide an important extra component with which to assess the metallation products: the TD-DFT calculation prediction of the spectral data. The calculation was set up using two different amino acid residue coordinations for the 4 Pb(II) ions in the α fragment domain. To mimic the neutral pH coordination, the authors chose to include a bridged or shared thiolate from cysteine18 (S18). There is no experimental evidence that cysteines bridge for As(III) or Pb(III), but while

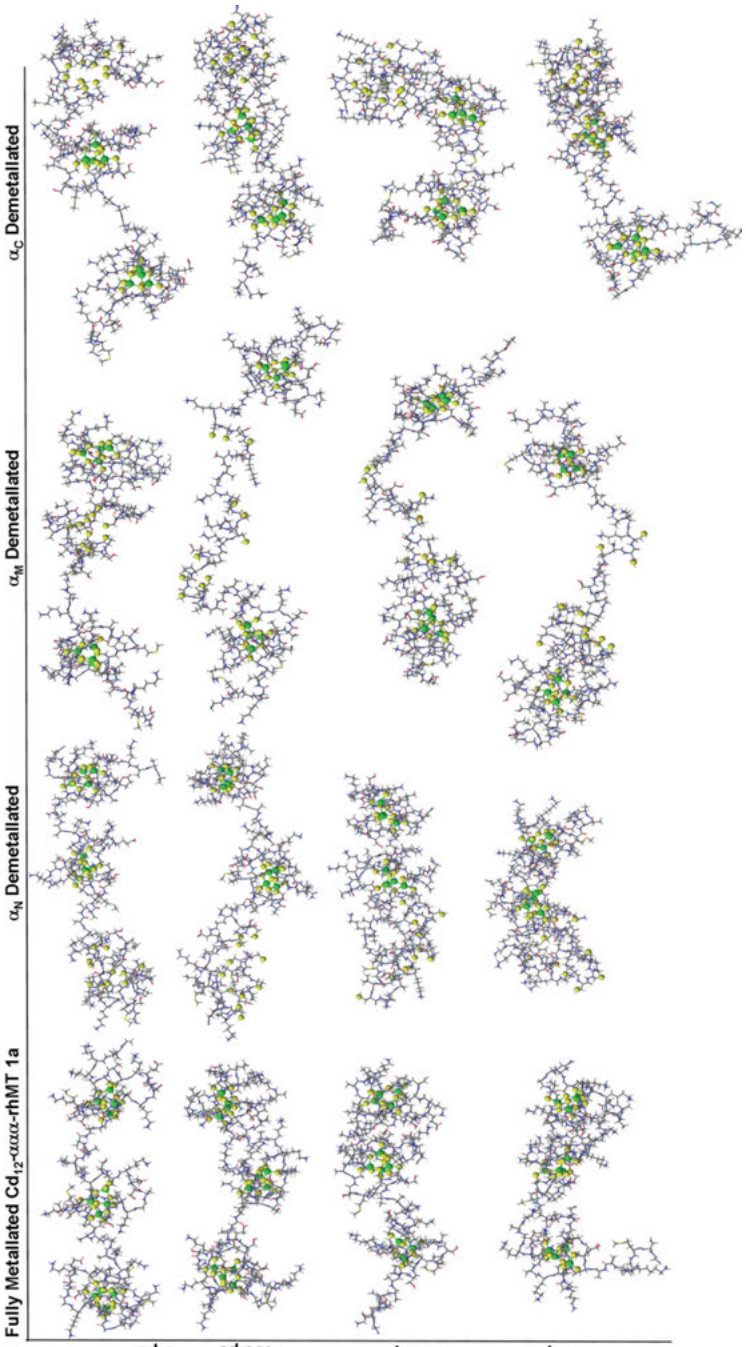

Figure 6. Conformers extracted from the MD trajectory change in secondary and tertiary structure of Cd_n-αααα-rhMT-1a (n = 12, 8, 8, and 8) at 0, 100, 400, and 500 ps, with a simulated temperature of 300 K. Structures are shown for Cd_{12}, $Cd_0Cd_4Cd_4$-, $Cd_4Cd_0Cd_4$-, and $Cd_4Cd_4Cd_0$-αααα-rhMT-1a. The protein residues are depicted in ball-and-stick form, and are color-coded by atom. The final structures are shown as space-filling images. Note: For the three domains (D1, D2, D3) we indicate which domain is demetallated by α_N for D1, α_M for D2, and α_C for D3. Reproduced from [79] with permission of Wiley, copyright 2008.

only 6 As(III) bind using up 18 cysteines clearly not involving cysteinyl bridging, ESI-MS data clearly show that 7 Bi(III) bind to the 20 cysteines of apo-MT-1a. This supports the optical spectroscopic data that indicates 7 Pb(II) bind to MT-2, so in each case one cysteine would need to bridge two Bi(III) and Pb(II) ions to maintain a purely thiolate coordination [38, 59]. The absence of an oxy donor atom was suggested by the ^{207}Pb NMR spectrum [71].

For the low pH model, He and coworkers chose to include the oxygen from aspartate56 [55]. Again, the rationale was from the ^{207}Pb NMR spectral data. The authors comment that the optical data predicted by the TD-DFT calculations for both these models were very sensitive to the functional used, namely B3LYP *versus* BP86. This, of course, introduces a current issue with DFT calculations: that the choice of parametrization can greatly influence the result, so to some extent one needs to know the answer prior to deciding on the details of the method to be used. In this case, the well-known B3LYP functional resulted in calculated absorption spectra that closely resembled the absorption spectra at both neutral and acidic pH values for the two coordination geometries chosen.

In summary, the computational contribution in the paper by He et al. is the most advanced to date for a metal other than Cd(II) or Zn(II) coordinated to metallothionein [55]. By using the detailed coordination information from ^{207}Pb NMR spectra, the authors built a structure with the extra computational power of the ONIOM method, and were able to provide calculated absorption spectra that resembled those recorded at neutral and acidic pH values. Together, the combination of spectroscopy and computational methods provided a much more secure analysis of the structural properties of Pb_7MT-2.

4. CONCLUSIONS

Studies of lead binding to metallothionein show that the metallation mechanism is dependent on experimental conditions. Acidic conditions provide a starkly different absorption spectrum and NMR signal than at neutral pH, indicating that a significant change in structure occurs. Additionally, Pb(II) reconstitution into apo-metallothionein appears to follow an alternative reaction pathway than replacement of Zn_7MT. ESI-MS shows that while Pb(II) displaces Zn(II) in Zn_7MT, this product does not remain stable over time. Isothermal titration calorimetry provides the thermodynamic parameters, indicating that the Pb(II) binding to apo-MT and replacement of Zn_7MT is favourable and exothermic, and that its binding constant is one magnitude higher than that of Zn(II) binding to MT. X-ray absorption data and NMR confirm a trigonal coordination as PbS_3 binding motif.

While the study of lead and its toxic effects on the body are not fully understood, the research studies carried out to date have provided a significant insight into how the metal sequestration of MT can capture lead and scavenge it efficiently. However, this still leaves the mechanism of toxic effects unknown. While metallothionein binds this toxic pollutant with high efficiency, it is still unclear how it acts to transport or detoxify the metal ion. Still, the progress in the study

of the metal-protein interaction shows the fluxionality with which MT is capable of sequestering a wide array of heavy metals.

ACKNOWLEDGMENTS

We gratefully acknowledge past and present members of the Stillman Bioinorganic Group, of which some contributed to the work is presented here. We thank NSERC of Canada for Discovery Grants to M. J. S., and financial assistance from an Ontario Graduate Scholarship to D. L. W.

ABBREVIATIONS

ALAD	δ-aminolevulinic acid dehydratase
CA	carbonic anhydrase
CD	circular dichroism
EDTA	ethylenediamine-N,N′,N″,N‴-tetraacetate
ESI-MS	electrospray ionization mass spectrometry
EXAFS	extended X-ray absorption fine structure
GSH	glutathione
ITC	isothermal titration calorimetry
LMTC	ligand-to-metal charge transfer
MCD	magnetic circular dichroism
MD	molecular dynamics
MM	molecular mechanics
MT	metallothionein
NMR	nuclear magnetic resonance
ONIOM	our own N-layered integrated molecular orbital and molecular mechanics
QM	quantum mechanics
rhMT	recombinant human metallothionein
ROS	reactive oxygen species
RP-HPLC-ICP-TOF-MS	reverse phase-high pressure liquid chromatography-inductively coupled plasma-time of flight-mass spectrometry
TD-DFT	time-dependent density functional theory
XANES	X-ray absorption near-edge structure
XAS	X-ray absorption spectroscopy

REFERENCES

1. J. Kägi, Y. Kojima, in *Chemistry and Biochemistry of Metallothionein*, Springer, Birkhäuser, Basel, Boston, 1987, pp. 25–61.

2. R. A. Festa, D. J. Thiele, *Curr. Biol.* **2011**, *21*, 877–883.
3. R. G. Pearson, *J. Chem. Educ.* **1968**, *45*, 581.
4. G. F. Nordberg, B. A. Fowler, M. Nordberg, *Handbook on the Toxicology of Metals*, Academic Press, London, UK, 2014, pp. 3–543.
5. R. A. Goyer, *Annu. Rev. Nutr.* **1997**, *17*, 37–50.
6. J. H. Kägi, B. L. Vallee, *J. Biol. Chem.* **1960**, *235*, 3460–3465.
7. M. J. Stillman, *Coord. Chem. Rev.* **1995**, *144*, 461–511.
8. D. E. Sutherland, M. J. Stillman, *Metallomics* **2011**, *3*, 444–463.
9. A. R. Leach, *Molecular Modelling: Principles and Applications*, Pearson, Essex, England, 2001, pp. 1–720.
10. J. Chan, Z. Huang, M. E. Merrifield, M. T. Salgado, M. J. Stillman, *Coord. Chem. Rev.* **2002**, *233*, 319–339.
11. F. A. Stennard, A. F. Holloway, J. Hamilton, A. K. West, *BBA-Gene Struct. Expr.* **1994**, *1218*, 357–365.
12. A. Miles, G. Hawksworth, J. Beattie, V. Rodilla, *Crit. Rev. Biochem. Mol. Biol.* **2000**, *35*, 35–70.
13. B. L. Vallee, in *Metallothionein: Historical Review and Perspectives*, Springer, Birkhäuser, Basel, 1979, pp. 19–40.
14. Schaffer, A., *Biochemistry* **1988**, *27*, 8509–8515.
15. M. J. Stillman, C. F. Shaw, K. T. Suzuki, *Metallothionein: Synthesis, Structure, and Properties of Metallothioneins, Phytochelatins, and Metal-Thiolate Complexes*, Wiley-VCH, New York, 1992, pp. 1–443.
16. M. J. Daniels, J. S. Turner-Cavet, R. Selkirk, H. Sun, J. A. Parkinson, P. J. Sadler, N. J. Robinson, *J. Biol. Chem.* **1998**, *273*, 22957–22961.
17. M. Vašák, D. W. Hasler, *Curr. Opin. Chem. Biol.* **2000**, *4*, 177–183.
18. M. E. Merrifield, J. Chaseley, P. Kille, M. J. Stillman, *Chem. Res. Toxicol.* **2006**, *19*, 365–375.
19. R. Prinz, U. Weser, *FEBS Lett.* **1975**, *54*, 224–229.
20. T. R. Butt, D. J. Ecker, *Microbiol. Rev.* **1987**, *51*, 351–364.
21. V. Calderone, B. Dolderer, H.-J. Hartmann, H. Echner, C. Luchinat, C. Del Bianco, S. Mangani, U. Weser, *Proc. Natl. Acad. Sci. USA* **2005**, *102*, 51–56.
22. A. Robbins, D. McRee, M. Williamson, S. Collett, N. Xuong, W. Furey, B. Wang, C. Stout, *J. Mol. Biol.* **1991**, *221*, 1269–1293.
23. R. Duncan, E. Kelly, C. W. Kirby, M. J. Stillman, *FEBS J.* **2008**, *275*, 2227–2239.
24. W. Feng, J. Cai, W. M. Pierce, R. B. Franklin, W. Maret, F. W. Benz, Y. J. Kang, *Biochem. Biophys. Res. Commun.* **2005**, *332*, 853–858.
25. M. M. Peña, J. Lee, D. J. Thiele, *J. Nutr.* **1999**, *129*, 1251–1260.
26. L. López-Maury, J. Giner-Lamia, F. J. Florencio, *Plant Signal. Behav.* **2012**, *7*, 1712–1714.
27. P. Aggett, *Clin. Endocrinol. Meta.* **1985**, *14*, 513–543.
28. G. W. Irvine, T. B. Pinter, M. J. Stillman, *Metallomics* **2016**, *8*, 71–81.
29. T. B. Pinter, M. J. Stillman, *Biochemistry* **2014**, *53*, 6276–6285.
30. R. A. Bernhoft, *Scientific World J.* **2013**, http://dx.doi.org/10.1155/2013/394652.
31. J. Godt, F. Scheidig, C. Grosse-Siestrup, V. Esche, P. Brandenburg, A. Reich, D. A. Groneberg, *J. Occup. Med. Toxicol.* **2006**, Sep 10, 1:22.
32. G. F. Nordberg, *Toxicol. Appl. Pharmacol.* **2009**, *238*, 192–200.
33. G. F. Nordberg, *Biometals* **2004**, *17*, 485–489.
34. G. Kazantzis, *Biometals* **2004**, *17*, 493–498.
35. T. B. Pinter, G. W. Irvine, M. J. Stillman, *Biochemistry* **2015**, *54*, 5006–5016.
36. D. E. Sutherland, M. J. Willans, M. J. Stillman, *J. Am. Chem. Soc.* **2012**, *134*, 3290–3299.

37. M. F. Hughes, B. D. Beck, Y. Chen, A. S. Lewis, D. J. Thomas, *Toxicol. Sci.* **2011**, *123*, 305–332.
38. T. T. Ngu, A. Easton, M. J. Stillman, *J. Am. Chem. Soc.* **2008**, *130*, 17016–17028.
39. G. W. Irvine, K. L. Summers, M. J. Stillman, *Biochem. Biophys. Res. Commun.* **2013**, *433*, 477–483.
40. N. J. Neustadt, S. Pieczenik, *Integr. Med.* **2011**, *10*, 45–51.
41. W. Cai and M. J. Stillman, *J. Am. Chem. Soc.* **1988**, *110*, 7872–7873.
42. M. J. Stillman, A. Presta, Z. Gui, D.-T. Jiang, *Metal-Based Drugs* **1994**, *1*, 375–394.
43. M. Sullivan, *NEW SOLUTIONS: A Journal of Environmental and Occupational Health Policy* **2015**, *25*, 78–101.
44. D. L. Eaton, N. H. Stacey, K.-L. Wong, C. D. Klaassen, *Toxicol. Appl. Pharmacol.* **1980**, *55*, 393–402.
45. O. Campana, C. Sarasquete, J. Blasco, *Ecotoxicol. Environ. Saf.* **2003**, *55*, 116–125.
46. S. J. Hamilton, P. M. Mehrle, *Trans. Am. Fish. Soc.* **1986**, *115*, 596–609.
47. B. A. Fowler, *Environ. Health Perspect.* **1998**, *106*, 1585.
48. E. Galano, A. Arciello, R. Piccoli, D. M. Monti, A. Amoresano, *Metallomics* **2014**, *6*, 587–597.
49. H. C. Gonick, *J. Toxicol.* **2011**, http://dx.doi.org/10.1155/2011/686050.
50. F. Jalilehvand, N. S. Sisombath, A. C. Schell, G. A. Facey, *Inorg. Chem.* **2015**, *54*, 2160–2170.
51. V. Mah, F. Jalilehvand, *Inorg. Chem.* **2012**, *51*, 6285–6298.
52. N. S. Sisombath, F. Jalilehvand, *Chem. Res. Toxicol.* **2015**, *28*, 2313–2324.
53. N. S. Sisombath, F. Jalilehvand, A. C. Schell, Q. Wu, *Inorg. Chem.* **2014**, *53*, 12459–12468.
54. W. Bernhard, M. Good, M. Vašák, J. H. Kägi, *Inorg. Chim. Acta.* **1983**, *79*, 154–155.
55. Y. He, M. Liu, N. Darabedian, Y. Liang, D. Wu, J. Xiang, F. Zhou, *Inorg. Chem.* **2014**, *53*, 2822–2830.
56. D. Chu, Y. Tang, Y. Huan, W. He, W. Cao, *Thermochim. Acta.* **2000**, *352*, 205–212.
57. A. Casini, A. Karotki, C. Gabbiani, F. Rugi, M. Vašák, L. Messori, P. J. Dyson, *Metallomics* **2009**, *1*, 434–441.
58. D. L. Wong, M. J. Stillman, *Chem. Commun.* **2016**, *52*, 5698–5701.
59. T. T. Ngu, S. Krecisz, M. J. Stillman, *Biochem. Biophys. Res. Commun.* **2010**, *396*, 206–212.
60. P. M. Gehrig, C. You, R. Dallinger, C. Gruber, M. Brouwer, J. H. Kägi, P. E. Hunziker, *Protein Sci.* **2000**, *9*, 395–402.
61. Y. Hathout, D. Fabris, C. Fenselau, *Int. J. Mass Spectrom.* **2001**, *204*, 1–6.
62. T. T. Ngu, M. J. Stillman, *J. Am. Chem. Soc.* **2006**, *128*, 12473–12483.
63. M. Knipp, A. V. Karotki, S. Chesnov, G. Natile, P. J. Sadler, V. Brabec, M. Vašák, *J. Med. Chem.* **2007**, *50*, 4075–4086.
64. C. P. Mercogliano, D. J. DeRosier, *J. Mol. Biol.* **2006**, *355*, 211–223.
65. H. G. Infante, F. Cuyckens, K. Van Campenhout, R. Blust, M. Claeys, L. Van Vaeck, F. C. Adams, *J. Anal. At. Spectrom.* **2004**, *19*, 159–166.
66. Ò. Palacios, À. Leiva-Presa, S. Atrian, R. Lobinski, *Talanta* **2007**, *72*, 480–488.
67. T.-Y. Li, A. J. Kraker, C. F. Shaw, D. H. Petering, *Proc. Natl. Acad. Sci.* **1980**, *77*, 6334–6338.
68. M. C. Carpenter, A. S. Shah, S. DeSilva, A. Gleaton, A. Su, B. Goundie, M. L. Croteau, M. J. Stevenson, D. Wilcox. R. N. Austin, *Metallomics* **2016**, *8*, 605–617.
69. J. S. Magyar, T.-C. Weng, C. M. Stern, D. F. Dye, B. W. Rous, J. C. Payne, B. M. Bridgewater, A. Mijovilovich, G. Parkin. J. M. Zaleski, *J. Am. Chem. Soc.* **2005**, *127*, 9495–9505.
70. S. S. Hasnain, G. Diakun, I. Abrahams, I. Ross, C. Garner, I. Bremner, M. Vasak, in *EXAFS Studies of Metallothionein*, Springer, Birkhäuser, Basel, 1987, pp. 227–236.

71. K. P. Neupane, V. L. Pecoraro, *J. Inorg. Biochem.* **2011**, *105*, 1030–1034.
72. S. P. de Visser, M. J. Stillman, *Int. J. Mol. Sci.* **2016**, *17*, 519–544.
73. T. Vreven, K. Morokuma, *Ann. Rep. Comput. Chem.* **2006**, *2*, 35–51.
74. D. A. Fowle, M. J. Stillman, *J. Biomol. Struct. Dyn.* **1997**, *14*, 393–406.
75. A. Presta, D. A. Fowle, M. J. Stillman, *J. Chem. Soc., Dalton Trans.* **1997**, 977–984.
76. W. Braun, M. Vasak, A. Robbins, C. Stout, G. Wagner, J. Kägi, K. Wüthrich, *Proc. Natl. Acad. Sci.* **1992**, *89*, 10124–10128.
77. J. Chan, M. E. Merrifield, A. V. Soldatov, M. J. Stillman, *Inorg. Chem.* **2005**, *44*, 4923–4933.
78. G. Yalovega, G. Smolentsev, A. Soldatov, J. Chan, M. Stillman, *Nuclear Instruments and Methods in Physics Research Section A: Accelerators, Spectrometers, Detectors and Associated Equipment* 2007, *575*, 162–164.
79. J. Chan, Z. Huang, I. Watt, P. Kille, M. Stillman, *Chem. Eur. J.* **2008**, *14*, 7579–7593.
80. J. Chan, Z. Huang, I. Watt, P. Kille, M. J. Stillman, *Can. J. Chem.* **2007**, *85*, 898–912.
81. K. E. Rigby, J. Chan, J. Mackie, M. J. Stillman, *Proteins: Struct. Funct. Bioinform.* **2006**, *62*, 159–172.
82. K. E. Rigby, M. J. Stillman, *Biochem. Biophys. Res. Commun.* **2004**, *325*, 1271–1278.
83. K. L. Summers, A. K. Mahrok, M. D. Dryden, M. J. Stillman, *Biochem. Biophys. Res. Commun.* **2012**, *425*, 485–492.
84. P. Greisen, J. B. Jespersen, K. P. Kepp, *Dalton Trans.* **2012**, *41*, 2247–2256.
85. K. P. Kepp, *J. Inorg. Biochem.* **2012**, *107*, 15–24.
86. J. D. Otvos, I. M. Armitage, *Proc. Natl. Acad. Sci.* **1980**, *77*, 7094–7098.

10

Lead(II) Binding in Natural and Artificial Proteins

Virginia Cangelosi, [1] ***Leela Ruckthong,*** [2] ***and Vincent L. Pecoraro*** [*2]

[1] Department of Chemistry, Michigan State University, 578 S. Shaw Ln., East Lansing, MI 48824-1322, USA
<vcangelo@msu.edu>

[2]Department of Chemistry, University of Michigan, 930 N. University, Ann Arbor, MI 48109-1055, USA
<vlpec@umich.edu>

Metal Ions in Life Sciences, Volume 17 Edited by Astrid Sigel, Helmut Sigel, and Roland K. O. Sigel

DOI 10.1515/9783110434330-010

Abstract: This article describes recent attempts to understand the biological chemistry of lead using a synthetic biology approach. Lead binds to a variety of different biomolecules ranging from enzymes to regulatory and signaling proteins to bone matrix. We have focused on the interactions of this element in thiolate-rich sites that are found in metalloregulatory proteins such as Pbr, Znt, and CadC and in enzymes such as δ-aminolevulinic acid dehydratase (ALAD). In these proteins, Pb(II) is often found as a homoleptic and hemidirectic $Pb(II)(SR)_3^-$ complex. Using first principles of biophysics, we have developed relatively short peptides that can associate into three-stranded coiled coils (3SCCs), in which a cysteine group is incorporated into the hydrophobic core to generate a $(cysteine)_3$ binding site. We describe how lead may be sequestered into these sites, the characteristic spectral features may be observed for such systems and we provide crystallographic insight on metal binding. The $Pb(II)(SR)_3^-$ that is revealed within these α-helical assemblies forms a trigonal pyramidal structure (having an *endo* orientation) with distinct conformations than are also found in natural proteins (having an *exo* conformation). This structural insight, combined with ^{207}Pb NMR spectroscopy, suggests that while Pb(II) prefers hemidirected $Pb(II)(SR)_3^-$ scaffolds regardless of the protein fold, the way this is achieved within α-helical systems is different than in β-sheet or loop regions of proteins. These interactions between metal coordination preference and protein structural preference undoubtedly are exploited in natural systems to allow for protein conformation changes that define function. Thus, using a design approach that separates the numerous factors that lead to stable natural proteins allows us to extract fundamental concepts on how metals behave in biological systems.

Keywords: lead · lead toxicity · metalloregulatory proteins · ^{207}Pb NMR · protein design

1. INTRODUCTION

Throughout history, lead (Pb) has been both an instrument for, and a hindrance to, human progress. It's been used as a wine preservative, in cosmetics, in cookware, in printing presses, in paint, and more [1, 2]. Utilizing tetraethyl lead as an antiknock gasoline additive in the 1920s improved the performance of engines, but it also introduced lead into the environment in unprecedented amounts. Since lead additives were phased out of gasoline, the average blood lead level (BLL) of children in the United States dropped significantly from 15.0 μg/dL between 1976–1980 to 1.84 μg/dL in 2009–2010 [3, 4]. The malleability of lead allowed for the first plumbing systems, yet contaminated drinking water from lead pipes and soldering is a problem that still haunts us today. At the time this chapter was written, the entire city of Flint, Michigan (population 100,000) in the United States is being advised to drink bottled water because of the contamination of the local water supply [5]. The city switched water sources in an attempt to save money, but failed to treat the new water with corrosion inhibitors, resulting in the leaching of lead from pipes. The Environmental Protection Agency (EPA) sets an acceptable threshold of 15 parts-per-billion (ppb) for drinking water, yet lead levels of over 1000 ppb were measured in water coming straight from the taps of some residents' homes. The problem was discovered by a doctor who noticed a doubling in the number of children with elevated BLLs (above 5 μg/dL) [6].

Unfortunately these children are already starting to experience the health problems associated with lead exposure. Lead causes a barrage of health problems including anemia, renal impairment, hypertension, infertility, violent behavior, decreased intelligence, and more [4, 7–11]. Lead causes developmental problems in fetuses and, even if a pregnant mother is not exposed to a new source, lead stored in the bones of women can be mobilized during pregnancy and lactation [12–14]. A recent study shows that the epigenetic consequences are even farther reaching than that. Lead exposure while pregnant affects the DNA methylation status of the fetal germ cells in not just her child, but her grandchildren [15]. The diversity of lead-related health problems result from lead's ability to bind to, and disrupt, the function of a multitude of biomolecules.

Many of the health problems caused by lead can be explained by studying the natural proteins to which it binds. The coordination of lead to δ-aminolevulinic acid dehydratase (ALAD) interrupts the biosynthesis of heme, causing anemia [16]. Memory and growth issues can result from lead coordinating to calcium-binding proteins [17]. Many of the neurological problems associated with lead exposure could result from Pb(II) coordination to zinc finger proteins [18]. There is still much to discover about how Pb(II) behaves in the body and one way to learn more is to study proteins that appear to have evolved specifically for Pb(II) coordination. One of the difficulties in studying natural proteins is that they are large and often difficult to isolate and characterize due to the specific conditions they require for folding. A way around this problem is to use simplified proteins, designed from scratch, to coordinate lead in its preferred geometry. In this chapter we will discuss the application of *de novo* protein design to lead binding and the characterization of these proteins by spectroscopic techniques including ^{207}Pb nuclear magnetic resonance spectroscopy (^{207}Pb NMR).

2. LEAD IN NATURAL SYSTEMS

The size, thiophilicity, and ability to bind many types of ligands in many coordination geometries makes Pb(II) a particularly problematic ion in biological systems. In many proteins and biomolecules it is able to replace physiologically relevant ions, but due to differences in chemistry, cannot carry out their functions. Lead complexes are kinetically labile and thermodynamically stable under aqueous conditions [19, 20]. In proteins, Pb(II) is coordinated by sulfur, oxygen, and nitrogen donors. Although coordination by cysteine (Cys) is preferred over glutamic acid (Glu) or histidine (His), mixed donor ligand environments, such as those found in many proteins, are harder to predict [19]. In a 2008 analysis of 48 lead-containing crystal structures in the Protein Data Bank, replacement of a native metal ion by lead was observed in one-third of the lead-containing sites [17]. The other two-thirds of the lead ions were coordinated to proteins opportunistically in sites that did not previously contain metal ions. Lead ions were observed with up to 9 ligands, but 2–5 were observed in three-quarters of the sites. In these structures, 59 % of the ligands were glutamate and aspartate side chains and another 20 % were water molecules. Side chain nitrogen atoms made up 5 %

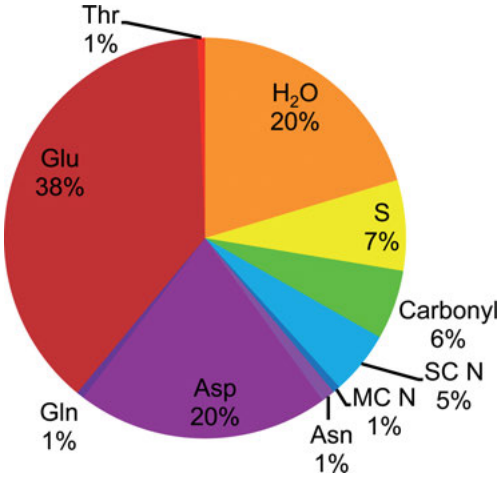

Figure 1. Distribution of Pb(II) in protein crystal structures by ligand (S = sulfur, SC N = side chain nitrogen, MC N = main chain nitrogen). (Adapted from [17]).

of the ligands whereas side chain and small molecule sulfur made up only 7 %. This may seem surprising considering the thiophilicity of lead, but it is impossible to determine which of these sites are relevant *in vivo* and which result from the crystallization process. Still, the analysis provides useful information on the diversity of ligands and coordination environments that are possible for lead within proteins (Figure 1).

Many of the best-studied natural protein systems described below do contain Pb(II) coordinated in Cys_3 environments, including the metalloregulatory proteins that appear to have evolved to control Pb(II) concentrations in cells (Section 2.5). One of the most-studied targets for Pb(II) toxicity, δ-aminolevulinic acid dehydratase contains a Zn(II)Cys_3 site that is substituted with Pb(II) (Section 2.2). Pb(II) also substitutes for Zn(II) in zinc finger proteins, with the affinity for this ion correlated with the total number of Cys residues at the metal binding site. Thus, zinc finger proteins containing three or more Cys are best able to bind Pb(II), with the canonical His_2Cys_2 having lower affinity for this protein class. Unfortunately, Pb(II) is not a functional substitute for Zn(II) (Section 2.4 below) in any of these systems, in part because it is believed not to bind well to histidine. Pb(II)'s radius (1.19 Å) is significantly larger than that of Zn(II) (0.74 Å), it is less acidic, and it has different coordination preferences. The Pb–S bond distances for Pb(II)Cys_3 sites are all between 2.6 and 2.8 Å [18, 21–24].

2.1. Glutathione and Other Small Peptides

In cells, glutathione (GSH) and thiol-rich proteins may act as a natural "buffering system" for lead *in vivo* [20]. GSH, which has concentrations of greater than 1 mM in most mammalian cells, coordinates toxic metal ions and transfers them

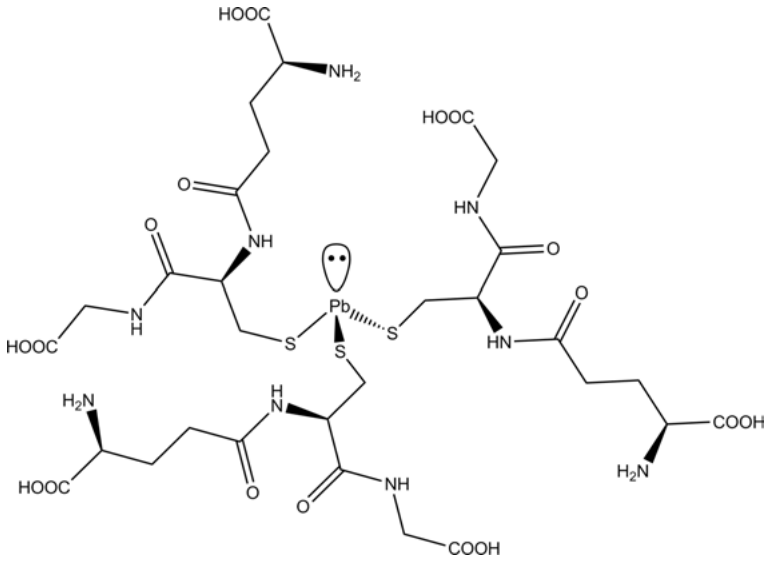

Figure 2. Predominant lead-glutathione complex $[Pb(II)(GS)_3]^-$.

to proteins, providing some protection against their toxic effects [25–27]. The cysteine-rich metallothioneins and phytochelatins are known to bind lead that has been transferred from lead complexes of GSH *in vitro* [25]. In humans, GSH likely complexes Pb(II) *in vivo*. This is supported by the observation that humans with work-related exposure to lead have decreased GSH levels and decreased GSH-dependent enzyme activities [28, 29]. GSH, which contains multiple potential donors, coordinates lead using its sulfur donor with additional minor interactions with the C-terminal carboxylate. In line with lead's coordination preferences discussed above, $[Pb(II)(GS)_3]^-$ is the predominately formed species in solution with Pb–S distances of 2.65 Å (Figure 2) [22, 30–33].

2.2. δ-Aminolevulinic Acid Dehydratase

In humans, the metalloenzyme δ-aminolevulinic acid dehydratase (ALAD), also known as porphyrobilinogen synthase) carries out the second step of heme biosynthesis. The condensation of two molecules of δ-aminolevulinic acid (ALA) to produce porphobilinogen, a precursor of heme, is catalyzed by a $Zn(II)$-Cys_3 site in ALAD. Inhibition of this enzyme process leads to hemoglobin deficiency which causes anemia. Pb(II), which is estimated to have a 25-fold greater affinity than Zn(II) for the active site of ALAD, can replace the Zn(II) ion and inhibit activity [34]. This occurs at concentrations as low as femtomolar lead ($K_i = 0.07$ pM) [34]. The consequences of inhibition are two-fold: not only is heme synthesis halted, but neurotoxic ALA accumulates in the system [16, 35].

The active site of ALAD contains a Zn(II) ion coordinated by three Cys residues and one exogenous water molecule in a pseudo-tetrahedral coordination

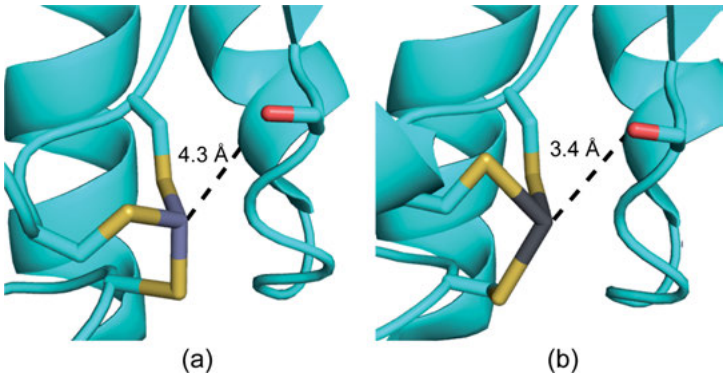

Figure 3. The active site of ALAD occupied by (**a**) Zn(II) and (**b**) Pb(II). (Prepared from PDB 1EB3 (a) and 1QNV (b) [36, 21]).

geometry. Thiophilic Pb(II) replaces the Zn(II) ion with minimal disruption to the fold of the protein or the structure of the active site [16, 21]. The crystal structure of Pb(II)-ALAD shows the Pb(II) ion coordinated in a trigonal pyramidal, hemidirected manner geometry to the Cys_3 site (Figure 3). Although the coordination geometries of the Zn(II) and Pb(II) ions to the endogenous protein ligands are similar, they are not identical and the chemistry of these ions is very different [21, 36]. Coordination of ALA to Zn(II) allows activation of the ketone group, which is essential to the reaction mechanism. Pb(II), which is a weaker Lewis acid than Zn(II), cannot activate ALA [37]. Additionally, the Pb–S bonds are an average of 0.54 Å longer than the Zn–S bonds, causing Pb(II) to protrude farther in to the substrate-binding cavity [16, 21]. Most significantly, Pb(II)'s lone pair of electrons blocks the incoming ALA substrate from binding at the required angle [37]. Finally, a normally non-bonding serine residue (Ser 179) is 0.9 Å closer to the metal ion in the lead structure than in the zinc structure [16, 21].

In addition to coordinating and inhibiting the active site of ALAD, Pb(II) ions can bind opportunistically (or non-specifically) to other parts of the protein. The crystal structure of lead-coordinated ALAD reveals a second ion bound within the substrate-binding pocket with a Pb–Pb distance of 4.4 Å [16, 21]. This non-specific binding increases the possibility of increased Pb(II) solubility and transport [17].

In erythrocytes, the majority of lead coordination occurs within ALAD. Workers who are occupationally exposed to lead often have elevated blood lead levels (BLLs). In samples of their blood, between 35 and 81 % of the detected lead was bound to ALAD [38]. In whole blood, ALAD was found to have a lead-binding capacity of ~40 μg/dL or 1.9 μM [38]. Each ALAD octamer was coordinated to an average of ~6 Pb(II) ions. Despite this being less than one ion per monomer, ALAD activity is greatly reduced. At BLLs of μg/dL (720 nM) there are only 1–2 bound lead atoms per octamer, yet ALAD activity is decreased by 50 % [38].

2.3. Calmodulin

Another family of metalloproteins that are known to be disrupted by lead are the calcium-binding proteins (CaBPs). CaBPs are signal transducers that use Ca(II) ions to govern cellular activities. One of the most heavily studied families of CaBPs is calmodulin (CaM) [39]. CaM is found in all eukaryotic cells and plays a role in the calcium signaling pathways for more than 100 biological processes. These include memory, growth, inflammation, immune response, and muscle contraction. Coordination and release of Ca(II) ions causes structural changes within CaM. This serves as an on/off switch for CaM to bind to and activate other proteins [40]. Calcium binding occurs to oxygen atoms from side chain and backbone residues within four highly conserved helix-loop-helix domains known as EF hand motifs [39]. Similar EF hand motifs are found in over half of all CaBPs, so CaM is prototypical for this class of proteins.

The four EF hand motifs in CaM can also bind Pb(II) ions and do so simultaneously and with high affinity [41, 42]. Crystal structures of calcium- and lead-bound CaM show that these two ions have almost identical coordinations and very similar occupancies within the metal-binding site (Figure 4) [43, 44]. Lead-for-calcium ion replacement causes minimal perturbation within the metal-binding sites and is not expected to cause major conformational changes to CaM. While the C-terminal domains of Ca(II)- and Pb(II)-bound CaM show close structural agreement, the N-terminal domain of Pb(II)-CaM participates in extensive Pb(II)-mediated contact with neighboring molecules and shows significant structural differences [44]. It is proposed that the changes in structure are due to the opportunistic coordination of 10 additional Pb(II) ions outside of the metal binding sites to the protein's surface (Figure 5). The conditions required for crystal growth of metalloproteins often involve high concentrations of metal ions, making surface binding a common phenomenon during crystallization and not necessarily representative of *in vivo* metal binding. In this case the surface binding occurs in areas of high electrostatic potential leading to the proposal that this high affinity binding causes conformational changes to the protein's structure [17, 44].

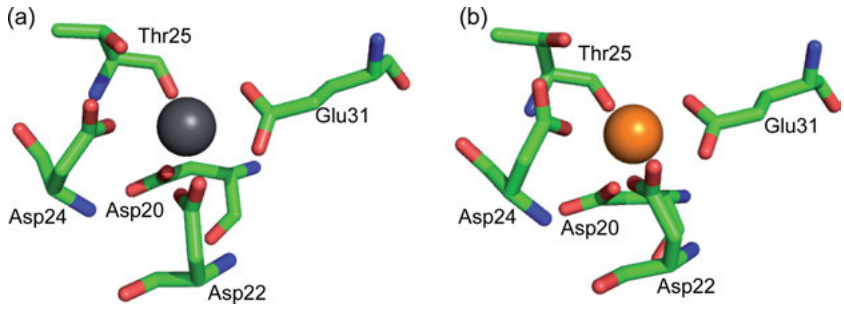

Figure 4. The CaM-binding site containing (**a**) Ca(II) and (**b**) Pb(II). (Prepared from PDB 1EXR (a) and PDB 1N0Y (b) [43, 44]).

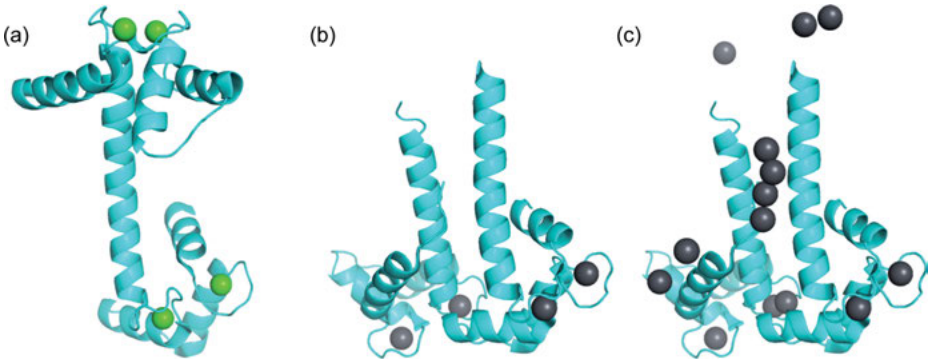

Figure 5. X-ray crystal structues of CaM proteins (**a**) Ca(II)-CaM (1EXR), (**b**) Pb(II)-CaM showing only the Pb(II) ions within the EF-binding sites (1N0Y), and (**c**) Pb(II)-CaM showing all of the coordinated Pb(II) ions including those that are bound opportunistically (1N0Y). (Prepared from PDB 1EXR (a) and PDB 1N0Y (b and c) [43, 44]).

Since these structural changes were observed *in vitro*, it is unclear what, if any, the effects of opportunistic Pb(II)-binding are on CaM *in vivo* or if it even occurs. It has been observed *in vitro* that in the presence of physiological concentrations of free Ca(II), CaM can be activated by Pb(II) at concentrations below 50 pM [45]. While lead is normally thought to inhibit protein function, this suggests that very low concentrations of Pb(II) may actually amplify intracellular Ca(II) signaling thus stimulating other cellular processes. This is further supported by the stimulatory effects of low concentrations of Pb(II) on the activation of myosin light-chain kinase by Pb(II)-CaM [46].

Lead ions coordinate to CaM with a higher affinity than Ca(II) [47]. Coordination at all four of the Ca(II)-binding sites within CaM has been observed, but with unequal affinities to the different sites [41, 48]. In the metal binding sites within the C-terminal domain, Pb(II) binds with a 3-fold higher affinity than Ca(II): $K_D = 0.73\ \mu M$ for Pb(II) and $K_D = 2.0\ \mu M$ for Ca(II)). In the N-terminal domain, there is an 8-fold preference for Pb(II): $K_D = 1.4\ \mu M$ for Pb(II) and $K_D = 11.5\ \mu M$ for Ca(II) [47]. This is consistent with observations of other CaBPs that coordinate Pb(II) with higher affinity than Ca(II). The measured dissociation constant for Pb(II) (6.2×10^{-8} M) is lower than that for Ca(II) (5×10^{-7} M) in bovine and chick intestinal CaBPs, indicating stronger lead binding [42]. In each case, the Pb(II) ions appear to bind directly to the calcium-binding sites. It should be noted, however, that these studies were carried out *in vitro* and the comparison *in vivo* is unknown.

2.4. Zinc Finger Proteins

Zinc finger proteins are one of the most abundant protein types in eukaryotic cells and have an extremely diverse set of roles. Best known as transcriptional regulators, zinc fingers are important for DNA recognition, transcriptional activation, mediation of protein-protein interactions, RNA packaging, and much

more [49]. Disruption of these processes in children would affect neurological development. Broadly defined, a zinc finger is a small protein domain that requires one or more Zn(II) ions for stabilization of the fold [50]. The classic zinc finger has a ββα structure that binds zinc ions in a tetrahedral geometry with four ligands composed of mixtures of Cys and His (two from within the turn of the β-hairpin and two from the C-terminal end of the α-helix). Residues on the exterior of the zinc finger (α-helix side chains) recognize and bind to specific DNA, RNA, or protein sequences.

Lead can cause misfolding when it interacts with zinc finger proteins in cell nuclei and the cytosol [51–53]. *In vitro* competition experiments with zinc finger consensus peptides show that Zn(II) and Pb(II) equilibrate rapidly [20]. Lead speciation appears to be under thermodynamic control and the relative binding affinities of the metals determine the ratio of the metals bound to the protein. This contradicts the previous assumption that lead is kinetically inert after binding non-specifically to cysteine-rich proteins. This suggests that under physiological conditions, Pb(II) should be able to compete effectively with Zn(II) for binding to cysteine-rich sites. Indeed, this is observed in both artificial and natural zinc finger proteins.

Even though four potentially chelating residues are present, only three Cys residues actually bind Pb(II) within Cys_4 and Cys_3His zinc fingers, resulting in a misfolding of the protein [18, 33, 54]. The number and positions of Cys and His residues within the zinc finger proteins affects the affinities of both Zn(II) and Pb(II) (Figure 6) [18, 20, 55]. Zinc finger consensus peptides containing four Cys residues (CP-CCCC) bind both Zn(II) and Pb(II) more strongly than those with only two or three Cys residues (Table 1). For lead, CP-CCCC binds about three orders of magnitude more strongly than the other peptides. The position of the Cys residues is also important. Although both contain one His and three Cys residues, Zn(II) binds an order of magnitude less strongly to CP-CCCH than it binds to CP-CCHC [18]. However, Pb(II) binds to CP-CCCH almost an order of magnitude *more* strongly than CP-CCHC. Taken together, there is a significant

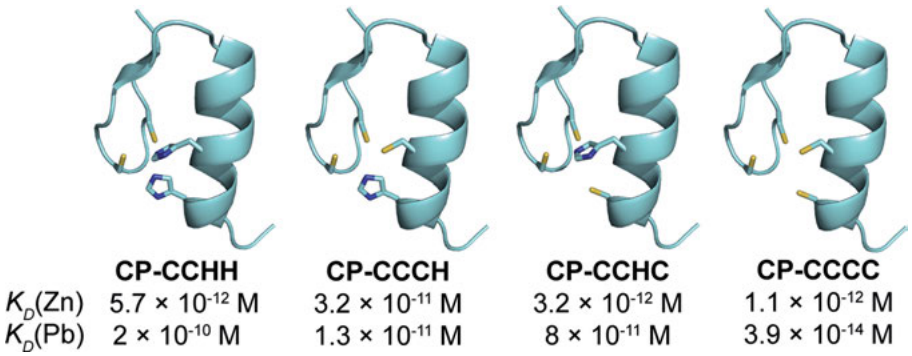

Figure 6. Models of apo-zinc finger consensus proteins. (Generated by modification of PDB 1MEY using PyMOL [55]). Dissociation constants K_D for Zn(II) and Pb(II) at pH 7.2 [18, 20].

Table 1. Zinc finger peptide sequences.[a]

Peptide		Sequence	
CP-CCCC		PYK**C**PE**C**GKSFSQKSDLVK**C**QRT**C**TG	
CP-CCCH		PYK**C**PE**C**GKSFSQKSDLVK**C**QRT**H**TG	
CP-CCHC		PYK**C**PE**C**GKSFSQKSDLVK**H**QRT**C**TG	
CP-CCHH		PYK**C**PE**C**GKSFSQKSDLVK**H**QRT**H**TG	
HIV-CCHC	AcHN	VK**C**FN**C**GKEG**H**IARN**C**RA	$CONH_2$
HIV-CCGC	AcHN	VK**C**FN**C**GKEG**G**IARN**C**RA	$CONH_2$
HIV-CCHH	AcHN	VK**C**FN**C**GKEG**H**IARN**H**RA	$CONH_2$

[a] Bold residues indicate substitutions.

difference in the competitiveness of these two peptides for lead based on the positions of the coordinating residues. This is likely because the first two cysteines are separated by only a proline residue and they are too close together to coordinate Pb(II) in a trigonal pyramidal geometry [18]. A peptide with CP-XCCC is predicted to form the most stable complex with lead because of the spacing of the Cys residues. Despite the fact that CP-CCCC only uses three Cys residues to do so, it coordinates Pb(II) 30-fold more strongly than Zn(II). Considering physiological concentrations and the rapid equilibration of these sites, this difference means that lead should be able to compete with zinc binding in cells [20, 56].

While most of the quantitative data on lead's interaction with zinc fingers comes from experiments with synthetic consensus peptides, natural zinc fingers are also known to bind Pb(II). One specific type of protein that binds GATA sequences within DNA using classic zinc fingers are GATA proteins. These transcription factors are critical for development of blood cells, the central nervous system, the genitourinary system, and cardiac health. Lead can displace the zinc ions within the Cys_4 binding sites within GATA proteins resulting in those proteins having a decreased DNA-binding affinity and a decreased ability to activate transcription [57]. Canonical zinc fingers containing Cys_2His_2 sites may also be targets. The transcription factors TFIIIA and Sp1 have inhibited DNA binding in the presence of micromolar lead, although Pb(II) may not compete effectively with Zn(II) for Cys_2His_2 sites *in vivo* [20, 58, 59]. The human protamine HP2 is inhibited upon binding Pb(II) at two different sites, possibly explaining the decreased fertility of men occupationally exposed to lead [60].

2.5. Metalloregulatory Proteins

Bacteria living in metal-rich environments have evolved defenses against the toxic effects of metals that range from storing them in inert forms within the cell to expelling them. Concentrations within the cell of purely toxic metals such as mercury, arsenic, cadmium, and lead as well as physiologically-necessary metals that are toxic in excess must be controlled [61–63].

2.5.1. *The Lead Resistance Operon pbr*

Some bacteria have evolved defenses for dealing with high concentrations of lead in the environment. The complex set of genes, *pbrRTUABCD*, encode lead resistance in the bacterium *C. metallidurans* strain CH34 [64]. Compared to the metalloregulation carried out by *znt* and *cad* (see below), the *pbr* operon is relatively complex (Figure 7). It is encoded for the regulatory protein PbrR, the uptake protein PbrT, the efflux ATPase PbrA, the inner-membrane fusion phosphatase PbrB/PbrC, and a lead-binding protein PbrD [64–66]. There may also be an inner membrane permease gene (*pbrU*) present [66, 67]. Regulation of lead starts with transport of Pb(II) into the cell by the uptake protein PbrT in order to protect the cell's exterior. Once within the cell, it is picked up by the metallochaperone PbrD and transported to the efflux ATPase PbrA (or ZntA) which exports it from the cytosol to the periplasm. In the periplasm, PbrB/PbrC produce phosphates that precipitate Pb(II), sequestering the ion from circulation [65]. On top of removing harmful Pb(II) ions from the external environment and storing them as inert lead phosphates within the cell, this process also protects *C. metallidurans* strain CH34 by increasing the pH around the external environ-

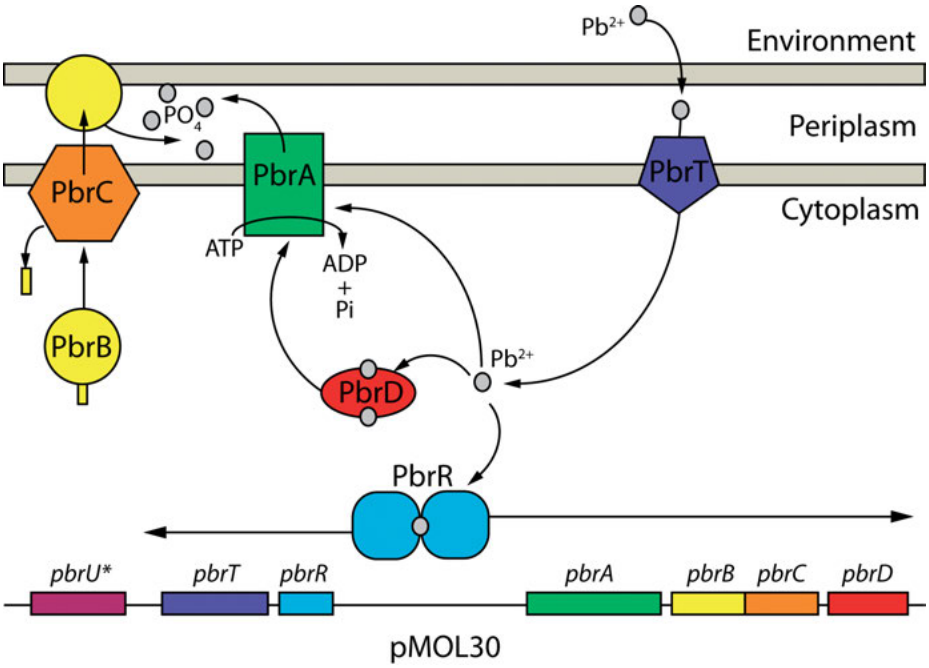

Figure 7. *pbr* resistance in *Cupriavidus metallidurans.* Pb(II) ions are transported into the cell by PbrT. From there they can be coordinated by PbrR, signaling expression of the resistance proteins or coordinated by the metallochaperone PbrD and transported to the efflux ATPase PbrA. PbrA exports Pb(II) into the periplasm when it is precipitated by phosphates produced by PbrB/C. (Adapted from [64, 67]).

ment of the cells. This results in the precipitation of lead in the local cell environment as lead hydroxide and lead carbonate which lowers the local concentration of Pb(II) [64]. Protecting cells in this manner is not a completely unknown phenomenon; the cadmium-zinc-cobalt resistance system *czc* protects *C. metallidurans* in a similar manner [68].

Transcription of the *pbrRTUABCD* genes is controlled by the lead regulatory protein PbrR, which is a member of the MerR family of metal-sensing regulatory proteins. PbrR is a homodimeric protein that binds to the promoter region of the *pbr* operon in the absence of lead [69]. When lead is present, it is thought to bind to three cysteine residues (Cys14, Cys79, and Cys134) in the protein, one of which is found in the helix-turn-helix DNA binding domain (Cys14). Binding changes the conformation of the protein and, as the concentration of Pb(II) increases, the affinity of PbrR for the promoter region decreases. Changes to the conformation of the DNA strand makes the area accessible to RNA polymerase and transcription of the genes follows [69].

Binding studies were carried out with a PbrR homologue, PbrR691, which is also found in *C. metallidurans* strain CH34. Each dimer binds one equivalent of Pb(II) with about 1000-fold selectivity over other divalent metals (Zn(II), Cu(II), Ni(II), Co(II), Hg(II), and Cd(II)) and a $K_D = 0.2\ \mu M$ [70]. In fact, this protein is so selective for Pb(II) that it was developed into a Pb(II) sensor [70]. The significant selectivity may come from the binding site being preorganized to coordinate Pb(II) in a hemidirected geometry, which is lead's preference at low coordination numbers [23]. Lead is coordinated by cysteine residues, probably Cys78, Cys113, and Cys122, which are conserved when aligning the sequence with MerR [23]. Publication of the X-ray crystal structure of PbrR-691 is anticipated soon as an unpublished structure has been deposited in the RCSB Protein Data Bank (unreleased structure ID 5DBZ) [71, 72].

The *pbr* operon encodes two different transmembrane transport proteins, PbrA and PbrT. Although it is not an ATPase, the inner-membrane protein PbrT appears to be a Pb(II)-uptake protein [64]. This is supported by hypersensitivity of the cell to Pb(II) when PbrT is expressed in isolation from the remainder of the *pbr* operon [64]. Once within the cell, Pb(II) appears to be transported by the ~200 amino acid protein PbrD. This metallochaperone has the potential binding site(s) Cys-7X-Cys-Cys-7X-Cys-7X-His-14X-Cys and theoretically sequesters Pb(II), transporting ions to the efflux ATPases and lowering cytoplasmic concentrations of free lead. This is supported by the observations that cells lacking PbrD have higher cytoplasmic lead levels and have higher rates of induction of efflux proteins such as PbrA and ZntA [66]. The influx of Pb(II) by PbrT is counteracted by the efflux of Pb(II) by the PbrA. PbrA is an ATPase with similar properties to CadA and ZntA (see Sections 2.5.2 and 2.5.3) [65]. While most P-type ATPases that transport soft metals contain the consensus Cys-X-X-Cys sequence, this is replaced in PbrA by two Cys-Pro-Thr-Glu-Glu metal-binding sites that may contribute to the selectivity of this protein for lead [64].

PbrR also controls the gene for the fusion protein PbrBC, an undecaprenyl pyrophosphate (C55-PP) phosphatase, found in the periplasm bound to the inner membrane [65–67]. Resistance appears to come from the *pbrB* portion of the

gene, because removal of the *pbrC* portion does not affect cell viability in the presence of lead [65]. When PbrBC is expressed, there is an increased production of phosphates in the periplasm which precipitate Pb(II), although the exact chemical composition of the precipitate is unknown. PbrBC works within the greater lead resistance mechanism of *C. metallidurans* strain CH34. If Pb(II) cannot reach the periplasm due to the absence of P-type ATPase efflux pumps (PbrA and ZntA), there is an overproduction of phosphate in the periplasm and a buildup of lead in the cytoplasm [65].

2.5.2. The Zinc Resistance Operon znt

In *Escherichia coli*, Pb(II) can be removed from cells by the P-type ATPase ZntA [73, 74]. The native substrate for ZntA is Zn(II), which, despite being an essential metal, is toxic in excess. However, in the presence of Pb(II), Zn(II) transport is inhibited [75]. Pb(II) activates the ATPase, increasing the rate of phosphorylation and conferring resistance to Pb(II) [76]. The highest ATPase activities are observed for Pb(II)-Cys and Pb(II)-GSH complexes, suggesting that thiolates may carry Pb(II) ions to ZntA and play an important role in the functioning of the enzyme *in vivo* [77]. This is supported by the fact that at a pH greater than 6, Cd(II) and Hg(II) inhibit ZntA activity while Cd(II)-thiolate and Hg(II)-thiolate complexes stimulate activity. Both of these metals have a higher affinity than Pb(II) or Zn(II) for ZntA and may form dead-end complexes upon coordinating Cys residues. However, the mechanism of binding, the exact binding mode of Pb(II), and the role of high affinity thiolate molecules are unclear.

ZntA expression is controlled by ZntR, a homodimeric member of the MerR family of transcriptional regulators that shares many characteristics with PbrR and responds to Zn(II), Cd(II), and Pb(II) binding [78, 79]. ZntR binds Zn(II) very strongly ($\log K_D = -14.8$ at pH 7.0), but the affinity of lead for the protein is unknown [80]. There is not yet an X-ray crystal structure showing Pb(II) bound to ZntR, but the structure of an N-terminally truncated Zn(II)-bound fragment of ZntR may give some insight. This structure reveals two metal-binding domains at the dimeric interface that are each bound to two tetrahedral Zn(II) ions [81]. Within each site, the ions are 3.6 Å apart and coordinated by two residues from one monomer (Cys114 and Cys124 for Zn1 and Cys115 and His119 for Zn2), a bridging Cys ligand from the other monomer (Cys79), and an oxygen atom from a bridging sulfate or phosphate ion (Figure 8). Neither Cys115 nor His119 are required for induction of ZntR by Pb(II), suggesting that Pb(II) could coordinate in a trigonal pyramidal geometry by Cys79, Cys114, and Cys124 in a similar position to Zn1 [82]. How the differences in size and acidity of the metals are affecting the conformation and the function of the protein is unknown.

While the binding of Zn(II) and Pb(II) may be slightly different, once bound the mechanism by which ZntR induces gene expression is likely similar (and reminiscent of transcriptional regulation by MerR). Apo-ZntR binds the ZntA-promoter region and distorts the DNA by bending the strand toward itself, caus-

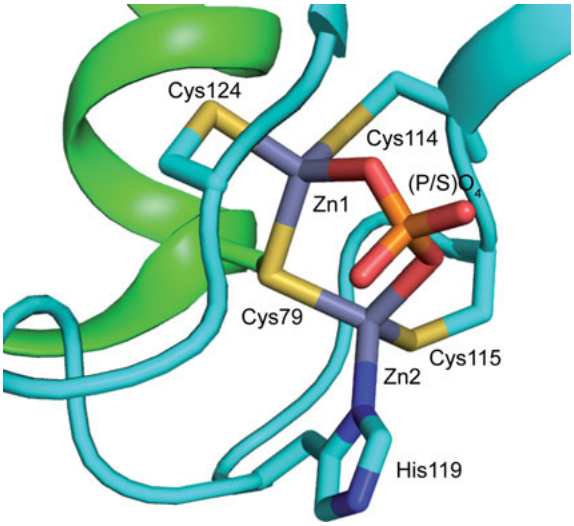

Figure 8. The metal-binding site of ZntR containing two Zn(II) ions in tetrahedral geometries. (Prepared from the 1.9 Å resolution X-ray crystal structure PDB 1Q08 [81]).

ing the formation of two kinks [83]. These kinks restrict access by RNA polymerase to the promoter site and transcription is repressed. Zn(II) coordination causes slight changes to the shape of ZntR, relaxing the bend in the DNA and unwinding the center of the promoter region. This allows RNA polymerase full access to the operator and transcription is activated.

2.5.3. The Cadmium Resistance Operon cad

The *cadCA* operon, consisting of the efflux ATPase CadA and the metalloregulatory protein CadC, provide heavy metal resistance to *Staphylococcus aureus* [84]. Homologous to ZntA, CadA is a P-type ATPase that exports Cd(II), Zn(II), and Pb(II) [75]. Unlike ZntR, the metalloregulatory CadC is a member of the ArsR/SmtB family of transcriptional regulators. In the absence of inducing cations, the homodimer CadC binds specifically to the cad operator on the DNA, suppressing transcription of CadA [85]. Upon binding to Pb(II), Cd(II), and Bi(III), CadC changes conformation and releases the DNA, allowing transcription of CadA. Complete derepression of *cadCA* occurs at lower concentrations of Pb(II) than Cd(II) (200 nM and 300 nM, respectively), suggesting that CadC is primarily a lead regulator [75].

The mechanism of transcriptional regulation is supported by the X-ray crystal structure of apo-CadC (1.9 Å resolution) (Figure 9) [86]. The putative DNA binding domains are helix-turn-helix motifs composed of helices 4 and 5 (and 4′ and 5′). The two metal binding sites, both of which are required for derepression, lie in the interface of the homodimer and are composed of two cysteine residues (Cys7 and Cys11) from helix 1′ (and 1) and two (Cys58 and Cys60) from helix

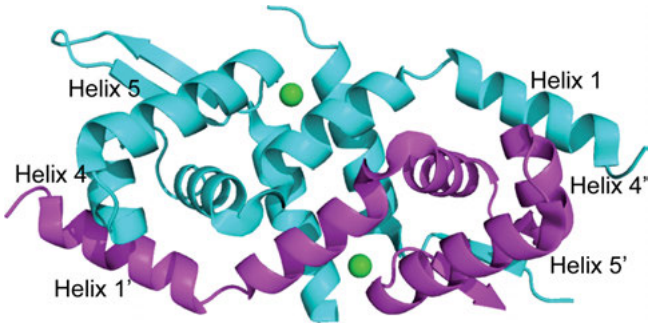

Figure 9. X-ray crystal structure of the CadC dimer. The inducing metal ions are absent. The green sphere represent the structural Zn(II) ions. (Prepared from PDB 1U2W [86]).

4 (and 4′) [87–90]. Within each site, all four Cys residues coordinate Cd(II) in a distorted tetrahedral geometry. An alternative idea is that this fourth thiolate ligand is easily displaced by water so that an equilibrium structure between $[Cd(II)(SR)_4]^{2-}$ and $[Cd(II)(SR)_3(H_2O)]^-$ is the best description. This idea is supported by ^{113}Cd NMR spectroscopy and the notion that having a more dynamic metal binding site would facilitate the rapid kinetics necessary for a metal responsive switch [91]. Lead, which prefers Cys_3 coordination, does not require Cys11 for derepression and instead forms a trigonal pyramidal $Pb(II)Cys_3$ complex [92, 93]. Metallation of the sites moves helix1′ toward helix 4 (and helix 1 toward helix 4′), which sterically blocks a section of the DNA-binding motif causing the protein to release from the DNA.

Metal binding to CadC occurs in two distinct kinetic phases [94]. First, there is a bimolecular encounter between CadC and the metal ion. The rate of this step is metal-dependent (Pb(II) > Bi(III) >> Co(II)). Next, a slower isomerization step occurs which is rate-independent of the type of metal bound and appears to utilize Cys7.

3. LEAD CHEMISTRY WITH DESIGNED PROTEINS

Until very recently, detailed structural information regarding the active site structure of many of the heavy metal binding proteins described in the previous sections was not existent. Even as more clarity on the natural systems is being revealed, there are still issues dealing with the fundamental interaction of heavy metals with proteins that are often difficult to assess in these systems. As mentioned above, there has been significant debate about the first coordination sphere ligands that bind to Cd(II) in CadC, and whether there may be multiple species that can exist in order to control exchange kinetics for this metalloregulatory switch [91–94].

We have been particularly interested in defining how heavy metals bind intrinsically to proteins, what their coordination preferences are and how well struc-

ture dictates function in these systems. Unfortunately, the answers to such fundamental questions may be obscured by the complexity of natural systems, which have to perform functions beyond the binding of the target metal. Thus, we have sought a simplified construct that may directly address the issues of structural preference, site stability, exchange kinetics and site selectivity by using *de novo* designed proteins that allow interrogation of the heavy metal protein relationship in a more detailed and precise fashion. The following section presents our strategy for achieving these objectives with the biologically important Pb(II) cation.

3.1. Design Strategy for Binding Lead

Our strategy to prepare small proteins to bind lead effectively began after more general advances in protein design had been established [95]. One of the most important concepts we utilize is that of exclusion of hydrophobes from water or "hydrophobic collapse" [96–101]. The aggregation of the peptides that we synthesize is dominated by the favorable energetics of desolvation of hydrophobic residues such as leucine, isoleucine or valine when the desired structure is formed. Our target scaffold was the three-stranded coiled coil motif (3SCC). To achieve such a structure, one should synthesize peptides that are amphipathic, meaning one side is hydrophobic and the opposite face is hydrophilic. In doing so, one can exploit the strong stabilization obtained from hydrophobic collapse, while generating an aggregate that is still water-soluble. Examination of the helical wheel diagram for a parallel 3SCC, shown as Figure 10, illustrates this point well. All of the hydrophobic residues are oriented toward the interior of the assembly, while hydrophilic residues point either to the helical interface, where they may form salt bridges with adjacent helices, or toward the solvent, providing for water solubility.

Of course, one must have a strategy to align these residues to adopt the desired positions shown in the helical wheel diagram. This is achieved by employing the concept of the "heptad repeat" [100, 102–105]. Seven amino acids, typically designated *abcdefg*, are repeated along the primary sequence of the desired peptide. The N- and C-terminal ends are capped with glycines that have been acetylated or amidated, respectively. These modifications to glycine induce the folding of the sequence into an α-helix and decrease the resultant helical dipole. Numerous studies have shown that a binary pattern, either using hydrophobic or hydrophilic residues, will lead to helical folding when one places these amino acids in the appropriate position of the heptad [106–110]. Thus, the *a* and *d* positions contain hydrophobes while *b*, *e*, *f* and *g* positions contain hydrophilic residues. The *c* position is neutral to hydrophilic/hydrophobic concerns and typically contains the helix inducing residue alanine.

The α-C positions in an α-helix rotate 100 degrees with respect to the previous amino acid in the sequence [111]. Thus, a heptad of amino acid rotates the α-C positions 700 degrees across its length. This is 20 degrees short of two full turns of the helix, therefore, to align residues in such a way to maximize hydrophobic

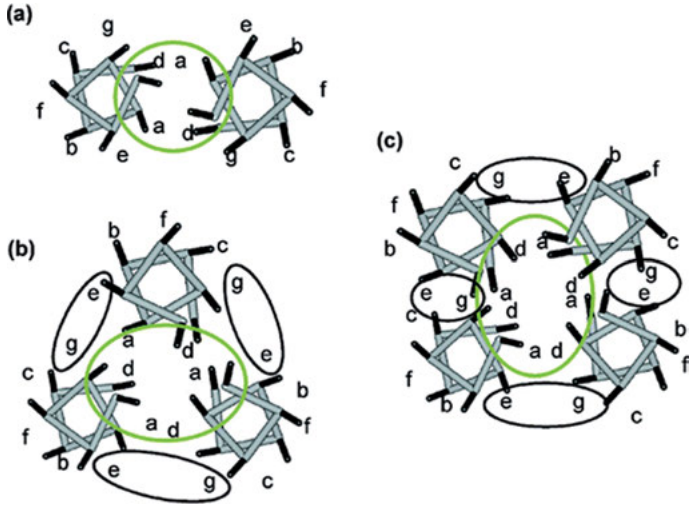

Figure 10. Helical wheel diagram for parallel (**a**) two, (**b**) three, and (**c**) four stranded coiled coil peptides. Reprinted with permission from [124]; copyright 2005 American Chemical Society.

contacts, the resultant α-helix must coil around the other helices forming the scaffold. It is this mismatch of rotation that leads to the supercoiling in these systems.

The typical sequence that we utilize is based on the heptad repeat LKALEEK [112]. Notice that the *a* and *d* positions contain the bulky hydrophobe leucine. Just as considered above, rotation from the *a* leucine to the *d* leucine requires 300 degrees, therefore, these residues do not lie directly above one another in the core of the 3SCC (Figure 11). Similarly, moving from the *d* leucine to the *a′* leucine (the first leucine in a subsequent heptad) requires 400 degrees, which is 40 degrees out of rotational phase. As will be demonstrated below, this rotational disparity has significant consequences for the binding of heavy metals. Another important consequence of the heptad repeat is that two residues intervene between the *a* and *d* layers, whereas three residues separate the *d* and *a* positions. This asymmetry results in different interlayer spacing of the hydrophobes, and subsequently, heavy metal binding ligands that will be placed within the hydrophobic interior.

The heptad orientation also has consequences for the amino acids in the hydrophilic positions. In this case, principles of "negative design" are utilized [102]. Typically, chemists think of building stable structures by minimizing energetic interactions; however, a negative design strategy attempts to generate a desired structure by destabilizing unwanted interactions. For this reason, the residues, particularly in the *e* and *g* positions, are chosen to select against anti-parallel helical orientations [113]. The number of strands in a bundle (2SCC, 3SCC, 4SCC or higher) is controlled by the choice of hydrophobe (e.g., by its size) and

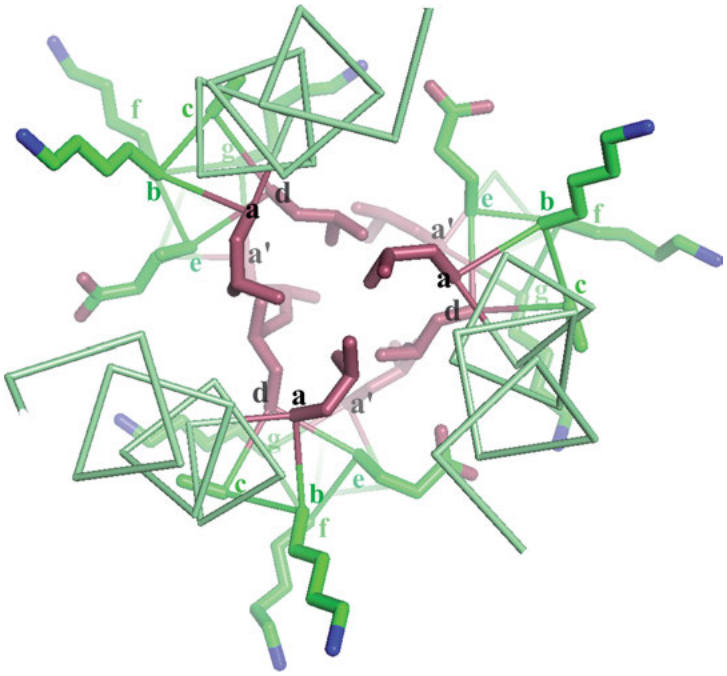

Figure 11. Twisting of the α-helices in a 3SCC along a superhelical axis causing an unalignment of Leu residues in the *a*, *d*, and *a′* layers in the hydrophobic center. Leu residues are represented as red sticks. Other residues at *b*, *c*, *e*, *f* and *g* are green (oxygen in red and nitrogen in blue). (Prepared from PDB 3LJM [155]).

the pattern of the chosen hydrophilic residues (charge, length) in the *e* and *g* positions [108, 114–117].

Once the heptad sequence is established, it is now necessary to determine the length of the peptide [118,119]. We have worked with three lengths containing three (Baby), four (TRI) or five (GRAND) heptads, which are generally referred to as the TRI family of peptides as these have been designed to assemble into parallel 3SCCs using the principles just described [120]. Representative sequences are presented in Table 2. The free energy of folding for these peptides increases as the length of the peptide increases [120]. Thus, GRAND peptides fold into 3SCCs at sub-nanomolar concentrations whereas the much shorter Baby peptides are only partially folded at micromolar levels. In addition to being important for allowing the preparation of stable aggregates to interrogate in solution, the added stability of GRAND peptides has been important for the growth of crystals using the related CoilSer peptides (CS or GRAND-CS, Table 2).

While this TRI family leads to very stable assemblies, they are not yet capable of high affinity and selective metal binding. To achieve this goal one must modify the sequence in order to incorporate a ligand that has a strong propensity to bind large, soft heavy metals such as Pb(II). The ligand of choice has been cysteine.

Table 2. TRI family peptide sequences.[a,b]

Peptide		a b c d e f g 2	a b c d e f g 9 12	a b c d e f g 16 19	a b c d e f g 26	a b c d e f g 30
BABY	Ac-G	LKALEEK	LKALEEK	LKALEEK	G-NH_2	
TRI	Ac-G	LKALEEK	LKALEEK	LKALEEK	LKALEEK	G-NH_2
TRIL9CL19C	Ac-G	LKALEEK	**C**KALEEK	LKA**C**EEK	LKALEEK	G-NH_2
TRIL12C	Ac-G	LKALEEK	LKA**C**EEK	LKALEEK	LKALEEK	G-NH_2
TRIL16C	Ac-G	LKALEEK	LKALEEK	**C**KALEEK	LKALEEK	G-NH_2
TRIL12AL16C	Ac-G	LKALEEK	LKA**A**EEK	**C**KALEEK	LKALEEK	G-NH_2
TRIL19C	Ac-G	LKALEEK	LKALEEK	LKA**C**EEK	LKALEEK	G-NH_2
TRIL2WL16C	Ac-G	WKALEEK	LKALEEK	**C**KALEEK	LKALEEK	G-NH_2
TRIL2WL12AL16C	Ac-G	WKALEEK	LKA**A**EEK	**C**KALEEK	LKALEEK	G-NH_2
GRAND	Ac-G	LKALEEK	LKALEEK	LKALEEK	LKALEEK	LKALEEK G -NH_2
CoilSer (CS)	Ac-E	WEALEKK	LAALESK	LQALEKK	LEALEHG	-NH_2
CSL9C	Ac-E	WEALEKK	**C**AALESK	LQALEKK	LEALEHG	-NH_2
CSL16C	Ac-E	WEALEKK	LAALESK	**C**QALEKK	LEALEHG	-NH_2
CSL19C	Ac-E	WEALEKK	LAALESK	LQA**C**EKK	LEALEHG	-NH_2
CSL12AL16C	Ac-E	WEALEKK	LAA**A**ESK	**C**QALEKK	LEALEHG	-NH_2
CSL12AL16CL26C	Ac-E	WEALEKK	LAA**A**ESK	**C**QALEKK	LEA**C**EHG	-NH_2
GRAND-CS	Ac-E	WEALEKK	LKALESK	LQALEKK	LQALEKK	LEALEHG -NH_2
GRAND-CSL16CL30H	Ac-E	WEALEKK	LAALESK	**C**QALEKK	LQALEKK	**H**EALEHG -NH_2

[a] Bold residues indicate substitutions.
[b] C- and N-termini are capped by Ac and NH_2 groups, respectively.

A substitution of a hydrophobic residue either at an *a* or *d* position allows for a three Cys binding site. The original designs were TRIL12C and TRL16C in which a Cys is replaced at the twelfth position (*d* site) and the sixteenth position (*a* site), respectively [24]. In solution studies, these Cys_3 binding sites were found to bind several types of heavy metal ions (e.g., Pb(II), Hg(II) Cd(II), As(III) and Bi(III)) [24,121–145]; however, only evidence of Pb(II) binding will be addressed in this chapter. Readers who are interested in Cd(II) and Hg(II) studies with these peptides are referred to other articles [146–149]. As will be demonstrated below, metal complexation at *a* sites is not necessarily equivalent to binding to *d* sites, which leads to interesting differences in structure, spectroscopy, and selectivity. While the vast majority of Pb(II) biological sites are substituted Ca(II) environments, complexes of lead with thiolate ligands will be emphasized in the following sections. This limitation is because most reported studies with designed proteins binding heavy metals have focused on soft metal complexation.

3.2. Lead Spectroscopic Features

The bioinorganic chemistry of Pb(II) interactions with sulfurs can be followed by a variety of spectroscopic methods. Previously, there was a widespread misconception that the filled d-shell of lead yields spectroscopically silent species impeding attempts to study lead binding to proteins. However, the presence of the $6s^2$ lone pair and the relativistic splitting of the empty 6p orbitals affects the electronic structures of the Pb(II) center when bound to different ligands. Currently, UV/VIS spectroscopy, X-ray absorption spectroscopy (XAS), and ^{207}Pb NMR spectroscopy are used to give complementary insight into the coordination environment of lead.

XAS is a synchrotron technique for investigating the local structural environments of the metal, geometry, and metal site ligation, while ^{207}Pb NMR spectroscopy is an excellent probe for the Pb(II) coordination environments through the large chemical shift range for this isotope based on different ligand environments of the Pb(II) centers. Though there are a few other techniques that have been used to determine Pb(II) complexes in proteins (e.g., photoelectron, Raman, infrared, and mass spectroscopies), in this chapter we will focus on the application of UV/VIS, XAS, and ^{207}Pb NMR spectroscopies that allow for better understanding of Pb(II)-thiolate interactions.

3.2.1. UV/VIS Spectroscopy of Pb(II) in Small Molecule and Protein Environments

The coordination of Pb(II) by three cysteinate residues causes charge-transfer electronic transitions in the UV region that can be used to directly monitor Pb(II)-peptide complexes [20]. When Pb(II) binds to cysteines, two intense absorption bands are observed in the UV region: a strong peak with an absorption

maximum around 240–280 nm and a moderate signal at a longer-wavelength around 300–350 nm. The molar absorptivity and energy of the latter absorption band can provide quantitative information about lead-protein interactions and are assigned to three or four thiolates bound to a Pb(II) center [20]. Competition experiments with other metal ions result in changes to the ligand-to-metal charge transfer (LMCT) bands when Pb(II) is replaced in the target site. Unfortunately, in most cases, determination of Pb(II) binding constants by direct titration is impossible because of the high affinity of this metal for thiolate ligation. Given the extinction coefficient at ~340 nm of 3,500–4,000 M^{-1} cm^{-1}, one can only directly determine dissociation constants on the order of ~20 μM; however, it is likely that Pb(II) binds to tris cysteinate sites with far greater affinities. Even fluorescence spectroscopy, which can monitor direct complexation of metals at nanomolar levels, has been inadequate to give reliable values. Despite these limitations, the ~340 nm absorption can be used to give relative affinities for Pb(II) as compared to other metals. In most cases, Pb(II) binds much more tightly. Examples of this phenomenon are affinities *versus* Co(II), Zn(II), and Fe(II) [150].

Changes to the binding site also affect the LMCT bands. In a CadC mutant in which one of the cysteines in the metal-binding site has been replaced with a glutamate (C50G), the band is ~15 nm blue shifted compared to the lead-bound wild-type protein [92]. This difference allows for the distinction of $Pb(II)S_3$ from $Pb(II)S_2O$ sites. A similar trend is observed in the UV/VIS spectroscopy of small molecule Pb(II) complexes containing inorganic thiolate ligands [22, 151, 152]. The spectroscopic fingerprints for Pb(II) bound to a series of small biomolecules (L-Cys, L-Pen, NAC and GSH) in alkaline aqueous solutions established that the environment of the metal center depends on ligand-to-metal ratios, concentrations, and the pH of the solution [22, 151, 152].

For the Cys ligands, the UV/vis spectra displayed absorption maxima at 298–300 nm for the dithiolate $Pb(II)S_2N(N/O)$ species at low Cys-to-Pb(II) ratios, while excess ligand led to the formation of tris thiolate $Pb(II)S_3N$ and $Pb(II)S_3$ (minor) complexes. These were red-shifted and appeared at ~330 nm. The Cys ligand is able to form a five-membered S,N-chelate ring; therefore, in order to shift the equilibrium from the $Pb(II)S_2N^-$ (N/O) to tris thiolate there must be a large excess of free ligand in solution [151]. The blocked amine group in GSH and N-acetylcysteine (NAC) make the Pb(II) coordination modes at low ligand/Pb(II) mole ratio different than the Cys ligand, in which the formation of dimeric or oligomeric $Pb(II)S_2S'$ was proposed. However, the corresponding bands are blue-shifted to the tris thiolate Pb(II) environment when a large excess of ligand was added into the solution ($[Pb(II)(S\text{-}NAC)_3]^{4-}$: λ_{max} = 335 nm, $Pb(II)(S\text{-}GSH)_3$: λ_{max} = 335 nm) [22, 152]. These studies showed that the LMCT bands of tris thiolate Pb(II) complexes give the most red-shifted spectra compared to the Pb(II)-sulfur centers that have lower numbers of coordinating thiol ligands. This characteristic is one of the spectroscopic features that has been used to probe the tris thiolate Pb(II) center, which is the most common coordination environment of Pb(II) found in proteins.

Glutathione (GSH) also preferentially binds to Pb(II) in a $Pb(II)S_3$ coordination geometry between pH 7.5–9.5 [22, 30–33]. However, the LMCT band at pH

7.5 shows the weakest intensity, suggesting an incomplete deprotonation of Cys residues upon Pb(II) binding [33]. When the pH is raised to 8.5 and higher, the thiols are deprotonated and the band becomes more pronounced with an observed λ_{max} of 334 nm ($\varepsilon_{334} = 3500 \pm 100\,M^{-1}\,cm^{-1}$). These parameters are close to the values reported for $Pb(II)S_3$ binding in zinc finger proteins and *de novo* 3SCC environments [20, 138].

The binding constants for the zinc finger proteins described in Section 2.4 were determined using UV/VIS spectroscopy. The series of proteins included the cysteine-rich zinc finger consensus domains: CP-CCHH (naturally occurring Cys_2His_2 site), CP-CCHC (consensus $Cys_2HisCys$ binding domain), CP-CCCC (consensus Cys_4 site), CP-CCHC, and HIV-CCHC (consensus and HIV nucleocapsid protein containing $Cys_2HisCys$ sites) [18, 20]. Only the binding sites that have three or four Cys ligands showed intense bands around 255 nm ($\varepsilon_{255} \cong 16{,}000\,M^{-1}\,cm^{-1}$) and a well-resolved peak near 330 nm ($\varepsilon_{330} \cong 4{,}000\,M^{-1}\,cm^{-1}$) suggesting $Pb(II)S_3$ coordination. When Pb(II) binds to CP-CCHH, the transitions appear blue-shifted [20]. The relative affinities of Zn(II) and Pb(II) for the sites (Figure 6) were determined by titrating Zn(II) into a solution of Pb(II)-zinc finger proteins and following the disappearance of the absorption band at 255 nm.

3.2.2. UV/VIS Spectroscopy of Pb(II) Within de novo Designed Peptides

UV/VIS spectroscopy was used to probe the interactions of Pb(II) with the *de novo* designed 3SCCs described in Section 3.2. The peptides TRIL12C and TRIL16C self-assemble to give 3SCCs with Cys residues in the *d* and *a* sites, respectively. Small aliquots of peptide were added into $Pb(II)(NO_3)_2$ solutions at pH 8.0 and the $RS^- \rightarrow Pb(II)$ LMCT bands were monitored by UV/Vis spectroscopy, confirming the chelation of lead in $Pb(II)S_3$ environments [24]. Two intense absorption bands in the UV region were observed: a strong peak with an absorption maximum at 260 nm for TRIL16C and 278 nm for TRIL12C, respectively, and a moderate signal at a longer-wavelength (346 nm for TRIL16C and 343 nm for TRIL12C). The molar absorptivity and energy of the latter absorption band can provide quantitative information about lead-protein affinity and are assigned to $Pb(II)Cys_{3/4}$ centers [20].

However, the 3 : 1 ratio of peptides-to-metal ion in the titration curves indicate $Pb(II)S_3$ coordination within $Pb(II)(TRIL12C)_3^-$ and $Pb(II)(TRIL16C)_3^-$ (Figure 12). The lower energy regions of these spectra are consistent with those observed for Pb(II)-substituted to the metalloregulatory proteins (wild-type *S. aureus* pI258 CadC, Pb(II)-PbrR691, and Pb(II)-AztR), consensus zinc finger peptides (CP-CCHC and CP-CCCC), and the HIV-nucleocapsoid protein (HIV-CCHC), implying similar Pb(II) geometries in each of these proteins [20, 23, 87, 153]. However, the higher energy region of the spectra for the Pb(II)-bound 3SCCs and Pb(II)-bound CadC are slightly shifted and show different intensities, indicating that the secondary protein structures around the metal sites may affect the spectroscopy or geometry of the $Pb(II)S_3$ sites [24].

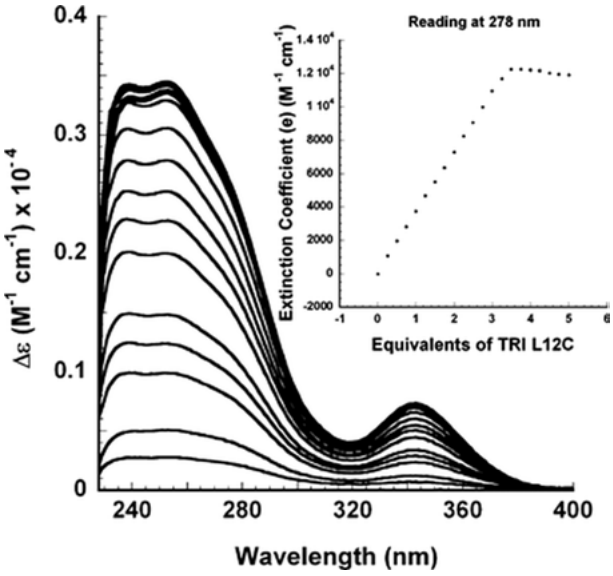

Figure 12. Difference titration of Pb(II) into TRIL12C. The change in the absorption at 278 nm is plotted as a function of the equivalents of peptide added in the inset. The experiment was performed at pH 8.0 in the presence of 100 mM tris(hydroxy-methyl)aminomethane buffer while the metal concentration was maintained at 20 μM. (Reproduced with permission from [24]; copyright 2006 Springer, Berlin, Heidelberg).

Soft metal ions, including Pb(II), are believed to bind to the TRI and GRAND peptides under slightly acidic conditions where these peptides have already formed 3SCCs (it should be noted that 2SCCs are the dominant species below pH 4.5). When Pb(II) is bound at pH 5.5, it is thought to be complexed by one thiolate ligand and two thiol groups, forming, for example, a Pb(II)(TRIL16C)(H-TRIL16C)$_2^+$ species that contains two coordinated thiols, rather than thiolate, ligands. As the pH is raised, the two bound thiols are deprotonated simultaneously to form Pb(II)(TRIL16C)$_3^-$. The pK_{a2} of these two bound thiol deprotonations can be determined by monitoring the growth of the 342 nm absorption. Figure 13 shows a comparison of the titration curves between Pb(II)(TRIL12C)$_3^-$ and Pb(II)(TRIL16C)$_3^-$. The curves were best fit with a non-linear regression model corresponding to a release of two protons (pK_{a2}) from the moiety Pb(II)(H-TRILXC)$_2$(TRILXC)$^+$, yielding Pb(II)(TRILXC)$_3^-$. As shown in Table 3, Pb(II) has a lower pK_{a2} of ~12.1 $\pm$ 0.2 binding to the *d* peptides (X = 12 or 19) compared to the *a* peptide (pK_{a2} of 12.6 $\pm$ 0.2, X = 9 or 16) [24]. These results indicated the protons of Cys residues at a *d* site can be released at a slightly lower pH. If one compares these pK_{a2} values to those determined previously for Cd(II) complexation, also given in Table 3, we see that the thiols are more acidic in the presence of Pb(II). Furthermore, we see the reverse trend in acidities for the *a* and *d* sites, with *a* sites being significantly more acidic (13.6 $\pm$ 0.2) than *d* sites (14.6 $\pm$ 0.2).

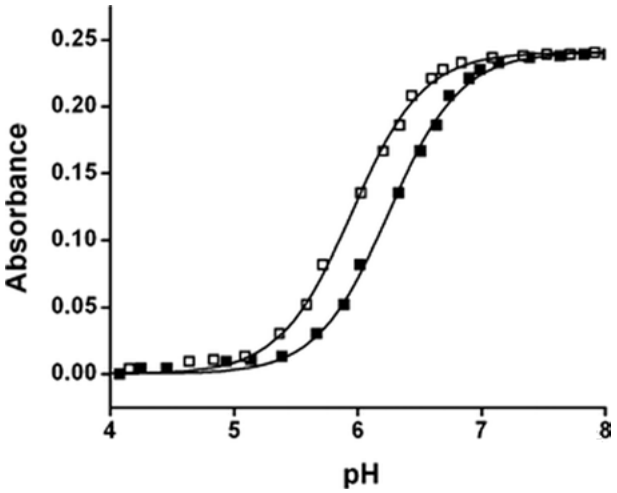

Figure 13. pH dependence of complex formation for $Pb(TRIL16C)_3^-$ (filled squares) and $Pb(TRIL12C)_3^-$ (open squares). The lines connecting the data points are the fits to the data to extract apparent pK_a values. Metal concentrations were 10 μM and peptide concentrations were 50 μM as monomer. (Reproduced with permission from [24]; copyright 2006 Springer, Berlin, Heidelberg).

Table 3. pK_a values for peptides.

Peptide	**Apparent pK_{a2}**			
	Pb(II)/TRILXC[a]	**Ref.**	**Cd(II)/TRILXC**[a]	**Ref.**
TRIL9C	12.5	[154]	13.7	[126]
TRIL12C	12.0	[24]	14.6	[24]
TRIL16C	12.6	[24]	13.4	[24]
TRIL19C	12.2	[154]	14.6[b]	[126]

[a] X refers to substitution in the peptide sequence.
[b] This value is for Cd(II)/CSL19C.

Not only are the pK_a values of the thiols different between TRIL12C *versus* TRIL16C, the affinities for Pb(II) binding are slightly different as well. The binding constant of metal binding to the peptides was analyzed using a non-linear least square algorithm with the model:

$$Pb(II) + (TRILXC)_3^{3-} \rightleftharpoons Pb(II)(TRILXC)^{3-} \quad (1)$$

where X is 12 or 16 [24].

Though Pb(II) binds to both peptides with high affinities ($>10^7$ in magnitude), initial determinations of these constants indicated that these values were slightly greater than 10^7; however, more recent determinations put a lower limit on these

values as high as 10^{16} [150]. TRIL12C shows slightly tighter binding than TRIL16C, which is a trend that is in contrast with Cd(II) in which the metal binds selectively to the *a* site with 6-fold stronger affinity than the *d* site [24]. It is, however, consistent with the lower pK_{a2} values for *d versus a* sites. The preference of Pb(II) for a *d* site was further confirmed by the Pb(II) titrations into TRIL9CL19C monitored by ^{1}H NOESY spectroscopy [154]. The di-substituted TRIL9CL19C has Cys residues incorporated at the ninth position (*a* site) and the nineteenth position (*d* site) simultaneously. Pb(II) was shown to bind preferentially to the L19C site (*d* site) over the L9C (*a* site). Only a 2-fold preference of *d* over *a* was seen for Pb(II) (with Cd(II) having a >10-fold preference for *a versus d*). The selectivity and affinities of metal binding to each of these sites were later proposed to depend on the size of the metal pocket, the orientations of the Cys ligands, and the packing of Leu residues all of which influence the accommodation of a metal lone pair or a fourth ligand if needed for a 4-coordinate metal center [33, 155].

Crystal structures of apo-CSL9C and apo-CSL19C, representing Cys orientations in *a* and *d* sites respectively, later suggested that the Cys pocket in the *d* sites peptide is larger than the *a* site [155]. It could be that the larger atomic radius of the Pb(II) ion (1.33 Å), along with its lone pair, fit better in a *d* site, while Cd(II) with a smaller atomic radius (0.92 Å) and a fourth ligand would bind to an *a* site. Despite the designed peptides being simpler than the natural proteins, these preliminarily observations inspired an idea that the relative affinities of different metals in metalloregulatory proteins may be different even though many of these proteins use three Cys ligands as a core feature to bind those metals. Moreover, different locations of the metal sites along a sequence can lead to different selectivities toward metals.

In addition to understanding the affinity and determining structural possibilities for Pb(II) in designed peptides, Zampella et al. subsequently proposed that not only the position along the primary sequence of the Cys pocket mattered for metal affinity, but also the steric considerations of the second coordination sphere for accepting the lone pair could affect the binding constant of complex formation [137]. To test this, a sterically bulky Leu side chain was replaced by Ala at the twelfth position above the metal binding site, yielding TRIL2WL12AL16C, which was thought to remove the steric constraints for metal binding (a Trp was included at the second position as a convenient spectroscopic tag for calibrating peptide concentration). Metal ions that do not have a lone pair (such as Cd(II)) but have a fourth ligand, that occupies the space where the lone pair would be found, should also exhibit this site selectivity.

It was shown that one exogenous water molecule was bound to yield a fully 4-coordinated Cd(II)S_3O species in TRIL12AL16C, whereas TRIL16C, which does not feature a hole above the metal binding site, bound Cd(II) as a mixture of 3- and 4-coordinate species [130, 131]. Parallel studies were done using a crystallographic analogue of the TRI family, called CoilSer (CS). The 3SCC CS derivatives have been shown spectroscopically to bind heavy metals in the interior in an analogous manner to TRI family designs [126]. The structural details of the designs will be discussed in detail in Section 3.4. The CSL12AL16C is about

4- to 5-fold higher in stability constant than CSL16C following the trend observed for TRIL2WL12AL16C and TRIL2WL16C [137]. Binding of lead to these peptides may be interpreted as indicating that peptides have a higher affinity for Pb(II) when alanine is in the layer above the *a* site, which was confirmed by ^{207}Pb NMR spectroscopy; however, the quantitative assessment presented in this study may underestimate the binding affinities of Pb(II) in both TRIL2WL12AL16C and TRIL2WL16C. These observations further emphasized that the steric encumbrance at the second coordination sphere of the metal binding site affects the metal affinities and coordination numbers.

DFT calculations were implemented to evaluate the viability of the model that steric hindrance associated with the lone pair of Pb(II)$(ACA)_3^-$ could lead to site and orientational preferences (ACA is a small modeled peptide with an ALAAACAALA sequence) [137]. When As(III) was examined, it was suggested that the observed *endo* conformation was adopted to minimize lone pair repulsions. An *endo* configuration is defined when both the β-carbon of Cys and the toxic ion are on the same side of the three atom sulfur plane, while an *exo* configuration refers to a conformation where the β-carbon of Cys is located on the opposite side of the three bound sulfur atoms with respect to the position of the metal. It was shown that without other factors, the preferred Pb(II) conformation was an *exo* isomer as has been seen in enzymes such as ALAD and it was

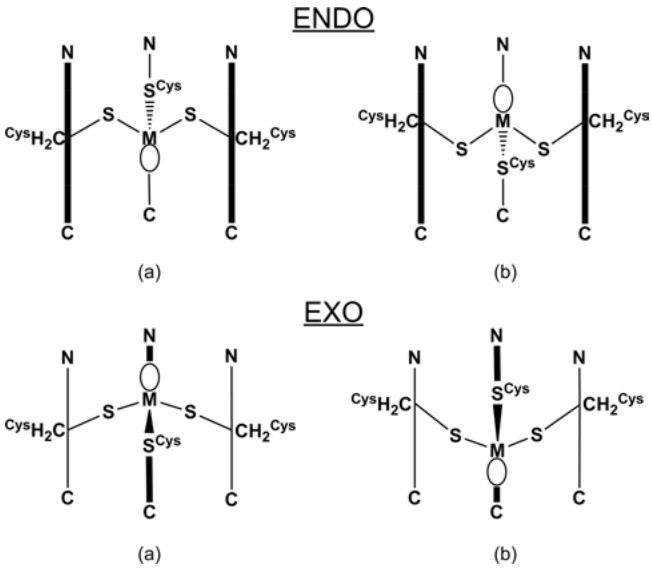

Figure 14. Scheme showing the four possible orientations of a lone pair-containing metal center within a three-stranded coiled coil. **Top panel**: Two possible orientations for the *endo* configuration in which both the β-carbon of Cys and the toxic ion are on the same side of the three atom sulfur plane. **Bottom panel**: Two possible orientations for the *exo* configuration where the β-carbon of Cys is located on the opposite side of the three bound sulfur atoms with respect to the position of the metal. (Reproduced with permission from [137]; copyright 2012 Wiley-VCH, Weinheim).

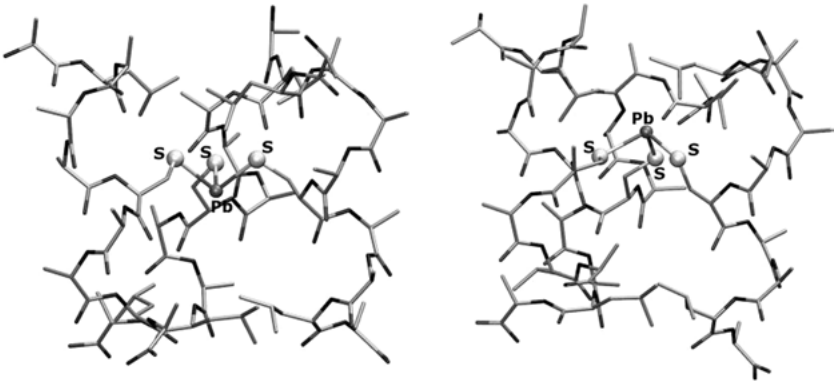

Figure 15. DFT-optimized geometries of $[Pb(II)(ACA)_3]^-$ isomers characterized for *endo* (**left**) and *exo* (**right**) coordination environments. (Reproduced with permission from [137]. Copyright 2012 Wiley-VCH, Weinheim).

suggested that the higher affinity observed when alanine occupied the layer above the cysteines was a consequence of less steric repulsion for the *exo* Pb(II). The $Pb(II)(ACA)_3^-$, thus, represented the $Pb(II)(CSL9C)_3^-$ system where Cys is occupied at an *a* site (ninth position). Depending on the Cys orientations, two possibilities of *endo* and two possibilities of *exo* might be envisioned in the system of studies (Figure 14).

DFT results revealed the *endo* conformation (*endo a*) that has the Pb(II) ion pointing down toward the C-terminus, but Cys rotamers pointing both of their sulfurs and β-carbons toward the N-terminus is highly preferred [137] (Figure 15). While these calculations gave a reasonable explanation of the data, they were limited in their scope as they only used DFT methods rather than a full bore quantum mechanics/molecular mechanics assessment of the 3SCC. Factors such as hydrogen bonding within the coiled coil or preferred rotamers for cysteines were not fully considered. Thus, the prediction obtained for the 3SCC with alanine above the layer was for conversion to the preferred *exo* conformation (*exo a*) as based solely on the chemical preferences of Pb(II) but, as will be described below, the protein environment contribution can generate other structures, especially as the energetic differences between *endo* and *exo* isomers is so small (< 4 kcal/mol) [137]. In fact, the crystallographic description found in the following section will challenge some of the conclusions based solely on the metal sulfur preferences for geometries.

3.2.3. ^{207}Pb NMR Spectroscopy of PbS_3 Centers

Nuclear magnetic resonance (NMR) spectroscopy has become one of the most important methods for evaluating structures of molecules. While many chemists think of this technique primarily for applications using ^{1}H, ^{13}C or ^{15}N isotopes, many other elements have NMR-sensitive nuclei that may provide outstanding

insight into their local structure. We have exploited ^{199}Hg and ^{113}Cd nuclei, often in conjunction with another nuclear technique known as perturbed angular correlation of γ-rays spectroscopy (PAC), to probe the binding of these elements to our designed peptides. Using this approach, we were able to distinguish 2- *versus* 3-coordinate Hg(II) structures and 3- versus 4-coordinate Cd(II) structures that exist at sulfur layers in proteins such as $(TRIL12C)_3$ or $(TRIL16C)_3$ [131].

The ^{207}Pb nucleus is also a promising candidate for NMR studies as it has a medium sensitivity (receptivity of the enriched isotope 9×10^{-3} *versus* ^{1}H) I = 1/2 nucleus with an extremely large chemical shift range (nearly 17,000 ppm) [156, 157]. While ^{207}Pb NMR spectroscopy has been used for some time, it is only recently that this nucleus has been used to examine homoleptic sulfur environments [41]. This is because for many years signals from a $Pb(II)S_3$ chromophore had not been detected since the chemical shift range that needed to be explored was so great and the specific resonance so small and narrow. Typical acquisition times, even with enriched samples, can be several hours. However, once the approximate region of the spectrum was established (5361 ppm *versus* $PbMe_4$ or 2961 ppm downfield of $Pb(NO_3)_2$) it has now become routine to acquire such spectra [22, 138, 151]. In the below discussion, the chemical shift will be given *versus* $PbMe_4$ with the $Pb(NO_3)_2$ value in parentheses.

Jahlilevand and coworkers examined the complexes of Pb(II) with penicillamine and cysteine using UV/VIS, XAS, and ^{207}Pb NMR to clarify this metal's interaction with these important cellular components [151]. In these studies, they found that Pb binds with mixed coordination modes including the thiolate sulfur, but also oxygen and nitrogen donors of the carboxylate and amines. These assignments were confirmed based on the relatively high upfield shifts for cysteine and penicillamine ranging from 4794 (1833) to 5252 (2291) ppm. This compares

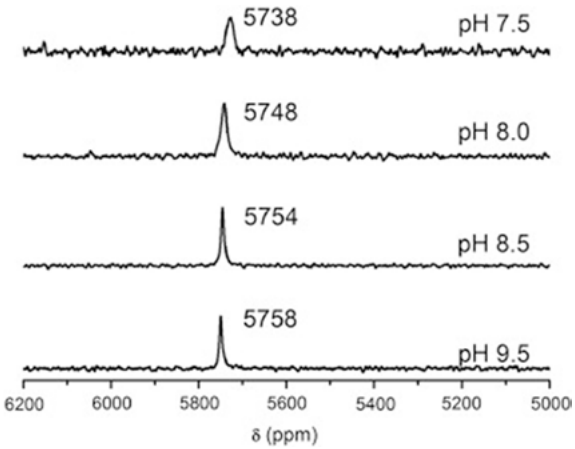

Figure 16. ^{207}Pb NMR spectra of Pb(II)-bound reduced glutathione (GSH) in a molar ratio of 1 : 3 (5 mM Pb(II) : 15 mM GSH) at different pHs. All spectra were recorded for 2 h using enriched $^{207}Pb(NO_3)_2$ (^{207}Pb = 92.4 %) at 25 °C. (Reprinted with permission from [33]; copyright 2011 Elsevier).

as shown in Figure 16 to 5754 (2793) at pH 8.5 for the PbS_3 values for glutathione [22, 33]. Thus, these small molecules may exhibit a range of different structures, including mixed ligand coordination modes.

A ^{207}Pb NMR spectroscopy study of zinc finger proteins was completed soon after it was realized that NMR could be used to examine such species. The protein fragments HIV-CCHC, HIV-CCGC, and HIV-CCHH (all based on zinc finger domains found in the HIV nucleocapsid protein) were tested [33]. Previously, Godwin et al. had completed a thorough UV/Vis and XAS study that showed that these peptides preferred PbS_3 structures [18]. The ^{207}Pb NMR data for HIV-CCHC exhibited resonances at 5744 to 5790 (2779 to 2829) ppm, values conclusive for the proposed PbS_3 geometry. Unexpectedly, there were two resonances for this protein rather than one as had been suggested by EXAFS and UV/VIS studies. This observation emphasizes the power of ^{207}Pb NMR, as it was able to identify two simultaneously existing conformations (Figure 17) that were undetectable by other probes of lead structure. Thus, while still a relatively slow technique, ^{207}Pb NMR spectroscopy may be useful to establish speciation of systems or longer timescale dynamics.

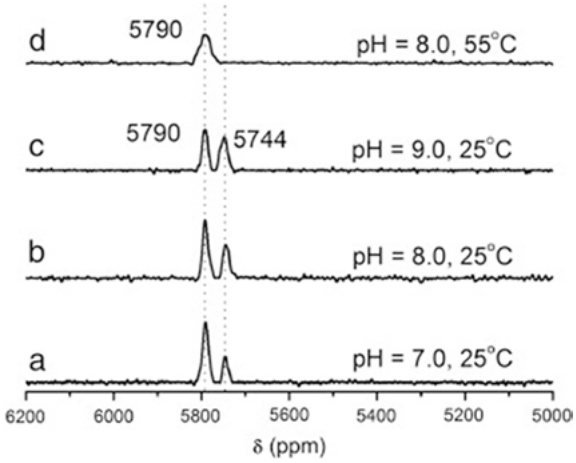

Figure 17. ^{207}Pb NMR spectra of Pb(HIV-CCHC) in a 1 : 1 molar ratio of Pb(II) : peptide at three different pH. The spectra (a) – (c) were recorded at 25 °C and spectrum (d) was recorded at 55 °C. All spectra were recorded for 2 h using enriched $^{207}Pb(NO_3)_2$ (^{207}Pb = 92.4 %). (Reprinted with permission from [33]; copyright 2011 Elsevier).

The first report of ^{207}Pb NMR spectroscopy performed on a $Pb(II)S_3$ chromophore appeared for designed peptides [138]. In these studies, variants of the cysteine-substituted TRI and CS peptides were interrogated to establish their chemical shift range and the utility of NMR spectroscopy in confirming Pb(II) binding to the peptide. As it turned out, the results were successful beyond our original hopes. Remarkably, these experiments were completed on natural abundance samples, suggesting that natural proteins isolated from cells may be

directly probed using this technique. As shown in Figure 18, with designed peptides there was a large chemical shift difference between samples that contained *a* layer cysteines *versus* those that utilized *d* layer substitutions. However, there were only small changes between peptides of different length or composition containing cysteines in the same *a* or *d* layer. Furthermore, while the greatest difference was observed between *a* or *d* layers, there was a useful separation of resonances within derivatives containing cysteine in the same layer and nearby modifications (e.g., $Pb(CSL12AL16C)_3^-$ at 5555 ppm *versus* $Pb(CSL16C)_3^-$ at 5612 ppm). Because of the differences, we were able to assess site-selective binding for Pb(II) to peptides containing two different cysteine layers. In Figure 18 spectrum f, one equivalent of Pb was added to the peptide CSL12AL16CL26C (a peptide containing cysteine in the 16 (*a*) and 26 (*d*) layers and alanine instead of leucine in the layer directly above the *a* site). When one equivalent of Pb(II) was added to this sample, the Pb(II) bound exclusively to the *a* site and when a second equivalent of Pb(II) was added the *d* position became occupied. This experiment elegantly demonstrated that the affinity of Pb(II) was L12AL16C > L26C.

Previous work, which was confirmed with ^{207}Pb NMR spectroscopy, indicated that Pb(II) had the preference L12C or L19C > L9C or L16C, suggesting that the binding order should be an *a* site with an alanine layer above the cysteines is

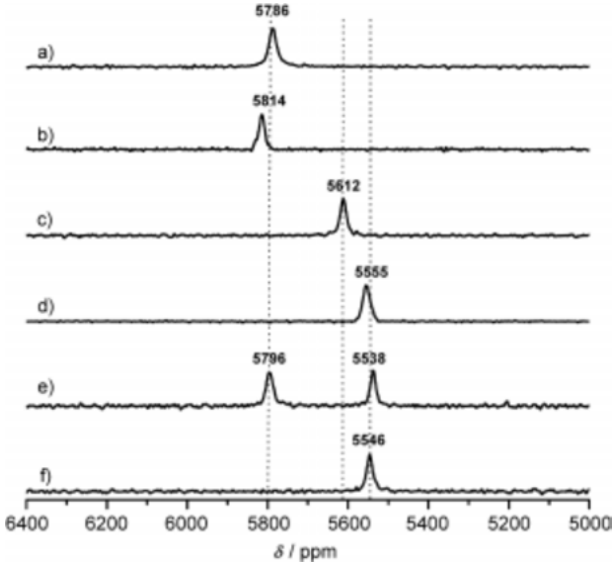

Figure 18. Natural-abundance ^{207}Pb NMR spectra (104.435 MHz) of Pb(II)-bound three-strand coiled-coil peptides (10–12 mM):
(**a**) $Pb(BabyL12C)_3^-$, (**b**) $Pb(CSL12C)_3^-$, (**c**) $Pb(CSL16C)_3^-$, (**d**) $Pb(CSL12AL16C)_3^-$, (**e**) $Pb_2(GrandL12AL16L26C)_3^{2-}$, (**f**) $Pb(GrandL12AL16L26C)_3^-$. All spectra were recorded for 10–12 hr using natural-abundance $Pb(NO_3)_2$ (^{207}Pb = 22.6 %), pH 7.35 $\pm$ 0.05, at 25 °C. (Reproduced with permission from [138]; copyright 2010 Wiley-VCH, Weinheim).

greater than a *d* site which is greater than an a standard *a* site (with leucine above) [24, 154]. This prediction was subsequently confirmed, although the intensity difference between $Pb(TRIL12AL16C)_3^-$ and $Pb(TRIL16C)_3^-$ was small. Therefore, even though absolute binding constants cannot yet be discerned for these peptides, relative affinities may be deduced from experiments such as these.

A related set of experiments, using both ^{113}Cd and ^{207}Pb NMR spectroscopy, has demonstrated that one can evaluate mixed metal selectivity for these systems [154]. It was shown that Cd(II) binds preferentially to *a* sites and Pb(II) goes to the *d* sites. Thus, one can imagine building designed proteins that can incorporate different metals into different sites selectively and also to measure rates of metal substitution between sites based on metal concentrations or pH.

3.2.4. X-Ray Absorption Spectroscopy of Designed Proteins

XAS experiments, especially extended X-ray absorption fine structure (EXAFS) spectroscopy, has been implemented to determine precise metrical parameters for the Pb(II) center. The technique can provide information on ligation type (O,N *versus* S,Cl ligands), coordination number, and metal ligand distances [158]. The Pb(II) L_{III}-edge EXAFS of Pb(II)-bound PbrR691 revealed that the Pb-S bond was 2.67 Å [23], which is in excellent agreement with the Pb(II)–S bond distances determined from in the X-ray diffraction results for $[Pb(II)(SPh)_3]^-$ (2.65 Å), $\{[Tm^{Ph}]Pb(II)\}[ClO_4]$ (2.69 Å) and other tris thiolate Pb(II) complexes [159–161]. These inorganic complexes illustrated a mononuclear trigonal pyramidal Pb(II) with three thiol-containing ligands arranged in a *hemidirected* fashion. Thus, it suggested that Pb(II) might be bound to native proteins in a similar fashion.

The EXAFS results (~2.64 Å) observed for the designed protein series that contain either three or four Cys residues (CP-CCCC, CP-CCHC, CP-CCCH, and HIV-CCHC) could be consistent with this viewpoint [20]. The EXAFS spectrum of Pb(II)-bound CP-CCCC is identical to that seen from the tris(2-mercapto-1-phenylimidazolyl)hydroborato Pb(II) complex, $[(Tm^{Ph})Pb][ClO_4]$, suggesting that while four cysteine sulfur atoms are available, the metal binds to only three Cys ligands. The CP-CCCH showed three-coordination; however, lower scattering intensity for peaks at the same distance were observed for Pb(II) bound to CP-CCHC and HIV-CCHC peptides, indicating there could be a mixture of $Pb(II)S_3$ and $Pb\text{-}(OH_2)_x$ species present in solution or a homogenous $Pb(II)S_2(O/N)$ species that exists. These results demonstrated that the relative positions of the three Cys ligands in the binding site plays a significant role in stabilizing tris thiolate complexes. The CP-CCCH peptide also shows a higher affinity for Pb(II) than those of CP-CCHC and HIV-CCHC, but surprisingly less than the CP-CCCC where all four thiol ligands are present.

Likewise, a single shell of three sulfurs at 2.63 Å was well-fit for Pb(II)–S bond distances in both 3SCC $Pb(II)(TRIL12C)_3^-$ and $Pb(II)(TRIL16C)_3^-$ peptides [24]. This strongly indicated that both the *d* site (TRIL12C) and *a* site (TRIL16C) Cys environments in 3SCCs bind to Pb(II) in trigonal pyramidal geometries. This coordination mode is also consistent with Pb(II) bound to CadC in which the

Pb(II)–S bond length is 2.66 Å, as reported by Giedroc and coworkers [87, 92]. Apparently, these 3SCC models provide an excellent peptidic environment for a tris thiolate site that could resemble the sites in native metalloregulators.

3.3. Structures of Pb(II) Designed Proteins

Protein X-ray crystallography is a powerful technique that allows one to illustrate the success of designed peptides at the molecular level. Crystal structures not only allow structural insight of the particular metal structure of interest, but could also reveal some hidden features in helical coiled coil scaffolds that may be critical for the metal-protein relationship. In this section, the structural details of a trigonal pyramidal Pb(II) center within a 3SCC is discussed along with an examination of ligand organization upon metal binding compared to the apo-form. Moreover, the comparison between the designed 3SCC crystal structure with the Pb(II)-bound to the Pb(II)-substituted native yeast ALAD aims to increase the understanding of Pb(II) binding in Cys-rich sites in different protein environments.

The crystallographic analogs of the designed TRI family variants have been obtained using a CS sequence (Table 2). CS was first designed based on TM29 and crystallized by Lovejoy et al., as an antiparallel triple-stranded coiled coil at low pH [162]. By substitution of one or two positions containing hydrophobic residues in the CS peptides with metal-binding ligands (e.g., Cys, Pen or His residue) the Pecoraro group has been able to show that at higher pH the peptides crystallized in a parallel 3SCC manner [127, 143, 145, 147, 155]. For example, the As(III)$(CSL9C)_3$ (PDB: 2JGO), apo-$(CSL9C)_3$ (PDB: 3LJM), and apo-$(CSL19C)_3$ (PDB: 2X6P) are all parallel 3SCCs [127, 155]. The interior metal binding between TRI and CS variants were shown to behave similarly; however, the distinct characteristics that makes CS capable of crystallization are the His residue on the *f* position and Glu residues usually from the *b* and *e* positions of the last heptad to ligate Zn(II) ions on the exterior of the scaffold. This allows for the 3D packing of the 3SCC helices within the lattice. In designs containing a high number of mutations or drastically destabilizing substitutions (e.g., D-amino acids), peptides containing an extra heptad, termed as GRAND-CS series, have been developed to provide more stability to the construct [143, 163].

GRAND-CSL16CL30H was designed as a representative model for Pb(II) bound to an *a* site in a designed 3SCC environment. $Pb(II)_SZn(II)_N(GRAND\text{-}CSL16CL30H)_3^+$ was solved at 2.13 Å resolution in the space group R32. It contains a Pb(II) ion bound as a *hemidirected* trigonal pyramidal $Pb(II)S_3$ using three Cys ligands at the sixteenth position and a tetrahedral $Zn(II)N_3O$ with three His ligands and a water at the thirtieth position (*a* site) close to the C-terminus (Figure 19) [143, 163]. The latter site was originally designed for catalysis, but that will not be emphasized in this chapter.

The bound Cys ligands interact with the Pb(II) center by directing the side chain to the core of the structure and toward the N-termini with an observed χ_1 value of –68.34° (Figure 20). This χ_1 angle is almost identical to the value of

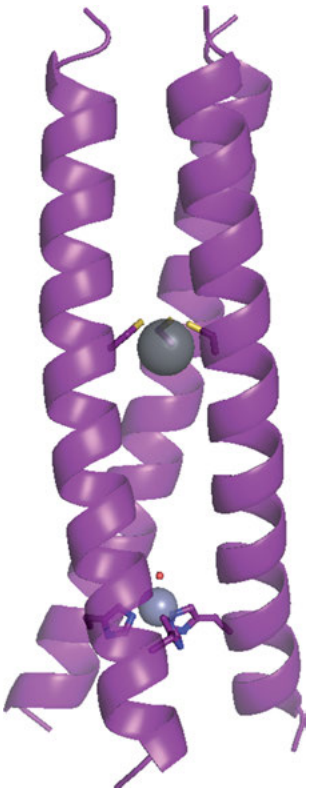

Figure 19. Side view of the trimeric $Pb(II)_SZn(II)_N(GRAND\text{-}CSL16CL30H)_3^+$ structure representing a trigonal pyramidal $Pb(II)S_3$ site at the 16^{th} position and a tetrahedral $Zn(II)N_3(H_2O)$ at the 30^{th} position. Main chain atoms are shown as purple ribbon diagram, Cys in the 16^{th} position and His in the 30^{th} position are present as sticks (sulfur = bright yellow, nitrogen = blue). The Pb(II) and Zn(II) ions are shown as a dark and light grey spheres, respectively. The water ligand of the $Zn(II)N_3(H_2O)$ site is shown as a small red sphere. (Reproduced from [143]).

–66.24° observed for the major conformation of the unmetallated Cys rotamers in the apo-$(CSL16C)_3$ (Figure 21), implying that the orientation of Cys in the apo-peptide is highly *preorganized* for Pb(II) to bind in this trigonal pyramidal geometry. This results in close values of Sγ-Sγ separation between the metallated $Pb(II)S_3$ structure (3.49 Å) and apo-$(CSL16C)_3$ (3.32 Å, average).

However, the apo-Cys ligands, in contrast, are *predisposed* for trigonal planar Hg(II) because both of the centers require the metal to bind relatively close to the sulfur plane. It would be impossible for Hg(II) to bind to the Cys ligands in the positions they are found in the apo-$(CSL16C)_3$ without steric clashing. Therefore, a significant rotation of the Cys rotamers to the helical interface is needed to open the metal pocket space for metal sequestration [143]. On the other hand, Pb(II) can accept the apo-structure conformations because the trigonal pyramidal polyhedron allows the metal to be positioned at a distance of 1.63 Å

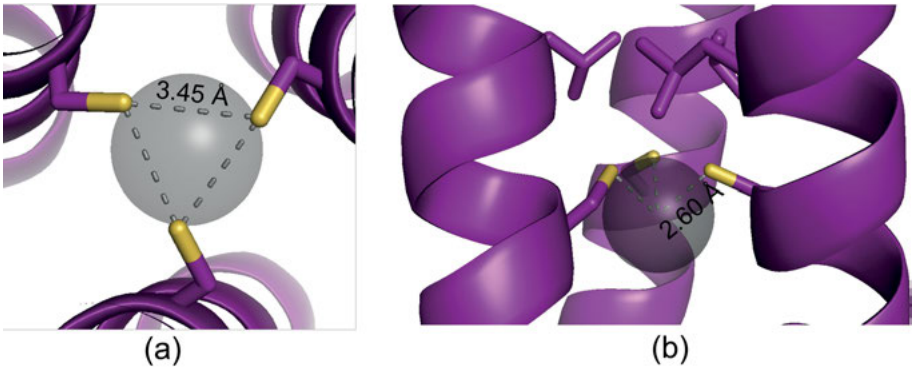

Figure 20. PyMOL visualization of the trigonal pyramidal $Pb(II)S_3$ in the $Pb(II)_SZn(II)_N$ $(GRAND\text{-}CSL16CL30H)_3^+$ structure [55]. (**a**) Top down view from the N-terminus and (**b**) side view of the binding site. Main chain atoms are shown as ribbon diagrams in purple, 12 Leu and 16 Cys side chains are shown as sticks (sulfur is yellow). The Pb(II) ion is shown as a grey sphere. (Reproduced from [143]).

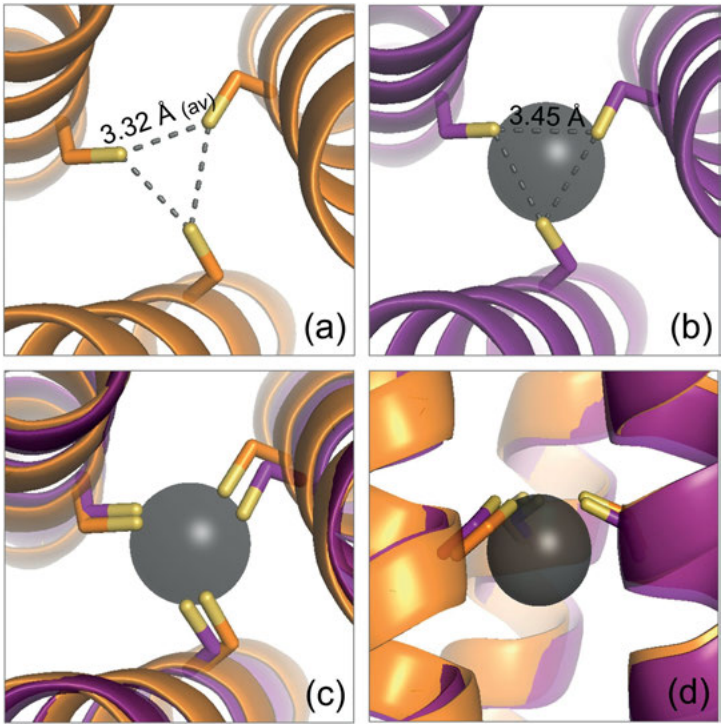

Figure 21. Preorganization of Cys arrangements upon trigonal pyramidal Pb(II) binding in the 3SCC environments. **Top panel**: Representing a top down view from the N-terminus of (**a**) the apo-protein environment from the apo-$(CSL16C)_3$ and (**b**) $Pb(II)_SZn(II)_N$ $(GRAND\text{-}CSL16CL30H)_3^+$. **Bottom panel**: An overlay between the apo-$(CSL16C)_3$ and $Pb(II)_SZn(II)_N(GRAND\text{-}CSL16CL30H)_3^+$ structures, in (**c**) a top down view and (**d**) a side on view. (Reproduced from [143]).

below the metal plane and toward the C-terminus of the 3SCC. The fact that both β-carbon planes of the Cys residues and the Pb(II) ion are on the same side of the three atom sulfur plane, this is considered as an *endo* configuration. The best crystallographic model gives the Pb(II)-S bond distance of 2.60 Å, which is within the error of the value determined from X-ray absorption spectroscopy reported for the $Pb(TRIL16C)_3^-$ (2.63 Å) [24]. Moreover, the fact that the bond length of the *endo* $Pb(II)_SZn(II)_N(GRAND\text{-}CSL16CL30H)_3^+$ is close to other *exo* structures of Pb(II), such as in ALAD and small molecule $Pb(II)S_3$ systems, indicates that the Pb(II)–S bond length does not distinguish between the *exo* and *endo* configurations.

Previously, the *endo* conformation was observed for the $As(III)S_3$ site of the $As(III)(CSL9C)_3$ crystal structure, while the $As(III)S_3$ complex had also been predicted to be in an *exo* form in computational studies and inorganic molecules [127]. The small As(III) ion with an atomic radius of As(III) = 0.72 Å (compared to Pb(II) = 1.33 Å) achieves a 2.28 Å As(III)–S bond distance. This shorter bond length does not require the As(III) to be positioned as far below the sulfur plane, with an observed out of plane distance of 1.30 Å. The arrangements of the bound thiols in the first coordination sphere of both structures are shown in Figure 22. In both cases, the ligands are directed toward the core of the structure and upward to the N-termini. The $As(III)S_3$ has a slightly shorter Sγ-Sγ separation (3.25 Å, average) than the $Pb(II)S_3$ (3.45 Å) as the size of the bound metal defines the necessary size of the thiol plane. As(III) requires the thiol ligands to orient 10 degrees inward toward the core compared to the ligands in the apoprotein in order to compress the diameter of the sulfur plane. On the other hand, the binding of the larger Pb(II) causes the thiols to move slightly outward from

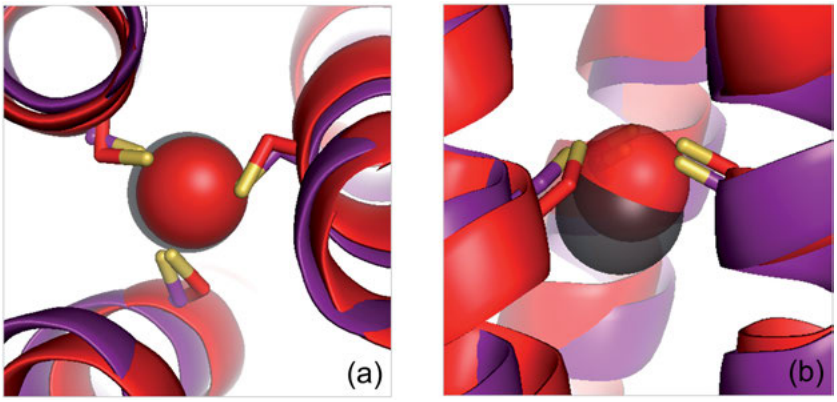

Figure 22. Comparison of trigonal pyramidal structures of the $Pb(II)(S)_3$ from $Pb(II)_SZn(II)_N(GRAND\text{-}CSL16CL30H)_3^+$ and $As(III)(S)_3$ from the published $As(III)(CSL9C)_3$ structure (PDB code 2JGO) [127]. Representation of (**a**) a top down view of the overlay from the N-terminus and (**b**) a side view of the binding sites. Main chain atoms of $Pb(II)_SZn(II)_N(GRAND\text{-}CSL16CL30H)_3^+$ are colored in purple and $As(III)(CSL9C)_3$ in red. The sulfur atoms are yellow. The Pb(II) and As(III) ions are shown as grey and red spheres, respectively. (Reproduced from [143]).

the core to accommodate a longer M–S bond distance. Regardless of the slight difference in χ_1 dihedral angle values of both structures, the Cys arrangements are almost identical. Both the Pb(II) and As(III) ions are oriented with their lone pairs pointing toward the C-termini of the 3SCC.

These crystallographic observations corroborate well with the reported DFT calculations of the small $Pb(ACA)_3^-$ and $As(ACA)_3$ models, respectively [137]. DFT suggested that the *endo* form is preferable over the *exo* when there are Leu residues above the metal site. Undoubtedly, the actual crystal structures proved this assumption. Analogously to the small ACA peptide used in the DFT experiments, both of the CSL9C and GRAND-CSL16CL30H derivatives used for X-ray crystallography contain Leu above the Cys site. Touw et al. discovered that the lone pair of As(III) may play an important role in influencing the As(III) coordination sphere within the 3SCC environment [127]. The poorer packing of the 12 Leu residues (one hydrophobic layer below the 9 Cys site) was reasoned to accommodate the lone pair of the *endo*-As(III) rather than the tighter packing of 5 Leu (side chains orienting more toward the helical core). As

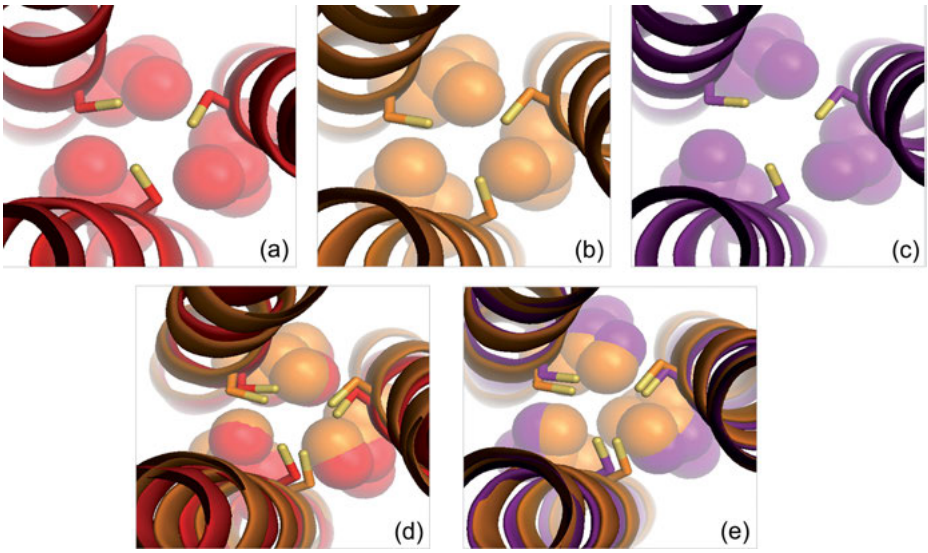

Figure 23. Comparison of the hydrophobic packing below the Cys site of the trigonal pyramidal metal structures compared to the apo-protein. **Top panels**: From top down view of the N-termini, representing the packing of (**a**) 12 Leu below the 9 Cys layer of As(III)$(CSL9C)_3$, (**b**) 19 Leu below the 16 Cys of apo-$(CSL16C)_3$ and (**c**) 19 Leu below the 16 Cys of $Pb(II)_SZn(II)_N(GRAND\text{-}CSL16CL30H)_3^+$. **Bottom panels**: Overlays (**d**) between the As(III)$(CSL9C)_3$ and apo-$(CSL16C)_3$, and (**e**) between $Pb(II)_SZn(II)_N(GRAND\text{-}CSL16CL30H)_3^+$ and apo-$(CSL16C)_3$. Main atoms of $Pb(II)_SZn(II)_N(GRAND\text{-}CSL16CL30H)_3^+$, apo-$(CSL16C)_3$ and As(III)$(CSL9C)_3$ are represented as purple, orange and red ribbon diagrams, respectively. Cys side chains are present as sticks in which the thiols are yellow. Leu residues are shown as spheres indicating the packing. Pb(II) and As(III) ions are omitted for clarity. The PDB code for As(III)$(CSL9C)_3$ is 2JGO [127]. (Reproduced from [143]).

a consequence, it was thought that As(III) had to orient the lone pair to the C-terminal side of the metal ion so that the lone pair will not suffer from steric clashes with the 5 Leu side chains. The alignment of the trigonal pyramidal $As(III)S_3$ and $Pb(II)S_3$ to the apo-structure suggested that metal binding and the effect of the second coordination sphere follow the same trend in both structures (Figure 23).

The fact that Pb(II) and As(III) can adopt the same structure, despite the difference in charge and size, illustrates the potential importance of *preorganization* of the Cys ligands prior to metal binding. While the size and lone pairs of the ions may be a contributing factor to metal site location, it is likely that the pre-arrangement of the ligands is the dominant factor for defining the metal position in these systems. This energetic preference potentially comes from the torsion angle restrictions for cysteines in an *a* site of the helical 3SCC system, which does not allow the ligands to orient in a way that can bind Pb(II) in an *exo* conformation nor to be situated on the N-terminal side of the 3SCC.

This torsion angle restriction for cysteines is likely a major factor for defining Pb(II) structures in helical assemblies. In contrast, other secondary or tertiary structures of proteins that are more flexible than the rigid α-helical scaffold may be able to accept the *exo* conformation of tris thiolate Pb(II) complexes more easily. The yeast ALAD X-ray crystal structure, featuring a TIM-barrel by an eight-membered β-sheet surrounded by eight α-helices, has an active site located in a loop connecting β5 with α4 at the C-terminal end of the β-barrel and oriented directly to the solvent region [164–166]. The site involves three Cys residues (Cys133, Cys135, and Cys143) which coordinate to Zn(II) with an intervening solvent ligand. However, Pb(II) inactivates the site activity by displacing the tetrahedral Zn(II) with a trigonal pyramidal geometry. The loop region allows Cys to bind Pb(II) in an *exo* configuration where the metal ion is positioned at the opposite side from the β-carbon with respect to the sulfur. The Pb(II) ion appears to be situated above the sulfur plane and is exposed to the solvent region.

The comparison of the *exo* conformation of Pb(II)-ALAD and *endo* conformation of Pb(II)-bound in 3SCC is illustrated in Figure 24. The torsion angles of Cys ligands in ALAD are –142.7° (Cys133), 41.4 ° (Cys135) and –53.2° (Cys143), which mostly are different from the dihedral angles observed in the $Pb(II)_S Zn(II)_N(GRAND\text{-}CSL16CL30H)_3^+$. The variation of the torsion angles in the Pb(II)-bound ALAD system strongly indicates that the loop region provides more flexibility for Cys rotamers to accept a wide range of orientations, rather than the rigidity of the helical 3SCC scaffold. The Pb(II)–S bond distances are 2.7, 2.8, and 2.8 Å for Cys133, Cys135, and Cys143, respectively. The mean Sγ-Sγ separation between three sulfur atoms is 4.23 ± 0.35 Å (determined from the actual crystal structure using PyMOL software) and the mean S-Pb(II)-S angle is $98.80 \pm 10.86°$ [55]. These observations strongly suggested that the secondary and tertiary protein structures serve significant roles in defining a specific conformation of the trigonal pyramidal geometry of Pb(II) centers in proteins.

Future models for lead interactions must, therefore, consider not only the first coordination sphere ligands, but also the secondary and tertiary structures in

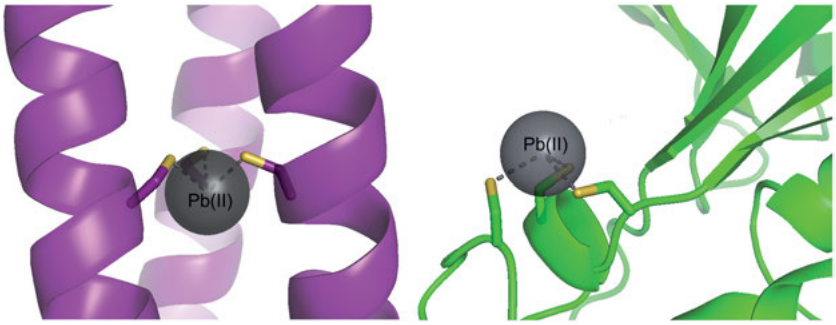

Figure 24. Crystal structures demonstrating (**a**) an *endo* configuration of a trigonal pyramid $Pb(II)S_3$ in the 3SCC $Pb(II)_SZn(II)_N(GRAND\text{-}CSL16CL30H)_3^+$ and (**b**) an *exo* configuration $Pb(II)S_3$ in the native ALAD. (Prepared (a) from [143] and (b) from PDB 1QNV [21]).

which metal binding ligands are located. As an example, Pb(II) bound to the metalloregulatory PbrR691 should take the rotamer restrictions of Cys based on different protein structures into consideration. The PbrR691 belongs to the MerR metalloregulatory protein class. It binds Pb(II) using three Cys residues (Cys78, Cys113, and Cys122) which are also conserved for Hg(II) binding in the MerR protein as determined from the sequence alignment between PbrR691 and MerR (Tn 501) [167]. The recent crystal structure of a Hg(II) bound to MerR (PDB: 4UA1) by Nei-Li Chan and coworkers showed that the trigonal planar Hg(II) site is close to a flexible connecting loop where one of the Hg(II) ligands is located. The second donor is from a helix-to-loop transition and the third Cys is more structurally constrained to the coiled coil dimerization module [168]. This suggests that the flexibility of the loop could possibly affect the Cys rotamers and *endo versus exo* conformations of the Pb(II) complex formed in this protein. On the other hand, the metalloregulatory protein ArsR, a member of the SmtB family which differs from MerR, is helical and must bind As(III) in an irregular C-X-C sequence. Previous models for As(III) binding to ArsR have proposed an *exo*-As(III) configuration [127]. However, the As(III) binding site (Cys32, Cys34, and Cys37) in this protein is in a helical region, so future models for this protein should reconsider the importance of the cysteine rotamers for metal binding. It is quite possible that in the ArsR sequence, the proper rotamers for metal binding cannot be adopted and that this restriction is a contributory factor to the unraveling of the 4-helix bundle upon As(III) association with the protein.

While these crystals structures of designed proteins may inform discussions of the native metalloregulators that have not been structurally characterized in their metallated forms, another important contribution of the studies comes from the perspective of supramolecular chemistry and molecular recognition. This crystallographic study provides structural insight for trigonal pyramidal metalloids that bind into a tris thiolate environment using self associating 3SCCs. As

described in the previous section on ^{207}Pb NMR, metal site selectivity along the primary sequence of a protein or spontaneously assembling group of peptides is a major unexplored research area. As we accumulate more structural information on metalloids in different environments, at different positions along the linear sequence, we will learn the code that helps define molecular recognition at its most basic level. Already, the analysis of metallated and unmetallated *de novo* designed 3SCC peptides allows one to evaluate the extent of ligand *preorganization* prior to metal complexation.

We may now attempt to exploit the clear preference of *a* sites that are *preorganized* for trigonal pyramidal Pb(II) and As(III) ions. Will this be the basis for Pb(II) having higher affinity for *d* versus *a* sites? Conversely, will tetrahedral ions be well accommodated in these different environments? And will these intrinsic apo-protein preferences allow for discrimination of element type, geometry, and coordination number? The answer to these questions should be critical for further understanding the structure-function relationships of metalloids such as Pb(II) and As(III) in biology.

4. GENERAL CONCLUSIONS

In this article we have attempted to integrate our knowledge of the structure and function of known cellular targets for Pb(II) binding to thiolate-rich sites with our fundamental studies aimed at clarifying the spectroscopic and structural behavior of this ion in non-natural constructs that have been prepared based on the first principle ideas. We have seen that using the simple concept of a heptad repeat, assemblies of α-helices (in the form of 3SCCs) serve as excellent vehicles for sequestering Pb(II) into first coordination environments that have either been identified or proposed for most lead-thiolate interactions in proteins and small molecules such as glutathione. Despite the similarity in the first coordination sphere ligand type, distances, and angles, a more comprehensive examination of these systems reveals that there are significant differences between the environments found for Pb in proteins such as ALAD or Zn fingers than coiled coil scaffolds.

First among these differences is that Pb(II) binding in 3SCCs appears to be preorganized with an *endo* conformer being the energetically lowest energy state, despite the apparent preference for *exo* configurations as seen in lead-substituted ALAD or in computational work. In fact, one often sees cysteines that coordinate to metals in β-sheet regions or within loop structures. This is likely because the rigid architecture available with an α-helical bundle requires specific cysteine rotamers to achieve the preferred homoleptic, hemidirected PbS_3-type environment so often found in biology. Furthermore, in metalloregulatory proteins, nature exploits the strong Pb-S bond strength to drive conformational changes to either twist DNA or disrupt helical structures. Such conformational control could not be achieved if a center was constructed within a well designed natural helical bundle. Therefore, we see that while there are apparently many ways that biolo-

gy could avail itself of binding lead, it is actually the function that drives the type (helix, sheet or loop) of binding site that is found in the protein.

In the case of lead inhibiting existing metalloenzymes the system may be more complicated in that the Pb(II) ion accepts the structure that was utilized by a different metal. Thus, we see that a tetrahedral Zn(II) ion, as found in ALAD, is replaced with a trigonal pyramidal Pb(II) bound in an *exo* conformation. The lead accepts this structure as the native protein presents an environment that had allowed for a fourth ligand to Zn(II). While it is conceivable that a tetrahedral ion could accept an *endo* conformation for cysteines, the resultant polyhedron would necessarily be somewhat distorted toward a more trigonal planar system. We conclude that lead is sufficiently promiscuous to complex in this zinc site with little hesitation.

We also see that zinc finger peptides have a strong preference for PbS_3 chromophores as compared to mixed systems that incorporate histidines. However, we also recognize from ^{207}Pb NMR spectroscopy that the types of complexes that form may not be unique, and that two or more conformations could exist. Future work will hopefully assess whether this conformational flexibility could have biological function.

Future work in protein design will need to examine whether the principles derived from the present study for metal binding to α-helices is only narrowly applicable to *a* sites in parallel coiled coils or whether similar chemistry is implicated when lead binds to cysteines in *d* sites or when one has a more natural antiparallel orientation of helices. While the UV/VIS parameters for these divergent centers appear to be similar, the ^{207}Pb NMR shifts are markedly different. Hence, structural studies of this wider range of synthetic constructs will be essential to inform new designs that allow Pb(II) to be understood fully in even these most simple of protein scaffolds.

ACKNOWLEDGMENT

V.L.P. thanks the National Institute of Health for support of this research (ES012236). L.R. thanks the Royal Thai Government for a full PhD scholarship.

ABBREVIATIONS AND DEFINITIONS

A	alanine
ALA	δ-aminolevulinic acid
ALAD	δ-aminolevulinic acid dehydratase
ArsR/SmtB	arsenic resistance regulatory protein family
Baby	peptide containing three heptads
BLL	blood lead level
CaBP	calcium binding protein
cad	cadmium resistance operon

CadA	cadmium resistance efflux ATPase
CadC	cadmium resistance regulatory protein
CaM	calmodulin
CP-CCCC	zinc finger consensus peptide with Cys_4 site
CP-CCCH	zinc finger consensus peptide with Cys_3His site
CP-CCHC	zinc finger consensus peptide with $Cys_2HisCys$ site
CP-XCCC	zinc finger consensus peptide with $XCys_3$ site
CS	CoilSer peptide containing four heptad repeats
Cys	cysteine
czc	cadmium-zinc-cobalt resistance system
DFT	density functional theory
E	glutamic acid
EPA	United States Environmental Protection Agency
EXAFS	extended X-ray absorption fine structure spectroscopy
GATA	guanine-adenine-thymine-adenine
Gln	glutamine
Glu	glutamic acid
Gly	glycine
GRAND	peptide containing five heptads
GRAND-CS	GRAND-CoilSer peptide containing five heptad repeats
GS	glutathione anion
GSH	glutathione
His	histidine
HIV-CCGC	zinc finger HIV domain with $Cys_2GlyCys$ site
HIV-CCHC	zinc finger HIV domain with $Cys_2HisCys$ site
HIV-CCHH	zinc finger HIV domain with Cys_2His_2 site
HP2	human protamine 2
K	lysine
K_D	dissociation constant
K_i	inhibition constant
L	leucine
LMCT	ligand-to-metal charge transfer
L-Cys	L-cysteine
L-Pen	L-penicillamine
MerR	mercury resistance regulatory protein
NAC	N-acetylcysteine
NMR	nuclear magnetic resonance spectroscopy
NOESY	nuclear Overhauser spectroscopy
PAC	perturbed angular correlation of γ-rays spectroscopy
pbr	lead resistance operon
PbrA	lead resistance efflux ATPase
PbrB/PbrC	lead resistance fusion phosphatase
PbrD	lead resistance lead-binding protein
PbrR	lead resistance regulatory protein
PbrR691	PbrR-homologue
PbrT	lead resistance uptake protein

pbrU	lead resistance inner membrane permease gene
pM	picomolar
ppb	parts-per-billion
Pro	proline
Ser	serine
Sp1	specificity protein1
TFIIIA	transcription factor IIIA
Thr	threonine
TIM	triosephosphate isomerase
TM-29	synthetic peptide analog of tropomyosin that contains 29 residues with the sequence Ac-(Lys-Leu-Glu-Ala-Leu-Glu-Gly)$_4$-Lys amide
TRI	peptide containing four heptads
XAS	X-ray absorption spectroscopy
znt	zinc resistance operon
ZntA	zinc resistance efflux ATPase
ZntR	zinc resistance regulatory protein
3SCC	three-stranded coiled coil

REFERENCES

1. J. Eisinger, *Med. Hist.* **1982**, *26*, 279–302.
2. G. Markowitz, D. Rosner, *Am. J. Public Health* **2000**, *90*, 36–46.
3. K. R. Mahaffey, J. L. Annest, J. Roberts, R. S. Murphy, *New. Eng. J. Med.* **1982**, *307*, 573–579.
4. N. Zhang, H. W. Baker, M. Tufts, R. E. Raymond, H. Salihu, M. R. Elliott, *Am. J. Public Health* **2013**, *103*, e72–e77.
5. The Virginia Tech Research Team "Flint Water Study," can be found under http://www.flintwaterstudy.org, **2016**. (accessed Apr. 17, 2016)
6. K. Drum, "Mother Jones 'Raw Data: Lead Poisoning of Kids in Flint,'" can be found under http://www.motherjones.com/kevin-drum/2016/01/raw-data-lead-poisoning-kids-flint, **2016**. (accessed Apr. 17, 2016)
7. M. F. Bouchard, D. C. Bellinger, J. Weuve, J. Matthews-Bellinger, S. E. Gilman, R. O. Wright, J. Schwartz, M. G. Weisskopf, *Arch. Gen. Psychiat.* **2009**, *66*, 1313–1319.
8. D. C. Bellinger, K. M. Stiles, H. L. Needleman, *Pediatrics* **1992**, *90*, 855–861.
9. H. W. Mielke, S. Zahran, *Environ. Int.* **2012**, *43*, 48–55.
10. B. P. Lanphear, R. Hornung, J. Khoury, K. Yolton, P. Baghurst, D. C. Bellinger, R. L. Canfield, K. N. Dietrich, R. Bornschein, T. Greene, S. J. Rothenberg, H. L. Needleman, I. Schnaas, G. Wassermann, J. Graziano, R. Roberts, *Environ. Health Persp.* **2005**, *113*, 894–899.
11. Agency for Toxic Substances and Disease Registry "Case Studies in Environmental Medicine (CSEM) Lead Toxicity", can be found under http://www.atsdr.cdc.gov/csem/csem.asp?csem = 7&po = 0, **2010**. (accessed Apr. 16, 2016)
12. J. G. Dorea, C. M. Donangelo, *Clin. Nutr.* **2006**, *25*, 369–376.
13. L. Patrick, *Altern. Med. Rev.* **2006**, *11*, 2–22.
14. J. G. Dorea, *Brit. J. Nutr.* **2004**, *92*, 21–40.
15. A. Sen, N. Heredia, M.-C. Senut, S. Land, K. Hollocher, X. Lu, M. O. Dereski, D. M. Ruden, *Sci. Rep.* **2015**, *5*, 14466.

16. M. J. Warren, J. B. Cooper, S. P. Wood, P. M. Shoolingin-Jordan, *Trends Biochem. Sci.* **1998**, *23*, 217–221.
17. M. Kirberger, J. J. Yang, *J. Inorg. Biochem.* **2008**, *102*, 1901–1909.
18. J. S. Magyar, T.-C. Weng, C. M. Stern, D. F. Dye, B. W. Rous, J. C. Payne, B. M. Bridgewater, A. Mijovilovich, G. Parkin, J. M. Zaleski, J. E. Penner-Hahn, H. A. Godwin, *J. Am. Chem. Soc.* **2005**, *127*, 9495–9505.
19. E. S. Claudio, H. A. Godwin, J. S. Magyar, *Prog. Inorg. Chem.* **2002**, *51*, 1–144.
20. J. C. Payne, M. A. ter Horst, H. A. Godwin, *J. Am. Chem. Soc.* **1999**, *121*, 6850–6855.
21. P. T. Erskine, E. M. H. Duke, I. J. Tickle, N. M. Senior, M. J. Warren, J. B. Cooper, *Acta Crystallogr. D* **2000**, *D56*, 421–430.
22. V. Mah, F. Jalilehvand, *Inorg. Chem.* **2012**, *51*, 6285–6298.
23. P. R. Chen, E. C. Wasinger, J. Zhao, D. van der Lelie, L. X. Chen, C. He, *J. Am. Chem. Soc.* **2007**, *129*, 12350–12351.
24. M. Matzapetakis, D. Ghosh, T.-C. C. Weng, J. E. Penner-Hahn, V. L. Pecoraro, *J. Biol. Inorg. Chem.* **2006**, *11*, 876–890.
25. R. K. Mehra, V. R. Kodati, R. Abdullah, *Biochem. Bioph. Res. Co.* **1995**, *215*, 730–736.
26. R. K. Singhal, M. E. Anderson, A. Meister, *FASEB J.* **1987**, *1*, 220–223.
27. J. Yang, R. Swati, T. L. Stemmler, B. P. Rosen, *Biochemistry* **2010**, *49*, 3658–3666.
28. A. Hunaiti, M. Soud, A. Khalil, *Sci. Total Environ.* **1995**, *170*, 95–100.
29. A. A. Hunaiti, M. Soud, *Sci. Total Environ.* **2000**, *248*, 45–50.
30. B. J. Fuhr, D. L. Rabenstein, *J. Am. Chem. Soc.* **1973**, *95*, 6944–6950.
31. L. A. P. Kane-Maguire, P. J. Riley, *J. Coord. Chem.* **1993**, *28*, 105–120.
32. B. K. Singh, R. K. Sharma, B. S. Garg, *J. Therm. Anal. Calorim.* **2006**, *84*, 593–600.
33. K. P. Neupane, V. L. Pecoraro, *J. Inorg. Biochem.* **2011**, *105*, 1030–1034.
34. T. J. B. Simons, *Eur. J. Biochem.* **1995**, *234*, 178–183.
35. A. Schütz, S. Skerfving, *Scand. J. Work Environ. Health* **1976**, *3*, 176–184.
36. P. T. Erskine, L. Coates, R. Newbold, A. A. Brindley, F. Stauffer, S. P. Wood, M. J. Warren, J. B. Cooper, P. M. Shoolingin-Jordan, R. Neier, *FEBS Lett.* **2001**, *503*, 196–200.
37. G. Parkin, *Chem. Rev.* **2004**, *104*, 699–767.
38. I. A. Bergdahl, M. Sheveleva, A. Schütz, V. G. Artamonova, S. Skerfving, *Toxicol. Sci.* **1998**, *46*, 247–253.
39. D. Chin, A. R. Means, *Trends Cell. Biol.* **2000**, *10*, 322–328.
40. J. A. Cowan, in *Binding, Transport, and Storage of Metal Ions in Biological Cells,* Eds W. Maret, A. G. Wedd, Royal Society of Chemistry, Cambridge, 2014, pp. 123–152.
41. J. M. Aramini, T. Hiraoki, M. Yazawa, T. Yuan, M. Zhang, H. J. Vogel, *J. Biol. Inorg. Chem.* **1996**, *1*, 39–48.
42. C. S. Fullmer, S. Edelstein, R. H. Wasserman, *J. Biol. Chem.* **1985**, *260*, 6816–6819.
43. M. A. Wilson, A. T. Brunger, *J. Mol. Biol.* **2000**, *301*, 1237–1256.
44. M. A. Wilson, A. T. Brunger, *Acta Crystallogr. D* **2003**, *D59*, 1782–1792.
45. M. Kern, M. Wisniewski, L. Cabell, G. Audesirk, *Neurotoxicology* **2000**, *21*, 353–363.
46. S. H. Chao, C. H. Bu, W. Y. Cheung, *Arch. Toxicol.* **1995**, *69*, 197–203.
47. M. Kirberger, H. C. Wong, J. Jiang, J. J. Yang, *J. Inorg. Biochem.* **2013**, *125*, 40–49.
48. H. Ouyang, H. J. Vogel, *Biometals* **1998**, *11*, 213–222.
49. J. H. Laity, B. M. Lee, P. E. Wright, *Curr. Opin. Struct. Biol.* **2001**, *11*, 39–46.
50. S. S. Krishna, I. Majumdar, N. V. Grishin, *Nucleic Acids Res.* **2003**, *31*, 532–550.
51. H. C. Gonick, *J. Toxicol.* **2011**, *2011*, Article ID 686050, 10 pages.
52. R. A. Goyer, D. L. Leonard, J. F. Moore, B. Rhyne, M. R. Krigman, *Arch. Environ. Health* **1970**, *20*, 705–711.
53. R. A. Goyer, P. May, M. M. Cates, M. R. Krigman, *Lab. Invest.* **1970**, *22*, 245–251.

54. A. A. Jarzęcki, *Inorg. Chem.* **2007**, *46*, 7509–7521.
55. *The PyMOL Molecular Graphics System, Version 1.5.0.4 Schrödinger, LLC.*
56. V. M. Cangelosi, V. L. Pecoraro, in *Binding, Transport, and Storage of Metal Ions in Biological Cells,* Eds W. Maret, A. G. Wedd, Royal Society of Chemistry, Cambridge, 2014, pp. 843–882.
57. A. B. Ghering, L. M. M. Jenkins, B. L. Schenck, S. Deo, R. A. Mayer, M. J. Pikaart, J. G. Omichinski, H. A. Godwin, *J. Am. Chem. Soc.* **2005**, *127*, 3751–3759.
58. N. H. Zawia, R. Sharan, M. Brydie, T. Oyama, T. Crumpton, *Brain Res. Dev. Brain Res.* **1998**, *107*, 291–298.
59. J. S. Hanas, J. S. Rodgers, J. A. Bantle, Y.-G. Cheng, *Mol. Pharmacol.* **1999**, *56*, 982–988.
60. B. Quintanilla-Vega, D. J. Hoover, W. Bal, E. K. Silbergeld, M. P. Waalkes, L. D. Anderson, *Chem. Res. Toxicol.* **2000**, *13*, 594–600.
61. C.-C. Chang, L. Y. Lin, X.-W. Zou, C. -C. Huang, N.-L. Chan, *Nucl. Acids Res.* **2015**, *43*, 7612–7623.
62. C. Rensing, M. Ghosh, B. P. Rosen, *J. Bacteriol.* **1999**, *181*, 5891–5897.
63. Z. Ma, F. E. Jacobsen, D. P. Giedroc, *Chem. Rev.* **2009**, *109*, 4644–4681.
64. B. Borremans, J. L. Hobman, A. Provoost, N. L. Brown, D. Van Der Lelie, *J. Bacteriol.* **2001**, *183*, 5651–5658.
65. A. Hynninen, T. Touzé, L. Pitkänen, D. Mengin-Lecreulx, M. Virta, *Mol. Microbiol.* **2009**, *74*, 384–394.
66. S. Taghavi, C. Lesaulnier, S. Monchy, R. Wattiez, M. Mergeay, D. van der Lelie, *Antonie Van Leeuwenhoek* **2009**, *96*, 171–182.
67. S. Monchy, M. A. Benotmane, P. Janssen, T. Vallaeys, S. Taghavi, D. van der Lelie, M. Mergeay, *J. Bacteriol.* **2007**, *189*, 7417–7425.
68. L. Diels, Q. Dong, D. van der Lelie, W. Baeyens, M. Mergeay, *J. Ind. Microbiol.* **1995**, *14*, 142–153.
69. J. L. Hobman, D. J. Julian, N. L. Brown, *BMC Microbiol.* **2012**, *12*, 109.
70. P. Chen, B. Greenberg, S. Taghavi, C. Romano, D. van der Lelie, C. He, *Angew. Chem. Int. Ed.* **2005**, *44*, 2715–2719.
71. H. M. Berman, J. Westbrook, Z. Feng, G. Gilliland, T. N. Bhat, H. Weissig, I. N. Shindyalov, P. E. Bourne, *Nucleic Acids Res.* **2000**, *28*, 235–242.
72. S. Q. Huang, W. Z. Chen, D. Wang, Q. Y. Hu, X. C. Liu, J. H. Gan, H. Chen, *Unreleased ID 5DBZ: Crystal Structure of the Transcription Regulator PbrR691 from Ralstonia Metallidurans CH34 in Complex with Lead(II)*, 2015.
73. S. J. Beard, R. Hashim, J. Membrillo-Hernández, M. N. Hughes, R. K. Poole, *Mol. Microbiol.* **1997**, *25*, 883–891.
74. C. Rensing, B. Mitra, B. P. Rosen, *Proc. Natl. Acad. Sci. USA* **1997**, *94*, 14326–14331.
75. C. Rensing, Y. Sun, B. Mitra, B. P. Rosen, *J. Biol. Chem.* **1998**, *273*, 32614–32617.
76. J. Okkeri, T. Haltia, *Biochemistry* **1999**, *38*, 14109–14116.
77. R. Sharma, C. Rensing, B. P. Rosen, B. Mitra, *J. Biol. Chem.* **2000**, *275*, 3873–3878.
78. K. R. Brocklehurst, J. L. Hobman, B. Lawley, L. Blank, S. J. Marshall, N. L. Brown, A. P. Morby, *Mol. Microbiol.* **1999**, *31*, 893–902.
79. M. R. Binet, R. K. Poole, *FEBS Let.* **2000**, *473*, 67–70.
80. Y. Hitomi, C. E. Outten, T. V O'Halloran, *J. Am. Chem. Soc.* **2001**, *123*, 8614–8615.
81. A. Changela, K. Chen, Y. Xue, J. Holschen, C. E. Outten, T. V O'Halloran, A. Mondragón, *Science* **2003**, *301*, 1383–1387.
82. S. Khan, K. R. Brocklehurst, G. W. Jones, A. P. Morby, *Biochem. Bioph. Res. Co.* **2002**, *299*, 438–445.
83. C. E. Outten, F. W. Outten, T. V O'Halloran, *J. Biol. Chem.* **1999**, *274*, 37517–37524.
84. K. P. Yoon, S. Silver, *J. Bacteriol.* **1991**, *173*, 7636–7642.
85. G. Endo, S. Silver, *J. Bacteriol.* **1995**, *177*, 4437–4441.

86. J. Ye, A. Kandegedara, P. Martin, B. P. Rosen, *J. Bacteriol.* **2005**, *187*, 4214–4221.
87. L. S. Busenlehner, N. J. Cosper, R. A. Scott, B. P. Rosen, M. D. Wong, D. P. Giedroc, *Biochemistry* **2001**, *40*, 4426–4436.
88. Y. Sun, M. D. Wong, B. P. Rosen, *Mol. Microbiol.* **2002**, *44*, 1323–1329.
89. Y. Sun, M. D. Wong, B. P. Rosen, *J. Biol. Chem.* **2001**, *276*, 14955–14960.
90. M. D. Wong, Y.-F. Lin, B. P. Rosen, *J. Biol. Chem.* **2002**, *277*, 40930–40936.
91. A. G. Tebo, L. Hemmingsen, V. L. Pecoraro, *Metallomics* **2015**, *7*, 1555–1561.
92. L. S. Busenlehner, T.-C. Weng, J. E. Penner-Hahn, D. P. Giedroc, *J. Mol. Biol.* **2002**, *319*, 685–701.
93. J. L. Apuy, L. S. Busenlehner, D. H. Russell, D. P. Giedroc, *Biochemistry* **2004**, *43*, 3824–3834.
94. L. S. Busenlehner, D. P. Giedroc, *J. Inorg. Biochem.* **2006**, *100*, 1024–1034.
95. F. Yu, V. M. Cangelosi, M. L. Zastrow, M. Tegoni, J. S. Plegaria, A. G. Tebo, C. S. Mocny, L. Ruckthong, H. Qayyum, V. L. Pecoraro, *Chem. Rev.* **2014**, *114*, 3495–3578.
96. B. J. Berne, J. D. Weeks, R. Zhou, *Annu. Rev. Phys. Chem.* **2009**, *60*, 85–103.
97. V. R. Agashe, M. C. Shastry, J. B. Udgaonkar, *Nature* **1995**, *377*, 754–757.
98. A. M. Gutin, V. I. Abkevich, E. I. Shakhnovich, *Biochemistry* **1995**, *34*, 3066–3076.
99. K. A. Dill, S. Bromberg, Y. Kaizhi, K. M. Fiebig, D. P. Yee, P. D. Thomas, H. S. Chan, *Protein Sci.* **1995**, *4*, 561–602.
100. F. H. C. Crick, *Acta Crystallogr.* **1953**, *6*, 689–697.
101. P. Palau, J. Puigdomenech, *J. Mol. Biol.* **1974**, *88*, 457–469.
102. W. F. DeGrado, C. M. Summa, V. Pavone, F. Nastri, A. Lombardi, *Annu. Rev. Biochem.* **1999**, *68*, 779–819.
103. R. S. Hodges, **1996**, *154*, 133–154.
104. B. Apostolovic, M. Danial, H.-A. Klok, *Chem. Soc. Rev.* **2010**, *39*, 3541–3575.
105. R. S. Hodges, A. K. Saund, P. C. S. Chong, S. A. St.-Pierre, R. E. Reid, *Biol. Chem.* **1981**, *256*, 1214–1224.
106. J. A. Talbot, R. S. Hodges, *Acc. Chem. Res.* **1982**, *15*, 224–230.
107. D. Eisenberg, W. Wilcox, A. D. Mclachlan, *J. Cell. Biochem.* **1986**, *31*, 11–17.
108. P. B. Harbury, T. Zhang, P. S. Kim, T. Alber, *Science* **1993**, *262*, 1401–1407.
109. A. Sikorski, A. Kolinski, J. Skolnick, *Biophys. J.* **1998**, *75*, 92–105.
110. W. DeGrado, J. Lear, *J. Am. Chem. Soc.* **1985**, *107*, 7684–7689.
111. P. B. Harbury, J. J. Plecs, B. Tidor, T. Alber, P. S. Kim, *Science* **1998**, *282*, 1462–1467.
112. G. Dieckmann, S. Heilman, W. DeGrado, V. L. Pecoraro, in *An Inorganic Perspective of Life*, Eds D. P. Kessissoglou, D. Coucouvanis, M. Kanatzidas, Elsevier, Amsterdam, 1995, p. 275.
113. D. L. Mcclain, H. L. Woods, M. G. Oakley, *J. Am. Chem. Soc.* **2001**, *123*, 3151–3152.
114. X. Zeng, H. Zhu, H. a Lashuel, J. C. Hu, *Protein Sci.* **1997**, *6*, 2218–2226.
115. L. Gonzalez, R. A. Brown, D. Richardson, T. Alber, *Nat. Struct. Biol.* **1996**, *3*, 1002–1009.
116. P. B. Harbury, P. S. Kim, T. Alber, *Nature* **1994**, *371*, 80–83.
117. J. D. Lear, Z. R. Wasserman, W. F. DeGrado, *Science* **1988**, *240*, 1177–1181.
118. J. Y. Su, R. S. Hodges, C. M. Kay, *Biochemistry* **1994**, *33*, 15501–15510.
119. S. C. Kwok, R. S. Hodges, *Biopolym.-Pept. Sci. Sect.* **2004**, *76*, 378–390.
120. D. Ghosh, K.-H. Lee, B. Demeler, V. L. Pecoraro, *Biochemistry* **2005**, *44*, 10732–10740.
121. G. R. Dieckmann, Ph.D. Dissertation, University of Michigan, **1995**.
122. G. R. Dieckmann, D. K. McRorie, J. D. Lear, K. A. Sharp, W. F. DeGrado, V. L. Pecoraro, *J. Mol. Biol.* **1998**, *280*, 897–912.
123. G. R. Dieckmann, D. K. Mcrorie, D. L. Tierney, L. M. Utschig, C. P. Singer, T. V O'Halloran, J. E. Penner-Hahn, W. F. Degrado, V. L. Pecoraro, *J. Am. Chem. Soc.* **1997**, *119*, 6195–6196.

124. D. Ghosh, V. L. Pecoraro, *Curr. Opin. Chem. Biol.* **2005**, *9*, 97–103.
125. D. Ghosh, V. L. Pecoraro, *Inorg. Chem.* **2004**, *43*, 7902–7915.
126. O. Iranzo, D. Ghosh, V. L. Pecoraro, *Inorg. Chem.* **2006**, *45*, 9959–9973.
127. D. S. Touw, C. E. Nordman, J. A. Stuckey, V. L. Pecoraro, *Proc. Natl. Acad. Sci. USA* **2007**, *104*, 11969–11974.
128. O. Iranzo, S. Chakraborty, L. Hemmingsen, V. L. Pecoraro, *J. Am. Chem. Soc.* **2011**, *133*, 239–251.
129. A. Dołęga, K. Baranowska, J. Gajda, S. Kaźmierski, M. J. Potrzebowski, *Inorganica Chim. Acta* **2007**, *360*, 2973–2982.
130. K.-H. Lee, M. Matzapetakis, S. Mitra, E. N. G. Marsh, V. L. Pecoraro, *J. Am. Chem. Soc.* **2004**, *126*, 9178–9179.
131. M. Matzapetakis, B. T. Farrer, T.-C. Weng, L. Hemmingsen, J. E. Penner-Hahn, V. L. Pecoraro, *J. Am. Chem. Soc.* **2002**, *124*, 8042–8054.
132. M. Matzapetakis, V. L. Pecoraro, *J. Am. Chem. Soc.* **2005**, *127*, 18229–18233.
133. O. Iranzo, P. W. Thulstrup, S.-B. Ryu, L. Hemmingsen, V. L. Pecoraro, *Chemistry* **2007**, *13*, 9178–9190.
134. O. Iranzo, C. Cabello, V. L. Pecoraro, *Angew. Chem. Int. Ed. Engl.* **2007**, *46*, 6688–6691.
135. S. Chakraborty, O. Iranzo, E. R. P. Zuiderweg, V. L. Pecoraro, *J. Am. Chem. Soc.* **2012**, *134*, 6191–6203.
136. O. Iranzo, T. Jakusch, K.-H. Lee, L. Hemmingsen, V. L. Pecoraro, *Chemistry* **2009**, *15*, 3761–3772.
137. G. Zampella, K. P. Neupane, L. De Gioia, V. L. Pecoraro, *Eur. J. Inorg. Chem.* **2012**, *18*, 2040–2050.
138. K. P. Neupane, V. L. Pecoraro, *Angew. Chem. Int. Ed.* **2010**, *49*, 8177–8180.
139. B. T. Farrer, N. P. Harris, K. E. Balchus, V. L. Pecoraro, *Biochemistry* **2001**, *40*, 14696–14705.
140. B. T. Farrer, C. P. McClure, J. E. Penner-Hahn, V. L. Pecoraro, *Inorg. Chem.* **2000**, *39*, 5422–5423.
141. B. T. Farrer, V. L. Pecoraro, *Proc. Natl. Acad. Sci. USA* **2003**, *100*, 3760–3765.
142. M. L. Zastrow, A. F. A. Peacock, J. A. Stuckey, V. L. Pecoraro, *Nat. Chem.* **2012**, *4*, 118–123.
143. Ruckthong, L., *Crystallographic Comparison of TRI-Thiolate Sites in Designed Proteins to Control Metal Geometries*, Ph.D. Thesis, University of Michigan, Ann Arbor, 2016.
144. K.-H. Lee, C. Cabello, L. Hemmingsen, E. N. G. Marsh, V. L. Pecoraro, *Angew. Chem. Int. Ed. Engl.* **2006**, *45*, 2864–2868.
145. A. F. A. Peacock, J. A. Stuckey, V. L. Pecoraro, *Angew. Chem. Int. Ed. Engl.* **2009**, *48*, 7371–7374.
146. A. F. A. Peacock, V. L. Pecoraro, in *Cadmium: From Toxicity to Essentiality*, Vol. 11 of *Metal Ions in Life Sciences*, Eds A. Sigel, R. K. O. Sigel, H. Sigel, Springer SBM, Dordrecht, The Netherlands, 2013, pp. 303–337.
147. M. Zastrow, V. L. Pecoraro, *Coord. Chem. Rev.* **2013**, 2565–2588.
148. V. L. Pecoraro, A. F. A. Peacock, O. Iranzo, M. Luczkowski, in *ACS Symposium Series*, Eds E. Long, M. J. Baldwin, 2009, pp. 183–198.
149. A. F. A. Peacock, O. Iranzo, V. L. Pecoraro, *Dalton Trans.* **2009**, 2271–2280.
150. C. S. Mocny, *Examining the Metal Selectivity of Thiol Rich de Novo Designed Peptides as a Strategy to Make Asymmetric Alpha- Helical Protein Assemblies*, Ph.D. Thesis, University of Michigan, 2016.
151. F. Jalilehvand, N. S. Sisombath, A. C. Schell, G. A. Facey, *Inorg. Chem.* **2015**, *54*, 2160–2170.
152. N. S. Sisombath, F. Jalilehvand, *Chem. Res. Toxicol.* **2015**, *28*, 2313–2324.

153. T. Liu, J. W. Golden, D. P. Giedroc, *Biochemistry* **2005**, *44*, 8673–8683.
154. D. Touw, *Structural and Spectroscopic Studies of Heavy Metal Binding to de Novo Designed Coiled Coil Peptides*, Ph.D. Thesis, University of Michigan, 2007.
155. S. Chakraborty, D. S. Touw, A. F. A. Peacock, J. Stuckey, V. L. Pecoraro, *J. Am. Chem. Soc.* **2010**, *132*, 13240–13250.
156. B. Wrackmeyer, *Annu. Reports NMR Spectrosc.* **2002**, *47*, 1–37.
157. B. Wrackmeyer, K. Horchler, *Annu. Reports NMR Spectrosc.* **1990**, *22*, 249–306.
158. J. E. Penner-Hahn, *Coord. Chem. Rev.* **2005**, *249*, 161–177.
159. G. Christou, K. Folting, J. C. Huffman, *Polyhedron* **1984**, *3*, 1247.
160. B. M. Bridgewater, G. Parkin, *J. Am. Chem. Soc.* **2000**, *122*, 7140–7141.
161. I. C. C. Z.-G. Ren, X.-Y. Tang, Li Li, G.-F. Liu, H.-X. Li, Y. Chen, Y. Zhang, J.-P. Lang, *Inorg. Chem. Commun.* **2007**, 1253.
162. B. Lovejoy, S. Choe, D. Cascio, D. K. Mcrorie, F. William, D. Eisenberg, W. F. Degrado, *Science* **1993**, *259*, 1288–1293.
163. L. Ruckthong, M. L. Zastrow, J. A. Stuckey, V. L. Pecoraro, *J. Am. Chem. Soc.* **2016**, *138*, 11979–11988.
164. P. T. Erskine, N. Senior, S. Awan, R. Lambert, G. Lewis, I. J. Tickle, M. Sarwar, P. Spencer, P. Thomas, M. J. Warren, P. M. Shoolingin-Jordan, S. P. Wood, J. B. Cooper, *Nat. Struct. Biol.* **1997**, *4*, 1025–1031.
165. P. T. Erskine, R. Newbold, A. A. Brindley, S. P. Wood, P. M. Shoolingin-Jordan, M. J. Warren, J. B. Cooper, *J. Mol. Biol.* **2001**, *312*, 133–141.
166. P. T. Erskine, E. M. H. Duke, I. J. Tickle, N. M. Senior, J. B. Cooper, **2000**, 421–430.
167. P. R. Chen, C. He, *Curr. Opin. Chem. Biol.* **2008**, *12*, 214–221.
168. C.-C. Chang, L.-Y. Lin, X.-W. Zou, C.-C. Huang, N.-L. Chan, *Nucleic Acids Res.* **2015**, 1–12.

11

Complex Formation of Lead(II) with Nucleotides and Their Constituents

Astrid Sigel, Bert P. Operschall, and Helmut Sigel

Department of Chemistry, Inorganic Chemistry, University of Basel,
Spitalstrasse 51, CH-4056 Basel, Switzerland
<astrid.sigel@unibas.ch> <helmut.sigel@unibas.ch>

Metal Ions in Life Sciences, Volume 17 Edited by Astrid Sigel, Helmut Sigel, and Roland K. O. Sigel

DOI 10.1515/9783110434330-011

Abstract: Lead is widely distributed in the environment; it is known to mankind for thousands of years and its toxicity is nowadays (again) well recognized, though on the molecular level only partly understood. One of the reasons for this shortcoming is that the coordination chemistry of the biologically important lead(II) is complicated due to the various coordination numbers it can adopt (CN = 4 to 10) as well as by the $6s^2$ electron lone pair which, with CN = 4, can shield one side of the Pb^{2+} coordination sphere. The chapter focuses on the properties of Pb^{2+} complexes formed with nucleotides and their constituents and derivatives. Covered are (among others) the complexes formed with hydroxy groups and sugar residues, the interactions with the various nucleobases occurring in nucleic acids, as well as complexes of phosphates. It is expeced that such interactions, next to those like with lipids and proteins, are responsible for the toxic properties of lead. To emphasize the special properties of Pb^{2+} complexes, these are compared as far as possible with the corresponding properties of the Ca^{2+}, Fe^{2+}, Cu^{2+}, Zn^{2+}, and Cd^{2+} species. It needs to be mentioned that the *hard-soft rule* fails with Pb^{2+}. This metal ion forms complexes with ligands offering O donors of a stability comparable to that of Cu^{2+}. In contrast, with aromatic N ligands, like imidazole or N7 sites of purines, complex stability is comparable to that of the corresponding Fe^{2+} complexes. The properties of Pb^{2+} towards S donor sites are difficult to generalize: On the one hand Pb^{2+} forms very stable complexes with nucleoside 5′-*O*-thiomonophosphates by coordinating to nearly 100 % at S in the thiophosphate group; however, on the other hand, once a sulfur atom replaces one of the terminal oxygen atoms in the phosphodiester linkage, macrochelate formation of the phosphate-bound Pb^{2+} occurs with the O and not the S site. Quite generally,

the phosphodiester linkage is a relatively weak binding site, but the affinity increases further to the mono- and then to the di- and triphosphate. The same holds for the corresponding nucleotides, though the Pb^{2+} affinity had to be estimated via that of the Cu^{2+} complexes for some of these ligands. Complex stability of the pyrimidine-nucleotides (due to their *anti* conformation) is solely determined by the coordinating tendency of the phosphate group(s); this also holds for the Pb^{2+} complex of adenosine 5′-monophosphate. For the other purine-nucleotides macrochelate formation takes place by the interaction of the phosphate-coordinated Pb^{2+} with the N7/(C6)O site of, e.g., the guanine residue. The extents of the formation degrees of these chelates are summarized. Unfortunately, information about mixed ligand (ternary) or other higher order comlexes is missing, but still it is hoped that the present overview will help to understand the interaction of Pb^{2+} with nucleotides and nucleic acids, and especially that it will facilitate further research in this fascinating area.

Keywords: cadmium · calcium · DNA · isomeric equilibria · lead · nucleic acids · ribozymes · RNA · stability constants · Stability Ruler

1. INTRODUCTION

Lead is certainly a toxic element [1–3]. Its essentiality has been discussed but not demonstrated [2, 4]. The toxicity of lead was recorded already by Greek and Arab scholars. Indeed, lead is one of the oldest metals known to man; e.g., it was known to the early Egyptians and Hebrews [2, 4]. There is a figure of lead in the British Museum that was crafted before 3800 B.C. and lead was mined in Spain as early as 2000 B.C. [2]. Thus, "lead has been mined and used for over 6000 years, spiking during Roman times and the Industrial Revolution" [5] (see also [6, 7]). During the past 100 years lead was extensively used in paint pigments, for electronic storage batteries, for toy manufacturing, etc., and as an additive to gasoline [2, 5], though the latter use is now banned (see Chapters 13 and 14 of this book). In any case, lead is a prominent toxic metal in natural and engineered systems [8].

Lead is the most abundant of the heavy metals in the Earth's crust [9]. It occurs in ores of zinc, silver, and copper [4]; its major sources are galena (PbS), cerrussite ($PbCO_3$), and anglesite ($PbSO_4$) [2–4]. Lead is transported in the ecosystem by precipitation from the atmosphere to soil and water, uptake by plants and animals, and re-entry to the atmosphere [2] (see also Chapter 2). The inputs of natural lead to ecosystems are mainly from geological erosion, yet inputs from industrial sources and human activities are by far the most important in industrialized areas of the world [2, 4, 6].

Maybe at this point one should add that a literature search in SciFinder for the metal lead is troubled by the verb "to lead" and as a result one feels insecure if all relevant publications have been caught (see also Chapter 1). Lead occurs in the oxidation states zero (i.e., as the metal), two and four; for biological systems Pb(II)/Pb^{2+} is relevant [10]. If the name "lead" is used in this chapter without an oxidation state, either the metal itself is addressed or Pb(II); which form is meant is always clear from the context.

As already indicated above, lead has been recognized as a toxic element for a long time [2] and the acute and chronic effects of lead poisoning have been

summarized [3] (see also Chapter 16). Lead produces adverse effects in mammals, e.g.,

- it acts on the central and peripheral nervous systems [1, 2, 11, 12].
- it leads to anemia [2, 13].
- it induces an inflammatory response [14, 15].
- it modulates immune functions [16, 17].
- it has genetic and reproductive effects [18–20].
- it affects the metabolism of other metal ions [1], like Ca^{2+}, Zn^{2+} or Cu^{2+}.

Interestingly, about 95 % of the body burden of lead is stored in bone [3] indicating a chemical relationship between Ca^{2+} and Pb^{2+}. Similarly, about 95 %

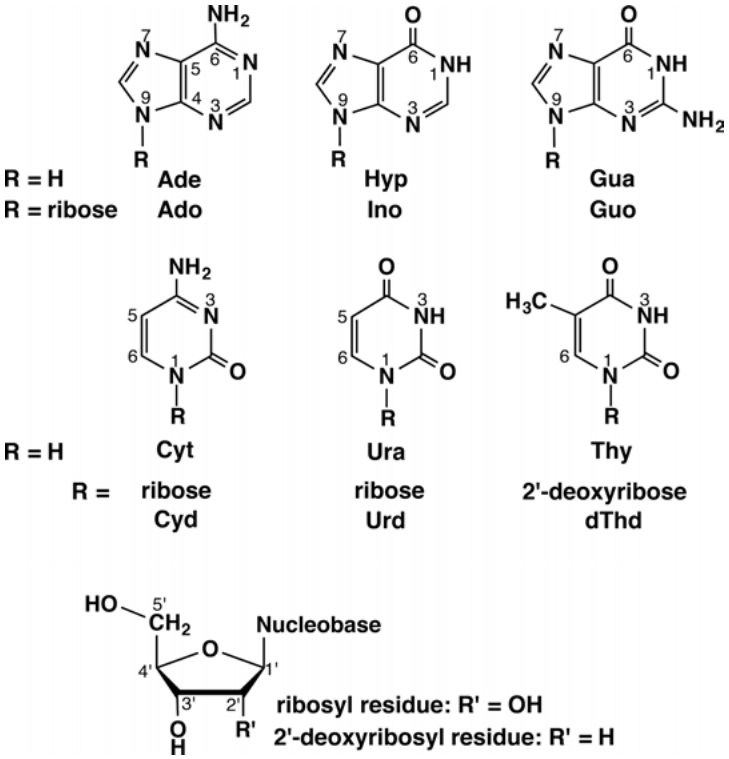

Figure 1. Chemical structures of the nucleobases (R = H) occurring in RNA: adenine (Ade), guanine (Gua), cytosine (Cyt), and uracil (Ura). Hypoxanthine (Hyp) is a rare nucleobase and shown for comparison with guanine. Thymine (Thy), which occurs in DNA, can also be addressed as 5-methyluracil. The corresponding nucleosides (R = ribosyl residue) are adenosine (Ado), inosine (Ino), guanosine (Guo), cytidine (Cyd), uridine (Urd), and thymidine (dThd); in thymidine R is the 2′-deoxyribosyl residue. The dominating conformation of the nucleosides is the *anti* one [22–25]; this conformation is obtained if the "Nucleobase" at C1′ of the ribosyl residue is replaced by the bases as they are depicted within the plane. This means, for the purines the aromatic rings are pointing away from the ribose plane; the same holds for the (C2)O group of the pyrimidines.

of Pb(II), which occurs in blood, is actually found in red cells [2]. In fact, the interaction of Pb^{2+} with many components in the body restricts the free Pb^{2+} concentration in blood or within cells to very low levels: Application of a procedure developed by Martin [21] for $Ca(HPO_4)$ solubility leads to the conclusion that at pH 7.4 and 2 mM total inorganic phosphate for the extracellular fluid, the allowed free Pb^{2+} concentration amounts to $2.5 \cdot 10^{-8}$ M [10]; for the intracellular fluid one obtains at pH 6.6 and 10 mM phosphate a free Pb^{2+} concentration of 10^{-8} M. From these very low free Pb^{2+} concentrations it follows that in body fluids Pb(II) must be complexed to a very large extent [10].

Such complexation reactions involving nucleotides and constituents thereof are in the center of this chapter (Sections 3 through 7). The structures of the relevant nucleobases, present in nucleosides and nucleotides, as well as the ribose residue are shown in Figure 1 [22–25].

Next to the nucleobases, the structures of the nucleosides are also indicated in Figure 1. There are many different nucleotides but all of them are phosphate esters formed with one of the ribosyl-hydroxyl groups [26–28]. One may add that the four main nucleosides of RNA are Ado, Guo, Cyd, and Urd, whereas those of DNA are the corresponding 2′-deoxy compounds, Urd being replaced by dThd [29].

This chapter is organized in part analogously to a chapter devoted to Cd^{2+} [30] and published in the book "Cadmium: From Toxicity to Essentiality" [31].

2. COMPARISONS OF THE PROPERTIES OF LEAD(II) WITH THOSE OF RELATED DIVALENT METAL IONS

2.1. Metal Ion Interdependencies

It has been indicated above that Pb^{2+} may affect the metabolism of other metal ions, especially of essential ones. Therefore it is of relevance to consider the interdependencies between Pb^{2+} and other elements as is outlined in Figure 2. Note, there may be more interdependencies; only some obvious ones are shown [32].

As summarized before in a different context [30], "an arrow from element A to B, $A \rightarrow B$, indicates that administration of element A may reduce toxicity due to element B." Hence, the toxicity of Pb^{2+} may be reduced by the ions of Ca, Zn, Cu, and Fe, as well as by phosphate (P); the metalloid Se may also have indirect effects. However, low levels of element A, e.g., of Ca^{2+}, Zn^{2+}, and Cu^{2+}, may increase the toxicity of element B (Pb^{2+}), or high levels of element B (Pb^{2+}) may inhibit salutary effects of element A (e.g., Zn^{2+}). "Such interrelations are common, though not easy to reveal and to understand" [30] (see also [1, 32]) .

Ignoring strontium from the eight metals shown in Figure 2, we are left with the essential divalent metal ions Mg^{2+}, Ca^{2+}, Fe^{2+}, Zn^{2+}, and Cu^{2+}, and the toxic Cd^{2+} [30]. In its binding strength to ligands Cd^{2+} is more like Zn^{2+}, at least in a first approximation, and Pb^{2+} more like Cu^{2+}, at least towards oxygen donor sites [1]. Based on the indicated observations, we focus in the sections to follow on the physical and chemical properties of Pb^{2+} in comparison to those

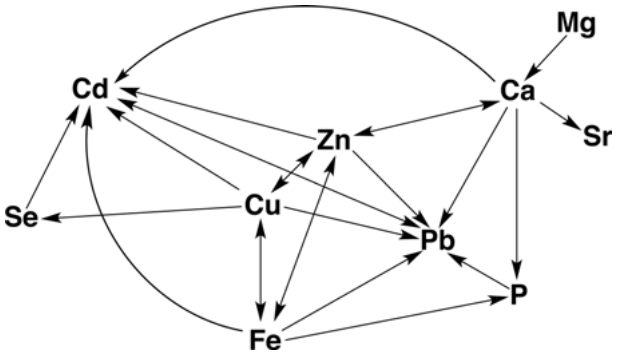

Figure 2. Interdependencies between several elements relevant for mammals. An arrow from element A → B indicates that administration of element A may reduce toxicity due to element B. Note, there may be further interdependencies which are not shown (see also text). This figure is based on information provided by Martin in Figure 2 of [32] and the connected text given there.

of Ca^{2+}, Fe^{2+}, Cu^{2+}, Zn^{2+}, and Cd^{2+}. The properties and complexes of Fe^{2+}, Cu^{2+}, Zn^{2+}, and Cd^{2+} will also allow, where needed, a more systematic type of comparisons.

2.2. Definition of the "*Stability Ruler*"

Contrary to some expectations, Pb^{2+} does not form extraordinarily stable complexes. In this context the *Stability Ruler* of Martin [1, 32–35] is helpful; it is based on the common Irving-Williams stability order of complexes [36, 37], $Mg^{2+} < Mn^{2+} < Fe^{2+} < Co^{2+} < Ni^{2+} < Cu^{2+}$ (> Zn^{2+}): With nitrogen donor ligands Pb^{2+} binds with about the same affinity as Fe^{2+}, e.g., for NH_3 $\log K^{Pb}_{Pb(NH_3)} = 1.6$ and $\log K^{Fe}_{Fe(NH_3)} = 1.7$ (25 °C; $I = 5$ M, NH_4NO_3) [38], whereas Zn^{2+} and Cd^{2+} bind more strongly to NH_3 than Pb^{2+} (Table 1; vide infra).

This result towards N ligands is confirmed by the complex stabilities of imidazole (Im), that is, $\log K^{Pb}_{Pb(Im)} = 1.28$ is significantly smaller than $\log K^{Zn}_{Zn(Im)} = 2.55$ or $\log K^{Cd}_{Cd(Im)} = 2.72$, and this is even more true for $\log K^{Cu}_{Cu(Im)} = 4.25$ (25 °C; $I = 0.5$ M) [38]. Of relevance in these comparisons is also the value for $Fe(Im)^{2+}$, $\log K^{Fe}_{Fe(Im)} = 1.81$ (30 °C; $I = 0.1$ M) [38], despite the somewhat different experimental conditions. Imidazole was included here because it mimics the imidazole part of purine-nucleosides well (see Figure 1).

However, with oxygen donor ligands Pb^{2+} moves strongly up the ruler and binds with about the same strength as Cu^{2+} (and more strongly than Zn^{2+} or Cd^{2+}), e.g., with methyl phosphate, $CH_3OPO_3^{2-}$ (MPO^{2-}), $\log K^{Pb}_{Pb(MPO)} = 2.98 \pm 0.10$ [39] and $\log K^{Cu}_{Cu(MPO)} = 2.94 \pm 0.03$ [40] (25 °C; $I = 0.1$ M, $NaNO_3$).

With sulfur donor ligands the situation is more complicated because with thiophosphate sites Cu^{2+} undergoes redox reactions [41, 42], but the inherent and significant affinity of Pb^{2+} for R-S^- sites is still evident from the Cd^{2+} and

Pb^{2+} complexes with methyl thiophosphate, $CH_3OP(O)_2(S)^{2-}$ (MPS^{2-}): $\log K^{Cd}_{Cd(MPS)} = 4.50 \pm 0.06$ [42] and $\log K^{Pb}_{Pb(MPS)} = 4.78 \pm 0.06$ [39] (25 °C; $I = 0.1$ M, $NaNO_3$); in other words, Pb^{2+} has certainly a significant affinity to sulfur sites [41], but dependent on the structure of the ligand, this affinity may be modulated, suppressed [43] and even dominated by oxygen donor sites [44] (see also Section 7.3).

Pb^{2+} exhibits coordination numbers between 4 and 10 having often an irregular coordination sphere [45]. Pb^{2+} can be stereochemically active, due to its $6s^2$ electron pair (see also Chapter 7 and Section 2.2 in Chapter 8), and with CN = 4 the liganding atoms can be on one side and on the other is then the $6s^2$ lone pair [46, 252]. This irregularity distinguishes Pb^{2+} from Cd^{2+} or Zn^{2+} and it is possibly the reason that allows Pb^{2+} to adapt to Zn^{2+} or Cd^{2+} sites even though these ions are much smaller [10].

2.3. Some Intrinsic Properties of Lead(II) and Related Metal Ions

Due to the indicated observations we compare now the properties of Pb^{2+} with those of Ca^{2+}, Fe^{2+}, Cu^{2+}, Zn^{2+}, and Cd^{2+}. To this end, the information assembled in Table 1 was collected [1, 30, 32, 38, 47–65]. Clearly, many comparisons are possible, some follow below.

Comparison of the radii shows (Table 1, columns 3–5) that those of Pb^{2+} and Ca^{2+} are most alike; hence, it is understandable that Pb^{2+} can replace Ca^{2+} in bone. However, due to the indicated "irregularity" of the coordination sphere of Pb^{2+}, it can also compete for Fe^{2+}, Cu^{2+}, and Zn^{2+} sites occurring in Nature. Ca^{2+} likes oxygen donor sites, as does Pb^{2+}, but so does Fe^{2+}. Among the free enthalpies of hydration the least pronounced one is that of Pb^{2+}, which is a result of its large size leading to a small charge density and thus a low affinity for the dipole-water molecules. In accord herewith are the ΔG_{hyd} values of Ca^{2+} and the other listed metal ions; the one for Cu^{2+} being most pronounced, as expected, due to its smallest size.

The solubility products of PbS and CdS are rather close to each other, in agreement with their related affinity for R-S^- sites according to the *Stability Ruler*. The smallest solubility product has CuS (Table 1, column 8) which therefore precipitates already in an acidic solution, reflecting the high affinity of Cu^{2+} for sulfur sites, whereas FeS forms a precipitate only in the alkaline pH range (that is, in the presence of NH_3), though the affinity of Fe^{2+} for sulfur is still pronounced enough to allow the formation of Fe-S clusters [66]. Interestingly, in contrast to Pb^{2+} with its large affinity for S^{2-} the corresponding affinity of Ca^{2+} is very low; based on the information given in [38] one calculates that saturated solutions of CaS are about 0.05 M in Ca^{2+} and S^{2-}.

Table 1. Comparison of some physico-chemical properties of metal ions (M^{2+}), that is, atomic numbers, preferred coordination numbers (CN) with the corresponding effective ionic radii,[a,b] preferred liganding atoms,[c] free enthalpies of hydration (ΔG_{hyd}),[d] negative logarithms of the solubility products for metal ion sulfides [$p(SP)_{MS}$],[e] negative logarithms of the acidity constants [$pK^{H}_{M(H_2O)_n}$; Eq. (1)] of a water molecule in the aqua complex,[f] and logarithms of the stability constants [Eq. (2)] of the 1 : 1 complexes formed with acetate, CH_3COO^- (Ac^-),[g] and ammonia, NH_3,[h] together with the logarithms of the apparent stability constants [Eq. (4)] of the $M(NH_3)^{2+}$ complexes at pH 7.5.[i]

M^{2+}	Atomic number	Ionic radius for CN			Preferred liganding atoms[c]	ΔG_{hyd} [kJ/mol][d]	$p(SP)_{MS}$[e]	$pK^{H}_{M(H_2O)_n}$[f]	$\log K^{M}_{M(Ac)}$[g]	$\log K^{M}_{M(NH_3)}$[h]	$\log K^{M}_{M(NH_3)app}$[i]
		4[a]	6[a]	8[a]							
Ca^{2+}	20		100	*112*	O	–1569/–1558	–	12.85	0.55 ± 0.05	0.1	–1.79
Fe^{2+}	26	63	*78*[b]	92	O, N	–1870/–1911	18.0 ± 0.8	9.5	0.83 ± 0.06	1.68 ± 0.11	–0.21
Cu^{2+}	29	57	73		N, O	– /–2059	36.1 ± 1.0	7.53	2.11 ± 0.01	4.18 ± 0.03	2.29
Zn^{2+}	30	60	*74*[b]	90	N, O, S	–1870/–2007	24.3 ± 1.0	8.96	0.85 ± 0.04	2.41 ± 0.09	0.52
Cd^{2+}	48	78	*95*	110	S, N, O	–1640/–1780	26.9 ± 0.7	10.08	1.08 ± 0.04	2.67 ± 0.03	0.78
Pb^{2+}	82	98	119	129	O, S	–1431/–1477	28.0 ± 0.6	7.78	1.91 ± 0.03	1.3	–0.59

[a] Effective ionic radii (pm); those with the more common coordination numbers are printed in *italics*. The values are taken from listings in [1] and [47].

[b] The high-spin value is given for Fe^{2+}; the low-spin value is 61 pm. Zn^{2+} has a chameleon-type coordination sphere; CN 4 (tetrahedral) is common as well [48].

[c] According to [1, 49] and our own intuition.

[d] All values refer to coordination number 6. The values at the left are calculated [51] with radii close to the effective ionic radii of Shannon [47]; those at the right are based [50] on the crystal radii also given by Shannon [47].

[e] Negative logarithm of the solubility product, $SP = [M^{2+}][S^{2-}]$. The given SP constants (error: 3σ) are the average of the values at 25 °C listed in [52–57, 65]; these are 8 values each for FeS and CuS, 15 for ZnS, 12 for CdS, and 14 for PbS.

[f] The values for Cu^{2+} and Pb^{2+} are from [58, 59]; the others are from [60, 61].

[g] Log $K^{Fe}_{Fe(Ac)} = 0.83$ is an estimated value [60], as is the given error limit of ±0.06 [30] (25 °C; $I = 0.1$ M). The value for Ca^{2+} is taken from table 4 in [62] (aq. sol.; 25 °C; $I = 0.1$ M, $NaNO_3$) (see also [38]); all the other values are abstracted from the data collected in table 8 of [62], including $pK^{H}_{H(Ac)} = 4.80 \pm 0.01$ (aq. sol.; 25 °C; $I = 2$ M, $NaClO_4$) (see also [63]).

[h] The values for $M(NH_3)^{2+}$, where $M^{2+} = Cu^{2+}$, Zn^{2+} or Cd^{2+} are from table 1 in [64] (aq. sol.; close to 25 °C and $I = 0.1$ M); these conditions also hold for $\log K^{Fe}_{Fe(NH_3)} = 1.68 \pm 0.11$, which is an estimate [30] based on $\log K^{Mn}_{Mn(NH_3)} = 1.27 \pm 0.10$ [64] and $\log K^{Co}_{Co(NH_3)} =$

2.08 ± 0.03 [64]. It holds further [64] $pK^{H}_{H(NH_3)} = 9.38 \pm 0.01$ (25 °C; $I = 0.1$ M, $NaNO_3$). The values for $Ca(NH_3)^{2+}$ (25 °C; $I = 0.5$ M) and $Pb(NH_3)^{2+}$ (25 °C; $I =$ ca 1 M) are from [38]. The value given above for $Pb(NH_3)^{2+}$ is based on $\log K^{Pb}_{Pb(NH_3)} = 1.55$ valid for 25 °C and $I = 5$ M [38]; from the ionic strength effects on the stabilities of the $Cu(NH_3)^{2+}$ and $Cd(NH_3)^{2+}$ complexes [38] it follows that for $I =$ ca 1 M $\log K^{Pb}_{Pb(NH_3)} = 1.3$ holds.

[i] The apparent stability constants [49] valid for pH = 7.5 were calculated with Eq. (4) and the stability constants listed in column 11 and the acidity constant given in footnote "h".

Column 9 of Table 1 provides the acidity constants for the hydrolysis reaction (1):

$$M(H_2O)_n^{2+} \rightleftharpoons M(OH)(H_2O)_{n-1}^{+} + H^+ \quad (1a)$$

$$K^{H}_{M(H_2O)_n} = \frac{[M(OH)(H_2O)_{n-1}^{+}][H^+]}{[M(H_2O)_n^{2+}]} \quad (1b)$$

As pointed out previously [30], "this hydrolysis reaction leads to hydroxo complexes and the coordinated OH^- species can act as nucleophiles [58, 67, 68] or participate in general base catalysis [58], important for metal ion-containing cores of ribozymes, where also large pK_a shifts can occur [69]." The acidity constants for the $M(H_2O)_n^{2+}$ species (Eq. (1b)) are very close for Pb^{2+} and Cu^{2+}, reflecting the discussed similarity, in the context of the *Stability Ruler*, of their affinities for oxygen donor sites. The latter is also born out from the size of the stability constants of the $Pb(Ac)^+$ and $Cu(Ac)^+$ complexes, which will be considered in the next section.

2.4. Complex Stabilities and the Effect of pH

The stability constants of 1 : 1 complexes are defined in a general manner (omitting charges) in Eq. (2), though for the present L = Ac^- or NH_3:

$$M^{2+} + L \rightleftharpoons M(L) \quad (2a)$$

$$K^{M}_{M(L)} = [M(L)]/([M^{2+}][L]) \quad (2b)$$

The size of the stability constants of the $Pb(Ac)^+$ and $Ca(Ac)^+$ complexes (Table 1, column 10) reflects the fact that in the calmodulin family Pb^{2+} binds more avidly to the Ca^{2+}sites of the protein, which are composed of oxygen donor sites, than does Ca^{2+} itself. As stated previously [10], "in oncomodulin and chick vitamin D-induced intestinal calcium-binding protein, Pb^{2+} binding occurs exclusively at the Ca^{2+} sites, despite the presence of a free sulfhydryl group on the proteins [70]," thus demonstrating the before mentioned "irregular" binding properties of lead(II).

The stabilities of the $Fe(Ac)^+$, $Zn(Ac)^+$, and $Cd(Ac)^+$ complexes, if compared to the corresponding Pb^{2+} and Cu^{2+} species, are lower, showing in a first approximation the same tendency as observed for the hydrolysis of $Fe(H_2O)_n^{2+}$, $Zn(H_2O)_n^{2+}$, and $Cd(H_2O)_n^{2+}$, if compared with the one of $Pb(H_2O)_n^{2+}$ and $Cu(H_2O)_n^{2+}$. Though it appears that the value for $Zn(H_2O)_n^{2+}$ ($pK^{H}_{Zn(H_2O)_n}$ = 8.96) is a bit low, the reason possibly being that with the formation of $Zn(OH)(H_2O)_{n-1}^{+}$ the Zn^{2+} system is already partly on the way to change the coordination number from 6 to 4, considering that $Zn(OH)_4^{2-}$ is tetrahedral [48].

At first sight the $M(NH_3)^{2+}$ complexes of the transition metal ions, including Zn^{2+} and Cd^{2+}, seem to be much more stable than those of the corresponding

$M(CH_3COO)^+$ complexes (Table 1, columns 10 and 11). However, in the physiological pH range around 7.5 one needs to take into account the competition between M^{2+} and H^+ for binding at the ligand, that is, the size of the acidity constant ([Eq. (3)]; charges omitted) of the protonated ligands is important:

$$H(L) \rightleftharpoons L + H^+ \tag{3a}$$

$$K^{H}_{H(L)} = [L][H^+]/[H(L)] = K_a \tag{3b}$$

Since the value of the acidity constant of acetic acid, CH_3COOH ($pK^{H}_{H(Ac)} = 4.8$), is much below the physiological pH range (pH 7.5), there is hardly any competition between H^+ and M^{2+} for binding at CH_3COO^-. This is evidently very different for NH_4^+ with $pK^{H}_{H(NH_3)} = 9.4$; in this case practically all ligand is present in its protonated form, and thus the competition of H^+ and M^{2+} for binding at NH_3 is very sincere. This competition can be accounted for by defining so-called conditional or apparent (app) stability constants [Eq. (4)], which then are valid only for a given pH [1, 30, 49]:

$$K^{M}_{M(L)app} = K^{M}_{M(L)} \frac{1}{1 + [H^+]/K^{H}_{H(L)}} \tag{4a}$$

$$= K^{M}_{M(L)} \frac{K^{H}_{H(L)}}{[H^+] + K^{H}_{H(L)}} \tag{4b}$$

$$\log K^{M}_{M(L)app} = \log K^{M}_{M(L)} + \log [K^{H}_{H(L)}/([H^+] + K^{H}_{H(L)})] \tag{4c}$$

For $pH \gg pK^{H}_{H(L)}$ the unbound ligand is present predominantly in its basic form and $\log K^{M}_{M(L)app} = \log K^{M}_{M(L)}$. For $pH \ll pK^{H}_{H(L)}$ the unbound ligand is predominantly protonated and Eq. (4c) reduces to $\log K^{M}_{M(L)app} = \log K^{M}_{M(L)} - pK^{H}_{H(L)} + pH$.

With the above reasonings in mind, columns 10 to 12 of Table 1 should be compared: For acetate $pH = 7.5 \gg pK^{H}_{H(Ac)} = 4.8$, that is, virtually all ligand is in its basic CH_3COO^- form and metal ion binding practically occurs without competition. For ammonia this is different: $\log K^{M}_{M(NH_3)app} < \log K^{M}_{M(NH_3)}$, the difference amounts to ca 1.9 log units. In fact, only for Cu^{2+} at pH 7.5 the affinity towards NH_3 is about equal to that of Ac^-. In all other instances the affinity towards the carboxylate group is more pronounced.

This result is of relevance for nucleotides and nucleic acids because some sites carry a proton at the physiological pH, e.g., (N1)H of a Guo derivative (pK_a ca 9.4 [71–73]), and others which are free, e.g., N7 also of a Guo derivative (pK_a ca 2.5 for $(N7)H^+$ [71–73]); hence, the N7 site is easily accessible, whereas the $(N1)^-$ site is not. Monoprotonated phosphate groups have pK_a values of about 6.2 to 6.5 [27, 28, 73], hence, there is some competition at pH 7.5 between H^+ and M^{2+}, but it is not very pronounced. Phosphodiester bridges, $RO\text{-}P(O)_2^-\text{-}OR'$, if protonated, lose their proton already with a pK_a of about 1 [74, 75]; hence there is no proton competition at all in the physiological pH range. These general considerations will be reflected in the discussions to follow [30].

3. LEAD(II) INTERACTIONS WITH HYDROXYL GROUPS AND SUGAR RESIDUES

3.1. Some General Reasonings

Pb^{2+} is effective in sequence-specific folding of DNA [76], and at pH values near 7 Pb^{2+} will cleave RNA at bound positions [58]. Nucleoside 2′,3′-cyclic monophosphates are effectively hydrolyzed by Pb^{2+} and Cu^{2+} [77], and for both ribo- and 2′-deoxyribonucleosides (see Figure 1) at pH > 6 Pb^{2+} promotes dephosphorylation of 2′-, 3′-, and 5′-monophosphates [77, 78]. Lead(II) also catalyzes the oligomerization of nucleoside 5′-phosphorimidazolides [79] to yield short oligonucleotides [80]; this allows the synthesis of 2′,5′-linked oligonucleotides [81], and there are indications based on UO_2(II) that the phosphate group and the deprotonated hydroxyl group of the sugar coordinate to the metal ion [82] (see also the related research in [83]).

From the above indications it is evident that Pb(II) plays an important role in engineered and artificial nucleotide and nucleic acid systems and that in these Pb(II)-sugar interactions occur. However, detailed knowledge on binding of Pb^{2+} to carbohydrates, especially in aqueous solution, is very scarce; this is even more true if one asks for quantitative information, i.e., stability constants of Pb^{2+} complexes. Therefore we begin the discussion with the three "simple" ligands seen in Figure 3. These ligands offer only oxygen donor atoms and therefore one may hope that the available information on their Cu^{2+} complexes sheds also some light on the expected properties of the Pb^{2+} species because based on the *Stability Ruler* (Section 2.2) this should be the case.

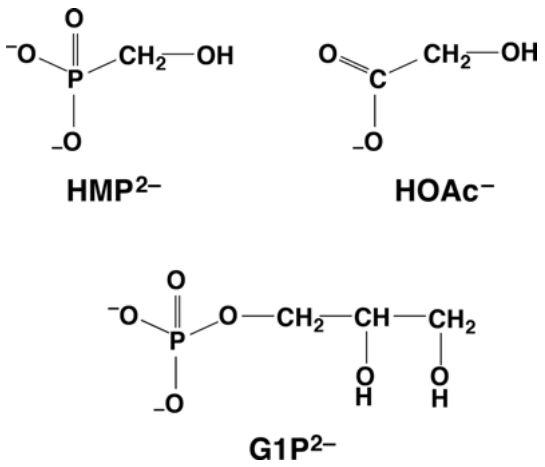

Figure 3. Chemical structures of ligands containing a primary binding site (PBS), which is negatively charged, and a hydroxyl group: hydroxymethylphosphonate (HMP^{2-}), hydroxyacetate ($HOAc^-$), and glycerol 1-phosphate ($G1P^{2-}$ = α-glycerophosphate; in many biochemistry texts also designated as glycerol 3-phosphate).

3.2. Quantification of Isomeric Equilibria and Chelate Formation

It is evident that all three ligands in Figure 3 have a primary binding site (PBS), that is, a carboxylate or a phosph(on)ate group, which will determine the stability of a metal ion complex to a very large part, because any interaction with a hydroxyl group will be weak [62]. However, if a hydroxyl group participates in metal ion binding the following intramolecular Equilibrium (5) must occur:

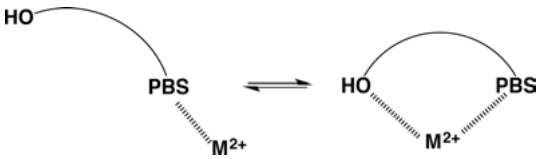

(5a)

$$M(PBS\text{-}OH)_{op} \rightleftharpoons M(PBS\text{-}OH)_{cl} \tag{5b}$$

If both isomers in Equilibrium (5) are formed, the stability constant given in Eq. (2b) needs to be redefined as given in Eq. (6):

$$K^{M}_{M(L)} = \frac{[M(L)_{op}] + [M(L)_{cl}]}{[M^{2+}][L]} = K^{M}_{M(L)exp} \tag{6}$$

Of course, if Equilibrium (5) is far on its left side and only the open (op) isomer exists and no closed (cl) or chelated species is formed, then Eq. (7) holds:

$$K^{M}_{M(L)op} = \frac{[M(L)_{op}]}{[M^{2+}][L]} \tag{7}$$

The total analytical concentration, $M(L)_{tot}$, one measures, of course, is the sum of the concentration of the isomers [Eq. (8)]:

$$[M(L)_{tot}] = [M(L)_{op}] + [M(L)_{cl}] \tag{8}$$

The intramolecular and dimension-less equilibrium constant K_I, which quantifies the position of Equilibrium (5), is defined by Eq. (9):

$$K_I = \frac{[M(PBS\text{-}OH)_{cl}]}{[M(PBS\text{-}OH)_{op}]} = \frac{[M(L)_{cl}]}{[M(L)_{op}]} \tag{9a}$$

$$= \frac{K^{M}_{M(L)}}{K^{M}_{M(L)op}} - 1 \tag{9b}$$

Values for $K^{M}_{M(L)}$ in the nominator of Eq. (9b) are experimentally measured, whereas values for the open isomers, $K^{M}_{M(L)op}$ need to be obtained in an indirect

manner. Commonly, one makes use of the observation [84] that for a family of structurally closely related ligands plots of $\log K^{M}_{M(L)}$ [Eqs (2b) and (7)] *versus* $pK^{H}_{H(L)}$ [Eq. (3)] result in straight lines [Eq. (10)]:

$$\log K^{M}_{M(L)} = m \cdot pK^{H}_{H(L)} + b \tag{10}$$

Once the parameters for m (slope of the straight line) and b (intercept of the straight line with the y-axis) are known, one may calculate the log stability constant of any related complex based on the also known acidity constant, $pK^{H}_{H(L)}$. With this information at hand, namely $K^{M}_{M(L)exp}$ and $K^{M}_{M(L)op}$, the intramolecular equilibrium constant K_I of Eq. (9) may be calculated, and this means further

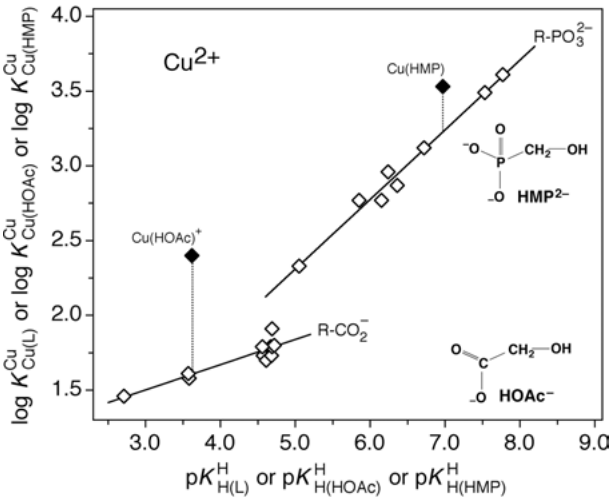

Figure 4. Evidence for an enhanced stability of the Cu^{2+} 1:1 complexes (◆) of $HOAc^{-}$ and HMP^{2-} (see Figure 3) based on the straight-line relationships for the primary binding sites (PBS) (◇) as they result from $\log K^{M}_{M(L)}$ *versus* $pK^{H}_{H(L)}$ plots, where L = simple carboxylate (CA^{-}) or phosph(on)ate ($R\text{-}PO_3^{2-}$) ligands. The simple carboxylate ligands ($R\text{-}CO_2^{-}$ from left to right) are: chloroacetate, formate, formate, acetate, acetate, 3-methylbutanoate, 4-methylvalerate (= 4-methylpentanoate), propanoate, 5-methylhexanoate, 2-methylpropanoate, and 6-methylheptanoate. The corresponding 11 data sets for the least-squares reference line [Eq. (10)] are from table 4 in [62]; the straight-line parameters are listed in table 5 of [62]. The simple phosphate monoester and phosphonate ligands ($R\text{-}PO_3^{2-}$; from left to right) are: 4-nitrophenyl phosphate ($NPhP^{2-}$), phenyl phosphate (PhP^{2-}), uridine 5′-monophosphate (UMP^{2-}), D-ribose 5-monophosphate ($RibMP^{2-}$), thymidine (= 1-(2′-deoxy-β-D-ribofuranosyl)thymine) 5′-monophosphate ($dTMP^{2-}$), *n*-butyl phosphate (BuP^{2-}), methanephosphonate (MeP^{2-}), and ethanephosphonate (EtP^{2-}). The least-squares reference line [Eq. (10)] is drawn through the corresponding eight data sets taken from [86] for the phosphate monoesters and from [87] for the phosphonates. The corresponding straight-line parameters are listed in [28, 85, 87]. The points due to the equilibrium constants for the $Cu^{2+}/HOAc^{-}$ and HMP^{2-} systems are based on the values listed in Table 2 (columns 2 and 4). The vertical dotted lines emphasize the stability differences to the reference lines; they equal $\log \Delta_{M/L}$ as defined in Eq. (12). All the plotted equilibrium constants refer to aqueous solutions at 25 °C and I = 0.1 M.

that also the formation degree of the closed (chelated) species becomes known [Eq. (11)]:

$$\% \, M(L)_{cl} = 100 \cdot K_I / (1 + K_I) \tag{11}$$

At this point it is important to emphasize that any formation of a chelate in Equilibrium (5) must be connected with a stability enhancement [84, 85]. This stability increase is defined by Eq. (12), where calc = calculated:

$$\log \Delta_{M/L} = \log K^{M}_{M(L)} - \log K^{M}_{M(L)op} \tag{12a}$$

$$= \log K^{M}_{M(L)exp} - \log K^{M}_{M(L)calc} \tag{12b}$$

The corresponding equality of the various terms in Eqs. (12a) and (12b) is evident, however, it is also clear that for any quantitative evaluation well-defined error limits are needed. It is obvious that based on Eq. (12), Eq. (9b) defining K_I, can be re-written as given in Eq. (13):

$$K_I = 10^{\log \Delta_{M/L}} - 1 \tag{13}$$

This form, in principle equivalent to Eq. (9), is more convenient to use as we will see below.

3.3. Copper(II) as a Mimic for Lead(II)

From Figure 4 [28, 62, 85–87], where we use the results of the Cu^{2+} complexes as mimics for Pb^{2+} complexes several conclusions are immediately evident, such as:

(i) For both complex systems, phosph(on)ates ($R\text{-}PO_3^{2-}$) and carboxylates ($R\text{-}COO^-$), straight lines are obtained from the $\log K^{Cu}_{Cu(L)}$ *versus* $pK^{H}_{H(L)}$ plots.

(ii) Hydroxymethylphosphonate (HMP^{2-}; Figure 3), forms a more stable Cu^{2+} complex compared to its simple $R\text{-}PO_3^{2-}$ relatives. The corresponding data point is well above the reference line.

(iii) Exactly the same observation, as described in (ii), is made for the Cu^{2+} systems of hydroxyacetate and the related carboxylates.

(iv) In both instances, the data points due to Cu(HMP) and $Cu(HOAc)^+$ are above their reference line and the vertical distance from such a data point to the reference line corresponds exactly to $\log \Delta_{M/L}$ as defined in Eq. (12).

(v) Why is the observed stability enhancement for $Cu(HOAc)^+$ clearly more pronounced than the one for Cu(HMP)? Well, the two complexes differ in their charge; the charge density on Cu^{2+} in $Cu(HOAc)^+$ being larger than it is the case in Cu(HMP). This higher charge density is responsible for a larger formation degree of the closed isomer and thus a more pronounced stability increase.

(vi) The same explanation holds for the different slopes of the two straight lines. The more the charge density on the metal of the complex is lowered the steeper the slope. Therefore, m for the $Cu(R\text{-}COO)^+$ complex family is smaller than the one for the $Cu(R\text{-}PO_3)$ family. There are more examples like this [62].

(vii) Finally one should note that the extent of chelate formation does not go parallel to the absolute stability of the complexes, $Cu(HOAc)^+$ is less stable than Cu(HMP), but the formation degree of its closed species (that is, of $\log \Delta_{M/L}$) is larger.

The quantitative evaluation of Figure 4 is summarized in Table 2 [38, 62], where in addition also some results for Ca^{2+} complexes are given. In all instances significant percentages of the chelated isomers are formed and therefore the same may be summarized for the Pb^{2+} complexes. We believe that these results speak for themselves and that no further comments are needed.

The two ligands we have dealt with up to now form with metal ions 5-membered chelates. Indeed, for $M(HOAc)^+$ complexes of 10 different metal ions it has been shown that the formation degree of the chelates is quite pronounced; it varies between 60 and 95 % [62]. It is therefore interesting to consider the corresponding complexes of 3-hydroxypropanoate, $HO\text{-}CH_2CH_2\text{-}COO^-$, which could give rise to 6-membered chelates. However, such chelates are not formed to any significant extent [62], and this is also true for the complexes of 4-hydroxybutanoate, $HO\text{-}CH_2CH_2CH_2\text{-}COO^-$, in which no indication for any hydroxyl group participation could be discovered [62]; hence, no 7-membered chelates occur to any significant extent either.

The instability of 7-membered chelates is confirmed by the 10 complexes formed with glycerol 1-phosphate ($G1P^{2-}$; Figure 3); no stability enhancement is observed [88]. In accord herewith one obtains [42, 88] in aqueous solution for Cu(G1P) $\log \Delta_{Cu/G1P} = -0.05 \pm 0.08$ (25 °C; $I = 0.1$ M, $NaNO_3$). However, a decrease in solvent polarity (i.e., a reduced dielectric constant or permittivity, ε [89, 90], by applying water containing 50 % 1,4-dioxane (v/v) as solvent gives for Cu(G1P) $\log \Delta_{Cu/G1P} = 0.24 \pm 0.04$ and % $Cu(G1P)_{cl} = 42 \pm 5$ % demonstrating that a decreasing solvent polarity favors the hydroxyl-metal ion interaction ([91], revised values in [85]). These results are corroborated by dihydroxyacetone phosphate ($DHAP^{2-}$; $HO\text{-}CH_2\text{-}C(O)\text{-}CH_2\text{-}O\text{-}PO_3^{2-}$) and its Cu^{2+} complex for which one obtains in aqueous solution $\log \Delta_{Cu/DHAP} = 0.04 \pm 0.06$ and in 50 % 1,4-dioxane $\log \Delta_{Cu/DHAP} = 0.26 \pm 0.03$ and % $Cu(DHAP)_{cl} = 45 \pm 4$ % [85]. These results show that a carboxyl group [(C2)=O of $DHAP^{2-}$] and a hydroxyl group [(C2)-OH of $G1P^{2-}$; Figure 3] bind with the same affinity to Cu^{2+} at the reduced solvent polarity, and the same may be surmised for Pb^{2+}. This is meaningful because $G1P^{2-}$ and $DHAP^{2-}$ are representatives for many sugar moieties.

For 3-hydroxypropanoate ($3\,HOPr^-$), $HO\text{-}CH_2\text{-}CH_2\text{-}COO^-$, we have seen that the formation of 6-membered rings occurs, if at all, only in trace amounts in aqueous solution (25 °C) [62]. It is therefore interesting to note that acetyl phosphate (AcP^{2-}; $CH_3\text{-}C(O)\text{-}O\text{-}PO_3^{2-}$) gives rise to 10 M(AcP) complexes (25 °C; $I = 0.1$ M, $NaNO_3$) [85, 92] which form 6-membered chelate rings with formation

Table 2. Comparison of the measured stability constants, $K^{M}_{M(L)exp}$ [Eqs (2) and (6)], of the 1 : 1 complexes formed between hydroxymethylphosphonate (HMP^{2-}) or hydroxyacetate ($HOAc^{-}$) (Figures 3 and 4) and Ca^{2+} or Cu^{2+}, and the corresponding stability constants $K^{M}_{M(L)op}$ [Eq. (7)], for the open isomers with a sole phosphonate or carboxylate coordination of M^{2+}, and extent of the intramolecular chelate formation according to Equilibrium (5) in the M(L) complexes as defined by K_I [Eqs (9) and (13)] and % $M(L)_{cl}$ [Eq. (11)] for aqueous solution at 25 °C and $I = 0.1$ M.[a]

L	$pK^{H}_{H(L)}$	M^{2+}	$\log K^{M}_{M(L)exp}$ [b]	$\log K^{M}_{M(L)op}$	$\log \Delta_{M/L}$	K_I	% $M(L)_{cl}$
HMP^{2-}	6.97 ± 0.04	Ca^{2+}	1.68 ± 0.06	1.55 ± 0.05	0.13 ± 0.08	0.35 ± 0.24	26 ± 13
		Cu^{2+}	3.53 ± 0.06	3.23 ± 0.06	0.30 ± 0.08	1.00 ± 0.39	50 ± 10
$HOAc^{-}$	3.62 ± 0.03	Cu^{2+}	2.40 ± 0.06	1.61 ± 0.05	0.79 ± 0.08	5.17 ± 1.11	84 ± 3
		Ca^{2+}	1.11 ± 0.06	0.33 ± 0.05	0.78 ± 0.08	5.03 ± 1.08	83 ± 3

[a] The listed data are compiled from tables 2 and 7 of [62]; see also Figure 4. The acidity constant [Eq. (3)] $pK^{H}_{H(HMP)} = 6.97$ is from [38]; the error limit is an estimation based on information given in [38].
[b] Calculated with the $pK^{H}_{H(L)}$ values of column 2 and the parameters for the straight-line equations [Eq. (10)] listed in tables 1 (phosphonates) and 5 (carboxylates) of [62].

degrees between $24 \pm 10\,\%$ (Mn^{2+}) and $76 \pm 4\,\%$ (Cu^{2+}). $Ca(AcP)_{cl}$ is with $48 \pm 8\,\%$ about mid-way. This comparison between the ligands $3\,HOPr^-$ and AcP^{2-} shows that small alterations can have remarkable effects on the participation of hydroxyl or carbonyl groups in metal ion binding.

3.4. The Lead(II)-Hydroxyacetate System

With hydroxyacetate ($HOAc^-$; Figure 3) the stability of the Pb(II) complex has been measured at an ionic strength (I) of 2 M (25 °C) [38, 63] and the straight-line correlations [Eq. (10)] $\log K^{Pb}_{Pb(L)}$ *versus* $pK^{H}_{H(L)}$ for simple carboxylate (CA) ligands have also been determined [62]. The same is true for the corresponding Cu^{2+} and Cd^{2+} systems. For all three metal ions the corresponding straight lines are plotted in Figure 5 together with the data points (full symbols) for the $M(HOAc)^+$ complexes.

The most satisfying result is that the straight lines for Cu^{2+} and Pb^{2+} are very similar. Obviously, only the Pb^{2+} points for formate and acetate are somewhat too low, all the other data points for Cu^{2+} and Pb^{2+} are nearly on top of each other. In fact, the straight-line parameters [62], summarized in Equations (14) and (15), are identical within their error limits:

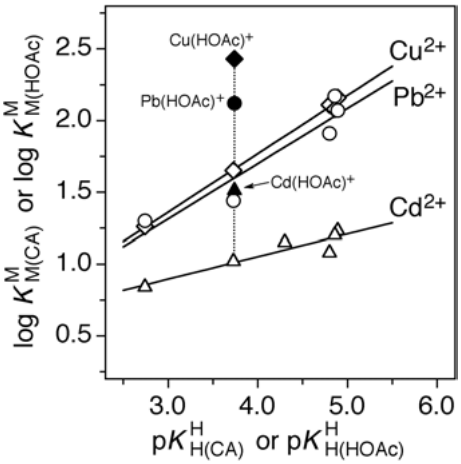

Figure 5. Evidence for an enhanced complex stability of the Pb^{2+} (●), Cu^{2+} (◆), and Cd^{2+} (▲) 1:1 complexes of $HOAc^-$ based on the relationship between $\log K^{M}_{M(CA)}$ and $pK^{H}_{H(CA)}$ for the simple carboxylate ($CA^- = R\text{-}CO_2^-$) ligands chloroacetate, formate, phenylacetate (where available), acetate, propanoate, and butanoate (from left to right); the corresponding data sets are listed in table 8 of [62] for Pb^{2+} (○), Cu^{2+} (◇), and Cd^{2+} (△). The parameters for the corresponding least-squares reference lines [Eq. (10)] are summarized in table 9 of [62]. The data for the points due to the equilibrium constants for the $M^{2+}/HOAc^-$ systems [Pb^{2+} (●), Cu^{2+} (◆), Cd^{2+} (▲)] are given in Table 3. The vertical dotted lines emphasize the stability differences to the reference lines; they equal $\log \Delta_{M/HOAc}$, as defined in Eq. (12) (see also Table 3, column 5). All plotted equilibrium constants refer to aqueous solutions at 25 °C and $I = 2$ M.

$$\log K^{Cu}_{Cu(CA)} = (0.408 \pm 0.016) \cdot pK^{H}_{H(CA)} + (0.139 \pm 0.067) \quad (14)$$

$$\log K^{Pb}_{Pb(CA)} = (0.385 \pm 0.075) \cdot pK^{H}_{H(CA)} + (0.159 \pm 0.322) \quad (15)$$

This result justifies the conclusions provided in Section 3.3, which are based on Figure 4, where Cu^{2+} is used as a mimic for Pb^{2+}. The stabilities of all the Cd^{2+} complexes are far below those of the corresponding Pb^{2+} and Cu^{2+} systems.

The quantitative evaluations that correspond to Figure 5 and $I = 2$ M are listed for the $M(HOAc)^{+}$ complexes in entries 3 through 6 of Table 3. Entries 1 and 2 contain the results for the Ca^{2+} and Cu^{2+} complexes of $HOAc^{-}$ at $I = 0.1$ M (25 °C). From the data for $Cu(HOAc)^{+}$, where results for both ionic strengths are available (entries 2, 3) it is evident that the numbers overlap within their error limits, meaning that the change in I has only a very minor or no effect at all. Only the acidity constant of H(HOAc) is somewhat affected: $pK^{H}_{H(HOAc)} = 3.74 \pm 0.03$ at $I = 2$ M (Table 3) and 3.62 ± 0.03 at $I = 0.1$ M (Table 2), giving the difference $\Delta\, pK_a = 0.12 \pm 0.04$.

Table 3. Comparison of the measured stability constants, $K^{M}_{M(HOAc)exp}$ [Eqs (2) and (6)], of the 1:1 complexes formed between hydroxyacetate ($HOAc^{-}$, Figure 5) and several divalent metal ions (M^{2+}) with the corresponding stability constants $K^{M}_{M(HOAc)op}$ [Eq. (7)] valid for the open isomers with a sole carboxylate coordination of M^{2+}, together with the extent of the intramolecular chelate formation according to Equilibrium (5) for the $M(HOAc)^{+}$ complexes as defined by K_I [Eqs (9) and (13)] and % $M(HOAc)^{+}_{cl}$ [Eq. (11)] for aqueous solution at 25 °C and $I = 0.1$ M (entries 1, 2) or $I = 2$ M (entries 3–6).[a]

No.	M^{2+}	log $K^{M}_{M(HOAc)exp}$	log $K^{M}_{M(HOAc)op}$ [b]	log $\Delta_{M/HOAc}$	K_I	% $M(HOAc)^{+}_{cl}$
1	Ca^{2+}	1.11 ± 0.06	0.33 ± 0.05	0.78 ± 0.08	5.03 ± 1.08	83 ± 3
2	Cu^{2+}	2.40 ± 0.06	1.61 ± 0.05	0.79 ± 0.08	5.17 ± 1.11	84 ± 3
3	Cu^{2+}	2.43 ± 0.03	1.66 ± 0.04	0.77 ± 0.05	4.89 ± 0.68	83 ± 2
4	Zn^{2+}	1.72 ± 0.06	0.67 ± 0.07	1.05 ± 0.09	10.22 ± 2.38	91 ± 2
5	Cd^{2+}	1.51 ± 0.02	1.01 ± 0.08	0.50 ± 0.08	2.16 ± 0.60	68 ± 6
6	Pb^{2+}	2.12 ± 0.10	1.60 ± 0.17	0.52 ± 0.20	2.31 ± 1.50	70 ± 14

[a] For entries 1 and 2 the data including the corresponding acidity constant $pK^{H}_{H(HOAc)} = 3.62 \pm 0.03$, are taken from table 7 in [62] ($I = 0.1$ M). Those for entries 3 through 6 and $pK^{H}_{H(HOAc)}$ 3.74 ± 0.03 are from table 11 in [62] ($I = 2$ M); see also Figure 5.
[b] Calculated with the parameters for the straight-line equations [Eq. (10)] listed in tables 5 ($I = 0.1$ M) and 9 ($I = 2$ M) of [62], together with the acidity constants for $pK^{H}_{H(HOAc)}$ (see footnote "a").

It thus follows that the formation degree of the closed $M(HOAc)^{+}_{cl}$ isomers is identical for the Ca^{2+} and Cu^{2+} complexes of $HOAc^{-}$ (Table 3, entries 1–3), despite the fact that the stability constants [$\log K^{M}_{M(HOAc)}$; Eqs (2, 6)] of the $Ca(HOAc)^{+}$ and $Cu(HOAc)^{+}$ complexes differ significantly. The reason for this is that K_I is an intramolecular and thus dimension-less equilibrium constant [Eqs (5, 9, 13)].

Of interest is further the result for $Pb(HOAc)^{+}_{cl}$ (entry 6), the formation degree of which (unfortunately) carries a large error limit (70 ± 14 %), though its formation still overlaps with the ca 83 ± 3 % obtained for $Ca(HOAc)^{+}_{cl}$ and $Cu(HOAc)^{+}_{cl}$. Remarkably, the most significant stability enhancement ($\log \Delta_{Zn/HOAc}$) is observed for $Zn(HOAc)^{+}$, which reaches also the highest formation degree of the studied chelates, i.e., of 91 ± 2 %. The lowest amount of chelate formation in Table 3 occurs with $Cd(HOAc)^{+}$ reaching only 68 ± 6 %.

To conclude, taking everything together, Pb^{2+} behaves in its affinity towards O donors just like Cu^{2+}. However, more important, provided a suitable primary binding site is available, then Pb^{2+} shows a remarkable affinity for hydroxyl groups; this is an important observation regarding nucleotides and nucleic acids.

3.5. Lead(II)-Sugar Interactions

In an earlier study employing electromagnetic field (emf) and NMR measurements, it was shown that Pb(II) forms weak complexes with pentoses. It was further shown that the complex formed between Pb(II) and neutral D-ribose is about five times more stable than those with *L*-arabinose and D-xylose; the stability constant for $Pb(ribose)^{2+}$ being about 1.9 M^{-1} [93]. The stability of the corresponding Ca^{2+} complex was determined by emf measurements as 1.6 M^{-1}. This value agrees well with 2.0 M^{-1} [93, 94], which is based on ^{1}H NMR spectroscopy [94]; in fact, by the same method a number of carbohydrate complexes with alkaline earth metal ions has been studied [94, 95]. By ion-exchange chromatography complex formation between Pb(II) and sugar molecules was also proven [96] and it was further shown that three vicinal hydroxyl groups [96, 97] are especially favorable for metal ion binding including Pb(II) [96].

A suitable primary binding site is helpful for hydroxyl coordination to metal ions as we have already seen above for various systems (e.g., Section 3.4) including G1P (Figure 3) which is often considered as a representative for many sugar moieties (Section 3.3). Indeed, this is also born out from a study based on FTIR, ^{1}H and ^{13}C NMR spectroscopy and molar conductivity measurements which includes also a crystal structure of Pb(II)-D-gluconate [98]: D-glucuronic acid coordinates to Pb(II) via the deprotonated carboxylate group. Furthermore, in the solid state Pb(II) is hexacoordinated by four D-glucuronates involving carboxylate oxygens and two hydroxyl groups [98,99].

A mass spectrometric study combined with semi-empirical and density functional theory (DFT) calculations [100] showed that Pb(II) reacts with monosaccharides, including D-ribose, to form the deprotonated [Pb(monosaccharide) – $H]^{+}$ complexes; this deprotonation reaction is important [100]. In this context one may also mention that the existence of a Pb(II)-sucrose complex was proven in strongly alkaline solution [101]; complex formation occurred via $Pb(OH)^{-}_{3}$ and one must assume that sucrose lost a proton.

Interesting and relevant observations are also the following ones: The *cis* arrangement of the 2- and 3-hydroxyl groups as present in a ribose moiety (see Figure 1) favors deprotonation of one of the two OH groups because in the result-

ing anion intramolecular hydrogen bond formation occurs [74, 102]. Clearly, this favored deprotonation with $pK_a = 12.5$ is far beyond the physiological pH range, meaning that it can occur in a biological system only in a very special environment [69]. However, this deprotonation reaction can be facilitated, e.g., by Cu^{2+}. The Cu^{2+} ion is able to bind to the *cis*-glycol unit of a ribose moiety in aqueous solution at high pH values [79, 103, 104] as proven in experiments with adenosine; 2′-deoxyadenosine (Figure 1) shows no deprotonation of its 3′-hydroxyl group under the corresponding conditions [103, 104]. Since the acidifying power of Pb^{2+} is comparable to that of Cu^{2+} (Table 1, column 9), one may assume that Pb^{2+} is well able to deprotonate and to coordinate also to the geminal 2-/3-hydroxyl unit of a ribose moiety. In fact, exactly this unit has been proposed to be involved in the Pb(II)-promoted cleavage reaction of a ribozyme, in a leadzyme, and in a DNAzyme as well [58, 105].

4. INTERACTIONS OF LEAD(II) WITH NUCLEOBASE RESIDUES

Table 4 contains the available stability constants [60, 106–117] for the Pb^{2+} complexes of several nucleosides, the nucleobases of which are shown in Figure 1. To allow comparisons, the corresponding values for the complexes of Zn^{2+}, Cu^{2+}, and Cd^{2+} are also given.

4.1. Complexes of Adenosine

If we begin our discussion with the adenosine complexes, it is important to note that the basicity of the aromatic-ring nitrogens in Ado increases in the order N3 < N7 < N1 [118] as reflected by the acidity constants $pK^{H}_{H_3(Ado)} = -4.02$, $pK^{H}_{H_2(Ado)} = -1.53$, and $pK^{H}_{H(Ado)} = 3.64 \pm 0.02$ (25 °C; $I = 0.5$ M, $NaNO_3$) [118]. However, these acidity constants do not quantify the true, intrinsic basicity of the three aromatic nitrogen atoms; note, the $(C6)NH_2$ group shows no proton affinity, it rather loses a proton with $pK_a = 16.7$ [74, 119]. In fact, there is evidence that this group may act as a H-donor in a hydrogen bond [120].

The problem regarding the aromatic N atoms is that the deprotonation of $(N3)H^+$ is facilitated by the repulsion of the $(N1)H^+$ and $(N7)H^+$ sites; the same is true regarding the deprotonation of $(N7)H^+$ and its repulsion by $(N1)H^+$ [118]. Only the deprotonation of the $(N1)H^+$ site remains largely unaffected by the other two uncharged N sites and thus the measured acidity constant reflects in this case well the basicity of N1. The true, that is, the intrinsic basicity of the other two N sites needs to be described by so-called micro acidity constants; these are $pk^{N7\text{-}N1}_{N7(Ado)N1\cdot H} = 3.63 \pm 0.02$, $pk^{N7\text{-}N1}_{H\cdot N7(Ado)N1} = 2.15 \pm 0.15$, and $pk^{N3\text{-}N1,N7}_{H\cdot N3(Ado)N1,N7} = 1.5 \pm 0.3$, and they reflect the decreasing basicity of the various nitrogen atoms, that is, N1 > N7 > N3 [118]. From these microconstants follow the formation degrees of the tautomers formed for monoprotonated $H(Ado)^+$,

Table 4. Logarithms of the measured stability constants [Eqs (2) and (6)] for several M^{2+} 1:1 complexes of nucleosides (Ns; Figure 1) in aqueous solution (25 °C).[a] In the bottom part the pK_a values [Eq. (3)] of the relevant (N)H^+/(N)H sites of the nucleosides are given (aq. sol.; 25 °C; I = 0.1 M).[a]

M^{2+}	$\log K^{M}_{M(Ns)}$ for Ns =					
	Ado	**Guo**	**(Guo – H)$^-$**	**Cyd**	**(Urd – H)$^-$**	**(dThd – H)$^-$**
Zn^{2+}	0.15 ± 0.04[b]	0.80 ± 0.06[d]		0.20 ± 0.11[f]	2.41 ± 0.14[h]	2.61 ± 0.07[h,j]
Cu^{2+}	0.84 ± 0.04[b]	2.15 ± 0.04[e]	4.34 ± 0.55[e]	1.56 ± 0.06[f]	4.13 ± 0.20[h,i]	4.36 ± 0.02[h,j]
Cd^{2+}	0.64 ± 0.03[b]	1.17 ± 0.06[d]		0.91 ± 0.07[f]	3.16 ± 0.04[h]	3.43 ± 0.05[h]
Pb^{2+}	0.4 ± 0.3[c]	1.25 ± 0.17[c]		1.20 ± 0.07[g]	3.35 ± 0.20[h,i]	3.60 ± 0.20[h,j]
pK_a values:	$pK^{H}_{HN1(Ado)}$ = 3.61 ± 0.03[k]	$pK^{H}_{HN7(Guo)}$ = 2.11 ± 0.04[l]	$pK^{H}_{HN1(Guo)}$ = 9.22 ± 0.02[l,m]	$pK^{H}_{HN3(Cyd)}$ = 4.14 ± 0.02[n]	$pK^{H}_{HN3(Urd)}$ = 9.18 ± 0.02[h]	$pK^{H}_{HN3(dThd)}$ = 9.67 ± 0.02[h]

[a] The errors given are three times the standard error of the mean value (3 σ) or the sum of the probable systematic errors, whichever is larger.
[b] L. E. Kapinos, H. Sigel, results to be published (25 °C; I = 0.5 M, $NaNO_3$); some values are also given in [60, 106].
[c] [107] (25 °C; I = 0.1 M, $NaNO_3$).
[d] From table VI of [108] [D_2O; 27 °C; I = 0.1 M ($NaNO_3$) to 4 M]; see also footnote "h" in table 2 of [108]. Related results are given in [109] (25 °C; I = 1 M, $NaClO_4$).
[e] Taken and partially calculated from the data given in [110] (20 °C; I = 1 M, $NaNO_3$); for the actual values see [111].
[f] [112, 113] (25 °C; I = 0.5 M, $NaNO_3$).
[g] [114] (25 °C; I = 0.1 M, $NaNO_3$).
[h] [115] (25 °C; I = 0.1 M, $NaNO_3$).
[i] Calculated with $pK^{H}_{Urd} = 9.18 \pm 0.02$ and the straight-line parameters listed in table 3 of [115].
[j] Calculated with $pK^{H}_{dThd} = 9.67 \pm 0.02$ and the straight-line parameters listed in table 3 of [115].
[k] [24]. [l] [116]. [m] [107]. [n] [112, 117].

which are 96.1, 3.2, and 0.7 % for N7(Ado)N1·H^+, $^+$H·N7(Ado)N1, and $^+$H·N3(Ado)N1,N7, respectively. In this context it is interesting to note that in the gas phase N3 of $H_3(AMP)^+$ and $H_3(2'\text{-deoxy-AMP})^+$ is the most basic ring nitrogen, i.e., it is present as $(N3)H^+$ in the indicated species, as was shown by infrared multiple photon dissociation (IRMP) spectroscopy combined with theoretical calculations [121]. It is not clear at present, if this change in N basicity is a solvation effect of water or if it is due to the presence of the $P(O)(OH)_2$ group or both. In any case, macrochelate formation in M(AMP) complexes occurs in aqueous solution via (N7)-coordination [122] (see also Section 6.3).

Based on the intrinsic basicity of the nitrogen atoms of Ado, as discussed above, N1 should have the highest affinity for metal ions in aqueous solution. However, the $(C6)NH_2$ unit (Figure 1) exercizes a significant steric hindrance towards M^{2+} coordination at N1 [123, 124], but also towards N7 [125]; yet, the hindrance at N1 is more pronounced than that at N7 [120, 126] and thus, the "positive" basicity effect cancels to some extent *versus* the "negative" steric effect, making the two binding sites relatively equal. The consequence of this situation is the existence of the following isomeric Equilibrium (16):

$$M(Ado{\cdot}\mathit{N1})^{2+} \rightleftharpoons M(Ado{\cdot}\mathit{N7})^{2+} \tag{16}$$

In a first approximation one may conclude that the formation degrees of the *N1*- and *N7*-coordinated isomers are about equal. In fact, over the years there have been many attempts to determine these formation degrees for various metal ions [123, 126–130]. The results vary significantly between the various sources due to different assumptions employed, but in all instances it was concluded that appreciable amounts of isomers of Equilibrium (16) exist. We believe that the most recent results [131] are the most reliable ones: For $Zn(Ado\cdot\mathit{N7})^{2+}$, $Cu(Ado\cdot\mathit{N7})^{2+}$, and $Cd(Ado\cdot\mathit{N7})^{2+}$ the formation degrees are 32 ± 11 %, 49 ± 7 %, and 35 ± 11 %, respectively. It should be noted that the ratio of the isomers in Equilibrium (16) is a dimension-less value and therefore independent of the concentration. Thus, despite the different absolute stabilities of the $Zn(Ado)^{2+}$ and $Cd(Ado)^{2+}$ complexes (Table 4, column 2), the formation degrees of their (N7)-isomers can be identical, as it is actually the case for $Zn(Ado\cdot\mathit{N7})^{2+}$ and $Cd(Ado\cdot\mathit{N7})^{2+}$ with about 30 to 35 %, what automatically means that $Zn(Ado\cdot\mathit{N1})^{2+}$ and $Cd(Ado\cdot\mathit{N1})^{2+}$ form to about 65 to 70 %.

The situation with $Pb(Ado)^{2+}$ is somewhat less satisfying because the stability constant, $\log K^{Pb}_{Pb(Ado)} = 0.4 \pm 0.3$ (Table 4), carries a rather large error, though overall this result appears to be in the correct order. In any case, one may still conclude that the affinity of Pb^{2+} towards the N sites of Ado is lower than it is with Cu^{2+}. In fact, this observation agrees with the *Stability Ruler* (Section 2.2) according to which a low affinity of Pb^{2+} towards N sites (including imidazole, a mimic of the imidazole part of Ado; Figure 1) is expected and indeed, also found for N7 of AMP^{2-} (Section 6.3).

Unfortunately the *N7 versus N1* isomeric ratio [Eq. (16)] cannot be calculated for $Pb(Ado)^{2+}$ because the necessary background information is missing [123], which means, the log *K versus* pK_a straight-line parameters [Eq. (10)] for

o-amino(methyl)pyridine-type ligands are not known. This shortcoming prevents the calculation of a value for the micro stability constant $\log k^{Pb}_{Pb(Ado \cdot N1)}$, what would otherwise have been possible with the indicated (and missing) straight-line parameters and the micro acidity constant $pk^{N7\text{-}N1}_{N7(Ado)N1 \cdot H}$ (= 3.63 [118]); of course, in case a value for $k^{Pb}_{Pb(Ado \cdot N1)}$ would be available, the equation $K^{Pb}_{Pb(Ado)exp} = k^{Pb}_{Pb(Ado \cdot N1)} + k^{Pb}_{Pb(Ado \cdot N7)}$ could be applied and then the formation degrees of the isomers could be calculated [130]. In the present situation it is only possible to assume in a first approximation that the isomeric ratio is similar to the one of the Zn^{2+} and Cd^{2+} complexes (despite the difference in the overall stability constants) meaning that Pb(Ado · *N7*) is expected to occur with a formation degree of about 30 %.

4.2. Complexes of Guanosine

In neutral guanosine (Figure 1) the N1 site is blocked for metal ion coordination as it carries a proton, i.e., metal ion binding at (N1)H can occur only after deprotonation; hence, M^{2+} is (N7)-bound and no dichotomy exists for $M(Guo)^{2+}$ complexes. With this reasoning in mind, a comparison of the stability constants listed in columns 2 and 3 of Table 4 reveals that the $M(Guo)^{2+}$ complexes are much more stable than the $M(Ado)^{2+}$ ones, even though the basicity of N7 is identical in both cases, that is, $pK^{H}_{HN7(Guo)} = 2.11 \pm 0.04$ (Table 4, bottom) and $pk^{N7\text{-}N1}_{H \cdot N7(Ado)N1} = 2.15 \pm 0.15$ (Section 4.1) [118]. Because the steric effect of the (C6)O carbonyl group is much lower or even not existent [123, 132], compared to that of the $(C6)NH_2$ unit, this observation is a clear indication that (C6)O participates in M^{2+} binding.

From solid state structures (for examples see [116]) it follows that transition metal ions coordinate generally innersphere to N7 and hydrogen bonds to (C6)O are formed outersphere via a metal ion-coordinated water molecule [133]. A direct 5-membered N7/(C6)O chelate is normally not observed because the N7/(C6)O bite is too wide (the angle is about 132°) [116]. Though the detailed structure of $Pb(Guo)^{2+}$ is not known, it is evident that the whole N7/(C6)O unit is important for its remarkable stability, which is comparable to that of $Cd(Guo)^{2+}$ but clearly higher than the one of $Zn(Guo)^{2+}$; this is in accord with the preference of Pb^{2+} for O donor sites, whereas Zn^{2+} prefers N sites (Section 2.2).

In this context one should note that studies of $Pb(H;dGMP)^{+}$ in the gas phase, as based on combined IMS (ion mobility spectrometry), infrared multiple photon dissociation (IRMPD), and MS/MS (tandem mass spectrometry) experiments in combination with theoretical calculations [134] have led to the conclusion that for the (rather large; see Table 1) Pb^{2+} ion the "most stable coordination mode is characterized by a tetradentate interaction involving two oxygens of the phosphate group $[P(O)^{-}_{2}(OH)]$ and N7 and the carbonyl group of the guanine residue. Both *syn* and *anti* forms were obtained"; for the *anti* macrochelate the Pb···(N7) and Pb···(O6) distances (see Figure 1) equal 2.467 Å and 2.669 Å, respectively [134]. This 5-membered chelate is clearly strained; in aqueous solution most likely one of the two sites will become outersphere.

A further important aspect is that (N7)-coordination of a M^{2+} ion facilitates (N1)H deprotonation in guanosine-type ligands is well known (e.g., [107, 111, 116]), though for $Pb(Guo)^{2+}$ the corresponding data are not known. However, such data exist for the $Cu(Guo)^{2+}$ system (Table 4, columns 3 and 4) and these allow to formulate the following Equilibrium scheme (17):

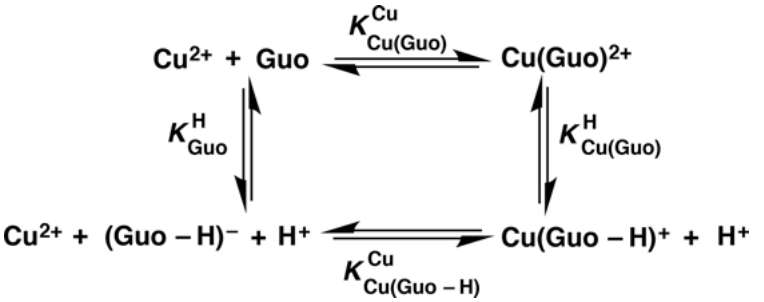

(17)

This scheme involves four equilibrium constants but because it is of a cyclic nature, only three constants are independent of each other; the fourth constant is automatically determined by the other three [Eq. (18)]:

$$\log K^{Cu}_{Cu(Guo)} - pK^{H}_{Cu(Guo)} = \log K^{Cu}_{Cu(Guo-H)} - pK^{H}_{Guo} \tag{18}$$

Rearranging Eq. (18) and inserting the known equilibrium constants of Table 4 (columns 3 and 4) leads to Eq. (19):

$$pK^{H}_{Cu(Guo)} = pK^{H}_{Guo} + \log K^{Cu}_{Cu(Guo)} - \log K^{Cu}_{Cu(Guo-H)} \tag{19a}$$

$$= (9.22 \pm 0.02) + (2.15 \pm 0.04) - (4.34 \pm 0.55) \tag{19b}$$

$$= 7.03 \pm 0.55 \tag{19c}$$

The acidification of the (N1)H site in the $Cu(Guo)^{2+}$ complex, as caused by the (N7)-coordinated metal ion, is defined by Eq. (20):

$$\Delta\, pK_a = pK^{H}_{Guo} - pK^{H}_{Cu(Guo)} \tag{20a}$$

$$= (9.22 \pm 0.02) - (7.03 \pm 0.55) \tag{20b}$$

$$= 2.2 \pm 0.6 \tag{20c}$$

The result of Eq. (20c) agrees with an earlier evaluation [111] and it fits also in a previously defined series in which the acidifying effect on (N1)H of the (N7)-coordinated divalent metal ion decreases [the $\Delta\, pK_a$ values, defined in analogy to Eq. (20a) are given in parentheses]: Cu^{2+} $(2.2 \pm 0.3) > Ni^{2+}$ $(1.7 \pm 0.15) \approx Cd^{2+}$ $(\approx Zn^{2+}) > Pt^{2+}$ $(1.4 \pm 0.1) \approx Pd^{2+}$ [30].

From the results listed in Table 4 and summarized in this section it follows unequivocally that Pb^{2+}, coordinated at N7/(C6)O, exercizes an acidifying effect as well. The exact acidifying power of Pb^{2+} is unknown at present, but it seems safe to predict that $\Delta\ pK_{a/Pb(II)} = 1.7 \pm 0.4$.

4.3. Complexes of Cytidine

In a review on the Cd^{2+}/Cyd system it was recently concluded [30] and this also holds here: "Among the three pyrimidine-nucleobase residues shown in Figure 1 only the cytosine moiety is not protonated at N3 in the physiological pH range and hence, freely available for metal ion coordination. Therefore, this residue will be discussed first. The cytosine residue is an ambivalent ligating site" [113] offering metal ions N3 and (C2)O for binding [30]. The $(C4)NH_2$ unit does not participate in metal ion coordination [74]; such an exocyclic amino group rather introduces steric hindrance [113] as already discussed for adenosine in Section 4.1. The stability constants for the $Pb(Guo)^{2+}$ and $Pb(Cyd)^{2+}$ complexes (Table 4; columns 3 and 5) are of the same size and this is a clear indication that also in $Pb(Cyd)^{2+}$ the complete N3/(C2)O unit participates, at least to some extent, in Pb^{2+} binding. Thus, for aqueous solution the intramolecular Equilibrium (21) involving (C2)O and N3 needs to be considered:

$$M(Cyd)^{2+}_{op} \rightleftharpoons M(Cyd)^{2+}_{cl} \qquad (21)$$

Of course, the M^{2+} interaction may be innersphere or outersphere; in any case a 'closed' (cl) chelated species results [30, 113]. The 'open' (op) species may be (N3)- or (C2)O-bound, depending on the metal ion involved. The various binding modes are summarized in Figure 6.

The structures A, B, and C of Figure 6 have been verified in the solid state by X-ray crystal structure studies [22, 23, 135]: Co^{2+}, Pd^{2+}, and Pt^{2+} bind in a monodentate fashion to N3 (Structure A), whereas Ba^{2+} and Mn^{2+} coordinate solely to the (C2)O carbonyl group (B). The 4-membered chelate seen in Structure C is observed for Zn^{2+}, Cu^{2+}, and Cd^{2+}; however, the 4-membered ring is distorted to varying extents and especially the bond of $(C2)O\cdots M^{2+}$ is commonly longer. Hence, one may suggest that in aqueous solution a water molecule is inserted leading to a 6-membered semi-chelate in which (C2)O is outersphere bound (Structure D), whereas for metal ions with a strong affinity for O and a weak one for N donors the semi-chelate seen in Structure E may form.

Any kind of chelate formation must give rise to an increased complex stability (see Section 3.2). Hence, if Equilibrium (21) is in action and if chelates with varying structures are formed (Structures C, D, E) such an enhanced stability should be observed [84]. Indeed, this is the case, and in agreement with the mentioned solid state structures one obtains for $Zn(Cyd)^{2+}_{cl}$ a formation degree of 31 ± 22 % [113]. For $Cd(Cyd)^{2+}_{cl}$ and $Cu(Cyd)^{2+}_{cl}$ the formation degrees are 58 ± 11 % and 83 ± 4 %, respectively [30, 113], and most satisfying the value for

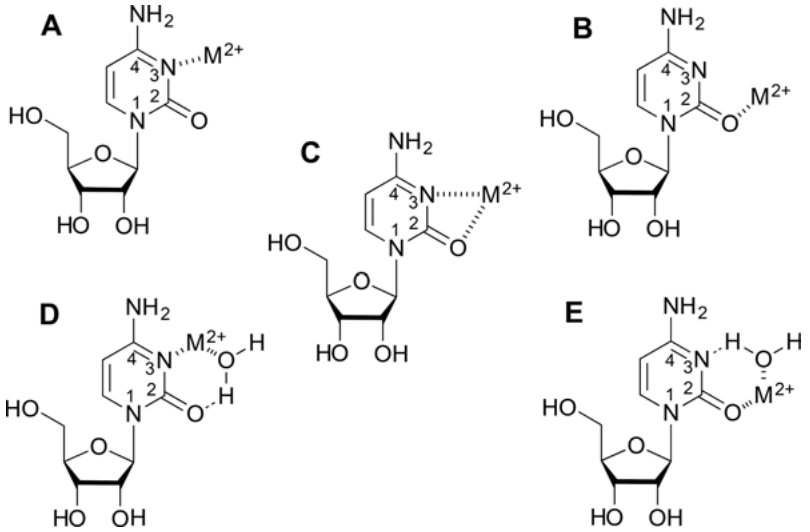

Figure 6. Possible metal ion-binding modes of the $Pb(Cyd)^{2+}$ complex in aqueous solution. According to Equilibrium (21) the two monodentate, 'open' species A and B (also known from the solid state) may occur. Both isomers may transform to the four-membered chelate C (also found in the solid state). However, in aqueous solution the formation of the two 6-membered chelates D and E involving hydrogen-bond formation of a coordinated water molecule seems quite likely; D and E form directly from A and B, respectively, or by insertion of a water molecule into C.

$Co(Cyd)_{cl}^{2+}$ is zero, in accord with the solid state structure, which revealed a $(N3)\cdots Co^{2+}$ bond only [22, 135].

Unfortunately, for $Pb(Cyd)^{2+}$ a corresponding evaluation is not possible because the necessary background information (straight-line correlation) is not available. However, based on the described results one may estimate for $Pb(Cyd)_{cl}^{2+}$ a formation degree of 50 ± 20 % because an interaction with both, (C2)O and N3 is expected (see also below).

Of interest in the present context is also a gas phase study of $Pb(H;CMP)^{+}$ and $Pb(H;dCMP)^{+}$, which was based on tandem mass spectrometry, DFT calculations, and infrared multiple-photon dissociation (IRMPD) spectra [136]. The result is that the most stable species have a "tetradentate coordination involving (two oxygens from) the phosphate group $[P(O)_2^-(OH)]$ and both (C2)O and N3 sites. The interaction with the (C2)O carbonyl group is strong as (is) attested by the important (and short) bond length" [136] of 2.295 Å compared to $(N3)\cdots Pb^{2+}$ with 3.332 Å; the distances of Pb^{2+} in this *syn* conformation to the phosphate oxygens are 2.315 Å and 2.331 Å. The energy difference between the *syn* and *anti* conformations is small. For the *anti* complex the $(C2)O\cdots Pb^{2+}$ and $(N3)\cdots Pb^{2+}$ distances are 2.303 Å and 3.131 Å, respectively [136]. Hence, based on these results one is tempted to suggest that in aqueous solution for the $Pb(Cyd)^{2+}$ complex Structure E of Figure 6 is of relevance.

4.4. Complexes of Uridine and Thymidine

Carbonyl oxygens may interact in the solid state with metal ions [22, 137], but in aqueous solution isolated carbonyl-oxygen interactions are not observed; metal ion binding occurs only if the (C)O group is supported and correctly positioned by a primary binding site [62, 85]. In accord herewith, in aqueous solution no interactions between M^{2+} ions and the (C2)O and (C4)O sites of neutral uracil or thymine residues are found [28, 86, 115] and this also holds for Pb^{2+} [114].

Therefore, we consider first some results obtained for $Pb(H;UMP)^{+}$ in the gas phase [138]. This study combined tandem mass spectrometry (MS/MS) experiments with theoretical density functional theory (DFT) calculations, also recording the IRMPD (infrared multiple-photon dissociation) spectra of the electrospray ionization (ESI)-generated complexes. The most stable structure is characterized by a tridentate coordination involving two oxygens of the $P(O)_2^-(OH)$-phosphate residue and the (C4)O carbonyl group of the nucleobase in the *anti* conformation. The calculated bond lengths of the two O(phosphate)–Pb^{2+} distances are 2.337 Å and 2.342 Å, the one of (C4)O–Pb^{2+} is 2.296 Å [138]. The strong Pb^{2+} interaction with (C4)O is also attested by the important bond lengthening of (C4)–O with 1.277 Å compared to 1.211 Å for the (C2)–O bond. The Pb^{2+} interactions involving the (C2)O carbonyl unit lead to less stable structures. However, most remarkable is that the overall results suggest that the oxo form is a minority population and that the most abundant species for the $Pb(H;UMP)^{+}$ ion is the enolic tautomer which formally arises by moving the proton of N3 to the adjacent (C4)O [138].

How is the situation in aqueous solution? Here complex formation between Pb^{2+} or other M^{2+} ions and Urd or dThd can only be observed, if (N3)H is deprotonated [115, 139]. A comparison of the stability constant listed in Table 4 (column 6) for the $Pb(Urd - H)^{+}$ complex with that of $Cd(Urd - H)^{+}$ shows that the two $M(Urd - H)^{+}$ complexes have within the error limits the same stability. The same observation is made (column 7) for the two corresponding $Pb(dThd - H)^{+}$ and $Cd(dThd - H)^{+}$ species. The somewhat higher stability of all the $M(dThd - H)^{+}$ complexes (column 7), compared to that of the $M(Urd - H)^{+}$ ones (column 6), is simply a matter of the somewhat increased basicity of $(dThd - H)^{-}$ (see the bottom row of Table 4 for the pK_a values).

Of relevance is now that for $Cd(Urd - H)^{+}$ and some related complexes an intramolecular equilibrium [Eq. (5)] exists between monodentately coordinated (op) and chelated (cl) isomers, the formation degree of $Cd(Urd - H)^{+}_{cl}$, which is most likely a mixture of chelates, amounting to 60 % (or more) [30, 115]. Hence, the same formation degrees need to be assumed for $Pb(Urd - H)^{+}_{cl}$ and $Pb(dThd - H)^{+}_{cl}$. Yet, structure-wise there appears to be a difference because for Cd^{2+} and the related transition metal ions $(N3)^{-}$ is the primary binding site [115], whereas for $Pb(Urd - H)^{+}$ and $Pb(dThd - H)^{+}$, due to the strong affinity of Pb^{2+} towards carbonyl groups [138] (see also Section 4.3) one is forced to assume that now the primary binding site is a (C)O unit. Furthermore, the gas phase results [138] have indicated that enolic forms are important and that these should actually be favored in aqueous solution. Therefore, we propose for $Pb(Urd - H)^{+}$, and analogously for $Pb(dThd - H)^{+}$, the structures seen in Figure 7.

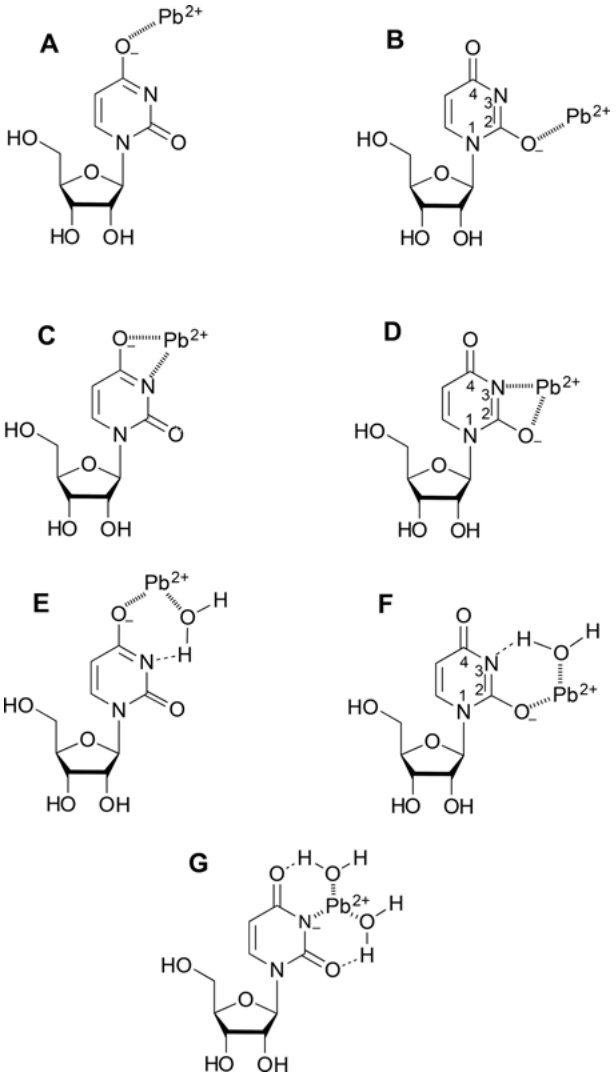

Figure 7. Possible metal ion-binding modes for the $Pb(Urd - H)^{+}$ complex in aqueous solution (for details see the text in Section 4.4). As far as the intramolecular Equilibrium (5) is concerned, we believe that the most relevant isomers are Structure A, which involves a monodentate binding mode, and Structure E containing a 6-membered semichelate.

Of course, the negative charge of $(N3)^{-}$ is in reality only partially displaced towards the (C)O units; in addition, further structures can be thought of. This is suggested already from the simple fact that for $Cu(Urd - H)^{+}_{cl}$ a formation degree of 80 % (or more) was derived and that for $Ca(Urd - H)^{+}_{cl}$ one of 50 % holds [30, 115] – and for the latter complex one must assume that outersphere interactions are also important [115].

To conclude, for aqueous solution and $Pb(Urd - H)^+$ we propose the structures seen in Figure 7. Monodentate binding occurs in our view via (C4)O (Structure A) and only to a small part via (C2)O (Structure B) because (C4)O is more easily accessible for metal ion coordination and in accord herewith this site is also favored by the gas phase considerations. Distorted 4-membered chelates, in analogy to the one seen in Figure 6, may also form (Structures C and D), yet, we believe that in aqueous solution their stability is not very high. This is different with the 6-membered semi-chelates shown in Structures E and F of Figure 7. Finally, one could imagine that there is a complex in which the charge on $(N3)^-$ is only little delocalized and Pb^{2+} coordinates at this site, supported by two 6-membered semi-chelates which involve (C2)O and (C4)O (Structure G). In summary, we believe that the most stable isomers of $Pb(Urd - H)^+$, which are most important in aqueous solution regarding the intramolecular Equilibrium (5), are those with Structures A and E; for Pb(dThd) the analogous situation holds.

4.5. Complexes of Some Less Common Natural and Artificial Purine-Nucleobase Residues

To the best of our knowledge for none of the ligands mentioned below have any Pb^{2+} complexes been studied. However, in most instances stability constants, especially for nucleosides, are known for Zn^{2+}, Cu^{2+} and Cd^{2+} complexes, and thus for the corresponding Pb^{2+} complexes educated guesses become possible. There exist also stability constants in the literature which cannot be recommended, because, e.g., metal ion hydrolysis has been overlooked. The sources we are listing appear to us as being reliable.

4.5.1. 2-Amino-9-methylpurine

2-Amino-9-methylpurine (2A9MP) is most close to 9-methyladenine (9MAde) (Figure 1) which can also be named 6-amino-9-methylpurine (6A9MP). The structures of these two isomeric compounds, together with the one for 2,9-dimethylpurine (2,9DMP), are shown in Figure 8. 2A9MP and its derivatives are traditionally used as probes due to their excellent fluorescent properties, that is, they are powerful reporter molecules, e.g., regarding enzyme interactions of DNA and RNA [140]. Since such systems commonly also contain metal ions, it is important to understand the coordination chemistry of 2A9MP.

In Table 5 some pertinent data are listed [141, 142]. It is impressive to see that the shift of the NH_2 group from C6 to C2 enhances the stability of the Ni^{2+} and Cu^{2+} complexes by about 0.7 log unit and this despite the fact that the basicity of N1 is reduced by $\Delta\ pK_a = 0.2$ due to this same NH_2 shift. What happens? The steric effect of an NH_2 group on (N1)-M^{2+} binding is identical in 9MAde and 2A9MP because the NH_2 group is *ortho* to N1 in both compounds. The crucial difference is that in 9MAde the (C6)NH_2 group sterically hinders M^{2+} binding at N7, whereas with 2A9MP the N7 site is freely accessible.

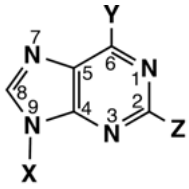

6A9MP: $X = CH_3$; $Y = NH_2$; $Z = H$
2A9MP: $X = CH_3$; $Y = H$; $Z = NH_2$
2,9DMP: $X = Z = CH_3$; $Y = H$

Figure 8. Chemical structures of the purine (Pu) derivatives 6-amino-9-methylpurine (6A9MP = 9-methyladenine = 9MeAde), 2-amino-9-methylpurine (2A9MP), and 2,9-dimethylpurine (2,9DMP) (see Section 4.5.1).

Table 5. Negative logarithms of the acidity constants [Eq. (3)] of three purine (Pu) derivatives (Figure 8) and logarithms of the stability constants [Eq. (2) and analogous to Eq. (6)] of their Ni^{2+} and Cu^{2+} 1:1 complexes, together with the percentage of the $M(Pu \cdot N7)^{2+}$ isomer which is part of the intramolecular Equilibrium (22) (aq. sol.; 25 °C; $I = 1$ M, $NaClO_4$).[a]

Pu	$pK^{H}_{H(Pu)}$	M^{2+}	$\log K^{M}_{M(Pu)}$	% $M(Pu \cdot N7)^{2+}$
6A9MP = 9MAde	4.45 ± 0.03	Ni^{2+}	0.71 ± 0.22	75 (60/85)
		Cu^{2+}	1.26 ± 0.12	59 (46/70)
2A9MP	4.26 ± 0.03	Ni^{2+}	1.45 ± 0.10	96 (94/97)
		Cu^{2+}	2.03 ± 0.09	94 (92/95)
2,9DMP	3.84 ± 0.01	Ni^{2+}	1.24 ± 0.04	94 (93/95)
		Cu^{2+}	1.78 ± 0.05	93 (92/94)

[a] The values are abstracted from tables 1 and 3 of [120] and the values there are based on the work of Arpalahti et al. [141, 142]. For details regarding the calculation of % $M(Pu \cdot N7)^{2+}$ see [120].

This view is in accord with the formation degree of the (N7)-coordinated isomers. As discussed before (Section 4.1), there is a N1 *versus* N7 dichotomy which is expressed by the intramolecular Equilibrium (22), where Pu = purine derivative:

$$M(Pu \cdot N1)^{2+} \rightleftharpoons M(Pu \cdot N7)^{2+} \quad (22)$$

The formation degree of the (N7)-coordinated isomer in the $M(9MAde)^{2+}$ systems increased from roughly 67 to 95 % in the $M(2A9MP)^{2+}$ species (see Table 5, column 5). Interestingly, replacement of the $(C2)NH_2$ group by a $(C2)CH_3$ unit has no significant effect: If the different basicities of N1 are taken into account, the stability of both types of complexes corresponds to each other and the formation degrees of the $M(Pu \cdot N7)^{2+}$ isomers is within the error limits also the same. In other words, the steric effects of NH_2 and CH_3 groups are quite alike.

As far as the properties of the corresponding Pb^{2+} complexes are concerned, we conclude that they are expected to be relatively close to those of the Ni^{2+} complexes. This conclusion is based on the following two observations: (i) The acidification of (N1) sites in Guo derivatives by (N7)-coordinated Ni^{2+} or Pb^{2+} is very similar (Section 4.2). (ii) The stability constant of the $Ni(Ado)^{2+}$ complex $\log K^{Ni}_{Ni(Ado)} = 0.32 \pm 0.12$ [130] / 0.4 ± 0.2 ([102], from [130] based on data in [143]), equals the one of $Pb(Ado)^{2+}$, $\log K^{Pb}_{Pb(Ado)} = 0.4 \pm 0.3$ (Table 4, column 2).

4.5.2. Inosine

The hypoxanthine residue is the only nucleobase shown in Figure 1, of which the metal ion-binding properties have so far not been dealt with, therefore, we consider next this purine derivative, i.e., inosine (Ino). Its nucleotides, that is, the inosine phosphates, have been well studied (e.g., [26–28, 30, 60, 102, 116, 144]) in contrast to inosine itself, though its acid-base properties have been discussed [145].

Information about inosine is scattered and not comprehensive. For example, the following constants are taken from different sources [102], that is, $pK^{H}_{HN7(Ino)} = 1.06 \pm 0.06$ and $pK^{H}_{HN1(Ino)} = 8.76 \pm 0.03$ (25 °C; $I = 0.1$ M, $NaNO_3$) [116], $\log K^{Ni}_{Ni(Ino)} = 1.15 \pm 0.13$ [Eq. (2)] (15 °C; $I = 1.0$ M, $NaClO_4$) [146], and $\log K^{Ni}_{Ni(Ino-H)} = 2.8 \pm 0.2$ (25 °C; $I = 1.0$ M, $NaClO_4$) [110] (the error limits of the log K values are estimates [102]). Application of an equation analogous to Eq. (19a) provides $pK^{H}_{Ni(Ino)} = 7.11 \pm 0.24$ and an acidification of the (N7)-coordinated Ni^{2+} on the (N1)H site of $\Delta\ pK_a = (8.76 \pm 0.03) - (7.11 \pm 0.24) = 1.65 \pm 0.24$. This result should be compared with $\Delta\ pK_a = 2.2 \pm 0.6$ for the Cu^{2+}/Guo system [Eq. (20)] and the related results of Section 4.2; this then suggests that for Pb^{2+}/Ino an acidification of $\Delta\ pK_a$ ca 1.4 to 1.6 is to be expected.

Values for the (Ba^{2+}, Ca^{2+}, Mg^{2+}, Mn^{2+}), Co^{2+}, Ni^{2+}, Cu^{2+}, and Zn^{2+} systems with Ino are also available [109] (see further in [147]); those for Ni^{2+}, Cu^{2+} and Zn^{2+} appear in addition in [128, 129]. Studies with $(Dien)Pd^{2+}$ and Ino also exist [111, 127, 129] as do those with $(Dien)Pt^{2+}$ [111, 129, 148, 149].

4.5.3. Tubercidin

Tubercidin (Tu) is also known as 7-deazaadenosine and this means that the (N7)-atom in the purine ring is replaced by a CH unit (Figure 9, Structure A). This nucleoside is synthesized by molds and fungi [150]; tubercidin and its derivatives have antibacterial, antiviral and also anticancer properties (see, e.g., Refs in [122, 151]). Furthermore, tubercidin and related analogues have inspired drug discovery for the past 50 years [152].

Replacement of N7 by CH makes the N1 site of tubercidin more basic, i.e., $pK^{H}_{H(Tu)} = 5.21 \pm 0.03$ [Eq. (3)] [151], compared with its parent compound adenosine, $pK^{H}_{H(Ado)} = 3.61 \pm 0.03$ [24] (25 °C; $I = 0.1$ M, $NaNO_3$). This increased basic-

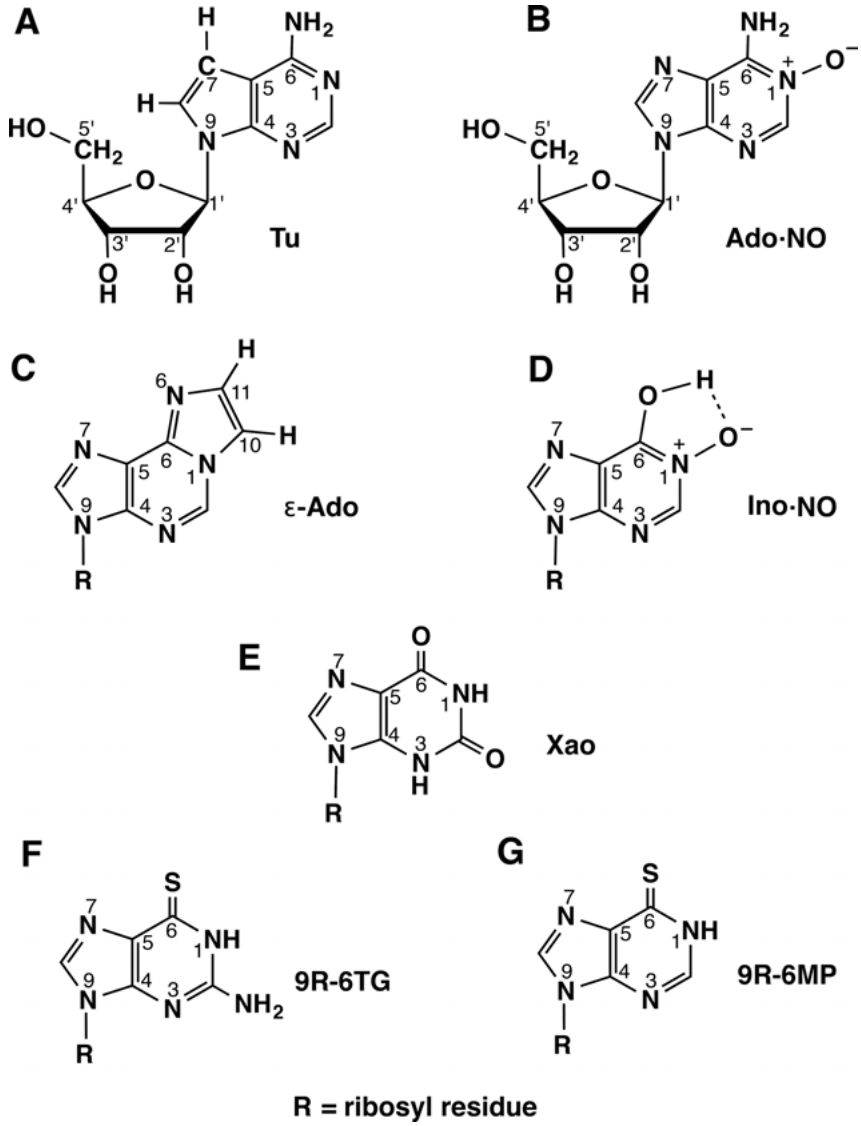

Figure 9. Chemical structures of some nucleosides considered in Sections 4.5.3 through 4.5.7 as well as in Section 4.5.9 (**A**) tubercidin (Tu) (= 7-deazaadenosine), (**B**) adenosine (N1)-oxide (Ado · NO), (**C**) (N)1,(N)6-ethenoadenosine = 1,N^6-ethenoadenosine (ε-Ado), (**D**) inosine (N1)-oxide (Ino · NO), (**E**) xanthosine (Xao), (**F**) 9-(β-D-ribofuranosyl)-6-thioguanine (9R-6TG), and (**G**) 9-(β-D-ribofuranosyl)-6-mercaptopurine (9R-6MP) [it may be noted that the nucleobase 6-mercaptopurine in 9R-6MP should more correctly be named 6-thiopurine or purine-6-thione (or even 6-thiohypoxanthine)]. – The two structures A and B at the top are shown in their dominating *anti* conformation [22–24]. For C through G R = ribosyl residue as shown in A and B; R is linked in all instances to N(9) of the purine-nucleoside as indicated in A and B via C(1′) of the ribosyl residue, also always in the *anti* conformation.

ity of $\Delta\, pK_a = 1.6$ over-compensates somewhat for the loss of the (N7)-coordination site in the $M(Tu)^{2+}$ complexes ($M^{2+} = Ca^{2+}$, Mg^{2+}, Mn^{2+}, Co^{2+}, Ni^{2+}, Cu^{2+}, Zn^{2+}, Cd^{2+}) [151]; these are therefore approximately 0.1 to 0.2 log unit more stable than the corresponding $M(Ado)^{2+}$ complexes ([106] and Table 4, column 2). For $Pb(Tu)^{2+}$ the stability constant $\log K^{Pb}_{Pb(Tu)} = 0.4 \pm 0.2$ is expected.

4.5.4. Adenosine (N1)-oxide

As is common with (artificial) nucleobase derivatives adenosine (N1)-oxide ($Ado \cdot NO$) shows biological activity, that is, it has antiinflammatory effects [153] and analogues of it inhibit orthopox virus replication [154]. The replacement of N1 in adenosine by a (N→O)-oxide group (Figure 9, Structure B) affects the acid-base properties strongly, that is, the (N1)-oxide derivative becomes more acidic: The values for $H(Ado)^+$, i.e., $pK^H_{HN1(Ado)} = 3.61$ (Table 4, bottom row) and $pK^H_{Ado[(C6)NH_2]} = 16.7$ [119], are significantly higher than those of $H(Ado \cdot NO)^+$: $pK^H_{HN1(Ado \cdot NO)} = 2.25$ and $pK^H_{Ado \cdot NO[(C6)NH_2]} = 12.86$ [155]. Complex formation occurs between the oxygen of the (N1)→O unit and the ionized $(C6)NH^-$ group [155] and as expected, the stability of these $M(Ado \cdot NO - H)^+$ complexes is much higher than that of the $M(Ado)^{2+}$ complexes (Section 4.1). Values for $\log K^M_{M(Ado \cdot NO - H)}$ (given in parenthesis) are for $M^{2+} = Mn^{2+}$ (5.27), Co^{2+} (7.01), Ni^{2+} (7.52), Cu^{2+} (11.32), and Zn^{2+} (7.50) [155] (see also [156]). A very rough guess for the Pb^{2+} complex is $\log K^{Pb}_{Pb(Ado \cdot NO - H)} = 9.5 \pm 2$.

It is evident that insertion of the (N1)-oxide group in AMP will change the metal ion-coordinating properties of this nucleotide dramatically; in fact, it does give rise to interesting structures and pH dependencies [156, 157].

4.5.5. (N)1,(N)6-Ethenoadenosine

The name of this nucleoside is also often written as $1,N^6$-ethenoadenosine (ε-Ado). In ε-Ado the N1 site and the $(C6)NH_2$ unit are linked by an etheno bridge and this leads to a 5-membered ring (Figure 9, Structure C). This compound and its derivatives exhibit excellent fluorescence properties [158] and if incorporated into macromolecules provide a powerful tool to obtain structural information [158, 159]).

While Ado is protonated at N1 ($pK^H_{HN1(Ado)} = 3.61$; Table 4, bottom row) (Section 4.1), in ε-Ado protonation occurs at N6 ($pK^H_{HN6(\varepsilon\text{-Ado})} = 4.05$ (25 °C; $I = 0.1$ M, $NaNO_3$) [160], though the positive charge can be redistributed giving rise to resonance structures. The (N6)–(N7) bite is relatively wide and thus less suitable for metal ion coordination than the one in 1,10-phenanthroline, but still the resulting metal ion complexes are roughly about 100 times more stable than those with Ado. Stability constants are available for the $M(\varepsilon\text{-Ado})^{2+}$ complexes, where $M^{2+} = Mg^{2+}$, Mn^{2+}, Co^{2+}, Ni^{2+}, Cu^{2+}, Zn^{2+}, Cd^{2+} [159–161].

To make an estimate for the stability of the $Pb(\varepsilon\text{-Ado})^{2+}$ complex is difficult; maybe due to the wide (N6)–(N7) bite the large Pb^{2+} (Table 1) fits relatively well, yet on the other hand the affinity of Pb^{2+} for N sites is not very pronounced (Section 2.2). Our tentative guess for the stability of $Pb(\varepsilon\text{-Ado})^{2+}$ is $\log K^{Pb}_{Pb(\varepsilon\text{-Ado})} = 2.2 \pm 0.6$; other related values are $\log K^{Cu}_{Cu(\varepsilon\text{-Ado})} = 2.81 \pm 0.09$ and $\log K^{Zn}_{Zn(\varepsilon\text{-Ado})} = 1.51 \pm 0.03$ [159, 160].

The properties of the M^{2+}/ε-Ado nucleotide systems differ significantly, at least for the 3d-transition metal ions, from those of the M^{2+}/Ado nucleotides [122, 159]. The extent of macrochelate formation [Eq. (5)] is much more pronounced for the complexes of the ε-Ado nucleotides [159].

4.5.6. Inosine (N1)-oxide

After having shortly discussed some adenosine derivatives we proceed now to inosine (N1)-oxide (Ino · NO) (Figure 9, Structure D). This nucleoside is synthesized by deamination of Ado · NO with nitrosyl chloride (NOCl) [162]. After deprotonation of the (C6)OH group ($pK_a = 5.40$ [163]) a powerful ligand results which forms 5-membered chelates, the structure of which is evident from D in Figure 9. The stabilities of $M(Ino \cdot NO - H)^{+}$ complexes have been determined for $M^{2+} = Ba^{2+}$, Ca^{2+}, Mg^{2+}, Mn^{2+}, Co^{2+}, Ni^{2+}, Cu^{2+}, Zn^{2+}) [156, 164].

Representative stability constants are $\log K^{Ni}_{Ni(Ino \cdot NO - H)} = 3.50 \pm 0.05$, $\log K^{Cu}_{Cu(Ino \cdot NO - H)} = 5.27 \pm 0.05$, and $\log K^{Zn}_{Zn(Ino \cdot NO - H)} = 3.60 \pm 0.05$ (aq. sol.; 25 °C; $I = 0.1$ M, $NaClO_4$) [156, 164]. Considering that $(Ino \cdot NO - H)^{-}$ is a ligand which offers two O donor sites giving rise to a 5-membered chelate (see Structure D in Figure 9), one expects (see Section 2.2) that Pb^{2+} behaves like Cu^{2+}, and thus we estimate for the stability of the $Pb(Ino \cdot NO - H)^{+}$ complex $\log K^{Pb}_{Pb(Ino \cdot NO - H)} = 4.8 \pm 0.4$.

Combination of the (N1)O/$(C6)O^{-}$ binding site with the phosphate group as it is the case in inosine 5′-monophosphate N(1)-oxide leads to a ligand with interesting properties. Depending on the pH of the aqueous solution the M^{2+} ions switch in this artificial nucleotide from the (N1)O/$(C6)O^{-}$ site to the phosphate group and *vice versa* [156, 164].

4.5.7. Xanthosine

Xanthosine (Xao) (see Figure 9, Structure E) and its derivatives are of relevance for the metabolism of purine-nucleosides/nucleotides in all kingdoms of life [165, 166]. Xanthosine is involved in very diverse reactions, it affects mammary stem cells [167] and it is also part of the purine catabolism in plants which leads (via Xao) to theobromine and caffeine [168]. That its acid-base and metal ion-binding properties need to be understood is evident.

Xanthosine can be protonated at N7 ($pK^{H}_{H(Xao)} = pK^{H}_{HN7(Xao)} = 0.74 \pm 0.06$ [117]), just like Guo or Ino (see Table 4, bottom line), but Xao is less basic. This is even more true for the deprotonation of the neutral nucleosides; deprotona-

tion for Xao occurs already with $pK_a = 5.47 \pm 0.03$, which is to be compared, e.g., with $pK^{H}_{HNI(Guo)} = 9.22$ (Table 4, bottom). Furthermore, for Xao deprotonation occurs from the (N1)H/(N3)H sites, meaning that there is evidence for a tautomeric equilibrium between $(N3)^-$/(N1)H and (N3)H/$(N1)^-$ with formation degrees of 70 and 30 %, respectively [169]. Hence, Xao is present in the physiological pH range in its anionic form $(Xao - H)^-$ whereas its relatives Guo and Ino exist in their neutral forms. Of course, once the $(Xao - H)^-$ anion is formed the negative charge can be distributed over many atoms, that is, N3, (C2)O, N1, and (C6)O [169].

Stability constants of $M(Xao - H)^+$ complexes have been determined [117] and there is evidence that a dichotomy for M^{2+} binding between N1 and N7 occurs [117, 125], as it has been described in Section 4.1 for $M(Ado)^{2+}$ complexes. For $Cd(Xao - H)^+$ it is concluded that about 75 % are (N7)-coordinated [117, 125]. The stability constants, $\log K^{M}_{M(Xao-H)}$, for $M(Xao - H)^+$ complexes are, e.g., 1.65 ± 0.05 (Co^{2+}), 2.09 ± 0.05 (Ni^{2+}), 2.58 ± 0.03 (Cu^{2+}), 1.32 ± 0.02 (Zn^{2+}), 1.96 ± 0.05 (Cd^{2+}) [117, 169]. Considering the involvement of N sites in complex formation, but also the negative charge and the presence of a carbonyl group, we estimate for the stability of the $Pb(Xao - H)^+$ complex $\log K^{Pb}_{Pb(Xao-H)} = 2.0 \pm 0.3$.

From the indicated results it is clear that the coordination chemistry of the xanthosine-phosphates is rich but also complicated. For example, for the nucleotide xanthosine 5′-monophosphate and its Cd^{2+} complex in aqueous solution 86.8 ± 4.2 % exist in a closed/chelated form [Eq. (5)]; the remaining 13.2 ± 4.2 % present in the open form are divided in two further isomers, that is, one where Cd^{2+} is phosphate-bound (9.0 %) and one where Cd^{2+} is at the deprotonated xanthine residue (4.2 %) [169, 170].

4.5.8. Benzimidazole Derivatives

The structure and size of benzimidazole (BI) is very similar to that of purine and indeed BI may also be named 1,3-dideazapurine. It is thus no surprise that many benzimidazole derivatives have been tested for their biological activity [171–173].

Figure 10 shows the structures of several such BI compounds for which the metal ion-binding properties have been determined, that is, for the alkaline earth ions and the second half of the divalent 3d-transition metal ions including Zn^{2+} and Cd^{2+}. To discuss all these results is beyond the limits of this review but the reader should be aware of their existence because there is a rich coordination chemistry hidden [174–176]. No stability constants for Pb^{2+} complexes have been determined but sophisticated estimates can be made based on the values given for the Ni^{2+}, Cu^{2+}, Zn^{2+}, and Cd^{2+} complexes. The data for Part I of Figure 10 are found in [177], those for Parts II and III in [124] and [178], respectively. The acidification of the benzimidazole (N3)H site by (N1)-coordinated M^{2+} ions is discussed in [179].

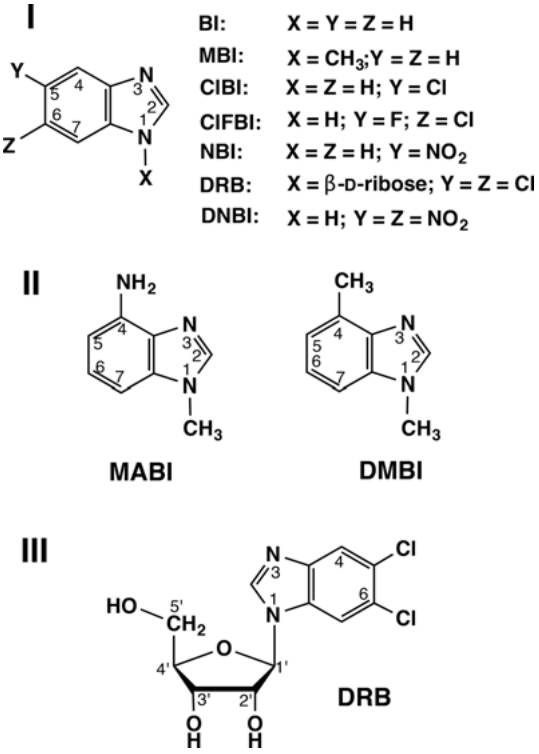

Figure 10. Part I:. Chemical structures of benzimidazole (BI) (= 1,3-dideazapurine) and its derivatives considered in Section 4.5.8: 1-methylbenzimidazole (MBI) (= 9-methyl-1,3-dideazapurine), 5(6)-chlorobenzimidazole (ClBI), 6-chloro-5-fluorobenzimidazole (ClFBI), 5(6)-nitrobenzimidazole (NBI), 5,6-dichloro-1-(β-D-ribofuranosyl)-benzimidazole (DRB; see also Part III), and 5,6-dinitrobenzimidazole (DNBI). **Part II**: Structures of 1-methyl-4-aminobenzimidazole (MABI) (= 9-methyl-1,3-dideazaadenine) and 1,4-dimethylbenzimidazole (DMBI) (= 6,9-dimethyl-1,3-dideazapurine). **Part III:** Structure of 5,6-dichloro-1-(β-D-ribofuranosyl)benzimidazole (DRB).

4.5.9. 6-Thiopurines

Thiopurines are widely used as immunosuppressant and anticancer drugs [180–183]. Among these is 6-mercaptopurine, more correctly named 6-thiopurine (see comment to Structure G in Figure 9), an antileukemic drug [184] with a role in tumor necrosis [183], that also owns antioxidant properties [185]. A relative is the S-(1-methyl-4-nitroimidazol-5-yl) derivative which is also known as azathiopurine (AZA) and used as an immunosuppressive agent [184, 186]. A further wellknown compound is 6-thioguanine (Structure F with R = H in Figure 9), also an antileukemic drug [184, 187], that, e.g., damages mitochondrial DNA and causes mitochondrial dysfunction in human cells [180].

Many X-ray crystal structures of complexes of 6-mercaptopurine (6MP) and 6-thioguanine (6TG) and derivatives thereof are available [184]. Among these

are complexes of Fe^{2+}, Co^{2+}, Cu^{2+}, Cd^{2+}, and Ru^{2+} with neutral 6MP, M^{2+} being coordinated to the (C6)S-N7 bite with hydrogens at N1 and N9. Hence, the structure of 6MP in these complexes is the one seen in Figure 9, i.e., Structure G with R = H. A corresponding structure exists for a Cu^{2+} complex of 6TG (Figure 9, Structure F with R = H). In a $Ru(9R\text{-}6MP)_2$ complex with (C6)S-N7 chelates and (N1)H sites the ligand has the form seen in Structure G (R = H) of Figure 9 [184]. A binuclear Ru^{5+} complex with 6TG is also known [188]. (N1)H-deprotonated complexes of 6MP have been studied as well [184], e.g., in $Pt(6MP - H)_2 \cdot 2\,H_2O$ the negative charge of $(N3)^-$ is shifted to $(C6)S^-$ and Pt^{2+} forms $(C6)S^-$-N7 chelates [184]. The distance between the S and N atoms in the (C6)S-N7 bite varies, depending on the metal ion, from 3.35 Å (in free 6MP) via 3.22 Å for a Cd^{2+} complex to 3.01 Å in the mentioned $Pt(6MP - H)_2$ species [184].

With the above information in mind it is interesting to consider the properties of 9R-6MP and 9R-6TG (see Figure 9) in aqueous solution. Deprotonation of the (N3)H site occurs with $pK_a = 7.50 \pm 0.04$ and 8.11 ± 0.01, respectively [189]. This deprotonation reaction shifts the negative charge to $(C6)S^-$ [43]; the stability constants of the corresponding Ni^{2+} and Cd^{2+} complexes have been measured [189]: $\log K^{Ni}_{Ni(9R\text{-}6MP - H)} = 4.18 \pm 0.05$ and $\log K^{Cd}_{Cd(9R\text{-}6MP - H)} = 5.32 \pm 0.05$ for the $M(9R\text{-}6MP - H)^+$ species; those for the $M(9R\text{-}6TG - H)^+$ complexes are $\log K^{Ni}_{Ni(9R\text{-}6TG - H)} = 4.40 \pm 0.04$ and $\log K^{Cd}_{Cd(9R\text{-}6TG - H)} = 5.18 \pm 0.26$. The stability of all four complexes is higher than the one of the corresponding thiouridine ligands [43, 189]; the reason is that the (C6)S-N7 bite allows formation of 5-membered chelates, whereas for the thiouridines only 4-membered chelates or semi-chelates involving an outersphere water molecule are possible (for details see [43]). Cu^{2+} undergoes in aqueous solution redox reactions with the two thiopurines [189] as it is also the case with most thiouridines [43, 189], and therefore no stability data exist.

As summarized before [43], "Pb^{2+} is known to bind to DNA giving rise to a destabilization of the double helix and to bind in an inter- and intra-chain fashion to phosphate groups as well as to nucleobase residues [190, 191]. Incorporation of a thionucleotide unit into DNA enhances the affinity of the modified nucleic acid for Cd^{2+} [192] and the same is expected for Pb^{2+}". Taking into account the *Stability Ruler* (Section 2.2) one may assume that the stability for the Pb^{2+} complexes is close to the ones of the Ni^{2+} and Cd^{2+} species, that is, $\log K^{Pb}_{Pb(9R\text{-}6MP - H)} = 4.7 \pm 0.6$ for $Pb(9R\text{-}6MP - H)^+$ and $\log K^{Pb}_{Pb(9R\text{-}6TG - H)} = 4.8 \pm 0.5$ for $Pb(9R\text{-}6TG - H)^+$.

4.6. Complexes of Some Less Common Pyrimidine-Nucleobase Residues

In contrast to the situation with the purine-nucleobase residues (Section 4.5), those of the pyrimidines discussed below occur to the largest part in Nature. However, direct knowledge about Pb^{2+} complexes is also in these cases rather redundant. Yet, the metal ion affinity of the pyrimidine-nucleobases is throughout best evaluated via their corresponding nucleosides.

4.6.1. Orotidine

Orotidine and its derivatives play an important role as intermediates in the metabolism of pyrimidine-nucleotides [165]. For example, orotidine 5′-monophosphate decarboxylase catalyzes the decarboxylation of orotidine [193], and there is evidence that the active-site residues in the orotidinate-binding site are of special importance for a high reaction rate [194].

The structure of orotidine, H(Or), is shown in Figure 11, together with the one of uridine, Urd. The remarkable point is that H(Or) exists predominantly in the *syn* conformation [195, 196], which is enforced by the (C6)COOH group and this is still true for orotidinate, Or^-, formed after deprotonation of the carboxylic acid group. In contrast, Urd is present in the *anti* conformation [22, 25].

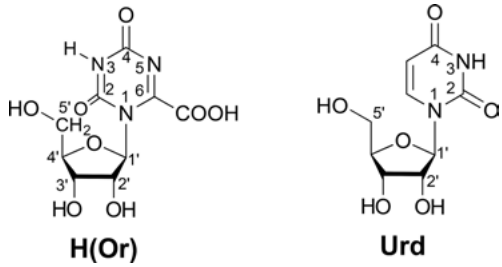

Figure 11. Chemical structures of orotidine, H(Or), and uridine, Urd. Note, H(Or) is shown in its dominating *syn* conformation (what also holds for Or^-, see text) and this contrasts with Urd, which prefers the *anti* conformation [25, 194, 195].

The (C6)COOH group of H(Or) is in aqueous solution with $pK_a = 0.5 \pm 0.3$ [197] strongly acidic, if compared to formic acid ($pK_a = 3.58 \pm 0.01$) and acetic acid ($pK_a = 4.57 \pm 0.01$) [198]. This differs for the deprotonation of the (N3)H site of Or^- which occurs with $pK_a = 9.12 \pm 0.02$ [197], a value which is quite close to the one of its parent nucleoside uridine with $pK_a = 9.18 \pm 0.02$ [115]. The reason is that in Or^- two opposite effects operate: The electronegative oxygen atoms of the carboxylate group are electron-withdrawing, leading to acidification, but this effect is largely offset by the negative charge of Or^-, if compared with the uncharged Urd.

In accord with the low basicity of the (C6)COO^- group of Or^- are the stability constants of the Mg^{2+}, Cu^{2+} and Zn^{2+} complexes (only these have been studied [197]) somewhat smaller than those for the corresponding $M(Ac)^+$ complexes, e.g., $\log K^{Mg}_{Mg(Or)} = -0.1 \pm 0.4$ [197] *versus* $\log K^{Mg}_{Mg(Ac)} = 0.51 \pm 0.05$ [62] [for the other $M(Or)^+$ species see [197]; cf. with the values in Table 1, column 10]. The stability constants for complexes with $(Or - H)^{2-}$, i.e., the carboxylic acid group and the (N1)H site (see Figure 11) are deprotonated, have not been measured, but the straight-line parameters [Eq. (10)] for $\log K$ *versus* pK_a plots have been determined for eleven M^{2+} 1 : 1 complexes of uridinate-type ligands, abbreviated as $(U - H)^-$ [115]. Hence, for these eleven metal ion complexes, including Pb^{2+},

stability constants can be calculated or at least estimated. This is done now for the $Pb(Or - H)^0$ complex; the needed straight-line parameters are given in Eq. (23):

$$\log K^{Pb}_{Pb(U-H)} = 0.514 \cdot pK^{H}_{U} - 1.373 \quad (23)$$

The error limit for calculations with Eq. (23) is ± 0.07 log unit (1 σ) [115]. Hence, one obtains with $pK^{H}_{Or} = 9.12$ for the $Pb(U - H)^+$ complex $\log K^{Pb}_{Pb(U-H)} = 3.31 \pm 0.21$ (3 σ).

However, there is a caveat in this result because the complexes $Pb(U - H)^+$ and $Pb(Or - H)^0$ carry different charges and this charge effect needs to be taken into account. We believe that this effect is well described by considering the acidity constants of the nucleotides, that is, of the 5′-monophosphates of Or^- and Urd, namely OMP^{3-} and UMP^{2-}; the acidity constants for $P(O)_2^-(OH)$ deprotonation are $pK^{H}_{H(OMP)} = 6.40 \pm 0.02$ and $pK^{H}_{H(UMP)} = 6.15 \pm 0.01$ [199]. This means, the release of the proton from the $P(O)_2^-(OH)$ group of $H(OMP)^{2-}$ is inhibited by the negative charge of the $(C6)COO^-$ group by 0.25 ± 0.02 pK unit. The generality of this result is corroborated by the release of the proton from $(N1)H^+$ in $H(Ado)^+$ (Figure 1) and $H_2(AMP)^{\pm}$ [24, 122]: $pK^{H}_{H_2(AMP)} - pK^{H}_{H(Ado)} = (3.84 \pm 0.02) - (3.61 \pm 0.03) = 0.23 \pm 0.04$. We thus obtain for the stability constant of the $Pb(Or - H)^0$ complex $\log K^{Pb}_{Pb(Or-H)} = (3.31 \pm 0.21) + (0.25 \pm 0.02) = 3.56 \pm 0.21$ and we consider as the final result $\log K^{Pb}_{Pb(Or-H)} = 3.6 \pm 0.3$.

One may add that the stabilities of the complexes formed with orotidinate 5′-monophosphate (OMP^{3-}) are determined by the basicity of the phosphate group [199]. No evidence was observed for macrochelate formation between the phosphate-coordinated metal ions and the carboxylate group [199, 200] (but there is a charge effect of about 0.4 log unit [199]). Hence, in $M(OMP)^-$ complexes no interaction with the pyrimidine ring occurs [199, 200] and this corresponds to the situation in the M(UMP) complexes [86].

4.6.2. 2-Thiocytidine

A large number of modifications of the four major nucleosides, that is of adenosine, guanosine, uridine, and cytidine, exist in Nature [201]. They have been characterized in tRNAs from all three domains of life [201, 202], bacteria, archaea, and eukaryota. One important subgroup of these modifications contains thiolated nucleosides, of which at least 10 have been characterized [201]. Among these is 2-thiocytidine (C2S) which is found, e.g., next to four more thionucleosides, in *Salmonella enterica* serovar Thyphimurium [203]. Considering that the reactions of RNAs (and DNA as well) are strongly affected and guided by the interactions with metal ions [69, 204, 205], it is important to understand the coordination chemistry of such thio derivatives [43, 206, 207].

Replacement of the carbonyl group (C2)O in cytidine (Cyd) by a thione (C2)S unit (see Figure 12; Part I) changes the properties of the resulting nucleoside very strongly. 2-Thiocytidine is remarkable because it loses a proton from the

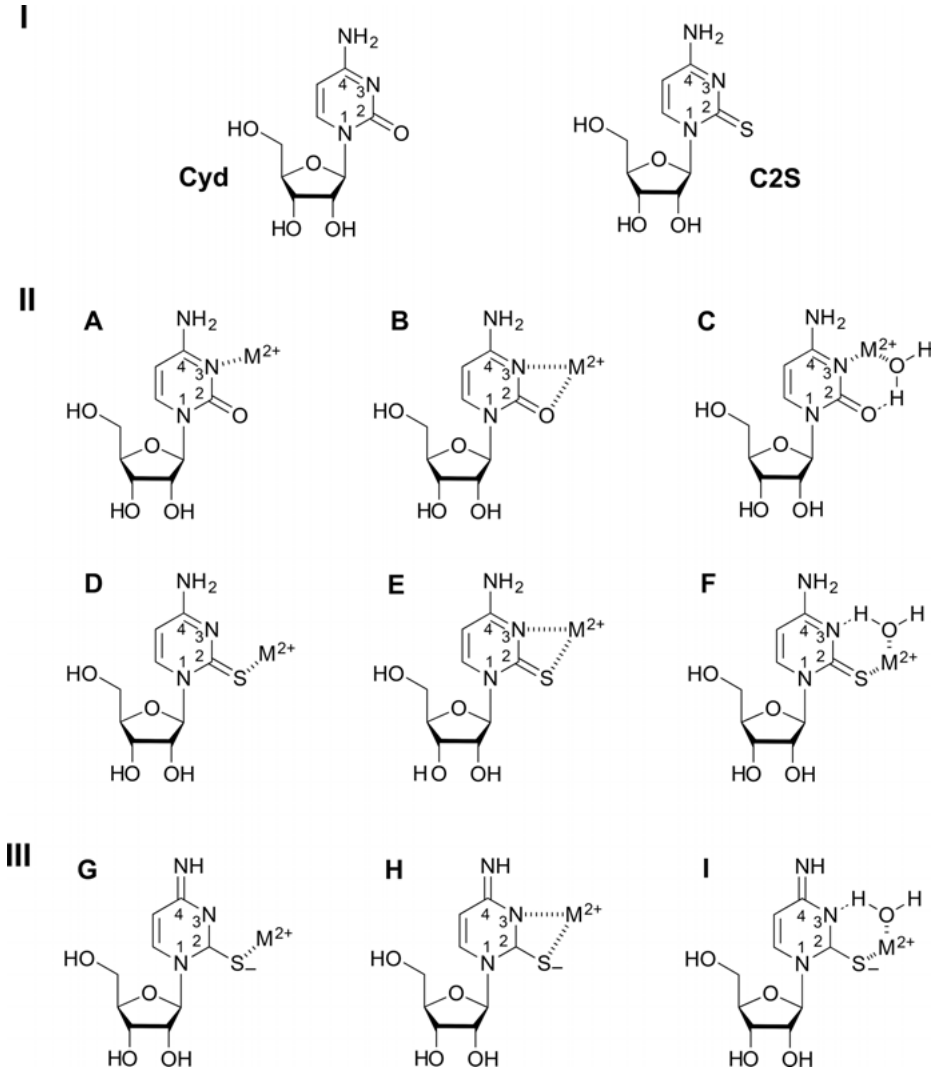

Figure 12. **Part I**: Chemical structures of cytidine (Cyd) and of its analogue 2-thiocytidine (C2S); both nucleosides are shown in their dominating *anti* conformation [22, 25]. **Part II**: Possible metal ion-binding modes in the chelates formed in equilibrium [Eq. (5)] in aqueous solution of the $M(Cyd)^{2+}$ (Structures B and C) and $M(C2S)^{2+}$ (E and F) complexes. Note the different primary binding sites in Structures A, B, C *versus* D, E, F (for details see [43]; further minority species are also possible [205]). **Part III**: Possible metal ion-binding modes of complexes formed with $(C2S - H)^{-}$ having a deprotonated $(C4)NH_2$ unit. In the $M(C2S - H)^{+}$ complexes is the charge mainly located on S, giving thus the primary $(C2)S^{-}$ binding site; this is emphasized in Structure G. Structures H and I indicate the two most likely chelated [Eq. (5)] species formed in aqueous solution [43, 206].

(C4)NH_2 group with pK_a = 12.65 [43, 206]; this contrasts with the properties of the parent nucleoside where the same reaction occurs with pK_a ca 16.7 [74]. The deprotonation and acidification of the (C4)NH_2 group by the (C2)S unit is connected with a redistribution of charge (cf. Part III of Figure 12) and the formation of a (C2)S^- site, which is attractive for metal ions (M^{2+}). Consequently, two types of complexes are formed, namely $M(C2S)^{2+}$ (Figure 12; Part II, Structures D, E, F) and $M(C2S - H)^+$ (Part III), whereas for the parent nucleoside only $M(Cyd)^{2+}$ species, formed with the neutral Cyd, exist (Part II; Structures A, B, C).

Evidently, for both types of C2S complexes N3 is no longer the primary binding site; this is now (C2)S (Figure 12; Part II; D, E, F) and (C2)S^- (Part III; G, H, I). Furthermore, it is clear that the stability of the $M(Cyd)^{2+}$ complexes is much lower than that of the C2S species; for example, $\log K^{Zn}_{Zn(Cyd)} = 0.20 \pm 0.11$, $\log K^{Zn}_{Zn(C2S)} = 2.53 \pm 0.04$, and $\log K^{Zn}_{Zn(C2S-H)} = 11.83 \pm 0.14$ [43]. Connected with the very high stability of the latter species is the fact that the $M(C2S - H)^+$ complexes form already at a very low pH. For example, the acidity constant for Equilibrium (24)

$$M(C2S)^{2+} \rightleftharpoons M(C2S - H)^+ + H^+ \qquad (24)$$

is pK_a ca 3.3 for Zn^{2+} and Cd^{2+} as metal ions (others have not been studied [206]). This demonstrates the very high affinity of Zn^{2+} and Cd^{2+} for thiolate sites. No values for the Pb^{2+}/C2S systems are available but one may assume that for Equilibrium (24) also a pK_a value close to 3.3 holds.

To conclude, the occurrence of C2S in tRNAs will strongly affect their properties, because, e.g., traces of Zn^{2+} will give rise to deprotonation reactions [Eq. (24)] already below the physiological pH range. In fact, even Mg^{2+} with a much smaller thiophilicity for (C)S^- sites is expected, due to electrostatic interactions, to achieve deprotonation in the physiological pH range [43].

4.6.3. Thiouridines

More than 100 different [208] modified derivatives of nucleosides are known from tRNAs and they occur in all organisms on this planet [209]. Thionucleosides are an important subgroup with 2-thiouridine (U2S) and 4-thiouridine (U4S) being especially prominent [208]. They occur, e.g., in *Escherichia coli* [210, 211] or in *Salmonella enterica* serovar Thyphimurium [203]. The ubiquitous presence of these modified nucleosides plays a pivotal role in the function of tRNAs [209] and therefore their coordination chemistry needs to be understood [43].

As can be seen from Part I in Figure 13, replacement of a carbonyl by a thione unit facilitates deprotonation of the (N3)H sites by about 1 to 2 pK units, the charge being then largely localized on the (C)S sites and this supports complex formation. For example [43], the stabilities of the $M(Urd - H)^+$ complexes with Ni^{2+}, Cu^{2+}, and Cd^{2+} are $\log K^M_{M(Urd-H)} = 1.70 \pm 0.07$, 4.13 ± 0.21, and 3.16 ± 0.04, respectively. The corresponding stabilities for the $M(U2S - H)^+$ complexes are again for Ni^{2+}, Cu^{2+} and Cd^{2+} $\log K^M_{M(U2S-H)} = 2.99 \pm 0.04$, 5.91 ± 0.06, and 4.11 ± 0.03, respectively. Hence, there is a stability enhancement

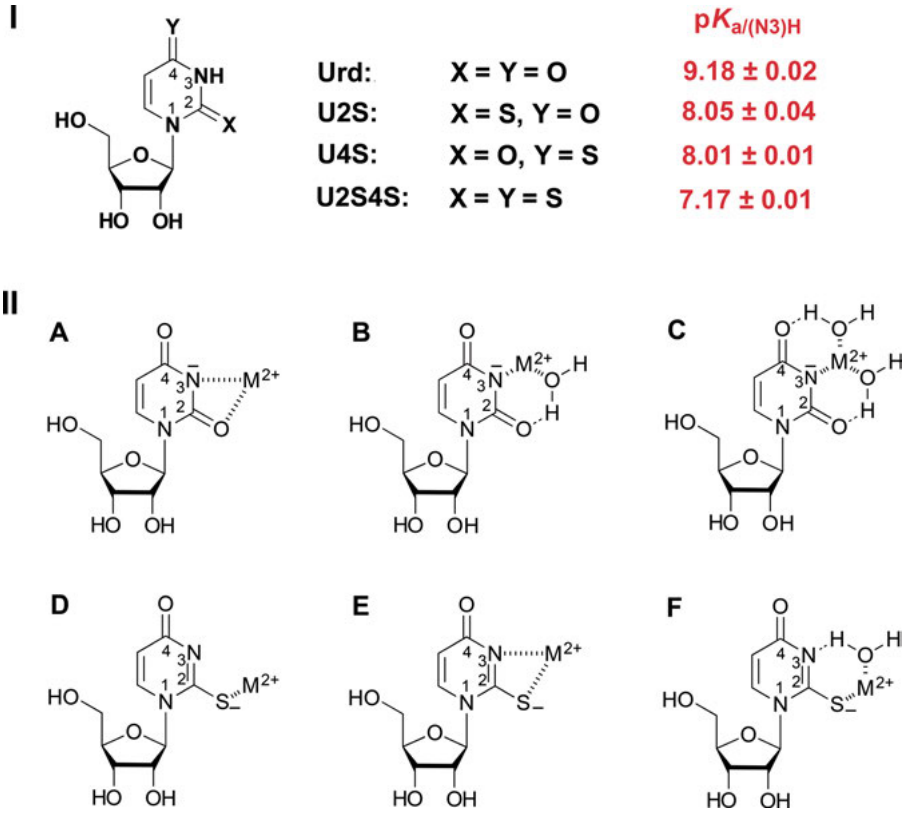

Figure 13. **Part I**: Chemical structures of uridine (Urd) (i.e., the parent nucleoside), 2-thiouridine (U2S), 4-thiouridine (U4S), and 2,4-dithiouridine (U2S4S). All nucleosides are shown in their dominating *anti* conformation [22, 25, 207]. The listed pK_a values refer for all uridines (U) shown to the deprotonation of the (N3)H site (the values are taken from a collection in [43]). The (N3)H deprotonated species are written in a general manner as $(U - H)^-$ to indicate that the uracil residue lost the proton. **Part II**: Possible metal ion-binding modes in the chelates formed in equilibrium [Eq. (5)] in aqueous solution of the $M(Urd - H)^+$ (Structures A, B, C) and $M(U2S - H)^+$ (E and F) complexes. The monodentate $(N3)^-$-M^{2+} isomer of $M(Urd - H)^+$ is not shown due to its expected low formation degree. Note the different primary binding sites in Structures A, B, C *versus* D, E, F (for details see [43]); further possible minority species are not shown [43, 115, 206].

of about 1 to 1.8 log units (despite the lower basicity of U2S compared to that of Urd). The difference is that in the $M(Urd - H)^+$ complexes $(N3)^-$ is the primary binding site (Figure 13, Part II; A, B, C), whereas in the $M(U2S - H)^+$ species it is the $(C2)S^-$ site (Part II; D, E, F).

With $(U4S - H)^-$ as ligand the situation is similar as described for $(U2S - H)^-$ except that Cu(II) is reduced to Cu(I) transforming the thiolate to a disulfide. This reduction also occurs with $(U2S4S - H)^-$. As indicated, in the $Cu(U2S - H)^+$

complex Cu(II) is stable, most likely due to steric constraints inhibiting disulfide formation [43].

The relatively high affinity of the (C)S sites for the indicated M^{2+} ions is reflected in the 2-thiouridine 5′-monophosphate ($U2SMP^{2-}$) and 4-thiouridine 5′-monophosphate ($U4SMP^{2-}$) complexes; in these complexes M^{2+} is located to more than 99 % at the thiouracil residue and only traces are coordinated at the phosphate group. In fact, in the $Cu[(U2S - H)MP]^-$ complex the ligand is partly transformed from the *anti* into the *syn* conformation allowing thus to some extent formation of a macrochelate [Eq. (5)]. The isomeric ligand $(U4S - H)MP^{3-}$ reduces Cu(II) again to Cu(I) [43, 207].

It is regrettable that no values for the corresponding Zn^{2+} complexes are available, but their properties are expected to be between those of the Ni^{2+} and Cd^{2+} complexes. The properties of the corresponding Pb^{2+} complexes are difficult to predict because Pb^{2+} is expected to be thiophilic and this would mean that the properties of its complexes are between those of the Cu^{2+} and Cd^{2+} complexes. To conclude, the presence of thiouridine residues in tRNAs will clearly affect the properties of these nucleic acids.

5. COMPLEXES OF LEAD(II) WITH PHOSPHATES

The structures of the phosphates to be discussed here are shown in Figure 14, that is, we consider the monoesters of triphosphate, diphosphate, and monophosphate (top to bottom). These residues may occur at the terminal end of nucleic acids [212, 213], but they are also part of nucleoside mono-, di-, or triphosphates (for the involved nucleobases see Figure 1) [27, 28]. The shorter the distance of the residue R to the (terminal) phosphate group, the larger is its influence on the basicity/acidity; e.g., monoprotonated phenylphosphate is less acidic ($pK_a = 5.85 \pm 0.01$ [86]) than monoprotonated 4-nitrophenyl phosphate ($pK_a = 5.05 \pm 0.01$ [86]) reflecting the influence of the residue R. This contrasts with the situation in a triphosphate where the residue R has practically no effect any more on the acid-base properties of the terminal γ-phosphate group [71, 73] (see Figure 14) which, in case it is protonated, has a pK_a of 6.50 ± 0.05 [71]. Note, the most basic phosphate group is always the terminal one, which therefore is also the most important one for metal ion coordination.

Of equal relevance, like the indicated mono-, di-, and triphosphates, is the phosphodiester bridge, which is part of the phosphate-sugar backbone of nucleic acids and of importance for metal ion binding of these macromolecules [106]. However, the basicity of such diester units, $(RO)_2P(O)_2^-$, is small, that is, for the corresponding monoprotonated unit the pK_a value is close to 1 [74, 75], whereas the pK_a values for monoprotonated mono-, di-, and triphosphate residues (Figure 14) are close to 6.2, 6.4, and 6.5, respectively [60].

In accord with the low basicity of the $(RO)_2P(O)_2^-$, unit is its small affinity for metal ions, which, in fact, is difficult to measure [106]. Experience shows [30, 60, 106] that the metal ion affinity of $(RO)_2P(O)_2^-$ is relatively well mimicked by acetate (Ac^-) or formate ($HCOO^-$), and this despite the relatively low acidity of

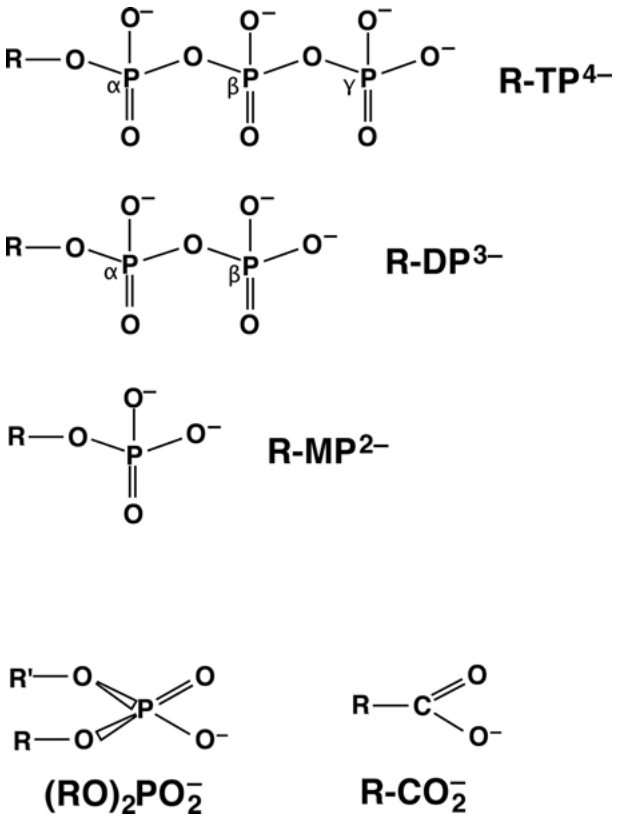

Figure 14. Chemical structures of simple monoesters of triphosphate ($R\text{-}TP^{4-}$), diphosphate ($R\text{-}DP^{3-}$), and monophosphate ($R\text{-}MP^{2-}$), as well as of the phosphodiester bridge ($(RO)_2PO_2^-$) as it occurs in nucleic acids and of its primitive and simple mimic carboxylate ($R\text{-}CO_2^-$). R represents in all instances a residue which does not affect metal ion coordination at the phosphate or carboxylate groups, i.e., neither in a positive nor negative sense. The labeling system of the di- and triphosphate chain is also indicated; note that e.g., the phosphate groups in $R\text{-}TP^{4-}$ are labeled α, β, γ, where γ refers to the terminal phosphate group.

H(Ac) ($pK^{H}_{H(Ac)}$ = ca 4.6 [62]) compared to that of $(RO)_2P(O)(OH)$ (pK_a ca 1; see above). The reason that this mimicry works is that the slopes of $\log K^{M}_{M(R\text{-}COO)}$ *versus* $pK^{H}_{H(R\text{-}COO)}$ plots are small, e.g., for the Ca^{2+}, Cu^{2+}, and Zn^{2+} complexes they are $m_{Ca} = 0.197 \pm 0.023$, $m_{Cu} = 0.169 \pm 0.025$, and $m_{Zn} = 0.060 \pm 0.022$, respectively [the intercepts b differ of course; see Eq. (10)] (25 °C, $I = 0.1$ M) [62]; no data are available for Pb^{2+} at this ionic strength [62] (see also Section 3.4). The fact that the slopes of the $Ca(R\text{-}COO)^+$ and $Cu(R\text{-}COO)^+$ complexes are within the error limits identical and, furthermore, the very low value for $Zn(R\text{-}COO)^+$ indicate that outersphere complexes are important. This suggestion agrees with the earlier conclusion [214], "the lower the charge, the more predominant are outersphere complexes".

To mediate a feeling for the stabilities of the complexes of the discussed ligands (Figure 14) we have plotted the log $K^{M}_{M(R\text{-}P)}$ values (R-P represents the ligands of Figure 14) in an Irving-Williams-type fashion in Figure 15. It is immediately evident that the Irving-Williams series [36, 37] is not strictly followed, but for phosph(on)ate ligands this was observed repeatedly before [49, 87, 143, 204, 215–217], that is, the Mn(R-P) complexes are more stable than the corresponding Ni(R-P) species. There are two points immediately evident from Figure 15: (i) Complex stability increases from the $M(Ac)^{+}$ complexes (the mimics) to the M(R-MP) complexes by about 1 log unit, the next step from M(R-MP) to $M(R\text{-}DP)^{-}$ encompasses about 2 log units and the final one to the triphosphate complexes, $M(R\text{-}TP)^{2-}$, amounts again to about 1 log unit. The large step of about 2 log units reflects the fact that from M(R-MP) to $M(R\text{-}DP)^{-}$ chelate formation becomes essential. (ii) The stabilities of the Cu^{2+} and Pb^{2+} complexes are in each series very close to each other, what confirms the conclusion of Section 2.2 that the affinity of Pb^{2+} towards O-donors is pronounced and comparable to that of Cu^{2+}. In other words, Cu(II)-O-donor complexes can be considered as mimics regarding the stabilities of the corresponding Pb^{2+} complexes if these are not known [10].

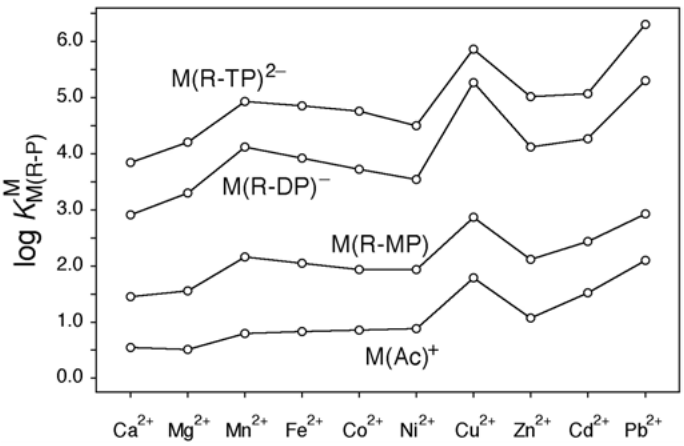

Figure 15. Irving-Williams sequence-type plots [36, 37] for the 1:1 complexes of Ca^{2+} through Zn^{2+} plus Cd^{2+} and Pb^{2+} formed with mono- ($R\text{-}MP^{2-}$), di- ($R\text{-}DP^{3-}$), and triphosphate monoesters ($R\text{-}TP^{4-}$) as well as of those for acetate (Ac^{-}), which is used as a simple mimic (see text) for the $(RO)_2PO_2^{-}$ unit. The abbreviation R-P represents all four ligands. The plotted data of the phosphate ligands are from table 13 of [144]; those for the corresponding Cd^{2+} and Pb^{2+} complexes are from [215] and [10], respectively. These values also represent the stability constants for the M^{2+} complexes of the pyrimidine-nucleoside 5′-mono-, di- or triphosphates (except for $Cu(CTP)^{2-}$ [113, 215]) (25 °C; $I = 0.1$ M, $NaNO_3$). The log stability constants of the $M(Ac)^{+}$ complexes are collected from [38]; log $K^{M}_{M(Ac)}$ is given in parentheses after the symbol of the metal ion: Ca^{2+} (0.55 ± 0.07), Mg^{2+} (0.51 ± 0.05), Mn^{2+} (0.80 ± 0.1; error estimated), Fe^{2+} (0.83 ± 0.06; estimated value), Co^{2+} (0.86 ± 0.05), Ni^{2+} (0.88 ± 0.05), Cu^{2+} (1.79 ± 0.06), Zn^{2+} (1.07 ± 0.07), Cd^{2+} (1.52 ± 0.10), and Pb^{2+} (2.10 ± 0.10) (25 °C; $I = 0.1$ M).

To emphasize the above conclusions somewhat further, the stability constants for most metal ions used in Figure 15 are listed in the top part of Table 6 [62, 74, 75, 106, 144, 218]. It may be mentioned here that pyrimidine-nucleoside 5′-phosphates furnish representative values for comparisons because the pyrimidine nucleobases do not participate in complex formation of the ligands in question (the sole exception being $Cu(CTP)^{2-}$ [216, 217]). In other words, the pyrimidine nucleobases fulfill the request made for R (see legend of Figure 14), that this residue does not affect complex formation at the phosphate residue, neither in a positive nor in a negative manner [144, 215–217].

Table 6. Comparison of the stability constants [Eq. (2)] of M^{2+} complexes formed with acetate (Ac^-), as a simple mimic of the phosphodiester bridge (Figure 14), mono- (R-MP^{2-}), di- (R-DP^{3-}), and triphosphate monoesters (R-TP^{4-}) in aqueous solution at 25 °C and $I = 0.1$ M ($NaNO_3$), together with the corresponding stability differences (lower part) as they follow from the data listed in neighboring columns.[a,b,c]

M^{2+}	log $K^{M}_{M(L)}$ [Eq. (2)] for L =			
	Ac^-	R-MP^{2-}	R-DP^{3-}	R-TP^{4-}
H^+	(4.56 ± 0.03)[d,e]	6.20[d]	6.40[d]	6.50[d]
Ca^{2+}	0.55 ± 0.07	1.45 ± 0.05	2.91 ± 0.03	3.84 ± 0.05
Mn^{2+}	0.80 ± 0.10	2.16 ± 0.05	4.12 ± 0.03	4.93 ± 0.03
Ni^{2+}	0.88 ± 0.05	1.94 ± 0.05	3.54 ± 0.06	4.50 ± 0.03
Cu^{2+}	1.79 ± 0.06	2.87 ± 0.06	5.27 ± 0.04	5.86 ± 0.03
Zn^{2+}	1.07 ± 0.07	2.12 ± 0.06	4.12 ± 0.03	5.02 ± 0.02
Cd^{2+}	1.52 ± 0.10	2.44 ± 0.05	4.27 ± 0.03	5.07 ± 0.03
Pb^{2+}	2.10 ± 0.10	2.93 ± 0.08	5.30 ± 0.15	6.30 ± 0.25

M^{2+}	log $\Delta_{R\text{-}MP/Ac}$	log $\Delta_{R\text{-}DP/R\text{-}MP}$	log $\Delta_{R\text{-}TP/R\text{-}DP}$
Ca^{2+}	0.90 ± 0.09	1.46 ± 0.06	0.93 ± 0.06
Mn^{2+}	1.36 ± 0.11	1.96 ± 0.06	0.81 ± 0.04
Ni^{2+}	1.06 ± 0.07	1.60 ± 0.08	0.96 ± 0.07
Cu^{2+}	1.08 ± 0.08	2.40 ± 0.07	0.59 ± 0.05
Zn^{2+}	1.05 ± 0.09	2.00 ± 0.07	0.90 ± 0.04
Cd^{2+}	0.92 ± 0.11	1.83 ± 0.07	0.80 ± 0.04
Pb^{2+}	0.83 ± 0.13	2.37 ± 0.17	1.00 ± 0.29

[a] For the error limits see footnote "a" of Table 4 as far as our own data are concerned; the error limits of the derived data were calculated according to the error propagation after Gauss.

[b] For the constants of the $M(Ac)^+$ complexes see legend of Figure 15.

[c] The values for the M(R-MP), the $M(R\text{-}DP)^-$, and the $M(R\text{-}TP)^{2-}$ complexes are from the same sources, given in the legend for Figure 15.

[d] These values are the acidity constants [144] of the monoprotonated ligands and refer to $pK^{H}_{H(L)}$ [Eq. (3)]. The value for $pK^{H}_{H(Ac)}$ is from [62].

[e] The pK_a value of $(RO)_2P(O)(OH)$ is ca 1 [74, 75, 218]; despite the pK_a difference acetate mimics the complex stabilities of the $M[(RO)_2(PO_2)]^+$ species relatively well [106] (see also text).

It is amazing to note that, despite the differences in the absolute stabilities of the complexes within a given series (upper part of Table 6), the differences between two neighboring columns (listed in the lower part) are quite constant. The average value for log $\Delta_{\text{R-MP/Ac}} = 1.03 \pm 0.20$ (3 σ) encompasses within the error limits all listed values. For the average of log $\Delta_{\text{R-DP/R-MP}} = 2.03 \pm 0.38$ (3 σ) the value for the Ca^{2+} complexes drops out somewhat and it is therefore not part of the given average. However, for log $\Delta_{\text{R-TP/R-DP}} = 0.90 \pm 0.10$ (3 σ) (calculated without the Cu^{2+} value) the difference is much smaller again and all values are quite alike despite the large span in complex stability between ca 3.8 and 6.3 log units which includes the value for Pb^{2+}. That log $\Delta_{\text{R-TP/R-DP}} = 0.59 \pm 0.05$ for the Cu^{2+} complexes is significantly smaller than the average value (0.90 ± 0.10) is understandable because due to steric reasons the equatorial sites of the Jahn-Teller-distorted Cu^{2+} coordination sphere cannot accommodate all three phosphate units of the triphosphate residue; this is possible for a metal ion with an octahedral or otherwise adaptable coordination sphere, like the one of Pb^{2+}.

6. LEAD(II) COMPLEXES OF NUCLEOTIDES

6.1. Some General Comments

The coordination of Mg^{2+} to ATP was depicted by Szent-Györgyi in the form of a macrochelate [219]. This suggestion from 1956 is by now 60 years old, but ever since it has fascinated coordination chemists, despite the fact that the structure shown by Szent-Györgyi has very little to do with reality because the Mg^{2+}-binding phosphate units are given in a protonated form and the $(C6)NH_2$ group is also employed as a binding site [106]. However, already more than 50 years ago the existence of macrochelates was proven by several methods [220–223]. Today, at least for kinetically labile metal ions, it is generally accepted that the phosphate residue is the primary binding site and that chelate formation, as indicated in Equilibrium (25), occurs via N7 in the case of purine derivatives (e.g., [116, 144, 217, 224]).

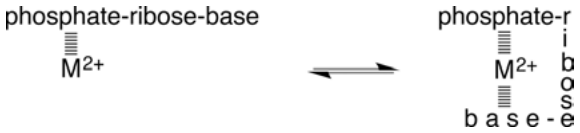

(25a)

$$M(NP)_{op} \rightleftharpoons M(NP)_{cl} \qquad (25b)$$

In this section Equilibrium (25), where NP = nucleoside phosphate, replaces Equilibrium (5) to make the actual structures more evident. In the previously defined Eqs (6) through (12), the general symbol L (for ligand) is to be replaced by NP = NMP^{2-}, NDP^{3-} or NTP^{4-} (Figure 16) to comply with the generally employed symbolism which is also used in this section in presenting the data.

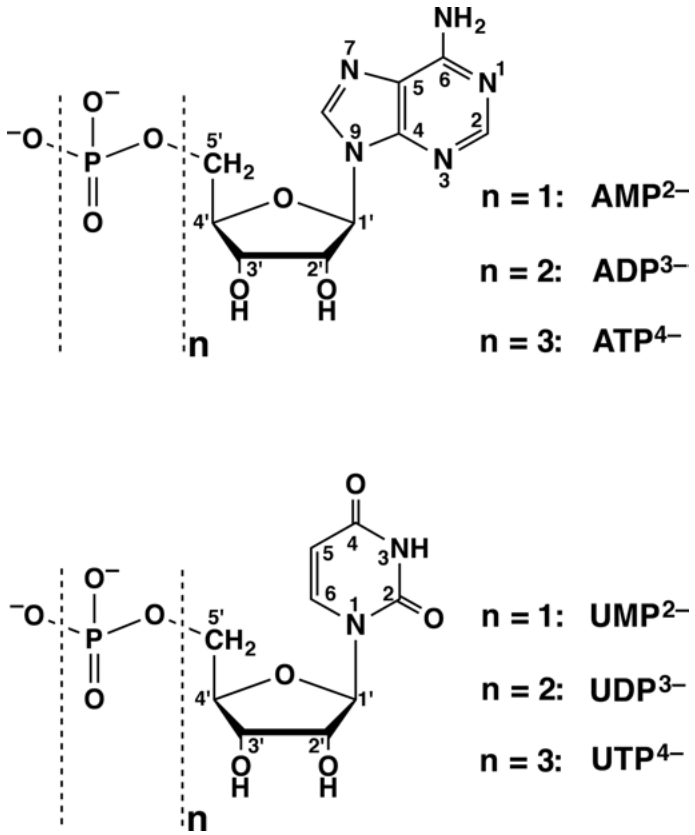

Figure 16. Chemical structures of adenosine 5′-monophosphate (n = 1: AMP^{2-}), adenosine 5′-diphosphate (n = 2: ADP^{3-}), and adenosine 5′-triphosphate (n = 3: ATP^{4-}) as well as of uridine 5′-monophosphate (n = 1: UMP^{2-}), uridine 5′-diphosphate (n = 2: UDP^{3-}), and uridine 5′-triphosphate (n = 3: UTP^{4-}) in their dominating *anti* conformation [22–25, 28]. Note, the triphosphate chain in nucleoside 5′-triphosphates (NTP^{4-}) is labeled α, β, and γ, where γ refers to the terminal phosphate group (see also Figure 14); for nucleoside 5′-diphosphates (NDP^{3-}) the situation is analogous with α and β (see Figure 14). The adenine and uracil residues in the nucleotide structures shown above may be replaced by one of the other nucleobase residues shown in Figure 1; if this substitution is done in the way the bases are depicted within the plane (Figure 1), then the *anti* conformation will also result for the corresponding nucleoside 5′-phosphates. The abbreviations AMP^{2-}, ADP^{3-}, ATP^{4-}, IMP^{2-}, etc. in this text always represent the 5′-derivatives; 2′- and 3′-derivatives are defined by $2'AMP^{2-}$, $3'AMP^{2-}$, etc.; in a few instances where uncertainties might otherwise occur, the abbreviations $5'AMP^{2-}$, $5'ADP^{3-}$, etc. are also used.

Figure 16 shows typical examples of purine and pyrimidine nucleotides in their dominating *anti* conformation (see legend of Figure 1). At a glance it is thus evident, that the adenosine and other purine-nucleoside phosphates may form macrochelates via N7, the extent being dependent on the metal ion involved [Eq. (25)]. This contrasts with the situation of the uridine and other pyrimidine-

nucleoside phosphates, which are also given in their dominating *anti* conformation, but now the potential binding sites at the nucleobase residue are pointing away from a metal ion coordinated at the phosphate residue, thus preventing macrochelate formation.

Generally speaking, purine nucleotides are in the conformation needed for macrochelate formation, whereas pyrimidine nucleotides are not. This implies that the pyrimidine nucleotides represent the stability of the open isomer in Equilibrium (25) (see also Section 5). In the next section we shall now first discuss pyrimidine derivatives.

6.2. Complexes of Pyrimidine-Nucleoside 5′-Monophosphates

Here cytidine 5′-monophosphate (CMP^{2-}), uridine 5′-monophosphate (UMP^{2-}) and thymidine [= 1-(2-deoxy-β-D-ribofuranosyl)thymine] 5′-monophosphate ($dTMP^{2-}$) plus D-ribose 5-monophosphate ($RibMP^{2-}$) are to be considered; the structures of all four phosphate monoesters are evident from the information provided in Figures 16 and 1. Because the distance between the nucleobase residue and the phosphate group is small, the acidity constants of the monoprotonated forms, $H(NMP)^-$, vary slightly; they are listed in column 2 of Table 7 and the stability constants of the corresponding Pb(NMP) complexes are provided in column 4.

With regard to the discussion in the preceding Section 6.1, the question to be asked first is: Does the pyrimidine residue participate in complex formation?

Table 7. Acidity constants of monoprotonated pyrimidine-NMPs [analogous to Eq. (3)] and stability constants of their Pb(NMP) complexes [Eq. (2)]. The corresponding data are also given for $H(RibMP)^-$ (aq. sol.; 25 °C; I = 0.1 M, $NaNO_3$).[a]

$H(NMP)^-$	$pK^H_{H(NMP)}$	pK^H_{NMP}	$\log K^{Pb}_{Pb(NMP)}$	$\log K^{Pb}_{Pb(NMP)calc}$	$\log \Delta_{Pb/NMP}$[e]
$H(RibMP)^-$	6.24 ± 0.01		3.01 ± 0.05	2.95 ± 0.08[d]	0.06 ± 0.09
$H(CMP)^-$	6.19 ± 0.02[b]		2.93 ± 0.04	2.93 ± 0.08[d]	0.00 ± 0.09
$H(UMP)^-$	6.15 ± 0.01	9.45 ± 0.02[c]	2.80 ± 0.04	2.91 ± 0.08[d]	–0.11 ± 0.09
$H(dTMP)^-$	6.36 ± 0.01	9.90 ± 0.03[c]	2.93 ± 0.03	3.01 ± 0.08[d]	–0.08 ± 0.09

[a] For the error limits see footnotes "a" of Tables 4 and 6. In this table NMP^{2-} includes $RibMP^{2-}$ = D-ribose 5-monophosphate. For the structures of the nucleobase residues see Figure 1; if the 5′(CH_2)-OH group of the ribosyl residue is phosphorylated, the NMPs are obtained. All constants listed above and also in the footnotes below are collected from information provided in [114], aside from the pK_a values given in the third column [86].

[b] In $H_2(CMP)^{\pm}$ the N3 site is protonated; deprotonation occurs with $pK^H_{H_2(CMP)}$ = 4.33 ± 0.04. The stability constant of the $Pb(H;CMP)^+$ complex and the acidity constant of the same species are also known, that is, $\log K^{Pb}_{Pb(H;CMP)} = 1.55 \pm 0.09$ and $pK^H_{Pb(H;CMP)} = 4.81 \pm 0.10$, respectively.

[c] These values refer to the deprotonation of the (N3)H sites in NMP^{2-} (see Figure 1).

[d] Calculated with the $pK^H_{H(NMP)}$ values (see above) and the straight-line parameters defined in Eq. (26). Note, $R\text{-}PO_3^{2-}$ is a phosphate monoester with a non-interacting residue R.

[e] See Eq. (12).

Because the parameters for the straight-line plot of log $K^{Pb}_{Pb(R\text{-}PO_3)}$ *versus* $pK^{H}_{H(R\text{-}PO_3)}$ have previously been determined [114] for R-PO_3^{2-} = phosphate monoesters or phosphonates, where R does not interact with Pb^{2+}, the expected values can be calculated (see below). The corresponding straight-line equation is defined by Eq. (26) [see also Eq. (10)]:

$$\log K^{Pb}_{Pb(R\text{-}PO_3)} = (0.493 \pm 0.033) \cdot pK^{H}_{H(R\text{-}PO_3)} - (0.122 \pm 0.213) \qquad (26)$$

Values calculated in the $pK^{H}_{H(R\text{-}PO_3)}$ range of about 4.5 to 8 for the stability of a Pb(R-PO_3) complex, log $K^{Pb}_{Pb(R\text{-}PO_3)}$, have an error of about ± 0.08 log unit (3σ).

Application of the acidity constants of column 2 in Table 7 to Eq. (26) leads to the calculated stability constants of the Pb(NMP) complexes listed in column 5. Comparison according to Eq. (12) between the measured and calculated stability constants leads to the log $\Delta_{Pb/NMP}$ values given in the terminating column of Table 7. It is evident that the measured and calculated constants being identical within their error limits prove that the pyrimidine residue does not affect metal ion coordination at the phosphate residue. This also holds for the sugar moiety in Pb(RibMP).

The $Pb^{2+}/CMP^{2-}/H^+$ system deserves a special comment: The acidity constant of $H_2(CMP)^{\pm}$ for the release of the proton from $(N3)H^+$ is $pK^{H}_{H_2(CMP)} = 4.33 \pm 0.04$ [114]. In fact, also a monoprotonated $Pb(H;CMP)^+$ complex exists from which the proton is released with $pK^{H}_{Pb(H;CMP)} = 4.81 \pm 0.10$ (see Table 7, footnote). This means, the complex is less acidic than the ligand; in other words, $pK^{H}_{Pb(H;CMP)} = 4.81$ is above $pK^{H}_{H_2(CMP)} = 4.33$ but below $pK^{H}_{H(CMP)} = 6.19$ (Table 7). This indicates that Pb^{2+} is largely coordinated at the N3/(C2)O site and the proton at the phosphate group. Indeed, a careful evaluation via micro stability constants [10] reveals that about 90 % of the protonated $Pb(H;CMP)^+$ species exist in form of the $(Pb \cdot CMP \cdot H)^+$ isomer, and the remaining 10 % are present as the $(CMP \cdot Pb \cdot H)^+$ isomer, with both, Pb^{2+} and H^+ at the phosphate group. This is different in the gas phase, as shown by combining electrospray ionization (ESI), tandem mass spectrometry, and mid-infrared multiple-photon dissociation (IRMPD) spectroscopy [136], where $Pb(H;CMP)^+$ forms a macrochelate "in which the Pb^{2+} ion not only interacts with the (monoprotonated) phosphate group but also with the carbonyl group", that is, (C2)O of the cytosine moiety [136] (see also Section 4.3).

In the above context it is also worthwhile to note that in aqueous solution "in a first approximation Pb^{2+} has comparable affinities for the single negatively charged" phosphodiester bridge of a nucleic acid backbone [114] and for the cytosine residue. This is evidenced by the stability constant of the $Pb(H_2PO_4)^+$ complex, log $K^{Pb}_{Pb(H_2PO_4)} = 1.5 \pm 0.5$ (25 °C; $I = 0$ M) [225], $(HO)_2P(O)_2^-$ being a mimic of $(RO)_2P(O)_2^-$, and the micro stability constant for Pb^{2+} binding to the N3/(C2)O site, log $k^{Pb}_{Pb \cdot CMP \cdot H} = 1.65 \pm 0.2$ (25 °C; $I = 0.1$ M) [114]. As far as the given estimate and mimic for the affinity of Pb^{2+} towards the phosphodiester bridge is concerned, log $K^{Pb}_{Pb[(RO)_2P(O)_2]} = 1.5 \pm 0.5$, a caveat is appropriate: The mentioned value is possibly too large due to its extrapolation towards an ionic strength of zero [10]; other values in the literature are 0.7 ± 0.4 (25 °C; $I = 0.1$ M)

[107] and 0.9 ($\pm$ 0.35) (25 °C; $I = 0.1$ M) [106], but see also Figure 15. Though lead(IV) is not in the focus here, we may add that the stability constant for the interaction between $(CH_3)_3Pb^+$ and HPO_4^{2-} has been determined: $\log K^{(CH_3)_3Pb}_{(CH_3)_3Pb(HPO_4)} = 1.88$ (aq. sol.; 25 °C; $I = 0.3$ M) [226].

Neutral uracil and thymine residues, in contrast to the neutral cytosine moiety ($\log K^{Pb}_{Pb(Cyd)} = 1.20 \pm 0.07$; 25 °C; $I = 0.1$ M) [114], have a vanishing affinity towards Pb^{2+} because "isolated" carbonyl units are quite generally poor binding sites; this changes only after deprotonation of the (N3)H site (Section 4.4). Yet, in the gas phase the situation is different [138]: By application of the already mentioned methods [136], it was concluded for $Pb(H;UMP)^+$ "that Pb^{2+} ions interact not only with the (monoprotonated) phosphate group but also with a carbonyl group of the nucleobase moiety by folding of the mononucleotide, resulting in macrochelates" [138]. It is further suggested "that the ESI-generated complex likely corresponds to a mixture of several structures", including enolic tautomers [138] (see also Section 4.4).

From the results summarized in Table 7 we have seen that in Pb(UMP) complexes the uracil residue is not involved in metal ion binding and this holds quite generally for M(UMP) species in aqueous solution. However, replacement of the (C2)O or (C4)O units by (C2)S or (C4)S changes (see Figure 17) the situation drastically [43]; now, dependent on the kind of metal ion the thionucleobase residues become heavily involved. Unfortunately, no data for Pb^{2+} complexes are available; only Ni^{2+} and Cd^{2+} complexes have been studied [43, 207], as well as some Cu^{2+} species but with Cu^{2+} the studies are hampered due to redox reactions [43, 192]. We concentrate now on a few results obtained for Cd^{2+}

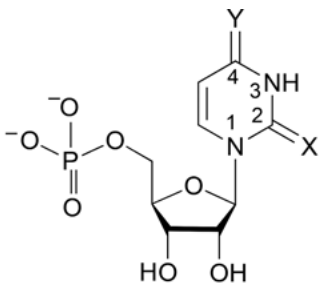

UMP^{2-}: X = Y = O
$U2SMP^{2-}$: X = S, Y = O
$U4SMP^{2-}$: X = O, Y = S

Figure 17. Chemical structures of uridine 5′-monophosphate (UMP^{2-}) and of its thio derivatives, 2-thiouridine 5′-monophosphate ($U2SMP^{2-}$) and 4-thiouridine 5′-monophosphate ($U4SMP^{2-}$) shown in their dominating *anti* conformation [22, 25]. Deprotonation of the thiouridine 5′-monophosphates ($USMP^{2-}$) at the (N3)H site leads to 3-fold negatively charged species which are written as $((US - H)MP)^{3-}$ to indicate that the proton is released from the thiouracil residue [206].

species though it is uncertain to which extent these are able to mimic the Pb^{2+} complexes (see also the two terminating paragraphs of Section 4.6.3).

The large affinity of Cd^{2+} for the thio sites becomes evident from the (N3)-deprotonated species which give rise to thiolate sites in the presence of a monoprotonated phosphate group; for U2SMP^{2-} (Figure 17) the complex is best written as Cd · (U2S – H)MP · H, to indicate that Cd^{2+} is at the deprotonated nucleobase and H^+ at the phosphate group. The indicated species reaches a formation degree of 99.2 ± 0.2 % [43]; that is, the (U2S)MP · Cd isomer occurs only in traces. For the Cd^{2+} nucleobase-bound Cd · (U4S – H)MP · H isomer the situation is very similar, with a formation degree of 99.5 ± 0.1 %. It is now interesting to note that deprotonation gives rise to [Cd(U4S – H)MP]$^-$ which occurs with a formation degree of 99 %, only 1 % being present as [(U4S – H)MP · M]$^-$ and no indication for any chelate formation involving both, the phosphate group and the nucleobase moiety, is observed [43]. The latter was only indicated with (U2S – H)MP^{3-}, where the chelated Cd[(U2S – H)MP]$^-_{cl}$ species occurs with roughly 22 % and the open one with 78 %; of these about 77 % are present as [Cd · (U2S – H)MP]$^-$ and only 1 % as [(U2S – H)MP · Cd]$^-$; note, two 'open' isomers occur here in contrast to the situation described in Equilibrium (25). From the indicated observations follows that a metal ion at the (C4)S site cannot reach the phosphate group, whereas a metal ion at the (C2S) site is able to do so; whether this latter interaction with the phosphate group occurs in an inner-sphere or outersphere manner is not known. How Pb^{2+} behaves is difficult to predict: Does its thiophilicity or its O donor affinity dominate?

6.3. Complexes of Purine-Nucleoside 5′-Monophosphates

The focus in this section is on adenosine 5′-monophosphate (AMP^{2-}) and guanosine 5′-monophosphate (GMP^{2-}) (Figures 16 and 1) because they are not only important nucleotides, but also important units in nucleic acids. For the evaluation of these systems we need the definitions summarized in Section 6.1, including the acidity constants to Eq. (3), plus two more acidity constants. These constants refer to $H_2(NMP)^{\pm}$, which carries the (N7)H^+ unit, as well as to NMP^{2-}, regarding the deprotonation of the (N1)H site (e.g., in GMP^{2-}), and they are defined according to Eqs (27) and (28), respectively:

$$H_2(NMP)^{\pm} \rightleftharpoons H(NMP)^- + H^+ \tag{27a}$$

$$K^H_{H_2(NMP)} = [H(NMP)^-][H^+]/[H_2(NMP)^{\pm}] \tag{27b}$$

$$NMP^{2-} \rightleftharpoons (NMP - H)^{3-} + H^+ \tag{28a}$$

$$K^H_{H_2(NMP)} = [(NMP - H)^{3-}][H^+]/[(NMP)^{2-}] \tag{28b}$$

To provide an impression of the situation we have plotted in Figure 18 log $K^M_{M(R\text{-}PO_3)}$/log $K^M_{M(NMP)}$ *versus* p$K^H_{H(R\text{-}PO_3)}$/p$K^H_{H(NMP)}$ for the metal ions Pb^{2+},

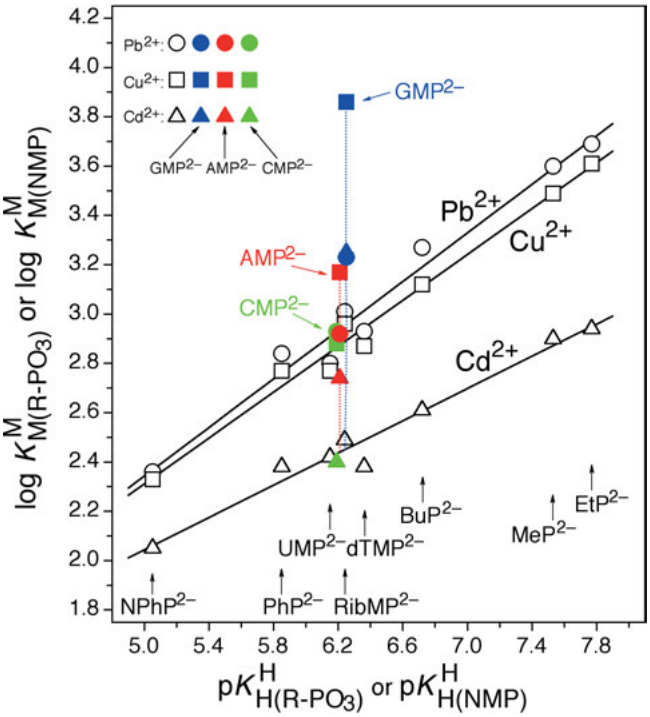

Figure 18. Evidence for an enhanced stability of the Pb^{2+}, Cu^{2+} and Cd^{2+} 1:1 complexes [Eqs (2) and (6)] of GMP^{2-} (blue) and AMP^{2-} (red), as well as evidence of a non-affected (i.e., not increased) complex stability with CMP^{2-} (green), based on the relationship between log $K^{M}_{M(R\text{-}PO_3)}$ and $pK^{H}_{H(R\text{-}PO_3)}$ for $M(R\text{-}PO_3)$ complexes of some simple phosphate monoester and phosphonate ligands ($R\text{-}PO_3^{2-}$) (empty symbols): 4-nitrophenyl phosphate ($NPhP^{2-}$), phenyl phosphate (PhP^{2-}), uridine 5′-monophosphate (UMP^{2-}), D-ribose 5-monophosphate ($RibMP^{2-}$), thymidine (= 1-(2′-deoxy-β-D-ribofuranosyl)thymine) 5′-monophosphate ($dTMP^{2-}$), *n*-butyl phosphate (BuP^{2-}), methanephosphonate (MeP^{2-}), and ethanephosphonate (EtP^{2-}) (from left to right). The least-squares straight lines [Eq. (10)] are drawn through the corresponding eight data sets (○,□,△) taken from [86] for the phosphate monoesters and from [87] for the phosphonates. The straight-line parameters are listed in [28, 85, 87, 116]. The points due to the equilibrium constants for the M^{2+}/NMP systems (colored symbols) are based on the values listed in Table 8; the M^{2+}/CMP values are from [86]. The equilibrium data for the Pb^{2+}/NMP systems (fully colored circles) are from [107]. These results are discussed in Section 6.3. The vertical dotted lines emphasize the stability differences to the reference lines; they equal log $\Delta_{M/NMP}$ as defined in Eq. (12) for the M(NMP) complexes. All the plotted equilibrium constants refer to aqueous solutions at 25°C and $I = 0.1$ M ($NaNO_3$).

Cu^{2+}, and Cd^{2+}. The straight-reference lines are defined by complexes of $R\text{-}PO_3^{2-}$ ligands, where R is a non-interacting residue (see legend of Figure 18). It is immediately evident that the reference lines for the Pb^{2+} and Cu^{2+} complexes are close together, in accord with observations described in Sections 3.3 and 3.4. The parameters of the straight-reference line for $Pb(R\text{-}PO_3)$ complexes are given in Eq. (26); those for $Cu(R\text{-}PO_3)$ complexes are provided in Eq. (29):

$$\log K^{Cu}_{Cu(R\text{-}PO_3)} = (0.465 \pm 0.025) \cdot pK^{H}_{H(R\text{-}PO_3)} - (0.015 \pm 0.164) \quad (29)$$

The error limits for stability constants calculated in the pK_a range seen in Figure 18 amount to ± 0.06 log unit (3σ) [87].

It is worth noting that the parameters for the slope *m* and the intercept *b* [Eq. (10)] for the two Eqs (26) and (29) overlap within their error limits in accord with the *Stability Ruler* (Section 2.2). To emphasize this fact further, we note that the data of Figure 18 span the pK_a range of about 5.0 to 7.8; therefore, we calculate for these two "extremes" the stability constants for the $Pb(R\text{-}PO_3)$ and $Cu(R\text{-}PO_3)$ complexes plus the ones for $pK_a = 6.2$ because this value is close to the acidity constants of many monoprotonated nucleoside 5′-monophosphates [27, 28, 85, 107, 114, 116] (see also Figure 18). The results of these calculations are given in Eqs (30) through (32):

$$pK^{H}_{H(R\text{-}PO_3)} = 5.00: \quad \log K^{Pb}_{Pb(R\text{-}PO_3)} = 2.34 \pm 0.08 \text{ and} \quad (30a)$$

$$\log K^{Cu}_{Cu(R\text{-}PO_3)} = 2.31 \pm 0.06 \quad (30b)$$

$$pK^{H}_{H(R\text{-}PO_3)} = 6.20: \quad \log K^{Pb}_{Pb(R\text{-}PO_3)} = 2.93 \pm 0.08 \text{ and} \quad (31a)$$

$$\log K^{Cu}_{Cu(R\text{-}PO_3)} = 2.87 \pm 0.06 \quad (31b)$$

$$pK^{H}_{H(R\text{-}PO_3)} = 7.80: \quad \log K^{Pb}_{Pb(R\text{-}PO_3)} = 3.72 \pm 0.08 \text{ and} \quad (32a)$$

$$\log K^{Cu}_{Cu(R\text{-}PO_3)} = 3.61 \pm 0.06 \quad (32b)$$

These results confirm the validity of the *Stability Ruler* (Section 2.2) and the conclusion that Pb^{2+} has about the same affinity towards O donor sites as Cu^{2+}. Furthermore, they provide the necessary confidence to derive stability constants for diphosphate ($R\text{-}DP^{3-}$) and triphosphate ($R\text{-}TP^{4-}$) monoesters (see Section 6.5).

For the complexes of pyrimidine-nucleoside 5′-monophosphates it was concluded in Section 6.2, in accord with results given in Section 5, that the stability of the complexes is solely determined by the metal ion affinity of the phosphate group and that the nucleobase residues do not participate in metal ion binding due to the *anti* conformation of these pyrimidine-NMPs (Figure 16, lower part). This is confirmed by the stability data for the M(CMP) complexes of Cd^{2+}, Cu^{2+}, and Pb^{2+}, which all fit on their reference lines in Figure 18 (green symbols).

The stabilities of the Cd^{2+}, Cu^{2+}, and Pb^{2+} complexes of AMP^{2-} and GMP^{2-}, these nucleotides being present in the *anti* conformation (Figure 16, upper part), are all larger than expected, that is, the corresponding data points are above the reference lines (red and blue symbols in Figure 18). Remarkably, the M(GMP) complexes are in all three instances more stable than the corresponding M(AMP) species. That the observed complex stabilities are not dictated by O donor interactions, follows, e.g., from the fact that the stability enhancement for Cu(GMP) (blue, filled square) is significantly larger than the one for Pb(GMP)

(blue, filled circle). This confirms an (N7) interaction because the affinity of Cu^{2+} towards N sites is very pronounced whereas that of Pb^{2+} is not (Section 2.2). The observed enhanced complex stabilities must be attributed to macrochelate formation [84] as is indicated in Equilibrium (25). It needs to be noted that the vertical distances of the data points (colored symbols) to the reference lines reflect the extent of chelation. These vertical distances can exactly be defined because the intercepts of the vertical lines with the reference lines represent the stabilities of the "open" complexes [Eq. (7)] and these intercepts can be calculated with the known straight-line parameters and the corresponding pK_a values [Eq. (10)]. In this way values for $\log \Delta_{M/NMP}$ [Eq. (12)] are obtained. The corresponding data are listed in columns 2 through 4 of Table 8.

Once values for $\log \Delta_{M/NMP}$ are known, those for the intramolecular dimension-less equilibrium constants, K_I, can be calculated [Eqs (9), (13)] and from these follow the formation degrees of the "closed" or macrochelated species. These results are listed in columns 5 and 6 of Table 8 for several M(AMP) and

Table 8. Logarithms of the stability constants [Eqs (2) and (6)] of several M(NMP) complexes as determined by potentiometric pH titration, together with the calculated stability constants of the 'open' forms [Eq. (7)], as well as with the enhanced complex stabilities, $\log \Delta_{M/NMP}$ [Eq. (12)], and the extent of intramolecular macrochelate formation according to Equilibrium (25) for aqueous solutions at 25 °C and $I = 0.1$ M ($NaNO_3$).[a,b]

M(NMP)	$\log K^{M}_{M(NMP)}$ [Eqs (2, 6)]	$\log K^{M}_{M(NMP)op}$ [Eq. (7)][c]	$\log \Delta_{M/NMP}$ [Eq. (12)]	K_I [Eqs (9, 13)]	% $M(NMP)_{cl}$ [Eqs (11, 25)]
Ca(AMP)	1.48 ± 0.03	1.45 ± 0.05	0.03 ± 0.06	0.07 ± 0.14	7 ± 13
Mn(AMP)	2.23 ± 0.02	2.16 ± 0.05	0.07 ± 0.05	0.17 ± 0.15	15 ± 11
Cu(AMP)	3.17 ± 0.02	2.87 ± 0.06	0.30 ± 0.06	1.00 ± 0.29	50 ± 7
Zn(AMP)	2.38 ± 0.07	2.13 ± 0.06	0.25 ± 0.09	0.78 ± 0.38	44 ± 12
Cd(AMP)	2.74 ± 0.05	2.44 ± 0.05	0.30 ± 0.07	1.00 ± 0.32	50 ± 8
Pb(AMP)	2.92 ± 0.08	2.94 ± 0.08	–0.02 ± 0.11	0 (< 0.23)	0 (< 19)
Ca(GMP)	1.57 ± 0.03	1.45 ± 0.05	0.12 ± 0.06	0.32 ± 0.18	24 ± 10
Mn(GMP)	2.42 ± 0.05	2.17 ± 0.05	0.25 ± 0.07	0.78 ± 0.29	44 ± 9
Cu(GMP)	3.86 ± 0.04	2.89 ± 0.06	0.97 ± 0.07	8.33 ± 1.55	89 ± 2
Zn(GMP)	2.83 ± 0.03	2.14 ± 0.06	0.69 ± 0.07	3.90 ± 0.76	80 ± 3
Cd(GMP)	3.25 ± 0.03	2.46 ± 0.05	0.79 ± 0.06	5.17 ± 0.83	84 ± 2
Pb(GMP)	3.23 ± 0.08	2.96 ± 0.08	0.27 ± 0.11	0.86 ± 0.47	46 ± 14

[a] For the error limits see footnotes "a" of Tables 4 and 6. The values for the Pb(NMP) complexes are from [107], those for the M(AMP) and M(GMP) complexes are from [224] and [28], respectively.

[b] The acidity constants are for $H_2(AMP)^{\pm}$ $pK^{H}_{H_2(AMP)} = 3.84 \pm 0.02$ [Eq. (27); $(N1)H^{+}$ site] and $pK^{H}_{H(AMP)} = 6.21 \pm 0.01$ [Eq. (3); R-$P(O)^{-}_2$(OH) group], and for $H_2(GMP)^{\pm}$ $pK^{H}_{H_2(GMP)} = 2.48 \pm 0.04$ [Eq. (27); $(N7)H^{+}$ site], $pK^{H}_{H(GMP)} = 6.25 \pm 0.02$ [Eq. (3); R-$P(O)^{-}_2$(OH) group] and $pK^{H}_{GMP} = 9.49 \pm 0.02$ [Eq. (28); (N1)H site] [116].

[c] The values in this column were calculated with $pK^{H}_{H(NMP)}$ and Eq. (10) by using the straight-line parameters listed in [28, 85, 87, 116].

M(GMP) complexes [values for M(IMP) species are also known [28, 107], but are not listed here]. What can we learn from these data?

If one compares for a given metal ion the values for K_I and % $M(NMP)_{cl}$ in columns 5 and 6 of Table 8, one notes that always the values for the M(AMP) complexes are smaller. Why? It cannot be a matter of different basicities of the N7 sites, though, as these units are responsible for chelate formation, this is the idea that comes first to mind. However, the acidity constants for the $(N7)H^+$ sites of adenosine and guanosine are $pk^{N7\text{-}N1}_{H\cdot N7(Ado)N1} = 2.15 \pm 0.15$ (micro acidity constant) [118] and $pK^{H}_{HN7(Guo)} = 2.11 \pm 0.04$ [116], respectively, that is, the basicities of these two N7 sites are identical within the error limits. Hence, there must be a different reason and this can only be a steric effect. Indeed, the $(C6)NH_2$ group is known to inhibit metal ion binding at N7 (and at N1 as well) [120, 125], whereas a (C6)O group rather promotes it by forming outersphere bonds to a water molecule at the (N7)-bound metal ion [116].

Further interesting conclusions that follow from Table 8 include the following ones:

(i) Pb(GMP) forms a macrochelate with a formation degree of about 46 %, whereas for Pb(AMP) at best only traces of a macrochelate occur [Eq. (25)]. The reason is probably the (C6)O unit of GMP^{2-} as Pb^{2+} likes to interact with O donor sites.

(ii) The highest formation degrees of the macrochelates occur with Cu(GMP) (89 %) and Cd(GMP) (84 %). The formation degrees of about 50 % for the corresponding M(AMP) complexes are also similar in both instances.

(iii) The extent of macrochelate formation for the M(GMP) complexes depends on the metal ion and decreases in the order $Cu^{2+} > Cd^{2+} > Zn^{2+} > Pb^{2+} \approx Mn^{2+} > Ca^{2+}$, which reflects the affinity of these metal ions towards N7. The order for the M(AMP) complexes is similar.

(iv) Most remarkable is the situation with Ca(AMP) and Pb(AMP); macrochelate formation occurs in both cases only in traces, if at all, indicating the already mentioned kinship (Sections 1 and 2), but note, the absolute stabilities differ by nearly 1.5 log units (see column 2 in Table 8).

Protonated complexes of the type $M(H;NMP)^+$ do not play any role in the physiological pH range, e.g., for the $M(H;GMP)^+$ complexes the release of the proton occurs in the pK_a range of about 4.5 (Pb^{2+}) [107] to 5.2 (Ba^{2+}) [28]. However, already with $Pb(H;CMP)^+$ we have seen (Section 6.2) that the question where Pb^{2+} and where H^+ bind is an interesting one. The formation degrees of the $(Pb\cdot NMP\cdot H)^+$ and $(NMP\cdot Pb\cdot H)^+$ isomers can be calculated via micro stability constants [10, 107]; the results for the ratios R, by repeating the one for $Pb(H;CMP)^+$, are as follows:

$$R = \frac{(Pb\cdot CMP\cdot H)^+}{(CMP\cdot Pb\cdot H)^+} \approx \frac{90}{10}$$

$$R = \frac{(Pb\cdot GMP\cdot H)^+}{(GMP\cdot Pb\cdot H)^+} \approx \frac{92}{8}$$

$$R = \frac{(\mathrm{Pb \cdot AMP \cdot H})^{+}}{(\mathrm{AMP \cdot Pb \cdot H})^{+}} \approx \frac{60}{40}$$

These ratios reflect the affinities of Pb^{2+} towards nucleoside residues (Table 4) and they are expecially remarkable for guanosine and cytidine. The result with $Pb(H;AMP)^{+}$ indicates that for Pb^{2+} the affinities of the adenine residue and that of a $-P(O)_2^-(OH)$ group are of a comparable size.

6.4. Complexes of Nucleoside 5′-*O*-Thiomonophosphates

Nucleotides altered at all three parts, that is, the nucleobase, the sugar, and the phosphate residues [41], have been used as probes in nucleic acid research as well as for studying enzymatic reactions involving nucleotides. The most popular alteration is the substitution of an oxygen by a sulfur atom at the phosphate group, giving the $-OP(O)_2^-(S)^-$ residue [227, 228]. The resulting nucleotide derivatives are commonly addressed as nucleoside phosphorothioates (abbreviated as PS) or (less precise) as thionucleotides (see Sections 4.6.2 and 4.6.3).

These nucleoside phosphorothioates are widely applied [229], including as therapeutics [230] and small interfering RNAs (siRNAs) [231], in studying the chemistry of ribozymes [228, 232]. Considering that all these reactions depend on the presence of metal ions [69], available quantitative information of metal ion binding to the $-OP(O)_2^-(S)^-$ residue is scarce [39, 41, 42, 233–235].

Replacement of O by S in the phosphate group of an NMP^{2-} ligand increases the acidity by about 1.4 pK units, that is, the $pK^{H}_{H(NMP)}$ value of about 6.2 (Table 7, Figure 18) drops to a $pK^{H}_{H(PS)}$ value of about 4.8 (Table 9, footnotes). The reason is that sulfur likes to form single P–S bonds and to carry a charge of –1; protonation in $-OP(O)_2^-(S)^-$ occurs at one of the two oxygens [236]. The acid-base properties of the nucleobase residues are only little affected [39].

The stabilities of several Pb(PS) complexes, where PS = methyl thiophosphate ($MeOPS^{2-}$), uridine 5′-*O*-thiomonophosphate ($UMPS^{2-}$) or adenosine 5′-*O*-thiomonophosphate ($AMPS^{2-}$), have been measured [39]. These values are listed in column 2 of Table 9, together with the results obtained for the corresponding complexes of Ca^{2+}, Zn^{2+}, and Cd^{2+} [41, 42]. As far as the M(AMPS) complexes are concerned, it is assumed that the extent of macrochelate formation in the M(AMP) and M(AMPS) complexes is the same; an assumption supported by the fact that the basicity of N1 remains unchanged (Tables 8 and 9, footnotes) and this must then also be the case for N7 [118, 236]. Application of the indicated correction due to macrochelate formation [column 3; Eq. (25)] provides the stability constant, $\log K^{M/cor}_{M(AMPS)}$ (column 4), which reflects now solely the influence in the M(AMPS) complexes due to the presence of sulfur in the thiophosphate group. Use of the parameters [28, 85, 87, 116] of the previously determined straight-line plots [Eq. (10); see, e.g., Figure 18] together with $pK^{H}_{H(PS)}$ values provides the stabilities of the complexes due to a (thio)phosphate coordination (column 5). With these values one can now quantify the effect of the sulfur substitution [Eq. (33)] (Table 9, column 6).

Table 9. Stability constant comparisons for M(PS) complexes formed by Ca^{2+}, Zn^{2+}, Cd^{2+} or Pb^{2+} and methyl thiophosphate ($MeOPS^{2-}$), uridine 5′-*O*-thiomonophosphate ($UMPS^{2-}$) or adenosine 5′-*O*-thiomonophosphate ($AMPS^{2-}$) between the measured stability constants, log $K^{M}_{M(PS)}$ [Eq. (2)], or the stability constants of M(AMPS) corrected for the macrochelate effect, log $K^{M/cor}_{M(AMPS)}$, and the calculated stability constants, log $K^{M}_{M(PS)calc}$, together with the stability difference [Eq. (12)] for aqueous solutions at 25 °C and I = 0.1 M ($NaNO_3$).[a,b]

M(PS)	log $K^{M}_{M(PS)}$	log $\Delta_{M/AMP}$[c]	log $K^{M/cor}_{M(AMPS)}$	log $K^{M}_{M(PS)calc}$[d]	log $\Delta_{M/PS}$	log $\Delta_{M/PS/av}$[e]
Ca(MeOPS)	1.25 ± 0.06			1.29 ± 0.05	–0.04 ± 0.08	
Ca(UMPS)	1.19 ± 0.10			1.26 ± 0.05	–0.07 ± 0.11	–0.04 ± 0.04
Ca(AMPS)	1.27 ± 0.06	0.03 ± 0.06	1.24 ± 0.08	1.25 ± 0.05	–0.01 ± 0.10	
Zn(MeOPS)	2.34 ± 0.05			1.69 ± 0.06	0.65 ± 0.08	
Zn(UMPS)	2.21 ± 0.06			1.63 ± 0.06	0.58 ± 0.08	0.63 ± 0.05
Zn(AMPS)	2.52 ± 0.18	0.25 ± 0.09	2.27 ± 0.20	1.61 ± 0.06	0.66 ± 0.21	
Cd(MeOPS)	4.50 ± 0.06			2.03 ± 0.05	2.47 ± 0.08	
Cd(UMPS)	4.37 ± 0.08			1.97 ± 0.05	2.40 ± 0.09	2.41 ± 0.06
Cd(AMPS)	4.62 ± 0.12	0.30 ± 0.07	4.32 ± 0.14	1.95 ± 0.05	2.37 ± 0.15	
Pb(MeOPS)	4.78 ± 0.06			2.32 ± 0.08	2.46 ± 0.10	
Pb(UMPS)	4.63 ± 0.03			2.23 ± 0.08	2.40 ± 0.09	2.48 ± 0.10
Pb(AMPS)[f]	4.77 ± 0.10	(–0.02 ± 0.11)	4.77 ± 0.15	2.20 ± 0.08	2.57 ± 0.17	

[a] For the error limits see footnotes "a" of Tables 4 and 6. The values for AMPS are from [39, 41], those for MeOPS and UMPS from [42].

[b] The acidity constants are for $H(MeOPS)^-$ $pK^{H}_{H(MeOPS)} = 4.96 \pm 0.02$ [Eq. (3)], for $H(UMPS)^-$ $pK^{H}_{H(UMPS)} = 4.78 \pm 0.02$ [Eq. (3)], and $pK^{H}_{UMPS} = 9.47 \pm 0.02$ [Eq. (28)] [42], and for $H_2(AMPS)^{\pm}$ $pK^{H}_{H_2(AMPS)} = 3.72 \pm 0.03$ [Eq. (27)] and $pK^{H}_{H(AMPS)} = 4.83 \pm 0.02$ [Eq. (3)] [236]; the micro acidity constants for $H_2(AMPS)^{\pm}$, the second one being needed for the straight-line calculation,[d] are $pk^{AMPS\cdot H}_{H\cdot AMP\cdot H} = 3.84 \pm 0.02$ [$(N1)H^+$ deprotonation] and $pk^{AMPS}_{AMPS\cdot H} = 4.71 \pm 0.04$ (deprotonation of the thiophosphate group) [236].

[c] See Table 8 in Section 6.3 or [41].

[d] The values in this column were calculated with the $pK^{H}_{H(PS)}$ values given above [b] and Eq. (10) by using the straight-line parameters listed in [28, 85, 87, 116] (for Pb^{2+} see [114]).

[e] Arithmetic mean with 2 σ as error limit.

[f] For consistency, Pb(AMPS) is treated in this table in the same way as the other three M(AMPS) complexes; however, in [114], together with the Pb(AMPS) system, $pk^{AMPS}_{AMPS\cdot H} = 4.75 \pm 0.05$ was determined and this leads to log $K^{Pb}_{Pb(AMPS)calc} = 2.22 \pm 0.08$ and to log $\Delta_{Pb/AMPS} = 2.55 \pm 0.13$; both values agree within the error limits with the above ones.

$$\log \Delta_{M/PS} = \log K^{M}_{M(PS)} - \log K^{M}_{M(PS)calc} \quad (33a)$$

$$= \log K^{M}_{M(PS)} - \log K^{M}_{M(R\text{-}PO_3)} \quad (33b)$$

Among the conclusions to be drawn from the stability differences (Table 9, column 6) are at least the following ones:

(i) The $\Delta_{Ca/PS}$ values for the Ca(PS) complexes are zero within the error limits and the identical observations have been made for the corresponding complexes of Mg^{2+}, Sr^{2+}, and Ba^{2+} [42]; hence, there is no sulfur effect in these instances.

(ii) Point (i) proves that these alkaline earth ions have the same affinity towards the $-OP(O)_2^-(S)^-$ and $-OP(O)_3^{2-}$ residues and this justifies the application of the straight-line plots based on $R\text{-}PO_3^{2-}$ complexes also for the other metal ions considered.

(iii) Comparison of the values for $\log \Delta_{M/MeOPS}$ and $\log \Delta_{M/UMPS}$ proves that the uracil residue in the M(UMPS) complexes, as expected (Section 6.2; Table 7), does not participate in complex formation. In fact, if there is any influence, it is a small inhibiting (steric) effect of the uracil residue (the uracil moiety is larger than the methyl group) of about –0.06 log unit, but this value is within the error limits.

(iv) In the M(PS) complexes of Zn^{2+}, Cd^{2+}, and Pb^{2+} the presence of the sulfur atom leads to a significantly enhanced complex stability of about 0.6 to 2.5 log units; this proves that the S atom participates in coordination of these metal ions.

From the discussed results it follows that two isomeric complexes occur, one where M^{2+} is O-coordinated, PO · M, and one where S-coordination occurs, PS · M. Because the formation of the PS · M isomer is linked to the stability enhancements $\log \Delta_{M/PS}$ and because these values are for a given M^{2+} identical within the error limits for the three thio ligands considered, we have calculated the average value, $\log \Delta_{M/PS/av}$, listed in column 7 of Table 9; the error limits of these averages encompass for a given metal ion the individual $\log \Delta_{M/PS}$ values. Considering that the stability enhancements $\log \Delta_{M/PS/av}$ are a reflection of the extent of the S interaction, one can apply Eq. (13) and calculate K_I for the intramolecular PO · M $\rightleftharpoons$ PS · M equilibrium, or to say it differently [42], calculate the ratio R = [PS · M]/[PO · M] from which the formation degree of PS · M, that is, % PS · M, follows.

For the $-OP(O)_2^-(S)^-$ residue, in the Zn^{2+} complexes of $MeOPS^{2-}$, $UMPS^{2-}$, and $AMPS^{2-}$, follows from $R = 10^{0.63} - 1$ [Eq. (13)] for Zn(PS) a formation degree of about 77 % for the S-coordinated PS · Zn isomer; the O-coordinated PO · Zn isomer occurs thus with a formation degree of about 23 %. For Cd^{2+} the PS · M isomer reaches a formation degree of 99.6 %, and the PO · Cd species occurs thus only in traces; hence, Cd^{2+} is considerably more thiophilic than Zn^{2+}. This is even more true for Pb^{2+} with a formation degree of 99.7 % for PS · Pb. If in the PS · M species the metal ions are coordinated only to S or if (outersphere) chelates involving also O atoms [86] of the $-OP(O)_2^-(S)^-$ residue

occur, is not known. In any case, the given formation degrees for the PS · M species reflect the solubility products, which increase in the order ZnS < CdS < PbS (see Table 1), PbS being the least soluble of these sulfides.

6.5. Complexes of Nucleoside 5′-Di- and Triphosphates

The results described in Section 6.3 in the context of Eqs (30) through (32) provide the necessary confidence to derive stability constants for Pb^{2+} complexes of diphosphate ($R\text{-}DP^{3-}$) and triphosphate ($R\text{-}TP^{4-}$) monoesters. To the best of our knowledge no such data have been measured for Pb^{2+} complexes [38, 52–55, 237]; this includes a SciFinder search from February/March 2016 that provided values for "mixed ligand complexes" [238, 239] as discussed below at the end of this section. Considering that the knowledge of stability data for $Pb(R\text{-}DP)^{-}$ and $Pb(R\text{-}TP)^{2-}$ complexes is highly desirable, the previous estimates [10] are summarized and also updated as far as possible (all values refer to 25 °C and $I = 0.1$ M).

For simple diphosphate monoesters ($R\text{-}DP^{3-}$), like methyl diphosphate, phenyl diphosphate, etc., log K *versus* pK_a straight-line plots have been established for 10 metal ions including Cu^{2+} [215]. The corresponding parameters [215], together with pK_a = 6.40 ± 0.05, which is valid for many monoprotonated nucleoside 5′-diphosphates [215, 240], were used to calculate [10] for $Cu(R\text{-}DP)^{-}$ complexes the data provided in Eq. (34):

$$pK^{H}_{H(R\text{-}DP)} = 6.40: \quad \log K^{Cu}_{Cu(R\text{-}DP)} = 5.27 \pm 0.04 \tag{34}$$

Hence it was concluded, in accord with the observations mentioned above as well as in Section 6.3, that for the stability of the $Pb(R\text{-}DP)^{-}$ complex Eq. (35) (with a generously estimated error limit) holds:

$$pK^{H}_{H(R\text{-}DP)} = 6.40 \pm 0.05: \quad \log K^{Pb}_{Pb(R\text{-}DP)} = 5.3 \pm 0.15 \tag{35}$$

For the complexes of CDP^{3-}, UDP^{3-}, and $dTDP^{3-}$ with Ba^{2+}, Sr^{2+}, Ca^{2+}, Mg^{2+}, Mn^{2+}, Co^{2+}, Ni^{2+}, Cu^{2+}, Zn^{2+}, and Cd^{2+} it has been shown that the nucleobase residues do not interact with a M^{2+} coordinated at the diphosphate residue [215], in fact, the corresponding data fit the reference lines; this is also expected for the corresponding Pb^{2+} complexes. Furthermore, the extent of macrochelate formation is commonly very similar for M(NMP), $M(NDP)^{-}$, and $M(NTP)^{2-}$ complexes [144, 224] and because for Pb(AMP) no adenine-Pb^{2+} interaction, that is, no macrochelate formation, was observed [107], the same is surmised for $Pb(ADP)^{-}$. Hence, the results of Eq. (35) hold for the $Pb(NDP)^{-}$ complexes of UDP^{3-}, $dTDP^{3-}$, CDP^{3-}, and ADP^{3-}.

Based on analogous reasonings [10] and taking into account that Cu^{2+} is hampered in coordinating equatorially (Jahn-Teller effect [241]) to all three phosphate units of a triphosphate chain (for details see [10]), compared to an octahedral or otherwise adaptable coordination sphere which is able to do so, and considering further that for $H(NTP)^{3-}$ species the pK_a is close to 6.50 [71, 216, 242], one obtains Eq. (36) (again a generous error limit is given):

$$pK^{H}_{H(R\text{-}TP)} = 6.50 \pm 0.05: \quad \log K^{Pb}_{Pb(R\text{-}TP)} = 6.3 \pm 0.25 \tag{36}$$

Thus, Eq. (36) provides estimated stabilities for the $Pb(NTP)^{2-}$ complexes, where $NTP^{4-} = UTP^{4-}$, $dTTP^{4-}$, CTP^{4-}, and ATP^{4-}, and where the nucleobase moiety has no effect. It is comforting to note in the context of Eq. (36) that for the Pb^{2+} complex of hydrogen triphosphate, $Pb(HP_3O_{10})^{2-}$, the stability constant has been measured, that is, $\log K^{Pb}_{Pb(HP_3O_{10})} = 6.32$ (30 °C; $I = 1$ M, $NaClO_4$) [53, 243], and this value is very close to the above estimate for the $Pb(R\text{-}TP)^{2-}$ [= $Pb(ROP_3O_9)^{2-}$] complexes.

Since, as already mentioned, the extent of chelate formation is about the same for a given metal ion in M(NMP), $M(NDP)^{-}$, and $M(NTP)^{2-}$ complexes, one can also estimate [10] complex stabilities for the Pb^{2+} complexes of IDP^{3-} [Eq. (37)], GDP^{3-} [Eq. (38)], ITP^{4-} [Eq. (39)], and GTP^{4-} [Eq. (49)], by taking into account the $\log \Delta_{Pb/NMP}$ values listed in Tables 3 and 4 of [107]:

$$\log K^{Pb}_{Pb(IDP)} = (5.3 \pm 0.15) + (0.12 \pm 0.09) = 5.42 \pm 0.18 \approx 5.4 \pm 0.2 \tag{37}$$

$$\log K^{Pb}_{Pb(GDP)} = (5.3 \pm 0.15) + (0.27 \pm 0.11) = 5.57 \pm 0.19 \approx 5.6 \pm 0.2 \tag{38}$$

$$\log K^{Pb}_{Pb(ITP)} = (6.3 \pm 0.25) + (0.12 \pm 0.09) = 6.42 \pm 0.27 \approx 6.4 \pm 0.3 \tag{39}$$

$$\log K^{Pb}_{Pb(GTP)} = (6.3 \pm 0.25) + (0.27 \pm 0.11) = 6.57 \pm 0.27 \approx 6.6 \pm 0.3 \tag{40}$$

These estimations are recommended for use as long as no measured values exist.

In a paper [239] dealing with the "mixed ligand complex(es) of … Pb(II) … with adenosine diphosphate and nitrilotriacetate" the stability constant for the $Pb(ADP)^{-}$ complex is given as $\log K^{Pb}_{Pb(ADP)} = 4.41$, and in a second, analogous report [238] the value for $Pb(ATP)^{2-}$ appears as $\log K^{Pb}_{Pb(ATP)} = 4.90$ (30 °C; $I =$ 0.1 M). Both values are much lower than the corresponding constants given in Eqs (35) ($\log K^{Pb}_{Pb(R\text{-}DP)} = 5.3 \pm 0.15$) and (36) ($\log K^{Pb}_{Pb(R\text{-}TP)} = 6.3 \pm 0.25$), respectively. That these results [238, 239] need to be ignored follows also from the stability constants measured for the corresponding Cu^{2+} complexes, that is, $\log K^{Cu}_{Cu(ADP)} = 5.61 \pm 0.03$ [224] and $\log K^{Cu}_{Cu(ATP)} = 6.34 \pm 0.03$ [144, 216]; both stability constants contain small contributions due to macrochelate formation [Eq. (25)], that is, $\log \Delta_{Cu/AP} = 0.34 \pm 0.05$ [224] and 0.48 ± 0.04 [144, 216], respectively (AP = adenosine phosphate). Hence, at this time only the estimates given in Eqs. (35) through (40) can be recommended.

7. LEAD(II) BINDING IN DINUCLEOTIDES

7.1. Coordinating Properties of the Phosphodiester Linkage

One of the important questions in nucleic acid research is to find out to which extent neighboring nucleotide units affect each other. Knowledge in this respect is still rather scarce [244]. To what extent does a neighboring phosphodiester

linkage contribute to metal ion binding? To find at least a partial answer to this question for several metal ions, including Pb^{2+}, the coordinating properties of uridylyl-(5′→3′)-5′-uridylate, $pUpU^{3-}$ (Figure 19) [236, 245, 246], were studied. This dinucleotide is ideal for such a study because the uracil residue is expected not to participate in metal ion binding (see Sections 4.4 and 6.2).

The measured stablity constants for the $M(pUpU)^{-}$ complexes of Mg^{2+}, Mn^{2+}, Zn^{2+}, Cd^{2+}, and Pb^{2+} are listed in column 3 of Table 10. To see, if next to the $-PO_4^{3-}$ residue, which is the primary binding site, a further metal ion interaction occurs, which, if present, must lead to an increased complex stability [84], the stability constants for simple $M(R\text{-}PO_3)$ complexes were calculated from the available straight-line plots (see, e.g., Figure 18) [28, 85, 87, 116]. These stability constants, which represent the stability of the 'open' isomer in equilibria analogous to Eqs (6) and (25), are listed in column 4 of Table 10, and the resulting stability enhancements according to Eq. (12) are provided in column 5.

A quick glance at the log $\Delta_{M(pUpU)}$ values shows that these are identical within the error limits for the metal ion complexes of Mg^{2+}, Mn^{2+}, and Cd^{2+}. Considering the very different metal ion-binding properties [38, 52–55] of these three metal ions, it is evident that this "equality" must originate in a general effect. Indeed, it is wellknown that metal ion coordination at a given site can be affected by a charge that is located at a distance (e.g., [170, 249–251]). Hence, it is concluded that the singly negatively charged phosphodiester bridge facilitates metal

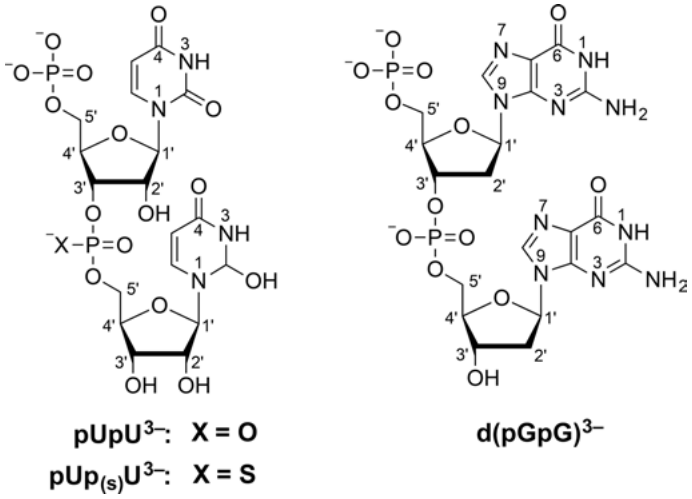

Figure 19. Chemical structures of the trianions of uridylyl-(5′→3′)-5′-uridylate ($pUpU^{3-}$) and of its thio derivative *P*-thiouridylyl-(5′→3′)-5′-uridylate ($pUp_{(s)}U^{3-}$) as well as of 2′-deoxyguanylyl-(5′→3′)-2′-deoxy-5′-guanylate ($d(pGpG)^{3-}$) with the two nucleoside units in each dinucleotide in the predominant *anti* conformation [22–25]. Regarding the thiophosphate diester bridge one may add that, if protonated, H^{+} is most likely bound at the terminal O atom of this bridge [39, 235]. After deprotonation the negative charge of the thiophosphate bridge is mainly located at the sulfur atom [235, 244, 245], as is depicted in the above $pUp_{(s)}U^{3-}$ structure.

Table 10. Logarithms of the stability constants [Eqs (2) and (6)] of several $M(pUpU)^-$ and $M[d(pGpG)]^-$ complexes as determined by potentiometric pH titration, together with the calculated stability constants of the "open" forms [Eq. (7)], as well as of the enhanced complex stabilities, $\log \Delta_{M/pNpN}$ [Eq. (12)], and the extent of intramolecular macrochelate formation as indicated in Equilibria (5), (25), and (41) (see text) (aq. sol.; 25 °C, $I = 0.1$ M, $NaNO_3$).[a]

$pNpN^{3-}$	M^{2+}	$\log K^{M}_{M(pNpN)}$	$\log K^{M}_{M(R\text{-}PO_3)}$[b]	$\log \Delta_{M/pNpN}$[c]	$\log \Delta^{*}_{M/pNpN}$[d]	K_I[e]	% $M(pNpN)^-_{cl}$[f]
$pUpU^{3-}$	Mg^{2+}	1.84 ± 0.04	1.61 ± 0.03	0.23 ± 0.05*	–0.01 ± 0.06	~0	~0 (< 11)
	Mn^{2+}	2.49 ± 0.05	2.22 ± 0.05	0.27 ± 0.07*	0.03 ± 0.08	~0	~0 (< 22)
	Zn^{2+}	2.57 ± 0.03	2.20 ± 0.06	0.37 ± 0.07	0.13 ± 0.08	0.35 ± 0.25	26 ± 14
	Cd^{2+}	2.75 ± 0.03	2.52 ± 0.05	0.23 ± 0.05*	–0.01 ± 0.06	~0	~0 (< 11)
	Pb^{2+}	4.45 ± 0.25	3.05 ± 0.08	1.40 ± 0.26	1.16 ± 0.26	13.45 ± 8.65	93 ± 4
$d(pGpG)^{3-}$	Mg^{2+}	2.43 ± 0.06	1.64 ± 0.03	0.79 ± 0.07	0.55 ± 0.08	2.55 ± 0.65	71.8 ± 5.2
	Zn^{2+}	3.66 ± 0.05	2.25 ± 0.06	1.41 ± 0.08	1.17 ± 0.09	13.791 ± 3.065	93.24 ± 1.40
	Cd^{2+}	4.01 ± 0.06	2.56 ± 0.05	1.45 ± 0.08	1.21 ± 0.09	15.22 ± 3.36	93.8 ± 1.3
	Pb^{2+}	4.14 ± 0.10	3.11 ± 0.08	1.03 ± 0.13	0.79 ± 0.14	5.17 ± 1.99	83.8 ± 5.2

[a] For the error limits see footnotes "a" of Tables 4 and 6. The values in column 3 for $pUpU^{3-}$ are from [75] and those for $d(pGpG)^{3-}$ from [247]. The relevant acidity constants of the $-P(O)_2^-(OH)$ residues [Eq. (3)] are $pK^{H}_{H(pUpU)} = 6.44 \pm 0.02$ [75] and $pK^{H}_{H[d(pGpG)]} = 6.56 \pm 0.03$ [248]. The values for the deprotonation of the (N3)H sites of $pUpU^{3-}$ [Eq. (28)] are available [75] but not of relevance in the present context because $pK_a \geq 9$. Similarly, the values for the deprotonation of the $(N7)H^+$ sites of $H_2[d(pGpG)]^-$ are also known [248] [Eq. (27)] ($pK_a \leq 3.0$), as are those for the (N1)H sites [Eq. (28)], where $pK_a \geq 9.5$ [248].

[b] The values in this column [see Eq. (7)] were calculated with $pK^{H}_{H(pNpN)}$ and Eq. (10) by using the straight-line parameters listed in [28, 85, 87, 116] (for Pb^{2+} see Eq. (26) or [114]).

[c] Calculated according to Eq. (12).

[d] Note, $\log \Delta^{*}_{M/pNpN} = \log \Delta_{M/pNpN} - \log \Delta_{M/pUpU/charge}$. The latter value is the average of the three marked values (*) in column 5, which amounts to 0.24 ± 0.04 [75], and which represents the charge effect that the negatively charged phosphodiester bridge exercizes on a metal ion coordinated at the terminal phosphate group (Figure 19).

[e] See Eqs (9) and (13). In the case of the $d(pGpG)^{3-}$ system $K_{I/tot}$ is given (see text) and Table 11.

[f] Calculated according to Eq. (11). In the case of % $M[d(pGpG)]^-$ the percentages refer to the total amount of closed/chelated species (see text and Table 11).

ion binding at the terminal phosphate group of $pUpU^{3-}$ by $\log \Delta_{M(pUpU)charge} = 0.24 \pm 0.04$ (average of the values for Mg^{2+}, Mn^{2+}, and Cd^{2+} in column 5) without a direct participation of the ester linkage in metal ion coordination. Deduction of this value from that of $\log \Delta_{M(pUpU)}$ (column 5) provides the charge-corrected $\log \Delta^{*}_{M/pUpU}$ values listed in column 6 of Table 10. These values reflect now the true stablity enhancement due to a further metal ion interaction, and of course, this can only be a coordination at the phosphodiester linkage because $pUpU^{3-}$ offers no other binding site; hence, an equilibrium analogous to Eqs (5) and (25) operates.

Application of Eq. (13) to the $\log \Delta^{*}_{M/pUpU}$values provides the intramolecular equilibrium constant K_I [Eq. (6)] and from this follows with Eq. (11) the formation degree of the $M(pUpU)^{-}_{cl}$ isomers. These results are given in the two terminating columns 7 and 8 of Table 10. In accord with the pronounced affinity of Pb^{2+} towards O donor sites (Sections 2.2 and 5) the stability enhancement for $Pb(pUpU)^{-}$ is more than one log unit and the macrochelated isomer with a 10-membered ring occurs thus with a formation degree of about 93 %. The affinity of Zn^{2+} towards the $(RO)_2P(O)^{-}_{2}$ bridge is with a formation degree of about 25 % rather moderate, but the interaction is certain. It is further certain that for the $M(pUpU)^{-}$ complexes of Mg^{2+}, Mn^{2+}, and Cd^{2+}, if at all, only traces of the macrochelated species occur in solution.

7.2. Intramolecular Equilibria in Dinucleotide Complexes Involving Guanosine Moieties

Because the N7 unit of a guanine residue has a rather pronounced affinity towards metal ions (Sections 4.2 and 6.3), the dinucleotide 2′-deoxyguanylyl-(5′→3′)-2′-deoxy-5′-guanylate, $(d(pGpG)^{3-}$, Figure 19), has previously been studied [247]. For simplicity we refer in this section always to N7, being aware, however, that for several metal ions actually the complete N7/(C6)O unit of the nucleobase is involved in binding, partly in an outersphere manner (Section 6.3). Considering further also the results discussed in the preceding Section 7.1, it is evident that for the $M[d(pGpG)]^{-}$ complexes the Equilibrium Scheme (41) needs to be considered:

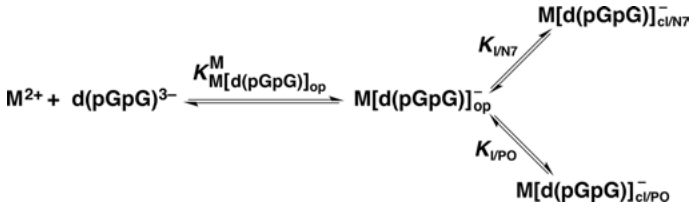

(41)

In this Equilibrium Scheme (41), $M[d(pGpG)]^{-}_{op}$ designates the 'open' complex in which M^{2+} is only bound to the terminal $-PO^{2-}_{3}$ group (Figure 19). The 'closed' macrochelated isomers, involving either the phosphodiester bridge or the N7 sites, are termed $M[d(pGpG)]^{-}_{cl/PO}$ or $M[d(pGpG)]^{-}_{cl/N7}$, respectively [106, 247].

A simultaneous binding to the bridge and N7 is for steric reasons not possible. However, it is believed [247] that due to self-stacking of the two guanine residues (Figure 19) a pre-orientation of the $d(pGpG)^{3-}$ ligand occurs and that therefore metal ions can bind simultaneously not only to the phosphate group, but also to both N7 sites, possibly involving even a (C6)O unit. Hence, two-, three- or even four-point interactions appear as possible giving thus rise to additional equilibria; note, the designation $M[d(pGpG)]^{-}_{cl/N7}$ represents all isomers containing next to the phosphate group a N7 interaction. Of course, in the measured stability constants, which are defined according to Eq. (2), [M(L)] is the analytical concentration and this is represented by $[M[d(pGpG)]^{-}]$, which encompasses the sum of all isomeric species in the Equilibrium Scheme (41) [see also below Eq. (42)]. These stability constants are listed in the lower part of Table 10 in column 3.

Figure 20 shows the straight-line reference plots for log $K^{M}_{M(R\text{-}PO_3)}$ *versus* $pK^{H}_{H(R\text{-}PO_3)}$ for the metal ions Mg^{2+}, Zn^{2+}, and Pb^{2+}, together with the data points representing the corresponding $M(pUpU)^{-}$ and $M[d(pGpG)]^{-}$ complexes. It is immediately evident that all six complexes own an increased complex stability. For the $M(pUpU)^{-}$ species with Mg^{2+} and Zn^{2+} the increase is small whereas for the same metal ions, but with $d(pGpG)^{3-}$, the stability increase is more pronounced indicating already at this point that the N7 isomer is of relevance. The largest stability increase is observed for $Pb(pUpU)^{-}$, its data point is far above the reference line; the stability increase for $Pb[d(pGpG)]^{-}$ seems to be a bit less pronounced.

For an evaluation of the constants listed in column 3 of Table 10 (lower part) regarding the Equilibrium Scheme (41), it seems helpful to write in analogy to Eq. (6) now Eq. (42) [247]; once $K_{I/tot}$ of Eq. (42) is known, the total concentration of closed species can be calculated with Eq. (11). Furthermore, Eq. (2) is best rewritten as given in Eq. (43). By taking Eq. (7) into account, one obtains Eqs (44) and (45). Finally, from Eqs (42) and (43) follows then Eq. (46). Eqs (42) through (46) are as follows:

$$K_{I/tot} = \frac{[M[d(pGpG)]^{-}_{cl/tot}]}{[M[d(pGpG)]^{-}_{op}]} \tag{42a}$$

$$= \frac{[M[d(pGpG)]^{-}_{cl/N7}] + [M[d(pGpG)]^{-}_{cl/PO}]}{[M[d(pGpG)]^{-}_{op}]} \tag{42b}$$

$$K^{M}_{M[d(pGpG)]} = \frac{[M[d(pGpG)]^{-}]}{[M^{2+}][d(pGpG)^{3-}]} \qquad (2) = (43a)$$

$$= \frac{[M[d(pGpG)]^{-}_{op}] + [M[d(pGpG)]^{-}_{cl/N7}] + [M[d(pGpG)]^{-}_{cl/PO}]}{[M^{2+}][d(pGpG)^{3-}]} \tag{43a}$$

$$= K^{M}_{M[d(pGpG)]op} + K_{I/N7} \cdot K^{M}_{M[d(pGpG)]op} + K_{I/PO} \cdot K^{M}_{M[d(pGpG)]op} \tag{43c}$$

$$= K^{M}_{M[d(pGpG)]op}(1 + K_{I/N7} + K_{I/PO}) \tag{43d}$$

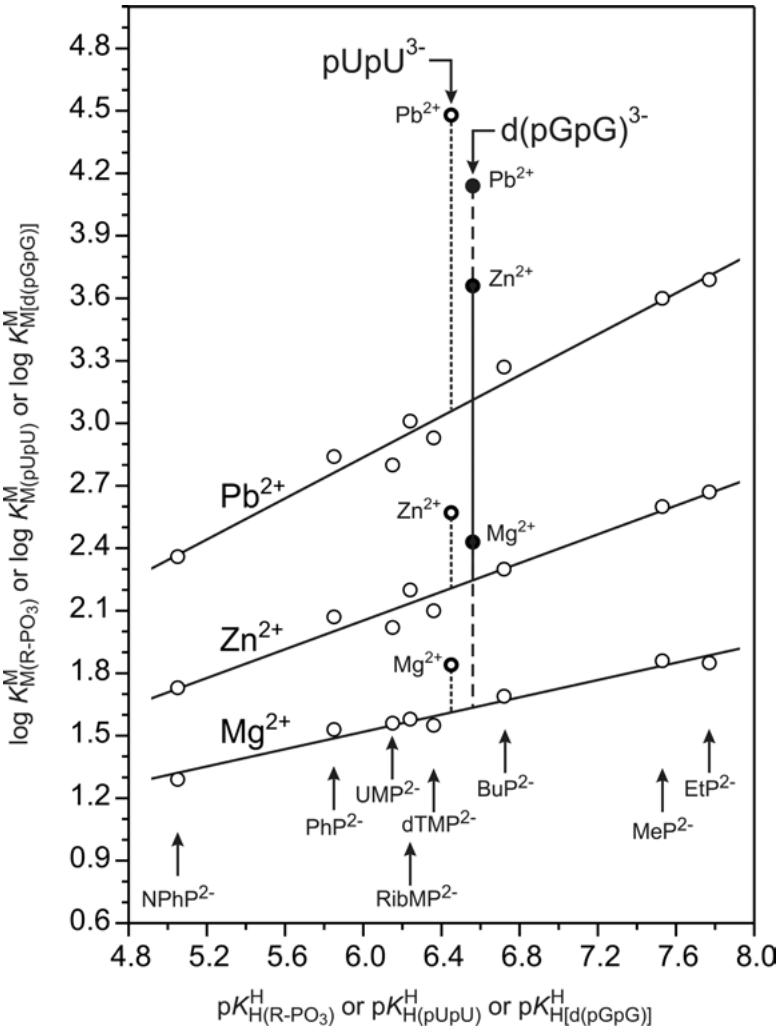

Figure 20. Evidence for an enhanced stability of the $M(pUpU)^-$ and $M[d(pGpG)]^-$ complexes of Mg^{2+}, Zn^{2+}, and Pb^{2+}, based on log $K^{M}_{M(R\text{-}PO_3)}$ *versus* p$K^{H}_{H(R\text{-}PO_3)}$ plots for $M(R\text{-}PO_3)$ complexes, where $R\text{-}PO_3^{2-}$ encompasses the same list of ligands given in the legend of Figure 18. The least-squares lines are drawn through eight data sets [86, 87]; the straight-line parameters are listed in [28, 85, 87, 116]. The data points for the $M^{2+}/H^+/pUpU^{3-}$ and $M^{2+}/H^+/d(pGpG)^{3-}$ systems are based on the values listed in Table 10 [75, 114, 247, 248]. The vertical dotted lines emphasize the stability differences to the reference lines, log $\Delta_{M/pUpU}$ [defined in Eq. (12)], for the $M(pUpU)^-$ complexes. The vertical solid (Zn^{2+}) and broken (Pb^{2+}, Mg^{2+}) lines describe the situation for the $M[d(pGpG)]^-$ complexes. All plotted constants refer to aqueous solutions at 25 °C and $I = 0.1$ M ($NaNO_3$). This is a framed version of Figure 2 in [247] ("Metal-Ion-Coordinating Properties of the Dinucleotide 2′-Deoxyguanylyl-(5′→3′)-2′-deoxy-5′-guanylate ($d(pGpG)^{3-}$): Isomeric Equilibria Including Macrochelated Complexes Relevant for Nucleic Acids"; *Chem. Eur. J.* 2007); reproduced with permission; copyright 2007 Wiley-VCH, Weinheim, Germany.

$$K_{I/N7} = [M[d(pGpG)]^{-}_{cl/N7}]/[M[d(pGpG)]^{-}_{op}] \quad (44)$$

$$K_{I/PO} = [M[d(pGpG)]^{-}_{cl/PO}]/[M[d(pGpG)]^{-}_{op}] \quad (45)$$

$$K_{I/tot} = K_{I/N7} + K_{I/PO} \quad (46)$$

Now the stability enhancements, log $\Delta_{M/d(pGpG)}$, seen in Figure 20 and listed in the lower part of Table 10 in column 5, can be evaluated. Once the charge effect, log $\Delta_{M/pUpU/charge} = 0.24 \pm 0.04$ as defined in Section 7.1, which of course is the same for the $M[d(pGpG)]^{-}$ complexes, is taken into account, one obtains the charge-corrected stability enhancements log $\Delta^{*}_{M/d(pGpG)}$, which are listed in column 6 of Table 10 in the lower part. Thereafter, $K_{I/tot}$ [Eq. (42)] and % $M[d(pGpG)]^{-}_{cl/tot}$ [Eq. (11)] can be calculated; these results are listed in the two terminating columns 7 and 8, respectively (Table 10, lower part).

With $K_{I/tot}$ and % $M[d(pGpG)]^{-}_{cl/tot}$ known, the formation degrees for the isomers occurring in the Equilibrium Scheme (47) can be calulated. The corresponding results are assembled in Table 11 and they are to the largest part self-explaining.

However, a few points need to be recalled:

(i) Mg^{2+} and Cd^{2+} did not show an interaction with the phosphodiester bridge (Table 10, upper part); consequently, the complete stability enhancements (of 0.55 and 1.21 log units, respectively) need to be attributed to macrochelate formation with N7 [please recall the caveats pointed out above together with the Equilibrium Scheme (41)].

(ii) The stability enhancement observed for the $Pb(pUpU)^{-}$ complex (1.16 ± 0.26 log units; Table 10) is larger than the one for the $Pb[d(pGpG)]^{-}$ species (0.79 ± 0.14 log unit), or at its best within its error limits the same. Consequently, there is no indication for the formation of a $Pb[d(pGpG)]^{-}_{cl/N7}$ isomer and the whole stability enhancement needs to be attributed to the formation of the $Pb[d(pGpG)]^{-}_{cl/PO}$ isomer, that is, to the lower branch of Eq. (41).

(iii) Only with $Zn[d(pGpG)]^{-}$ all the isomers seen in the Equilibrium Scheme (41) occur: The value of $K_I = 0.35 \pm 0.25$ determined for $Zn(pUpU)^{-}$ (Table 10; upper part) can safely be assumed to hold also for $K_{I/PO}$ of $Zn[d(pGpG)]^{-}$ (Table 11, colum 6) because the phosphodiester linkage is identical in both dinucleotides. Hence, from Eq. (46) $K_{I/N7}$ follows and thus the percentage for the upper part in Scheme (41). To conclude, for $Zn[d(pGpG)]^{-}$ the upper branch of Eq. (41) dominates with a formation degree of 91 (± 0.25)%, followed by the open isomer with about 6.8 (± 1.4)%, and the 10-membered macrochelate $Zn[d(pGpG)]^{-}_{cl/PO}$ with 2.4 (± 1.8)% (lower branch).

The only other metal ion for which most likely all three isomers of the Equilibrium Scheme (41) occur, is Ca^{2+}; this suggestion appears as valid, even though the given values are only estimates for the various $Ca[d(pGpG)]^{-}$ isomers. Because Ca^{2+} can be a mimic of Pb^{2+} (Sections 1 and 2), the indicated suggestions are worthwhile to be considered.

Table 11. Evaluation of Equilibrium Scheme (41) for the various isomers formed in $M[d(pGpG)]^-$ systems, based on $K_{I/tot}$ (taken from Table 10), together with the percentages in which the isomers occur in aqueous solution at 25 °C and $I = 0.1$ M ($NaNO_3$).[a]

M^{2+}	$K_{I/tot}$ [Eqs (42), (46)]	% $M[d(pGpG)]^-_{cl/tot}$ [Eq. (11)]	% $M[d(pGpG)]^-_{op}$ [Eqs (41), (42a)][b]	$K_{I/N7}$ [Eqs (44), (46)]	$K_{I/PO}$ [Eqs (45), (46)]	% $M[d(pGpG)]^-_{cl/N7}$ [Eq. (44)]	% $M[d(pGpG)]^-_{cl/PO}$ [Eq. (45)]
Mg^{2+}	2.55 ± 0.65	71.8 ± 5.2	28.2 ± 5.2	2.6 ± 0.7[c]	~0[d]	72 ± 5.5[c]	~0[d]
Ca^{2+}			~39			~47	~14
Zn^{2+}	13.791 ± 3.065	93.24 ± 1.40	6.76 ± 1.40	13.44 ± 3.08[e]	0.35 ± 0.25[f]	91 ± 2.5[g]	2.4 ± 1.8[g]
Cd^{2+}	15.22 ± 3.36	93.8 ± 1.3	6.2 ± 1.3	15.2 ± 3.4[c]	~0[d]	94 ± 1.5[c]	~0[d]
Pb^{2+}	5.17 ± 1.99	83.8 ± 5.2	16.2 ± 5.2	~0[h]	5.2 ± 2.0	~0[h]	84 ± 5.5

[a] For the error limits see footnotes "a" in Tables 4 and 6. The estimated values for the $Ca[d(pGpG)]^-$ system are from Table 5 in [106]. The other data are collected from Table 5 in [247].
[b] These values follow from 100 – % $M[d(pGpG)]^-_{cl/tot}$.
[c] Rounded values from columns 2 and 3. No significant amounts of the $M[d(pGpG)]^-_{cl/PO}$ isomers are formed in these cases as is evidenced from the corresponding $M(pUpU)^-$ results listed in the upper part of Table 10.
[d] These values are zero within the error limits as follows from the $M(pUpU)^-$ data in the upper part of Table 10.
[e] Calculated from $K_{I/tot}$ and $K_{I/PO}$ according to Eq. (46).
[f] This value refers to $Zn(pUpU)^-$ and is taken from column 7 in the upper part of Table 10.
[g] % $Zn[d(pGpG)]^-_{cl/PO}$ was calculated from $K_{I/PO}$ and % $Zn[d(pGpG)]^-_{op}$ according to Eq. (45). The value for % $Zn[d(pGpG)]^-_{cl/N7}$ follows from the difference % $Zn[d(pGpG)]^-_{cl/tot}$ – % $Zn[d(pGpG)]^-_{cl/PO}$; it may also be calculated via Eq. (44) which gives the same result but understandably with a larger error; for further details see [247].
[h] Since $K_{I/tot/Pb[d(pGpG)]} = 5.17 \pm 1.99$ appears to be smaller than $K_{I/Pb(pUpU)} = 13.45 \pm 8.65$ (Table 10, upper part, column 7; the errors just overlap), there is no indication for any Pb^{2+} interaction with the N7/(C6)O site in the $Pb[d(pGpG)]^-$ complexes (see also text).

As far as $Pb[d(pGpG)]^-$ is concerned, it seems appropriate to consider the above mentioned stability enhancements again, that is, $\log \Delta_{Pb/pUpU} = 1.16 \pm 0.26 \geq \log \Delta_{Pb/d(pGpG)} = 0.79 \pm 0.14$. We are inclined to consider the indicated difference as real, that is, $\log \Delta\Delta = 0.37 \pm 0.30$. The explanation for the different stability enhancements is that $pUpU^{3-}$ is more flexible than the "stacked" $d(pGpG)^{3-}$ species and that therefore it is easier for Pb^{2+} to form the 10-membered macrochelate with $pUpU^{3-}$ than with $d(pGpG)^{3-}$ in which the intramolecular stack first needs to be disrupted.

7.3. Effect of a Terminal Sulfur Atom in the Phosphodiester Linkage on Metal Ion Coordination

Phosphorothioates are popular alterations of nucleotides in nucleic acid research (Section 6.4). Therefore, complex formation of *P*-thiouridylyl-(5′→3′)-5′-uridylate, $pUp_{(s)}U^{3-}$ (Figure 19), had been studied with several metal ions including Pb^{2+}. The available information [44] is summarized in Table 12, where the arrangement of the data is in analogy to Table 10.

The measured stability constants of the $M(pUp_{(s)}U)^-$ complexes with Mg^{2+}, Mn^{2+}, Zn^{2+}, Cd^{2+}, and Pb^{2+} are listed in the second column of Table 12 and in the third column the calculated stabilities of the $M(R\text{-}PO_3)$ complexes are given; from these data the stability enhancements $\log \Delta_{M/pUp_{(s)}U}$ (column 4) follow. These values need to be corrected for the charge effect of the negatively charged phosphodiester linkage, which is defined as $\log \Delta_{M/pUpU/charge} = 0.24 \pm 0.04$ in Section 7.1, giving thus the corrected values, $\log \overset{*}{\Delta}_{M/pUp_{(s)}U}$, (Table 12, column 5). Here two comments are needed:

(i) The $\log \Delta$ values of 0.26 ± 0.08 and 0.23 ± 0.09 for $Mg(pUp_{(s)}U)^-$ and $Mn(pUp_{(s)}U)^-$, respectively, confirm the mentioned charge effect of 0.24 ± 0.04, and consequently,

(ii) there is no indication for macrochelate formation in $Mg(pUp_{(s)}U)^-$ and $Mn(pUp_{(s)}U)^-$; these complexes occur only in the 'open' form, meaning that M^{2+} is solely coordinated to the terminating 5′-phosphate group (Figure 19).

Most interesting is the situation for the $M(pUp_{(s)}U)^-$ complexes with Zn^{2+} and Cd^{2+}; both have within the error limits the same properties and form macrochelates involving the diester unit with a formation degree of about 65 % (Table 12, column 7). Here it needs to be emphasized that this formation degree may encompass two different 10-membered macrochelates, one formed with S, $M(pUp_{(s)}U)^-_{cl/PS}$, and one with O, $M(pUp_{(s)}U)^-_{cl/PO}$ (cf. Figure 19); this is expressed in the Equilibrium Scheme (47).

Table 12. Logarithms of the stability constants [Eqs (2) and (6)] of several $M(pUp_{(s)}U)^-$ complexes as determined by potentiometric pH titration, together with the calculated stability constants of the 'open' forms [Eq. (7)], as well as of the enhanced complex stabilities, log $\Delta_{M/pNp_{(s)}N}$ [Eq. (12)], due to the extent of the total intramolecular macrochelate formation involving the non-bridging oxygen or sulfur atoms of the phosphodiester linkage [Equilibria (5), (25), and (47)] (aq. sol.; 25 °C; $I = 0.1$ M, $NaNO_3$).[a]

M^{2+}	log $K^{M}_{M(pUp_{(s)}U)}$	log $K^{M}_{M(R\text{-}PO_3)}$ [b]	log $\Delta_{M/pUp_{(s)}U}$ [c]	log $\Delta^{*}_{M/pUp_{(s)}U}$ [d]	$K_{I/tot}$ [e]	% $M(pUp_{(s)U)cl/tot}^{-}$ [f]
Mg^{2+}	1.85 ± 0.08	1.59 ± 0.03	0.26 ± 0.08	0.02 ± 0.09	~0	~0 (<22)
Mn^{2+}	2.42 ± 0.07	2.19 ± 0.05	0.23 ± 0.09	–0.01 ± 0.10	~0	~0 (<19)
Zn^{2+}	2.88 ± 0.07	2.16 ± 0.06	0.72 ± 0.09	0.48 ± 0.10	2.02 ± 0.68	67 ± 8
Cd^{2+}	3.16 ± 0.07	2.48 ± 0.05	0.68 ± 0.09	0.44 ± 0.10	1.75 ± 0.62	64 ± 8
Pb^{2+}	3.49 ± 0.11	2.99 ± 0.08	0.50 ± 0.14	0.26 ± 0.15	0.82 ± 0.61	45 ± 18

[a] For the error limits see footnotes "a" in Tables 4 and 6. The above data are collected from tables 2 and 3 of [44]. For the acidity constant of the $-P(O)_2^-(OH)^-$ residue holds $pK^{H}_{H(pUp_{(s)}U)} = 6.32 \pm 0.03$ [Eq. (3)] [44]. The values for the deprotonation of the (N3)H sites (Figure 19) are $pK^{H}_{pUp_{(s)}U} = 9.29 \pm 0.04$ [Eq. (28)] and $pK^{H}_{[(pUp_{(s)}U)-H]} = 9.98 \pm 0.12$ [44].

[b] See footnote "b" in Table 10.

[c] Calculated according to Eq. (12).

[d] Here the charge of the phosphodiester bridge, exercized on a metal ion coordinated at the terminal phosphate group (Figure 19), is taken into account, that is, $\log \Delta^{*}_{M/pNp_{(s)}N} = \log \Delta_{M/pNp_{(s)}N} - \log \Delta_{M/pUpU/charge}$ and $\log \Delta_{M/pUpU/charge} = 0.24 \pm 0.04$ [75]. See also the above values for Mg^{2+} and Mn^{2+} in column 4, which confirm the size of the charge effect.

[e] See Eqs (9) and (13).

[f] Calculated according to Eq. (11); see also text with regard to the individual isomers of Eq. (47).

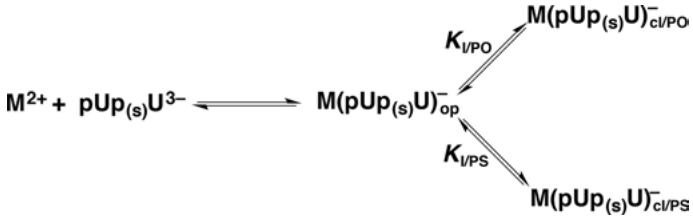

(47)

For $Pb(pUp_{(s)}U)^-$ the formation degree of the 10-membered macrochelate is with about 45 % not very large, meaning that the affinity of Pb^{2+} towards the terminal S atom of the diester bridge (Figure 19) cannot be very pronounced.

The percentages of the two closed isomers defined in the Equilibrium Scheme (47) can be calculated [44] by applying procedures as described for the intramolecular equilibrium $PO \cdot M \rightleftharpoons PS \cdot M$ considered for nucleoside 5′-*O*-thiomonophosphate complexes in Section 6.4 or for the N1 *versus* N7 dichotomy described in Section 4.5.1. The corresponding results are summarized in Table 13 for the $M(pUp_{(s)}U)^-$ complexes of Zn^{2+}, Cd^{2+}, and Pb^{2+}, that is, for these three metal ions for which Equilibrium (47) operates (Table 12). As already mentioned, in the complexes of Mg^{2+} and Mn^{2+} no macrochelates are formed, that is, such species occur at best in traces.

In the second column of Table 13 the values for % $M(pUp_{(s)}U)^-_{cl/tot}$ are repeated from Table 12. A remarkable observation from the data in Table 13 is that Cd^{2+} forms no $Cd(pUp_{(s)}U)^-_{cl/PO}$ isomer, which is in accord with the 0 % observed for $Cd(pUpU)^-$ (Table 10), that is, the lower branch of Equilibrium (47) does not occur, only the $Cd(pUp_{(s)}U)^-_{cl/PS}$ isomer with a formation degree of about 64 % is formed. Consequently, the remaining 36 % are attributed [44] to the 'open' isomer in Eq. (47). The reverse observation is made with Pb^{2+}, and this is rather surprising, considering the situation with $UMPS^{2-}$ (Section 6.4), where S binding is favored; now only $Pb(pUp_{(s)}U)^-_{cl/PO}$ forms with about 45 %, no indication for a S interaction is found. It seems that an initial O donor coordination, as it takes place with the PO_3^{2-} residue, does not favor S coordination but it rather facilitates binding of another O site.

Similar to the observations described in Section 7.2 for the Equilibrium Scheme (41) (Table 11), Zn^{2+} is the most adaptable of the considered metal ions, also for Equilibrium (47). In the present case with $Zn(pUp_{(s)}U)^-$ there are

Table 13. Percentages of isomeric species formed in intramolecular equilibria according to Scheme (47) with $M(pUp_{(s)}U)^-$ complexes (aq. sol.; 25 °C, $I = 0.1$ M, $NaNO_3$).[a]

M^{2+}	% $M(pUp_{(s)}U)^-_{cl/tot}$	% $M(pUp_{(s)}U)^-_{op}$	% $M(pUp_{(s)}U)^-_{cl/PO}$	% $M(pUp_{(s)}U)^-_{cl/PS}$
Zn^{2+}	67 ± 8	33 ± 8	12	55
Cd^{2+}	64 ± 8	36 ± 8	~0	64
Pb^{2+}	45 ± 18	55 ± 18	45	0

[a] The results are based on Tables 10 (upper part) and 12; they are abstracted from table 4 in [44].

55 % present as a macrochelate involving the S atom (lower branch in Eq. (47)), 12 % with an O coordination (upper branch), and 33 % occur as the open isomer. Maybe here is one of the reasons for the immense role that Zn^{2+} plays in bio-systems, that is, its adaptability to different situations [48] without being too one-sided as it is the case for the toxic Cd^{2+} [31].

8. CONCLUDING REMARKS

Humans have used lead for more than 6000 years and its toxicity was known already to Greek and Arab scholars and nowadays, one is again very well aware of this negative effect, yet on a molecular level the toxicity of lead is only partly understood. One of the reasons is that the coordination chemistry of lead(II), this is the relevant oxidation state for bio-systems, is rather complicated. For example, it does not fit the simple *hard-soft principle*: It forms rather insoluble sulfides and appears thus as "soft", yet very often it favors O donor sites, which are "hard" and where it mimics Cu(II) regarding the stability of the complexes (Section 2.2 and 3.3). Furthermore, towards aromatic N sites, like those in imidazole or the N7 site in purines, its affinity is comparable to that of Fe(II). Thus, stability predictions are difficult to make. Moreover, Pb(II) can adopt the coordination numbers between 4 and 10. However, its coordination chemistry is further complicated by the stereochemically active $6s^2$ electron pair, that is, at coordination number 4 the $6s^2$ lone pair is on one side and the liganding atoms on the other (Section 2.3).

Lead(II) is stored in bone replacing Ca(II), but it also interferes with the metabolism of other metal ions including essential ones, like iron, copper or zinc, but also with that of the toxic Cd(II) (Section 2.1). Because this chapter has nucleotides in the focus, we have collected data, as far as available, for the complexes formed by the mentioned metal ions and the individual constituents, i.e., sugars, nucleobases, and phosphates (Sections 3 to 5), and of course, nucleotides themselves (Section 6). It is hoped that the comparisons between the properties of Pb(II) complexes and those of related metal ions that become possible in this way, are of help and contribute to our understanding of the special coordination chemistry of lead(II).

How difficult it is to reach reliable conclusions for a system with unknown properties, shows the following example: With nucleoside 5′-*O*-thiomonophosphates, where the PO_3^{2-} group is replaced by $P(O)_2^-(S)^-$, Pb^{2+} coordinates to nearly 100 % to the sulfur atom (Section 6.4). On the other hand, with a dinucleotide that contains instead of the common phosphodiester linkage one where a terminal O is replaced by a S atom (Section 7.3), Pb^{2+} already coordinated to the terminal 5′-phosphate group (Figure 19), interacts with the O atom of the S-altered diester bridge. In other words, the 10-membered macrochelate that is formed between the phosphate-bound Pb^{2+} and the altered diester linkage, is formed with the O and not the S atom of the linkage, as one might (naively) have predicted.

To conclude, despite all progress made in understanding the formations and stabilities of Pb^{2+} complexes with nucleotides and their constituents, more work is needed to allow fine-tuning of our knowledge as the preceding thio example shows. Most important, no information regarding Pb^{2+} exists yet on the formations and preferred stabilities of mixed ligand or ternary and other higher order complexes – after all, in bio-systems binary complexes are the exceptions, mostly two (or more) different ligands coordinate to a given metal ion.

ACKNOWLEDGMENT

The support of our work by the Department of Chemistry of the University of Basel is gratefully acknowledged.

ABBREVIATIONS AND DEFINITIONS

The abbreviations for the nucleobases and nucleosides are defined in Figure 1 and the labeling systems for the di- and triphosphate residues in Figure 14. Other abbreviations are defined in the legends of Figures 3 to 5, 8 to 13, and 16 to 19. Further abbreviations together with their definitions are listed below.

Species written in the text without a charge do not carry one or represent the species in general (i.e., independent of the protonation degree); which of the two possibilities applies is always clear from the context. In formulas such as $M(H;NMP)^{+}$ the H^{+} and NMP^{2-} are separated by a semicolon to facilitate reading; yet they appear within the same parenthesis to indicate that the proton is at the ligand without defining its location. A formula like $(C2S - H)^{-}$ means that the ligand, here 2-thiocytidine, has lost a proton and it is to be read as C2S *minus* H^{+}. The term (aq) is used to indicate that water is acting as a ligand.

Ac^{-}	acetate
AcP^{-}	acetyl phosphate
Ade	adenine (Figure 1)
Ado	adenosine (Figure 1)
Ado · NO	adenosine (N1)-oxide (Figure 9)
ε-Ado	(N)1,N(6)-ethenoadenosine (= 1,N^{6}-ethenoadenosine) (Figure 9)
ADP^{3-}	adenosine 5′-diphosphate (Figure 16)
AMP^{2-}	adenosine 5′-monophosphate (Figure 16)
2A9MP	2-amino-9-methylpurine (Figure 8)
6A9MP	6-amino-9-methylpurine = 9-methyladenine = 9MeA (Figure 8)
$AMPS^{2-}$	adenosine 5′-*O*-thiomonophosphate
ATP^{4-}	adenosine 5′-triphosphate (Figure 16)
AZA	azathiopurine
BI	benzimidazole (Figure 10, including BI derivatives)
C2S	2-thiocytidine (Figure 12)
CA^{-}	general carboxylate ligand

CMP^{2-}	cytidine 5′-monophosphate
CN	coordination number
CTP	cytidine 5′-triphosphate
Cyd	cytidine (Figures 1 and 12)
Cyt	cytosine (Figure 1)
DFT	density functional theory
DHAP	dihydroxyacetone phosphate
Dien	diethylenetriamine = 1,4,7-triazaheptane
DMBI	1,4-dimethylbenzimidazole (Figure 10)
2,9DMP	2,9-dimethylpurine (Figure 8)
DP	diphosphate
$d(pGpG)^{3-}$	see Figure 19
DRB	5,6-dichloro-1-(β-D-ribofuranosyl)benzimidazole (Figure 10)
dThd	thymidine [= 1-(2-deoxy-β-D-ribofuranosyl)thymine] (Figure 1)
$dTMP^{2-}$	thymidine 5′-monophosphate
emf	electromagnetic field
ESI	electrospray ionization
FTIR	Fourier transform infrared spectroscopy
$G1P^{2-}$	glycerol 1-phosphate = α-glycerophosphate (Figure 3)
Gua	guanine (Figure 1)
Guo	guanosine (Figure 1)
H(Or)	orotidine (Figure 11)
HMP^{2-}	hydroxymethylphosphonate (Figure 3)
$HOAc^{-}$	hydroxyacetate
$3\,HOPr^{-}$	3-hydroxypropionate
Hyp	hypoxanthine (Figure 1)
I	ionic strength
Im	imidazole
IMS	ion mobility spectrometry
Ino	inosine (Figure 1)
Ino · NO	inosine (N1)-oxide (Figure 9)
IRMPD	infrared multiple-photon dissociation
K	(macro) equilibrium constant [see Eqs. (1), (2), (3), etc.)]
k	micro equilibrium constant
K_I	intramolecular dimension-less equilibrium constant
MABI	1-methyl-4-aminobenzimidazole (Figure 10)
9MAde	9-methyladenine = 6-amino-9-methylpurine = 6A9MP (Figure 8)
$MeOPS^{2-}$	methyl thiophosphate
MP	monophosphate
6MP	6-mercaptopurine (see also Figure 9)
MPO^{2-}	methyl phosphate
MPS^{2-}	methyl thiophosphate
MS/MS	tandem mass spectrometry
NDP^{3-}	nucleoside diphosphate
NMP^{2-}	nucleoside monophosphate
NMR	nuclear magnetic resonance

NS	nucleoside
NTP^{4-}	nucleoside triphosphate
OMP^{3-}	orotidinate 5′-monophosphate
Or–	orotidinate; see also H(Or)
PBS	primary binding site
$pNpN^{3-}$	dinucleotide (see Figure 19)
PS	nucleoside phosphorothioates (= thionucleotides)
Pu	purine derivative
$pUp_{(s)}U^{3-}$	see Figure 19
$pUpU^{3-}$	see Figure 19
$(RO)_2PO_2^-$	phosphodiester linkage/bridge (Figure 14)
$R\text{-}DP^{3-}$	diphosphate monoester (Figure 14)
$R\text{-}MP^{2-}$	monophosphate monoester (Figure 14)
9R-6MP	9-(β-D-ribofuranosyl)-6-mercaptopurine (Figure 9)
9R-6TG	9-(β-D-ribofuranosyl)-6-thioguanine (Figure 9)
$R\text{-}TP^{4-}$	triphosphate monoester (Figure 14)
$RibMP^{2-}$	D-ribose 5-monophosphate
siRNA	small interfering RNA
6TG	6-mercaptoguanine (see also Figure 9)
Thy	thymine (Figure 1)
TP	triphosphate
Tu	tubercidin (= 7-deazaadenosine) (Figure 9)
U	uridine-type ligand
$(U - H)^-$	uridinate-type ligand
U2S	2-thiouridine (Figure 13)
U2S4S	2,4-dithiouridine (Figure 13)
$U2SMP^{2-}$	2-thiouridine 5′-monophosphate (Figure 17)
U4S	4-thiouridine (Figure 13)
$U4SMP^{2-}$	4-thiouridine 5′-monophosphate (Figure 17)
UDP^{3-}	uridine 5′-diphosphate (Figure 16)
UMP^{2-}	uridine 5′-monophosphate (Figures 16 and 17)
$UMPS^{2-}$	uridine 5′-thiomonophosphate
Ura	uracil (Figure 1)
Urd	uridine (Figures 11 and 13)
$(Urd - H)^-$	uridinate
UTP^{4-}	uridine 5′-triphosphate (Figure 16)
Xao	xanthosine (Figure 9)

REFERENCES

1. R. B. Martin, *Met. Ions Biol. Syst.* **1986**, *20*, 21–65.
2. R. A. Goyer, in *Handbook on Toxicity of Inorganic Compounds*, Eds H. G. Seiler, H. Sigel, A. Sigel, Dekker, New York, 1988, pp. 359–382.
3. J. Molin Christensen, J. Kristiansen, in *Handbook on Metals in Clinical and Analytical Chemistry*, Eds H. G. Seiler, A. Sigel, H. Sigel, Dekker, New York, 1994, pp. 425–440.

4. K. Deibler, P. Basu, *Eur. J. Inorg. Chem.* **2013**, 1086–1096.
5. N. M. Roy, S. DeWolf, B. Carneiro, *Aquatic Toxicology* **2015**, *158*, 138–148.
6. S. Tiwari, I. P. Tripathi, H. L. Tiwari, *Res. J. Chem. Sci.* **2013**, *3*, 86–88.
7. S. Hernberg, *Am. J. Ind. Med.* **2000**, *38*, 244–254.
8. L. Yuan, W. Zhi, Y. Liu, S. Karyala, P. J. Vikesland, X. Chen, H. Zhang, *Environ. Sci. Technol.* **2015**, *49*, 824–830.
9. M. Alushllari, *J. Internat. Environmental Application & Science* **2015**, *10*, 108–112.
10. H. Sigel, C. P. Da Costa, R. B. Martin, *Coord. Chem. Rev.* **2001**, *219–221*, 435–461.
11. J. Arora, A. K. Choudhary, S. S. Kishanrao, J. Gumashta, *Int. J. Pharma Bio Sciences* **2015**, *6*, 600–605.
12. J.-H. Yoon, Y.-S. Ahn, *J. Affective Disord.* **2016**, *190*, 41–46.
13. W.-H. Jang, K.-M. Lim, K. Kim, J.-Y. Noh, S. Kang, Y.-K. Chang, J.-H. Chung, *Toxicol. Sciences* **2011**, *122*, 177–184.
14. G. T. Ramesh, S. K. Manna, B. B. Aggarwal, A. L. Jadhav, *Toxicol. Appl. Pharmacol.* **1999**, *155*, 280–286.
15. U. Bergstroem, B. Ekstrand-Hammarstroem, L. Haegglund, H. Wingfors, *J. Toxicol. Environm. Health*, *Part A* **2015**, *78*, 645–661.
16. M. J. McCabe, Jr., D. A. Lawrence, *J. Immunol.* **1990**, *145*, 671–677.
17. H. Haase, L. Rink, *Metallomics* **2014**, *6*, 1175–1180.
18. F. M. Johnson, *Mutation Res.* **1998**, *410*, 123–140.
19. L. Zhen, Y. Yu, L. Xiaohong, W. Aimin, M. Mingdao, L. Nana, D. Ying, J. Xi, L. Shengli, L. Yuan, C. Xinlin, W. Fudi, Z. Jun, *Reproductive Toxicol.* **2015**, *51*, 1–6.
20. L. Xu, J. Ge, X. Huo, Y. Zhang, A. T. Y. Lau, X. Xu, *Sci. Total Environment* **2016**, *550*, 1163–1170.
21. R. B. Martin, *Met. Ions Biol. Syst.* **1984**, *17*, 1–49.
22. K. Aoki, *Met. Ions Biol. Syst.* **1996**, *32*, 91–134.
23. R. B. Martin, Y. H. Mariam, *Met. Ions Biol. Syst.* **1979**, *8*, 57–124.
24. R. Tribolet, H. Sigel, *Eur. J. Biochem.* **1987**, *163*, 353–363.
25. D. B. Davies, P. Rajani, H. Sadikot, *J. Chem. Soc. Perkin Trans. 2*, **1985**, 279–285.
26. H. Sigel, *ACS Symp. Series* **1989**, *402*, 159–204.
27. H. Sigel, *Chem. Soc. Rev.* **1993**, *22*, 255–267.
28. H. Sigel, B. Song, *Met. Ions Biol. Syst.* **1996**, *32*, 135–205.
29. W. Saenger, *Principles of Nucleic Acid Structure*, Springer-Verlag, New York, 1984, pp. 1–556.
30. R. K. O. Sigel, M. Skilandat, A. Sigel, B. P. Operschall, H. Sigel, *Met. Ions Life Sci.* **2013**, *11*, 191–274; see also Chapter 8 in [31].
31. *Cadmium: From Toxicity to Essentiality*, Vol. 11 of *Metal Ions in Life Sciences*, Eds A. Sigel, H. Sigel, R. K. O. Sigel, Springer, Dordrecht, Heidelberg, New York, London, 2013, pp. 1–560.
32. R. B. Martin, in *Handbook on Toxicity of Inorganic Compounds*, Eds H. G. Seiler, H. Sigel, A. Sigel, Dekker, New York, 1988, pp. 9–25.
33. R. B. Martin, in *Encyclopedia of Inorganic Chemistry*, Vol. 4, Ed. R. B. King, Wiley, Chichester, U.K., 1994, pp. 2185–2196.
34. R. B. Martin, in *Molecular Biology and Biotechnology*, Ed. R. A. Meyers, VCH Publishers, New York, 1995, pp. 83–86.
35. R. B. Martin, in *Encyclopedia of Molecular Biology and Molecular Medicine*, Vol. 1, Ed. R. A. Meyers, VCH, Weinheim, Germany, 1996, pp. 125–134.
36. H. M. Irving, R. J. P. Williams, *Nature* **1948**, *162*, 746–747.
37. H. M. Irving, R. J. P. Williams, *J. Chem. Soc.* **1953**, 3192–3210.
38. *NIST Critically Selected Stability Constants of Metal Complexes*, Reference Database 46, Version 6; data collected and selected by R. M. Smith and A. E. Martell, U. S.

Department of Commerce, National Institute of Standards and Technology, Gaithersburg, MD, USA, 2001.
39. C. P. Da Costa, D. Krajewska, A. Okruszek, W. J. Stec, H. Sigel, *J. Biol. Inorg. Chem.* **2002**, *7*, 405–415.
40. A. Saha, N. Saha, L.-n. Ji, J. Zhao, F. Gregán, S. A. A. Sajadi, B. Song, H. Sigel, *J. Biol. Inorg. Chem.* **1996**, *1*, 231–238.
41. R. K. O. Sigel, B. Song, H. Sigel, *J. Am. Chem. Soc.* **1997**, *119*, 744–755.
42. C. P. Da Costa, A. Okruszek, H. Sigel, *ChemBioChem* **2003**, *4*, 593–602.
43. A. Sigel, B. P. Operschall, A. Matera-Witkíewícz, J. Swiatek-Kozlowska, H. Sigel, *Coord. Chem. Rev.* **2016**, *327–328*, 200–220.
44. B. Knobloch, B. Nawrot, A. Okruszek, R. K. O. Sigel, *Chem. Eur. J.* **2008**, *14*, 3100–3109.
45. P. G. Harrison, *Coord. Chem. Rev.* **1976**, *20*, 1–36.
46. L. Shimoni-Livny, J. P. Glusker, C. W. Bock, *Inorg. Chem.* **1998**, *37*, 1853–1867.
47. R. D. Shannon, *Acta Cryst.* **1976**, *A32*, 751–767.
48. H. Sigel, R. B. Martin, *Chem. Soc. Rev.* **1994**, *23*, 83–91.
49. H. Sigel, D. B. McCormick, *Acc. Chem. Res.* **1970**, *3*, 201–208.
50. K. B. Yatsimirskii, *Theoret. Exper. Chem.* **1994**, *30*, 1–9.
51. W. E. Morf, W. Simon, *Helv. Chim. Acta* **1971**, *54*, 794–810.
52. L. G. Sillén, A. E. Martell, *Stability Constants of Metal-Ion Complexes*, Special Publication 17, The Chemical Society, London, 1964.
53. L. G. Sillén, A. E. Martell, *Stability Constants of Metal-Ion Complexes*, *Supplement No. 1*, Special Publication 25, The Chemical Society, London, 1971.
54. E. Högfeldt, *Stability Constants of Metal-Ion Complexes, Part A: Inorganic Ligands*, IUPAC Chemical Data Series 21, Pergamon Press, Oxford, New York, 1982.
55. R. M. Smith, A. E. Martell, *Critical Stability Constants, Vol. 4: Inorganic Complexes*, Plenum Press, New York, London, 1976.
56. N. Wiberg, *Holleman-Wiberg, Lehrbuch der Anorganischen Chemie*, Aufl. 91–100, Walter de Gruyter, Berlin, New York, 1985, p. 213.
57. *Handbook of Chemistry and Physics, 74th ed.*, Ed. D. R. Lide, CRC Press, Boca Raton, FL, Ann Arbor, MI, London, Tokyo, 1993, pp. 8–49.
58. A. M. Pyle, *Met. Ions Biol. Syst.* **1996**, *32*, 479–520.
59. J. E. Huheey, *Inorganic Chemistry*, Harper and Row, New York, 1983.
60. R. K. O. Sigel, H. Sigel, in *Bioinorganic Fundamentals and Applications: Metals in Natural Living Systems and Metals in Toxicology and Medicine*, Eds V. L. Pecoraro, T. Hambley, in Volume 3 of *Comprehensive Inorganic Chemistry II*, Eds J. Reedijk, K. Poeppelmeier; Elsevier, Oxford, UK, 2013, pp. 623–660.
61. C. F. Baes, Jr., R. E. Mesmer, *The Hydrolysis of Cations*, Krieger Publishing Co., Malabar, Florida, 1976, pp. 1–496.
62. F. M. Al-Sogair, B. P. Operschall, A. Sigel, H. Sigel, J. Schnabl, R. K. O. Sigel, *Chem. Rev.* **2011**, *111*, 4964–5003.
63. I. Filipović, T. Matusinović, B. Mayer, I. Piljac, B. Bach-Dragutinović, A. Bujak, *Croat. Chem. Acta* **1970**, *42*, 541–549.
64. N. Saha, H. Sigel, *J. Am. Chem. Soc.* **1982**, *104*, 4100–4105.
65. A. I. Vogel, *A Text-Book of Macro and Semimicro Qualitative Inorganic Analysis*, 4th ed.; Longmans, Green and Co., London, 1957, p. 40.
66. A. C. Dlouhy, C. E. Outten, *Met. Ions Life Sci.* **2013**, *12*, 241–278.
67. H. Sigel, F. Hofstetter, R. B. Martin, R. M. Milburn, V. Scheller-Krattiger, K. H. Scheller, *J. Am. Chem. Soc.* **1984**, *106*, 7935–7946.
68. H. Sigel, *Coord. Chem. Rev.* **1990**, *100*, 453–539.
69. R. K. O. Sigel, A. M. Pyle, *Chem. Rev.* **2007**, *107*, 97–113.
70. C. S. Fullmer, S. Edelstein, R. H. Wasserman, *J. Biol. Chem.* **1985**, *260*, 6816–6819.

71. H. Sigel, E. M. Bianchi, N. A. Corfù, Y. Kinjo, R. Tribolet, R. B. Martin, *J. Chem. Soc., Perkin Trans. 2* **2001**, 507–511.
72. C. P. Da Costa, H. Sigel, *Inorg. Chem.* **2003**, *42*, 3475–3482.
73. A. Mucha, B. Knobloch, M. Jeżowska-Bojczuk, H. Kozlowski, R. K. O. Sigel, *Chem. Eur. J.* **2008**, *14*, 6663–6671.
74. B. Lippert, *Prog. Inorg. Chem.* **2005**, *54*, 385–447.
75. B. Knobloch, D. Suliga, A. Okruszek, R. K. O. Sigel, *Chem. Eur. J.* **2005**, *11*, 4163–4170.
76. I. Smirnov, R. H. Shafer, *J. Mol. Biol*. **2000**, *296*, 1–5.
77. S. Kuusela, H. Lönnberg, *Met. Ions Biol. Syst.* **1996**, *32*, 271–300.
78. J. J. Butzow, G. L. Eichhorn, *J. Inorg. Biochem.* **1986**, *28*, 21–31.
79. S. Yano, M. Otsuka, *Met. Ions Biol. Syst.* **1996**, *32*, 27–60.
80. H. Sawai, *J. Am. Chem. Soc.* **1976**, *98*, 7037–7039.
81. H. Sawai, T. Shibata, M. Ohno, *Tetrahedron* **1981**, *37*, 481–485.
82. H. Sawai, K. Kuroda, T. Hojo, *Bull. Chem. Soc. Jpn.* **1989**, *62*, 2018–2023.
83. M. Shimazu, K. Shinozuka, H. Sawai, *Angew. Chem. Int. Ed. Engl.* **1993**, *32*, 870–872.
84. R. B. Martin, H. Sigel, *Comments Inorg. Chem.* **1988**, *6*, 285–314.
85. H. Sigel, L. E. Kapinos, *Coord. Chem. Rev.* **2000**, *200–202*, 563–594.
86. S. S. Massoud, H. Sigel, *Inorg. Chem.* **1988**, *27*, 1447–1453.
87. H. Sigel, D. Chen, N. A. Corfù, F. Gregáň, A. Holý, M. Strašák, *Helv. Chim. Acta* **1992**, *75*, 2634–2656.
88. H. Sigel, B. Song, G. Liang, R. Halbach, M. Felder, M. Bastian, *Inorg. Chim. Acta* **1995**, *240*, 313–322.
89. H. Sigel, R. B. Martin, R. Tribolet, U. K. Häring, R. Malini-Balakrishnan, *Eur. J. Biochem.* **1985**, *152*, 187–193. See also the comment in the footnote on p. 258 in [90].
90. M. Bastian, H. Sigel, *Inorg. Chim. Acta* **1990**, *178*, 249–259.
91. G. Liang, D. Chen, M. Bastian, H. Sigel, *J. Am. Chem. Soc.* **1992**, *114*, 7780–7785.
92. H. Sigel, C. P. Da Costa, B. Song, P. Carloni, F. Gregáň, *J. Am. Chem. Soc.* **1999**, *121*, 6248–6257.
93. L.-G. Ekström, A. Olin, *Acta Chem. Scand. A* **1977**, *31*, 838–844.
94. S. J. Angyal, *Aust. J. Chem.* **1972**, *25*, 1957–1966.
95. S. J. Angyal, *Pure Appl. Chem.* **1973**, *35*, 131–146.
96. M. M. Hämäläinen, H. Lönnberg, *Carbohydrate Res.* **1991**, *215*, 357–360.
97. S. J. Angyal, J. A. Mills, *Aust. J. Chem.* **1979**, *32*, 1993–2001.
98. H.-A. Tajmir-Riahi, *Bull. Chem. Soc. Jpn.* **1989**, *62*, 1281–1286.
99. T. Lis, *Acta Crystallogr., Sect. C* **1984**, *40*, 374–376.
100. J. Y. Salpin, J. Tortajada, *Adv. Mass. Spectrometry* **2001**, *15*, 735–736.
101. F. Coccioli, M. Vicedomini, *Ann. Chim. (Rome)* **1974**, *64*, 513–522.
102. R. K. O. Sigel, H. Sigel, *Met. Ions Life Sci.* **2007**, *2*, 109–180.
103. H. Reinert, R. Weiss, *Hoppe-Seylers Z. Physiol. Chem.* **1969**, *350*, 1321–1326.
104. Y.-Y. H. Chao, D. R. Kearns, *J. Am. Chem. Soc.* **1977**, *99*, 6425–6434.
105. T. Lan, Y. Lu, *Met. Ions Life Sci.* **2012**, *10*, 217–248.
106. R. K. O. Sigel, H. Sigel, *Acc. Chem. Res.* **2010**, *43*, 974–984.
107. C. P. Da Costa, H. Sigel, *Inorg. Chem.* **2000**, *39*, 5985–5993.
108. K. H. Scheller, F. Hofstetter, P. R. Mitchell, B. Prijs, H. Sigel, *J. Am. Chem. Soc.* **1981**, *103*, 247–260.
109. H. Lönnberg, P. Vihanto, *Inorg. Chim. Acta* **1981**, *56*, 157–161.
110. A. M. Fiskin, M. Beer, *Biochemistry* **1965**, *4*, 1289–1294.
111. B. Song, J. Zhao, R. Griesser, C. Meiser, H. Sigel, B. Lippert, *Chem. Eur. J.* **1999**, *5*, 2374–2387.
112. Y. Kinjo, L.-n. Ji, N. A. Corfù, H. Sigel, *Inorg. Chem.* **1992**, *31*, 5588–5596.

113. B. Knobloch, H. Sigel, *J. Biol. Inorg. Chem.* **2004**, *9*, 365–373.
114. C. P. Da Costa, H. Sigel, *J. Biol. Inorg. Chem.* **1999**, *4*, 508–514.
115. B. Knobloch, W. Linert, H. Sigel, *Proc. Natl. Acad. Sci.* **2005**, *102*, 7459–7464.
116. H. Sigel, S. S. Massoud, N. A. Corfù, *J. Am. Chem. Soc.* **1994**, *116*, 2958–2971.
117. Y. Kinjo, R. Tribolet, N. A. Corfù, H. Sigel, *Inorg. Chem.* **1989**, *28*, 1480–1489.
118. L. E. Kapinos, B. P. Operschall, E. Larsen, H. Sigel, *Chem. Eur. J.* **2011**, *17*, 8156–8164.
119. R. Stewart, M. G. Harris, *Can. J. Chem.* **1977**, *55*, 3807–3814.
120. A. Sigel, B. P. Operschall, H. Sigel, *Coord. Chem. Rev.* **2012**, *256*, 260–278.
121. R. R. Wu, C. C. He, L. A. Hamlow, Y.-w. Nei, G. Berden, J. Oomens, M. T. Rodgers, *J. Phys. Chem. B* **2016**, *120*, 4616–4624.
122. H. Sigel, S. S. Massoud, R. Tribolet, *J. Am. Chem. Soc.* **1988**, *110*, 6857–6865.
123. Y. Kinjo, R. Tribolet, N. A. Corfù, H. Sigel, *Inorg. Chem.* **1989**, *28*, 1480–1489.
124. L. E. Kapinos, H. Sigel, *Inorg. Chim. Acta* **2002**, *337*, 131–142.
125. L. E. Kapinos, A. Holý, J. Günter, H. Sigel, *Inorg. Chem.* **2001**, *40*, 2500–2508.
126. R. B. Martin, *Met. Ions Biol. Syst.* **1996**, *32*, 61–89.
127. K. H. Scheller, V. Scheller-Krattiger, R. B. Martin, *J. Am. Chem. Soc.* **1981**, *103*, 6833–6839.
128. S.-H. Kim, R. B. Martin, *Inorg. Chim. Acta* **1984**, *91*, 19–24.
129. R. B. Martin, *Acc. Chem. Res.* **1985**, *18*, 32–38.
130. H. Sigel, N. A. Corfù, L.-n. Ji, R. B. Martin, *Comments Inorg. Chem.* **1992**, *13*, 35–59.
131. L. E. Kapinos, H. Sigel, results to be published.
132. M. D. Reily, T. W. Hambley, L. G. Marzilli, *J. Am. Chem. Soc.* **1988**, *110*, 2999–3007.
133. M. A. Salam, K. Aoki, *Inorg. Chim. Acta* **2001**, *314*, 71–82.
134. J.-Y. Salpin, L. MacAleese, F. Chirot, P. Dugourd, *Phys. Chem. Chem. Phys.* **2014**, *16*, 14127–14138.
135. R. W. Gellert, R. Bau, *Met. Ions Biol. Syst.* **1979**, *8*, 1–55.
136. J.-Y. Salpin, L. Gamiette, J. Tortajada, T. Besson, P. Mâitre, *Internat. J. Mass Spectrometry* **2011**, *304*, 154–164.
137. H. Einspahr, C. E. Bugg, *Met. Ions Biol. Syst.* **1984**, *17*, 51–97.
138. J.-Y. Salpin, S. Guillaumont, D. Ortiz, J. Tortajada, P. Mâitre, *Inorg. Chem.* **2011**, *50*, 7769–7778.
139. B. Knobloch, C. P. Da Costa, W. Linert, H. Sigel, *Inorg. Chem. Commun.* **2003**, *6*, 90–93.
140. Y. Saito, A. Suzuki, I. Saito, *Fluorescent Purine Nucleosides and Their Applications*, in *Modified Nucleic Acids*, Vol. 31 of „Nucleic Acids and Molecular Biology“, Eds K. Nakatani, Y. Tor, Springer International Publishing, Switzerland, 2016, pp. 27–61.
141. J. Arpalahti, H. Lönnberg, *Inorg. Chim. Acta* **1983**, *78*, 63–68.
142. J. Arpalahti, E. Ottoila, *Inorg. Chim. Acta* **1985**, *107*, 105–110.
143. H. Lönnberg, J. Arpalahti, *Inorg. Chim. Acta* **1981**, *55*, 39–42.
144. H. Sigel, R. Griesser, *Chem. Soc. Rev.* **2005**, *34*, 875–900.
145. G. Kampf, L. E. Kapinos, R. Griesser, B. Lippert, H. Sigel, *J. Chem. Soc., Perkin Trans. 2* **2002**, 1320–1327.
146. A. Nagasawa, H. Diebler, *J. Phys. Chem.* **1981**, *85*, 3523–3528.
147. B. Knobloch, A. Okruszek, H. Sigel, *Inorg. Chem.* **2008**, *47*, 2641–2648.
148. J. Arpalahti, P. Lehikoinen, *Inorg. Chem.* **1990**, *29*, 2564–2567.
149. R. Griesser, G. Kampf, L. E. Kapinos, S. Komeda, B. Lippert, J. Reedijk, H. Sigel, *Inorg. Chem.* **2003**, *42*, 32–41.
150. H. R. Mahler, E. H. Cordes, *Biological Chemistry*, Harber and Row, New York, 1966.
151. L.-n. Ji, N. A. Corfù, H. Sigel, *J. Chem. Soc. Dalton Trans.* **1991**, 1367–1375.
152. V. A. Mulamoottil, *Current Organic Chem.* **2016**, *20*, 830–838.

153. K. Kohno, E. Ohashi, O. Sano, H. Kusano, T. Kunikata, N. Arai, T. Hanaya, T. Kawata, T. Nishimoto, S. Fukuda, *J. Inflammation* **2015**, *12*, 2, DOI: 10.1186/s12950-014-0045-0.
154. A. L. Khandazhinskaya, E. A. Shirokova, A. V. Shipitsin, I. L. Karpenko, E. F. Belanov, M. K. Kukhanova, M. V. Yasko, *Collect. Czech. Chem. Commun.* **2006**, *71*, 1107–1121.
155. D. D. Perrin, *J. Am. Chem. Soc.* **1960**, *82*, 5642–5645.
156. H. Sigel, *Met. Ions Biol. Syst.* **1979**, *8*, 125–158.
157. H. Sigel, H. Brintzinger, *Helv. Chim. Acta* **1964**, *47*, 1701–1717.
158. E. Sharon, S. A. Lévesque, M. N. Munkonda, J. Sévigny, D. Ecke, G. Reiser, B. Fischer, *ChemBioChem* **2006**, *7*, 1361–1374.
159. H. Sigel, *CHIMIA* **1987**, *41*, 11–26.
160. K. H. Scheller, H. Sigel, *J. Am. Chem. Soc.* **1983**, *105*, 3005–3014.
161. H. Sigel, K. H. Scheller, *Eur. J. Biochem.* **1984**, *138*, 291–299.
162. H. Sigel, H. Brintzinger, *Helv. Chim. Acta* **1965**, *48*, 433–437.
163. H. Sigel, *Helv. Chim. Acta* **1965**, *48*, 1513–1518.
164. H. Sigel, *Helv. Chim. Acta* **1965**, *48*, 1519–1524.
165. J. D. Rawn, *Biochemistry*, Neil Patterson Publ., Burlington, North Carolina, USA, 1989.
166. R. Hille, *Met. Ions Life Sci.* **2009**, *6*, 395–416.
167. R. K. Choudhary, A. V. Capuco, *BMC Cell Biology* **2012**, *13*, 14; DOI: 10.1186/1471-2121-13-14.
168. H. Ashihara, T. Yokota, A. Crozier, *Adv. Botanical Res.* **2013**, *68*, 111–138; DOI: 10.1016/B978-0-12-408061-4. 00004-3.
169. H. Sigel, B. P. Operschall, R. Griesser, *Chem. Soc. Rev.* **2009**, *38*, 2465–2494.
170. H. Sigel, S. S. Massoud, B. Song, R. Griesser, B. Knobloch, B. P. Operschall, *Chem. Eur. J.* **2006**, *12*, 8106–8122.
171. B. Maiti, K. Chanda, *RSC Advances* **2016**, *6*, 50384–50413.
172. M. Gaba, C. Mohan, *Med. Chem. Res.* **2016**, *25*, 173–210.
173. A. A. Spasov, K. Y. Kalitin, O. Y. Grechko, V. A. Anisimova, *Bull. Exper. Biol. Medicine* **2016**, *160*, 336–339.
174. A. Ashraf, W. A. Siddiqui, J. Akbar, G. Mustafa, H. Krautscheid, N. Ullah, B. Mirza, F. Sher, M. Hanif, C. G. Hartinger, *Inorg. Chim. Acta* **2016**, *443*, 179–185.
175. Y. Shin, J. Suchomel, M. Cardozo, J. Duquette, X. He, K. Henne, Y.-L. Hu, R. C. Kelly, J. McCarter, L. R. McGee, J. C. Medina, D. Metz, T. San Miguel, D. Mohn, T. Tran, C. Vissinga, S. Wong, S. Wannberg, D. A. Whittington, J. Whoriskey, G. Yu, L. Zalameda, X. Zhang, T. D. Cushing, *J. Med. Chem.* **2016**, *59*, 431–447.
176. W. Han, Y. Ding, Y. Xu, K. Pfister, S. Zhu, B. Warne, M. Doyle, M. Aikawa, P. Amiri, B. Appleton, D. D. Stuart, A. Fanidi, C. M. Shafer, *J. Med. Chem.* **2016**, *59*, 3034–3045.
177. L. E. Kapinos, B. Song, H. Sigel, *Chem. Eur. J.* **1999**, *5*, 1794–1802.
178. L. E. Kapinos, B. Song, H. Sigel, *Z. Naturforsch.* **1998**, *53b*, 903–908.
179. L. E. Kapinos, H. Sigel, *Eur. J. Inorg. Chem.* **1999**, 1781–1786.
180. I. Daehn, R. Brem, E. Barkauskaite, P. Karran, *FEBS Lett.* **2011**, *585*, 3941–3946.
181. K. E. La Duke, S. Ehling, J. M. Cullen, W. Baumer, *Amer. J. Veter. Res.* **2015**, *76*, 649–655.
182. A. A. Fernandez-Ramos, V. Poindessous, C. Marchetti-Laurent, N. Pallet, M. A. Loriot, *Biochimie* **2016**, *127*, 23–36.
183. M. P. Burke, K. M. Borland, V. A. Litosh, *Curr. Topics Med. Chem.* **2016**, *16*, 1231–1241.
184. E. Dubler, *Met. Ions Biol. Syst.* **1996**, *32*, 301–338.
185. G.-X. Li, Z.-Q. Liu, *Eur. J. Med. Chem.* **2009**, *44*, 4841–4847.

186. N. M. Heerasing, J. F. Ng, D. Dowling, *Internal Med. J.* **2016**, *46*, 465–469.
187. U. Krug, W. E. Berdel, R. P. Gale, C. Haferlach, S. Schnittger, C. Müller-Tidow, J. Braess, K. Spiekermann, P. Staib, D. Beelen, H. Serve, C. Schliemann, M. Stelljes, L. Balleisen, G. Maschmeyer, A. Grüneisen, H. Eimermacher, A. Giagounidis, H. Rasche, R. Hehlmann, E. Lengfelder, E. Thiel, A. Reichle, C. Aul, W.-D. Ludwig, W. Kern, T. Haferlach, W. Köpcke, D. Görlich, M. C. Sauerland, A. Heinecke, B. J. Wörmann, W. Hiddemann, T. Büchner, *Leukemia* **2016**, *30*, 1230–1236.
188. R. Ilavarasi, *Asian J. Chem.* **2015**, *27*, 4505–4509.
189. T. Kowalik-Jankowska, K. Varnagy, J. Swiatek–Kozłowska, A. Jon, I. Sóvágó, E. Sochacka, A. Malkiewicz, J. Spychala, H. Kozłowski, *J. Inorg. Biochem.* **1997**, *65*, 257–262.
190. J. Swiatek, B. Gulanowski, *Acta Biochim. Pol.* **1990**, *37*, 7–20.
191. J. Swiatek, *J. Coord. Chem.* **1990**, *22*, 121–130.
192. O. Iranzo, H. Khalili, D. M. Epstein, J. R. Morrow, *J. Biol. Inorg. Chem.* **2004**, *9*, 462–470.
193. M. Fujihashi, T. Ishida, S. Kuroda, L. P. Kotra, E. F. Pai, K. Miki, *J. Am. Chem. Soc.* **2013**, *135*, 17432–17443.
194. V. Iiams, B. J. Desai, A. A. Fedorov, E. V. Fedorov, S. C. Almo, J. A. Gerlt, *Biochemistry* **2011**, *50*, 8497–8507.
195. H. Follmann, R. Pfeil, H. Witzel, *Eur. J. Biochem.* **1977**, *77*, 451–461.
196. F. E. Hruska, *J. Am. Chem. Soc.* **1971**, *93*, 1795–1797.
197. M. Bastian, H. Sigel, *Inorg. Chim. Acta* **1990**, *178*, 249–259.
198. G. Liang, R. Tribolet, H. Sigel, *Inorg. Chem.* **1988**, *27*, 2877–2887.
199. M. Bastian, H. Sigel, *J. Coord. Chem.* **1991**, *23*, 137–154.
200. M. Bastian, H. Sigel, *Inorg. Chim. Acta* **1991**, *187*, 227–237.
201. D. Bouvier, N. Labessan, M. Clémancey, J.-M. Latour, J.-L. Ravanat, M. Fontecave, M. Atta, *Nucleic Acids Res.* **2014**, *42*, 7960–7970.
202. H. Grosjean, C. Gaspin, C. Marck, W. A. Decatur, V. de Crécy-Lagard, *BMC Genomics* **2008**, *9*, 470; DOI: 10.1186/1471-2164-9-470; available from http://www.biomedcentral.com/1471-2164/9/470
203. R. Leipuviene, Q. Qian, G. R. Björk, *J. Bacteriol.* **2004**, *186*, 758–766.
204. J. Schnabl, R. K. O. Sigel, *Curr. Opinion Chem. Biol.* **2010**, *14*, 269–275.
205. E. Freisinger, R. K. O. Sigel, *Coord. Chem. Rev.* **2007**, *251*, 1834–1851.
206. J. Brasún, A. Matera, E. Sochacka, J. Swiatek-Kozlowska, H. Kozlowski, B. P. Operschall, H. Sigel, *J. Biol. Inorg. Chem.* **2008**, *13*, 663–674.
207. A. Odani, H. Kozlowski, J. Swiatek-Kozlowska, J. Brasún, B. P. Operschall, H. Sigel, *J. Inorg. Biochem.* **2007**, *101*, 727–735.
208. I. Deb, J. Sarzynska, L. Nilsson, A. Lahiri, *J. Chem. Information Modeling* **2014**, *54*, 1129–1142.
209. G. R. Björk, T. G. Hagervall, *EcoSal Plus* **2014**, 1–68; DOI: 10.1128/ecosalplus.ESP-0007-2013.
210. K. C. Rogers, A. T. Crescenzo, D. Söll, *Biochimie* **1995**, *77*, 66–74.
211. L. Aravind, E. V. Koonin, *Trends Biochem. Sci.* **2001**, *26*, 215–217.
212. M. C. Erat, R. K. O. Sigel, *Inorg. Chem.* **2007**, *46*, 11224–11234.
213. M. C. Erat, J. Coles, C. Finazzo, B. Knobloch, R. K. O. Sigel, *Coord. Chem. Rev.* **2012**, *256*, 279–288.
214. H. Brintzinger, G. G. Hammes, *Inorg. Chem.* **1966**, *5*, 1286–1287.
215. S. A. A. Sajadi, B. Song, F. Gregán, H. Sigel, *Inorg. Chem.* **1999**, *38*, 439–448.
216. H. Sigel, R. Tribolet, R. Malini-Balakrishnan, R. B. Martin, *Inorg. Chem.* **1987**, *26*, 2149–2157.

217. H. Sigel, E. M. Bianchi, N. A. Corfù, Y. Kinjo, R. Tribolet, R. B. Martin, *Chem. Eur. J.* **2001**, *7*, 3729–3737.
218. A. Mucha, B. Knobloch, M. Jeżowska-Bojczuk, H. Kozłowski, R. K. O. Sigel, *Dalton Trans.* **2008**, 5368–5377.
219. A. Szent-Györgyi, in *Enzymes: Units of Biological Structure and Function.* Ed. O. H. Gaebler, Academic Press, New York, 1956, p. 393–397.
220. M. Cohn, T. R. Hughes, Jr., *J. Biol. Chem.* **1962**, *237*, 176–181.
221. P. W. Schneider, H. Brintzinger, H. Erlenmeyer, *Helv. Chim. Acta* **1964**, *47*, 992–1002.
222. (a) H. Sternlicht, R. G. Shulman, E. W. Anderson, *J. Chem. Phys.* **1965**, *43*, 3133–3143. (b) R. G. Shulman, H. Sternlicht, *J. Mol. Biol.* **1965**, *13*, 952–955.
223. (a) H. Sigel, *Experientia* **1966**, *22*, 497–499. (b) H. Sigel, H. Erlenmeyer, *Helv. Chim. Acta* **1966**, *49*, 1266–1274.
224. E. M. Bianchi, S. A. A. Sajadi, B. Song, H. Sigel, *Chem. Eur. J.* **2003**, *9*, 881–892.
225. J. O. Nriagu, *Inorg. Chem.* **1972**, *11*, 2499–2503.
226. E. K. Millar, C. A. Evans, D. L. Rabenstein, *Can. J. Chem.* **1978**, *56*, 3104–3108.
227. M. C. Erat, R. K. O. Sigel, *Met. Ions Life Sci.* **2011**, *9*, 37–100.
228. L. Claus, S. Vortler, F. Eckstein, *Methods Enzymol.* **2000**, *317*, 74–91.
229. P. Guga, M. Koziołkiewicz, *Chem. Biodiv.* **2011**, *8*, 1642–1681.
230. F. Eckstein, *Nucleic Acid Ther.* **2014**, *24*, 374–387.
231. H. Jahns, M. Roos, J. Imig, F. Baumann, Y. Wang, R. Gilmour, J. Hall, *Nature Commun.* **2015**, *6*, Article No. 6317; DOI 10.1038/ncomms7317.
232. R. K. O. Sigel, *Eur. J. Inorg. Chem.* **2005**, 2281–2292.
233. V. L. Pecoraro, J. D. Hermes, W. W. Cleland, *Biochemistry* **1984**, *23*, 5262–5271.
234. L. L. Slavin, E. H. Cox, R. N. Bose, *Bioconjugate Chem.* **1994**, *5*, 316–320.
235. N. A. Kratochwil, J. A. Parkinson, C. Sacht, P. D. S. Murdoch, T. Brown, P. J. Sadler, *Eur. J. Inorg. Chem.* **2001**, 2743–2746.
236. B. Song, R. K. O. Sigel, H. Sigel, *Chem. Eur. J.* **1997**, *3*, 29–33.
237. R. M. Smith, A. E. Martell, Y. Chen, *Pure Appl. Chem.* **1991**, *63*, 1015–1080.
238. S. Yadav, K. L. Yadava, *Asian J. Chem.* **2001**, *13*, 249–254.
239. S. Yadav, *Asian J. Chem.* **2001**, *13*, 309–314.
240. E. M. Bianchi, S. A. A. Sajadi, B. Song, H. Sigel, *Inorg. Chim. Acta* **2000**, *300–302*, 487–498.
241. H. Sigel, R. B. Martin, *Chem. Rev.* **1982**, *82*, 385–426.
242. H. Sigel, *Eur. J. Biochem.* **1987**, *165*, 65–72.
243. P. S. Shetty, P. R. Subbaraman, J. Gupta, *Indian J. Chem.* **1964**, *2*, 8–11.
244. A. Dominguez-Martin, S. Johannsen, A. Sigel, B. P. Operschall, B. Song, H. Sigel, A. Okruszek, J. M. González-Pérez, J. Niclós-Gutiérrez, R. K. O. Sigel, *Chem. Eur. J.* **2013**, *19*, 8163–8181.
245. P. A. Frey, R. D. Sammons, *Science* **1985**, *228*, 541–545.
246. P. A. Frey, *Adv. Enzymol. Relat. Areas Mol. Biol.* **1989**, *62*, 119–201.
247. B. Knobloch, H. Sigel, A. Okruszek, R. K. O. Sigel, *Chem. Eur. J.* **2007**, *13*, 1804–1814.
248. B. Knobloch, H. Sigel, A. Okruszek, R. K. O. Sigel, *Organ. Biomolec. Chem.* **2006**, *4*, 1085–1090.
249. A. Fernández-Botello, A. Holý, V. Moreno, H. Sigel, *Polyhedron* **2003**, *22*, 1067–1076.
250. A. Fernández-Botello, R. B. Gómez-Coca, A. Holý, V. Moreno, H. Sigel, *Inorg. Chim. Acta* **2002**, *331*, 109–116.
251. B. Song, D. Chen, M. Bastian, R. B. Martin, H. Sigel, *Helv. Chim. Acta* **1994**, *77*, 1738–1756.

252. Added in proof: M. J. Romero, R. Carballido, L. Rodríguez-Silva, M. Maneiro, G. Zaragoza, A. M. González-Noya, R. Pedrido, *Dalton Trans.* **2016**, *45*, 16162–16165.

12

The Role of Lead(II) in Nucleic Acids

Joana Palou-Mir, [1] ***Miquel Barceló-Oliver,*** [1*] ***and Roland K. O. Sigel*** [2*]

[1]University of the Balearic Islands, Department of Chemistry, Bldg. Mateu Orfila i Rotger, Carretera Valldemossa km 7.5, E-07122 Palma (Mallorca), Spain
<joana.palou@uib.es>,<miquel.barcelo@uib.es>

[2] University of Zurich, Department of Chemistry, Winterthurerstrasse 190, CH-8057 Zurich, Switzerland
<roland.sigel@chem.uzh.ch>

Metal Ions in Life Sciences, Volume 17 Edited by Astrid Sigel, Helmut Sigel, and Roland K. O. Sigel

DOI 10.1515/9783110434330-012

Abstract: Although lead(II) is naturally not associated with nucleic acids, this metal ions has been applied with DNA and RNA in various contexts. Pb^{2+} is an excellent hydrolytic metal ion for nucleic acids, which is why it is mainly used as probing agent for secondary structure and to determine metal ion binding sites both *in vitro* and *in vivo*. A further application of lead(II) is in structural studies, i.e., NMR, but also in X-ray crystallography, mostly using this heavy metal to solve the phase problem in the latter method. The structures of $tRNA^{Phe}$, RNase P, HIV-1 DIS, and the leadzyme are discussed here in detail. A major part of this review is devoted to the cleavage properties of lead(II) with RNA because of its excellence in catalyzing phosphodiester cleavage. Metal ion binding sites in large naturally occurring ribozymes are regularly determined by Pb^{2+} cleavage, and also in the *in vitro* selected so-called leadzyme, this metal ion is the decisive key to backbone cleavage at a specific site. Lead(II) was used in the first *in vitro* selection that yielded a catalytic DNA, i.e., the DNAzyme named GR5. Next to the GR5, the so-called 8-17E is the second most prominent DNAzyme today. Derivatives of these two lead(II)-dependent DNAzymes, as well as the G-quadruplex forming PS2.M have been applied to detect lead(II) in the lower nanomolar range not only in the test tube but also in body fluids. Due to the toxicity of lead(II) for living beings, this is a highly active research field. Finally, further applications of lead(II)-dependent DNAzymes, e.g., in the construction of nanocomputers, are also discussed.

Keywords: DNAzyme · hydrolytic cleavage · leadzyme · nucleic acids · RNA · sensing

1. INTRODUCTION

In order to properly fold to a functionally correct three-dimensional structure, any nucleic acid has to associate in a tight interaction with metal ions. Not only to properly compensate for the accumulated negative charge of the phosphate sugar backbone, which is mainly done by an excess of monovalent ions, but also to stabilize local structural motifs [1]. Over the past decades, thousands of studies have focused on RNA as well as DNA in the context of metal ions taken from the whole periodic table of elements [2, 3]. While each metal ion has small or large differences in binding properties, often the comparison and accumulated data with different metal ions is key in a proper understanding of the role of metal ions in functional nucleic acids.

Among all metal ions, also Pb^{2+} has been employed for various kinds of experiments in the context of nucleic acids [2, 4]. As a heavy metal with a large number of electrons, it is regularly used in crystallographic studies in order to solve the phase problem, and/or to identify metal ion binding sites by difference Fourier maps. A highly favourable property of Pb^{2+} in the context of nucleic acids, is the pK_a of coordinated water which is around 7.8. Hence, a $Pb(OH)^+$ species is present to considerable amounts at physiological pH. Pb^{2+} is thus a very good hydrolytic metal ion, promoting backbone cleavage. On the one hand, this is used to identify metal ion binding sites in large RNAs by hydrolysis assays followed by footprinting gel electrophoresis, and on the other hand, Pb^{2+}-dependent and specific DNAzymes and artificial ribozymes have been selected by

in vitro evolution experiments. One of the most prominent artificial ribozymes is the so-called leadzyme, a small motif comprising an internal bulged loop of ten nucleotides. While so-far no natural interaction or role of Pb^{2+} with nucleic acids has been found in living cells, the leadzyme motif occurs rather frequently in some genomes, raising the question about a possible natural role of this ribozyme.

DNAzymes and their application are probably the most prominent research field encompassing nucleic acids and Pb^{2+}: Due to the toxicity of Pb^{2+}, its accurate detection at highest dilution and exact concentration determination is highly desired. DNAzymes provide a perfect mean because of their high specificity and selectivity for Pb^{2+}. Several different approaches in the past years have led to highly sensitive fluorescent, electrochemical and colorimetric detection methods, the newest ones even in form of easy-to-use dipstick tests. Related techniques and approaches have in addition led to the development of logical gates based on Pb^{2+}/DNA interactions with the vision to build nanocomputers in the near future.

In this review, we summarize the available literature on Pb^{2+}-nucleic acid interactions, focusing especially on the points mentioned above, but we also refer the interested reader to the respective publications for more details.

2. RELEVANT PROPERTIES OF LEAD(II) IN COMPARISON TO OTHER DIVALENT METAL IONS

Mg^{2+} and K^{+} are those two metal ions that are considered to be majorily, if not exclusively, involved with RNA in living cells. Both are decisive for each nucleic acid to reach its active three-dimensional state and perform its assigned function, e.g., catalysis [1]. Nevertheless, a multitude of further metal ions are present in the cell and are also used regularly in *in vitro* experiments to mimic the spectroscopically silent Mg^{2+} [2, 4]. Several examples are known where metal ions other than Mg^{2+} can fine tune, or even largely accelerate RNA catalysis, e.g., in group II introns or the hammerhead ribozyme [5, 6].

In combination with RNA, Pb^{2+} is mostly used as hydrolytic metal ion in order to determine metal ion binding sites in larger RNAs but also in the context of crystal structures, where it has been shown that Pb^{2+} preferably replaces Mg^{2+} at sites where the Mg^{2+} is partially dehydrated. In general, Pb^{2+} is not considered to be a very good mimic of Mg^{2+} as its physico-chemical properties differ more than those of, e.g., Cd^{2+} or Mn^{2+} [2]. It is rather considered a mimic of Ca^{2+} in the context of proteins (see also Chapter 10) [7, 8]. The most relevant physico-chemical properties of Mg^{2+}, Ca^{2+}, and Pb^{2+} in the context of nucleic acids are summarized in Table 1.

The ionic radii and the coordination number are (aside from the twofold positive charge) two principle properties that govern together with the nature of the ligands the choice of the metal ion binding pocket. While Mg^{2+} is strictly octahedral, Pb^{2+} can also accommodate eight ligating atoms in its inner shell. The water exchange rate and the pK_a of coordinated water molecules on the other hand are important for the acceleration of backbone hydrolysis. Oxidation state +IV

Table 1. Comparison of some physico-chemical properties of Mg^{2+}, Ca^{2+}, and Pb^{2+} in aqueous solution. Given are the ionic radii and the preferred coordination number (CN) of the M^{2+} ions, the enthalpy of hydration (ΔH_{Hydr}), the acidity constant ($pK^{H}_{M(H_2O)_n}$) of a water molecule in the aqua complex, the ligand exchange rate from the first coordination sphere of the metal ion (k_{exch}), the logarithm of the affinity towards acetate (log K_O), and the affinity towards NH_3 (log K_N). The data in this table is abstracted from Table 1 in [2].

	Mg^{2+}	Ca^{2+}	Pb^{2+}	Ref.
Ionic radius (Å)	0.72	1.00 (1.12)[a]	1.19	[9]
CN	6	6 (8)[a]	6 (8)[a]	
Preferred ligands	O	O	O	
ΔH_{Hydr} ($kJmol^{-1}$)	1858	1570 (1657)[a]	1432 (1524)[a]	[10]
$pK^{H}_{M(H_2O)_n}$ (25 °C)	11.44 ± 0.1	12.85 ± 0.1	7.8	[11]
k_{exch} (s^{-1})	$6.7 \cdot 10^5$	$\approx 5 \cdot 10^8$		[12–14]
log K_O	0.49 ± 0.04	0.52 ± 0.05	2.08 ± 0.04	[15]
log K_N	0.22 ± 0.02	0.1	1.3	[15]

[a] The numbers in brackets refer to CN = 8.

seems so far not to be of relevance in the context of nucleic acids. More details can be found in [2] as well as in Chapter 11 in this book.

3. STRUCTURES OF LEAD(II) BINDING SITES IN NUCLEIC ACIDS

The number of three-dimensional structures solved by NMR and X-ray crystallography and deposited in the PDB (including the NDB) [16] has strongly increased over the past decade. A keyword search for nucleic acids in the PDB yields > 13,000 hits for "DNA" and > 9500 hits for "RNA", either alone or in the context of other biomacromolecules, i.e., mostly proteins.

Naturally, all these nucleic acid structures must exist in the presence of metal ions. While in the case of solution structures, metal ions are only exceptionally included in structure determination, in the vast majority of solid state structures, at least some metal ions are localized and included: However, even in macromolecular structures of good resolution (~2 Å), at most 10 % of the negative charge from the phosphate sugar backbone is formally compensated by specifically bound metal ions [17]. The MINAS (*M*etal *I*ons in *N*ucleic *A*cid*S*) database [3] contains all structures that encompass metal ions and complexes thereof, allowing for a rigorous search of their coordination environment. Surprisingly, only very few PDB files contain Pb^{n+} ions: while in numerous studies, Pb^{2+} salts (mostly the acetate salt) are used in co-crystallization and soaking in order to gain phasing information for solving the crystal structures, these additional data sets are not included in the PDB, but at best only shortly discussed in the respective publication. In fact, neither MINAS nor a search in the PDB shows up a

single DNA structure in the presence of lead(II/IV). However, a handful of structures are known of RNA that also contain Pb^{2+} ions:

(i) In 1983, Klug and coworkers discovered that $tRNA^{Phe}$ is cleaved at specific sites by Pb^{2+}, also describing a first crystal structure containing three Pb^{2+} ions (PDB ID 1TN2) [18]. In the same year, another low resolution structure at 5.5 Å revealed the same three Pb^{2+} ions [19]. This PDB and follow-up entries (2TNA, 7TNA, 8TNA) [19] have been replaced by 1TRA [20], but none lists coordinates for Pb^{2+}, which prevents a detailed analysis. Two years later, the higher resolution crystal structure of $tRNA^{Phe}$ in the presence of three Pb^{2+} ions was discussed in more detail by Brown et al. (PDB ID 1TN2) [21].

(ii) Mondragon and coworkers published the crystal structure of the specificity domain of a bacterial RNase P that contained two independent units of the RNA in the presence of 11 and 12 Pb^{2+} ions, respectively (PDB ID 1NBS) [22]. Shortly thereafter, Pace and coworkers published a structure of a 417 nucleotide long RNase P RNA. While they used osmium(III) hexammine and Pb^{2+} derivatives for phasing, only the coordinates of the Mg^{2+}-containing RNase P structure were deposited (PDB ID 2A64) [23].

(iii) The HIV-1 dimerization initiation site (HIV-1 DIS) was cocrystallized by Dumas and coworkers [24] in the presence of 13 different metal ions, among them Pb^{2+} (PDB ID 1Y95).

(iv) The leadzyme is an *in vitro* selected catalytic RNA that functions best in the presence of Pb^{2+}. It is well investigated and also two crystal structures are known [25, 26]. The so-called LZ4 leadzyme was crystallized in the presence of Mg^{2+}, Ba^{2+}, and Pb^{2+}, but only coordinates for the Mg^{2+}-containing structure were deposited (PDB ID 429D) [25]. The same leadzyme was later on solved at higher resolution in the presence of Mg^{2+} and Sr^{2+} [26]. The structures of the leadzyme are discussed in more detail in Section 5.2 (see also Chapter 7 by Aoki, Murayama, and Hu).

(v) Recently, the structure of the paramyxovirus parainfluenza virus 5 (PIV5) nucleoprotein-RNA complex was solved upon soaking with lead(II) acetate [27]. This large RNA-protein complex consists of 13 subunits, arranged in a large circle around the single-stranded RNA genome. However, the 14 Pb^{2+} ions localized are all exclusively bound to the protein subunits, each too far away for even an outer-sphere coordination to the RNA. Consequently, we will not discuss this structure here in more detail. Below we will thus concentrate on the structures in the above points (i) to (iii), especially those where the Pb^{2+} coordinates are included in the PDB files.

3.1. Lead(II) Binding to $tRNA^{Phe}$

Within the ribosomal translation machinery, tRNA mediates the genetic information encoded on the mRNA into the growing peptide chain. tRNA is different from most other functional RNAs in so far that its three-dimensional structure

shows very little to no dynamics, and that it contains a high number of modified nucleotides. Its rigidity and stability, again in the context of specifically bound Mg^{2+} ions, makes this RNA as one of the earliest and best investigated RNAs. Still, replacement of Mg^{2+} with other metal ions can lead to hydrolytic cleavage.

Incubation of $tRNA^{Phe}$ with Pb^{2+} at pH 7.4 led to cleavage at two sites, a major one between residues D17 and G18, and a minor one between G22 and A23. This cleavage is strictly pH-dependent, as at pH 5.0 no cleavage was observed [18]. This is a clear indication that a lead(II) hydroxide species is directly involved, solvated Pb^{2+} having a pK_a of around 7.8 (Table 1). A crystal structure of the same $tRNA^{Phe}$ revealed three localized Pb^{2+} ions (PDB ID 1TN2, Figure 1) [18, 21]. The first $Pb^{2+}(1)$ is bound in the single stranded region of the C-loop at residues U59 and C60, replacing a known Mg^{2+} in the native structure [18, 28]. The second $Pb^{2+}(2)$ is bound to G45 replacing a spermine in the native structure, and the third $Pb^{2+}(3)$ to Y37 in the anticodon loop. The second and third Pb^{2+} are bound to the Hoogsteen face of the purine rings, i.e., N7 and O6, the distances indicating respective inner-sphere as well as outer-sphere coordina-

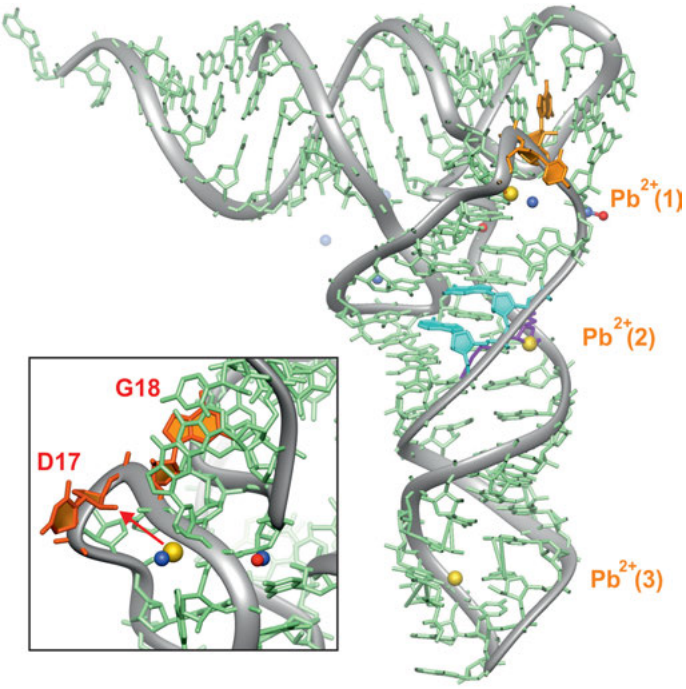

Figure 1. $tRNA^{Phe}$ structure in the presence of Pb^{2+}. The three Pb^{2+} ions are shown as yellow spheres. The Mg^{2+} ions (blue spheres) and the spermidine (magenta) present in the native structure are also shown. The major cleavage site between nucleotides D17 and G18 flanking the major cleavage site are shown in dark orange, the minor cleavage between G22 and A23 is shown in turquoise. The inset shows a detailed view on the major cleavage site, the 6 Å between $Pb^{2+}(1)$ and the D17 2′-OH indicated by a red arrow. This figure was prepared using MOLMOL [29] and the PDB ID 1TN2 [18, 21].

tion to these and nearby residues (no water molecules could be located in the coordination sphere of the Pb^{2+} ions) [18, 21].

The major cleavage site is close to $Pb^{2+}(1)$ and the minor cleavage site to $Pb^{2+}(2)$. Cleavage at site (1) proceeds by proton abstraction from the 2′-OH of the D17 ribose, resulting in a 2′-3′-cyclic phosphate at the same residue. $Pb^{2+}(1)$ is about 6 Å from the D17 2′-OH (Figure 1, inset), which corresponds quite well to an outer-sphere distance. The second cleavage site observed in gel electrophoresis experiments (but not in the crystal) is rather close to $Pb^{2+}(2)$, although too far away and on the wrong side of the strand to directly derive a cleavage mechanism from this structure.

3.2. Lead(II) Binding to RNase P

Ribonuclease P (RNase P) cleaves a specific phosphodiester bond in precursor tRNA to form a 5′-phosphorylated tRNA. RNase P is a large RNA-protein complex of which homologues exist in all organisms. While RNA and protein(s) are crucial for cell viability, *in vitro* the RNA alone is active at high salt concentrations [30]. Hence, RNase P is a true multiple-turnover ribozyme, which is dependent on divalent ions for catalysis [31].

The crystal structure of RNase P RNA from *Bacillus stearothermophilus* was solved at 3.3 Å resolution based on Os(III) hexammine and Pb^{2+} derivatives for phasing [23]. Unfortunately, only the native structure without the coordinates for Pb^{2+} was deposited (PDB ID 2A64), preventing a detailed analysis. 27 Os(III) hexammine and two Pb^{2+} binding sites were identified. One Pb^{2+} is located in the major groove of the highly conserved P4 helix, which is distorted from the regular A-form, and overlaps with one $[Os(NH_3)_6]^{3+}$ (the so-called A site in [23]).

Previously, Mondragon and coworkers had crystallized the specificity domain (S domain) of *Bacillus subtilis* RNase P, comprising nucleotides 86-239, and refined the structure to 3.15 Å (PDB ID 1NBS) [22]. The S domain crystallizes as two independent molecules per asymmetric unit, both showing a very similar over-all structure but with slightly different local conformations. Cocrystallization with Pb^{2+} yielded a multitude of Pb^{2+} binding sites, 12 in molecule A (Pb241-Pb252) and 11 in molecule B (Pb301-Pb312) (Figure 2).

The obtained resolution did not allow for an identification of water molecules in the lead(II) coordination sphere and hence a detailed investigation of the coordination pockets. Nevertheless, using the distances provided by MINAS [3] from the individual Pb^{2+} ions to potential coordinating heteroatoms on the nucleotides, some conclusions can be drawn. Out of the 23 Pb^{2+} ions identified, 13 show a close enough distance to either nucleobase heteroatoms or phosphate oxygens to allow an inner-sphere coordination. The major groove, i.e., the Hoogsteen side, of guanine nucleobases is thereby the most prominent one with five occurrences (Pb312, Pb303, Pb302, Pb212, Pb203). Five other Pb^{2+} ions show inner-sphere contacts to phosphate oxygens of A, G, and C (Pb306, Pb213, Pb210, Pb206, Pb201). The remaining three Pb^{2+} are in close proximity to the

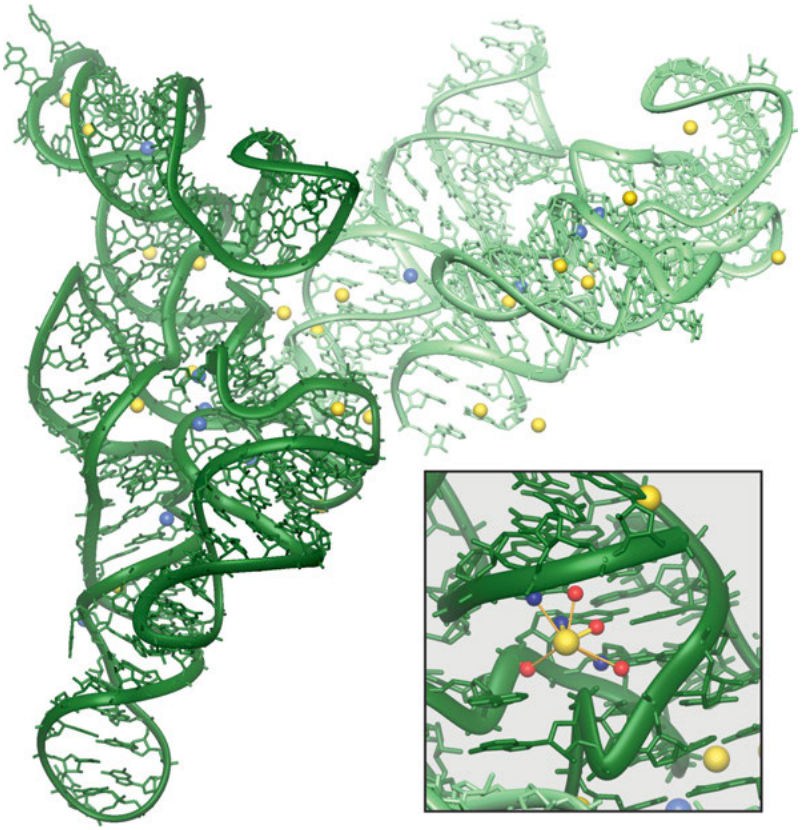

Figure 2. The two independent molecules of the *Bacillus subtilis* specificity domain of RNase P are shown, molecule A binding 12 Pb^{2+} ions (light green), and molecule B with 11 coordinated Pb^{2+} ions. Lead(II) ions are shown as yellow, Mg^{2+} ions as light blue spheres. The inset shows the coordination environment of Pb302. Inner-sphere connections to N7 and O6 of G132 are shown as thick solid yellow lines, outer-sphere connections to N7 and O6 of the adjacent G90 and G133, as well as to the R_P phosphate oxygen of G132 are shown as thin yellow lines. Two further Pb^{2+} ions (Pb303 and Pb305) are also shown. This figure was prepared using MOLMOL [29] and the PDB ID 1NBS [22].

Watson-Crick faces of C186 and G168, as well as the 2′-OH of C134. All other Pb^{2+} ions are of a distance to the RNA that allows for outer-sphere coordination exclusively (with a cut-off at 3.2 Å). An example of such a Pb^{2+} binding site encompassing both inner-sphere and outer-sphere distances is given in the inset of Figure 2. It should be noted that the positions of the Pb^{2+} ions have to be taken with care as some of the Pb^{2+}-RNA distances are actually too short. Nevertheless, from the general positioning of the metal ions it becomes clear that the major groove of guanines as well as phosphate groups are the primary coordination sites of Pb^{2+} in RNA, a picture that actually corresponds very well to the one for Mg^{2+} [15].

3.3. Lead(II) Binding to the HIV-1 Dimerization Initiation Site

Metal ions are key to RNA structure and function. While mostly K^+ and Mg^{2+} are assumed to play the decisive roles within a cellular environment, it is open if also other metal ions are involved with RNA in the cell [6]. Uncountable *in vitro* studies made use of almost all metal ions of the periodic table, using, e.g., their different coordination, electronic, and spectroscopic properties [2, 4]. Dumas and coworkers presented a systematic crystallographic study, analyzing the metal ion binding sites of 11 metal ions and two metal ion complexes in the HIV-1 dimerization initiation site (HIV-1 DIS) [24]. Two slightly different fragments of 23 nucleotides in length were examined, the so-called subtypes A and B from the HIV-1 RNA genome. Only subtype A showed coordination of three Pb^{2+} ions (Figure 3), although none of them at full occupancy.

The DIS can either form a loop-loop complex by homodimerization, or can form an extended duplex. Here we concentrate only on the extended duplex of

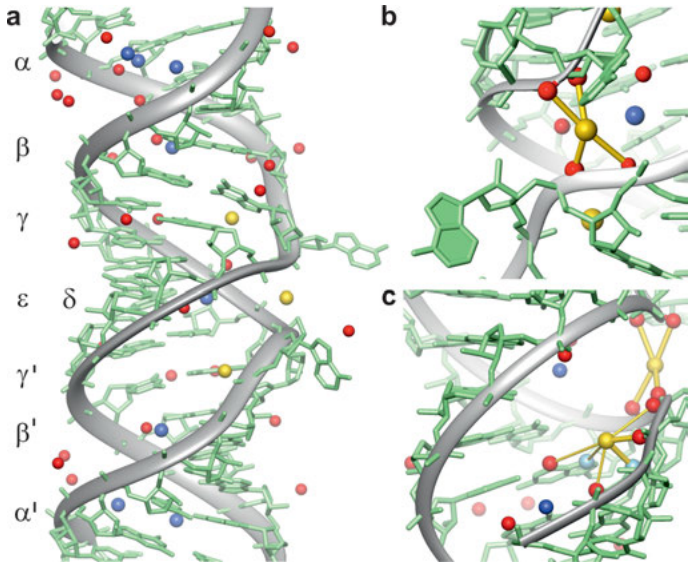

Figure 3. **(a)** Structure of the HIV-1 dimerization initiation site, subtype A, together with the three Pb^{2+} ions shown as yellow spheres and the Mg^{2+} ions overlaid as blue spheres. Water molecules are shown as red spheres. The HIV-1-DIS is sequence-symmetric yielding two sequence-identical metal ion binding sites above and below the central part with the two flipped out adenines. In the flanking arms, the sites are named α/α′, β/β′, and γ/γ′, the central part having two binding sites, ε within the helix, and δ between the two backbones. **(b)** Close up of binding site δ, the Pb^{2+} ion showing four inner-sphere coordinations to four phosphate oxygens on the two strands, as typical for a "Mg-clamp" motif. **(c)** Close up of the γ binding site, with the δ site in the background. Inner-sphere coordinations are indicated by thick yellow bonds, outer-sphere distances by thinner ones. The coordinated N7 atoms of G9 and G10 are shown as light blue spheres. This figure was prepared using MOLMOL [29] and the PDB ID 1TN2 [18, 21].

subtype A, which shows eight specific Mg^{2+} binding sites (Figure 3a). The central part around the flipped out adenines encompasses two M^{n+} binding sites, so-called ε and δ sites. The two flanking duplex arms, both identical in sequence, each harbor three binding sites α/α′, β/β′, and γ/γ′. While these are located at the same respective sequences, their binding patterns do not exactly match in all cases with all metal ions. In general, binding of the different metal ions does not change the overall structure of the HIV-1 DIS. Pb^{2+} binding occurs at sites γ/γ′ and δ, partially replacing Mg^{2+} upon soaking with lead(II) acetate. Interestingly, Pb^{2+} shows a preference for the γ′ site, as is judged on a higher occupancy factor, and all three sites stand out by being partially dehydrated Mg^{2+} sites. The δ site is located between the two phosphate sugar backbones, the Pb^{2+} ion coordinating in a roughly square-planar geometry four phosphate oxygens (Figure 3b). This pattern very closely resembles the classical Mg^{2+}-clamp motif, in which Mg^{2+} trans-coordinates the two strands [15]. The γ/γ′ site is located in the major groove, the Pb^{2+} undergoing inner-sphere coordination to N7 of G9 and the R_P oxygen of A8. Further ligands in an outer-sphere distance are the R_P oxygen and O6 of G9, as well as N7 and O6 of G10 (Figure 3c). Lead(II) probing with the dissolved crystals revealed two cleavage sites, a stronger one between G7 and A8, and a weaker one between G8 and G9. As Pb^{2+} is coordinated in the major groove, both cleavages can occur only after minor rearrangements, as it has already been observed with the above described $tRNA^{Phe}$ (see Section 3.1) [24].

4. LEAD(II) AS HYDROLYTIC CLEAVAGE AGENT TO PROBE DIVALENT METAL ION BINDING SITES AND SINGLE-STRANDED RNA REGIONS

RNA functionality is related to its capacity to adopt different conformations by varying the tertiary interactions between distant parts of a long sequence and/or by interacting with other molecules such as small ligands or proteins [32]. Obviously, such interactions, rearrangements, together with the three-dimensional structure of the RNA molecule are crucial for its biological function [33]. While the total number of RNA structures that have been determined by X-ray crystallography and NMR have increased exponentially over the past years, secondary structure prediction of a long RNA is still difficult. Chemical and enzymatic structural probes are mostly the method of choice for a rapid secondary structure analysis. Numerous nucleases with different nucleotide specificity and chemical reagents, such as dimethylsulfoxide and lead(II) are frequently used to map RNA structures [34, 35].

Metal ions in general catalyze the cleavage of phosphodiester bonds, playing one or several roles in this mechanism. It is believed that usually at least two metal ions are involved, be it in the cleavage of a diphosphate bond [36, 37] or of a phosphodiester [38, 39]. In such a classical S_N^2 reaction the nucleophile (2′-OH or a solvent water molecule) needs to be in an in-line geometry with the leaving group (5′-OH) yielding either 2′,3′-cyclic phosphate or a 2′-/3′-phosphate

together with a free 5′-hydroxyl group as cleavage products. Metal ions thereby activate the nucleophile, stabilize the transition state and/or stabilize the leaving group prior to protonation. Hydrated metal ions act as Brønsted bases that activate the 2′-OH group of the respective ribose and consequently, the cleavage rate of the reactions is often pH-dependent with an inverse correlation between the pK_a value of the coordinated water molecule and the observed reaction rate. Similarly, a low pK_a value promotes leaving group protonation [4, 40, 41].

Lead(II) is commonly used as a chemical reagent to analyze RNA structures due to its capacity to penetrate into folded structures in solution where nucleases cannot access for steric reasons [35]. Nucleases thus provide information on the solvent accessibility of a given nucleotide, whereas lead(II) does not, although secondary structure information is gained (see below). Furthermore, lead(II) has no sequence selectivity compared with enzymatic or other chemical methods [42]. A distinct advantage of lead(II) cleavage is the short incubation time (comparable to lanthanide(III) cleavage) [43] in comparison with the ones used for other metal ions such as Mg^{2+}. Aside from its use in predicting metal ion binding sites and probing RNA secondary structure, lead(II) has recently also increasingly been used to map RNA-ligand interactions *in vivo* as this ion is able to penetrate the cell membrane [33, 40].

As an in-line geometry around the cleavable phosphate is required, cleavage occurs preferentially in bulges, loops, and other single-stranded RNA regions but not in double-stranded helixes. Similarly, "single-strands" involved in stacking or tertiary interactions by base pairing are also not cleaved. A highly specific and distinct metal ion-induced cleavage site suggests the presence of a tight metal ion binding site. On the other hand, a cleavage region is no proof for a direct coordination of the metal ion at that site as cleavage can occur based on a local structural change upon metal ion binding nearby. Similarly, metal ion coordination in a rigid environment but unfavorable geometry and/or in the major groove might not show up in a cleavage assay [4, 40]. For a geometry-independent metal ion-induced cleavage, one would have to apply radical-based cleavage, i.e., through Fenton reaction [4]. Although Pb^{2+}-induced cleavage is in general sequence-independent, cleavage patterns of a single nucleotide bulge depend on the adjacent base pairs. For example, it has been shown that phosphodiester bonds are preferentially cleaved 3′ to pyrimidines [35]. In the case of terminal loops, cleavage intensities increase with loop size and depend on the nucleotide composition. Tetraloops are resistant to Pb^{2+} cleavage because of their conformational rigidity as are single-stranded G tracts and junctions of paired and unpaired regions. All these specific effects are probably due to extensive stacking interactions that cause conformal rigidity and reduce cleavage probability [35, 40].

Comparison of the cleavage patterns obtained by this technique under different conditions provides information on local structural changes, metal ion binding sites, secondary structure motifs, and RNA-ligand interactions, often in combination with other techniques, like nuclease digestion and/or selective 2′-hydroxyl acylation analysed by primer extension (SHAPE) [44]. Moreover, coupling the obtained data with computer folding programs based on energy minimization, stochastic simulations, as well as phylogenetic and sequence comparison enables the construction of a plausible secondary structure [32, 41].

4.1. *In vitro* Applications

Lead(II)-induced cleavage has been applied *in vitro* for various purposes. Analysis of the cleavage pattern is thereby mostly dependent on the RNA length. Therefore, 3′- or 5′-endlabelling is used for structural probing of RNA sequences usually not exceeding 150 nt, although it also works well with longer sequences [45]. Longer RNA sequences, especially in related experiments like SHAPE, are commonly analyzed by primer extension using inverse transcription. In the latter case differently labelled primers can be used covering each between 100 and 200 nt of the whole sequence. Labelled RNA or cDNA fragments can then be separated and analyzed by polyacrylamide gel electrophoresis, band intensities quantified using image-processing tools. The results can then be used as constraints for computational structure calculations [42].

Probably the most common applications of lead(II)-induced cleavage is the study of metal ion-binding sites and the determination of relative metal ion affinities [40, 41]. Two main approaches are used; firstly, metal ion-induced cleavage of phosphodiester bonds to compare the cleavage patterns of different metal ions, e.g., in a large group II intron [45], and secondly, competitive cleavage inhibition to probe for relative binding affinities. In the latter case increasing amounts of metal ion are added to a sample containing a constant concentration of Pb^{2+} [46]. An intense cleavage band suggests the presence of a specific metal ion-binding site close-by [40, 41]. However, it should be noted that the intensity of cleavage is not necessarily in accord with the affinity, as the local geometry plays an important role [4, 43]. This approach has for example been used to determine Mg^{2+} binding sites in the M1 RNA of RNase P where increasing Mg^{2+} concentrations supress Pb^{2+} cleavage indicating that Mg^{2+} competes with Pb^{2+} binding [47]. Similarly, specific metal ion-binding sites in the bulge region of HIV-1 TAR and in the extended hairpin structure of the HIV-2 TAR domain have been detected [46, 48]. With the above mentioned M1 RNA of RNaseP, it has been observed that Mn^{2+} has a higher affinity compared to Mg^{2+} or Ca^{2+} although similar cleavage patterns are observed [47]. The HIV-1 TAR bulge exhibits a higher specificity for $[Co(NH_3)_6]^{3+}$ than for Mg^{2+} or Ca^{2+} [46]. The same approach has been also used to study Mg^{2+} binding sites in the catalytic aminoacyl-transferase ribozyme [49].

Pb^{2+}-induced cleavage can be used in RNA structure analysis to identify similarities and differences in related RNA molecules. It has been demonstrated that equivalent structural motifs in different RNAs result in essentially identical patterns, which can be used to identify the same motifs in RNA molecules of unknown structure. Furthermore, the structural integrity of fragments from a larger RNA can be verified by comparison of the cleavage patterns [40]. In addition, the results from such Pb^{2+} cleavage experiments (mostly in combination with other techniques) provide important constraints for *in silico* folding programs used to create secondary structure models based on the energy minimization and stochastic simulations [32]. For example, the comparison of the Pb^{2+} cleavage patterns illustrated that the secondary structures of the 3′- and 5′-UTRs of the HCV RNA genome do not fold into “mirror images”, but sup-

port a three-stem-loop model for the 5′-UTR and most likely a two-hairpin pseudoknot for the 3′-UTR [50]. Further examples of such an experimental combination are the structure of the 5′-terminal loop of the *Klebsiella pneumoniae* Ibi RNA [51], the 3′-terminal HCV sequence [52], as well as the HIV-2 TAR [48]. Periodic conformational changes of the ribosomal 23S RNA and the tRNA during the different translation stages have been also analyzed by comparing the RNA cleavage patterns: Ribosome-bound tRNA exhibits a different conformation than tRNA free in solution and the 23S RNA exists in two different conformations in the PRE and POST translation state suggesting a periodical change between these two stages during elongation [53].

Another application of Pb^{2+} cleavage combined with the introduction of point mutations has been used to provide information of long-range interactions in RNA. Similarly, changes in Pb^{2+}-induced cleavage intensities are applied to detect RNA interactions with low-molecular-weight ligands, proteins, RNA, DNA or distinct motifs of the same molecule. However, conformational rearrangements of the RNA caused by the interaction with the ligand cannot be distinguished from effects of direct binding [40, 41]. Aminoglycoside binding to a tRNA prevents Pb^{2+} cleavage and it has been suggested that the aminoglycoside displaces the divalent metal ions bound to the RNA, i.e., the aminoglycoside binding site corresponds to the metal ion binding sites [54]. In the case of the antigenomic hepatitis delta virus ribozyme, it was shown that different antibiotics and their Cu^{2+} complexes interact and bind the ribozyme at different places and with differing affinities, the affinity of the interaction being the decisive factor for inhibiting the ribozyme [55]. Another example is the study of the 5′-UTR of the p53 mRNA where Pb^{2+}-induced cleavage was used to verify the binding of an antisense oligonucleotide and to monitor accompanied structural rearrangements. Upon hybridization, the observed cleavage pattern of the free RNA disappears due to the formation of base pairs [56].

Similarly, long-range RNA interactions between 5′- and 3′-ends of the DENV-MINI RNA using mutants and Pb^{2+} probing were studied and the formation of a pseudoknot between two distant PK1 and TL2 regions identified, underlining the importance of the structure and the sequence composition of the PK1 region for the correct 5′-3′ terminal RNA-RNA interaction [57]. The 3′-UTR of the TCF21 mRNA (a gene associated with coronary heart disease) interacts with miR-224 as has been shown by Pb^{2+}-induced cleavage providing the first example of miRNA mediated transcriptional regulation of this gene [58].

4.2. *In vivo* Applications

While *in vitro* studies of RNA structures have been essential to understand biological functions and structures of RNA, it is undeniable that *in vitro* conditions are far from a cellular environment where also a multitude of processes occurs simultaneously. For instance, the directionality and transcription or translation rates can influence RNA folding *in vivo*. It is also important to take into account the presence of proteins and other cofactors that can interact with RNA *in vivo*

[34]. The capacity of Pb^{2+} to easily penetrate into the cells has been taken as an advantage to perform the Pb^{2+}-induced cleavage *in vivo* to map RNA structure [32, 33, 40].

The *in vivo* procedure is not so much different from the *in vitro* one. Two different approaches have been used: either a fixed concentration of Pb^{2+} is added to the cell culture and incubated for different periods of time (from 3 to 20 min) or the incubation time is fixed, but the Pb^{2+} concentration is varied from 25 to 200 mM in order to monitor the correlation of the cleavage intensity pattern with time or concentration [33]. After incubation, the reaction is stopped with EDTA and the cells are submitted to a RNA extraction procedure followed by primer extension analysis using appropriately labelled primers to map all sequences of interest [33, 34, 40]. It is important to note that RNA samples from untreated cells have to be analyzed in parallel to the RNA from Pb^{2+}-treated cells [33].

This technique has been successfully applied in the determinations of metal ion-binding sites in the Sc.ai5γ intron in order to evaluate the influence of the Mss116p in the formation of metal ion-binding sites *in vivo*. The correlation of the Pb^{2+} cleavage patterns from the *in vivo* and *in vitro* experiments suggests that Mss116p may not influence binding site formation [34]. *In vivo* Pb^{2+}-induced cleavage was also used in tmRNA, CopT, and ompF mRNAs where good correlations between the *in vivo* and *in vitro* results were observed [33].

5. LEAD(II) AS CATALYTIC AND STRUCTURAL METAL ION

There are numerous hypotheses for the origins of life or ambiogenesis. As part of the RNA World hypothesis, a way to synthesize the first RNA polymers and their replication is needed [59]. The presence of low concentrations of Pb^{2+} or Mg^{2+} to catalyze the condensation of the four phosphoimidazolide-activated nucleobases to form mixed RNA oligomers in the eutectic phase in water ice at –18 °C is one possible explanation. Product yields correspond to a monomer incorporation of 80–90 % into oligomers up to 22-mer in length and with a high fraction of natural 3′-5′ RNA linkages [60].

The second step after oligomer formation is the extension of the chain in an enzyme-free reaction. The same water/ice eutectic system showed that the Pb^{2+}/Mg^{2+} pair can catalyze the extension of a primer in a one-pot synthesis across sequences, i.e., AA, AU, and AG [61]. Template-directed extension occurs both across pyrimidine- and purine-rich sequences and insertions of pyrimidines did not inhibit the subsequent insertions. Products were mainly formed with 2′-5′-phosphodiester linkages, however, the abundance of 3′-5′-linkages was higher than previously reported for pyrimidine insertions [61].

The final step for the RNA World initiation is the ligation of two previously formed oligomers. Although ligation requires the formation of double strands, oligonucleotides containing 2′,3′-cyclic phosphates readily ligate in the presence

of Mg^{2+}, Mn^{2+}, Co^{2+}, Zn^{2+}, and Pb^{2+}. Experiments at pH 7.2 showed that Pb^{2+} as the catalyst for this reaction yields an 8 % ligation product, 7 % is obtained with Mn^{2+} and roughly 6 % for the other tested M^{2+} ions. On the other hand, at pH 8.8 Mg^{2+} is the best cofactor, yielding 16.5 % ligation, 6.3 % with Mn^{2+} and about 5 % with Pb^{2+} and other M^{2+} [62]. Once these three steps are completed, the length of the formed oligomers is sufficient to form ribozymes, and hence, being the prerequisite for the RNA World.

In the following sections we will summarize the effect of lead(II) for the catalysis in *in vitro* selected DNAzymes, in the artificial ribozyme named leadzyme, and in naturally occurring ribozymes. In addition, opportunities arising from the structural capabilities of Pb^{2+} as a highly efficient stabilizer for quadruplex structures [63–65] will be discussed, which will lead to the preparation of lead(II) sensors.

5.1. Lead(II)-Dependent DNAzymes and Aptamers

DNA has been considered for a long time as the sole hard-drive for our genetic information. Due to its limited number of functional groups compared to proteins and to its stable double-helical structure, DNA was considered incapable of catalyzing chemical reactions. The discovery of ribozymes, RNAs that catalyze chemical or biological reactions [30, 66], implied that also DNA is able to perform catalysis [67]. In 1994 Breaker and Joyce presented the first DNAzyme isolated by *in vitro* selection that catalyzes a phosphodiester bond cleavage in the presence of lead(II) [68]. This DNAzyme, later named GR5, shows a rate enhancement of 10^5 compared to the non-catalyzed reaction. The reported lead(II)-dependent cleavage site in GR5 is situated at the 5′-aG-3′ junction, where the "a" denotes the single embedded ribonucleotide adenosine within a DNA substrate (Figure 4). Although GR5 is unable to cleave an all-RNA substrate from this initial DNA catalyst, numerous successor DNAzymes now offer highly useful and differing properties [69]. Later, it was shown that GR5 shows an exceptionally high selectivity of 400,000-fold for Pb^{2+} over other M^{2+} ions [70]. Slight modifications of the sequence, mainly at position 12, modulate the metal ion cofactor requirements [69].

All DNAzymes known today are artificial nucleic acid sequences isolated by *in vitro* selection from random pools of DNA sequences. They all use metal ions to obtain the best rate enhancement, often in the presence of a selected metal ion. These DNAzymes catalyze many different reactions, like DNA/RNA cleavage or ligation, DNA phosphorylation, capping, depurination, Diels-Alder reaction, porphyrin metalation, etc. [67]. Nevertheless, the lead(II)-dependent DNAzymes mainly catalyze RNA cleavage.

The two DNAzymes which have been widely used and best-studied are the 10-23 and the 8-17 DNAzymes, which are named according to their selection round and clone number [71]. The 17E variant of the 8-17 DNAzyme is lead(II)-dependent and has been repeatedly used for the design of lead(II)-sensors (*vide infra*). According to its predicted secondary structure, the 8-17 DNAzyme has a

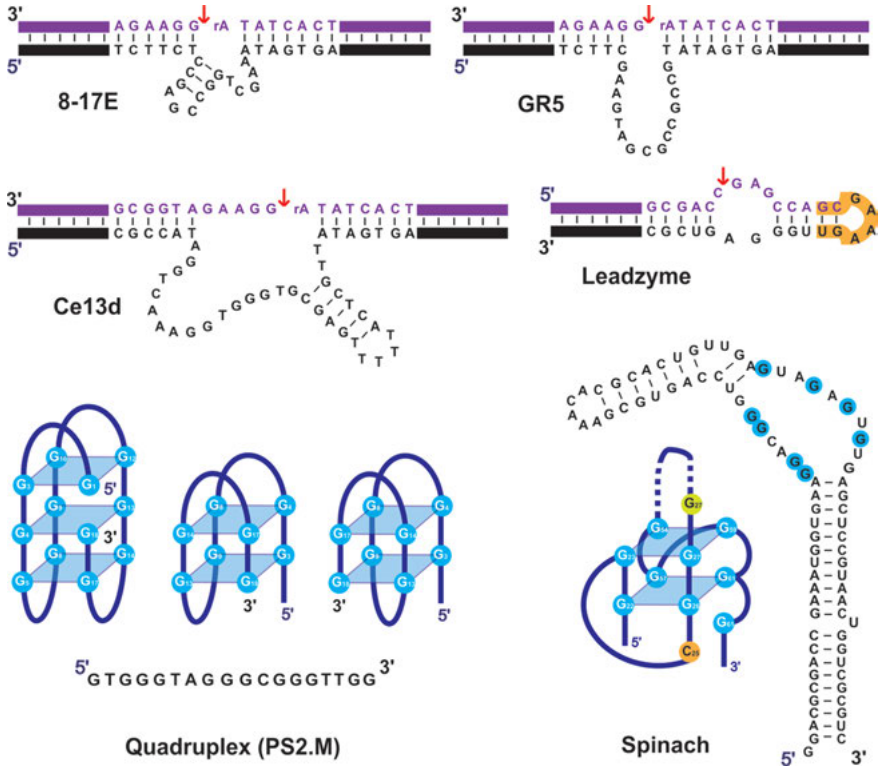

Figure 4. Secondary structures of the DNAzymes 8-17E, GR5, Ce13d, and the G-quadruplex forming PS2.M. Included are also the leadzyme and so-called spinach RNAs, the latter also forming a quadruplex with the Gs indicated by blue spheres. Substrate strands are shown in magenta, cleavage sites are in each case indicated by a red arrow.

small catalytic core of 13–15 nucleotides composed of a 3 base-pair stem, a triloop, and an AGGA(A) loop (Figure 4). The phosphodiester bond 3′ to an unpaired nucleotide with a G·T wobble pair immediately downstream is cleaved. Catalytic cleavage proceeds in a similar way to the one described for naturally occurring ribozymes with a metal ion-assisted deprotonation of the 2′-OH and the subsequent nucleophilic attack of the neighboring phosphate. A surprising aspect of the 8-17 DNAzyme is that it has been independently isolated by different groups under different conditions, subsequent selections leading to numerous 8-17 variants [72–74].

Mechanistic studies by FRET of the 8-17 DNAzymes family have revealed that the transesterification rate following the order $Pb^{2+} \gg Zn^{2+} \gg Mg^{2+}$ for the 17E DNAzyme is accompanied by a difference in global folding. In the presence of Zn^{2+} and Mg^{2+} the DNAzyme folds into a compact structure with a correlation between metal ion-induced folding and activity, and global folding preceding cleavage activity. Surprisingly, no differences in global folding were found upon addition of Pb^{2+}, suggesting this step is not necessary, and possibly

being the reason for Pb^{2+} preference [75]. An extended review on the 8-17 DNAzyme family was written by Schlosser and Li [76] to which we refer the interested reader.

Splitting (cleavage) experiments of both DNAzymes, GR5 and 8-17 (17E), have been performed to investigate the metal ion binding modes and the retaining activity. These results showed completely different patterns of enzyme activity as a function of the split site, thus indicating two different modes of binding the same metal cofactor for cleaving the same bond [77]. More recently, a comparison between the two classic lead-dependent DNAzymes, GR5 and 8-17E, has been published by Saran and Liu [78]. Both enzymes show the highest activity in the presence of lead(II) and share the same substrate sequence but they also contain conserved nucleotides in the catalytic core. A similar binding pocket for Pb^{2+} and the same mechanism has been proposed, also suggesting that the 8-17E is a special form of the GR5 DNAzyme. Both DNAzymes contain the simple sequence requirements needed for lead(II)-dependent cleavage, but 17E is also active with other metal ions, maybe because of some additional motifs in its sequence.

Apart of the well-studied GR5 and 8-17E, also other DNAzymes have been found to be active upon addition of lead(II). For instance, the Ce13 DNAzyme was isolated in the presence of cerium(III) by gel-based methods (Figure 4). This Ce13 DNAzyme is active with trivalent lanthanide ions and Y^{3+}, as well as moderately with Pb^{2+} [79]. On the other hand, DNAzymes with smaller enzyme loops are desirable to evolve. Both the GR5 and 8-17E have around 15 nucleotides in the enzyme loop, as do most of the metal-dependent RNA-cleaving DNAzymes. In contrast, the leadzyme, an *in vitro* selected RNAzyme (*vide infra*), is able to cleave a RNA substrate with just two unpaired nucleotides. Replacement of the ribonucleotides in the leadzyme by deoxyribonucleotides failed to produce an active enzyme.

In vitro selection in the presence of lead(II) and deep sequencing yielded the PbE22 DNAzyme, which contains just 5 nucleotides in the enzyme loop. This shorter DNAzyme version shows a 200-fold rate enhancement and good specificity for lead(II), lacking Mg^{2+}-induced activity. The lower catalytic efficiency suggests that site-specificity and metal ion-specificity is feasible with shorter loops, but extra nucleotides are probably important for better folding and optimal activity [80].

5.1.1. Lead(II) Sensors

Lead toxicity is well known, some effects having been linked to nucleic acids. For example, RT-qPCR has been applied to study the effect of lead(II) exposure on the transcription of certain genes in nitrifying bacteria [81] and in human epidermoid carcinoma cells [82, 83].

The mechanism of lead toxicity presumably involves cross reactions between Pb^{2+} and Ca^{2+} in calmodulin-dependent systems [7, 8]. On the other hand, lead(II) acetate exposure promotes structural changes in the liver of prepubescent rats accompanied by a decrease of DNA, total proteins, aminic nitrogen,

and glycogen [84]. Consequently, the development of lead(II) sensors allowing for on-site and real-time monitoring is a vivid research area. RNA-cleaving DNAzymes possess a high metal selectivity combined with a high stability and low cost DNA synthesis providing a new opportunity for biosensing applications [67]. The different approaches described in the literature are summarized below.

5.1.1.1. Fluorescence Sensors

Fluorescence is a highly sensitive technique and has early been used for lead(II) sensing. The first fluorescent DNAzyme Pb^{2+}-sensor reported was based on the 8-17 DNAzyme with the fluorophore TAMRA attached to the 5′-end of the substrate strand and the quencher Dabcyl to the 3′-end of the enzyme strand. In the absence of Pb^{2+} the Watson-Crick pairing of both strands results in a low fluorescence quenched state while, in the presence of Pb^{2+} the cleaved substrate is released from the enzyme strand, resulting in a fluorescence increase. Although the background fluorescence is rather high due to partially unbound substrate strand, this sensor can detect 10 nM lead(II) with 80- to 1,000-fold selectivity over other metal ions [85].

Background fluorescence was later reduced by introducing a second quencher at the 3′-end of the substrate strand, which quenches fluorescence of the free substrate strand [86]. Lan et al. presented a slight modification of this sensor based on a temperature-independent variant of 8-17 DNAzyme, the +5-17E, carrying a quencher in the enzyme strand and both the fluorophore and a second quencher in the substrate strand. This new construct yields a 40,000-fold improvement in metal ion selectivity [70]. Further modification ensured a preformed Pb^{2+}-binding pocket by linking the strands with a hairpin, resulting in higher cleavage efficiency. Such, the detection limit was decreased 167 fold to 2 nM, with a maximum of 20 μM, making this probe suitable for microscope-detection in solution [87].

Further improvement was achieved by replacing the organic fluorophores with quantum dots (QDs), having the advantages of size-dependent emission, single wavelength excitation, higher quantum yield, and higher photo stability, hence, allowing for higher sensitivity multiplex detection [67]. By attaching QDs with different emissions to the substrates of the 8-17 DNAzyme and a Cu^{2+}-sensitive DNAzyme, and two quenchers, one at the substrate 3′-end and the second at the 5′-end of the enzyme strand, it has been possible to simultaneously detect 0.2 nM Pb^{2+} and 0.5 nM Cu^{2+} [88]. Detection efficiency was improved by using gold nanoparticles (AuNPs) as quenchers. The fluorescence energy that is transferred from a fluorophore to AuNP is less dependent on the distal separation than that of the organic quenchers. Therefore, the fluorescence donor in the substrate and AuNP can be directly paired by immobilizing the substrates on the AuNPs (Figure 5) [89]. The combination of gold nanoparticles and the GR5 DNAzyme with both strands linked together and using carboxyfluorescein (FAM) as fluorophore leads to an improved detection limit at the picomolar level (250 pM) and with a linear range from 1 to 100 nM [90]. The use of gold nanorods (GNRs) as quencher lowered the lead(II) detection limit to 61.8 pM, showing a linear response between 0.1 and 100 nM [91].

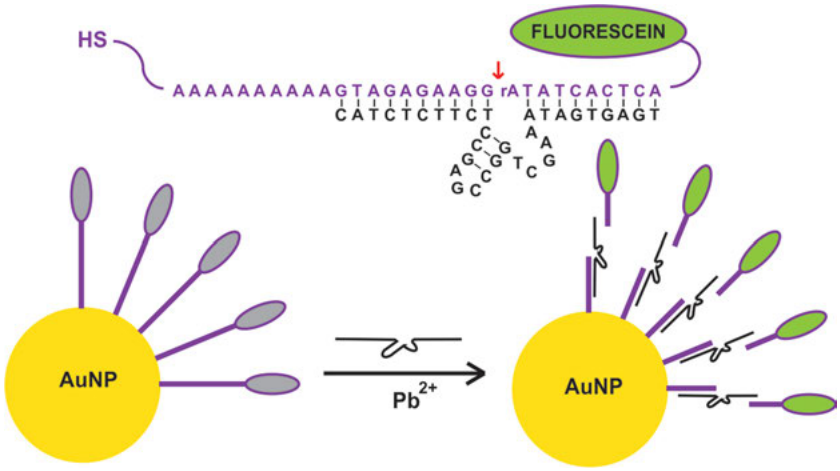

Figure 5. Pb^{2+} sensing with the 8-17E DNAzyme. The 8-17E is attached to gold nanoparticles (AuNP) via a terminal SH group on the substrate strand. Upon substrate cleavage in the presence of Pb^{2+}, fluorescein is released into solution and becomes fluorescent, previously being quenched by the AuNP.

A further elegant approach was the modification of the Ce13d DNAzyme, which is lanthanide(III)-dependent and working best with Lu^{3+}, with a phosphorothioate (PS) to render the DNAzyme towards thiophilic metal ions. With a single-quencher design a Pb^{2+} sensitivity of 0.1 nM was reached [92].

Surface-immobilized DNAzyme-based sensors also show a low background as unhybridized cleaved substrate can be washed away, in addition to possible sensor regeneration. Such a 8-17 DNAzyme covalently attached to a gold surface achieved a 1 nM detection limit and retained a long-lived activity [93].

DNAzymes with covalently bound fluorophores are rather expensive and have the further disadvantage of a possible interference with enzyme activity. Hence, label-free fluorescence sensors were developed making use of the different fluorescence properties of fluorophores when bound to or released from DNA. For example, 2-amino-5,6,7-trimethyl-1,8-naphthyridine (ATMND) was used with a 8-17 DNAzyme to detect lead(II) with high sensitivity and selectivity. An abasic site or single nucleotide bulge in the double-stranded region of the 8-17 DNAzyme-substrate complex selectively binds the fluorophore. Bound ATMND is quenched, but upon strand cleavage, ATMND is released into solution accompanied by fluorescence enhancement [94]. In a second approach, the DNA-chelating dye Picogreen is highly fluorescent when bound to a double-stranded region within the 17E DNAzyme. Pb^{2+}-dependent catalytic cleavage of the substrate strand causes dissociation of the enzyme-substrate complex, release of Picogreen, and a reduction of the fluorescence, yielding a detection limit of 10 nM [95]. The unique optical properties of water-soluble cationic polythiophene (PT) are the basis of a further approach: PT wraps around dsDNA as in the hybridized 17E-substrate complex, the nonplanar conformation being highly fluorescent.

Lead(II) leads to catalytic cleavage, dissociation of the dsDNA, release of PT, which adopts now a planar conformation, and hence, a lower fluorescence signal. Pb^{2+} concentrations could be detected from 10 nM to 100 μM [96].

Apart from using DNAzymes, two different approaches of label-free fluorescent sensors for Pb^{2+} have been developed based on G-quadruplex stabilization: (i) Spinach RNA is an *in vitro* selected aptamer with an unstructured region that forms a two-layer G-quadruplex motif in the presence of millimolar amounts of Na^+, K^+ or NH_4^+ (Figure 4). Pb^{2+} also induces G-quadruplex formation at the nanomolar level, allowing the RNA to bind the fluorophore DFHBI and activate its fluorescence. In this way 6 nM lead(II) can be detected with a >17,000-fold selectivity for Pb^{2+} compared to Ca^{2+}, the most competing ion [97]. (ii) Similarly, Pb^{2+} compacts an intramolecular G-quadruplex, called PS2.M (Figure 4). This structural change can be detected by hemin (Fe(III) protoporphyrin IX), which is weakly fluorescent by itself, but exhibits a dramatic fluorescence enhancement upon binding to quadruplex DNA formed in the presence of K^+ only. In the presence of Pb^{2+} hemin is released, providing a detection limit of 1 nM lead(II) and a linear response from 5 to 1000 nM with good selectivity [98].

5.1.1.2. Colorimetric Sensors

Fluorescence enhancement offers a high sensitivity and selectivity but requires an instrument for signal output, which can be a limitation for on-site and real-time detection. In contrast, a colorimetric change can often be detected by eye. AuNPs show strong distance-dependent optical properties and very high extinction coefficients: The change from a disperse state to an aggregate state of 13 nm AuNPs is accompanied by a color change from red to blue [67]. AuNPs carrying 8-17 DNAzymes with extended complementary strands on both sides of the substrate aggregate yielding a blue color. In the presence of Pb^{2+}, the substrate strand is cleaved and the AuNPs dissociate resulting in a change to red color that can be observed by eye. While the first colorimetric sensor with a 100 nM detection limit had some limitations due to the need of repeated annealing and reheating steps [99], several improvements could be made:

(i) Tail-to-tail arrangement of AuNPs eliminated the need of the heating-and-cooling process, while the increase of the AuNPs size from 13 nm to 42 nm decreased the detection time to 5 minutes, but changed the original "turn-on" sensor to a "turn-off" one [100];
(ii) small fragments of invasive DNA have been used to assist disassembly of the DNA-AuNP aggregates, allowing for a fast "turn-on" sensor [101, 102];
(iii) the use of asymmetric substrate-binding arms enabled the disassembly of the DNA-AuNP aggregate without the presence of invasive DNA at room temperature [103].

A system working the opposite way was presented by Brook et al. where 8-17 DNAzymes are immobilized on well-dispersed gold nanoparticles [104]. After catalytic cleavage of the nucleic acids by Pb^{2+}, the AuNPs aggregate rapidly

driven by van der Waals attraction and a red-to-purple color change [104]. Also the higher affinity of unmodified AuNPs for ssDNA *versus* dsDNA has been explored: Citrate-protected AuNPs absorb ssDNA, but not dsDNA. Upon substrate cleavage of the 8-17E DNAzyme in the presence of Pb^{2+}, the AuNPs absorb ssDNA losing their aggregation property and yielding a color change. This detection assay is performed in 20 minutes and shows a detection limit of 500 nM, providing a simple and cost-effective measurement tool for lead(II) detection [105]. A similar system with the 8-17 DNAzyme, but using salt-induced aggregation of the 13 nm AuNPs after quenching the cleavage reaction with EDTA detects 3 nM Pb^{2+} [106].

A more complex system encompasses the coupling of a metal ion-specific DNA/RNA-cleaving DNAzyme and a G-quadruplex DNAzyme. The substrate of the DNA/RNA-cleaving DNAzyme is designed as an intramolecular stem-loop structure, and a G-rich sequence caged in the double-stranded stem not able to form the catalytically active G-quadruplex DNAzyme structure [107]. Upon metal ion-dependent cleavage of the substrate, the G-rich sequence is released and the catalytic G-quadruplex DNAzyme structure formed. G-quadruplex formation is monitored by hemin, which binds to the quadruplex yielding a catalytically active G-quadruplex DNAzyme, resulting in an increase of the absorbance signal in the ABTS-H_2O_2 system. This dual DNAzyme system allows for the detection of 14 nM lead, although the linear relationship extends from 20 to 200 nM lead(II) [107].

The same approach was used for a dipstick test to detect lead(II) in paints, based on the 8-17 DNAzyme and AuNP conjugates. The substrate carries a 3′-biotin modification and a 5′-extension with a thiol group, which is used to conjugate the substrate to the AuNPs. The dipstick is made of four overlapping pads on a backing sheet: a wicking pad, a conjugation pad, where the annealed enzyme-substrate is spotted, a lateral flow membrane, where a control zone is made with streptavidin and a test zone is made with capture DNA, complimentary to the cleaved substrate, and an absorption pad. If no lead(II) is present, the DNA is captured by streptavidin and a red line appears in that region. In the presence of lead(II), the cleaved substrate crosses the control zone and is caught by the capture DNA, yielding a red line in the test zone. While the reaction yield is mostly not 100 %, the appearance of two lines is common, but this dipstick device can detect 500 nM Pb^{2+} in solution [108].

5.1.1.3. Electrochemical Sensors

Apart from optical detection, also electrochemical DNAzyme sensors have been developed with the aim to provide a higher sensitivity, lower cost, and easy miniaturization [67]. The first electrochemical sensor presented was based on the 8-17 DNAzyme carrying methylene blue (MB) at the 3′-end. The DNAzyme is attached to the gold electrode via a 5′-end thiol group. In the absence of lead(II), the rigidity of the enzyme-substrate complex prevents MB to reach the electrode and thus also electron transfer is inhibited. Upon lead(II)-catalyzed cleavage of the substrate MB can interact with the electrode transferring electrons, providing a 500 nM detection limit [109].

Another electrochemical sensor is based on the 8-17 DNAzyme in combination with $[Ru(NH_3)_6]^{3+}$ and DNA-AuNPs for signal amplification. $[Ru(NH_3)_6]^{3+}$ binds to the phosphate sugar backbones of the DNAzyme-AuNP assemblies, which amplifies the electron transfer from the ruthenium(III) complex to the electrode. Substrate cleavage by lead(II) release the DNA-AuNP conjugate reducing the number of ruthenium(III) complexes close to the electrode surface and resulting in a loss of the amplification. Even being a "turn-off" sensor, 1 nM detection limit was reached because of signal amplification [110].

More recently, Zhang et al. reported a photoelectrochemical sensor based on flower-like ZnO nanostructures, using the 8-17E DNAzyme as the recognition unit and a dsDNA intercalator, $[Ru(bpy)_2(dppz)]^{2+}$ as the photoelectrochemical signal reporter [111]. After DNAzyme reaction, the electrode was rinsed and $[Ru(bpy)_2(dppz)]^{2+}$ added and allowed to react for 30 minutes. In the presence of lead(II), substrate cleavage and release yields a dissociation of the ruthenium(II) complex from the DNA and a decrease of the photocurrent. A linear relationship is obtained between 0.5 to 20 nM, with a detection limit of 0.1 nM, able to measure the lead(II) level in human serum and in lead(II)-spiked water as a proof of concept [111].

Lastly, prone for low cost and mass production, an impedance biosensor based on gold interdigitated electrodes has been developed by immobilizing the GR5 DNAzyme onto the electrode surface through Au-S bonding. The lead(II)-catalyzed cleavage of the substrate strand causes changes in the interfacial properties of the electrode. The resulting decrease of the impedance magnitude allows for the detection of 6.61 nM lead(II), a linear range between 10 to 100 nM and a good selectivity based on the GR5 DNAzyme [112].

5.1.2. Lead(II)-Dependent DNAzymes for Further Applications

The inherent lead(II) interaction with DNA has also been used for molecular computing research, i.e., to develop molecular computers. The idea is to design logic gates that could mimic the Boolean logic system with the aid of functional nucleic acids. One example is to use the lead(II)-enforced stabilization of G-quadruplexes. Few G-quadruplexes have been found to mimic peroxidases in the presence of K^+ with hemin as cofactor, by catalyzing the H_2O_2-mediated oxidation of 2,2′-azino-bis(3-ethylbenzothiazoline-6-sulfonic acid) diammonium salt (ABTS), which can be followed spectroscopically [113]. The PW17 G-quadruplex DNAzyme was selected as logic device, showing a parallel topology, good hemin binding, and DNAzyme activity in the presence of K^+. After addition of Pb^{2+}, the G-quadruplex topology changes to antiparallel, releasing the hemin and inhibiting catalysis. In other words, K^+ and Pb^{2+} switch PW17 between "active" and "inactive" states, performing as a two-input INHIBIT logic gate. EDTA can remove lead(II) from PW17, resetting the system to its initial stage, yielding a second logic gate with a reversible two-input IMPLICATION logic gate behavior [114].

The same G-quadruplex DNAzyme was immobilized on a gold electrode and the reduction potential of lead(II) in the quadruplex was measured by differen-

tial pulse voltammetry (DPV). This reduction potential works as electric pulse for the logic gate (–0.365 V), being different from the hemin reduction potential once bound to the G-quadruplex (–0.359 V). Using lead(II), EDTA, and hemin as inputs a series of simple and reversible logic gates were fabricated, such as one-input (YES and NOT), two-input (INHIBIT, AND, IMPLICATION and OR) and three-input logic gates [115].

Finally, the use of a lead(II)-specific DNAzyme combined with a T-rich DNA sequence, a Hg^{2+}-specific aptamer, yielded a multiplex logic gate. In that probe three different fluorophores were introduced to allow for multistep FRET among the FAM, ALEXA, and TAMRA dyes. FAM was introduced at the 5′-end of the substrate probe P1, while TAMRA was introduced at the 3′-end of the P2, consisting in a DNAzyme followed by a T-rich sequence, and ALEXA was labelled in the middle of P2 to realize FRET with FAM. This construct presents four situations in response to Pb^{2+} and Hg^{2+}, which can be distinguished by their fluorescence emissions at different wavelengths. Without any extra stimulation, a FRET signal between FAM and ALEXA is observed. In the presence of Pb^{2+} the substrate is cleaved and the emission of FAM detected. On the other hand, the addition of Hg^{2+} yields a very close distance between the three dyes, allowing for an intermolecular multistep FRET. Finally, when both metal ions are simultaneously added, the FAM-labelled DNA was cleaved and ALEXA and TAMRA showed a FRET signal as a result of the formed T-Hg^{2+}-T structure. The combination of Hg^{2+}-DNAzyme and T-rich sequence thus enables the construction of three different logic gates: NOT, NOR and INHIBIT, although this system is not reversible [116].

5.2. The Leadzyme

Catalytic cleavage of RNA by Pb^{2+} was first discovered in 1976 with yeast $tRNA^{Phe}$ [117]. Cleavage occurs between D17 and G18 in the D-loop and seems to be more dependent on the conformation than on the sequence [21], yielding a useful probing reaction method for tRNA structure [118–120]. After the discovery of this $tRNA^{Phe}$ self-cleavage, Pan and Uhlenbeck performed an *in vitro* selection scheme on libraries of $tRNA^{Phe}$ to find molecules able to self-cleave in the presence of lead(II) faster than tRNAs themselves [121]. Six rounds of *in vitro* selection yielded a small lead-dependent self-cleaving ribozyme, named the leadzyme motif, specifically the LZ4 construct thereof [122]. The selected leadzyme motif does not fold like any tRNA element. The cleavage site is located in a 4-by-2 purine-rich internal loop flanked by helices at both sides, between C6 and G7, in the longer strand [123]. Most of the structural and mechanistic studies have been made either with a unimolecular hairpin construct capped with a stable GAAA tetraloop or in a two-piece duplex form [120].

The LZ4 leadzyme construct has been successfully crystallized by Wedekind and McKay [25, 26]. First in the presence of either Mg^{2+}, Ba^{2+}, or Pb^{2+} [25], and in a second attempt in the presence of Mg^{2+} and Sr^{2+} (Figure 6) [26]. Problems with the refinement and interpretation of the Pb^{2+} dataset persisted

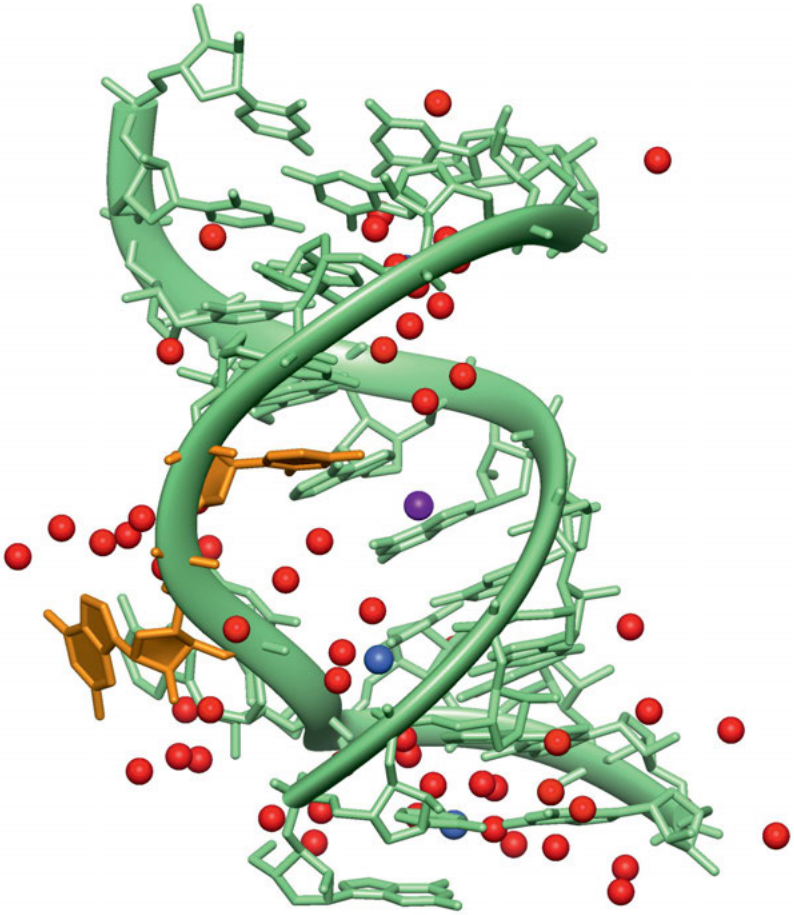

Figure 6. One out of four independent leadzyme molecules from the crystal structure in the presence of Sr^{2+} is shown. The Sr^{2+} ion is given as a magenta sphere, the Mg^{2+} ions in dark blue. Water molecules are shown as red spheres. The cleavage site is located between residues C6 and G7, both shown in orange. These two nucleotides are part of the purine-rich internal loop (Figure 4) and are flipped out because of intermolecular contacts with other leadzyme molecules within the crystal lattice. This figure was prepared using MOLMOL [29] and the PDB ID 1NUV [26].

due to the immediate Pb^{2+}-induced cleavage of the backbone and the resulting disorder in the catalytic core [25]. Hence, unfortunately only the coordinates of the native construct in the presence of Mg^{2+} (PDB ID 429D) and Mg^{2+}/Sr^{2+} were deposited (PDB ID 1NUV). NMR investigations [124] as well as the soaking experiments with Ba^{2+}, Sr^{2+}, and Pb^{2+} revealed that no structural change upon different metal ion binding occurs, suggesting that the global fold is already preformed [125]. Nevertheless, the leadzyme seems rather flexible as two conformations crystallized in the asymmetric unit, only one of which binds Ba^{2+} or Sr^{2+} ions.

Mg^{2+} is required for leadzyme function, but too high concentrations above 10 mM lead to inhibition, either due to competition with Pb^{2+} or by inducing an inactive fold. Ba^{2+} and Sr^{2+} are both potent inhibitors of leadzyme cleavage, possibly because they are similar in size to Pb^{2+}. Using Sr^{2+} in crystallization trials resulted in an improvement to 1.8 Å resolution, whereby one Sr^{2+} is located rather close to the attacking 2′-OH of cytosine 6 (Figure 6). Nevertheless, although Sr^{2+} might coordinate to relevant ligand atoms also for Pb^{2+} coordination, the catalytically active Pb^{2+} must coordinate to a different structure, as in none of the crystallized constructs, the correct geometry of an in-line attack is given. A possible reason for this is the fact that the bulged loop nucleotides undergo contacts with their respective nucleotides from other leadzyme molecules within the crystal structure, i.e., they are flipped out and lose their dynamics and flexibility (Figure 6). A detailed summary of the two structures [25, 26] for the interested reader is provided in [125].

An interesting fact is that the leadzyme motif and some of its variants have been found in eukaryotic genomes and in their mRNA sequences, i.e., humans, *Drosophila melanogaster*, *Caenorhabditis elegans*, and *Arabidopsis thaliana* show an average of 2–9 leadzyme motifs per 1 Mbp of DNA sequence [126]. These sequences can potentially self-cleave in the presence of lead(II) ions and have been related with lead toxicity *in vivo*, giving rise to cancer and other important human disorders [126]. On the other hand, a preliminary therapeutic use of the leadzyme has been reported based on the leadzyme interference. It was found that a leadzyme formed *in vivo* was able to interfere with the tobacco mosaic virus infecting *Nicotiana tabacum*. For that use, a synthetic 16-mer RNA, designed to form a leadzyme motif with an identified target sequence in the genomic mosaic virus RNA, was applied with a nontoxic, catalytic amount of lead(II) to infected tobacco leaves. The authors observed a significant reduction in mosaic virus accumulation even when the leadzyme was applied up to 2 hours after inoculation of leaves with tobacco mosaic virus [127].

Mechanistic studies have shown that the leadzyme follows a 2-step cleavage mechanism with very similar catalytic rate constants. The first step is similar to the bond-scission reaction characteristic of small ribozymes, where the 2′-OH nucleophile of the C6 ribose attacks the adjacent phosphate, forming a 2′,3′-cyclic phosphate (on the C6) and a free 5′-OH (at G7) [122]. This 2′,3′-cyclic intermediate is the final product in the hammerhead, hairpin, and hepatitis delta virus ribozymes [120]. Nevertheless, in the leadzyme cleavage reaction the 2′,3′-cyclic intermediate evolves in a second lead-dependent hydrolysis step to yield the 3′-monophosphate product, like in RNase A strand cleavage [122].

The cleavage reaction is highly specific for lead(II) and the cleavage reaction rate is exponentially dependent on pH between 5.5 and 7.0, which suggests that a lead(II)-hydroxide species acts as a general base in the rate-limiting step, abstracting a proton from the C6 2′-OH [120, 123]. The leadzyme is highly lead(II)-specific as studies have shown that about 25 different divalent and trivalent metal ions were not able to induce specific cleavage. Only neodymium(III) and some other rare metals enhance the cleavage reaction, which hints at a two-metal ion mechanism in which Pb^{2+} and Nd^{3+} play the roles of base and acid catalyst, respectively [128, 129].

5.3. Lead(II) in Ribozymes

Often described as relics from a primitive world based solely on RNA, RNA enzymes are naturally occurring, as well as artificial, catalysts involved in a variety of chemical reactions, such as autolytic cleaving and splicing, hydrolysis, peptide bond formation, tRNA aminoacylation, Diels-Alder chemistry, RNA-dependent RNA polymerization, redox activity, and many more [1]. Natural RNA enzymes, or ribozymes, are classified according to their size. Large ribozymes include self-splicing introns, the spliceosome, and RNase P, while small ribozymes are around 150 nts and include the hammerhead, hairpin, Varkud satellite (VS), hepatitis delta virus (HDV), and glucosamine-6-phosphate activated (*glmS* riboswitch) ribozymes [125]. Monovalent and divalent metal ions are required for all ribozymes in order to achieve efficient catalytic activity [2].

As already commented above, lead(II)-dependent hydrolytic cleavage is a powerful technique to study structure and metal ion binding sites in RNA, and as such it has been applied to study an aminoacyltransferase ribozyme [49], a Diels-Alder ribozyme [130], and the antigenomic hepatitis delta virus ribozyme [55].

Although lead(II) is not a natural metal cofactor in ribozymes, it has been applied regularly in order to study the catalytic mechanisms and their metal ion requirements. One of the first studies involving lead(II) and ribozymes concerned the metal ion requirements of the M1 subunit of RNase P from *Escherichia coli*. This RNA subunit catalytically cleaves precursor tRNA, without being self-cleaved nor forming any covalent bond with its substrate. The study showed that just Mg^{2+} and in a lesser extent Mn^{2+} can function at the catalytic core of M1 RNA, but Pb^{2+} failed to function as divalent cation cofactor in M1 cleavage [131]. Nevertheless, more recent studies revealed some RNase P RNA-mediated cleavage promoted by Pb^{2+} resulting in a 5′-phosphate and a 3′-OH as cleavage products. The authors suggest that lead(II) activates a water molecule to act as the nucleophile and they have identified residues both in the substrate and RNase P RNA that most likely position Pb^{2+} at the cleavage site [132].

On the other hand, a new cleavage site between G8 and A9 yielding a free 5′-hydroxyl and a 2′,3′-cyclic phosphate, has been identified in the hammerhead ribozyme. The metal dependence studies showed that Zn^{2+} is the preferred metal ion, but cleavage was also observed in the presence of Ni^{2+}, Co^{2+}, Mn^{2+}, Cd^{2+}, and Pb^{2+}, while being negligible with alkaline earth metal ions only. Among these metal ions, Pb^{2+} was almost as efficient as Zn^{2+} at pH 7.5 but, at pH 8.6 the cleavage activity in the presence of Pb^{2+} was just between 5 and 8 % compared with Zn^{2+} [133].

A similar study was carried out with the self-splicing reaction of the yeast mitochondrial group II intron *Sc*.ai5γ, which is highly sensitive to the presence of divalent metal ions others than Mg^{2+}. The first step of the splicing reaction was used to test the effect of different metal ions. Catalytic activity was not detected as both Zn^{2+} and Pb^{2+} lead to a fast nonspecific degradation of the RNA. Both metal ions have a high affinity for phosphate residues and a significant tendency to form hydroxo complexes, being ideal cations for hydrolytic cleavage of the phosphate sugar backbone at physiological pH [5].

6. CONCLUDING REMARKS AND FUTURE DIRECTIONS

The most important property of lead(II) in the context of nucleic acids is the pK_a of its coordinated water molecules near the physiological pH range. Aside from its use in X-ray crystallography to produce crystals containing heavy metals needed for solving the phase problem, all other applications of Pb^{2+} with nucleic acids involve hydrolytic backbone cleavage catalyzed by Pb^{2+}. The determination of metal ion binding sites in large RNAs both *in vitro* and *in vivo*, the detection of nanomolar amounts of Pb^{2+} by fluorescence assays using DNAzymes, as well as the construction of logic gates for the construction of nanocomputers are just a few examples.

The full potential of lead(II) has certainly not yet been exploited in the context of nucleic acids: The usage of Pb^{2+}-dependent DNAzymes will continue to be optimized for various applications, e.g., not only for sensing Pb^{2+} ions in solution, but also for the construction of nanocomputers, a field which is only at the very beginning. Similarly, one could also imagine the *in vitro* selection of new types of DNAzymes, using Pb^{2+} as cofactor for organic synthesis, similar to the Diels-Alder ribozyme.

Most interesting is the fact that the leadzyme motif, which has been found in *in vitro* selection experiments independently by various groups and under different selection conditions, also occurs regularly in various genomes of organisms. This raises the question if within the cell, upon exposure to Pb^{2+}, these motifs also get catalytically cleaved. The potential benefit of such a metal ion-selective and specific cleavage is open and it has actually been proposed that such a cleavage is one of the origins of Pb^{2+} toxicity [126, 132, 134]. On the other hand, one could also imagine that such a cleavage on the RNA level induces a signal cascade or upregulates, similar to a riboswitch, the production of proteins involved in Pb^{2+} detoxification. While all of this is speculation, the future will certainly have several surprises for us with regard to the interaction of Pb^{2+} with nucleic acids.

ACKNOWLEDGMENTS

Financial support from the Swiss National Science Foundation (to RKOS), the Swiss State Secretariat for Education, Research and Innovation (SBFI, COST Action CM1105) (RKOS), the COST Action CM1105 (short-term scientific mission, JPM), the University of Zurich (RKOS), and the *Govern de les Illes Balears* (FEDER AAEE68/2015 to MBO) is gratefully acknowledged.

ABBREVIATIONS AND DEFINITIONS

A	adenine
ABTS	2,2′-azino-bis(3-ethylbenzothiazoline-6-sulfonic acid) diammonium salt

ATMND	2-amino-5,6,7-trimethyl-1,8-naphthyridine
ATP	adenosine 5′-triphosphate
AuNP	gold nanoparticle
bipy	2,2′-bipyridine
C	cytosine
cDNA	complementary DNA
D	dihydrouridine
dabcyl	4-((4-(dimethylamino)phenyl)azo)benzoic acid
DENV-MINI	Dengue virus minigenome
DFHBI	3,5-difluoro-4-hydroxybenzylidene imidazolinone
DMS	dimethylsulfoxide
dppz	dipyrido[3,2-a:2′,3′-c]phenazine
DPV	differential pulse voltammetry
EDTA	ethylenediamine-N,N,N′,N′-tetracetate
FAM	fluorescein
FRET	Förster resonance energy transfer
G	guanine
glmS	glucosamine-6-phosphate
GNR	gold nanorod
HCV	hepatitis C virus
HDV	hepatitis delta virus
HIV-1/2 TAR	human immunodeficiency virus 1 (or 2) trans-activation response element
HIV-1 DIS	human immunodeficiency virus type 1 dimerization initiation site
MB	methylene blue
miRNA	microRNA
NDB	nucleic acid database
nt	nucleotide
PDB	protein database
PIV5	parainfluenza virus 5
PS	phosphorothioate
PT	polythiophene
QD	quantum dot
RNase P	ribonuclease P
RT-qPCR	real-time quantitative polymerase chain reaction
TAMRA	5-(and 6-)carboxytetramethylrhodamine
$tRNA^{Phe}$	transfer RNA encoding for phenylalanine
SHAPE	selective 2′-hydroxyl acylation analysed by primer extension
tmRNA	transfer-messenger RNA
U	uridine
UTR	untranslated region
VS	Varkud satellite
XAS	X-ray absorption spectroscopy
Y	pseudouridine

REFERENCES

1. *Structural and Catalytic Role of Metal Ions in RNA*, Vol. 9 of *Metal Ions in Life Sciences*, Eds A. Sigel, H. Sigel, R. K. O. Sigel, Royal Society of Chemistry, Cambridge UK, 2011.
2. M. C. Erat, R. K. O. Sigel, *Met. Ions Life Sci.* **2011**, *9*, 37–100.
3. J. Schnabl, P. Suter, R. K. O. Sigel, *Nucleic Acids Res.* **2012**, *40*, D434–D438.
4. M. Pechlaner, R. K. O. Sigel, *Met. Ions. Life Sci.* **2012**, *10*, 1–42.
5. M. C. Erat, R. K. O. Sigel, *J. Biol. Inorg. Chem.* **2008**, *13*, 1025–1036.
6. J. Schnabl, R. K. O. Sigel, *Curr. Opin. Chem. Biol.* **2010**, *14*, 269–275.
7. S. Li, X.-L. Liu, X.-L. Zhou, S.-J. Jiang, H. Yuan, *Interdisc.Toxicol.* **2016**, *8*, 155–158.
8. R. Sunkar, B. Kaplan, N. Bouché, T. Arazi, D. Dolev, I. N. Talke, F. J. M. Maathuis, D. Sanders, D. Bouchez, H. Fromm, *Plant J.* **2016**, *24*, 533–542.
9. R. D. Shannon, *Acta Crystallogr.* **1976**, *A32*, 751–767.
10. W. E. Morf, W. Simon, *Helv. Chim. Acta* **1971**, *54*, 794–810.
11. C. F. Baes, Jr., R. E. Mesmer, *The Hydrolysis of Cations*, Krieger Publishing Co., Malabar, Florida, 1976, pp. 1–496.
12. L. Helm, A. E. Merbach, *Coord. Chem. Rev.* **1999**, *187*, 151–181.
13. Y. Inada, A. M. Mohammed, H. H. Loeffler, S. Funahashi, *Helv. Chim. Acta* **2005**, *88*, 461–469.
14. S. F. Lincoln, *Helv. Chim. Acta* **2005**, *88*, 523–545.
15. R. K. O. Sigel, H. Sigel, in *Comprehensive Inorganic Chemistry II*, Vol. 3, Eds J. Reedijk, K. Poeppelmeier, Elsevier, Oxford, 2013, pp. 623–660.
16. H. M. Berman, T. N. Bhat, P. E. Bourne, Z. K. Feng, G. Gilliland, H. Weissig, J. Westbrook, *Nature Struct. Biol.* **2000**, *7*, 957–959.
17. E. Freisinger, R. K. O. Sigel, *Coord. Chem. Rev.* **2007**, *251*, 1834–1851.
18. R. S. Brown, B. E. Hingerty, J. C. Dewan, A. Klug, *Nature* **1983**, *303*, 543–546.
19. J. R. Rubin, M. Sundaralingam, *J. Biomol. Struct. Dyn.* **1983**, *1*, 639–646.
20. E. Westhof, M. Sundaralingam, *Biochemistry* **1986**, *25*, 4868–4878.
21. R. S. Brown, J. C. Dewan, A. Klug, *Biochemistry* **1985**, *24*, 4785–4801.
22. A. S. Krasilnikov, X. J. Yang, T. Pan, A. Mondragon, *Nature* **2003**, *421*, 760–764.
23. A. V. Kazantsev, A. A. Krivenko, D. J. Harrington, S. R. Holbrook, P. D. Adams, N. R. Pace, *Proc. Natl. Acad. Sci. USA* **2005**, *102*, 13392–13397.
24. E. Ennifar, P. Walter, P. Dumas, *Nucleic Acids Res.* **2003**, *31*, 2671–2682.
25. J. E. Wedekind, D. B. McKay, *Nat. Struct. Biol.* **1999**, *6*, 261–268.
26. J. E. Wedekind, D. B. McKay, *Biochemistry* **2003**, *42*, 9554–9563.
27. M. Alayyoubi, G. P. Leser, C. A. Kors, R. A. Lamb, *Proc. Natl. Acad. Sci. USA* **2015**, *112*, E1792–E1799.
28. A. Jack, J. E. Ladner, D. Rhodes, R. S. Brown, A. Klug, *J. Mol. Biol.* **1977**, *111*, 315–328.
29. R. Koradi, M. Billeter, K. Wüthrich, *J. Mol. Graphics* **1996**, *14*, 29–32 & 51–55.
30. C. Guerrier-Takada, K. Gardiner, T. Marsh, N. Pace, S. Altman, *Cell* **1983**, *35*, 849–857.
31. D. Donghi, J. Schnabl, *Met. Ions Life Sci.* **2011**, *9*, 197–234.
32. C. Chevalier, T. Geissmann, A.-C. Helfer, P. Romby, *Methods Mol. Biol.* **2009**, *540*, 215–232.
33. M. Lindell, P. Romby, E. G. H. Wagner, *RNA* **2002**, *8*, 534–541.
34. M. Wildauer, G. Zemora, A. Liebeg, V. Heisig, C. Waldsich, *Methods Mol. Biol.* **2014**, *1086*, 159–176.
35. K. Sobczak, G. Michlewski, M. de Mezer, J. Krol, W. J. Krzyzosiak, *Anal. Biochem.* **2010**, *402*, 40–46.
36. H. Sigel, *Coord. Chem. Rev.* **1990**, *100*, 453–539.

37. H. Sigel, *Inorg. Chim. Acta* **1992**, *198–200*, 1–11.
38. A. M. Pyle, *J. Biol. Inorg. Chem.* **2002**, *7*, 679–690.
39. T. A. Steitz, J. A. Steitz, *Proc. Natl. Acad. Sci. USA* **1993**, *90*, 6498–6502.
40. L. A. Kirsebom, J. Ciesiolka, *Handbook of RNA Biochemistry, Vols 1 and 2, 2nd Ed.*, 2014, pp. 269–283.
41. M. Forconi, D. Herschlag, *Methods Enzymol.* **2009**, *468*, 91–106.
42. J.-V. Philippe, L. Ayadi, C. Branlant, I. Behm-Ansmant, *Small Non-Coding RNAs: Methods and Protocols* **2015**, *1296*, 119–136.
43. R. K. O. Sigel, A. M. Pyle, *Met. Ions Biol. Syst.* **2003**, *40*, 477–512.
44. E. J. Merino, K. A. Wilkinson, J. L. Coughlan, K. M. Weeks, *J. Am. Chem. Soc.* **2005**, *127*, 4223–4231.
45. R. K. O. Sigel, A. Vaidya, A. M. Pyle, *Nat. Struct. Biol.* **2000**, *7*, 1111–1116.
46. M. Olejniczak, Z. Gdaniec, A. Fischer, T. Grabarkiewicz, L. Bielecki, R. W. Adamiak, *Nucleic Acids Res.* **2002**, *30*, 4241–4249.
47. M. Brannvall, N. E. Mikkelsen, L. A. Kirsebom, *Nucleic Acids Res.* **2001**, *29*, 1426–1432.
48. K. Pachulska-Wieczorek, K. J. Purzycka, R. W. Adamiak, *Nucleic Acids Res.* **2006**, *34*, 2984–2997.
49. A. Flynn-Charlebois, N. Lee, H. Suga, *Biochemistry* **2001**, *40*, 13623–13632.
50. M. Dutkiewicz, J. Ciesiolka, *Nucleic Acids Res.* **2005**, *33*, 693–703.
51. J. M. Warnecke, M. Nitschke, C. E. C. Moolenaar, E. T. Rietschel, R. K. Hartmann, U. Mamat, *Mol. Microbiol.* **2016**, *36*, 697–709.
52. M. Dutkiewicz, A. Swiatkowska, M. Figlerowicz, J. Ciesiolka, *Biochemistry* **2008**, *47*, 12197–12207.
53. N. Polacek, S. Patzke, K. H. Nierhaus, A. Barta, *Mol. Cell* **2000**, *6*, 159–171.
54. N. E. Mikkelsen, K. Johansson, A. Virtanen, L. A. Kirsebom, *Nat. Struct. Biol.* **2001**, *8*, 510–514.
55. J. Wrzesinski, L. Blaszczyk, M. Wronska, A. Kasprowicz, K. Stokowa-Soltys, J. Nagaj, M. Szafraniec, T. Kulinski, M. Jezowska-Bojczuk, J. Ciesiolka, *FEBS J.* **2013**, *280*, 2652–2664.
56. A. Swiatkowska, P. Zydowicz, A. Gorska, J. Suchacka, M. Dutkiewicz, J. Ciesiolka, *PLoS One* **2015**, *10*, e0141676.
57. J. Sztuba-Solinska, T. Teramoto, J. W. Rausch, B. A. Shapiro, R. Padmanabhan, S. F. J. Le Grice, *Nucleic Acids Res.* **2013**, *41*, 5075–5089.
58. C. L. Miller, U. Haas, R. Diaz, N. J. Leeper, R. K. Kundu, B. Patlolla, T. L. Assimes, F. J. Kaiser, L. Perisic, U. Hedin, L. Maegdefessel, H. Schunkert, J. Erdmann, T. Quertermous, G. Sczakiel, *PLoS Genetics* **2014**, *10*, e1004263.
59. R. F. Gesteland, T. R. Cech, J. F. Atkins, *The RNA World*, Cold Spring Harbor Press, 2006, pp. 1–768.
60. P.-A. Monnard, D. W. Deamer, J. W. Szostak, *Third European Workshop on Exo-Astrobiology* **2004**, *545*, 145–148.
61. P. M. Loffler, J. Groen, M. Dorr, P. A. Monnard, *PLoS One* **2013**, *8*, e75617.
62. A. V. Lutay, E. L. Chernolovskaya, M. A. Zenkova, V. V. Vlassov, *Biogeosciences* **2006**, *3*, 243–249.
63. C. C. Hardin, A. G. Perry, K. White, *Biopolymers* **2000**, *56*, 147–194.
64. P. R. Majhi, R. H. Shafer, *Biopolymers* **2006**, *82*, 558–569.
65. I. C. Kwan, X. Mo, G. Wu, *J. Am. Chem. Soc.* **2007**, *129*, 2398–2407.
66. K. Kruger, P. J. Grabowski, A. J. Zaug, J. Sands, D. E. Gottschling, T. R. Cech, *Cell* **1982**, *31*, 147–157.
67. T. Lan, Y. Lu, *Met. Ions Life Sci.* **2012**, *10*, 217–248.
68. R. R. Breaker, G. F. Joyce, *Chem. Biol.* **1994**, *1*, 223–229.

69. P. I. Pradeepkumar, C. Höbartner, in *From Nucleic Acids Sequences to Molecular Medicine*, Eds V. A. Erdmann, J. Barciszewski, Springer-Verlag, 2012, pp. 371–410.
70. T. Lan, K. Furuya, Y. Lu, *Chem. Commun.* **2010**, *46*, 3896–3898.
71. S. W. Santoro, G. F. Joyce, *Proc. Natl. Acad. Sci. USA* **1997**, *94*, 4262–4266.
72. J. Li, W. Zheng, A. H. Kwon, Y. Lu, *Nucleic Acids Res.* **2000**, *28*, 481–488.
73. D. Faulhammer, M. Famulok, *Angew. Chem. Int. Ed.* **2016**, *35*, 2837–2841.
74. R. P. Cruz, J. B. Withers, Y. Li, *Chem. Biol.* **2004**, *11*, 57–67.
75. H.-K. Kim, J. Liu, J. Li, N. Nagraj, M. Li, C. M.-B. Pavot, Y. Lu, *J. Am. Chem. Soc.* **2007**, *129*, 6896–6902.
76. K. Schlosser, Y. Li, *ChemBioChem* **2010**, *11*, 866–879.
77. P.-J. J. Huang, J. Liu, *Chem. Commun.* **2014**, *50*, 4442–4444.
78. R. Saran, J. Liu, *Inorg. Chem. Front.* **2016**, *3*, 494–501.
79. P.-J. J. Huang, J. Lin, J. Cao, M. Vazin, J. Liu, *Anal. Chem.* **2014**, *86*, 1816–1821.
80. R. Saran, Q. Chen, J. Liu, *J. Mol. Evol.* **2015**, *81*, 235–244.
81. V. Kapoor, X. Li, M. Elk, K. Chandran, C. A. Impellitteri, J. W. S. Domingo, *Env. Sci. Technol.* **2015**, *49*, 13454–13462.
82. Y.-T. Tsai, C.-M. Chang, J.-Y. Wang, M.-F. Hou, J.-M. Wang, R. Shiurba, W.-C. Chang, W.-C. Chang, *Env. Toxicol.* **2015**, *30*, 1024–1032.
83. C. P. Chan, Y. T. Tsai, Y. L. Chen, Y. W. Hsu, J. T. Tseng, H. Y. Chuang, R. Shiurba, M. H. Lee, J. Y. Wang, W. C. Chang, *Env. Toxicol.* **2016**, *30*, 129–136.
84. J. Stela-Gabriela, *Bulletin UASVM, Veterinary Medicine* **2008**, *65*, 16–19.
85. J. Li, Y. Lu, *J. Am. Chem. Soc.* **2000**, *122*, 10466–10467.
86. J. Liu, Y. Lu, *Anal. Chem.* **2003**, *75*, 6666–6672.
87. H. Wang, Y. Kim, H. Liu, Z. Zhu, S. Bamrungsap, W. Tan, *J. Am. Chem. Soc.* **2009**, *131*, 8221–8226.
88. C.-S. Wu, M. K. K. Oo, X. Fan, *ACS Nano* **2010**, *4*, 5897–5904.
89. J. H. Kim, S. H. Han, B. H. Chung, *Biosensors & Bioelectronics* **2011**, *26*, 2125–2129.
90. H.-B. Wang, L. Wang, K.-J. Huang, S.-P. Xu, H.-Q. Wang, L.-L. Wang, Y.-M. Liu, *New J. Chem.* **2013**, *37*, 2557–2563.
91. L. Wang, Y. Jin, J. Deng, G. Chen, *Analyst* **2011**, *136*, 5169–5174.
92. P.-J. J. Huang, J. Liu, *Anal. Chem.* **2014**, *86*, 5999–6005.
93. C. B. Swearingen, D. P. Wernette, D. M. Cropek, Y. Lu, J. V. Sweedler, P. W. Bohn, *Anal. Chem.* **2004**, *77*, 442–448.
94. Y. Xiang, A. Tong, Y. Lu, *J. Am. Chem. Soc.* **2009**, *131*, 15352–15357.
95. L. Zhang, B. Han, T. Li, E. Wang, *Chem. Commun.* **2011**, *47*, 3099–3101.
96. X. Chen, H. Guan, Z. He, X. Zhou, J. Hu, *Anal. Methods* **2012**, *4*, 1619–1622.
97. S. DasGupta, S. A. Shelke, N.-s. Li, J. A. Piccirilli, *Chem. Commun.* **2015**, *51*, 9034–9037.
98. L. Guo, D. Nie, C. Qiu, Q. Zheng, H. Wu, P. Ye, Y. Hao, F. Fu, G. Chen, *Biosensors & Bioelectronics* **2012**, *35*, 123–127.
99. J. Liu, Y. Lu, *J. Am. Chem. Soc.* **2003**, *125*, 6642–6643.
100. J. Liu, Y. Lu, *Chem. Mater.* **2004**, *16*, 3231–3238.
101. J. Liu, Y. Lu, *J. Am. Chem. Soc.* **2004**, *126*, 12298–12305.
102. J. Liu, Y. Lu, *J. Am. Chem. Soc.* **2005**, *127*, 12677–12683.
103. J. Liu, Y. Lu, *Org. Biomol. Chem.* **2006**, *4*, 3435–3441.
104. W. Zhao, J. C. F. Lam, W. Chiuman, M. A. Brook, Y. Li, *Small* **2008**, *4*, 810–816.
105. H. Wei, B. Li, J. Li, S. Dong, E. Wang, *Nanotechnology* **2008**, *19*, 095501.
106. Z. Wang, J. H. Lee, Y. Lu, *Adv. Mater.* **2016**, *20*, 3263–3267.
107. Q. Zhang, Y. Cai, H. Li, D.-M. Kong, H.-X. Shen, *Biosensors & Bioelectronics* **2012**, *38*, 331–336.
108. D. Mazumdar, J. Liu, G. Lu, J. Zhou, Y. Lu, *Chem. Commun.* **2010**, *46*, 1416–1418.
109. Y. Xiao, A. A. Rowe, K. W. Plaxco, *J. Am. Chem. Soc.* **2007**, *129*, 262–263.

110. L. Shen, Z. Chen, Y. Li, S. He, S. Xie, X. Xu, Z. Liang, X. Meng, Q. Li, Z. Zhu, M. Li, X. C. Le, Y. Shao, *Anal. Chem.* **2008**, *80*, 6323–6328.
111. B. Zhang, L. Lu, Q. Hu, F. Huang, Z. Lin, *Biosensors & Bioelectronics* **2014**, *56*, 243–249.
112. H. Cui, X. Xiong, B. Gao, Z. Chen, Y. Luo, F. He, S. Deng, L. Chen, *Electroanalysis* **2016**, *28*, 2000–2006.
113. P. Travascio, Y. F. Li, D. Sen, *Chem. Biol.* **1998**, *5*, 505–517.
114. T. Li, E. Wang, S. Dong, *J. Am. Chem. Soc.* **2009**, *131*, 15082–15083.
115. W. Zhai, C. Du, X. Li, *Chem. Commun.* **2014**, *50*, 2093–2095.
116. J. Tao, J. Zheng, J. Li, P. Zhao, J. Li, C. Ma, M. Yi, R. Yang, *Science China-Chemistry* **2014**, *57*, 453–458.
117. C. Werner, B. Krebs, G. Keith, G. Dirheimer, *Biochim. Biophys. Acta* **1976**, *432*, 161–175.
118. W. J. Krzyzosiak, T. Marciniec, M. Wiewiorowski, P. Romby, J. P. Ebel, R. Giege, *Biochemistry* **1988**, *27*, 5771–5777.
119. L. S. Behlen, J. R. Sampson, A. B. DiRenzo, O. C. Uhlenbeck, *Biochemistry* **1990**, *29*, 2515–2523.
120. X. Qi, T. Xia, *Biomol. Concepts* **2011**, *2*, 305–314.
121. T. Pan, O. C. Uhlenbeck, *Biochemistry* **1992**, *31*, 3887–3895.
122. T. Pan, O. C. Uhlenbeck, *Nature* **1992**, *358*, 560–563.
123. T. Pan, B. Dichtl, O. C. Uhlenbeck, *Biochemistry* **1994**, *33*, 9561–9565.
124. P. Legault, C. G. Hoogstraten, E. Metlitzky, A. Pardi, *J. Mol. Biol.* **1998**, *284*, 325–335.
125. J. E. Wedekind, *Met. Ions Life Sci.* **2011**, *9*, 299–345.
126. M. Z. Barciszewska, M. Szymanski, E. Wyszko, J. Pas, L. Rychlewski, J. Barciszewski, *Mutat. Res.* **2005**, *589*, 103–110.
127. E. Wyszko, M. Nowak, H. Pospieszny, M. Szymanski, J. Pas, M. Z. Barciszewska, J. Barciszewski, *FEBS J.* **2006**, *273*, 5022–5031.
128. T. Ohmichi, N. Sugimoto, *Biochemistry* **1997**, *36*, 3514–3521.
129. N. Sugimoto, T. Ohmichi, *FEBS Lett.* **1996**, *393*, 97–100.
130. A. M. Chiorcea-Paquim, J. A. Piedade, R. Wombacher, A. Jaschke, A. M. Oliveira-Brett, *Anal. Chem.* **2006**, *78*, 8256–8264.
131. M. E. Glasner, N. H. Bergman, D. P. Bartel, *Biochemistry* **2002**, *41*, 8103–8112.
132. E. Kikovska, N. E. Mikkelsen, L. A. Kirsebom, *Nucleic Acids Res.* **2005**, *33*, 6920–6930.
133. J. C. Markley, F. Godde, S. T. Sigurdsson, *Biochemistry* **2001**, *40*, 13849–13856.
134. M. Z. Barciszewska, E. Wyszko, R. Bald, V. A. Erdmann, J. Barciszewski, *J. Biochem.* **2003**, *133*, 309–315.

13

Historical View on Lead: Guidelines and Regulations

Hana R. Pohl, [*] ***Susan Z. Ingber, and Henry G. Abadin***

Agency for Toxic Substances and Disease Registry (ATSDR),
US Department of Health and Human Services, 1600 Clifton Road, Atlanta, GA 30333, USA
<hpohl@cdc.gov> <singber@cdc.gov> <habadin@cdc.gov>

* Corresponding author

The findings and conclusions in this report are those of the authors and do not necessarily represent the views of the Agency for Toxic Substances and Disease Registry.

Metal Ions in Life Sciences, Volume 17 Edited by Astrid Sigel, Helmut Sigel, and Roland K. O. Sigel

DOI 10.1515/9783110434330-013

Abstract: Lead has been used in many commodities for centuries. As a result, human exposure has occurred through the production and use of these lead-containing products. For example, leaded gasoline, lead-based paint, and lead solder/pipes in water distribution systems have been important in terms of exposure potential to the general population. Worker exposures occur in various industrial activities such as lead smelting and refining, battery manufacturing, steel welding or cutting operations, printing, and construction. Some industrial locations have also been a source of exposure to the surrounding communities. While the toxicity of relatively high lead exposures has been recognized for centuries, modern scientific studies have shown adverse health effects at very low doses, particularly in the developing nervous system of fetuses and children. This chapter reflects on historical and current views on lead toxicity. It also addresses the development and evolution of exposure prevention policies. As discussed here, these lead policies target a variety of potential exposure routes and sources. The changes reflect our better understanding of lead toxicity. The chapter provides lead-related guidelines and regulations currently valid in the U. S. and in many countries around the world. The reader will learn about the significant progress that has been made through regulations and guidelines to reduce exposure and prevent lead toxicity.

Keywords: lead blood levels · lead toxicity · U. S. lead regulations · World lead regulations

1. INTRODUCTION

Lead is a naturally occurring metal found in the Earth's crust at about 15–20 mg/kg [1]. Lead rarely occurs in its elemental state. The most important lead containing ores are galena (PbS), anglesite ($PbSO_4$), and cerussite ($PbCO_3$). Levels of lead in the environment (not contained in ore deposits) have increased over the past three centuries as a result of human activity. Human exposure to lead has resulted from the many uses of this metal. The most sensitive targets for lead toxicity are the developing nervous system, the hematological and cardiovascular systems, and the kidneys. However, due to the multi-modes of action of lead in biological systems, lead could potentially affect any system or organs in the body. Lead exposure may also cause anemia and high blood pressure, as well as reproductive effects in both sexes. Even at low doses, lead has been found to be detrimental to the developing nervous systems of young children [1]. The National Toxicology Program (NTP) concluded that, overall, there is sufficient evidence that blood lead (PbB) levels < 5 μg/dL are associated with adverse health effects in children (decreased academic achievement, IQ, and specific cognitive measures; increased incidence of attention-related and problem behaviors) [2]. Approximately half a million U. S. children ages 1–5 have PbB levels above 5 μg/dL, the reference level at which the United States (U. S.) Centers for Disease Control and Prevention (CDC) recommends public health actions be initiated.

Workers are exposed in the lead smelting and refining industries, battery manufacturing plants, steel welding or cutting operations, construction, rubber prod-

ucts and plastics industries, printing industries, firing ranges, radiator repair shops, and other industries requiring flame soldering of lead solder.

The greatest potential for lead exposure in the general population has been from its previous use as an additive in gasoline (which resulted in its widespread dispersal throughout the environment), and its use as a pigment in both interior and exterior paints. The U. S. gradually phased out lead use in gasoline in the 1980s and by 1996, banned its use in motor vehicles, except for certain uses; its use in consumer paints was banned in 1978. Consequently, PbBs in the U. S. general population have decreased over the past three decades [1]. PbBs measured as a part of the National Health and Nutrition Examination Surveys (NHANES) indicated that, from 1976 to 1991, levels in the U. S. population aged from 1 to 74 years dropped 78 %, from 12.8 to 2.8 μg/dL. The prevalence of PbBs ≥10 μg/dL also decreased sharply from 77.8 to 4.3 % [3]. Data from NHANES 2009–2010 reported a geometric mean PbB of 1.12 μg/dL.

The largest amounts of lead in occupational settings (two-thirds) are used in the manufacture of electric storage batteries. Surveillance data on storage battery manufacturers show mean airborne lead levels ranging from 50 to 5,400 μg/m^3; in the smelting and refining industries, mean air lead concentrations can reach 4,470 μg/m^3, and the average concentration in the breathing zone of structural steel welders is 1,200 μg/m^3 [1].

2. HISTORICAL VIEWS ON LEAD TOXICITY

Lead is one of the first metals used by humans and has been utilized for millennia. The oldest documented use of lead occurred in Asia Minor from about 6000 to 4000 B.C. [4]. The Egyptians and Hebrews also used lead; Phoenicians mined lead in modern-day Spain around 2000 B.C. More information comes from ancient Greece and the Roman Empire, where it was widely used in consumer products such as piping, cooking utensils, and in pottery glazing. Leaching of lead from these products may have resulted in poisoning. In addition, the Romans used lead as an additive, a syrup called sapa, to sweeten and preserve sour wines [5]. They also used lead in cosmetics and topical medications. In contrast, the Chinese used it in oral herbal medicines [6]. Spain and Britain, in particular, acquired large quantities of lead as a by-product in the mining of silver for coins. The Roman Empire produced 60,000 tons of lead per year for 400 years [4]. For comparison, in 2012, total worldwide lead production (primary and secondary) was over 10.5 million tons [7].

Historical accounts of lead poisoning signs and symptoms abound, beginning with the work of Hippocrates in 370 B.C. [8]. Although Hippocrates may have been the first to describe lead colic, Dioscorides, in 1 AD may have been the first to connect toxicity to lead exposure [4]. During the Middle Ages, the use of lead as a sweetener in drinks was wide-spread; however, the contemporary medical literature did not discuss lead poisoning. In the 16th century, Paracelsus

described a "miner's disease" and in the early 18th century, Ramazzini described lead toxicity in potters who worked with lead during glazing. An association between lead exposure in contaminated cider and development of "Devonshire colic" was reported in the late 18th century [9]. Laennec recognized anemia as a consequence of lead exposure in 1831, and Thackrah described "plumbism" as a clinical entity a year later [8]. By the 1800s, the many uses of lead resulted in an increased demand for the associated skilled trades needed to supply lead and lead containing products. Occupational lead poisoning cases began to be reported in the 1800s and into the 1900s. Subsequently, poisoning of lead workers was recognized as a significant health problem which resulted in exposure prevention strategies in many countries.

3. DEVELOPMENT OF GUIDELINES AND REGULATIONS IN THE U. S.

3.1. Historical Guidelines and Regulations

Hazardous substances (including lead) are regulated by a number of U. S. statutory requirements that govern the amount of allowable lead in air, water, paint, soil, and consumer products. Unfortunately, despite the abundant evidence of the toxicity of lead, many of these guidelines and regulations were not implemented until the latter part of the twentieth century. Nevertheless, the effects of these regulations have resulted in a stark reduction in blood lead levels in the U. S. as documented in survey data from the National Health and Nutrition Surveys (1971–2008) (Figure 1) [10]. The prevalence of children aged 1–5 years with PbB levels ≥ 10 μg/dL has decreased from 2.2 % in the 1991–1994 NHANES survey to 0.8 % in the 2007–2008 survey [11]. Estimated geometric mean PbB levels in 1–5 year olds have declined from 15 μg/dL (1976–1980) to 1.17 μg/dL (2009–2010) [11, 12].

Lead-specific guidelines and regulations were promulgated as the understanding of lead toxicity and exposure advanced. For example, the Lead Contamination Control Act of 1988 gave authority to the Centers for Disease Control and Prevention to develop and initiate programs aimed at eliminating lead poisoning in the U. S., such as developing targeted screening and case management guidelines for children with elevated PbB levels. In 1991, CDC defined PbB ≥ 10 μg/dL as the "level of concern" for children aged 1–5 years [13], down from 25 μg/dL in 1985 (Figure 2). In 2012, CDC accepted the recommendations of its Advisory Committee on Childhood Lead Poisoning Prevention (ACCLPP) that the term "level of concern" be replaced with an upper reference interval value defined as the 97.5th percentile of blood lead levels (BLLs) in U. S. children aged 1–5 years from two consecutive cycles of NHANES [14]. The current upper reference interval value of the 97.5th percentile of the distribution of the combined 2007–2008 and 2009–2010 cycles of NHANES was calculated as 5 μg/dL.

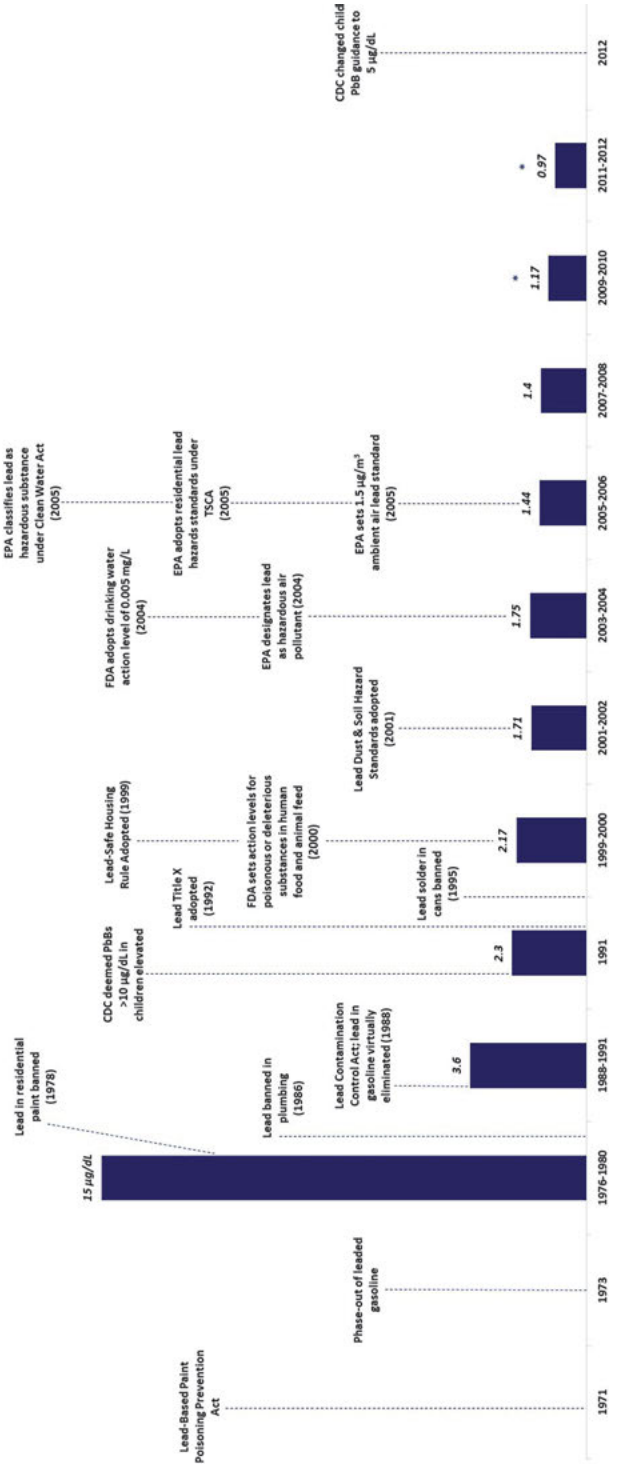

Figure 1. Timeline of U.S. lead policies and geometric mean PbBs (µg/dL) of children aged 1–5 years. National Health and Nutrition Examination Survey, United States, 1971–2014. Adapted from [10]. *unadjusted geometric mean

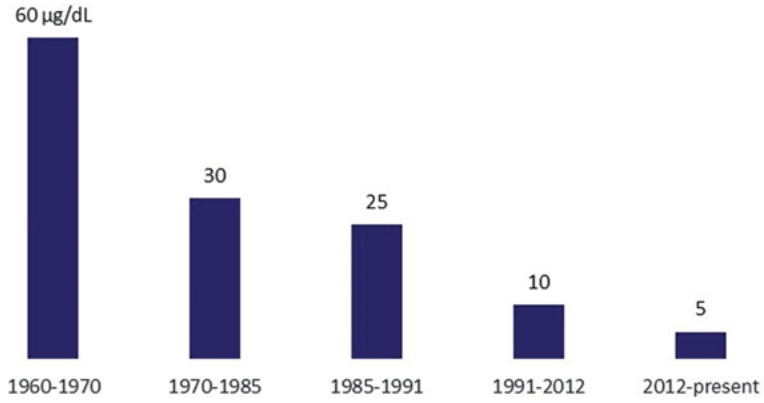

Figure 2. U. S. Blood lead action levels (µg/dL).

3.2. Current Guidelines and Regulations

Numerous lead guidelines and regulations have been developed in the U. S. Many of the more important of these are described and discussed in the following narrative and in Table 1.

3.2.1. Occupational

For workers, the Occupational Safety and Health Administration (OSHA) has developed regulations designed to protect workers. These include regulating the permissible air lead levels allowed, requiring engineering controls and work practices to reduce exposure, and requiring high exposure employees to be enrolled in medical surveillance programs. OSHA requires the employer to use engineering controls and work practices to achieve a permissible exposure limit (PEL) of 50 µg/m^3 or lower, based on an 8-hour time-weighted average (TWA) [15]. When employee lead exposures ≤ 50 µg/m^3 cannot be maintained, the employer must provide employees with respirators for supplemental control. Prevailing OSHA lead standards require medical removal from lead exposures only after a construction worker's BLL reaches or exceeds 50 µg/dL or a general industry worker's BLL reaches or exceeds 60 µg/dL, and allow workers to return to work when the BLL is below 40 µg/dL. OSHA lead standards also give the examining physician broad flexibility to tailor special protective procedures to the needs of individual employees, including consideration of removal from lead exposure at lower levels than the current OSHA lead standards require [15, 16]. In 2015, the National Institute of Occupational Safety and Health (NIOSH) designated 5 µg/dL of whole blood, in a venous blood sample, as the reference blood lead level for adults. An elevated BLL is defined as a BLL ≥ 5 µg/dL [17].

Table 1. Current U. S. lead regulations and guidelines.[a]

Agency	Description	Information	Ref.
Air			
EPA	Hazardous air pollutant	Yes	[77]
	National primary and secondary ambient air quality standards	0.15 μg/m^3	[19]
NIOSH	REL (TWA)	50 μg/m^3	[78]
	IDLH	100 mg/m^3	
OSHA	PEL (8-hour TWA) for toxic and hazardous substances for lead	50 μg/m^3	[15]
	PEL (8-hour TWA) for general industry for tetraethyllead	75 μg/m^3	[79]
	PEL (8-hour TWA) for construction industry for tetraethyllead	100 μg/m^3	[80]
	PEL (8-hour TWA) for shipyard industry for tetraethyl lead	100 μg/m^3	[81]
Water			
EPA	Designated as hazardous substances in accordance with Section 311(b)(2)(A) of the Clean Water Act lead acetate, lead chloride, leadfluoroborate, lead iodide, lead nitrate, lead sulfate, lead sulfide, and tetraethyllead	Yes	[82]
	National primary drinking water standards		[83]
	MCLG	Zero	
	MCL	Treatment[b]	
	action level	15 μg/L	
	Reportable quantities of hazardous substances designated pursuant to Section 311 of the Clean Water Act lead acetate, lead chloride, lead fluoroborate, lead iodide, lead nitrate, lead sulfate, lead sulfide, and tetraethyllead	10 pounds	[84]
EPA	Residential lead hazards standards – TSCA Section 403		[85]
	Floors	40 μg/ft^2	
	Interior window sills	250 μg/ft^2	
	Bare soil in children's play area	400 ppm	
	Bare soil in rest of yard	1200 ppm average	

Agency	Description	Information	Ref.
Food			
FDA	Action level (μg/mL leaching solution)		[86]
	Ceramicware		
	Flatware (average of 6 units)	3.0 μg/mL	
	Small hollowware (other than cups and mugs) (any 1 of 6 units)	2.0 μg/mL	
	Large hollowware (other than pitchers) (any 1 of 6 units)	1.0 μg/mL	
	Cups and mugs (any 1 of 6 units) and pitchers (any 1 of 6 units)	0.5 μg/mL	
	Silver-plated hollowware		
	Product intended for use by adults (average of 6 units)	7 μg/mL	
	Product intended for use by infants and children (any 1 of 6 units)	0.5 μg/mL	
	Bottled drinking water	5 μg/L	[87]
Other			
CDC	Reference value for children	5 μg/dL	[10]
CDC	Nationally notifiable non-infectious condition for children and adults	5 μg/dL	[88]
CPSC	The CPSIA limits lead in paint and substrates	0.009 %	[24]
EPA	Lead Renovation, Repair and Painting Program Rules	To protect the public from lead-based paint hazards associated with renovation, repair and painting activities.	[89]
EPA	Carcinogenicity classification	Probable human carcinogen	[90]
	Superfund, emergency planning, and community right-to-know		
	Designated CERCLA hazardous substance		
	Reportable quantity		
	Lead, lead acetate, lead chloride, lead fluoroborate, lead iodide, lead nitrate, lead phosphate, lead sulfate, lead sulfide, and tetraethyllead	10 pounds	[91]

	Effective date of toxic chemical release reporting for lead	01/01/87	[92]
	Extremely hazardous substances		[93]
	Tetraethyllead		
	Reportable quantity	10 pounds	
	Threshold planning quantities	100 pounds	
	Threshold amounts for manufacturing (including importing), processing, and otherwise using such toxic chemicals	100 pounds	[94]
AOEC	Clinical recommendations for patient care		[95]
NTP	Carcinogenicity classification	Reasonably anticipated to be human carcinogens	[96]

[a] Adapted from [1].
[b] Lead is regulated by a treatment technique that requires water distribution systems to control the corrosiveness of the water.
AOEC = Association of Occupational and Environmental Health Clinics; CDC = Centers for disease Control and Prevention; CERCLA = Comprehensive Environmental Response, Compensation, and Liability Act of 1980; CPSC = Consumer Product Safety Commission; CPSIA = Consumer Product Safety Improvement Act; EPA = Environmental Protection Agency; FDA = Food and Drug Administration; IDLH = immediately dangerous to life or health; MCL = the highest level of a contaminant that is allowed in drinking water; MCLG = a level of a contaminant in drinking water below which there is no known or expected risk to human health. MCLGs are non-enforceable public health goals; NTP = National Toxicology Program; OSHA = Occupational Safety and Health Administration; PEL = permissible exposure limits; REL = recommended exposure limits; TLV = threshold limit values; TSCA = Toxic Substances Control Act; TWA = time-weighted average

3.2.2. Water

The Clean Water Effluent Guidelines and Standards, which are promulgated under the authority of the Clean Water Act (CWA), provide limitations on pollutant concentrations in waste water discharges from point source categories and represent the degree of reduction in pollutant concentration that is attainable through demonstrated technologies for new and existing sources. The Lead and Copper Rule requires drinking water distribution systems to monitor drinking water at home taps. If lead concentrations exceed an action level of 15 ppb in more than 10 % of samples, the system must undertake a number of additional actions to control corrosion. In addition, the Reduction of Lead in Drinking Water Act (RLDWA) in 2011 strengthened the SDWA of 1986, which prohibited the use of pipes and solder/flux that was not "lead-free" (0.2 % solder or flux; 8 % for pipes) [18]. The RLDWA lowered the maximum lead content of plumbing products to a weighted average of 0.25 %.

3.2.3. Air

Under the Clean Air Act (CAA) of 1970, the Environmental Protection Agency (EPA) has set a national ambient air quality standard (NAAQS) for lead. CAA requires that the NAAQSs be revisited on a periodic basis to ensure the protection of human health and the environment. In 2008, EPA strengthened the NAAQS for lead from 1.5 $\mu g/m^3$ to 0.15 $\mu g/m^3$ [19].

Historically, the major sources of lead emissions to air have been from fuels in on-road motor vehicles (such as cars and trucks) and industrial sources. As a result of regulatory efforts to remove lead from on-road motor vehicle gasoline, emissions of lead from the transportation sector declined by 95 percent between 1980 and 1999, and levels of lead in the air decreased by 94 percent between 1980 and 1999. The highest air concentrations of lead are usually found near lead smelters [20]. Based on emission estimates, EPA reports a 98 % reduction in lead emissions to the atmosphere between 1980 and 2014 (Figure 3) [21].

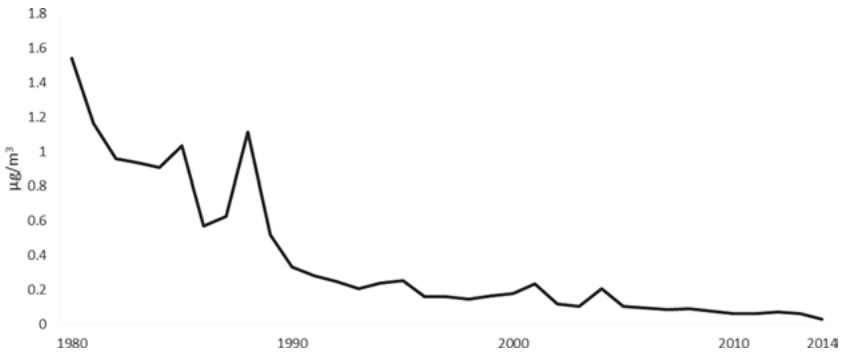

Figure 3. Average air levels ($\mu g/m^3$) decreased 98 % between 1980 and 2014; annual maximum three months average, trend based on 11 sites. Adapted from [21].

3.2.4. Waste and Soil

The EPA also regulates lead content in hazardous wastes as prescribed by the Resource Conservation and Recovery Act (RCRA). A solid waste may be defined as hazardous if it exhibits any of the four characteristics (ignitability, corrosiveness, reactivity, and toxicity) used to identify hazardous wastes. EPA set the RCRA lead threshold at 5.0 mg/L waste sample extract [22]. Lead has been identified in at least 1272 of the 1684 hazardous waste sites proposed for inclusion on the EPA National Priorities List (NPL) [23].

3.2.5. Paint

The Consumer Product Safety Improvement Act of 2008 authorized regulations pertaining to consumer products including specific requirements for children's products; these are enforced by the Consumer Product Safety Commission (CPSC). With certain exemptions, the CPSC now limits lead in consumer paints to 0.009 % (90 ppm). The CPSC further limits the lead content of children's products to less than 100 ppm of total lead content in accessible parts [24]. The Residential Lead-Based Paint Hazard Reduction Act of 1992 (also known as Title X of the Housing and Community Development Act) requires sellers, landlords, and agents to notify potential purchasers or tenants if a dwelling may contain lead-based paint and to provide information concerning the hazards of lead.

3.2.6. Food

In 1995, the use of lead-soldered cans was banned by the Food and Drug Administration (FDA) [25]. The FDA also establishes regulatory limits for lead levels in bottled water and in certain food ingredients, as well as guidance values for lead in certain foods, such as candy and juice. For juice, FDA states that lead levels in juice above 50 ppb may constitute a health hazard; for candy, FDA lowered its recommended maximum level of lead consumed by young children to 100 ppb. Where it has not established regulations, FDA assesses the significance of lead levels found in food on a case-by-case basis [26].

4. DEVELOPMENT OF GUIDELINES AND REGULATIONS AROUND THE WORLD

4.1. Historical Guidelines and Regulations

Historical records show the earliest lead regulations began in Germany, where Germanic tribes outlawed Roman wines because of the colic that occurred in those that had consumed the wine [27]. In the Middle Ages, lead was again used throughout Europe to preserve and sweeten wine. However, in 1696, Duke

Ludwig of Ulm in Germany issued a decree forbidding lead-based additives in wine products for economic rather than health-based reasons. If consumers were to learn that lead-treated local wine caused colic, they would not buy it. In the 19th century, the main concern about lead toxicity was in regards to occupational exposure from industrial activities such as mining, smelting, scrapping, printing, pottery, and the manufacture of batteries. There were many cases of poisoning and fatalities among workers in Europe and the U.S., even at the beginning of the 20th century [28, 29].

One of the major problems recognized at the time was poisoning caused by painting doors and windows with white lead paint. Consequently, the International Labour Conference (ILC) organized a meeting in 1921 to address this problem. The negotiations resulted in a recommendation to prohibit the indoor use of white lead and lead sulfate-containing paint with greater than 2 % metallic lead by weight [30]. However, railroad and industrial establishment applications were exempted. The ILC's proposal was ratified by 63 countries [31], including Czechoslovakia and Sweden (1923), Austria, Poland, and Spain (1924), and Finland and Norway (1929) [32]. However, Great Britain and the U.S. did not adopt the decision. For workers, European experts of the time recommended safe levels for lead exposure as: blood lead 80 μg/100 mL, urinary lead 150 μg/L, urinary coproporphyrin 500 μg/L, and urinary ALA 20 mg/L [33]. In 1978, the World Health Organization (WHO) recommended a health-based limit of 40 μg/100 mL lead in blood [34].

Other countries began passing additional lead laws starting in the 1960s. Australia first adopted its Uniform Paint Standard for lead in 1965 as part of its Standard for the Uniform Scheduling of Drugs and Poisons (SUSDP) policy [35]. Initially, the standard only applied to architectural paint and decorative paint (including children's toy applications) manufactured in Australia, thus excluding imported paints. Originally set at 1 % by weight, the lead limit decreased to 0.25 % in 1992 [35]. Prior to adopting its current hazardous substance regulation [Registration Evaluation, Authorisation and Restriction of Chemicals (REACH)] in 2006, the European Union (EU) passed Directive 1999/45/EC ("relating to the classification, packing, and labelling of dangerous preparations") [36]. The law included a provision for lead in paint and varnishes, establishing that paints with lead levels exceeding 0.15 % by weight must contain a warning with the following words:

> "Contains lead. Should not be used on surfaces liable to be chewed or sucked by children."

However, the law exempted packages containing less than 125 mL, which must instead indicate:

> "Warning! Contains lead."

In the initial REACH legislation, the EU included a ban only on lead carbonates and lead sulfates in paints [37]. It did, however, allow Member States to permit exemptions for use in historic buildings and artwork restoration projects.

Starting in the 1980s, some countries also began to pass legislation aimed at children's toys. The EU adopted its first toy lead legislation in 1988 (Council Directive 88/378/EEC of 3 May 1988). The law set a maximum bioavailability level of 0.7 μg/day from toy exposure without proposing a per-article exposure limit, such as a migration limit or percentage weight standard [38]. Canada's 2002 Hazardous Products Act (R.S.C., 1985, c. H-3; oldest version available on website) prohibited toys with decorative or protective coatings containing lead pigments or greater than 0.5 % lead by weight (total solids) [39]. In 2005, Health Canada added Surfaces Coating Materials Regulations to the Hazardous Products Act and set a maximum 600 mg/kg total lead limit for surface coating materials, "including paints or other similar materials that dry to a solid film when a layer of it is applied to a surface, but not including materials that become a part of the substrate" [40].

4.2. Current Guidelines and Regulations

Tables 2–6 below summarize the existing international lead legislation according to type of lead application, excluding lead paint laws. Overall, these regulations address the inhalation (occupational and environmental monitoring policies) and oral (children's toys, food, water/infrastructure, consumer products policies) exposure routes. Lead paint laws, which primarily focus on oral exposure in children, were catalogued by the United Nations Environmental Programme (UNEP) and the WHO [41]. They are discussed separately.

4.2.1. Paint

In 2014, during the Third Meeting of the Global Alliance to Eliminate Lead Paint, the UNEP and the WHO documented all of the lead paint laws passed across the globe [41]. They found a total of 43 existing, legally enforceable lead paint laws outside the United States, 13 of which set specific lead limits. Two countries (Philippines, Canada) set the most conservative limit of 90 ppm. Switzerland prohibits paint, varnishes, or products treated with coatings containing more than 100 ppm (0.01 %) lead or lead compounds by weight. The majority of lead limits (in Argentina, Brazil, Chile, Costa Rica, Oman, Panama, South Africa, Uruguay) set the lead threshold at 600 ppm, while the least protective limits were established in Belarus (150,000 ppm) and Australia (1000 ppm). In addition to these regulations, the EU's complete ban of lead carbonates and lead sulfates in paints (REACH) was adopted by 28 countries. However, the EU recently granted authorizations for six industrial paint applications for lead sulfochromate yellow and lead chromate molybdate sulfate red (total of 12 uses) [42]. Potential allowances include industrial uses in non-consumer paints, industrial articles, metal surfaces (e.g., road signs, machines vehicles), and hotmelt road marking. In contrast, India chose to adopt a voluntary paint limit, lowering it from 1000 ppm (in 2004) to 90 ppm in 2013 [43, 44]. While this conservative

threshold is more protective, the lack of regulatory authority to enforce it undermines its potential public health impact [45].

For most of these laws and standards, documentation on the scientific basis of these threshold levels was not available. Uruguay considered "international standards," as well as the interests of private industries (namely feasibility) and non-governmental organizations when deriving its paint threshold (Decreto 069/2011) [46]. Both The Philippines and Canada chose their 90 ppm paint threshold to be consistent with the United States' paint law [40, 47]. The Philippines also based their lead threshold on evidence that unleaded paint contains less than 90 ppm "and usually under 45 ppm" [47]. Canada's threshold also applies to other coatings found in children's toys (see Section 4.2.3. below).

4.2.2. Occupational

As shown in Table 2, Australia, Singapore, and South Africa currently have occupational lead standards in place. Notably, unlike Singapore's and South Africa's laws, Australia's lead policies are guidelines, not regulations.

In 1994, Australia passed the National Standard for the Control of Inorganic Lead at Work [NOHSC:1012(1994)] [48], which established health guidance values to help employers (particularly in the mining industry) determine when to place workers on medical leave, how long to monitor their PbBs, and when to allow them to return to work. The policy also accounted for the increased susceptibility of fetuses to the effects of lead exposure by setting more protective standards for women of childbearing age, pregnant, and breastfeeding women. According to the official guidance document, the Commonwealth based the PbBs on available studies showing health effects occurring at or below 30 μg/dL, but ultimately "lean[ed] towards what is currently achievable rather than strictly health effects" [48].

The following year, Australia adopted its current occupational ambient air lead exposure standards [49, 50]. They based all of their lead compound (tetraethyl lead, tetramethyl lead, lead arsenate, inorganic lead) limits on the American Conference of Governmental American Hygienists' (ACGIH's) threshold limit values (TLVs) and biological exposure indices (BEIs) (5^{th} [1986] and 6^{th} [1991] editions) [50]. Singapore set occupational ambient air lead levels in 2006. The regulatory language did not include the scientific basis for their air levels, but the policy's inorganic lead and lead arsenate limits are nearly identical to Australia's air guidance levels. In contrast to Australia, Singapore published their lead limits as permissible exposure levels (PELs); these permissible exposure *levels* are analogous to OSHA's permissible exposure *limits*. Singapore also adopted a more conservative PEL specifically for lead chromate.

Unlike Australia and Singapore, South Africa created a separate, more conservative inhalation limit for tetraethyl and tetramethyl lead (see Table 2). However, they did not establish separate PbBs for female workers. Moreover, their PbBs are considerably less conservative (i.e., less health-protective) than Australia's guidance.

Table 2. Current non-U.S. occupational lead regulations and recent amendments excluding paint laws as of February 2016.

Country	Name of policy (reference)	Year adopted	Regulatory or guidance?	Compound targeted	Exposure route targeted	Description/ exposure source	Exposure limit	Other details
Australia	National Standard for the Control of Inorganic Lead at Work [48]	1994	Guidance	Inorganic lead	NS	Blood lead level standard (PbB) for "Lead-risk Job"	> 30 μg/dL	
						PbB for 6 month follow-up biomonitoring of workers	< 30 μg/dL	Specific to those "not of reproductive capacity," "males of reproductive capacity" in a "lead-risk job" (see above)
						PbB for 3 month follow-up	30–39 μg/dL	Specific to those "not of reproductive capacity," "males of reproductive capacity"
							< 10 μg/dL	Specific to "females of reproductive capacity"
						PbB for 6 week follow-up	≥ 40 μg/dL	Specific to those "not of reproductive capacity" and "males of reproductive capacity"
							≥ 10 μg/dL	Specific to "females of reproductive capacity"
						PbB for "Medical Removal"	≥ 50 μg/dL	Specific to those "not of reproductive capacity" and "males of reproductive capacity"
							≥ 20 μg/dL	Specific to "females of reproductive capacity"
							≥ 15 μg/dL	Specific to pregnant or breastfeeding females
							< 40 μg/dL	Specific to those "not of reproductive capacity," "males of reproductive capacity"; stipulates ≥ 6 week follow-up

Country	Name of policy (reference)	Year adopted	Regulatory or guidance?	Compound targeted	Exposure route targeted	Description/ exposure source	Exposure limit	Other details
						PbB for allowing employee to return to work	< 10 μg/dL	Specific to "females of reproductive capacity"; stipulates ≥ 6 week follow-up
Australia	National Exposure Standards for Atmospheric Contaminants in the Occupational Environment [50]	1995	Guidance	Tetramethyl lead	Inhalation	Occupational ambient air exposure standards	0.15 mg/m^3	TWA, level at which no adverse effects or discomfort expected for "nearly all workers"; last reviewed January 18, 2005.
				Tetraethyl lead			0.1 mg/m^3	TWA (see above)
				Lead arsenate			0.15 mg/m^3	TWA (see above)
				Inorganic lead			0.15 mg/m^3	TWA (see above), specific to dusts and fumes
Singapore	Permissible Exposure Levels of Toxic Substances, Workplace Safety and Health Regulations [97]	2006	Regulation	Inorganic lead	Inhalation	Occupational exposure standard	0.15 mg/m^3	Specific to dusts and fumes; PEL, based on chronic exposure
				Lead arsenate			0.15 mg/m^3	PEL, based on long-term exposure
				Lead chromate			0.05 mg/m^3	
South Africa	Lead Regulations, 2001; Occupational Health and Safety Act of 1993 [98]	2002	Regulation	Tetraethyl and tetramethyl lead	Inhalation	Occupational exposure limit	0.10 mg/m^3	
				Lead (other than tetraethyl lead)			0.15 mg/m^3	
				Lead (other than tetraethyl lead)	NS	PbB for "Medical Removal"	75 μg/dL	Sets the following targets for future implementation: 70 μg/dL (2003), 65 μg/dL (2004), 60 μg/dL (2005)

	PbB for allowing employee to return to work	65 μg/dL	Sets the following targets: 60 μg/dL (2003), 55 μg/dL (2004), 50 μg/dL (2005)
	PbB for ≤ 12 month intervals for biomonitoring of workers	< 20 μg/dL	
	PbB for ≤ 6 month intervals	20–39 μg/dL	
	PbB for ≤ 3 month intervals	40–59 μg/dL	
	PbB for intervals at clinician's discretion	≥ 60 μg/dL	
	Urinary lead level for ≤ 6 week intervals	< 120 μg/dL	
	Urinary lead level for ≤ 1 week intervals	120–149 μg/dL	
	Urine Pb levels for intervals at clinician's discretion	≥ 150 μg/dL	

PbB = blood lead level; NS = not specified; PEL = permissible exposure level; TWA = time-weighted average (assumed 8 hour workday, 40 days/week)

4.2.3. Children's Toys

Uruguay, Australia, the EU, and Canada have lead laws specific to children's toys (see Table 3). The oldest of the current laws was adopted by Uruguay in 2004, and it appears to have established a complete ban of lead in toys, "as well as elements naturally exposed to direct and potentially frequent contact by children and adolescents" [51]. However, Uruguay's 2011 paint law sets a 600 ppm threshold that applies to surface coating materials and children's paints, which seems to conflict with the broad language of the 2004 legislation.

In contrast to Uruguay, Australia established a lead migration limit for its toy legislation. Under the authority of its Trade Practice Act 1974, Australia set a temporary ban in 2007 on lead-containing children's toys whose lead migration exceeded 90 mg/kg [52]. The Commonwealth based the migration limit on the Australian/New Zealand/International Standards Organisation Standard for lead [52]. This level was calculated from a toy bioavailability value of 0.7 μg/day and assumed an average daily intake of 8 mg/day [53]. The resulting limit level was further adjusted to "minimize children's exposure to toxic elements in toys and to ensure analytical feasibility, taking into account limits achievable under current manufacturing conditions" [53].

The EU derived its Safety of Toys (Directive 2009/48/EC) lead migration levels from estimated adult weekly dietary intake levels, which were then divided in half to predict a child's tolerable daily intake (TDI). The child TDI estimate was further adjusted by a factor of 0.1 % to estimate the intake level resulting from contact with lead-containing toys and account for children's high sensitivity to lead's neurotoxicity. These allowable intake levels were then converted to migration levels in milligrams per kilogram (mg/kg) of toy material, assuming a daily intake of 8 mg of toy material (consistent with Australia's methods above) and an average body weight of 12 kg [54, 55]. Unlike Australia, the EU adopted distinct migration limits for different types of toy materials.

However, the EU has recently proposed reduced lead migration limits in toys based on adoption of a Benchmark Dose Limit ($BMDL_{01}$), as recommended by the European Food Safety Agency (EFSA) [56]. EFSA derived the $BMDL_{01}$ based on data showing a one-point decrease in IQ from a daily intake of 0.5 μg/kg/day, as measured in the blood of six-year old children [57, 58]. The resulting migration levels would be seven times lower than the 2009 standards.

In 2010, Canada revised its *Surfaces Coating Materials Regulations* (under the Hazardous Products Act) for lead, decreasing the threshold from 600 mg/kg (in 2005) to 90 mg/kg, effectively updating the *Hazardous Products (Toys) Regulations* (renamed *Toys Regulations* (SOR/2011–17) in 2011). According to the policy's corresponding Regulatory Impact Statement, Health Canada based its lead limit on the United States' Consumer Product Safety Improvement Act's (CPSIA's) lead paint law (16 C.F.R. 1303) adopted two years earlier, and emphasized evidence of "severe" health effects in children [40, 59].

Overall, the EU has the most conservative toy migration limits (see Table 3). However, their scraped toy material standard (160 mg/kg) is less protective than Australia and Canada's single 90 mg/kg limit, as well as the U. S. lead paint stan-

Table 3. Current non-U. S. children's toy lead regulations and recent amendments excluding paint laws as of February 2016.

Country	Name of policy (reference)	Year adopted	Regulatory or guidance?	Compound targeted	Exposure route targeted	Description/ exposure source	Exposure limit	Other details
Australia	Trade Practices Act 1974, temporary ban on lead-containing children's toys (updated) [52]	2007	Regulation	Lead	Oral	Toy material migration limit	90 mg/kg	
Canada	Consumer Products Containing Lead (Contact with Mouth) Regulations (SOR/ 2010-273), Canada Consumer Product Safety Act [99]	2010	Regulation	Lead	Oral	Toy accessible parts	90 mg/kg	
Canada	Toys Regulations (SOR/2011-17), Section 23 (Specific substances in surface coatings) [100]	2011	Regulatory	Lead	Oral	Toy surface material coating	90 mg/kg	Effective through July 20, 2013
European Union	Directive 2009/48/EC (Safety of toys) [101]	2009	Regulatory	Lead	Oral	Dry, brittle, powder-like or pliable toy material Liquid or sticky toy material Scraped-off toy material	13.5 mg/kg 3.4 mg/kg 160 mg/kg	"Toys must not contain substances classified as CMR [carcinogenic, mutagenic, or toxic to reproductive system], Cat 1A, 1B or 2, at higher concentrations than the classification limit. This affects all lead compounds but not metallic lead. Cf. section C." [65]
Uruguay	Law N°17.775: Prevención de la contaminación por Plomo **[51]**	2004	Regulatory	Lead	Oral	Toys, products frequently used by children and adolescents	0 (Banned)	

dard. If the EU adopts its proposed migration limits, they will have the most protective toy lead regulations of any country. Though Uruguay's complete ban of lead in toys is the most conservative policy, it poses a potential implementation obstacle because it does not account for the industry feasibility issues expressed in Australia and the EU's regulatory guidance documents.

4.2.4. Food

The EU, Singapore, and Uruguay have lead laws addressing oral exposures from food. The EU passed its first food lead regulation in 1984, adopting lead migration limits in ceramics intended to contact food (see Table 4). However, the EU Commission has recently proposed new migration limits up to 1000 times lower than the current thresholds, based on the same EFSA $BMDL_{01}$ behind the draft toy surface migration limits (see Table 4) [60, 61]. Decades after passing their ceramics regulations, the EU adopted a law limiting lead in a specific plastic used in food packaging (see Table 4). The EU began to address food lead content in 1988, with their adoption of a food flavorings lead limit of 10 mg/kg [62]. Then in 2006, they broadened the scope of their food lead regulations, adopting more conservative thresholds ranging from 0.02 (milk and infant formula) to 1.5 mg/kg (seafood and shellfish). They based their lead levels in part on the WHO's provisional tolerable weekly intake (PTWI) of 25 μg/kg [63].

As shown in Table 4, Uruguay's 1994 policy (Decreto 315/94) sets somewhat less protective lead limits in food, ranging from 0.1 (in oils, fats, refined emulsions) to 2 mg/kg (all other foods excluding citrus fruit juice and chocolate). In 2004, Uruguay adopted a separate policy banning the use of lead in food packaging and containers [51], surpassing the EU's plastic and ceramic food packaging and utensil laws in terms of safety.

Singapore's 2005 Food Regulations policy established a larger set of lead limits targeting additional, more specific food categories, ranging from 0.1 ppm (oils and fats) to 20 ppm (various food colorings). In contrast to Uruguay, but similar to the EU, Singapore established a specific, more health-protective infant formula and baby food standard (0.2 ppm) relative to most of their other food limits, thus addressing children's increased susceptibility to lead poisoning. In 2014, Singapore added bottled water and ice lead limits (0.01 ppm) to their import regulations [64].

4.2.5. Other Consumer Products

The EU, Australia, and Uruguay adopted gasoline lead thresholds (Table 5). The EU was the first to adopt its 0.005 g/L limit in 1998 [65], followed by Australia in 2002 [66]. Uruguay passed its leaded gasoline limit in 2004, setting it at 13 mg/L (0.013 g/L). Australia also adopted a limit of 0.06 % lead by weight in candles and candlewicks in 2002 [67]. In their *Explanatory Statement* justifying the threshold, they asserted that, "when burned in an enclosed area for a long time," candles with more than 0.06 % lead "can release high levels of lead into the atmosphere" that can cause adverse health effects to those exposed, "particularly

Table 4. Current non-U.S. food lead regulations and recent amendments as of February 2016.

Country	Name of policy (reference)	Year adopted	Regulatory or guidance?	Compound targeted	Exposure route targeted	Description/ exposure source	Exposure limit	Other details
European Union	Directive 84/500/EEC [62]	1984	Regulatory	Lead	Oral	Ceramic articles which cannot be filled or can be filled ≤25 mm	0.8 mg/dm^2	2012 proposed draft legislation, if adopted, would repeal this law, amend Article (5) of EC No 1935/2004, and establish the below lead migration limits: (1) 0.002 mg/dm^2 (2) 0.0038 mg/L (3) 0.01 mg/L [60]
						Ceramic cooking utensils; packaging, storage vessels fillable >3 L	1.5 mg/L	
						Other ceramic articles	4.0 mg/L	
European Union	Directive 88/388/EEC [102]	1988	Regulatory	Lead	Oral	Food flavorings	10 mg/kg	
European Union	Commission Regulation (1881/2006) [63]	2006	Regulatory	Lead	Oral	Milk, Infant formula	0.02 mg/kg	
						Meat (cow, sheep, pig, poultry)	0.1 mg/kg	
						Offal (cow, sheep, pig, poultry)	0.5 mg/kg	
						Seafood	0.3–1.5 mg/kg	
						Cereals, legumes, pulses	0.2 mg/kg	
						Produce	0.1–0.3 mg/kg	
						Fats and oils (including milk fat)	0.1 mg/kg	
						Fruit juices	0.05 mg/kg	
						Wine	0.20 mg/kg	

Country	Name of policy (reference)	Year adopted	Regulatory or guidance?	Compound targeted	Exposure route targeted	Description/ exposure source	Exposure limit	Other details
European Union	Commission Regulation (EU) No 10/2011 [65, 103]	2011	Regulatory	Lead	Oral	Specific plastic material that comes into contact with foods	2 mg/kg plastic	Plastic material: Poly(3-D-hydroxybutanoate-co-3-D-hydroxypentanoate) (FCM substance 744)
Singapore	"Maximum Amounts of Arsenic, Lead, and Copper Permitted in Food", Regulation 31(1), Sale of Food Act [104]	2005	Regulation	Lead	Oral	Soft drinks and concentrates	1–2 ppm	
						Fruit and vegetable juice	0.3–1 ppm	
						Alcoholic and other beverages	0.2 ppm	
						Baking powder, cream of tartar, canned fish and meat, meat extract, hydrolyzed protein	2 ppm	
						Caramel	5 ppm	
						Chemicals used as ingredients or in food preparation/ processing	10 ppm	
						Herbs/spices	2 ppm	
						Coffee beans	2 ppm	
						Edible oils/fats	0.1 ppm	
						Coloring matter (for food)	10–20 ppm	
						Infant formula and baby food	0.2 ppm	

						Fruits and vegetables	1 ppm	
						Refined sugar, dextrose (anhydrous, monohydrate)	0.5 ppm	
						Eggs, fish, other food	2 ppm	
Singapore	Food Regulations (Chapter 283, Section 56(1)), Sale of Food Act [104]	2014	Regulatory	Lead	Oral	Packaged mineral, drinking water (imports)	0.01 ppm	Singapore's food authority (AVA) added these lead limits to their Import Requirements on January 6, 2014 [64]
						Ice (imports)	0.01 ppm	
Uruguay	Decreto 315/94 [105]	1994	Regulatory	Lead	Oral	Oils, fats, and refined emulsions	0.1 mg/kg	
						Sweetened chocolate	1 mg/kg	
						Citrus fruit juices	0.3 mg/kg	
						Other foods	2 mg/kg	
						Utensils, other objects having contact with food	1 % by weight	
						Alcoholic beverages	1 mg/L	
Uruguay	Law N°17.775: Prevención de la contaminación por Plomo [51]	2004	Regulatory	Lead	Oral	Food containers/ packaging	0 (Banned)	

Table 5. Current non-U.S. other consumer products lead regulations and recent amendments as of February 2016.

Country	Name of policy (reference)	Year adopted	Regulatory or guidance?	Compound targeted	Exposure route targeted	Description/ exposure source	Exposure limit	Other details
Australia	Fuel Standard (Petrol) Determination 2001 [66]	2002	Regulatory	Lead	Inhalation	Gasoline	0.005 g/L	
Australia	Trade Practices Act 1974 [67]	2002	Regulation	Lead	NS	Candles and candlewicks	>0.06 % lead by weight	Maximum allowable lead level
Denmark	Statutory order: BEK nr. 856 af 05/09/2009 [69]	2009	Regulatory	Lead	Oral	Consumer products	100 mg/kg	Specific to homogenous components
European Union	Packaging and Packaging Waste Directive (94/62/EC) [65]	1994	Regulatory	Lead	Oral	Packaging and packaging components	100 mg/kg	
European Union	Fuel Quality Directive (98/70/EC) [65]	1998	Regulatory	Lead	Inhalation	Gasoline	0.005 g/L	Exempts aircraft fuel
European Union	ELV (End-of-life Vehicle) Directive (2000/53/EC) [65]	2000	Regulatory	Lead	NS	Cars, goods transport vehicles <3.5 tons	0.1 % by weight	Applies to each homogenous material/ component; includes exemptions for alloys, batteries, and "various components"

European Union	RoHS Directive (2011/65/EU) [65]	2011	Regulatory	Lead	NS	Electric and electronic equipment	0.1 % by weight	Applies to each homogenous material/ component in the equipment; includes exemptions for lead solder in "various applications"
						Can copper alloys	4 % by weight	
European Union	Registration, Evaluation, Authorisation, and Restriction of Chemicals (REACH) [70, 106]	2012	Regulatory	Lead	Oral	Jewelry, Jewelry-making parts (placed on market)	0.05 % by weight	Exempt if lead release is ≤ 0.05 μg/cm^2 per hour (0.05 μg/g/h)
		2015	Regulatory	Lead	Oral	Consumer products, accessible parts children can mouth	0.05 % by weight	Able to be placed in children's mouths if < 5 cm; Exempt if lead release is ≤ 0.05 μg/cm^2 per hour (0.05 μg/g/h)
Uruguay	Law N°17.775: Prevención de la contaminación por Plomo [51]	2004	Regulatory	Lead	Oral	Consumer products (under NAFTA)	13 mg/L	
					Inhalation	Gasoline	13 mg/L	

NAFTA = North American Free Trade Agreement

for unborn babies, small children and pregnant women [68]." In addition, Uruguay adopted a NAFTA (North American Free Trade Agreement) consumer product lead limit of 13 mg/L in 2004 [51]. In 2009, Denmark adopted its own consumer product lead limit of 100 mg/kg (in homogenous components), exempting hobby and decoration products (such as jewelry and bijouterie) [69].

The EU added a jewelry lead limit to its REACH legislation in 2012 [70]. The regulation exempts antique jewelry and crystal glass. It used EFSA's BMDL value of 12 μg/L – the same one used in its proposed lead migration limits for toy surfaces – and applied a Margin of Exposure (MoE) of 10 to "produce no appreciable risk" [65]. The law also established a 0.05 μg/g/hour migration rate limit, derived as follows:

> "Considering an exposure scenario in which a child of 10 kg bw mouths a piece of jewellery [jewelry] for 1 hour with a surface of 10 cm^2 and a weight of 10 g a tolerable migration rate from the jewellery [jewelry] of 0.05 μg Pb/cm^2/hr or 0.05 μg Pb/g/hr is estimated … With a general assumption that the ratio between surface (in cm^2) and the weight (in g) of the jewellery [jewelry] is 1 …" [71].

In 2015, the EU amended its REACH policy to include a provision for lead in consumer products and objects able to be placed in children's mouths. The regulation applied the same risk assessment methodology used for the jewelry limits [58]. Consistent with the world's most conservative lead policies, the EU based its consumer product and jewelry lead limits on children's susceptibility. In addition to the consumer product policies listed in Table 5, the EU has adopted legislation prohibiting the use of lead in cosmetic products (EC/1223/2009) [72]. Other EU country-specific regulations on lead in consumer products (current in 2012) are summarized in the REACH Annex XV Restriction Report – Lead and its Compounds in Articles Intended for Consumer Use [65].

4.2.6. Air and Water

As shown in Table 6, both the EU and Australia adopted a regulatory ambient air lead limit of 0.5 μg/m^3 while Uruguay adopted a 30 μg/m^3 guidance value for air monitoring.

Table 7 presents the water lead laws currently enforced in Australia, the EU, and Uruguay. The EU adopted a water lead limit of 10 μg/L in 1998 [65]. In 1989, Australia banned the use of lead-based solder in drinking pipes (> 0.1 % lead by weight) in 1998 and decreased its drinking water limit from 0.05 mg/L to 0.01 mg/L in 2004 [73, 74]. However, Australia's water lead limit is not a mandatory standard [75]. By contrast, Uruguay adopted a less protective limit of 0.05 mg/L [35, 76].

Table 6. Current non-U.S. environmental and biological lead monitoring regulations and recent amendments as of February 2016.

Country	Name of policy (reference)	Year adopted	Regulatory or guidance?	Compound targeted	Exposure route targeted	Description/ exposure source	Exposure limit	Other details
Australia	National Environment Protection Measure for Ambient Air Quality [110]	1998	Regulation	Lead	Inhalation	Maximum ambient air concentration	0.5 μg/m^3	
European Union	Directive 86/278/EC [65]	1986	Regulation	Lead	Oral	Sewage sludge for agricultural use	1000–1750 mg/kg	Applies to dry matter
European Union	Council Directive 1999/30/EC [111]	1999	Regulation	Lead	Inhalation	Ambient air limit value	0.5 μg/m^3	
Uruguay	Decreto 64/004 [112]	2004	Regulatory	Lead	NS	Declaration standard (PbB) for lead-associated diseases	>15 μg/dL	
Uruguay	Ordenanza 337 [113]	2004	Guidance	Lead	NS	Lead biomonitoring standard	>30 μg/dL	

Table 7. Current non-U.S. water and infrastructure lead regulations and recent amendments as of February 2016.

Country	Name of policy (reference)	Year adopted	Regulatory or guidance?	Compound targeted	Exposure route targeted	Description/ exposure source	Exposure limit	Other details
Australia	Australian Drinking Water Guidelines [74, 75]	2004	Guidance	Lead	Oral	Drinking water	10 μg/L	
Australia	Australian Standard AS 3500 Part 1.2 (adopted in Plumbing and Drainage Code of Practice) [73]	1998	Regulation	Lead	Oral	Soft solder (water infrastructure)	0.1 % by weight	
European Union	Directive 98/83/EC on quality of water intended for human consumption [65]	1998	Regulation	Lead	Oral	Drinking water	10 μg/L	Revised in 2011
Uruguay	Decreto 315/94 (2nd Edition, Capitulo 25, Seccion 1) [76, 107]	2000	Regulatory	Lead	Oral	Drinking water	0.05 mg/L	Updated in 2002
Uruguay	Law N°17.775: Prevención de la contaminación por Plomo [51]	2004	Regulatory	Lead	Oral	Water pipes and fittings	0 (Banned)	

						Water pipes and fittings with lead-alternative materials	< 8 % of the metal content	
						Solder, or flux (for water distribution)	0.2 % of metal content (solder)	
Uruguay	Decreto 375/11 [108, 109]	2011	Regulatory	Lead	Oral	Drinking water	0.03 mg/L	Also sets target value of 0.01 mg/L that must be met within 10 years.

5. CONCLUSION

Lead is an important metal used by human populations for millennia. The toxicity of lead is well established, and numerous lead exposure regulations and guidelines have been developed throughout the world to protect people from lead's harmful effects. It is especially important to protect developing fetuses and children because of their susceptibility to be harmed by very low lead levels. While some countries have implemented regulatory policies, others have adopted voluntary guidelines to manage specific lead exposures. Some of these guidelines, such as Australia's occupational lead monitoring policy and India's lead paint policy, present relatively more conservative lead limits relative to their regulatory counterparts in other countries. However, the lack of authority to enforce health guidelines may reduce their impact on exposure reduction relative to less protective regulatory policies. Nevertheless, significant progress has been made through regulations and guidelines to reduce exposure and prevent lead toxicity. To ensure public health protection from lead exposures, in addition to continued vigilance, enforcement of current regulations and implementation of current guidelines are needed.

ABBREVIATIONS

ACCLPP	Advisory Committee on Childhood Lead Poisoning Prevention
ACGIH	American Conference of Governmental Industrial Hygienists
ALA	δ-aminolevulinic acid
BEI	biological exposure limit
BLL	blood lead level
CAA	Clean Air Act
CDC	Centers for Disease Control and Prevention
CPSC	Consumer Product Safety Commission
CPSIA	Consumer Product Safety Improvement Act
CWA	Clean Water Act
EPA	Environmental Protection Agency
EU	European Union
FDA	Food and Drug Administration
ILC	International Labour Conference
IQ	intelligence quotient
MoE	Margin of Exposure
NAAQA	National Air Quality Standard
NAFTA	North American Free Trade Agreement
NHANES	National Health and Nutrition Examination Survey
NIOSH	National Institute for Occupational Safety and Health
NPL	National Priorities List
NTP	National Toxicology Program
OSHA	Occupational Safety and Health Administration
PbB	blood lead

PEL	permissible exposure limit/level
PTWI	provisional tolerable weekly intake
RCRA	Resource Conservation and Recovery Act
REACH	Registration, Evaluation, Authorization and Restriction of Chemicals
RLDWA	Reduction of Lead in Drinking Water Act
SDWA	Safe Drinking Water Act
SUSDP	Standard for the Uniform Scheduling of Drugs and Poisons
TDI	tolerable daily intake
TLV	threshold limit value
TSCA	Toxic Substances Control Act
TWA	time-weighted average
UNEP	United Nations Environmental Programme
WHO	World Health Organization

REFERENCES

1. ATSDR, *Toxicological Profile for Lead*. Agency for Toxic Substances and Disease Registry, Atlanta, 2007, pp. 1–582.
2. Health effects of low-level lead evaluation. Research Triangle Park, NC: US Department of Health and Human Services, National Toxicology Program, 2013. (Accessed April 13, 2016, at http://ntp.niehs.nih.gov/go/36443)
3. J. Pirkle, D. Brody, E. Gunter, R. Kramer, D. Paschal, K. Flegal, T. Matte, *J. Am. Med. Ass.* **1994,** *272*, 284–291.
4. S. Hernberg, *Am. J. Ind. Med.* **2000,** *38*, 244–254.
5. J. Eisinger, *Med. Hist.* **1982,** *3,* 279–302.
6. J. J. Chisolm, *West. J. Med.* **1985,** *143,* 380–381.
7. Lead Production and Statistics. London: International Lead Association. (Accessed April 18, 2016, at http://www.ila-lead.org/lead-facts/lead-production--statistics)
8. D. Hunter, *The Disease of Occupations.* 4th edn., English Universities Press, Aulesbury, 1969, pp. 1–1259.
9. G. Baker, *Med. Trans. Royal Coll. Phys.* **1772,** *2,* 419–470.
10. CDC, *Morbidity and Mortality Weekly Report, Supplements* **2012,** *61*, 1–9.
11. CDC, *Morbidity and Mortality Weekly Report,* **2013,** *62*, 245–248.
12. National Report on Human Exposure to Environmental Chemicals, Updated Tables. Atlanta, GA: Centers for Disease Control and Prevention, 2015. (Accessed March 11, 2016, at http://www.cdc.gov/exposurereport/)
13. Preventing lead poisoning in young children. Atlanta, GA: Centers for Disease Control and Prevention, 1991.
14. CDC Response to Advisory Committee on Childhood Lead Poisoning Prevention Recommendations in "Low Level Lead Exposure Harms Children: A Renewed Call of Primary Prevention". Atlanta, GA: Centers for Disease Control and Prevention, 2012. (Accessed April 15, 2016, at http://www.cdc.gov/nceh/lead/acclpp/cdc_response_lead_exposure_recs.pdf)
15. OSHA, 29 CFR 1910.1025. *Code of Federal Regulations*, Washington, D.C., 2005.
16. OSHA, 29 CFR 1926.62. *Code of Federal Regulations*, Washington, D.C., 2005.
17. Adult Blood Lead Epidemiology and Surveillance (ABLES) Program. Cincinnati, OH: US Department of Health and Human Services, CDC, National Institute for

Occupational Safety and Health, 2015. (Accessed April 13, 2016, at http://www.cdc.gov/niosh/topics/ables/description.html)
18. Section 1417 of the Safe Drinking Water Act: Prohibition on Use of Lead Pipes, Solder, and Flux. Washington, D.C.: U. S. Environmental Protection Agency, 2015. (Accessed April 18, 2016, at https://www.epa.gov/dwstandardsregulations/section-1417-safe-drinking-water-act-prohibition-use-lead-pipes-solder-and)
19. EPA. *Federal Register Notice*, Washington, D.C., 2008, *73*(219): 66964–67062.
20. Basic Information about Lead Air Pollution. Washington, D.C.: U. S. Environmental Protection Agency, 2016. (Accessed April 19, 2016, at https://www.epa.gov/lead-air-pollution/basic-information-about-lead-air-pollution#how)
21. National Trends in Lead Levels. Washington, D.C.: U. S. Environmental Protection Agency, 2016. (Accessed December 2, 2016, at https://www.epa.gov/air-trends/lead-trends)
22. EPA, 40 CFR 261.24. *Code of Federal Regulations*, Washington, D.C., 1990.
23. HazDat database: ATSDR's Hazardous Substance Release and Health Effects Database. Atlanta, GA: Agency for Toxic Substances and Disease Registry, 2006.
24. CPSC, 16 CFR Part 1303. *Code of Federal Regulations*, 2008.
25. FDA, 21 CFR 189.240. *Code of Federal Regulations*, Washington, D.C., 1995.
26. Reported Findings of Low Levels of Lead in Some Food Products Commonly Consumed by Children. Washington, D.C.: U. S. Food and Drug Administration, 2015. (Accessed April 18, 2016, at http://www.fda.gov/Food/FoodborneIllnessContaminants/Metals/ucm233520.htm)
27. History of Lead Poisoning in the World. Electronic report: http://www.biologicaldiversity.org/campaigns/get_the_lead_out/pdfs/health/Needleman_1999.pdf
28. T. Legge, K. Goadby, *Lead Poisoning and Lead Absorption*. Longman, New York, 1919.
29. T. Lloyd Davies, *The Practice of Industrial Medicine.* J&A Churchill, London, 1957, 1–282.
30. General Conference of the International Labour Organization, ILC Session 3. *Information System on International Labour Standards*, 1921.
31. Asia Regional Paint Report. 2014.
32. E. Silverberg, *Annu. Rev. Public Health* **1997,** *18,* 187–210.
33. R. Lane, D. Hunter, D. Malcolm, M. Williams, T. Hudson, R. Browne, R. McCallum, A. Thompson, A. de Kretser, R. Zielhuis, K. Cramer, P. Barry, A. Goldberg, T. Beritic, *Br. Med. J.* **1968,** *4,* 501–504.
34. Recommended Health-Based Limits in Occupational Exposures to Heavy Metals. Technical Report Series 647. Geneva: World Health Organization, 1980.
35. Lead in house paint. Australian Government, Department of the Environment (Accessed February 19, 2016, at http://www.environment.gov.au/protection/chemicals-management/lead/lead-in-house-paint)
36. European Parliament; Council of the European Union, Directive 1999/45. *Official Journal of the European Communities*, 1999, L 200.
37. European Parliament; Council of the European Union, Regulation (EC) No 1907/2006. *Official Journal of the European Union*, 2006, L 396.
38. Council of the European Communities, Council Directive 88/378/EEC. *Official Journal of the European Communities*, 1988, L 187.
39. Government of Canada, R.S.C., 1985, c. H-3. *Consolidated Acts*, Minister of Justice: 2002.
40. Government of Canada. *Canada Gazette*, 2010, Volume 144, Issue 9.

41. Information about the status in countries of legally-binding legislation, regulation and standards for lead in decorative paint. New Delhi: Third Meeting of the Global Alliance to Eliminate Lead Paint, 2014.
42. Commission Implementing Decision of 7.9.2016. C(2016) 5644. Brussels: European Commission, 2016. (Accessed December 1, 2016, at http://ec.europa.eu/DocsRoom/documents/18670/attachments/1/translations/en/renditions/native)
43. C. M. Department, Subject: Implementation of revised STI for IS 133(Part 1):2013 for Enamel, Interior: (a) Undercoating (b) Finishing — Specification Part 1 For Household and Decorative Purposes. (FCT), C. M. D., Ed. 2014.
44. Bureau of Indian Standards (BIS) notifies lead standards in paints to 90 ppm. (Accessed February 25, 2016, at http://toxicslink.org/?q=content/bureau-indian-standards-bis-notifies-lead-standards-paints-90-ppm)
45. Lead in Enamel Decorative Paints. National Paint Testing Results in a Nine Country Study. 2013.
46. Module H.iii Lead in Paint − Case Study − Uruguay. GAELP, DINAMA, Ministerio de Relaciones Exteriores, 2015.
47. Module H.iv. Lead in Paint − Case Study − The Philippines. GAELP, Phillipines Department of Environment and Natural Resources, 2015.
48. Commonwealth of Australia, NOHSC:1012(1994). *Australian Government Publishing Service*, 1994.
49. Hazardous Substances Information System (HSIS). (Accessed February 19, 2016, at http://hsis.safeworkaustralia.gov.au/)
50. Adopted National Exposure Standards for Atmospheric Contaminants in the Occupational Environment [NOHSC:1003(1995)]. Safe Work Australia, 1995. (Accessed April 17, 2016, at http://www.safeworkaustralia.gov.au/sites/SWA/about/Publications/Documents/237/AdoptedNationalExposureStandardsAtmosphericContaminants_NOHSC1003-1995_PDF.pdf)
51. República Oriental del Uruguay, Ley N°17.775. *Diario Oficial*, 2004.
52. Explanatory Statement: Consumer Protection Notice No. 1 of 2009, Trade Practices Act 1974, Consumer Product Safety Standard – Limits on the migration of lead and certain elements in children's toys. Minister for Competition Policy and Consumer Affairs, 2009. (Accessed April 17, 2016, at https://www.comlaw.gov.au/Details/F2009L00223/9f205513-8b77-4bd3-87ea-d4422c40fde4)
53. Joint Technical Committee CS-018, AS/NZS ISO 8124.3:2012. *Standards Australia*, 2012.
54. Evaluation of the Migration Limits for Chemical Elements in Toys, 1 July 2010. Brussels: Scientific Committee on Health and Environmental Risks, 2010. (Accessed April 18, 2016, at http://ec.europa.eu/health/scientific_committees/environmental_risks/docs/scher_o_126.pdf)
55. RIVM report 320003001/2008. Bilthoven, The Netherlands: National Institute for Public Health and the Environment (RIVM) & Voedsel en waren autoriteit, 2015.
56. EU Proposes to Reduce the Migration Limits of Lead in Toys. Bureau Veritas, 2014. (Accessed February 25, 2016, at http://www.bureauveritas.com/6320593f-8357-44b5-bf09-9863777f1917/Newsbyte_14NB-061.pdf?MOD=AJPERES)
57. Draft: Commission Directive ../…/EU of XXX amending, for the purpose of adapting to technical progress, Annex II to Directive 2009/48/EC of the European Parliament and of the Council on the safety of toys. Brussels: European Commission, 2014. (Accessed April 17, 2016, at https://members.wto.org/crnattachments/2014/tbt/EEC/14_4268_00_e.pdf)
58. European Chemicals Agency. Background document to the Opinion on the Annex XV dossier proposing restrictions on Lead and its compounds in articles intended for

consumer use (Accessed April 17, 2016, at http://echa.europa.eu/documents/10162/10a7006f-1342-40ad-8aa3-c28365d0faca)
59. L. Smith, R. Ross, S. Weihrer, in "*Canadian Safety Requirements for Children's Toys*"", *Health Canada Information Session, Consumer Product Safety*, 2013; Health Canada: 2013.
60. Draft Commission Regulation (EU) No …/… of XXX on ceramic materials and articles intended to come into contact with food. Brussels: European Commission, 2012. (Accessed April 17, 2016, at http://fera.co.uk/about-us/nationalReferenceLaboratory/materialsContact/documents/draftCommissionRegulationCeramicMaterials.pdf)
61. SME panel consultation. On new limits for the release of metals from ceramic materials and articles into food. Brussels: European Commission, 2012. (Accessed April 17, 2016, at http://fera.co.uk/about-us/nationalReferenceLaboratory/materialsContact/documents/smeConsultationBackgroundDocument.pdf)
62. Council of the European Communities, Council Directive 84/500/EEC. *Official Journal of the European Communities*, 1984, 1984L0500.
63. Council of the European Communities, Commission Regulation (EC) No 1881/2006. *Official Journal of the European Union*, 2006, L 364.
64. AVA, Import Requirements of Specific Food Products (Updated 6 January 2014). Singapore, Agri-Food & Veterinary Authority, Ed. 2014.
65. Annex XV Restriction Report − Proposal For A Restriction: Lead and It's Compounds In Articles Intended For Consumer Use. Swedish Chemicals Agency, 2012. (Accessed April 17, 2016, at http://echa.europa.eu/documents/10162/80f7edca-b6c1-4433-8734-854594530db2)
66. Australian Government, F2008C00344. *Federal Register of Legislation*, 2008.
67. Commonwealth of Austalia, Consumer Protection Notice No 7 of 2002. *Federal Register of Legislative Instruments*, 2002.
68. Explanatory Statement: Nine permanent bans on unsafe goods under the Trade Practices Act 1974. Australian Government, 2010. (Accessed April 17, 2016, at https://www.comlaw.gov.au/Details/F2010L03296/386b6be3-8512-4a5d-8f74-30269ecfaeaa)
69. Miljøministeriet, BEK nr 856 af 05/09/2009 (Gældende). *Miljøstyrelsen*, 2009, MST-6220-00158
70. European Commission, Commission Regulation (EU) No 836/2012. *Official Journal of the European Union*, European Commission: 2012, L 252.
71. Background document to the opinions on the Annex XV dossier proposing restrictions on Lead and its compounds in jewellery. European Chemicals Agency, 2011. (Accessed April 17, 2016, at http://www.echa.europa.eu/documents/10162/c9388bba-2660–4c0e-946b-c3bbe5539940)
72. European Parliament; Council of the European Union, Regulation (EC) No 1223/2009. *Official Journal of the European Union*, 2009, L 342.
73. Lead in Drinking Water in Australia. *Hazards associated with lead based solder on pipes*. Summer Hill, NSW: Lead Advisory Service Australia (Accessed February 26, 2016, at https://www.lead.org.au/lanv8n1/l8v1-11.html)
74. Australian Drinking Water Guidelines 6. National Water Quality Management Strategy: 2004. (Accessed April 17, 2016, at http://www.nhmrc.gov.au/_files_nhmrc/publications/attachments/eh34_adwg_11_06.pdf)
75. Australian Drinking Water Guidelines 6. National Water Quality Management Strategy: 2011. (Accessed April 17, 2016, at https://www.nhmrc.gov.au/_files_nhmrc/file/publications/nhmrc_adwg_6_february_2016.pdf)
76. Monitoreo de Metales Pesados en Suelos de Montevideo: Informe de Actuaciones 2010–2011. Servicio de Evaluación de la Calidad y Control Ambiental, 2012.

(Accessed April 17, 2016, at http://www.montevideo.gub.uy/sites/default/files/monitoreo_metales_suelos_2010-2011.pdf)
77. The Clean Air Act Amendments of 1990 List of Hazardous Air Pollutants. Washington, D.C.: U.S. Environmental Protection Agency. (Accessed April 15, 2016, at https://www3.epa.gov/ttn/atw/orig189.html)
78. NIOSH Pocket Guide to Chemical Hazards. Atlanta, GA: National Institute for Occupational Safety and Health, 2015. (Accessed April 1, 2016, at http://www.cdc.gov/niosh/npg/npgd0368.html)
79. OSHA, 29 CFR 1910.1000. *Code of Federal Regulations*, Washington, D.C., 2005.
80. OSHA, 29 CFR 1926.55, Appendix A. *Code of Federal Regulations*, Washington, D.C., 2005.
81. OSHA, 29 CFR 1915.1000. *Code of Federal Regulations*, Washington, D.C., 2005.
82. EPA, 40 CFR 116.4. *Code of Federal Regulations*, Washington, D.C., 2005.
83. National Primary Drinking Water Regulations Washington, D.C.: U.S. Environmental Protection Agency, 2002. (Accessed April 15, 2016, at https://www.epa.gov/your-drinking-water/table-regulated-drinking-water-contaminants)
84. EPA, 40 CFR 117.3. *Code of Federal Regulations*, Washington, D.C., 2005.
85. Residential lead hazards standards − TSCA Section 403. Washington, DC: U.S. Environmental Protection Agency, 2005. (Accessed April 1, 2016, at https://www.epa.gov/lead/hazard-standards-lead-paint-dust-and-soil-tsca-section-403)
86. Guidance for Industry: Action Levels for Poisonous or Deleterious Substances in Human Food and Animal Feed. Washington, DC: Food and Drug Administration, 2000. (Accessed April 18, 2016, at http://www.fda.gov/food/guidanceregulation/guidancedocumentsregulatoryinformation/chemicalcontaminantsmetalsnaturaltoxinspesticides/ucm077969.htm#lead)
87. FDA, 21 CFR 165.110. *Code of Federal Regulations*, 2004.
88. National Notifiable Diseases Surveillance System (NNDSS). Lead, elevated blood levels; 2016. Atlanta, GA: Centers for Disease Control and Prevention, 2016. (Accessed April 14, 2016, at http://www.cdc.gov/nndss/conditions/lead-elevated-blood-levels)
89. Lead Renovation, Repair and Painting Rule (April 22, 2008). Washington, D.C.: U.S. Environmental Protection Agency, 2008. (Accessed April 13, 2016, at https://www.epa.gov/lead/lead-renovation-repair-and-painting-program-rules#rrp)
90. Lead. Washington, D.C.: Integrated Risk Information System, U.S. Environmental Protection Agency. (Accessed March 2, 2016, at http://www.epa.gov/iris/)
91. EPA, 40 CFR 50.12. *Code of Federal Regulations*, Washington, D.C., 2005.
92. EPA, 40 CFR 372.65. *Code of Federal Regulations*, Washington, D.C., 2005.
93. EPA, 40 CFR 355. Appendix A. *Code of Federal Regulations*, Washington, D.C., 2005.
94. EPA, 40 CFR 372.28. *Code of Federal Regulations*, Washington, D.C., 2005.
95. Medical management guidelines for lead-exposed adults. Washington, DC. (Accessed April 14, 2016, at http://www.aoec.org/documents/positions/mmg_revision_with_cste_2013.pdf)
96. Report on carcinogens. 13th edn. Research Triangle Park, NC: U.S. Department of Health and Human Services, National Toxicology Program, 2014.
97. Government of Singapore, Cap. 354A, Rg 1, Regulations 2 and 40. *Singapore Statutes Online*, 2006.
98. Department of Labor. *Government Notice*, 2002, R. 236.
99. Government of Canada, SOR/2010-273. *Consolidated Acts*, Minister of Justice: 2010.
100. Government of Canada, SOR/2011-17. *Consolidated Acts*, Minister of Justice: 2011.
101. European Parliament; Council of the European Union, Directive 2009/48/EC. *Official Journal of the European Union*, 2009, L 170.

102. Council of the European Communities, 88/388/EEC. *Official Journal of the European Communities*, 1988, 1988L0388.
103. European Commission, Commission Regulation (EU) No 10/2011. *Official Journal of the European Commission*, 2011, 2011R0010.
104. Government of Singapore, Regulation 31(1); Revised Edition 2005. *Singapore Statutes Online*, 2005, Cap. 283, Rg 1.
105. Ministerio de Salud Pública, Decreto 315/994. *Diario Oficial*, Montevideo, 1994.
106. European Commission, Commission Regulation (EU) 2015/628. *Official Journal of the European Union*, 2015, L 104.
107. República Oriental del Uruguay, Decreto Nº 315/994. *IMPO*, 2 ed.; Montevideo, 2005, pp. 211-213.
108. UNIT 833:2008 "Agua potable. Requesitos," Tabla 4 – Requisitos para los parámetros de control químico inorgánico y métodos de ensayo. Montevideo: Instituto Uruguayo de Normas Técnicas, 2010. (Accessed April 18, 2016, at http://www.ose.com.uy/descargas/clientes/reglamentos/unit_833_2008_.pdf)
109. Ministerio de Salud Pública, Decreto 375/011. *Diario Oficial*, 2011, N°28.348.
110. Commonwealth of Australia, National Environment Protection Council Act 1994 (Cwlth), Section 20. *Gazette*, 1998
111. Council of the European Union, Council Directive 1999/30/EC. *Official Journal of the European Communities*, 1999, L 163.
112. Ministerio de Salud Pública, Decreto 64/004. *Diario Oficial*, Montevideo, 2004.
113. Ministerio de Salud Pública, Ordenanza 337/2004. *Diario Oficial*, Montevideo, 2004, 001-1190/2004.

14

Environmental Impact of Alkyl Lead(IV) Derivatives: Perspective after Their Phase-out

Montserrat Filella [1,2] ***and Josep Bonet*** [2]

[1]Institute F.-A. Forel, University of Geneva,
Boulevard Carl-Vogt 66, CH-1211 Geneva 4, Switzerland
<montserrat.filella@unige.ch>

[2]SCHEMA, Rue Principale 92, L-6990 Rameldange, Luxembourg

Metal Ions in Life Sciences, Volume 17 Edited by Astrid Sigel, Helmut Sigel, and Roland K. O. Sigel

DOI 10.1515/9783110434330-014

Abstract: The use of alkyl lead derivatives as antiknock agents in gasoline can be considered as one of the main pollution disasters of the 20th century because of both the global character of the pollution emitted and the seriousness of the impact on human health. Alkyl lead derivatives in themselves cannot be considered to be persistent pollutants because they readily degrade either before being released from the tailpipes or soon afterwards in the atmosphere. However, the inorganic lead they produced has been deposited in soils all over the planet, largely, but not exclusively in urban areas and along motorways, since the direct emission of lead into the atmosphere favored its dispersal over great distances: The signal of the massive use of alkyl lead derivatives has been found all over the world, including in remote sites such as polar areas. The short residence time of lead in the atmosphere implies that this compartment is highly responsive to changes in emissions. This was demonstrated when leaded gasoline was phased-out and is in striking contrast to the very long permanence of inorganic lead in soils, where resuspension is a permanent source of toxic lead.

Keywords: alkyl lead(IV) · organolead · phase-out · tetraethyl lead · tetramethyl lead

1. INTRODUCTION

Alkyl lead(IV) derivatives are man-made compounds in which a carbon atom of one or more alkyl groups, usually methyl or ethyl, is bound to a lead(IV) atom. For over 70 years, tetraethyl lead (TEL) and tetramethyl lead (TML) derivatives were the additives of choice for reducing engine knock. These compounds raise the ignition point of fuel so that it does not pre-ignite under compression before the spark plugs fire during the ignition cycle (i.e., the engine does not knock). TEL was first introduced in 1923 and 90 % of the gasoline sold in the USA contained it by 1936. TML was introduced in 1960. The two compounds were added to gasoline either singly or as mixtures to achieve desired octane numbers. In the early 1970s, 200,000 tons of lead were emitted from automobiles in the United States alone each year, mostly in urban areas.

The widespread use of leaded gasoline caused the massive dispersion of lead throughout the environment along the 20th century, resulting in serious exposure for humans and ecosystems. Strictly speaking, alkyl lead compounds themselves cannot be considered persistent environmental pollutants because they mostly degrade to other forms of lead before being emitted or soon thereafter, eventually forming inorganic lead compounds, which are much more persistent. The inorganic lead generated through the use of organic lead in gasoline was deposited all over the planet and, in particular, on urban soils. Dusts with high concentrations of legacy lead are still present in many soils, mostly in cities and close to motorways.

Although an occasional mention is unavoidable, the focus of this chapter is not on inorganic lead pollution and environmental fate. Readers are kindly asked to consult, e.g., Chapters 1 and 2 in this book. Toxicology of alkyl lead is not discussed either, since a previous chapter in this book series [1] was dedicated to it (but see also Chapter 13), and direct environmental or occupational exposure to these compounds is rare today.

Table 1. Recommended reading about the development, use and phase-out of alkyl lead compounds.

Contents	Comment	Number of references	References' year of publication	Ref.
Historical account of the use and phase-out of lead additives in gasoline	Highly cited (more than 200 citations), easy-to-read early account written from the environmental/public health point of view.	39	1916–1988	[2]
Account of the historical and personal reflections of the author	Historical review of the steps towards the total ban on TEL. Clear insights on the role of the different stakeholders.	39	1953–1998	[3]
Focus on the chemistry of TEL and TML: their synthesis, reactions, and commercial applications	Historical account of the rise and fall of TAL from a dispassionate chemical point of view. Only a minimal reference is made to the root causes of its fall, the bulk of the article describing over 50 years of predominance of the product in the world and the chemists behind it.	80	1853–2003	[4]
Description of the controversy about the use of TEL as a gasoline additive	Description of the struggle between health and environmental concerns, and industrial concerns. The approach can be summarized in the sentence: "U.S. historians have regarded the invention of ethylleaded gasoline as a heroic episode in the history of technology rather than a public health disaster that could have been averted."	110	c.1700–2005	[5]
Description of the personal experience and perspective of the authors, who had primary responsibility for drafting the initial health-based regulation limiting lead content of gasoline during the early 1970s while employed by the U.S. EPA	An inspirational account of how two very young scientists were able to bring forward the ground-breaking regulation that banned lead in gasoline in the US against the combined efforts of the oil and lead industries. The importance of having independent scientists and government officials conducting research, using a great variety of data sources, and the key role played by U.S. EPA are important take aways.	56	1962–2009	[6]
History of lead-containing organometallic additives	Excellent, very detailed account, including exhaustive history of the phase-down (and -out) of lead in gasoline and a review of lead alternatives used in the past.	328	1923–2010	[7]

The phase-out of organic lead in gasoline has been accompanied by a steady decrease in the number of studies devoted to these compounds. This means that (i) most of the existing data on environmentally-relevant alkyl lead processes are not recent and have not benefitted from the possibilities offered by current state-of-the-art analytical methods; (ii) most of the many published chapters, review articles, and reports devoted to the development, use, and phase-out of organolead compounds – a particularly well-covered subject – cannot be considered as being necessarily superseded. Table 1 contains a selection of them [2–7]. Their contents will not be repeated here, where the focus will be on chemical and environmental issues linked to the phase-out for lead in gasoline additives.

2. THE PAST

The history of the use of leaded gasoline worldwide can be divided into two phases: The rise in total lead emissions between the 1930s and the 1970s and the lead phase-out from the 1970s to today. After the 1970s, different countries phased out gasoline lead at different times with the process taking several steps. For instance, the USA began in 1972, with the introduction of air pollution controlling catalytic converters that required unleaded fuel, followed by a rapid phase-down from 1986 leading to a total ban in 1996. The first country to completely switch to unleaded gasoline was Japan in 1988, followed by Brazil in 1990. Leaded gasoline was withdrawn entirely from the European Union on 1 January 2000, although it had been banned much earlier in most member states. A history of leaded gasoline use can be found in [7]. Figure 1 shows lead air emissions in the UK and China [8, 9]. It illustrates the profound effect that the 1984–1999 reduction of lead and eventual ban on lead in gasoline had on lead emissions in the UK. In contrast, the ban in China also produced a decrease in lead emissions but these remain high because of other sources such as smelting and coal combustion.

The toxicity of TEL was noted soon after its production began. Several very serious cases of lead poisoning occurred in all operating plants, and a number of workers died following acute psychosis with hallucinations due to exposure to TEL gas. In spite of this, the oil and lead industries managed to tout TEL as safe and successfully thwarted efforts to limit lead in gasoline for 50 years. For many years, the industry claimed that airborne lead was a negligible contributor to the exposure of the population to lead, while at the same time funding nearly all research on lead's effects on health and controlling dissemination of the results. Excellent accounts of the history of TAL use and the complicated process leading towards its phase-out can be found in Table 1.

It is difficult to find reliable estimates of the total world-wide consumption and emission of lead from leaded gasoline. Values from Australia, for instance, have just been published in 2015 [10], with atmospheric emissions of lead from leaded gasoline of 240,000 metric tons over seven decades of use (1936–2002), peaking at 7869 tons in 1974. Comparing this with the emission of 200,000 tons estimated for China during the period 1990–2009 [9] provides a striking image

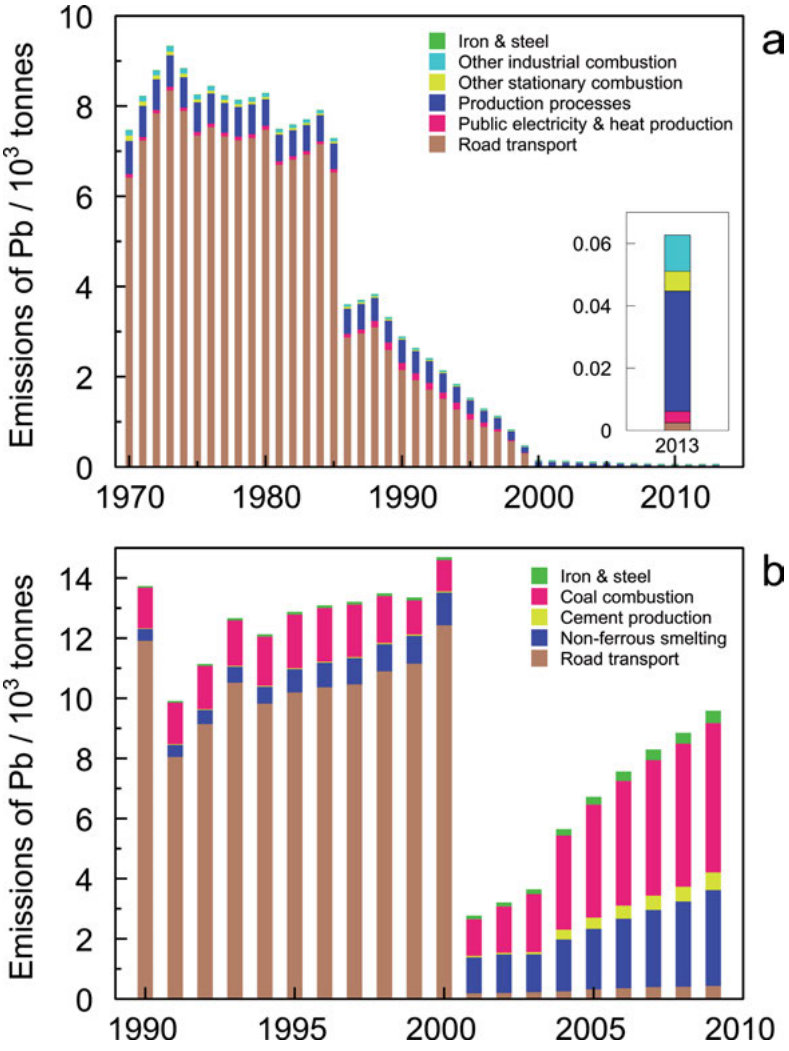

Figure 1. Temporal trends in lead emissions in (**a**) the UK [8] and (**b**) China [9]. Categories considered in both countries are not exactly the same but the abrupt decrease of lead in gasoline as well as the different trends in both countries are clearly observed. China data show that, contrary to more developed countries, the ban of lead in gasoline has not necessarily implied a permanent decrease in total emissions in other economies.

of the difference in automobile use in both countries (periods considered are different but populations in 2000 were: 19.15 million in Australia and 1.263 billion in China). According to Mielke and co-workers [11], in the USA, considered responsible for 80 % of all leaded gasoline sold globally prior to 1970 [2], 5.4 million tons of lead were used in gasoline beginning in 1927 through to 1994, of which about 75 % were released into the atmosphere.

3. CURRENT USES

Currently, the largest uses of alkyl lead are in aviation and racing gasoline. Neither of these are subject to any of the regulations that restrict leaded motor gasoline use.

TEL remains an ingredient of 100 octane Avgas (aviation gas) for piston-engine aircraft. Decades of research to find an unleaded replacement fuel that works without an adverse impact on engines and fuel systems and which can be certificated for fleet-wide use have proved only that the issue is difficult to solve. Lead emitted from aircraft using Avgas was the largest source of lead in air in the United States in 2005, constituting about 50 % of all lead emissions [12]. Children living within 500 m of an airport at which planes use leaded Avgas have higher blood lead levels than other children [13].

Older race cars also still use TEL, though other race cars have switched to unleaded fuel.

It is difficult to obtain complete, verified information on the current use of leaded gasoline for motor vehicles. The more recent map entitled “Leaded Petrol Phase-out: Global Status as at January 2016” on the UNEP (United Nations Environment Programme) website [14] shows only three countries as using both leaded and unleaded (Iraq, Yemen and Algeria) while the text on the webpage mentions six (North Korea, Myanmar, and Afghanistan, in addition to these three). However, this probably refers to the situation as of April 2014. Innospec Specialty Chemicals (formerly Octel Corporation and Associated Octel Company, Ltd), the world's only manufacturer of TEL outside China, has reported that it sells it for automotive use nowhere except for Algeria as of late 2014. Up to 2011, Innospec sold TEL to Iraq and Yemen but after head executives were charged for bribing various state-owned oil companies, the situation is now unclear. It should be mentioned that a product called TetraBOOST, “the only additive that makes real leaded fuel from the unleaded pump”, is freely available on the internet [15].

4. CHEMISTRY

Appraisal of the environmental impact of the use and phase-out of alkyl lead compounds requires sufficient knowledge of the chemical processes taking place. Unfortunately, no new research on the subject seems to have been significantly produced in the last 30 years. Thus, our knowledge of the subject, although satisfactory, is based on a relatively limited number of publications and probably suffers from the limitations of the analytical methods available at that time.

4.1. Compound Characteristics

Organolead compounds are covalent, containing a σ bond between a single carbon atom and the lead(IV) atom. This bond is polarized, the metal being less electro-negative than the carbon. The organolead compounds of interest are all

Table 2. Physical characteristics of the main alkyl lead(IV) derivatives [16, 17].

Name	Tetraethyl lead	Tetramethyl lead
Formula	$(C_2H_5)_4Pb$	$(CH_3)_4Pb$
CAS number	78-00-2	75-74-1
Molecular weight/g mol^{-1}	323.44	267.33
Boiling point/°C	200	109
Melting point/°C	–137.5 to –130.16 (depending on form)	–30.2
Vapor pressure/torr 20°C	0.26	22.5
Specific gravity (d^{20}_4)	1.66	2.00
Water solubility/mg L^{-1}	0.25	15

alkyl lead(IV) derivatives: tetralkyls (TAL), trialkyls (TrAL), dialkyls (DAL), etc. with methyl and ethyl groups as alkyl moieties. Compounds with methyl and ethyl groups in the same molecule have also been synthetized and used.

The environmentally-relevant physical characteristics of the main TAL are shown in Table 2 [16, 17]. Under ambient conditions, tetraethyl lead (TEL, $(CH_3CH_2)_4Pb^0$) is a viscous colorless liquid. It is an apolar molecule, highly lipophilic and soluble in gasoline and solvents. Its products of degradation (triethyl lead, TrEL, $(CH_3CH_2)_3Pb^+$; diethyl lead, DEL, $(CH_3CH_2)_2Pb^{2+}$; very unstable monoethyl lead, $(CH_3CH_2)Pb^{3+}$) are cations, readily soluble in water. They were often grouped as "ionic alkyl lead". Methylated compounds are more volatile and water-soluble.

Thermodynamic stabilities of organometallic compounds depend mainly on the strength of the bonds between metal and carbon atoms. Since free energies of formation are rarely known, the bond enthalpy is usually used for comparison of thermodynamic stabilities. Values can be found in [18]. The caveats of the meaning and use of such values are also discussed in this reference. However, thermodynamic stabilities are usually of little use in the environmental context because (i) thermodynamic stabilities consider the decomposition of the substances into its elements, which usually does not happen; (ii) in practice, the lack of observed stability is not due to weak metal-carbon bonds but to kinetic reasons. This is the case, for instance, of TEL, a stable compound in gasoline, whose environmental decay is mediated by oxygen, free radicals, etc., leading to its complete disappearance in a few days in the atmosphere.

Organometallic compounds in natural waters, sediments, and soils interact with naturally-occurring ligands. The Hard and Soft Acid and Base principles [19] apply to coordination preferences in the environment. Methyl groups are more electro-negative than metals and withdraw electron density from metals, increasing hardness. Larger aliphatic groups (i.e., ethyl groups) are more electron-releasing than methyl groups and give softer organometallic molecules than the corresponding methyl compounds. In the case of lead, $(CH_3)_nPb^{(4-n)+}$ are classified as borderline acids [18].

It is necessary to mention that alkyl lead compounds were not used alone. Bromine- and chlorine-containing compounds (e.g., 1,2-dibromoethane and 1,2-dichloroethane) were added as scavengers to prevent lead oxide deposits from forming during combustion, which could damage combustion chambers, valves, and spark plugs. These additives strongly influenced the chemical processes taking place in the engines. Detailed information about these and other scavenger compounds as well as about so-called extenders (compounds that increase octane ratings) and the composition of mixtures of TEL and TML used in gasoline can be found in [7].

4.2. Chemical Processes in Engines

About three-fourths of the lead burned in an engine is emitted from the tailpipe in the form of inorganic lead compounds. The primary inorganic lead compounds that leave the engine are $PbCl_2$, $PbBr_2$ – volatiles when formed in the hot engine – and PbClBr. Lead halides are formed by reaction with the corrective agents 1,2-dichloro- and 1,2-dibromoethane present in the lead antiknock mix. The main lead compound in exhaust emissions is lead chlorobromide, PbClBr, present in equilibrium with the mixture of $PbCl_2$ and $PbBr_2$ [20]. Basic lead halides may also be formed in the engine. This complex mixture of lead compounds leaves the exhaust system with the hot combustion gases as an aerosol.

Even if some doubts exist about the structural assignments [21], early electron microprobe results of airborne lead samples taken in a black plastic bag from a car exhaust nicely illustrate the complex composition of the emitted lead: $PbCl_2$, $PbBr_2$, PbClBr, Pb(OH)Cl, Pb(OH)Br, $(PbO)_2PbCl_2$, $(PbO)_2PbBr_2$, $(PbO)_2PbClBr$, $PbCO_3$, PbO_x, $(PbO)_2PbCO_3$, $PbSO_4$, with PbClBr and $(PbO)_2PbClBr$ as main components [22]. Rapid changes seem to occur after emission to the atmosphere. The authors observed that the halogen content of the lead particulates dropped with a corresponding increase in the concentration of lead as oxides and carbonates in only 18 h, even in the absence of light. The Br:Pb ratio has been used as an indication of aging of the lead aerosol [23]. The ratio measured is generally lower than that expected from primary exhaust particulates, with higher loss of bromine in summer than in winter [24]. As early as 1969, Pierrard suggested a photochemical decomposition of PbClBr to form lead oxide and bromine and chlorine gas [25]. The loss of halogen, but not the photochemical mechanism, was supported by other researchers [22, 26]. X-ray powder diffraction (XRD) detected $PbSO_4 \cdot (NH_4)_2SO_4$ as the predominant form of lead in ambient air polluted by vehicle exhaust [27, 28]. $PbSO_4$ was found to be the major component in soils [29].

The remaining lead is retained in the automobile: in deposits in the exhaust system, motor oil, and oil filter. This also ultimately ends up in the environment when the oil and oil filter are discarded or when the exhaust system deposits are lost mechanically during driving. Finally, only a very small amount, 0.3–3 % of the lead emitted, leaves the tailpipe as undecomposed TEL and TrEL and DEL compounds [30].

4.3. Chemical Processes in Nature

4.3.1. Atmosphere

Alkyl lead in the atmosphere degrades mainly by reacting with hydroxyl compounds, while removal by photolysis and direct reactions with ozone and $O(^3P)$ (= atomic oxygen) take place to a much lesser extent [31]. Decomposition rates in a non-polluted atmosphere in sunny summer conditions were 21 % h^{-1} for TML and 88 % h^{-1} for TEL (half-lives of 41 h and 8 h, respectively) with increasing rates in the presence of O_3, no decomposition in the dark and much lower decomposition rates in winter. Other decomposition rate estimates can be found in the literature but they all are in the same order of magnitude [32]. Decomposition products are TrAL and DAL in both gaseous and particulate phases, together with inorganic lead in particulate phases. Hydroxyl radicals decompose TrAL and DAL, but at slower rates (half-lives of 126 h and 34 h) [33]. TrAL and DAL are water-soluble and will dissolve in rainwater. The complete decomposition pathway in the atmosphere may thus be written as:

$$\text{TAL} \rightarrow \text{TrAL} \rightarrow \text{DAL} \rightarrow \text{inorganic lead}$$

All these compounds have been measured in the atmosphere (see [34] for values). Airborne particles containing inorganic lead may remain airborne for about 10 days and, therefore, be transported far from the original source. Lead is removed from the atmosphere and deposited on soil and water surfaces via wet or dry deposition.

Airborne lead-containing particles originating from leaded gasoline are typically smaller than a micron. Interestingly, a review of the literature on the concentrations and size distributions of airborne lead particles revealed that during the era of leaded gasoline airborne particle-bound lead was typically submicron sized whereas after the withdrawal of leaded gasoline, the largest mode of the size distribution of particles shifted to particles > 2.5 μm, typically associated with soil dust [35].

4.3.2. Water

With the development of more sensitive analytical techniques in the late 1970s and early 1980s, alkyl lead compounds were found to be ubiquitous in waters: surface water [36], rain [37, 38], snow [39]. Ionic TrEL and trimethyl lead (TrML) were the major species found, which is in accordance with insignificant atmospheric deposition of TAL due to their instability in the atmosphere.

Experiments of abiotic decomposition of TAL in an aqueous medium at concentration levels close to environmental concentrations (low μg L^{-1}) [40] show that 100 % of TAL decomposed within 5 days even in the dark. Inorganic lead, but not DAL, was the major decomposition product. It is important to stress that these results are not in accordance with those previously obtained at much higher – and impossible in nature – concentrations [41]. This shows, once more,

the need to work at the right concentration level and the impossibility of extrapolating from higher ones. Therefore, in water, probably it holds:

$$\text{TAL} \rightarrow \text{TrAL} \rightarrow \text{inorganic lead}$$

The DAL measured in water might originate from DAL produced in the atmosphere.

The acceleration of the disappearance of TAL when nutrient was added to polluted groundwater was interpreted as an indication of co-metabolic microbial attack [42]. However, these often mentioned results do not seem relevant in natural conditions.

4.3.3. Soils

Even though most of the lead from car exhausts reached the soil as inorganic lead, low concentrations of organolead compounds were also deposited in the upper layers of soils and, like with waters, were detected when analytical techniques became available [43]. Organolead compounds may persist over decades in soils, as the natural chemical and biological degradation is limited in this medium. The mobility of organolead compounds in the subsurface is dominated both by sorption and degradation reactions: while TAL tend to be immobile and adsorbed into soil particles, TrAL and DAL are quite mobile.

In addition to chemical transformation, microbial degradation may occur in soils. Published studies show that biologically mediated multiple dealkylations resulted finally in the formation of inorganic lead [44–47]. However, these and later experiments have always been performed in spiked soils in the context of bioremediation studies. From these data, it is difficult to extrapolate regarding microbial degradation in non-heavily polluted soils.

In some cases, the long persistence of TEL in polluted soils might need some reappraisal. Recently, a gas chromatography electron capture detector analysis of soils supposedly polluted with TEL in a refinery that operated before 1950 showed that lead was most probably present as inorganic lead bound to humic and fulvic acids in soil matter and not as organolead [48] as had been initially detected by an approved test (California method HML-939-M) based on an initial extraction with xylene. This method is not specific for TEL.

5. AFTER THE PHASE-OUT

The generalized use of leaded gasoline led to the dispersion of inorganic lead over the entire planet, causing serious exposure to humans. Spillages of large quantities of TEL during production, transportation or blending at oil refineries, and delivery to petrol stations resulted in several cases of severe soil and groundwater contamination [49] but remained a minor problem. Because of the type of environmental dispersion, the phase-down of alkyl lead compounds was rapidly

followed by decreases in lead concentrations in humans and in some environmental compartments, alongside accumulations in others, which acted as sinks.

The concentrations generally measured have been those of 'total' lead (i.e., inorganic lead) and alkyl lead compounds as such have rarely been quantified. Since there are multiple sources of lead (e.g., volcanic emissions, natural soil, industrial pollution, gasoline, etc.), source attribution needs to be based on the establishment of correlations (e.g., changes in atmospheric lead concentration *versus* changes in lead use) with its concomitant limitations [50]. Luckily, the isotopic composition of lead is an extremely useful tool as a potential tracer for identifying provenance [51, 52]. Lead isotopic fingerprinting is based on: (i) lead having four different naturally occurring isotopes: ^{204}Pb, ^{206}Pb, ^{207}Pb, ^{208}Pb, with ^{204}Pb's abundance remaining essentially constant (1.4 %) and the other three varying strongly depending on the origin of the ore; (ii) no isotopic fractionation occurring in industrial and environmental processes. As a fingerprinting technique, isotopic abundance ratios of lead have been used in a number of studies on many types of environmental samples, such as aerosols, lake and estuary sediments, snow, tree rings, mosses, etc. When the sources of the lead are well-known and their isotopic signature well-characterized, the relative contribution of each source to the global lead inventory can be quantitatively evaluated with the use of two or more component mixing models [53].

5.1. Environmental Compartments

5.1.1. Atmosphere

Since lead in gasoline was directly emitted to the atmosphere, the introduction, use, and ban of lead in gasoline were immediately reflected in lead concentrations in air. For instance, ambient lead concentrations in the USA decreased by 97 % between 1990 and 2014 [54] (Figure 2). The number of published studies and reports corroborating this effect all over the world is huge. It should be mentioned, however, that strong decreases in lead in aerosol samples following bans on leaded gasoline have not been observed everywhere. For instance, in places where automobile use was relatively low and other sources important (Figure 1b), such as in China, monitoring data indicate that despite the slightly decreasing trends, the lead concentrations remain relatively high in aerosol samples collected in cities after the phase-out [55]. In this case, isotopic fingerprinting made it possible to evaluate the efficacy of the leaded gasoline ban on curbing atmospheric lead pollution in Shanghai [56] and Tianjin [57]. Figure 3 shows that the increase of ^{206}Pb/^{207}Pb ratios and the decline of atmospheric lead concentrations in Shanghai and Tianjin are similar to the trends observed in Europe when leaded gasoline was phased-out [58]. Although the origins of the lead additives varied slightly from one European country to another, lead from the Broken Hill ores in Australia had been in heavy use for many years. For this reason, China and Europe showed the same increasing trends in ^{206}Pb/^{207}Pb ratios during the phase-out of leaded gasoline. In contrast, an opposite trend in the lead

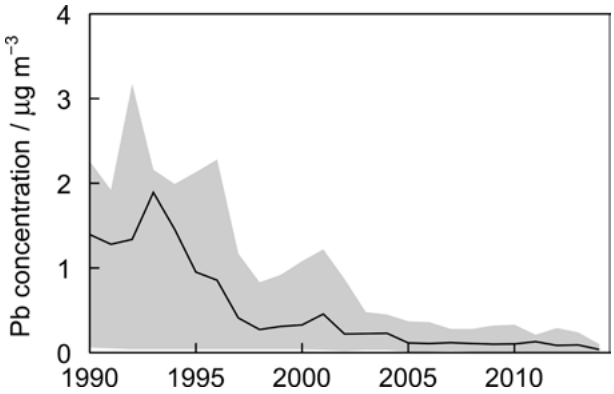

Figure 2. Temporal trends of lead concentrations in the atmosphere in the USA from 1990 to 2014 [54]. Values are annual maximum 3-months averages for 22 sites. The grey area covers the 10–90th percentiles and the black line represents the average among all the sites. The data in [54] are in the public domain.

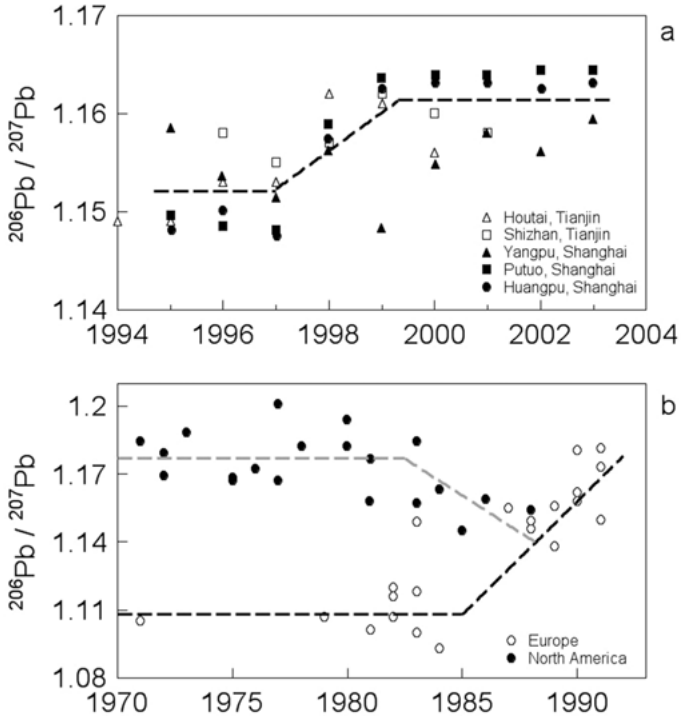

Figure 3. Evolution trends of the ^{206}Pb/^{207}Pb ratios of atmospheric aerosols during leaded gasoline phase-out (**a**) observations in Shanghai and Tianjin, China [56, 57]; (**b**) observations in Europe and North America [58]. The dashed lines have no statistical meaning, they just roughly help to follow the trends of changes in ^{206}Pb/^{207}Pb ratio. Adapted from [55] by permission; copyright 2010 Elsevier.

isotopic ratio was observed during the phase-out of leaded gasoline in North America where the primary source for alkyl lead additives before the mid-1970s were Missouri Mississippi ore deposits, which are significantly more radiogenic.

5.1.2. Water

It is not clear whether temporal trends of lead concentrations in aquatic systems might reflect massive lead emissions from leaded gasoline. Long-term trends of metal concentrations in streams and rivers are generally lacking, especially on broader spatial scales. In one of the few published studies [59], lead concentrations in 139 stream sites in Sweden showed mostly negative trends in the north (75 %) and nearly all positive trends in the south (93 %) in the period 1996–2009. This was in contrast to the depositional pattern of lead, which declined by a factor of 11.3 between 1975 and 2000 [60]. The difference in trends between regions may be partially explained by the difference in historical deposition, storage, and delayed response in catchments due to strong element sorption on soil solids.

5.1.3. Soils

The accumulated lead emitted from automotive tailpipes was deposited largely on urban soils. Dusts with a legacy of lead are present in the top layer of soils all over the world and will remain present for many years: lead residues remain until geological processes gradually cover or remove it, with an expected 'half-life' of 700 years [61]. Soils are not passive repositories, and re-suspension of fine lead-contaminated soil dust occurs [62]. The decline in deposition of trace elements is generally lower than the decline in emissions, possibly due to the contribution of wind-blown dust to their deposition. In some areas, the flux of soil lead is seasonal, being higher during periods of high evapotranspiration potential and low soil moisture [63, 64]. The seasonal flux of soil lead re-entrainment is reflected in the seasonal flux of children's blood lead levels [65]. Direct contact with soil, particularly in the case of children, remains an important cause for concern [66].

5.2. Human Blood

As expected, given the short residence time of lead in blood (less than a month, e.g., [67]), a fast human response to the reduction of air lead after the 1 January 1986 rapid phase-down of tetralkyl lead as a fuel additive in the USA was observed, with a 90 % decline of USA children's blood lead levels between 1976–1980 and 1988–1991, i.e., before and after the rapid phase-down of TAL in the country [68] (Figure 4). The average American child's blood lead level in 1976 was 13.7 μg dL^{-1} while by 1991 it had dropped to 3.2 μg dL^{-1}. The phasing-out of leaded gasoline has been closely matched by a clear decrease in lead in blood

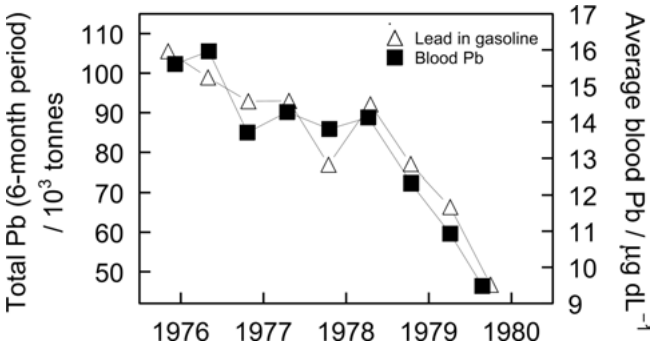

Figure 4. Parallel decreases of concentrations of lead in human blood and contents of lead in gasoline between 1976 and 1980 in the USA [68]. The data in [68] are in the public domain.

all over the world [69–73]. Analogous trends have been observed in a comparison of lead in deciduous teeth in the 1970s *versus* the 1990s [74]. The effect of the phase-out of alkyl lead compounds has also been found in other mammals (e.g., a 73 % decline in lead measured in otter bones between 1992 and 2004 [75]).

5.3. Environmental Archives

Natural environment archives, such as ice, ombrotrophic peat bogs, and lake sediments, offer a useful means of tracing lead use and dispersion. They store signals resulting from a flux from another reservoir (e.g., the atmosphere) and build up a time record of the changes. To be meaningful, this signal should ideally be well preserved, with no post-depositional remobilization.

5.3.1. Ice

Dated ice cores from the polar ice caps and high mountains have strongly contributed to the understanding of anthropogenic influences in the biogeochemical cycles of trace elements. The use of lead additives in gasoline has led to the highest recorded levels of lead pollution occurring during the mid-20th century in Greenland [76–79]. For instance, from 1970 to 1991, annual average concentrations dropped by 85 %, from 335.0 to 19.0 pg g^{-1}, in an ice core from south-central Greenland [79]. The study of Pb isotopic patterns in Greenland snow explained the sources and dispersal of gasoline-derived Pb, showing that the $^{206}Pb/^{207}Pb$ ratio increased from the 1960s (~1.16), reaching a peak value (~1.18) between 1975 and 1980, and then declined to its earlier values by the mid-1980s [80]. This change was attributed to varying contributions from the deposition of more radiogenic Pb from the USA and relatively constant levels of Pb from Eurasia arriving in central Greenland between 1960 and 1988. Since polar ice

cores are far removed from human activity, they mostly reflect long-range transport pollution. This is less the case for high mountain ice cores. Isotopic signatures in high altitude Mt. Everest ice cores (dated 1205–2002) show that, from 1970 to 1997, lead's origin was increasingly leaded gasoline from India (and possibly Bangladesh and Nepal) but for 1997–2002 a shift was observed to a less radiogenic signature but with very high levels of lead, probably coming from fossil combustion and non-ferrous metal production [81].

5.3.2. Ombrotrophic Peat Bogs

Ombrotrophic peat bogs have been used to study the changing rates and sources of atmospheric metal deposition as they receive all their nutrient, pollutant, and water inputs solely through dry and wet deposition from the atmosphere [82]. Lead is by far the most intensively studied trace element in peat bogs and cores from such bogs have proved especially useful as archives of atmospheric lead deposition since prehistoric times [83]. Lead profiles in ombrotrophic peat bogs reflect the contribution from leaded gasoline in the 20^{th} century but have been shown to be very sensitive to other lead sources such as coal combustion or local mining and smelting activities in many different locations all over the world: Scotland [84], Poland [85], Australia [86], Belgium [87], China [88], etc.

A peat core collected in an ombrotrophic bog in the Jura Mountains, Switzerland (Etang de la Gruère), was analyzed for organolead species (DEL, TrEL, DML, and TrML) [89]. Total alkyl lead never accounted for more than 0.02 % of total lead in any sample. The earliest occurrence of quantifiable alkyl lead was found at a depth of 24 cm, dated to AD 1946 ± 3, which is consistent with the introduction of leaded gasoline in Switzerland in 1947. The decline in anthropogenic Pb pre-dates the maximum in total alkyl lead and minimum $^{206}Pb/^{207}$ Pb, indicating that atmospheric Pb emissions had already begun their decline prior to the introduction of unleaded gasoline and responded to the introduction of legislation in Europe establishing a maximum allowable concentration of Pb in gasoline. These results are very interesting because they confirm that concentrations of organolead compounds in the atmosphere are very low compared with total lead as well as the extreme sensitivity of lead concentrations in the atmosphere to lead emissions.

5.3.3. Freshwater and Estuarine Sediments

Sediment records have been widely used to trace pre-industrial pollution [90] in the same way as ombrotrophic peat bogs, with the same experimental methods and data treatment methods being applied. As in the case of peat bogs, the lead present reflects gasoline-derived lead along with local sources. For instance, mixing models based upon Pb isotopic data have shown variable contributions from petrol-derived Pb in modern river sediments of up to 50–67 % [91–93].

5.3.4. Moss Surveys

The moss survey technique provides a time-integrated measure of the spatial pattern of trace element deposition from the atmosphere to terrestrial systems. It is based on the fact that mosses, especially carpet-forming species, obtain most of their nutrients directly from precipitation and dry deposition with little uptake from the substrate. The European moss survey has been repeated at five year intervals since 1990 [94], with the most recent survey reported conducted in 2010 [95]. Between 1990 and 2010, the average median Pb concentration in mosses across Europe has declined by 77 %. These declines are similar to those reported by EMEP (Environmental Monitoring and Evaluation Programme) for the modelled deposition across Europe, i.e., 74 % [96, 97] (Figure 5), and they reflect leaded gasoline phase-out but also fuel switching and the introduction of environmental legislation.

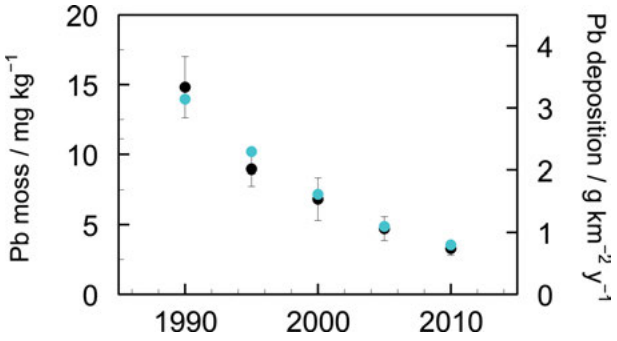

Figure 5. Average median lead concentration in mosses for European countries (n = 15–19, depending on year) that reported lead data for at least four survey years since 1990 (black dots); the blue dots indicate the average lead deposition flux modelled by EMEP [96]. Reproduced from [97]. The data in [96] and [97] are in the public domain.

6. LESSONS AND PERSPECTIVES

The use and subsequent complete ban of alkyl lead derivatives can be considered an interesting "global geophysical experiment" [98]. Never before had pollution created by the massive use of man-made compounds containing a toxic chemical element been so global, neither by how widespread the use was, nor by the type of release (i.e., directly to the atmosphere, a fast and efficient transport system). Lead had been used since Antiquity but never at the scale of its usage in gasoline additives. Alkyl lead compounds have a very short life in the environment but the inorganic lead they gave will remain in soils "forever", as a perfect example of the impossibility of remedying the effects of diffuse pollution. Major environmental accidents (e.g., Seveso, Chernobyl, Fukushima) and acute pollution episodes (e.g., London Great Smog, Minamata) have always been a source of in-

valuable scientific knowledge. This is also the case for lead, whose use in gasoline has fostered knowledge about global versus local pollution transport mechanisms. Other lessons learned relate to the behaviour and role of industry but these aspects are beyond science.

ABBREVIATIONS

DAL	dialkyls
DEL	diethyl lead
EMEP	Environmental Monitoring and Evaluation Programme
EPA	Environmental Protection Agency
TAL	tetralkyls
TEL	tetraethyl lead
TML	tetramethyl lead
TrAL	trialkyls
TrEL	triethyl lead
TrML	trimethyl lead
UNEP	United Nations Environment Programme
XRD	X-ray powder diffraction

REFERENCES

1. H. G. Abadin, H. R. Pohl, *Met. Ions Life Sci.* **2010**, *7*, 153–164.
2. J. O. Nriagu, *Sci. Total Environ.* **1990**, *92*, 13–28.
3. H. L. Needleman, *Environ. Res.* **1997**, *74*, 95–103.
4. D. Seyferth, *Organometallics* **2003**, *22*, 5154–5178.
5. W. Kovarik, *Int. J. Occup. Environ. Health* **2005**, *11*, 384–397.
6. K. Bridbord, D. Hanson, *Environ. Health Perspect.* **2009**, *117*, 1195–1201.
7. G. Oudijk, *Environ. Forensics* **2010**, *11*, 17–49.
8. http://naei.defra.gov.uk/about/methodology, last accessed 22 April 2016.
9. Q. Li, H. Cheng, T. Zhou, C. Lin, S. Guo, *Atmos. Environ.* **2012**, *60*, 1–8.
10. L. J. Kristensen, *Atmos. Environ.* **2015**, *111*, 195–201.
11. H. W. Mielke, M. A. S. Laidlaw, C. Gonzales, *Sci. Total Environ.* **2010**, *408*, 3965–3975.
12. U. S. EPA, *Advance Notice of Proposed Rulemaking on Lead Emissions from Piston-Engine Aircraft using Leaded Aviation Gasoline*. Office of Transportation and Air Quality, EPA-420-F-10-013, April 2010.
13. M. L. Miranda, R. Anthopolos, D. Hastings, *Environ. Health Perspect.* **2011**, *119*, 1513–1516.
14. http://www.unep.org/Transport/new/PCFV/pdf/Maps_Matrices/world/lead/MapWorldLead_January2016.pdf; last accessed 22 April 2016.
15. http://tetraboost.com/; last accessed 22 April 2016.
16. *Gmelin Handbook of Inorganic Chemistry. Pb Organolead compounds.* Vol. 1. Tetramethyllead, 8th ed., Springer-Verlag, 1987.
17. *Gmelin Handbook of Inorganic Chemistry. Pb Organolead compounds.* Vol. 2. Tetraethyllead, 8th ed., Springer-Verlag, 1990.

18. P. J. Craig, G. Eng, R. O. Jenkins, in *Organometallic Compounds in the Environment,* 2nd ed., Ed. P. J. Craig, Wiley, Chichester, 2003, pp. 1–55.
19. R. G. Pearson, *J. Am. Chem. Soc.* **1963**, *85*, 3533–3539.
20. H. Bloom, J. W. Hastie, *J. Phys. Chem*. **1967**, *71*, 2360–2361.
21. R. H. Heidel, G. A. Desborough, *Environ. Pollut.* **1975**, *8*, 185–191.
22. G. L. Ter Haar, M. A. Bayard, *Nature* **1971**, *232*, 553–554.
23. J. J. Paciga, T. M. Roberts, R. E. Jervis, *Environ. Sci. Technol.* **1975**, *9*, 1141–1144.
24. P. A. Cawse, *Chemosphere* **1975**, *2*, 107-112.
25. J. M. Pierrard, *Environ. Sci. Technol.* **1969**, *3*, 48–51.
26. J. A. Robbins, F. L. Snitz, *Environ. Sci. Technol.* **1972**, *6*, 164–169.
27. P. D. E. Biggins, R. M. Harrison, *Nature* **1978**, *272*, 531–532.
28. P. D. E. Biggins, R. M. Harrison, *Environ. Sci. Technol.* **1979**, *13*, 558–565.
29. K. W. Olson, R. K. Skogerboe, *Environ. Sci. Technol.* **1975**, *9*, 227–230.
30. C. N. Hewitt, M. B. Rashed, *Appl. Organomet. Chem.* **1988**, *2*, 95–100.
31. R. M. Harrison, D. P. H. Laxen, *Environ. Sci. Technol.* **1978**, *12*, 1384–1392.
32. O. J. Nielsen, D. J. O'Farrell, J. J. Treacy, H. W. Sidebottom, *Environ. Sci. Technol.* **1991**, *25*, 1098–1103.
33. C. N. Hewitt, R. M. Harrison, *Environ. Sci. Technol.* **1986**, *20*, 797–802.
34. J. Yoshinaga, in *Organometallic Compounds in the Environment,* 2nd ed., Ed. P. J. Craig, Wiley, Chichester, 2003, pp. 151–194.
35. S.-H. Cho, J. Richmond-Bryant, J. Thornburg, J. Portzer, R. Vanderpool, K. Cavender, J. Rice, *Atmos. Environ.* **2011**, *45*, 5005–5015.
36. Y. K. Chau, P. T. S. Wong, G. A. Bengert, O. Kramar, *Anal. Chem.* **1979**, *51*, 186–188.
37. R. M. Harrison, M. Radojević, S. J. Wilson, *Sci. Total Environ.* **1986**, *50*, 129–137.
38. M. Radojević, R. M. Harrison, *Atmos. Environ.* **1987**, *21*, 2403–2411.
39. R. Van Cleuvenbergen, D. Chakraborti, F. C. Adams, *Environ. Sci. Technol.* **1986**, *20*, 589–593.
40. R. Van Cleuvenbergen, W. Dirkx, P. Quevauviller, F. Adams, *Int. J. Environ. Anal. Chem.* **1992**, *47*, 21–32.
41. A. W. P. Jarvie, R. N. Markall, H. R. Potter, *Environ. Res.* **1981**, *25*, 241–249.
42. R. D. Fallon, J. B. Obrigawitch, *Bull. Environ. Contam. Toxicol.* **1994**, *53*, 603–609.
43. J. S. Blais, W. D. Marshall, *J. Environ. Qual.* **1986**, *15*, 255–260.
44. J. S. Blais, C. A. Doige, W. D. Marshall, R. Knowles, *Arch. Environ. Contam. Toxicol.* **1990**, *19*, 227–234.
45. L. E. Macaskie, A. C. R. Dean, *Appl. Microbiol. Biotechnol.* **1990**, *33*, 81–87.
46. L.-T. Ou, J. E. Thomas, W. Jing, *Bull. Environ. Contam. Toxicol.* **1994**, *52*, 238–245.
47. H. Teeling, H. Cypionka, *Appl. Microbiol. Biot.* **1997**, *48*, 275–279.
48. G. Kipp, A. Davis, K. Patel-Coleman, L. Klinchuch, *Environ. Forensics* **2013**, *14*, 204–214.
49. C. Gallert, J. Winter, *Water Res.* **2002**, 36, 3130–3140.
50. T. Vigen, *Spurious Correlations: Correlation Does Not Equal Causation,* Hachette Books, New York, 2015.
51. M. Komárek, V. Ettler, V. Chrastný, M. Mihaljevič, *Environ. Int.* **2008**, *34*, 562–577.
52. G. Bird, *Environ. Int.* **2011**, 37, 802–819.
53. I. Renberg, M.-L. Brännvall, R. Bindler, O. Emteryd, *Sci. Total Environ.* **2002**, *292*, 45–54.
54. https://www.epa.gov/air-trends/lead-trends; last accessed 2 May 2016.
55. H. Cheng, Y. Hu, *Environ. Pollut.* **2010**, *158*, 1134–1146.
56. J. Chen, M. Tan, Y. Li, Y. Zhang, W. Lu, Y. Tong, G. Zhang, Y. Li, *Atmos. Environ.* **2005**, *39*, 1245–1253.

57. W. Wang, X. Liu, L. Zhao, D. Guo, X. Tian, F. Adams, *Sci. Total Environ.* **2006**, *364*, 175–187.
58. F. E. Grousset, C. R. Quétel, B. Thomas, P. Buat-Ménard, O. F. X. Donard, A. Bucher, *Environ. Sci. Technol.* **1994**, *28*, 1605–1608.
59. B. J. Huser, S. J. Köhler, A. Wilander, K. Johansson, J. Fölster, *Biogeosciences* **2011**, *8*, 1813–1823.
60. A. Rühling, G. Tyler, *Environ. Pollut.* **2004**, *131*, 417–423.
61. R. M. Semlali, J.-B. Dessogne, F. Monna, J. Bolte, S. Azimi, N. Navarro, L. Denaix, M. Loubet, C. Chateau, F. van Oort, *Environ. Sci. Technol.* **2004**, *38*, 1513–1521.
62. M. A. S. Laidlaw, S. Zahran, H. W. Mielke, M. P. Taylor, G. M. Filippelli, *Atmos. Environ.* **2012**, *49*, 302–310.
63. K. C. Wells, M. Witek, P. Flatau, S. M. Kreidenweise, D. L. Westphal, *Atmos. Environ.* **2007**, *41*, 6585–6597.
64. M. A. S. Laidlaw, G. M. Filippelli, *Appl. Geochem.* **2008**, *23*, 2021–2039.
65. M. A. S. Laidlaw, H. W. Mielke, G. M. Filippelli, D. L. Johnson, C. R. Gonzales, *Environ. Health Perspect.* **2005**, *113*, 793–800.
66. H. W. Mielke, M. A. S. Laidlaw, C. R. Gonzales, *Environ. Int.* **2011**, *37*, 248–257.
67. M. B. Rabinowitz, G. W. Wetherill, J. D. Kopple, *J. Clin. Invest.* **1976**, *58*, 260–270.
68. U. S. EPA, *Air Quality Criteria for Lead*, Vol I. EPA-600/8-83/028aF, Washington DC, U. S. Environmental Protection Agency, 1986.
69. V. M. Thomas, R. H. Socolow, J. J. Fanelli, T. J. Spiro, *Environ. Sci. Technol.* **1999**, *33*, 3942–3948.
70. A. K. Singh, M. Singh, *Sci. Total Environ.* **2006**, *368*, 686–694.
71. K. He, S. Wang, J. Zhang, *Sci. Total Environ.* **2009**, *407*, 3986–3993.
72. J. Tuakuila, M. Kabamba, H. Mata, G. Mata, *Arch. Public Health* **2013**, *71*, 5.
73. U. Strömberg, T. Lundh, A. Schütz, S. Skerfving, *Occup. Environ. Med.* **2003**, *60*, 370–372.
74. H. M. Tvinnereim, R. Eide, T. Riise, G. R. Wesenberg, G. Fosse, E. Steinnes, *Sci. Total Environ.* **1997**, *207*, 165–177.
75. E. A. Chadwick, V. R. Simpson, A. E. L. Nicholls, F. M. Slater, *Environ. Sci. Technol.* **2011**, *45*, 1911–1916.
76. M. Murozumi, T. J. Chow, C. Patterson, *Geochim. Cosmochim. Acta* **1969**, *33*, 1247–1294.
77. C. F. Boutron, U. Görlach, J.-P. Candelone, M. A. Bolshov, R. J. Delmas, *Nature* **1991**, *353*, 153–155.
78. J.-P. Candelone, S. Hong, C. Pellone, C. F. Boutron, *J. Geophys. Res. Atmos.* **1995**, *100*, 16605−16616.
79. J. R. McConnell, R. Edwards, *PNAS* **2008**, *105*, 12140−12144.
80. K. J. R. Rosman, W. Chisholm, C. F. Boutron, J. P. Candelone, U. Görlach, *Nature* **1993**, *362*, 333–334.
81. K. Lee, S. D. Hur, S. Hou, L. J. Burn-Nunes, S. Hong, C. Barbante, C. F. Boutron, K. J. R. Rosman, *Sci. Total Environ.* **2011**, *412–413*, 194–202.
82. W. Shotyk, *Environ. Rev.* **1996**, *4*, 149–183.
83. W. Shotyk, D. Weiss, P. G. Appleby, A. K. Cheburkin, R. Frei, M. Gloor, J. D. Kramers, S. Reese, W. O. Van Der Knaap, *Science* **1998**, *281*, 1635–1640.
84. J. M. Cloy, J. G. Farmer, M. C. Graham, A. B. MacKenzie, G. T. Cook, *J. Environ. Monit.* **2005**, *7*, 1137–1147.
85. F. De Vleeschouwer, N. Fagel, A. Cheburkin, A. Pazdur, J. Sikorski, N. Mattielli, V. Renson, B. Fialkiewicz, N. Piotrowska, G. Le Roux, *Sci. Total Environ.* **2009**, *407*, 5674–5684.
86. S. K. Marx, B. S. Kamber, H. A. McGowan, A. Zawadzki, *Environ. Poll.* **2010**, *158*, 1615–1628.

87. M. Allan, G. Le Roux, F. De Vleeschouwer, R. Bindler, M. Blaauw, N. Piotrowska, J. Sikorski, N. Fagel, *Environ. Poll.* **2013**, *178*, 381–394.
88. K. Bao, J. Shen, G. Wang, G. Le Roux, *Atmosphere* **2015**, *6*, 380–409.
89. W. Shotyk, D. Weiss, M. Heisterkamp, A. K. Cheburkin, P. G. Appleby, F. C. Adams, *Environ. Sci. Technol.* **2002**, *36*, 3893–3900.
90. M.-L. Brännvall, R. Bindler, I. Renberg, O. Emteryd, J. Bartnicki, K. Billström, *Environ. Sci. Technol.* **1999**, *33*, 4391–4395.
91. C. E. Dunlap, R. Bouse, A. R. Flegal, *Environ. Sci. Technol.* **2000**, *34*, 1211–1215.
92. C. E. Dunlap, C. N. Alpers, R. Bouse, H. E. Taylor, D. M. Unruh, A. R. Flegal, *Geochim. Cosmochim. Acta* **2008**, *72*, 5935–5948.
93. M. F. Soto-Jiménez, F. Páez-Osuna, G. Scelfo, S. Hibdon, R. Franks, J. Aggarawl, A. R. Flegal, *Mar. Environ. Res.* **2008**, *66*, 451–458.
94. H. Harmens and 33 authors, *Environ. Pollut.* **2010**, *158*, 3144–3156.
95. H. Harmens and 34 authors, *Environ. Pollut.* **2015**, *200*, 93–104
96. O. Travnikov, I. Ilyin, O. Rozovskaya, M. Varygina, W. Aas, H. T. Uggerud, K. Mareckova, R. Wankmueller, *Long-term Changes of Heavy Metal Transboundary Pollution of the Environment (1990–2010)*, EMEP Status Report 2/2012, 2012.
97. H. Harmens, D. Norris, G. Mills, and the participants of the moss survey, *Heavy Metals and Nitrogen in Mosses: Spatial Patterns in 2010/2011 and Long-Term Temporal Trends in Europe*, ICP Vegetation Programme Coordination Centre, Centre for Ecology and Hydrology, Bangor, UK, 2013, 63 pp.
98. Y. Echegoyen, E. A. Boyle, J.-M. Lee, T. Gamo, H. Obata, K. Norisuye, *PNAS* **2014**, *111*, 15328–15331.

15

Lead Toxicity in Plants

Hendrik Küpper [1,2]

[1]Biology Center of the Czech Academy of Sciences, Institute of Plant Molecular Biology, Department of Plant Biophysics & Biochemistry, České Budějovice, Czech Republic
and
[2]University of South Bohemia, Department of Experimental Plant Biology; České Budějovice, Czech Republic
<hendrik.kuepper@umbr.cas.cz>

Abstract: This review looks critically at the relevance of lead (Pb^{2+}) toxicity and proposed mechanisms of Pb^{2+}-induced stress in algae and higher plants. As a basis, the current main sources of Pb^{2+} contamination in the environment are presented, which include agriculture, industry, and road traffic. Further, bioavailability of lead is discussed as a basis for evaluating the environmental relevance of the many studies on lead toxicity that have been published in the past decades. These studies suggest three main mechanisms of toxicity of Pb^{2+}: inhibition of photosynthesis, oxidative stress, and "genotoxicity" including DNA damage and defects in mitosis. Looking at the applied concentration ranges in these studies reveals that likely the defects in mitosis are the environmentally most relevant effects. In contrast, inhibition of photosynthetic light reactions is far less efficient with Pb^{2+} compared to other metal ions, so that for Pb^{2+} toxicity it seems environmentally not relevant. As a conclusion and outlook, a

Metal Ions in Life Sciences, Volume 17 Edited by Astrid Sigel, Helmut Sigel, and Roland K. O. Sigel

DOI 10.1515/9783110434330-015

direction of future studies towards establishment of reliable concentration thresholds of the various toxic effects and their causal interconnection is suggested.

Keywords: defects in mitosis · environmental relevance · genotoxicity · mutagenic effect · oxidative stress · photosynthesis

1. INTRODUCTION: ENVIRONMENTAL RELEVANCE OF LEAD TOXICITY IN PLANTS

Lead has been a very popular topic of research on metal toxicity, mainly because its use in additives for car fuel. Since this has been stopped already in the 1980s–1990s around the world, lead pollution in towns and near roads has dropped drastically. For example, in Hongkong there was an over 7-fold decrease of Pb in urban dust between studies from 1987 [1] and 2001 [2]. While this figure still includes Pb emissions from other sources, looking at traffic alone the reduction by the ban of Pb in fuel led to an almost 100-fold decrease of Pb emissions according to a study in Denmark [3]. As a consequence, contaminations along roadsides have dropped drastically, but are sometimes still considerable [4]. Another source of severe Pb pollution, which was important only in the past (until the 1970s), but the contamination of the environment still persists, is the use of lead arsenate as a pesticide to treat various fruits [5].

Contamination with lead can also result from its ongoing use in car batteries. This starts with lead production as the best investigated source of lead pollution [5–8]. But in recent years another problem came into focus. High Pb concentrations are found near e-waste dumps and recycling sites in poor countries where such works are still being done without proper safety precautions [9]. Finally, careless application of sewage sludge and municipal compost without properly testing it for toxic ingredients led to an increase of toxic metals, including Pb, in agricultural soils [10, 11].

However, most of the Pb that entered soils in the ways just discussed is not readily bioavailable, but it is present in insoluble form or it is strongly bound to soil particles [12–14]. Therefore, the concentration of Pb in agricultural field runoff is very low, actually irrelevant compared to the much more plant-toxic Cu [15]. This has to be taken into account when experiments on lead toxicity in plants are performed. Unfortunately, in most studies on lead toxicity in plants the extreme difference between plant-available lead and the total lead concentration in soil is completely ignored. Looking at field data, toxicity of lead to plants seems not to occur to a significant extent even in highly polluted areas along roadsides or e-waste recycling areas. However, the amount of lead that is taken up by the plants without causing toxicity there, can be dangerous for consumption by animals including humans – in the recent study on an e-waste recycling site in China, mean Pb levels in rice near this site exceeded the allowed limit 3.5 times [9]. To a lesser extent, also earlier studies on various horticultural crops showed that on some fields the lead concentrations exceed allowed limits as well [16–18].

In aquatic ecosystems, lead may sometimes exceed concentrations that are toxic to algae, as revealed already in 1979 by Christensen et al. [19] who found a 50 % reduction in total algal cell volume in response to only 140 $\mu g \cdot L^{-1}$ (0.68 μM) lead. Unfortunately, the mechanism was not investigated, and almost all later studies used orders of magnitude higher concentrations of Pb^{2+}. A recent study found even lower (down to 20 ppb = 0.1 μM Pb^{2+}) LC50 thresholds for some phytoplankton communities, but again did not investigate the mechanism [20]. A study investigating the synthesis of detoxifying ligands (phytochelatins) as a defence against Pb^{2+} toxicity in the aquatic shoot model plant *Ceratophyllum demersum*, using a range of 1–100 μM Pb^{2+}, found a statistically significant reduction of biomass after one week with 1 μM Pb^{2+} [21]. A very recent study on the model plant *Arabidopsis thaliana*, has shown that already sub-micromolar concentrations of Pb^{2+} can inhibit growth and induce phytochelatins in terrestrial plants [22].

2. CRITICAL REVIEW OF PROPOSED MECHANISMS OF LEAD TOXICITY IN PLANTS

2.1. General Aspects

Likely out of the knowledge that lead is toxic to humans, authors engaged on lead toxicity studies in plants. Lead toxicity in plants has been investigated in hundreds of studies over many years. However, by far most of them, including the highest cited ones [23], have been performed with environmentally not relevant, far too high lead concentrations. Clearly, this has been done because lead is overall not very toxic to plants, far less than most other metals that are important in environmental pollution, in particular cadmium and copper that are toxic to sensitive plants already in the low nanomolar range [24].

Further, looking at the literature about metal toxicity in plants in general, unfortunately many authors tend to choose concentrations that lead to effects very quickly and drastically, rather than waiting for those effects that occur already at much lower concentrations that are environmentally much more relevant (general review, e.g., by Küpper and Andresen [24]). Forcing fast drastic effects with a metal that only has low toxicity for plants yields the typical Pb concentrations in published studies, which are almost never below the range of hundreds of micromoles per liter and very often even in the millimolar range. This choice of concentration range may be understandable from the point of view of producing results quickly, but unfortunately it drastically reduces the value of the results in terms of understanding the effects of Pb contamination in the environment. Unfortunately, since previous reviews about lead toxicity in plants were written by the same people who published those studies based on environmentally irrelevant conditions, these problems were not discussed. Further, often actual mechanisms of toxicity (e.g., inhibition of an enzyme by binding

of Pb^{2+} to it) are confused with final unspecific outcomes such as reduced growth or diminished seed yield or necrotic lesions, which are a consequence of toxicity mechanisms. These final outcomes will not be discussed in the current review, which aims at looking at actual mechanisms that could cause such reductions in growth and yield.

Before Pb^{2+} can lead to toxicity inside the plant, it first needs to enter the plant. And already at this point, in most cases Pb^{2+} is excluded; it has been observed that the endodermis in the roots is the main barrier for uptake into the plant [25], which is not surprising because it is generally known to prevent unselective uptake of all kinds of solutes. For this reason, studies on the effects of lead in aerial parts of the plants have often been performed on detached leaves or isolated cells [26], but such studies have even less environmental relevance for environmental effects of lead.

2.2. Inhibition of Photosynthesis

Once in the plant, lead has been associated with various detrimental effects. In the following, the most discussed inhibitory effects of lead on plant metabolism will be critically discussed. An overview of concentration ranges where various effects of lead toxicity were observed is given in Figure 1.

Contrary to other metals, and contrary to some claims in earlier reviews on lead toxicity, photosynthetic light reactions are not very sensitive to lead. Studies reporting lead toxicity on photosynthesis are all based on enormous concentrations in the range of hundreds of μM or even mM, which are never environmentally relevant (even less inside the leaf as simulated by detached leaves, e.g., [26]). One reason for this insensitivity could be the almost absent tendency of Pb^{2+} to be bound in chlorophyll (Chl) [27], which efficiently happens with other toxic metals such as Cu^{2+} or Cd^{2+} (see review [24]). Highly toxic lead concentrations of 100 μM (however, lower and thus more relevant compared to most other concentrations used in Pb^{2+} toxicity studies in plants) were found to cause a decrease of pigment concentrations via an unknown mechanism [28, 21]. But in competition to toxic effects of Mn^{2+}, Zn^{2+} or Cu^{2+}, these 100 μM Pb^{2+} was observed not to cause any effect on Chl biosynthesis [28], which is in line with the early observation of Christensen et al. in 1979 [19] that the growth inhibition of algae by sub-micromolar sublethal Pb^{2+} concentrations can be at least partially offset by addition of Mn^{2+}.

In contrast to the light reactions, the light-independent reactions of the Calvin-Benson cycle (former called "dark reactions") that lead to carbon fixation are more sensitive to Pb^{2+}, as compared in a recent study [29]. Already 10 ppm total lead in soil (an environmentally common level), of which only a small part will be bioavailable as discussed before, led to a significant decrease of carbon fixation and maximal RuBisCo activity.

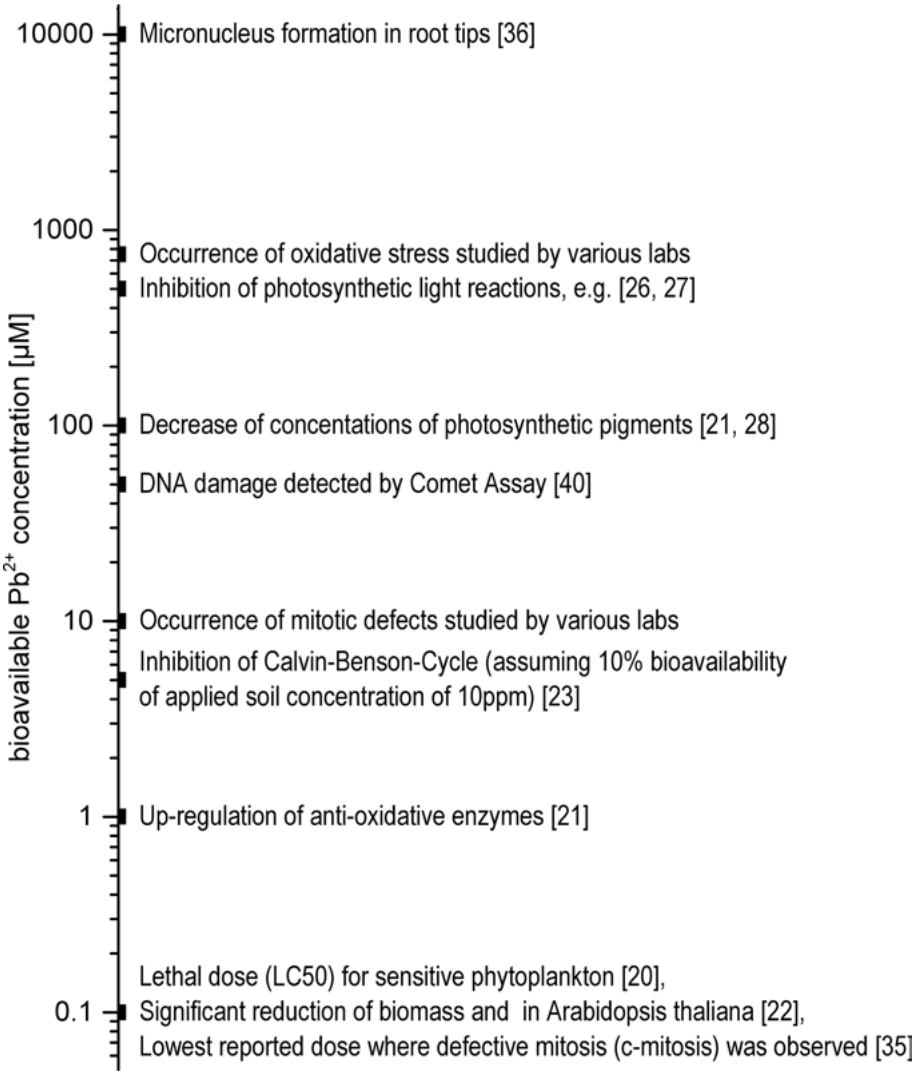

Figure 1. Scheme displaying the lowest respective concentrations where various effects of lead toxicity have been found in plants. Since for most mechanisms a determination of concentration thresholds has not been done (see text), unfortunately this does not necessarily mean that a certain effect does not occur at lower concentrations, but only that it has not yet been studied at lower concentrations.

2.3. Oxidative Stress

Lead has been suggested to cause oxidative stress in plants by a highly cited study [23]. This study is, however, typical for investigations of lead toxicity in plants as already mentioned: The authors used extremely high, environmentally completely irrelevant lead concentrations of 500 μM and 1000 μM. Further, as most other studies on lead toxicity, it describes the effect of reactive oxygen species (ROS) production without analyzing how the biologically redox-inactive lead causes the increase of ROS in the plants. It does show, however, that even at these extreme lead concentrations the ROS-removing enzymes superoxide dismutase (SOD), glutathione reductase (GR) and ascorbate peroxidase (APX) are not inhibited but up-regulated. Similar results were obtained at the same lead concentrations in pea root cells [30].

Later, at lower Pb^{2+} concentrations starting from 1 μM a similar response was observed in the aquatic shoot model plant *C. demersum* [21]. The increase of lipid peroxidation despite up-regulation of the antioxidative system as a result of toxicity of redox-inert Pb^{2+} suggests indirect formation of ROS during Pb toxicity via Pb-induced malfunction of electron transport in respiration or photosynthesis. The source of ROS remains unsolved, however, because of the low sensitivity of photosynthesis to Pb^{2+} at environmentally more relevant Pb^{2+} concentrations.

2.4. Genotoxicity and Effects on Mitosis

Another mode of lead toxicity that was often discussed after it was found in various studies are genotoxic effects. These can be based on various targets, which were reviewed including their concentration range of observation by Patra et al. [31]. In many cases, genotoxicity was studied in terms of looking for defects in mitosis, although here it is possible that Pb^{2+} actually only disturbed proteins, not nucleic acids. A recent study observing Pb-induced defects in the cytoskeleton, which changed chloroplast movement [32], could indicate that also mitosis is affected by a defective cytoskeleton.

One of the first studies of mitotic defects induced by Pb^{2+} in plants was performed by Chakravarty and Srivastava [33], who found defects in mitosis already at their lowest applied Pb^{2+} concentration, 10 μM, and noted that for this type of toxicity Pb^{2+} had stronger effects than all other studied metals (Al^{3+}, Cd^{2+}, Cu^{2+}, Ni^{2+}, Zn^{2+}). Another early study in this field was by Wierzbicka [34], who worked with 12.5 μM (2.5 ppm) Pb^{2+} and showed that c-mitoses were the first microscopically observable genotoxic effects. This was confirmed by other authors, covering a very wide range of lead concentrations [35]. Unfortunately, statistics is deficient in that study with error bars and tests of significant differences missing. Nevertheless, some trends of sensitivity of genotoxic effects like anormally dividing cells (in prophase, metaphase, and anaphase), mitotic anomalies like c-mitosis, chromosome bridges, and chromosome stickiness can be observed. Of these six parameters measured, chromosome bridges and c-mitosis

were the most sensitive, with small effects visible already at 10^{-7} M (0.1 μM) Pb^{2+}. Of all effects of Pb^{2+} on plants reported in literature, this is the one at lowest concentrations. Maybe it could explain the growth reduction that was observed by Christensen et al. in 1979 [19] at sub-micromolar Pb^{2+} concentrations without investigation of its mechanism.

Other effects on mitosis were observed only at much higher concentrations, as they were unfortunately used in almost all studies. For example, in one publication that is often cited for a comparison of micronucleus (MCN) bioassays of metal toxicity, Pb^{2+} was only observed to cause MCN formation above 1 mM Pb^{2+}, for root tip cells even above 10 mM Pb^{2+} [36]. Thus, based on the data available so far, it clearly has to be judged as environmentally not relevant. The effects on this parameter in soils from contaminated sites [37] can be attributed to other toxic components in these soils, in particular Cd^{2+} as a known highly genotoxic metal ion.

Although all the effects on mitosis mentioned above are usually regarded as "genotoxicity" as discussed also in the most popular review on that mode of action of Pb^{2+} in plants [31], a malfunctioning mitosis does not necessarily mean that the genome is modified in an inheritable way (mutation). In two studies of the mutagenic effect of metal-polluted soil, DNA damage was observed by the "Comet assay", but no mutations could be detected in the genome of the stressed plants [38, 39]. Therefore, the "genotoxic" effect of Pb^{2+} in plants should be regarded as a toxic, but not a mutagenic effect.

A recent (2014) study, using concentrations between 50 and 1,000 μM Pb^{2+}, correlated inhibition of mitosis, DNA damage measured by the Comet Assay, and increases in antioxidative enzymes with lipid peroxidation and leakiness of membranes [40]. Because all these alterations were observed together, it was concluded that oxidative stress would be the reason for DNA damage. This study is clearly much more comprehensive than the earlier ones on Pb^{2+}-induced oxidative stress and genotoxicity discussed above, and the lowest applied concentrations were at least somewhat lower than those in most previous studies. However, even these concentrations were still far too high compared to those in the environment, and 500 times higher than the lowest tested concentration that still induced an elevated percentage of mitotic defects in the study of Liu et al. [35]. Further, the otherwise comprehensive study of Kaur et al. [40] unfortunately failed to prove a causal relationship between the oxidative stress and DNA damage. The observed occurrence of both effects at the same concentrations can have many different reasons, and as mentioned at the beginning of this review, highly toxic concentrations lead to unspecific effects.

3. CONCLUSIONS AND OUTLOOK

A few studies, like those of Christensen et al. [19], Liu et al [35], Echeveste et al. [20], and Fischer et al. [22] indicate that lead toxicity may occur at much lower concentrations than those typically investigated in other Pb^{2+} toxicity studies – even in the sub-micromolar range. Future studies on lead toxicity

should be based on this concentration range. Furthermore, future studies should focus on finding causal relationships between the measured effects.

Currently, it seems that the most urgent need would be for a study that determines not only the concentration thresholds for the two effects that are currently most discussed, i.e., various types of "genotoxicity" including defects of mitosis, and oxidative stress. Further, the reason for the oxidative stress needs to be found, as Pb^{2+} itself is redox-inert in plants so that Fenton-type reactions can be excluded and an indirect mechanism has to be the reason. Finally, it should be investigated whether the oxidative stress causes the DNA damage and defects in mitosis, or which other mechanism is leading to these effects.

In addition to establishing a truly mechanistic insight into lead toxicity at environmentally relevant concentrations, studies on transfer of Pb into the food chain by plants will be a very important, environmentally and agriculturally relevant research topic.

ACKNOWLEDGMENTS

The author would like to thank the Biology Centre of the Czech Academy of Sciences and project No.: CZ.02.1.01/0.0/0.0/15_003/0000336 from the Ministry of Education, Youth and Sports of the Czech Republic, co-financed by the European Union, for financial support.

ABBREVIATIONS

APX	ascorbate peroxidase
Chl	chlorophyll
LC50	concentration at which half of a population dies
GR	glutathione reductase
MCN	micronucleus
ROS	reactive oxygen species
RuBisCo	ribulose-1,5-bisphosphate carboxylase/oxygenase
SOD	superoxide dismutate

REFERENCES

1. W. W. S. Yim, P. S. Nau, *Hong Kong Engineer* **1987**, 15, 7–14.
2. X. D. Li, C. S. Poon, P. S. Liu, *Appl. Geochem.* **2001**, *16*, 1361–1368.
3. K. Kemp, *Nucl. Instrum. Meth. Phys. Res. Sect. B-Beam Interact. Mater. Atoms* **2002**, *189*, 227–232.
4. D. Hjortenkrans, B. Bergbäck, A. Häggerud, *Environ. Monit. Assess.* **2006**, *117*, 85–98.
5. B. Freedman, T. C. Hutchinson, in *Effect of Heavy Metal Pollution on Plants: Metals in the Environment*, Vol. 2, Ed. N. W. Lepp, Applied Sci. Publ., London and New Jersey, 1981, pp. 35–94.

6. M. C. Jung, I. Thornton, *Appl. Geochem.* **1996**, *11*, 53–59.
7. A. N. Kachur, V. S. Arzhanova, P. V. Yelpatyevsky, M. C. von Braun, I. H. von Lindern, *Sci. Total Environ.* **2003**, *303*, 171–185.
8. U. Herpin, U. Siewers, B. Markert, V. Rosolen, G. Breulmann, M. Bernoux, *Environ. Sci. Pollut. Res. Int.*, **2004**, *11*, 57–66.
9. J. Fu, Q. Zhou, J. Liu, W. Liu, T. Wang, Q. Zhang, G. Jiang, *Chemosphere* **2008,** *71*, 1269–1275.
10. M. B. McBride, *Commun. Soil Sci. Plant Anal.* **2004**, *35*, 517–535.
11. S. R. Smith, *Environ. Intern.* **2009**, *35*, 142–156.
12. W. L. Lindsay, *Chemical Equilibria in Soils*, John Wiley and Sons Ltd., Chichester, UK, 1979, pp. 449.
13. R. D. Harter, *Soil Sci. Soc. Am. J.* **1983**, *47*, 47–51.
14. J. Y. Yang, X. E. Yang, Z. L. He, G. C. Chen, J. L. Shentu, T. Q. Li, *J. Environ. Sci. Health* **2004**, *39*, 1083–1087.
15. Z. L. He, M. K. Zhang, D. V. Calvert, P. J. Stoffella, X. E. Yang, S. Yu, *Soil Sci. Soc. Am. J.* **2004**, *68*, 1662–1669.
16. J. V. Lagerwerff, *Soil Sci.* **1971**, *111*, 129–133.
17. M. Peris, C. Micó, L. Recatalá, R. Sánchez, J. Sánchez, *Sci. Total Environ.* **2007**, *378*, 42–48.
18. M. Marković, S. Cupać, R. Durović, J. Milinović, P. Kljajić, *Arch. Environ. Contam. Toxicol.* **2010**, *58*, 341–351.
19. E. R. Christensen, J. Scherfig, P. S. Dixon, *Water Res.* **1979**, *13*, 79–92.
20. P. Echeveste, S. Agustí, A. Tovar-Sánchez, *Environ. Toxicol. Chem.* **2012**, *31*, 1887–1894.
21. S. Mishra, S. Srivastava, R. D. Tripathi, R. Kumar, C. S. Seth, D. K. Gupta, *Chemosphere* **2006**, *65*, 1027–1039.
22. S. Fischer, T. Kühnlenz, M. Thieme, H. Schmidt, S. Clemens, *Environ. Sci. Technol.* **2014**, *48*, 7552–7559.
23. S. Verma, R. S. Dubey, *Plant Science* **2003**, *164*, 645–655.
24. H. Küpper, E. Andresen, *Metallomics* **2016**, *8*, 269–285.
25. M. Sobotik, V. B. Ivanov, N. V. Obroucheva, I. V. Seregin, M. L. Martin, O. V. Antipova, H. Bergmann, *J. App. Bot.* **1998**, *72*, 144–147.
26. E. Parys, E. Romanowska, M. Siedlecka, J. W. Poskuta, *Acta Physiol. Plant.* **1998**, *20*, 313–322.
27. H. Küpper, F. Küpper, M. Spiller, *J. Exper. Bot.* **1996**, *47*, 259–266.
28. S. K. Sinha, H. S. Srivastava, R. D. Tripathi, *Bull. Environ. Contam. Toxicol.* **1993**, *51*, 241–246.
29. E. Rodriguez E, M. da Conceição Santos, R. Azevedo, C. Correia, *J. Environ. Sci. Pollut. Res. Int.* **2015**, *22*, 574–585.
30. A. Małecka, W. Jarmuszkiewicz, B. Tomaszewska, *Acta Biochim. Pol.* **2001**, *48*, 687–698.
31. M. Patra, N. Bhowmik, B. Bandopadhyay, A. Sharma, *Environ. Exper. Bot.* **2004**, *52*, 199–223.
32. S. Samardakiewicz S, W. Krzeszowiec-Jeleń, W. Bednarski, A. Jankowski, S Suski, H. Gabryś, A. Woźny, *PLoS One* **2015**, *10*, e0116757. DOI: 10.1371/journal.pone.0116757.
33. B. Chakravarty, S. Srivastava, *Mutat. Res.* **1992**, *283*, 287–294.
34. M. Wierzbicka, *Environ. Exper. Bot.* **1994**, *34*, 173–180.
35. D. Liu, W. Jiang, F. Zhao, C. Lu, *Environ. Pollut.* **1994**, *86*, 1–4.
36. H. Steinkellner, K. Mun-Sik, C. Helma, S. Ecker, T. H. Ma, O. Horak, M. Kundi, S. Knasmüller, *Environ. Mol. Mutagen.* **1998**, *31*, 183–191.

37. B. J. Majer, D. Tscherko, A. Paschke, R. Wennrich, M. Kundi, E. Kandeler, S. Knasmüller, *Mutat. Res.* **2002**, *515*, 111–124.
38. T. Gichner, Z. Patková, J. Száková, K. Demnerová, *Ecotoxicol. Environ. Saf.* **2006**, *65*, 420–426.
39. T. Gichner, I. Znidar, J. Száková, *Mutat. Res.* **2008**, *652*, 186–190.
40. G. Kaur, H. P. Singh, D. R. Batish, R. K. Kohli, *Ecotoxicology* **2014**, *23*, 1292–1304.

16

Toxicology of Lead and Its Damage to Mammalian Organs

Samuel Caito, [1] ***Ana Carolina B. Almeida Lopes,*** [2] ***Monica M. B. Paoliello,*** [2] ***and Michael Aschner*** [1*]

[1]Department of Molecular Pharmacology, Albert Einstein College of Medicine, Bronx, NY 10461, USA, <michael.aschner@einstein.yu.edu>

[2]Graduate Program in Public Health, Center of Health Sciences, State University of Londrina, Londrina, Parana, Brazil

Metal Ions in Life Sciences, Volume 17 Edited by Astrid Sigel, Helmut Sigel, and Roland K. O. Sigel

DOI 10.1515/9783110434330-016

Abstract: The toxicity of lead has been appreciated for centuries. Lead is a commonly used metal in industrialized nations, which results in the release of lead into the environment. Governmental agencies regulate the amount of lead permissible for workers to be exposed to; however, unregulated environmental lead exposure is a high concern. While essential metals have physiologic roles, there are no health benefits from lead intake. In this chapter, we discuss sources of lead exposure, the absorption, distribution, and elimination of lead from the human body, and molecular mechanisms of lead-induced toxicity. We also discuss the evidence on the association between lead exposure and blood pressure, and the influence of sociodemographic, lifestyle and environmental determinants of lead exposure in the general population. We highlight the effects on the nervous system, kidney, immune system, blood, reproductive system, and bones.

Keywords: anemia · bone · hypertension · lead · neurotoxicity

1. INTRODUCTION

1.1. History and Uses of Lead

Lead is a common metal in the Earth's crust that is widely used in industrial settings, but causes toxicity in exposed individuals. Lead is rarely found naturally as a metal, but is usually combined with two or more elements to form lead compounds or ores. Mining of lead is only one source of the metal used in industry. Lead is commonly recycled from scrap metal or batteries. The chemical properties of lead make it an easily workable metal which is highly valued for its softness, low melting temperature, malleability, ductility, poor conductivity, and resistance to corrosion. Lead is easily combined with other metals to form alloys.

While there are many beneficial uses of lead for industry and consumer products, lead is a persistent contaminant in our environment. Lead has to be mined and is therefore not a common element on the Earth's surface. Unlike other heavy metals, such as iron, cobalt or copper, there are no physiological processes in living organisms that are dependent on lead. Lead contamination of the polar regions of Greenland have been dated back to 500 B.C.–300 A.D., when an estimated 400 tons of lead was deposited in the environment by the Greeks and Romans [1]. In the ancient world lead was used for pipes, kitchen utensils and

tableware, ceramic pigments, cosmetics, and due to its sweet taste, a wine sweetener.

In modern times, lead was used in paints, stain glass, book printing, and anti-knock agents [2]. Lead was used in paints and stained glass for its pigment (white from lead(II) carbonate or yellow from lead chromate), opacity and insolubility in water. Leaded paints were vibrant in color, could cover a larger area than nonleaded paints, and had a highly water-resistant, durable, washable finish. The amount of lead used in paints and dyes has been greatly reduced in the past thirty years to minimize lead's harmful effect on people. Lead paint chips accounts for the majority of exposure to children, which remains a common occurrence in older homes and low-income urban dwellings where leaded paint has not been removed. The organolead compound tetraethyl lead was widely used as an anti-knock fuel additive for automobiles, but was banned by the United States in 1996. However, tetraethyl lead and other organolead compounds still can be added to aviation fuels. The largest use for lead currently is in batteries, and the most common non-battery use for lead is in ammunition. Additionally, lead is used in electrodes for electrolysis, radiation shielding and reactor coolant, semiconductors, polyvinyl chloride (PVC) plastics, and sailing ballasts.

1.2. Exposures to Lead

Exposure to lead can either occur occupationally or from environmental sources. The professions that have the highest risk for lead exposure include manufacturing of lead-containing products, recycling of batteries, car repair, lead paint removal, demolition, refining, welding, and smelting. In the United States the National Institute for Occupational Safety and Health (NIOSH) has set a recommended exposure limit (REL) for lead as 50 $\mu g/m^3$ over a 8 hour period. The Occupational Safety and Health Administration (OSHA) sets their permissible exposure limit (PEL) at 30 $\mu g/m^3$ averaged over 8 hours, with a reduction in the PEL for shifts longer than 8 hours. Regulations from OSHA have reduced the amount of lead poisonings in the workplace; however, these regulations are not always strictly followed. In professions that are not considered as high of a risk for lead exposure, monitoring of lead levels in the working environment may not take place. Sen et al. have found significant blood lead levels in scaffolders who erected and dismantled scaffolding on lead-painted structures and were not monitored for lead by their employers [3]. Exposure to lead occupationally is primarily inhalational. Many professions in which lead is used create dusts or aerosols that contain lead.

Environmental exposure to lead is of major concern. Lead enters the soil around sources of contamination, such as mines, industrial sites, power plants, incinerators, and hazardous waste sites. Lead in soil can leech into ground water and be taken up by plants. Food crops grown under these conditions can be tainted with lead. Lead can become air-born and available for inhalation from natural sources, such as volcanic eruption, but the majority of lead in the air comes from anthropogenic sources. Until the mid-1990s, the single largest source

of lead in the environment was from leaded gasoline, however, due to banning the additives, this is no longer the case. Living near industries involved in iron and steel production, lead-acid-battery manufacturing and nonferrous (brass and bronze) foundries increases the risk of exposure to lead. Drinking water is another source of environmental lead exposure. Very little lead is found naturally in fresh water and ground water used for the public drinking supply, however acid (soft) water can be corrosive to lead pipes and solder, resulting in lead dissolving into the water. Finally, living in older homes that contain lead paint increases one's exposure to lead. Leaded paint chips and dusts can be ingested either voluntarily or involuntarily. Eating lead paint chips is of great concern for young children, especially since children under the age of 5 absorb triple the amount of lead in their gastrointestinal tract than adults [4].

Finally, lead can be transmitted from mother to child both through the placenta and through breast milk. Measurements using stable isotope ratios of lead in pregnant women as they encounter novel environmental lead exposure showed that 80 % of lead in fetal cord blood derives from maternal bone stores whereas 20 % derive from the more recent exposure [5]. Factors that increase lead deposition from the mother into cord blood include alcohol consumption late in pregnancy and high blood pressure, whereas high hemoglobin content or sickle cell trait decrease the cord blood levels of lead [6]. Lead can be transferred to infants in breast milk. The concentration of lead in breast milk is more influenced by maternal blood lead concentrations than by maternal bone lead levels [7].

1.3. Absorption, Distribution, and Excretion

1.3.1. Absorption

Upon ingestion, lead absorption occurs primarily in the duodenum [8]. Transport of lead (ionized or complexed) may involve active transport, diffusion through intestinal epithelial cells or between cells. Lead phosphate and bile acid complexes are the dominant forms of lead observed following lead exposure in humans, however, inorganic lead salts, such as lead nitrate or ionized lead can be observed in the chime. Ionized lead has been observed only with concentrations of lead in the chime greater than 10^{-3} M [9]. However, ionized lead may be produced in the intestines due to the lability of bile acid complexes [10]. Observations of nonlinear relationships between blood lead concentration and lead intake in humans suggest a saturable absorption mechanism in the distribution of lead [11, 12]. This may be due to the activity of specific proteins in the intestinal mucosa that transport lead into the cells.

As lead is not an essential metal, the mechanism by which it enters mammalian cells is through mimicry to essential metals. Pb^{2+} is larger than both Ca^{2+} and Fe^{2+}, however, it shares similar valence chemistry; therefore, transporter proteins involved in moving divalent metals across membranes are capable of translocating lead. These include Ca^{2+} channel, Ca^{2+}-Mg^{2+} ATPase, Ca^{2+}/Na^{+} transporter, and possibly the divalent metal transporter (DMT1) [13, 14]. High levels of dietary calcium or iron have an inverse relationship with blood lead

concentration [15]. This is due to competition to the same transporters in the gastrointestinal (GI) tract between calcium and lead or iron and lead. Additionally, lead absorption is enhanced by dietary calcium depletion or in iron deficiency. Iron deficiency is the most common nutrient deficiency in the world, affecting close to 3 million people in the United States alone. In rat models of iron deficiency, the gastrointestinal absorption of lead is increased due to enhanced binding of lead to iron-binding proteins [16]. The type of lead that enters the body will affect its absorption. Only around 20 % of ingested inorganic lead is absorbed through the GI tract, while nearly all the organic lead is absorbed.

Absorption of inhaled lead occurs occupationally when there are aerosols of particulate lead. Size and solubility of the inhaled particle will determine its deposition in the lung. Large particles (>2.5 μm) are deposited in the ciliated airways and can be transferred by mucociliary transport into the esophagus and swallowed, whereas smaller particles (<1 μm), can be deposited in the alveoli, and be absorbed after extracellular dissolution or ingestion by phagocytic cells. Around 95 % of inhaled submicron inorganic lead is absorbed [17], while larger particles that are swallowed in the mucus have the same absorption as ingested lead.

1.3.2. Distribution

Upon absorption, lead is rapidly taken into the blood, where it accumulates in red blood cells. Lead enters the erythrocytes using multiple mechanisms. Over 90 % of lead enters red blood cells dependent upon bicarbonate (HCO_3) anion exchangers, which is completely blocked by anion exchange inhibitors such as 4,4′-diisothiocyanostilbene-2,2′-disulfonic acid, 4-acetamido-4′-isothiocyanostilbene-2,2′-disulfonic acid, phloretin, furosemide, and bumetanide [18]. The remaining 10 % of lead that enters erythrocytes may enter through Ca^{2+} channels [19]. Lead has been shown to be actively transported out of red blood cells by Ca^{2+}-Mg^{2+}-ATPase [20]. Inside red blood cells, δ-aminolevulinic acid dehydratase (ALAD) is the primary binding site for lead. Binding of lead to ALAD is saturable; with a dissociation constant approximately 1.5 μg/L [21]. Lead also binds to the pyrimidine 5′-nucleotidase [21]. ALAD has the strongest affinity for lead [21], binding up to 85 % of the total lead in the erythrocyte at blood lead levels below 40 μg/dL [22].

While the red blood cell binds the majority of lead in the blood, plasma proteins have been observed to also bind lead. Lead can loosely bind to serum albumin, complex to amino acids and carboxylic acids, bind tightly to circulating metalloproteins, or exist as free ionized lead (Pb^{2+}). Ionized lead has been measured to be the least abundant, with an estimated 1/5000 of total serum lead, as measured by ion-selective lead electrode [23]. Lead in serum that is not bound to albumin complexes with sulfhydryl groups present on proteins (e.g., cysteine) or small molecules (glutathione (GSH) or citrate) [23].

While there are strong binding interactions with proteins in the blood, lead accumulates predominantly in mineralized tissues (bone and teeth). The fraction of lead in the blood is small, serving the purpose to distribute lead to storage

sites or for excretion. Lead has a half-life in blood of adult humans between 28–36 days [24]. This is important as many studies report or make correlations with blood lead levels, which do not accurately estimate total body burden. Mineralized tissues make up the primary site of lead body burden, containing approximately 95 % of body lead in adults and 75 % in children. The process of calcification of bones allows for lead to take the place of calcium in the bone matrix and be stored for the individual's lifetime. Lead trapped in bone is considered to be inert, however, there are conditions that can cause the release of lead back into the blood stream and expose soft tissues (brain, liver, kidneys, etc.). These include pregnancy, lactation, menopause, broken bones, physiologic stress, osteoporosis, calcium deficiency, hyperthyroidism, and kidney disease. Distribution to soft tissues (not mineralized), such as the brain, kidney, and gonads is under 5 % for all tissues. The toxicity observed from lead exposure demonstrates how susceptible the nervous system, kidneys, reproductive system, and immune system are to lead toxicity (to be further discussed below).

1.3.3. Excretion

The excretion of lead is primarily through the kidneys in urine as well as in feces. Molecular mechanisms by which lead is excreted are not well characterized. In an early study, renal plasma clearance was approximated as 20–30 mL/minute in an adult human subject injected with a lead chloride tracer [4]. Lead undergoes glomerular filtration and net tubular reabsorption in mammalian models [25–27]. Interestingly, renal clearance of blood lead increases with increasing blood lead levels above 25 μg/dL [28]. This may be due to a variety of reasons, including lead forming low-molecular weight complexes with proteins and shift its glomerular filtration rate, a saturable reabsorption of lead in the glomerulus leading to less filtration of lead, or maybe an effect of lead-induced nephrotoxicity. As with the absorption of lead in the gastrointestinal tract, the protein transporters involved in lead trafficking in the kidney are thought to be transporters involved in calcium and iron transport. Excretion of lead in feces is less well characterized. Lead may enter the feces either through secretion of lead into bile, gastric fluid, and saliva [4, 24]. The form of lead will determine its excretion route. Inorganic lead is primarily cleared by the kidneys and does not pass through the liver to enter the feces via bile. Organic lead compounds are metabolized in the liver and excreted primarily in the feces complexed to bile.

1.4. Mechanisms of Lead Toxicity

While lead targets many organ systems in mammals, many of its diverse toxic effects share common mechanisms of action. Lead mimics the action of calcium and iron in several systems, which can perturb tightly regulated homeostatic processes. For example, the protein kinase C (PKC) family of kinases is composed of diacylglycerol- and/or calcium-dependent enzymes responsible for signaling through a variety of receptors. Calcium-dependent PKCs have a specific

C2 calcium-binding protein domain which also binds lead. By binding lead, the Ca-dependent PKCs can be activated or inactivated depending on the lead exposure. Low concentrations of lead causes activation of PKC, while high concentrations of lead antagonizes calcium and binds to a different site on the enzyme leading to inhibition [29, 30]. Lead can displace metals in metalloproteins, leading to alteration in protein function. Lead inhibits the Cys_2/His_2 zinc finger transcription factors TFIIIA and Sp1 *in vitro* competing for zinc binding sites [31, 32].

Lead is a potent inducer of oxidative stress, leading to damage to lipids and DNA. Lead decreases the activity of several antioxidant enzymes, creating an oxidizing environment. Inhibition of Cu/Zn-superoxide dismutase (SOD), Mn-SOD, and glutathione peroxidase (GPx) 1 and GPx4 following lead exposure is primarily due to lead substituting for the divalent metals contained in the enzymes. Lead also decreases the most abundant reactive thiol in cells, glutathione leading to increased oxidant burden. Finally, lead severely alters mitochondrial function. Lead enters the mitochondria using the Ca^{2+} uniporter. Ca^{2+} dysregulation can induce the generation of reactive oxygen species (ROS), lose mitochondrial membrane potential, and initiate apoptosis. Lead also decreases cellular ATP levels by inhibiting the Na^{+}/K^{+} ATPase activity [33].

2. NEUROTOXICITY OF LEAD

Lead enters the brain through both the blood-cerebrospinal fluid (CSF) barrier and the blood-brain barrier (BBB). Both the BBB and blood-CSF barrier are targets of lead toxicity. Lead causes the microvasculature of these barriers to become leaky, resulting in increased permeability of the barriers, brain swelling, herniation, ventricular compression, petechial and cerebral hemorrhages, thrombosis, and arteriosclerosis [34]. Additionally, the endothelial cells in the BBB microvasculature and the choroid plexus cells that comprise the blood-CSF barrier accumulate lead. This allows for an alteration of calcium homeostasis and signaling in these cells. Lead activates protein kinase C signaling by disrupting intracellular Ca^{2+} levels, which in turn increases endothelial permeability [35]. Accumulation of lead by the choroid plexus causes a decrease in transthyretin production [36], which disrupts thyroid hormone signaling.

While the nervous system does not accumulate similar levels of lead that mineralized tissue does, lead severely affects these tissues. In our discussion on the neurotoxicity of lead, we will highlight three distinct facets of lead neurotoxicity: damage to the developing brain, damage to the adult brain and peripheral neuronal effects.

2.1. Damage to the Adult Brain

Damage to the adult brain by lead is determined by the dose of lead and duration of lead an individual is exposed to. The most severe effect of lead on the developed brain is encephalopathy. Symptoms that initially develop within weeks

of initial exposure include dullness, poor attention span, irritability, headache, muscular tremor, hallucinations, and memory loss. As the condition worsens, one can also develop delirium, convulsions, paralysis, coma, and death [37]. Encephalopathy occurs in adults following extremely high lead exposure, with blood lead levels reaching over 400 μg/dL.

Neurobehavioral and psychiatric effects of lead have been observed in adults exposed to lead both occupationally and environmentally. In lead workers numerous reports describe malaise, forgetfulness, irritability, lethargy, headache, fatigue, impotence, decreased libido, dizziness, weakness, and paresthesia in individuals with blood lead levels from 40 to 120 μg/dL following either acute or chronic exposures. Psychiatric effects of lead include disturbances in reaction time, visual motor performance, hand dexterity, IQ test and cognitive performance, nervousness, mood, or coping ability [38–41]. These symptoms were observed in lead workers with blood lead levels of 50–80 μg/dL. Additionally, lead workers were found to exhibit greater levels of conflict in interpersonal relationships compared with unexposed workers [42]. Similar losses in neurobehavioral and psychiatric function have been observed in environmental exposures to lead. A study examining 141 male participants in the Normative Aging Study found blood and bone levels of lead correlated with memory loss, decreased reaction time, and decreased cognitive skills [43]. Further analysis of the Normative Aging Study participants found patellar lead levels associated with anxiety, depression, and phobic anxiety in elderly individuals (mean age 67.1 years) [44].

Lead causes cognitive impairment and has been associated with neurodegenerative diseases, such as Alzheimer's disease (AD). Cognitive deficits measured in lead-exposed workers include impaired visual contrast sensitivity, decrements in visuo-spatial abilities and executive functions related to the prefrontal cortex, impaired central information processing and short-term verbal memory [45–47]. Environmentally exposed individuals show similar trends in cognitive losses from lead. In a study examining participants in the Normative Aging Study, both blood and bone lead levels were associated with poor cognitive test performance [48]. Similar findings were described in diverse urban-dwelling population [49], however, in this population the normal age-related decrements in cognitive function were far worse in the lead-exposed individuals. High levels of both bone and blood lead levels are associated with decreased spatial copying skills, reduced pattern memory, and declines in cognitive functions [43, 50] from studies conducted using participants of the Veteran's Affairs normative aging study. This is a longitudinal cohort of men disease-free at time of recruitment in 1963. As lead affects cognition, it is currently being investigated whether lead is a risk factor for the development of AD. However, these studies are performed primarily in laboratory animals, as there have not been studies in lead-exposed workers correlating to development of AD. Pb exposure increases amyloid precursor protein (APP) mRNA and aggregated Aβ in rats, and increased amyloidogenesis, senile plaque deposition and up-regulates APP proteins in nonhuman primates [51–53]. Recent studies in mice show that early life exposure to lead enhances the expression of AD associated protein tau and alters epigenetic markers associated with the development of AD [54, 55].

2.2. Damage to the Developing Brain

The developing brain of children is highly susceptible to lead and more vulnerable than the adult brain. The high susceptibility and vulnerability as compared to adults is due to differences in exposure and toxicokinetics. Outside of occupational settings, children are more likely to have contact with contaminated surfaces due to playing on the ground and hand-to-mouth exposures. As mentioned previously, children absorb a larger fraction of lead from their GI tract. The brain of an adult is fully developed, however, in a developing brain there are many activities in which lead can interfere. Lead has been shown to interrupt trimming and pruning of synapses, migration of neurons, and formation of neuron-glia interactions, all of which can result in failure to establish the proper connections between structures and lead to functional deficits. Time of exposure will determine the extent of damage as brain development occurs over a long period of time and different brain areas mature at varying rates. This means that exposure *in utero* can have a completely different effect on the developing brain than a pediatric exposure.

Similar to adults, high level exposure to lead in children may result in encephalopathy. Encephalopathy in children has been observed with blood lead levels between 60–300 μg/dL. Symptomatically, children with encephalopathy present with hyperirritability, ataxia, convulsions, stupor, coma, and death. Pathologically debilitating and fatal encephalopathy in lead-exposed children is characterized by endothelial cell swelling and necrosis of the cerebral and cerebellar capillaries, capillary leakage and cerebral edema, loss of neuronal cells, cytoplasmic vacuolization, interstitial edema, and demyelination of nerve fibers. While encephalopathy is observed with high lead exposure, many nonfatal neurobehavioral effects occur at much lower blood lead levels. There is debate as to what the lowest observable adverse effect level (LOAEL) of lead on the nervous system is in children and whether there is a no observable adverse effect level (NOAEL).

Lead exposure has been associated with delinquent behavior and decrements in IQ. Studies of lead effects on IQ have shown that low exposures of lead (<60 μg/dL blood lead level) early in life can cause a decrease in IQ around the time children enter school even though at school age blood lead levels are lower than at the time of exposure. For example, in a study of 780 children treated for elevated blood lead levels (20–44 μg/dL) approximately 2 years of age that were followed until the age of 7 years, serial IQ tests showed decreases while lead level at age 7 was 8 μg/dL [56]. Furthermore, *in utero* exposures to lead as early as during the first trimester of pregnancy have been associated with decreases in intelligence scores [57]. Areas of intelligence that have shown decrements include arithmetic skills, reading skills, nonverbal reasoning, reaction time, visual-motor integration, fine motor skills, attention, and short-term memory. While multiple studies have examined the effects of lead on IQ in various locations around the globe, there are variables that affect the effects of lead. These include gender, socio-economic status, prenatal smoking, maternal age, and prenatal alcohol use [58]. The amount of IQ points that are decreased in lead-exposed children on an individual looks small; however the shift in a population's

IQ by lead is more detrimental, with fewer individuals in the higher end of the IQ spectrum and more individuals in the lower end.

The effects of lead on antisocial behavior have been investigated in school children. Studies performed on children in the Pittsburgh (PA) school system have associated bone lead levels with aggression, attention, and delinquency as well as with arrest and adjudication as a delinquent in the juvenile court system [59]. Prenatal lead exposure has also been associated with delinquent behavior and drug use in teenagers [60]. Lead air pollution from gasoline has been associated with incidence of homicides and violent crimes in the Unites States [61, 62] after adjusting for unemployment and percent of population in the high-crime age group.

2.3. Peripheral Nervous System Effects

A peripheral neuropathy is a classic symptom of lead toxicity. These were first characterized in house painters and other lead workers; manifestations including footdrop and wrist drop. Other symptoms may include extensor weakness of the distal upper limbs and weakness in dorsiflexion of the foot, which was measured in workers from a battery recycling plant [63]. Motor nerve dysfunction is typically assessed by nerve conduction velocities (NCV) of electrically stimulated nerves in arms or legs. Several studies have assessed NCV in workers exposed to lead occupationally. Decreased NCV have been found in median and ulnar nerves after 1 year of exposure to lead (blood lead levels 30–48 μg/dL) in newly hired employees [64]. Long-term exposures (1–28 years) to lead have shown decreased NCV in ulnar and median nerves, but not in fibular or sural nerves [65]. Decreases in NCV have also been observed in children exposed to lead environmentally. Damage to children's peripheral nerves occurs at blood lead levels similar to that of adults (20–30 μg/dL) [66].

It is important to note that the decreases in NCV that have been recorded fall within the range of normal variation, therefore, the effects of lead on peripheral nerves may not be clinically significant for a particular individual, but are significant when viewed over a population. Additionally, while changes in NCV usually indicate neurotoxicity, significant nerve damage can occur without an effect on conduction velocity.

Of the different kinds of peripheral nerves (sensory, motor, etc.), the motor neurons are more susceptible to lead. This has been speculated to be due to different structures of the neurons, however it has not been substantially confirmed. Lead induces Schwann cell degeneration, leading to segmental demyelination and/or axonal degeneration. Wallerian degeneration of posterior roots of the sciatic and tibial nerves has been observed.

3. IMMUNO- AND HEMATOTOXICITY OF LEAD

Once absorbed, lead enters the circulatory system and accumulates in erythrocytes. As little as 1 % of blood lead resides in the plasma. Around 80 % of lead in erythrocytes is bound to ALAD [67]. ALAD catalyzes the second step in the

synthesis of porphyrin and heme, and is a metalloenzyme, which utilizes zinc in its catalytic reaction. Lead has 20-fold greater affinity for ALAD *versus* zinc, which leads to the replacement of zinc with lead, thus inhibiting the reaction. There are two polymorphic alleles of ALAD (ALAD 1 and ALAD 2) and therefore, three possible genotypes: ALAD 1-1, ALAD 1-2, and ALAD 2-2 [68].

Higher lead blood levels have been observed in individuals with the ALAD 1-2 and ALAD 2-2 genotypes as compared to similarly exposed individuals with the ALAD 1-1 genotype [69–71] This suggests that the ALAD 2 allele may have a higher binding affinity for lead than the ALAD 1 allele [72], which may make carriers for this allele have a higher body burden of lead. Several studies have dealt with this hypothesis, investigating whether ALAD genotypes are associated with differences in partitioning of lead between red blood cells and plasma, differences in distribution of lead to other tissue compartments, or altered susceptibility to lead toxicity. To date there has been no association with higher susceptibility to lead in ALAD 2 carrying individuals [73–75].

Lead exposure is associated with high levels of oxidative stress in the blood. In a study on workers employed in zinc and lead production facilities, erythrocyte and leukocyte malondialdehyde (MDA) levels positively correlated with blood lead levels [76]. Similarly, in a study conducted on children with no reported accidental exposure to lead, there was a strong correlation between blood lead levels and increased MDA levels and decreased GSH levels [77]. There was also higher catalase activity in erythrocytes in the higher lead-exposed children, possibly due to high levels of H_2O_2 in their blood.

Elevated catalase activity, increased MDA, and decreased GSH levels have also been observed in rats exposed to 2000 ppm lead for 9 weeks [78]. The mechanisms by which lead causes oxidative stress are both enzymatic and non-enzymatic. The binding of lead to functional thiol groups in antioxidant enzymes, such as glutathione reductase, results in diminished enzymatic activity, and therefore increased ROS [79]. Lower selenium levels have been observed in workers chronically exposed to lead, which results in decreased activity of the selenoenzyme glutathione peroxidase [80]. Additionally, inhibition of ALAD by lead increases the levels of its substrate ALA and generates H_2O_2, $O_2^{-\bullet}$, and $OH^{\bullet}$ [81]. ROS are produced as a result of lead interacting with oxyhemoglobin, allowing for autooxidation of the protein [82]. Interestingly, lead can either increase or suppress blood levels of the antioxidant enzymes superoxide dismutase and catalase. Pb exposure causes an increase in the activity of both enzymes due to elevated ROS that the enzymes detoxify. High levels of lead can result in the replacement of the metals inside the enzymes (such as zinc in SOD), which suppresses the activities of these enzymes.

3.1. Anemia

Lead has been shown to cause anemia at levels that were once considered safe ($< 10\ \mu g/dL$). Anemia results from the direct inhibition of ALAD by lead, thereby increasing the activity of the upstream rate-limiting enzyme of the pathway,

δ-aminolevulinic acid synthetase (ALAS), which is normally feedback inhibited by the newly synthesized heme. This results in increased urinary porphyrins, coproporphyrin, and δ-aminolevulinic acid (ALA); increased blood and plasma ALA; and increased erythrocyte protoporphyrin (EP). ALA, in particular has been used for biomonitoring lead in exposed individuals. Lead also shortens the lifespan of red blood cells. The anemia of acute high-level lead exposure is characterized as hemolytic, while the anemia of chronic lead intoxication is hypochromic and normocytic or microcytic with a reticulocytosis.

3.2. Immunosuppression

Lead has been shown to be an immunosuppressant by impairing antibody production and altering the number of immune cells. As an immunosuppressant, lead levels between 20 and 85 μg/100 mL are associated with an increased susceptibility to colds and influenza infections [83]. Lead affects the levels of circulating antibodies in experimental animals, especially IgG. In humans the data is contradictory. Four independent studies performed in lead factory workers show no significant changes in serum IgG, IgA, or IgM [84–87], however, Ewers et al. [83] found decreased salivary IgA and Heo et al. [88] described decreased serum IgE levels in lead-exposed workers. B lymphocytes, which produce antibodies have been observed to be increased in workers with blood lead levels > 50 mg/100 mL [89].

Lead affects the number and function of immune cells. In studies examining immune cell function, lead decreased T-cell lymphocyte proliferation to phytohemagglutinin or concanavalin A and did not affect natural killer cell activity in three groups of workers (n = 84) who had mean blood lead levels of 6.5, 17.8, and 128 μg/dL [90]. However, studies performed in firearm instructors with mean blood lead levels between 34.8–39 μg/dL found no alterations in T-cell or NK cell activities in response to phytomegaglutinin or tetanus toxoid [85, 86]. The T-cell subpopulations are also altered by lead. Both $CD3^+$ and $CD4^+$ cells were found to be decreased in workers with a mean blood lead level of 74.8 μg/dL [84, 87]. $CD8^+$ cells, along with NK cells and B-cells were unaffected in these populations [89]. Lead's effects on macrophages were investigated in a small study of 10 occupationally-exposed workers (mean PbB of 33 μg/dL), showing impaired chemotaxis [91].

4. NEPHROTOXICITY OF LEAD

4.1. Nephropathies

Lead exposure can produce renal dysfunction upon acute or chronic exposure. Acute lead-induced nephropathy is characterized by Fanconi syndrome, a generalized deficit in tubular transport that allows for the transport of glucose, amino

acids, uric acid, phosphate, and bicarbonate into the urine rather than being reabsorbed. The continual loss of bicarbonate may result in renal tubular acidosis, while the loss of phosphates can lead to osteomalacia (bone demineralization), a process than can release lead back into circulation and exacerbate damage. Several studies in lead-exposed workers have shown a linear correlation between blood lead levels and renal dysfunction.

Kidney damage has been observed at blood lead levels in the range >60 μg/dL blood, but damage has also been reported at lower levels [92], suggesting that there may not be a level at which lead has no adverse effect on kidney function. It is important to note, blood lead levels are a poor indicator of body lead burden, whereas bone lead content may offer a better correlation. However, there are few studies which investigated the correlation between bone lead levels and kidney function in human individuals. Chronic exposure to low levels of lead has shown associations with decreased renal function in longitudinal studies. The Normative Aging Study, a population that has been continuously monitored since 1963, has shown that a 10 μg/dL increase in blood lead levels results in 9 % reduction in creatinine clearance [93]. Additionally it has been found that a 10-fold increase in blood lead levels can predict a 0.08 mg/100 mL increase in serum creatinine levels [94]. Additionally, chronic exposure to lead from childhood has been shown to cause chronic renal disease later in life.

Pathologically, the damage done to the kidney by lead is primarily to the proximal tubules of the nephron. While the exact mechanisms for toxicity are not fully appreciated, lead may damage the tubule epithelium in four ways. First, kidney damage associated with lead exposure is characterized by an accumulation of nuclear inclusion bodies in the proximal tubule cells. These inclusion bodies are intracellular protein aggregates composed of lead-protein complexes. Second, lead accumulates in the mitochondria of the tubule cells, which impairs energy production. As the proximal tubule is involved in the active transport of small molecules, decreases in ATP production severely affects the functional ability of the tubule cells. Third, lead exposure increases oxidative stress in the kidney. Lipid peroxidation byproducts have been observed in *in vivo* experiments and in workers exposed to lead [79, 95]. ROS react with lipids to produce oxidation byproducts, which results in loss of membrane integrity and dampens tubule function. Increased levels of renal thiobarbituric acid reactive substances (TBARS), a lipid peroxidation byproduct, has been observed with both acute lead exposure in mice (10 and 150 mg/kg body weight for 24 hours) [96], and chronic exposure of lead in rats (8 weeks of 500 mg lead/L drinking water or oral dose of 50 mg lead/kg body weight for 40 days) [97, 98]. Lead exposure has been shown to increase reactive nitrogen species in the kidney as a result of activation of inducible nitric oxide synthase (iNOS) [99]. The antioxidant enzymes SOD and catalase have been observed in kidneys of chronically exposed rodents [100, 101], which may represent a compensatory mechanism for the lead-induced oxidative stress. Fourth, alterations in mitochondrial function and increased oxidative stress are both triggers for apoptosis. Studies by Sujatha et al. have shown that treatment of rats with lead acetate over 12 weeks increased the number of apoptotic bodies in proximal tubular cells [102]. The use of the calci-

um channel blockers verapamil and nimodipine in mice prevented nephrotoxicity of lead by decreasing the amount of apoptosis [103], suggesting that lead-induced apoptosis is calcium-dependent. Activation of the PI3K/AKT signaling pathway has been shown to be protective against nephrotoxicity and apoptosis in lead-exposed rats [104].

4.2. Effects on Blood Pressure

Numerous experimental studies in animals have shown clear evidence that chronic exposure to low lead levels causes arterial hypertension that persists long after the cessation of exposure [105]. However, the precise mechanisms associated with the hypertensive effect of low chronic exposure to environmental lead are unknown.

Chronic lead exposure causes hypertension in rats through diverse mechanisms. Lead affects the adrenergic system, increasing central sympathetic nervous system activity, elevating plasma norepinephrine, leading to increased blood pressure [106–108]. Increased sympathetic nervous system activity activates the renin-angiotensin-aldosterone system, increasing plasma renin activity, leading to increased plasma angiotensin-converting-enzyme (ACE), which converts angiotensin I to angiotensin II, a vasoconstricting peptide that increases blood pressure. Lead also increases plasma aldosterone levels in rats, which increase blood volume and pressure [109, 110]. Lead also decreases the vasodilator nitric oxide (NO) in rats [111, 112]. Additionally, lead exposure in rats causes the expression of guanylate cyclase to decrease [113]. Guanylate cyclase is an enzyme that produces cyclic GMP, which mediates NO-induced vasodilation.

Epidemiological studies in occupational lead exposures have shown correlations between blood lead levels and blood pressure. A study conducted in 220 former lead battery workers in New Jersey showed a strong association between blood lead and hypertension in 30 % of the study population. These individuals possessed a particular variant of the sodium-potassium adenosine triphosphatase (Na^+-K^+ATPase) gene (ATP1A2), which is more prevalent among African Americans than Caucasians [114]. How lead interacts with ATP1A2 to produce higher blood pressure has yet to be determined.

Epidemiological studies on exposures to low levels of lead and their effects on blood pressure are discussed in Section 7.

5. REPRODUCTIVE TOXICITY OF LEAD

5.1. Effects on Females

The effects of lead on the female reproductive system have been documented since antiquity. At very high blood lead levels, lead is a powerful abortifacient. At lower levels ($> 10\ \mu g/100\ mL$), lead has been associated with stillbirths, mis-

carriages, and reduced fertility [115–117]. It is estimated that maternal blood lead levels of 5–9 μg/100 mL doubles the risk of spontaneous abortion [118]. Lead is extremely genotoxic to the developing fetus, due to the ability of lead to cause chromosomal aberrations, chromosome and chromatid breaks in the fetus. Lead exposure also increases the risk of preterm delivery and causes lower birth weight in infants [119]. How this occurs has yet to be determined, although it has been observed that lead does not cause disruption of membranes [120].

5.2. Effects on Males

Lead is a strong spermicidal agent. Blood lead levels in men > 40 μg/100 mL are associated with low libido, low semen volume and sperm counts, increased abnormal sperm morphology, and decreased sperm motility [121, 122]. Decreased endocrine function in males is related to duration of exposure [123]. In a study of lead workers from the UK, Belgium, and Italy, there was a 49 % reduction in the median sperm concentration in men with blood lead levels > 50 μg/100 mL with a likely threshold for effects of 44 μg/100 mL [124]. Examining physical characteristics of the specimens revealed that there was deterioration in sperm chromatin in men with the highest concentration of lead in spermatozoa [124]. Likewise, in a different study conducted in the UK, 33 % of occupationally exposed men had both low sperm counts and decreased motility [125].

6. OSTEOTOXICITY OF LEAD

Bone is the major site of lead distribution in the mammalian body, storing around 95 % of lead in adult tissues and around 70 % in children. Lead gets deposited in the bone during the process of calcification. Bone calcification is a process by which calcium is deposited in the formation of bone, where calcium forms a phosphate salt, called hydroxyapatite, which constitutes the primary crystalline matrix of bone. When an individual is exposed to lead, lead replaces calcium, forming highly stable phosphate salts that deposit in the forming bone. During bone remodeling, a process that repairs bone or mobilized calcium, lead can be released into the blood [126, 127]. Pregnancy, lactation, and menopause are times when there is increased bone resorption to allow for increased calcium mobilization, resulting in increased lead levels in exposed individuals. Disease conditions such as osteoporosis also will promote release of lead from bone. Lead is found highly concentrated on bone surfaces where growth and remodeling are highly active. During infancy and childhood the trabecular bone has the most growth, whereas in adults both the trabecular bone and cortical bone have more active calcification and remodeling. Individuals exposed to high levels of lead (> 40 μg/dL lead in blood) report muscle weakness, frequent pain, soreness, cramps and joint pain [128–131], suggesting that lead may damage the skeletal system.

Damage to the skeletal system by lead progresses as one ages. Children exposed prenatally to lead show delayed skeletal muscle development [132]. High levels of lead have been correlated with decrements in skeletal growth, such as height, weight, and chest circumference [133, 134]. Adult lead exposure has been correlated to osteoporosis, delayed fracture healing and osteoarthritis [135]. *In vivo* studies performed in rodents have observed similar effects of lead on bones. Oral exposure of rats to lead impairs normal bone growth and remodeling. The bones of exposed rats show decreased bone density and calcium content, decreased trabecular bone volume, increased bone resorption activity, and altered growth plate morphology. However, rats appear to be less sensitive than humans to lead's effects on bone, and therefore require larger doses to observe analogous effects. Mice, in contrast, are more sensitive to lead's effects on bone than rats. Using environmentally relevant doses of lead, Carmouche et al. found that mice exposed to lead had delays in fracture healing [136]. Furthermore, at higher doses lead induced fibrous nonunions by the progression of endochondral ossification [136].

At the cellular level, lead disrupts the function of several bone cell types. Osteoblasts, the cells responsible for bone formation, show disrupted intracellular calcium and 1,25-dihydroxyvitamin D signaling [137]. Lead also inhibits the synthesis of osteocalcin, a protein constituent of bone that is involved in normal mineralization of the tissue. Indeed, reduced plasma levels of osteocalcin have been observed in children exposed to lead [138]. Chondrocytes, cells that produce cartilage matrix, show decreased transforming growth factor β (TGF-β) activity upon lead exposure [139]. This can alter bone morphogenic protein (BMP) expression, and therefore reduce collagen production and cause an osteoarthritis phenotype [139, 140]. Lead inclusion bodies are commonly found in the cytoplasm and nuclei of osteoclasts, but not other bone cells, following *in vivo* lead exposure [138]. In mesenchymal stem cells, lead increases TGF-β signaling, allowing for increased chondrogenesis [141]

Interestingly, a study that investigated the association between lead exposure and bone density found that subjects with high cumulative lead exposure had a higher bone mineral density than subjects with low-lead cumulative exposure [142]. The authors speculated that lead accelerated skeletal maturation by inhibiting proteins that decrease the rate of maturation of chondrocytes in endochondral bone formation [143]. The increased bone volume was accompanied by evaluations in osteoclast (cells responsible for bone resorption) numbers with high Pb exposure, but a deficiency in osteoclastic activity. These studies highlight the dose-dependent nature of lead exposure on bone health.

Teeth are another mineralized tissue affected by lead. Lead exposure has been associated with periodontal bone loss. Analysis in the NHANES III cohort found blood lead levels of 2.5 μg/dL correlate with periodontal bone loss in 10,033 people, 20–69 years of age [144]. Additionally, lead exposure increases the occurrence of dental caries. In a study that examined blood lead levels and dental caries in over 24,000 people, 6541 of which were children between the ages of 2 and 11, there was an increased number of dental caries with blood lead levels of 2.9 μg/dL in children 2–5 years of age and 2.1 μg/dL in children 6–11 years of age [145].

7. EPIDEMIOLOGICAL STUDIES AND VARIABLES ASSOCIATED WITH LOW BLOOD LEAD LEVELS

7.1. Factors Associated with Blood Lead Levels

Several studies have reported that lead concentration in the environment has decreased since regulations were enacted to ban the use of lead in gasoline, in paints, and in soldering of cans [146]. However, lead exposure remains a public health concern because lead has been widely dispersed in the environment as a result of industrial use. In addition, some populations are still exposed to potential sources of lead as in food and beverages, medicines, and tobacco [147, 148].

Despite the decline in environmental lead concentrations observed over the last decades, studies evaluating the risk factors for lead exposure and the adverse effects of the metal in the general population, have reported positive associations between lead exposure and some morbidities, including kidney disease, hypertension, and peripheral arterial disease. Therefore, studies on risk factors in the general population represent an invaluable tool for identifying risk factors and trends of lead concentrations [146, 149].

Most studies with distinct populations have found significantly increased BLL in older *versus* younger individuals, and in men *versus* women, as shown in Table 1. Higher BLL associated with older age may reflect lead stored over decades in the bones and then released to the bloodstream due to absorption and resorption processes [150, 151]. Men have been reported to have higher BLL than women, possibly as a consequence of greater frequency of smoking and drinking habits. In addition, men usually have higher concentrations of hemoglobin than women, and lead is mostly bound to erythrocytes [152].

Combined with age and sex, smoking and alcohol consumption may significantly contribute to variations in BLL in the general population. Falq et al. [153] reported that 51 % of the total variations in BLL might be accounted for by older age, sex (male), as well as drinking and smoking habits. The same authors also reported increased BLL among people drinking tap water compared with those drinking bottled water (GM = 2.71 μg/dL; 2.59–2.84) and (2.47 μg/dL; 2.36–2.59), respectively.

Several studies found positive associations between BLL and the dietary consumption of shellfish and crustaceans, red meat, and milk. Crustaceans and mollusks represent food products with considerable lead contamination, and individuals consuming these foods have higher BLL than non-consumers [153, 154]. Almeida Lopes et al. [155] observed a positive association between BLL and more frequent red meat consumption in the unadjusted analysis, while the adjusted findings revealed a trend towards significant association in adults 40 years or older eating red meat five to seven days a week (ratio GM = 1.18; 95 % CI, 0.99–1.40), compared with those never eating red meat (reference group). This study also showed an inverse association between BLL and frequency of milk consumption. In the adjusted analysis, BLL were lower in people drinking milk five to seven days a week (ratio GM = 0.74; 95 % CI, 0.68–0.80), compared with non-consumers of milk.

Table 1. Epidemiological Studies of Lead Exposure in General Populations.

Ref.	City, Country	Study design Statistical analysis	Population		Lead assessment Mean ± SD in μg/dL	Main results
			Setting Number of subjects	Age range or mean (years)		
[161]	Monterrey, Mexico	Cross-sectional *t*-Student and ANOVA	Monterrey area 671	10–80	BLL Workers: male (14.38); female (13.11) Non-workers: male (14.08); female (13.35) Smokers: 15.11 Non-smokers: 12.92	No significant differences were found between BLL and alcoholism as well as "lead glazed pottery" used as food ware. Sex, smoking, and place of residence were significantly associated with BLL
[156]	Italy	Cross-sectional, AM, SD, Fisher's test and multiple regression analysis	1164 adults of seven different regions in Italy	18–64	BLL Males: 4.51 Females: 3.06	Sex, age, BMI, outdoor sport practice, alcohol intake, and smoking habits were associated with BLL
[162]	Germany	Cross-sectional Median, GM and AM	4646 adults	18–69	BLL GM: 3.07	BLL were significantly higher in men than in women
[163]	Canada	Cross-sectional Based on weighted data, bootstrap technique	8 data collection sites in Canada 2678 subjects	6–79	BLL 6 to 19 years: GM (0.88) 20 to 79 years: GM (1.50) Overall: GM (1.37)	BLL have fallen substantially since 1978 in the Canadian population. BLL were slightly lower than NHANES (2001–2002) data for ≥ 20 years (1.56) and than 3.07 μg/dL of GerES (1988 and 2003–2006)

[164]	Antwerp and Ghent cities, Belgium	Cross-sectional Weighted analysis, ANOVA and multiple regression analysis	1679 randomly selected adolescents	13.8–16.5	BLL 2.17	Adolescents of Antwerp region had higher exposure to heavy metals (BLL = 2.75) compared to the reference mean value of 2.17
[153]	France	Cross-sectional Multivariate analysis	Adults aged 18–74 2029 subjects	44.9	BLL GM: 2.59 (2.51–2.67)	Older age, male sex, smoking habits, alcohol intake, occupation, birth place, age of housing, leisure activity, type of drinking water, and shellfish/crustacean consumption were positively associated with BLL
[165]	Mexico City	Prospective study *t*-test, Pearson's chi-square test, simple and multiple linear regression analysis	Mother-child pairs drawn from longitudinal study 457 mothers	25.6 ± 5.4	Tibia 9.3 (3.3–16.1 μg/g) Patella 11.6 (4.5–19.9 μg/g)	Maternal tibia lead was significantly associated with SBP and DBP among female children
[166]	South Korea	Cross-sectional Based on weighted data, GM, AM, *t*-test and ANOVA	Non-institutionalized Korean adults 5087 subjects	≥20	BLL 1.91 (1.82–2.01)	GM BLL increased with age, was higher in men than in women, and in smokers compared with non-smokers
[167]	Czech Republic	Cross-sectional, AM, GM, median, percentiles and range	Urban/suburban population Adults blood donors: 4472 Children: 3798 Breastfeeding primiparas: 5667	Adults: 18–58 Children: 8–10	BLL and urine Male adults: 2.3 Female adults: 1.4 Boys: 2.2 Girls: 1.9	Men had higher BLL than women. BLL declined in the Czech population, but not sufficient for public health purposes

Ref.	City, Country	Study design Statistical analysis	Population Setting Number of subjects	Age range or mean (years)	Lead assessment Mean ± SD in μg/dL	Main results
[168]	United States	Cross-sectional analysis of the longitudinal study NHANES (2009–2010); Median, 95 % percentile	Non-institutionalized US population 8793 subjects	≥ 1	BLL GM: 1.1 (0.18 to 43.52)	BLL has declined comparing with previous NHANES data
[169]	Spain	Cross-sectional Weighted and multivariate analysis	Volunteers workers residing in Spain for five years or more 1880 subjects	≥ 16	BLL GM: 2.40 (2.29–2.51)	Older age, male sex and occupational background were positively associated with BLL. Small differences in BLL were found among distinct geographical areas
[155]	Brazil	Cross-sectional Student's *t*-test, Kruskal-Wallis test and multivariable analysis	Randomly selected Brazilian adults aged ≥ 40 959	54.6	BLL GM: 1.97	BLL were positively associated with male sex, older age, non-white participants, less frequent consumption of milk, with drinking and smoking habits, and with occupation background. Spatial analysis showed that subjects residing in areas with more Pb industries had higher BLL than those living in other areas

Abbreviations: SD standard deviation, BLL blood lead levels, AM arithmetic mean, BMI body masss index, GM geometric mean, NHANES National Health and Nutrition Examination Survey, GerES German Environmental Survey III and IV, SBP systolic blood pressure, DBP diastolic blood pressure, CDC Center for Disease Control and Prevention, US United States.

Other factors contributing to higher BLL were place of residence, including age of dwelling, and leisure activities exposing people to lead, such as renovation of old houses, painting, pottery, shooting and outdoor sports activities. Among French adults, a difference of 3.5 μg/dL higher BLL were found in those who reported several leisure activities [153]. In addition, higher BLL were found in subjects who practiced outdoors sports compared with those who did not (5.01 μg/dL and 3.74 μg/dL, $p < 0.0001$), respectively [156] (see also Table 1).

7.2. Lead Exposure and Blood Pressure

The hypertensive effects of lead have been widely documented both in workers exposed to high concentrations of lead as well as in experimental animals chronically exposed to high levels of lead [157].

The association between lead exposure and blood pressure has been found in populations with diverse geographic, ethnic, and socioeconomic background. Residual confounding by socioeconomic variables is a concern with the interpretation of the results; however, studies that have adjusted for a variety of socioeconomic indicators have identified an association between lead exposure and blood pressure [158].

Table 2 shows that the association between BLL and elevated blood pressure is inherent not only in cross-sectional, but also in longitudinal studies. These studies establish that changes in BLL result in elevated systolic and diastolic blood pressure. Increased risk for hypertension was associated with blood lead levels, with higher risks in postmenopausal women than in premenopausal women [159]. Additionally, it has been shown that environmental lead exposure can increase blood pressure during pregnancy, labor, and delivery [160]. The association between lead exposure and blood pressure may be underestimated because of errors in measurements of blood pressure. Single measurements are not as reproducible as multiple measurements or 24-hour ambulatory measurements, which many studies have performed.

Sufficient evidence exists to infer a causal relationship between lead exposure and high blood pressure. However, further research is needed to determine the precise dose–response relationship, the relevant mechanisms of lead toxicity at environmental levels of exposure, and whether the magnitude of the association is different in children or in other vulnerable population subgroups [158].

8. CONCLUDING REMARKS

Lead is a highly toxic metal that is regulated to prevent exposures in the work place. Environmental exposures to lead remain a continued problem in communities with old homes and water systems. The recent mass exposure to lead in drinking water in Flint, Michigan (USA), illustrates the importance of monitoring environmental lead levels.

Table 2. Epidemiological Studies of Lead Exposure and Blood Pressure in General Populations.

Ref.	City, Country	Study design Statistical analysis	Population		Lead assessment mean ± SD in µg/dL or range in µg/g (bone)	Outcome	Change in BLL (µg/dL)[a]	Change in mm Hg (95 % CI)[a]	Main results
			Setting	Age range or mean (years)					
[170]	United States	Longitudinal Multiple linear regression, multiple logistic regression	Civilian, NI US population NHANES II (1976–1980) 564 white male	40–59	BLL 16.7 (1976) 10.5 (1985)	SBP DBP Fatal/ nonfatal MI Fatal/ nonfatal stroke Death from all causes	↓37 % (1976 to 1980)	↓17.5 % in white males with HP	BLL were significantly associated with both SBP and DBP. The ↓37 % in mean BLL resulted in 17.5 % fewer white males with HP, ↓4.7 % and ↓6.7 % in incident fatal/nonfatal MI and stroke
[171]	Boston, MA, United States	Longitudinal Multivariate analysis	Policemen 89	46	BLL <20: 36 men 20–29: 33 men ≥30: 26 men	SBP DBP	20–29 ≥30	SBP: ↑5.8 (90 % CI, 1.5, 11.5)	High BLPL (≥30 µg/dL) were statistically associated with SBP
[172]	United States	Cross-sectional Correlation and regression analysis	Civilian, NI US population NHANES II (1976–1980)	12–74	BLL 2.45	SBP DBP HP	14–30	SBP: ↑7 DBP: ↑3	BLL were significantly associated with SBP and DBP in males but not in females
[173]	Zutphen, Netherlands	Longitudinal Means, SD, correlation analysis, analysis of variance, multiple	152 random sampled men	57–76	BLL 18.3 ± 7.4	SBP DBP CHD	↑1.0	SBP: ↑0.6 DBP: ↑0.3	BLL was significantly associated with SBP and DBP. The relation was stronger for SBP than for DBP

		regression analysis, Mantel-Haenszel test and Cox survival regression							
[174]	Unites States	Cross-sectional Regression analysis	Civilian, NI US population NHANES II (1976–1980) 9932 people	20–74	BLL –	SBP DBP	↓18 to 10	↓DBP by 2 mm Hg	BLL was significantly associated with SBP and DBP even after adjustment
[175]	San Francisco, United States	Cross-sectional Mean, SD, variance analysis and multiple regression analysis	Male (261)/ Female (27) Bus drivers	Male (261)/ Female (27) Bus drivers	BLL 2 to 15 (median 6.4)	SBP DBP	Per ln in μg/dL	SBP (↑1–2 mm Hg/ln, –2.0, 5.0) DBP (↑2–3 mm Hg/ln, 0.1, 4.9)	Low BLL was associated with DBP
[176]	Copenhagen County, Denmark	Longitudinal Multiple regression analysis and Cox proportional hazards model	1052 participants Male (504) Female (548)	40–51	BLL Male 1976 (13.6 ± 5.7) 1981 (9.6 ± 4.3) 1987 (8.3 ± 4.1) Female 1976 (9.6 ± 3.8) 1981 (6.8 ± 3.5)	SBP DBP CHD	↓4.0	SBP: ↓1.0[b]	For women, BLL were significantly associated with DBP even after adjustment. A doubling BLL represents a relative hazard of 2.14 for CHD
[177]	England	Cross-sectional Pearson correlation and multiple linear regression analysis	Representative sample of adults English population Male: 2563 Female: 2763	Male: 47.5 Female: 47.7	BLL Male: 3.7 Female: 2.6	SBP DBP Pulse pressure	↓at any level	DBP: ↓0.88 (0.13, 1.63) in men	A halving in prevalent BLL is associated with a ↓ in DBP in men

Ref.	City, Country	Study design Statistical analysis	Population		Lead assessment mean ± SD in µg/dL or range in µg/g (bone)	Outcome	Change in BLL (µg/dL)[a]	Change in mm Hg (95 % CI)[a]	Main results
			Setting	Age range or mean (years)					
[178]	United States	Cross-sectional Kolmogorov-Smirnov test, median, IQR, single and multiple regression analysis	Adults aged ≥ 20 (NHANES III) White males: (WM) 4685 White females: (WF) 5138 Black males: (BM) 1761 Black females: (BF) 2197	WM: 44.3 WF: 46.2 BM: 40.5 BF: 41.5	BLL WM: 3.6 WF: 2.1 BM: 4.2 BF: 2.3	SBP DBP	↑Doubling	SBP: WM 0.3 (–0.2, 0.7) WF 0.1 (–0.4, 0.5) BM 0.6 (–0.3, 1.5) BF 1.2 (0.4, 2.0) DBP: WM –0.6 (–0.9, –0.3) WF –0.2 (–0.5, –0.1) BM 0.3 (–0.3, 1.0) BF 0.5 (0.01, 1.1)	BLL were weakly associated with BP only in blacks, but not in whites
[179]	–	Meta-analysis Joint *p*-values, Fisher's and Stouffer's procedure	Articles were selected from January 1980 to February 2001 58,518 subjects	–	BLL	SBP DBP	↑ 2-fold	SBP: ↑1.0 (+0.5 to +1.4) DBP: ↑0.6 (+0.4 to +0.8)	A two-fold increase in BLL was associated with a 1.0 mm Hg and 0.6 mm Hg in SBP and DBP, respectively
[180]	United States	Cross-sectional Multiple linear regression and multiple logistic regression analysis	2165 women NHANES III (1988–1994)	40 to 59	BLL 2.9	SBP DBP HP	Quartile 1 (0.5–1.6) to quartile 4 (4.0–31.1)	SBP: 1.7 difference between quartiles 1–4 DBP: 1.4 difference between quartiles 1–4	BLL were positively associated with both SBP and DBP, and with increased risk for HP
[181]	Eastern, United States	Longitudinal Generalized estimating equation models	496 current and former employees of a chemical-manufacturing facility	55.8	BLL: 4.6 ± 2.6 Tibia lead: 14.7 ± 9.4	SBP DBP	Per every ↑SD	SBP: 0.64 (0.14, 1.14) for every SD ↑in BLL SBP: 0.73 (0.23, 1.23) for every SD ↑in tibia lead	SBP was associated with lead during the study, with an average annual increase in SBP of 0.64 mm Hg

[182]	Baltimore, Maryland, United States	Cross-sectional Multiple linear regression, multiple logistic regression analysis and propensity scoring	964 men and women	50 to 70	BLL: 3.5 ± 2.3 Tibia lead: 18.8 ± 12.4	SBP DBP HP	↑1.0	SBP: ↑0.99 (0.47, 1.51) DBP: ↑0.51 (0.24, 0.79)	BLL were associated with SBP and DBP, but not with HP. Tibia lead was borderline associated with HP after adjustment for race/ethnicity
[158]	–	Systematic Review –	Observational studies on lead exposure and CV endpoints through August 2006 Data bases: PubMed, EMBASE and TOXLINE	–	BLL Urine Job exposure matrix Job title/ symptoms Airborne Bone lead Area of residence	SBP DBP HP CHD Stroke CVD BFD AMI PAD Effort angina ECG	–	–	Lead exposure is positively associated with BP. The evidence is sufficient to infer a causal relationship of lead exposure with HP. The evidence is suggestive but insufficient to infer a causal relationship of lead with clinical CV outcomes
[183]	United States	Cross-sectional Multivariable logistic and linear regression analysis	6016 NI US population NHANES III (1988–1994)	44	BLL 2.98 ± 0.09	SBP DBP HP	BLL quartiles 1 reference 2 (1.5–2.3) 3 (2.4–3.7) 4 (3.8–52.9)	SBP: ↑ 1.76 (1.06, 2.47) in non-Hispanic blacks ↑ 0.72↑ (0.19, 1.26) in whites	BLL were significantly associated with SBP in non-Hispanic whites and with HP and SBP and DBP in non-Hispanic blacks

Ref.	City, Country	Study design Statistical analysis	Population		Lead assessment mean ± SD in µg/dL or range in µg/g (bone)	Outcome	Change in BLL (µg/dL)[a]	Change in mm Hg (95 % CI)[a]	Main results
			Setting	Age range or mean (years)					
[184]	United States	Cross-sectional Weighted analysis, multivariable linear regression, logistic regression, Pearson correlation	16,222 NI US population NHANES 1999–2006	Whites men: 47.14 women: 49.64 Blacks men: 42.86 women: 45.10 Mex-Am men: 37.64 women: 40.67	BLL 1999–2000: 1.75 2005–2006: 1.41	SBP DBP HP Pulse pressure	↑2-fold	SBP: ↑1.59 (0.61, 2.57) in black men ↑1.66 (0.07–3.25) black women DBP: ↑1.91 (0.76, 3.29) black men ↑0.62 (0.00, 1.25) white men ↑0.65 (0.13, 1.18) white women –0.92 (–1.84, –0.01) Mexican-American	BLL were significantly associated with higher SBP among black men and women, but not white or Mexican-Americans. Higher DBP was associated with BLL among white men and women and black men. A negative association was found in Mexican-American men
[185]	United States	Cross-sectional z test, Turkey test, χ^2 test with Bonferroni correction, multivariable analysis	12,725 Americans	>18	BLL Whites 1.46 No whites 1.57	SBP DBP HP	↑Doubling	SBP: ↑0.76 (0.38, 1.13) DBP: ↑0.43 (0.18, 0.68) HP: ↑0.95 (0.90, 1.01)	BLL were associated with SBP and DBP in the overall population, but not with the odds for HP

Abbreviations: SD standard deviation, BLL blood lead levels, CI confidence interval, NI noninstitutionalized, US United States, NHANES National Health and Nutrition Examination Survey, SBP systolic blood pressure, DBP diastolic blood pressure, MI myocardial infarction, HP hypertension, MA Massachusetts, CHD coronary heart disease, ln logarithm, IQR interquartile range, CV cardiovascular, CVD cardiovascular disease, BFD black foot disease, AMI acute myocardial infarction, PAD peripheral arterial disease, ECG electrocardiogram, SE standard errors.

[a]Considered the ↑ or ↓ in BLL (µg/dL) associated with ↑ in SBP and/or in DBP (mm Hg).

[b]Only in unadjusted analysis anal.

The effects of lead on the nervous system, kidneys, reproductive system, immune and hematological system, and skeleton have been defined but many of their underlying molecular mechanisms still need to be characterized. Regulatory and public health interventions must be developed and implemented to prevent and reduce lead exposure beyond current levels.

ACKNOWLEDGMENTS

This chapter has been supported in part by grants from the National Institute of Environmental Health Sciences (NIEHS) 1R01 ES020852, R01 ES07331, and R01 ES10563.

ABBREVIATIONS

Aβ	amyloid beta
ACE	angiotensin-converting enzyme
AD	Alzheimer's disease
ALA	δ-aminolevulinic acid
ALAD	δ-aminolevulinic acid dehydratase
ALAS	δ-aminolevulinic acid synthase
APP	amyloid precursor protein
ATP	adenosine 5′-triphosphate
BBB	blood brain barrier
BLL	blood lead level
BMP	bone morphologic protein
CSF	cerebrospinal fluid
DMT	divalent metal transporter
EP	erythrocyte protoporphyrin
GI	gastrointestinal tract
GMP	guanosine monophosphate
GPx	glutathione peroxidase
GSH	glutathione
Ig	immunoglobulin
iNOS	inducible nitric oxide synthase
IQ	intelligence quotient
LOAEL	lowest observable adverse effect level
MDA	malondialdehyde
NCV	nerve conduction velocity
NHANES	National Health and Nutrition Examination Survey
NIOSH	National Institute for Occupational Safety and Health
NOAEL	no observable adverse effect
OSHA	Occupational Safety and Health Administration
PEL	permissible exposure limit

PKC	protein kinase C
PVC	polyvinyl chloride
REL	recommended exposure limit
ROS	reactive oxygen species
SOD	superoxide dismutase
TBARS	thiobarbituric acid reactive substance
TGF-β	transforming growth factor β

REFERENCES

1. H. Needleman, *Annu. Rev. Med.* **2004**, *55*, 209–222.
2. S. Hernberg, *Am. J. Ind. Med.* **2000**, *38*, 244–254.
3. D. Sen, H. Wolfson, M. Dilworth, *Occup. Med.*, **2002**, *52*, 49–54.
4. A. Chamberlain, C. Heard, M. Little, *Philos. Trans R. Soc. Lond. A*, **1978**, *290*, 557–589.
5. B. L. Gulson, K. J. Mizon, M. J. Korsch, J. M. Palmer, J. B. Donnelly, *Sci. Total Environ*. **2003**, *303*, 79–104.
6. E. W. Harville, I. Hertz-Picciotto, M. Schramm, M. Watt-Morse, K. Chantala, J. Osterloh, P. J. Parsons, W. Rogan, *Occup. Environ. Med*. **2005**, *62*, 263–269.
7. A. S. Ettinger, M. M. Tellez-Rojo, C. Amarasiriwardena, K. E. Peterson, J. Schwartz, A. Aro, H. Hu, M. Hernandez-Avila, *Am. J. Epidemiol*. **2006**, *163*, 48–56.
8. P. Mushak, *Chem. Speciat. Bioavail*. **1991**, *3*, 87–104.
9. A. G. Oomen, J. Tolls, A. J. Sips, M. A. Van den Hoop, *Arch. Environ. Contam. Toxicol*. **2003**, *44*, 107–115.
10. A. G. Oomen, C. J. Rompelberg, M. A. Bruil, C. J. Dobbe, D. P. Pereboom, A. J. Sips, *Arch. Environ. Contam. Toxicol*. **2003**, *44*, 281–287.
11. S. J. Pocock, D. Ashby, M. A. Smith, *Int. J. Epidemiol*. **1987**, *16*, 57–67.
12. J. C. Sherlock, M. J. Quinn, *Food Addit. Contam*. **1986**, *3*, 167–176.
13. J. P. Bressler, L. Olivi, J. H. Cheong, Y. Kim, D. Bannona, *Ann. NY Acad. Sci*. **2004**, *1012*, 142–152.
14. F. D. Bronner, D. Pansu, W. D. Stein, *Am. J. Physiol*. **1986**, *250*, G561–569.
15. K. R. Mahaffey, P. S. Gartside, C. J. Glueck, *Pediatrics*, **1986**, *78*, 257–262.
16. J. N. Morrison, J. Quarterman, *Biol. Trace Elem. Res.* **1987**, *14*, 115–126.
17. J. B. Hursh, A. Schraub, E. L. Sattler, H. P. Hofmann, *Health Phys.* **1969**, *16*, 257–267.
18. T. J. Simons, *J. Physiol*. **1986**, *378*, 287–312.
19. J. V. Calderon-Salinas, M. A. Quintanar-Escorcia, M. T. Gonzalez-Martinez, C. E. Hernandez-Luna, *Hum. Exp. Toxicol.* **1999**, *18*, 327–332.
20. T. J. Simons, *J. Physiol.* **1988**, *405*, 105–113.
21. I. A. Bergdahl, M. Sheveleva, A. Schutz, V. G. Artamonova, S. Skerfving, *Toxicol. Sci*. **1998**, *46*, 247–253.
22. I. A. Bergdahl, A. Schutz, A. Grubb, *J. Anal. Atom. Spectrom*. **1996**, *11*, 735–738.
23. A. J. Al-Modhefer, M. W. Bradbury, T. J. Simons, *Clin. Sci. (Lond)* **1991**, *81*, 823–829.
24. M. B. Rabinowitz, G. W. Wetherill, J. D. Kopple, *J. Clin. Invest*. **1976**, *58*, 260–270.
25. S. Araki, H. Aono, K. Yokoyama, K. Murata, *Arch. Environ. Health* **1986**, *41*, 216–221.
26. S. Araki, F. Sata, K. Murata, *Int. Arch. Occup. Environ. Health* **1990**, *62*, 471–477.
27. W. Victery, A. J. Vander, D. R. Mouw, *Am. J. Physiol*. **1979**, *237*, F398–407.

28. A. Chamberlain, *Atmos. Environ*. **1983**, *17*, 677–692.
29. J. L. Tomsig, J. B. Suszkiw, *J. Neurochem*. **1995**, *64*, 2667–2673.
30. X. Sun, X. Tian, J. L. Tomsig, J. B. Suszkiw, *Toxicol. Appl. Pharmacol*. **1999**, *156*, 40–45.
31. J. S. Hanas, J. S. Rodgers, J. A. Bantle, Y. G. Cheng, *Mol. Pharmacol.* **1999**, *56*, 982–988.
32. J. S. Rodgers, J. R. Hocker, R. J. Hanas, E. C. Nwosu, J. S. Hanas, *Biochem. Pharmacol.* **2001**, *61*, 1543–1550.
33. I. Baranowska-Bosiacka, I. Gutowska, C. Marchetti, M. Rutkowska, M. Marchlewicz, A. Kolasa, A. Prokopowicz, I. Wiernicki, K. Piotrowska, M. Baskiewicz, K. Safranow, B. Wiszniewska, D. Chlubek, *Toxicology*, **2011**, *280*, 24–32.
34. W. Zheng, M. Aschner, J. F. Ghersi-Egea, *Toxicol. Appl. Pharmacol*. **2003**, *192*, 1–11.
35. J. Markovac, G. W. Goldstein, *Nature*, **188**, *334*, 71–73.
36. W. Zheng, H. Shen, W. S. Blaner, Q. Zhao, X. Ren, J. H. Graziano, *Toxicol. Appl. Pharmacol*. **1996**, *139*, 445–450.
37. S. Kumar, S. Jain, C. S. Aggarwal, G. K. Ahuja, *Jpn. J. Med*. **1987**, *26*, 253–254.
38. E. Arnvig, P. Grandjean, J. Beckmann, *Toxicol. Lett.* **1980**, *5*, 399–404.
39. H. Haenninen, S. Hernberg, P. Mantere, R. Vesanto, M. Jalkanen, *J. Occup. Med*. **1978**, *20*, 683–689.
40. C. Hogstedt, M. Hane, A. Agrell, L. Bodin, *Br. J. Ind. Med*. **1983**, *40*, 99–105.
41. P. Mantere, H. Hanninen, S. Hernberg, *Neurobehav. Toxicol. Teratol*. **1982**, *4*, 725–727.
42. D. K. Parkinson, C. Ryan, E. J. Bromet, M. M. Connell, *Am. J. Epidemiol*. **1986**, *123*, 261–269.
43. M. Payton, K. M. Riggs, A. Spiro, 3rd, S. T. Weiss, H. Hu, *Neurotoxicol. Teratol*. **1998**, *20*, 19–27.
44. D. Rhodes, A. Spiro, 3rd, A. Aro, H. Hu, *J. Occup. Environ. Med*. **2003**, *45*,1144–1151.
45. R. Lucchini, E. Albini, I. Cortesi, D. Placidi, E. Bergamaschi, F. Traversa, L. Alessio, *Neurotoxicology* **2000**, *21*, 805–811.
46. A. Barth, A. W. Schaffer, W. Osterode, R. Winker, C. Konnaris, E. Valic, C. Wolf, H. W. Rudiger, *Int. Arch. Occup. Environ. Health* **2002**, *75*, 394–398.
47. M. Meyer-Baron, A. Seeber, *Arch. Toxicol*. **2000**, *73*, 510–518.
48. M. G. Weisskopf, R. O. Wright, J. Schwartz, A. Spiro, 3rd, D. Sparrow, A. Aro, H. Hu, *Am. J. Epidemiol*. **2004**, *160*, 1184–1193.
49. R. A. Shih, T. A. Glass, K. Bandeen-Roche, M. C. Carlson, K. I. Bolla, A. C. Todd, B. S. Schwartz, *Neurology* **2006**, *67*, 1556–1562.
50. B. S. Schwartz, W. F. Stewart, K. I. Bolla, P. D. Simon, K. Bandeen-Roche, P. B. Gordon, J. M. Links, A. C. Todd, *Neurology* **2000**, *55*, 1144–1150.
51. M. R. Basha, M. Murali, H. K. Siddiqi, K. Ghosal, O. K. Siddiqi, H. A. Lashuel, Y. W. Ge, D. K. Lahiri, N. H. Zawia, *FASEB J.* **2005**, *19*, 2083–2084.
52. M. R. Basha, W. Wei, S. A. Bakheet, N. Benitez, H. K. Siddiqi, Y. W. Ge, D. K. Lahiri, N. H. Zawia, *J. Neurosci.* **2005**. *25*, 823–829.
53. J. Wu, M. R. Basha, B. Brock, D. P. Cox, F. Cardozo-Pelaez, C. A. McPherson, J. Harry, D. C. Rice, B. Maloney, D. Chen, D. K. Lahiri, N. H. Zawia, *J. Neurosci.* **2008**, *28*, 3–9.
54. S. W. Bihaqi, A. Bahmani, A. Adem, N. H. Zawia, *Neurotoxicology* **2014**, *44*,114–120.
55. A. M. Masoud, S. W. Bihaqi, J. T. Machan, N. H. Zawia, W. E. Renehan, *J. Alzheimers Dis.* **2016**; DOI: 10.3233/JAD–151018.

56. A. Chen, K. N. Dietrich, J. H. Ware, J. Radcliffe, W. J. Rogan, *Environ. Health Perspect*. **2005**, *113*, 597–601.
57. H. Hu, M. M. Tellez-Rojo, D. Bellinger, D. Smith, A. S. Ettinger, H. Lamadrid-Figueroa, J. Schwartz, L. Schnaas, A. Mercado-Garcia, M. Hernandez-Avila, *Environ. Health Perspect*. **2006**, *114*, 1730–1735.
58. B. P. Lanphear, R. Hornung, J. Khoury, K. Yolton, P. Baghurst, D. C. Bellinger, R. L. Canfield, K. N. Dietrich, R. Bornschein, T. Greene, S. J. Rothenberg, H. L. Needleman, L. Schnaas, G. Wasserman, J. Graziano, R. Roberts, *Environ. Health Perspect*. **2005**, *113*, 894–899.
59. H. L. Needleman, C. McFarland, R. B. Ness, S. E. Fienberg, M. J. Tobin, *Neurotoxicol. Teratol.* **2002**, *24*, 711–717.
60. K. N. Dietrich, M. D. Ris, P. A. Succop, O. G. Berger, R. L. Bornschein, *Neurotoxicol. Teratol*. **2001**, *23*, 511–518.
61. R. Nevin, *Environ. Res.* **2000**, *83*, 1–22.
62. P. B. Stretesky, M. J. Lynch, *Arch. Pediatr. Adolesc. Med*. **2001**, *155*, 579–582.
63. J. H. Yeh, Y. C. Chang, J. D. Wang, *Occup. Environ. Med*. **1995**, *52*, 415–419.
64. A. M. Seppalainen, S. Hernberg, R. Vesanto, B. Kock, *Neurotoxicology* **1983**, *4*, 181–192.
65. G. Triebig, D. Weltle, H. Valentin, *Int. Arch. Occup. Environ. Health* **1984**, *53*, 189–203.
66. J. Schwartz, P. J. Landrigan, R. G. Feldman, E. K. Silbergeld, E. L. Baker, Jr., I. H. von Lindern, *J. Pediatr*. **1988**, *112*, 12–17.
67. S. N. Kelada, E. Shelton, R. B. Kaufmann, M. J. Khoury, *Am. J. Epidemiol*. **2001**, *154*, 1–13.
68. G. Battistuzzi, R. Petrucci, L. Silvagni, F. R. Urbani, S. Caiola, *Ann. Hum. Genet*. **1981**, *45*, 223–229.
69. K. H. Astrin, D. F. Bishop, J. G. Wetmur, B. Kaul, B. Davidow, R. J. Desnick, *Ann. NY Acad. Sci*. **1987**, *514*, 23–29.
70. L. L. Hsieh, S. H. Liou, Y. H. Chen, L. C. Tsai, T. Yang, T. N. Wu, *J. Occup. Environ. Med*. **2000**, *42*, 151–155.
71. J. G. Wetmur, G. Lehnert, R. J. Desnick, *Environ. Res.* **1991**, *56*, 109–119.
72. I. A. Bergdahl, L. Gerhardsson, A. Schutz, R. J. Desnick, J. G. Wetmur, S. Skerfving, *Arch. Environ. Health* **1997**, *52*, 91–96.
73. A. Leroyer, B. Leleu, B. Dehon, P. Frimat, F. Broly, C. Nisse, *J. Toxicol. Environ. Health A* **2013**, *76*, 895–906.
74. A. da Cunha Martins, Jr., G. R. Mazzaron Barcelos, A. L. Jacob Ferreira, M. F. de Souza, I. M. de Syllos Colus, L. M. Greggi Antunes, M. M. Bastos Paoliello, J. A. Adeyemi, F. Barbosa, Jr., *J. Toxicol. Environ. Health A* **2015**, *78*, 1073–1081.
75. N. Pawlas, K. Broberg, E. Olewinska, A. Prokopowicz, S. Skerfving, K. Pawlas, *Neurotoxicology* **2012**, *33*, 37–43.
76. S. Kasperczyk, M. Dobrakowski, A. Kasperczyk, G. Machnik, E. Birkner, *Environ. Toxicol. Pharmacol.* **2014**, *37*, 638–647.
77. M. Ahamed, S. Verma, A. Kumar, M. K. Siddiqui, *Sci. Total Environ*. **2005**, *346*, 48–55.
78. S. K. Tandon, S. Singh, S. Prasad, S. Srivastava, M. K. Siddiqui, *Environ. Res.*, **2002**, *90*, 61–66.
79. H. Gurer-Orhan, H. U. Sabir, H. Ozgunes, *Toxicology* **2004**, *195*, 147–154.
80. N. Pawlas, M. Dobrakowski, A. Kasperczyk, A. Kozlowska, A. Mikolajczyk, S. Kasperczyk, *Biol. Trace Elem. Res.* **2015**, DOI: 10.1007/s12011–015–0435-z.
81. E. J. Bechara, *Braz. J. Med. Biol. Res.* **1996**, *29*, 841–851.
82. H. Gurer, N. Ercal, *Free Radic. Biol. Med*. **2000**, *29*, 927–945.
83. U. Ewers, R. Stiller-Winkler, H. Idel, *Environ. Res.* **1982**, *29*, 351–357.

84. N. Basaran, U. Undeger, *Am. J. Ind. Med*. **2000**, *38*, 349–354.
85. I. Kimber, M. D. Stonard, D. A. Gidlow, Z. Niewola, *Int. Arch. Occup. Environ. Health* **1986**, *57*, 117–125.
86. L. E. Pinkerton, R. E. Biagini, E. M. Ward, R. D. Hull, J. A. Deddens, M. F. Boeniger, T. M. Schnorr, B. A. MacKenzie, M. I. Luster, *Am. J. Ind. Med*. **1998**, *33*, 400–408.
87. U. Undeger, N. Basaran, H. Canpinar, E. Kansu, *Toxicology* **1996**, *109*, 167–172.
88. Y. Heo, B. K. Lee, K. D. Ahn, D. A. Lawrence, *Hum. Exp. Toxicol*. **2004**, *23*, 209–213.
89. A. Fischbein, P. Tsang, J. C. Luo, J. P. Roboz, J. D. Jiang, J. G. Bekesi, *Clin. Immunol. Immunopathol*. **1993**, *66*, 163–168.
90. K. P. Mishra, V. K. Singh, R. Rani, V. S. Yadav, V. Chandran, S. P. Srivastava, P. K. Seth, *Toxicology* **2003**, *188*, 251–259.
91. M. Valentino, M. Governa, I. Marchiseppe, I. Visona, *Arch. Toxicol*. **1991**, *65*, 685–688.
92. V. Matovic, A. Buha, D. Ethukic-Cosic, Z. Bulat, *Food Chem. Toxicol*. **2015**, *78*, 130–140.
93. M. Payton, H. Hu, D. Sparrow, S. T. Weiss, *Am. J. Epidemiol*. **1994**, *140*, 821–829.
94. R. Kim, A. Rotnitsky, D. Sparrow, S. Weiss, C. Wager, H. Hu, *JAMA* **1996**, *275*, 1177–1181.
95. M. Ahamed, M. K. Siddiqui, *Clin. Chim. Acta* **2007**, *383*, 57–64.
96. S. Sharma, B. Sinhg, *Int. J. Sci. Res.* **2014**, *3*, 1564–1566.
97. V. Sharma, A. Sharma, L. Kansal, *Food Chem. Toxicol*. **2010**, *48*, 928–936.
98. J. Wang, Z. Yang, L. Lin, Z. Zhao, Z. Liu, X. Liu, *Biol. Trace Elem Res.* **2012**, *146*, 354–359.
99. A. E. Abdel Moneim, M. A. Dkhil, S. Al-Quraishy, *J. Hazard Mater*. **2011**, *194*, 250–255.
100. F. Farmand, A. Ehdaie, C. K. Roberts, R. K. Sindhu, *Environ. Res.* **2005**, *98*, 33–39.
101. N. D. Vaziri, C. Y. Lin, F. Farmand, R. K. Sindhu, *Kidney Int.* **2003**, *63*,186–194.
102. K. Sujatha, C. H. Srilatha, Y. Anjaneyulu, P. Amaravathi, *Int. J. Pharm. BioSci.* **2011**, *2*, B458–B468.
103. J. Zhang, H. Cao, Y. Zhang, Y. Zhang, J. Ma, J. Wang, Y. Gao, X. Zhang, F. Zhang, L. Chu, *Toxicol. Lett*. **2013**, *218*, 273–280.
104. C. M. Liu, J. Q. Ma, Y. Z. Sun, *Toxicol. Appl. Pharmacol*. **2012**, *258*, 330–342.
105. EPA, *Air Quality Criteria for Lead*, U. S. Environmental Protection Agency, 2006.
106. M. Carmignani, A. R. Volpe, P. Boscolo, N. Qiao, M. Di Gioacchino, A. Grilli, M. Felaco, *Life Sci*. **2000**, *68*, 401–415.
107. H. R. Chang, S. S. Chen, T. J. Chen, C. H. Ho, H. C. Chiang, H. S. Yu, *Toxicol. Appl. Pharmacol*. **1996**, *139*, 1–5.
108. D.-A. Tsao, H.-S. Yu, J.-T. Cheng, *Toxicol. Appl. Pharmacol*. **2000**, *163*, 127–133.
109. P. Boscolo, M. Carmignani, *Environ. Health Perspect*. **1988**, *78*, 101–106.
110. M. Carmignani, P. Boscolo, P. Preziosi, *Arch. Toxicol. Supp*. **1988**, *12*, 326–329.
111. H. C. Gonick, Y. Ding, S. C. Bondy, Z. Ni, N. D. Vaziri, *Hypertension* **1997**, *30*, 1487–1492.
112. N. D. Vaziri, Y. Ding, Z. Ni, H. C. Gonick, *Kidney Int*. **1997**, *52*, 1042–1046.
113. M. Marques, I. Millas, A. Jimenez, E. Garcia-Colis, J. A. Rodriguez-Feo, S. Velasco, A. Barrientos, S. Casado, A. Lopez-Farre, *J. Am. Soc. Nephrol*. **2001**, *12*, 2594–2600.
114. B. S. Glenn, W. F. Stewart, B. S. Schwartz, J. Bressler, *Am. J. Epidemiol*. **2001**, *153*, 537–545.
115. M. Edwards, *Environ. Sci. Technol.* **2014**, *48*, 739–746.
116. I. Lancranjan, H. I. Popescu, O. Gavanescu, I. Klepsch, M. Serbanescu, *Arch. Environ. Health* **1975**, *30*, 396–401.

117. S. Nordstrom, L. Beckman, I. Nordenson, *Hereditas* **1979**, *90*, 291–296.
118. V. H. Borja-Aburto, I. Hertz-Picciotto, M. Rojas Lopez, P. Farias, C. Rios, J. Blanco, *Am. J. Epidemiol*. **1999**, *150*, 590–597.
119. A. J. McMichael, G. V. Vimpani, E. F. Robertson, P. A. Baghurst, P. D. Clark, *J. Epidemiol. Community Health* **1986**, *40*, 18–25.
120. K. W. Andrews, D. A. Savitz, I. Hertz-Picciotto, *Am. J. Ind. Med*. **1994**, 26, 13–32.
121. P. Apostoli, P. Kiss, S. Porru, J. P. Bonde, M. Vanhoorne, *Occup. Environ. Med*. **1998**, *55*, 364–374.
122. A. R. Chowdhury, N. J. Chinoy, A. K. Gautam, R. V. Rao, D. J. Parikh, G. M. Shah, H. N. Highland, K. G. Patel, B. B. Chatterjee, *Adv. Contracept. Deliv. Syst*. **1986**, *2*, 208–210.
123. G. Assennato, C. Paci, M. E. Baser, R. Molinini, R. G. Candela, B. M. Altamura, R. Giorgino, *Arch. Environ. Health* **1986**, *41*, 387–390.
124. J. P. Bonde, M. Joffe, P. Apostoli, A. Dale, P. Kiss, M. Spano, F. Caruso, A. Giwercman, L. Bisanti, S. Porru, M. Vanhoorne, F. Comhaire, W. Zschiesche, *Occup. Environ. Med*. **2002**, *59*, 234–242.
125. N. Cherry, A. C. Povey, R. McNamee, H. Moore, H. Baillie, J. A. Clyma, M. Dippnall, A. A. Pacey, participating centres of CHAPS-UK, *Occup. Environ. Med*. **2014**, *71*, 598–604.
126. E. J. O'Flaherty, *Toxicol. Appl. Pharmacol.* **1993**, *118*, 16–29.
127. E. J. O'Flaherty, *Toxicol. Appl. Pharmacol*. **1991**, *111*, 313–331.
128. P. E. Marino, A. Franzblau, R. Lilis, P. J. Landrigan, *Arch. Environ. Health* **1989**, *44*, 140–145.
129. T. D. Matte, J. P. Figueroa, G. Burr, J. P. Flesch, R. A. Keenlyside, E. L. Baker, *Am. J. Ind. Med*. **1989**, *16*, 167–177.
130. A. Pagliuca, G. J. Mufti, D. Baldwin, A. N. Lestas, R. M. Wallis, A. J. Bellingham, *J. Clin. Pathol*. **1990**, *43*, 277–281.
131. K. D. Rosenman, A. Sims, Z. Luo, J. Gardiner, *J. Occup. Environ. Med*. **2003**, *45*, 546–555.
132. M. Pearl, L. M. Boxt, *Radiology* **1980**, *136*, 83–84.
133. R. Shukla, R. L. Bornschein, K. N. Dietrich, C. R. Buncher, O. G. Berger, P. B. Hammond, P. A. Succop, *Pediatrics* **1989**, *84*, 604–612.
134. R. Shukla, K. N. Dietrich, R. L. Bornschein, O. Berger, P. B. Hammond, *Pediatrics* **1991**, *88*, 886–892.
135. J. D. Holz, T. J. Sheu, H. Drissi, M. Matsuzawa, M. J. Zuscik, J. E. Puzas, *Birth Defects Res. C Embryo Today* **2007**, *81*, 41–50.
136. J. J. Carmouche, J. E. Puzas, X. Zhang, P. Tiyapatanaputi, D. A. Cory-Slechta, R. Gelein, M. Zuscik, R. N. Rosier, B. F. Boyce, R. J. O'Keefe, E. M. Schwarz, *Environ. Health Perspect*. **2005**, *113*, 749–755.
137. G. J. Long, J. F. Rosen, *Life Sci*. **1994**, *54*, 1395–1402.
138. J. G. Pounds, G. J. Long, J. F. Rosen, *Environ. Health Perspect*. **1991**, *91*, 17–32.
139. J. D. Holz, E. Beier, T. J. Sheu, R. Ubayawardena, M. Wang, E. R. Sampson, R. N. Rosier, M. Zuscik, J. E. Puzas, *J. Orthop. Res.* **2012**, *30*, 1760–1766.
140. X. Li, A. M. Ionescu, E. M. Schwarz, X. Zhang, H. Drissi, J. E. Puzas, R. N. Rosier, M. J. Zuscik, R. J. O'Keefe, *J. Orthop. Res.* **2003**, *21*, 908–913.
141. M. J. Zuscik, L. Ma, T. Buckley, J. E. Puzas, H. Drissi, E. M. Schwarz, R. J. O'Keefe, *Environ. Health Perspect*. **2007**, *115*, 1276–1282.
142. J. R. Campbell, R. N. Rosier, L. Novotny, J. E. Puzas, *Environ. Health Perspect.* **2004**, *112*, 1200–1203.
143. E. E. Beier, J. D. Holz, T. J. Sheu, J. E. Puzas, *Toxicol. Sci.* **2016**, *149*, 277–288.
144. B. A. Dye, R. Hirsch, D. J. Brody, *Environ. Health Perspect*. **2002**, *110*, 997–1002.
145. M. E. Moss, B. P. Lanphear, P. Auinger, *JAMA* **1999**, *281*, 2294–2298.

146. P. Muntner, A. Menke, K. B. DeSalvo, F. A. Rabito, V. Batuman, *Arch. Intern. Med*. **2005**, *165*, 2155–2161.
147. M. M. Paoliello, E. M. De Capitani, *Rev. Environ. Contam. Toxicol*. **2005**, *184*, 59–96.
148. WHO, *Burden: Mortality, Morbidity and Risk Factors*, 2010, pp. 9–31.
149. A. Navas-Acien, M. Tellez-Plaza, E. Guallar, P. Muntner, E. Silbergeld, B. Jaar, V. Weaver, *Am. J. Epidemiol*. **2009**, *170*, 1156–1164.
150. E. K. Silbergeld, *Environ. Health Perspect.* **1991**, 63–70.
151. E. J. O'Flaherty, *Toxicol. Sci.* **2000**, *55*, 171–188.
152. M. Vahter, M. Berglund, A. Åkesson, C. Lidén, *Environ. Res.* **2002**, *88*, 145–155.
153. G. Falq, A. Zeghnoun, M. Pascal, M. Vernay, Y. Le Strat, R. Garnier, D. Olichon, P. Bretin, K. Castetbon, N. Frery, *Environ. Int.* **2011**, *37*, 565–571.
154. J. C. Leblanc, T. Guerin, L. Noel, G. Calamassi-Tran, J. L. Volatier, P. Verger, *Food Addit. Contam*. **2005**, *22*, 624–641.
155. A. C. B. Almeida Lopes, A. Navas-Acien, R. Zamoiski, E. K. Silbergeld, Mde. Carvalho, M. L. Buzzo, M. R. Urbano, C. Martins Ada, Jr., M. M. Paoliello, *J. Toxicol. Environ. Health A* **2015**, *78*, 92–108.
156. P. Apostoli, A. Baj, P. Bavazzano, A. Ganzi, G. Neri, A. Ronchi, L. Soleo, L. Di Lorenzo, P. Spinelli, T. Valente, C. Minoia, *Sci. Total Environ.* **2002**, *287*, 1–11.
157. R. Poreba, P. Gac, M. Poreba, R. Andrzejak, *Toxicol. Appl. Pharmacol*. **2010**, *249*, 41–46.
158. A. Navas-Acien, E. Guallar, E. K. Silbergeld, S. J. Rothenberg, *Environ. Health Perspect*. **2007**, *115*, 472–482.
159. Y. Cheng, J. Schwartz, D. Sparrow, A. Aro, S. T. Weiss, H. Hu, *Am. J. Epidemiol*. **2001**, *153*, 164–171.
160. E. M. Wells, A. Navas-Acien, J. B. Herbstman, B. J. Apelberg, E. K. Silbergeld, K. L. Caldwell, R. L. Jones, R. U. Halden, F. R. Witter, L. R. Goldman, *Environ. Health Perspect*. **2011**, *119*, 664–669.
161. P. Junco-Munoz, N. Arrieta Alcalde, *Gac. Med. Mex*. **1993**, *129*, 63–67.
162. K. Becker, S. Kaus, C. Krause, P. Lepom, C. Schulz, M. Seiwert, B. Seifert, *Int. J. Hyg. Environ. Health* **1998**, *205*, 297–308.
163. S. L. Wong, E. J. D. Lye, *Statistics Canada, Catalogue no. 82–003-XPE. Health Reports*, **2008**, *19*, 31–35.
164. C. Schroijen, W. Baeyens, G. Schoeters, E. Den Hond, G. Koppen, L. Bruckers, V. Nelen, E. Van De Mieroop, M. Bilau, A. Covaci, H. Keune, I. Loots, J. Kleinjans, W. Dhooge, N. Van Larebeke, *Chemosphere* **2008**, *71*, 1317–1325.
165 A. Zhang, B. N. Sanchez, A. S. Ettinger, S. K. Park, D. Cantonwine, L. Schnaas, R. O. Wright, H. Lamadrid-Figueroa, M. M. Tellez-Rojo, *Environ. Health Perspect.* **2012**, *120*, 445–450.
166. J. W. Lee, C. K. Lee, C. S. Moon, I. J. Choi, K. J. Lee, S. M. Yi, B. K. Jang, B. J. Yoon, D. S. Kim, D. Peak, D. Sul, E. Oh, H. Im, H. S. Kang, J. Kim, J. T. Lee, K. Kim, K. L. Park, R. Ahn, S. H. Park, S. C. Kim, C. H. Park, J. H. Lee, *Int. J. Hyg. Environ. Health* **2012**, *215*, 449–457.
167. M. Cerna, A. Krskova, M. Cejchanova, V. Spevackova, *Int. J. Hyg. Environ. Health* **2012**, *215*, 109–119.
168. CDC. Fourth National Report on Human Exposure to Environmental Chemicals Updated Tables, Centers for Disease Control and Prevention, 2013.
169. A. I. Cañas, M. Cervantes-Amat, M. Esteban, M. Ruiz-Moraga, B. Perez-Gomez, J. Mayor, A. Castano, BIOAMBIENT.ES, *Int. J. Hyg. Environ. Health* **2014**, *217*, 452–459.
170. J. L. Pirkle, J. Schwartz, J. R. Landis, W. R. Harlan, *Am. J. Epidemiol.* **1985**, *121*, 246–58.

171. S. T. Weiss, A. Munoz, A. Stein, D. Sparrow, F. E. Speizer, *Environ. Health Perspect.* **1988**, *78*, 53–56.
172. W. R. Harlan, *Environ. Health Perspect.* **1988**, *78*, 9–13.
173. D. Kromhout, *Environ. Health Perspect.* **1988**, *78*, 43–46.
174. J. Schwartz, *Environ. Health Perspect.* **1988**, *78*, 15–22.
175. D. S. Sharp, J. Osterloh, C. E. Becker, B. Bernard, A. H. Smith, J. M. Fisher, S. L. Syme, B. L. T. Holman, *J. Environ. Health Perspect.* **1988**. *78*, 131–137.
176. L. Moller, T. S. Kristensen, *Am. J. Epidemiol.* **1992**, *136*, 1091–1100.
177. L. Bost, P. Primatesta, W. Dong, N. Poulter, *N. J. Hum. Hypertens.* **1999**, *13*, 123–128.
178. E. E. Den Hond, T. Nawrot, J. A. Staessen, *J. Hum. Hypertens.* **2002**, *16*, 563–568.
179. T. S. Nawrot, L. Thijs, E. M. Den Hond, H. A. Roels, J. A. Staessen, *J. Hum. Hypertens.* **2002**, *16*, 123–131.
180. D. Nash, L. Magder, M. Lustberg, R. W. Sherwin, R. J. Rubin, R. B. Kaufmann, E. K. Silbergeld, *JAMA* **2003**, *289*, 1523–1532.
181. B. S. Glenn, W. F. Stewart, J. M. Links, A. C. Todd, B. S. Schwartz, *Epidemiology* **2003**, *14*, 30–36.
182. D. Martin, T. A. Glass, K. Bandeen-Roche, A. C. Todd, W. Shi, B. S. Schwartz, *Am. J. Epidemiol.* **2006**, *163*, 467–478.
183. F. Scinicariello, A. Yesupriya, M. H. Chang, B. A. Fowler, *Environ. Health Perspect.* **2010**, *118*, 259–264.
184. F. Scinicariello, H. G. Abadin, E. Murray, *H. Environ. Res.* **2011**, *111*, 1249–1257.
185. A. Hara, L. Thijs, K. Asayama, Y. M. Gu, L. Jacobs, Z. Y. Zhang, Y. P. Liu, T. S. Nawrot, J. A. Staessen, *Hypertension* **2015**, *65*, 62–69.

Subject Index

A

Metal Ions in Life Sciences, Volume 17 Edited by Astrid Sigel, Helmut Sigel, and Roland K. O. Sigel

DOI 10.1515/9783110434330-017

B

C

D

E

F

G

H

I

J

K

L

M

N

O

P

Q

R

S

T

U

V

W

X

Y

Z